Non-Gaussian resources for photonic quantum technologies

Mattia Walschaers

Non-Gaussian resources for photonic quantum technologies

Habilitation à Diriger des Recherches
Sorbonne Université

Mattia Walschaers
Laboratoire Kastler Brossel

2 October 2023

Composition du jury :

- Alexia Auffèves (Président)
- Chiara Macchiavello (Rapporteur)
- Gerardo Adesso (Rapporteur)
- Peter van Loock (Rapporteur)
- Alexei Ourjoumtsev (Examinateur)
- Kae Nemoto (Examinateur)

PROLOGUE AND STRUCTURE

In January 2015, I visited a conference on "quantum cybernetics and control" in Nottingham. I had convinced my PhD advisor to send me there to present our recent results on statistical benchmarks for Boson Sampling—we will discuss that more extensively in Section 2.1. The conference was a motley mix of optical control theory, quantum metrology, complex systems, and quantum computing. As a relatively inexperienced PhD student, several of the talks passed over my head. However, near the end of the workshop two talks captured my attention. One of them was by IBM, the other by Google. The speakers presented results on a four- and nine-qubit device, respectively. During the conference dinner, I ended up at the table with Rami Barends from Google, who told me about their plans for scaling up to larger devices. At that time, my mind was blown.

Every now and then a conference or a workshop leaves a deep and lasting impression. They can inspire new research directions or connect us to new collaborators. For me, the above anecdote marks such an event which caused a genuine shift in my personal point of view on quantum technologies. I had started working on Boson Sampling because it allowed me to combine random matrix theory with the operator algebra generated by the canonical commutation relation, mathematical tools that have always been dear to me. Frankly, I did not care about the implications for computational complexity theory, since I did not really believe a quantum computer would ever be built. This conference in 2015 challenged my view and marked an important turning point in my research career: it is the moment I genuinely started believing in quantum computing as a viable future technology.

Once I was convinced of the quantum future, a much harder personal question remained to be answered: what would be my role in this story? I decided to cultivate my love for the mathematical aspects bosonic systems and shift my research focus to continuous-variable quantum optics. When I started my postdoc in 2016, this niche field combined an enormous potential for scalability with major challenges and many unexplored avenues. Most of these challenges are related to the need of non-Gaussian features, which would become the cornerstone of my future research.

I never imagined that by 2023 several platforms would claim to have reached a quantum computational advantage, nor did I expect that continuous-variable systems would become a big topic of research, mainly because the surge in interest for bosonic error-correction codes. Throughout this manuscript, I present an overview of my own contributions to this field. I also describe my growing interest in quantum metrology

as both a tool and an application for my research.

More specifically, this Habilitation thesis is organised as follows. In the introductory Chapter 1, we will establish basic notions of continuous variable quantum optics. Section 1.1 is devoted to presenting a clear distinction between modes and states in quantum optics, whereas Section 1.2 contrasts the discrete- and continuous-variable approach for treating the states in these systems.

Chapter 2 reviews results about the quest for a quantum computational advantage in bosonic systems. In this context, we will discuss some of my older work on benchmarks for Boson Sampling in Section 2.1. This work highlights that, to fully understand bosonic sampling problems, we need a good understanding of the physical resources that fuel bosonic quantum computers. In Section 2.2 we review the search for such resources, which culminates in a very recent paper.

Once we have a clear idea of the required resources for bosonic quantum computing, Chapter 3 takes a more detailed dive into the field of quantum state engineering. In Section 3.1 we first explore photon subtraction as a typical tool for creating non-Gaussian quantum states of light. Subsequently, in Section 3.2, we explore the conditional generation of Wigner negativity from a more fundamental point of view.

In Chapter 4 we take a detour into the adjacent field of quantum(-inspired) metrology. In Section 4.1 we review some key results and important tools from this field. They will be applied to estimate the distance between two point sources in Section 4.2.

The pathways set out in all of the previous chapters coincide at the crossroad that is Chapter 5, where we study quantum states for which the quantum correlations themselves have non-Gaussian properties. This recent research topic is still in its infancy and thus very much a work in progress. We divide it in two parts. Section 5.1 contains preliminary results of our theoretical framework to describe non-Gaussian entanglement. Section 5.2 presents new protocols, based on quantum metrology, that we develop in order to detect non-Gaussian entanglement in continuous-variable quantum optics experiments.

CONTENTS

1

INTRODUCTION

The field of quantum optics studies the quantum properties of light and ways to detect them. In this first chapter, we introduce the basic concepts that will be used throughout this habilitation thesis and fix notation.

In the first section, we use two dual Hilbert spaces to describe the properties of light. The first Hilbert space is given by Maxwell's equations and describes the optical modes. These are the physical canisters in which energy can be stored. The statistical properties of these modes are determined by a quantum state which "lives" in the second Hilbert space. This chapter takes inspiration from (Fabre and Treps, 2020) and summarises key points from the included tutorial (Walschaers, 2021). Furthermore, this introduction is intended to offer some complementary elements that have not received much attention in these previous works.

1.1 OPTICAL MODES AND STATES

1.1.1 *Modes*

Quantum optics is in the first place the study of light. The behaviour of light is determined by the wave-like solutions of Maxwell's equations for the electromagnetic field. In this text, we focus primarily on quantum optics in free space, which means that we ignore the presence of any charges or currents in Maxwell's equations. They thus take the form

$$\nabla \cdot \boldsymbol{E}(\boldsymbol{r},t) = 0, \tag{1.1a}$$

$$\nabla \times \boldsymbol{E}(\boldsymbol{r},t) = -\frac{1}{c}\frac{\partial}{\partial t}\boldsymbol{B}(\boldsymbol{r},t), \tag{1.1b}$$

$$\nabla \cdot \boldsymbol{B}(\boldsymbol{r},t) = 0, \tag{1.1c}$$

$$\nabla \times \boldsymbol{B}(\boldsymbol{r},t) = \frac{1}{c}\frac{\partial}{\partial t}\boldsymbol{E}(\boldsymbol{r},t). \tag{1.1d}$$

In this particular case, knowledge of the electric field immediately implies full knowledge of the magnetic field and vice-versa. It is therefore common to restrict to the complex representation of the electric field and study the wave equation

$$\nabla \cdot \boldsymbol{E}^{(+)}(\boldsymbol{r},t) = 0, \tag{1.2a}$$

$$\left(\Delta - \frac{1}{c^2}\frac{\partial^2}{\partial t^2}\right)\boldsymbol{E}^{(+)}(\boldsymbol{r},t) = 0. \tag{1.2b}$$

The complex field $\boldsymbol{E}^{(+)}(\boldsymbol{r},t)$ is related to the real physical electric field via the identity $\boldsymbol{E}(\boldsymbol{r},t) = \boldsymbol{E}^{(+)}(\boldsymbol{r},t) + [\boldsymbol{E}^{(+)}(\boldsymbol{r},t)]^*$. Henceforth, we will refer to $\boldsymbol{E}^{(+)}(\boldsymbol{r},t)$ simply as the electric field.

The system of equations (1.2a) and (1.2b) now can be seen as an eigenvalue problem which generates a Hilbert space of solutions. It is convenient to define a basis $\{\boldsymbol{u}_k(\boldsymbol{r},t)\}$ of this Hilbert space and use it to describe the electric field as

$$\boldsymbol{E}^{(+)}(\boldsymbol{r},t) = \sum_k \mathcal{E}_k \alpha_k \boldsymbol{u}_k(\boldsymbol{r},t). \tag{1.3}$$

where we introduce the dimensionless complex coefficient α_k and the real coefficient $\mathcal{E}_k$ that carries the dimension of the electric field. The elements of the basis $\{\boldsymbol{u}_k(\boldsymbol{r},t)\}$ are known as optical modes and $\mathcal{E}_k$ can be interpreted as the electric field of the specific mode $\boldsymbol{u}_k(\boldsymbol{r},t)$. Typically, this mode basis is constructed such that the modes are orthonormal, meaning they satisfy the relation

$$\frac{1}{V}\int_V [\boldsymbol{u}_k(\boldsymbol{r},t)]^* \boldsymbol{u}_l(\boldsymbol{r},t) d^3\boldsymbol{r} = \delta_{k,l}, \tag{1.4}$$

where V is a volume that is sufficiently large tho contain the full experimental setup. Note, moreover, that we do not integrate over time. The mode is thus expected to be spatially normalised for every instant in time.

As for any vector space, the choice of mode basis is not unique. In optics experiments, it is mainly the desired application that determine in which mode basis we decide to work (we will highlight this in Section 4.2). Changing from one mode basis $\boldsymbol{u}_k(\boldsymbol{r},t)$ to another mode basis $\boldsymbol{v}_k(\boldsymbol{r},t)$ can be done via a unitary transformation. Simply expressing the modes on the "$\boldsymbol{v}$ mode basis" in terms of the modes in the "$\boldsymbol{u}$ mode basis" leads to the identity

$$\boldsymbol{v}_k(\boldsymbol{r},t) = \sum_l U_{kl} \boldsymbol{u}_k(\boldsymbol{r},t). \tag{1.5}$$

Via the inner product structure that is implicitly introduced in (1.4), we find that

$$U_{kl} = \frac{1}{V}\int_V [\boldsymbol{u}_l(\boldsymbol{r},t)]^* \boldsymbol{v}_k(\boldsymbol{r},t) d^3\boldsymbol{r}. \tag{1.6}$$

Furthermore, this expression, together with the normalisation condition in (1.4) and the completeness relation $\sum_k \boldsymbol{u}_k(\boldsymbol{r},t)\boldsymbol{u}_k^*(\boldsymbol{r}',t) = \delta^{(3)}(\boldsymbol{r}-\boldsymbol{r}')$, allows us to directly verify

that $U^\dagger U = UU^\dagger = \mathbb{1}$ and thus that U is indeed a unitary transformation.

Note that all of the above is the foundation of multimode classical optics. Hitherto we have not invoked a single quantum phenomenon. Yet we use a Hilbert space framework to describe the solutions to Maxwell's equations. This structure of the electromagnetic field is often a source of confusion in literature where properties that derive from the modal structure of light tend to be presented as quantum mechanical effects. In what follows, we will emphasise that the actual quantum properties of light are hidden away in the coefficients α_k that were introduced in (1.3). This becomes apparent when we quantize the field.

1.1.2 *Quantisation*

Quantisation of the electromagnetic field is a topic that is covered at length in most quantum optics textbooks such as (Grynberg et al., 2010) and introductory classes. We will not go through the whole derivation in full detail, but rather emphasise key points in relation to the modal structure of the field.

The energy contained within the electromagnetic field is given by the Hamiltonian

$$H = \frac{\epsilon_0}{2V} \int_V \left[\|\boldsymbol{E}(\boldsymbol{r},t)\|^2 + c^2 \|\boldsymbol{B}(\boldsymbol{r},t)\|^2 \right] d^3\boldsymbol{r}. \tag{1.7}$$

Using Maxwell's equations (1.1a - 1.1d) and Fourier analysis, we can ultimately relate the Hamiltonian H to the modal decomposition (1.3):

$$H = 2\epsilon_0 \sum_k \mathcal{E}_k^2 \left|\alpha_k\right|^2. \tag{1.8}$$

We thus see that the coefficients $|\alpha_k|^2$ relate directly to the amount of energy that is contained in the specific mode $\boldsymbol{u}_k(\boldsymbol{r},t)$.

Because the coefficient α_k are complex, it is useful to rewrite them as

$$\alpha_k = \frac{1}{2}(q_k + ip_k), \tag{1.9}$$

where we introduce the factor 2 for future convenience. The Hamiltonian now takes the form

$$H = \frac{\epsilon_0}{2} \sum_k \mathcal{E}_k^2 (q_k^2 + p_k^2), \tag{1.10}$$

where notation was chosen rather suggestively to make it apparent that every optical mode effectively behaves as a harmonic oscillator. The real and imaginary part of α_k are known as the *field quadratures*. The real part q_k is commonly referred to as the *amplitude quadrature*, whereas the imaginary part p_k goes by the name *phase quadrature*.

More detailed derivations in standard textbooks show that, indeed, the quadratures q_k and p_k are the canonical coordinates that appear in Hamilton's equations of motion

(Grynberg et al., 2010). This means that these variables form a phase space and satisfy the relations $\{q_k, p_l\} = \delta_{k,l}$, $\{q_k, q_l\} = 0$, and $\{p_k, p_l\} = 0$, where $\{.,.\}$ denotes the Poisson bracket. We can thus quantise the electromagnetic field through canonical (Dirac, 1925) or deformation quantisation (Moyal, 1949). This leads us to introduce the quadrature operators via

$$\{q_k, p_l\} = \delta_{k,l} \mapsto [\hat{q}_k, \hat{p}_l] = 2i\delta_{k,l}, \tag{1.11a}$$

$$\{q_k, q_l\} = 0 \mapsto [\hat{q}_k, \hat{q}_l] = 0, \tag{1.11b}$$

$$\{p_k, p_l\} = 0 \mapsto [\hat{p}_k, \hat{p}_l] = 0. \tag{1.11c}$$

Notice that we use a quantisation rule that suggests setting $\hbar = 2$. In practice, this choice is motivated by experiments where quadrature measurements are usually expressed in units of vacuum noise. We thus find that the quantum mechanical Hamiltonian of the field reads

$$\hat{H} = \frac{\epsilon_0}{2} \sum_k \mathcal{E}_k^2 (\hat{q}_k^2 + \hat{p}_k^2). \tag{1.12}$$

Because the canonical position (amplitude quadrature) and canonical momentum (phase quadrature) are physical observables, they must be hermitian, *i.e.* $\hat{q}_k = \hat{q}_k^\dagger$ and $\hat{p}_k = \hat{p}_k^\dagger$.[1] The quantised version of the electric field becomes

$$\hat{\boldsymbol{E}}^{(+)}(\boldsymbol{r}, t) = \frac{1}{2} \sum_k \mathcal{E}_k (\hat{q}_k + i\hat{p}_k) \boldsymbol{u}_k(\boldsymbol{r}, t), \tag{1.13}$$

where we note that the modes $\{\boldsymbol{u}_k(\boldsymbol{r}, t)\}$ have not been touched by the quantisation procedure and all the quantum properties of the light are governed by the field quadratures. We can also introduce the quantised version of the coefficients α_k by identifying with the annihilation operators

$$\alpha_k \mapsto \hat{a}_k = \frac{1}{2}(\hat{q}_k + i\hat{p}_k). \tag{1.14}$$

the canonical commutation relations (1.11a - 1.11c) directly implies that the creation and annihilation operators satisfy

$$[\hat{a}_k, \hat{a}_l^\dagger] = \delta_{k,l} \tag{1.15a}$$

$$[\hat{a}_k, \hat{a}_l] = [\hat{a}_k^\dagger, \hat{a}_l^\dagger] = 0. \tag{1.15b}$$

1 Because these operators are unbounded, the claim that these operators are hermitian is not very rigorous. More exact would be to claim that the operators are self-adjoint on their domain (Reed and B. Simon, 1980). Alternatively, one could use the formalism of C*-algebras and focus on a specific representation of the algebra of canonical commutation relations (Petz, 1990). In practice, our choice of working in a finite volume V effectively tames most of the wild mathematical behaviour of these operators. Unless they have an important physical impact, we will consider these mathematical subtleties beyond the scope of this work.

We can thus alternatively write the field as

$$\hat{\boldsymbol{E}}^{(+)}(\boldsymbol{r},t) = \sum_k \mathcal{E}_k \hat{a}_k \boldsymbol{u}_k(\boldsymbol{r},t). \tag{1.16}$$

At this point some readers may start to feel uncomfortable because equations (1.13) and (1.16) rely on a specific mode basis. In other words, the quadrature operators, and creations and annihilation operators, are basis dependent. This problem can be resolved via the mode basis change introduced in (1.5). Given that we have a set of annihilation operators $\{\hat{a}_k\}$ in mode basis $\{\boldsymbol{u}_k(\boldsymbol{r},t)\}$, we can find a transformation rule for the annihilation operators by demanding that the electric field operator $\hat{\boldsymbol{E}}^{(+)}(\boldsymbol{r},t)$ remains the same regardless of the mode basis. If we now denote $\{\hat{b}_k\}$ as the annihilation operators in mode basis $\{\boldsymbol{v}(\boldsymbol{r},t)\}$, this constraint implies that the creation and annihilation operators must transform as

$$\hat{b}_k^\dagger = \sum_l U_{kl} \hat{a}_l^\dagger, \tag{1.17a}$$

$$\hat{a}_k = \sum_l U_{lk} \hat{b}_l. \tag{1.17b}$$

Combining these transformation rules also leads to a transformation rule for the quadrature operators. For convenience, we introduce the vector of quadratures in the modes basis $\{\boldsymbol{u}(\boldsymbol{r},t)\}$ as

$$\vec{\hat{x}} = (\hat{q}_1, \hat{p}_1, \ldots, \hat{q}_m, \hat{p}_m)^\top, \tag{1.18}$$

where m denotes the number of modes in the system. The vector of quadratures $\vec{\hat{x}}'$ in the mode basis $\{\boldsymbol{u}(\boldsymbol{r},t)\}$ is now given by

$$\vec{\hat{x}}' = O\vec{\hat{x}}, \tag{1.19}$$

where O is an orthonormal matrix with components that are related to the unitary matrix of mode basis changed U via

$$O_{2i-1,2j-1} = \frac{1}{2}(U_{ij} + U_{ij}^*), \tag{1.20a}$$

$$O_{2i-1,2j} = -\frac{1}{2i}(U_{ij} - U_{ij}^*), \tag{1.20b}$$

$$O_{2i,2j-1} = \frac{1}{2i}(U_{ij} - U_{ij}^*), \tag{1.20c}$$

$$O_{2i,2j} = \frac{1}{2}(U_{ij} + U_{ij}^*). \tag{1.20d}$$

The unitarity of U imprints an additional symplectic structure on O. This structure makes sure that amplitude and phase quadratures that belonged to the same mode transform "together" when we apply the mode basis change. Formally this symplectic structure is fixed by a matrix

$$\Omega = \bigoplus_{j=1}^{m} \omega, \text{ with } \omega = \begin{pmatrix} 0 & -1 \\ 1 & 0 \end{pmatrix}, \tag{1.21}$$

for which we find that $O^T \Omega O = \Omega$. This symplectic structure lies at the basis on the optical phase space which is commonly used to describe states and observables in quantum optics through quasi-probability distributions. We will come back to this point in Section 1.2.2.

1.1.3 *States and observables*

The expression (1.13) and (1.16) for the quantised electric field only tell part of the story. In typical quantum experiments, we measure specific observables that are somehow related to the field, and upon measurements we accumulate a distribution of measurement outcomes, rather than fixed values. To describe all of this, we provide a more formal introduction of observables and states in such a bosonic quantum system.

From an algebraic point of view, the quadrature operators (or equivalently the creation and annihilation operators) are the generators of the algebra of observables $\mathcal{A}$ in our system. This means that any observable can be approximated by a polynomial of such operators. A more convenient representation (Neumann, 1931; Weyl, 1927) relies on a family of operators operators of the form

$$\hat{\chi}(\vec{\alpha}) = \frac{1}{(2\pi)^m} \exp(i\vec{\alpha}^\top \vec{\hat{x}}), \tag{1.22}$$

where $\vec{\hat{x}}$ is given by (1.18) and $\vec{\alpha}$ can be any vector in $\mathbb{R}^{2m}$. The bounded operators $\hat{\chi}(\vec{\alpha})$ can now be used as a basis (Hall, 2013) in which we can expand any other operator $\hat{A} \in \mathcal{A}$ as given by

$$\hat{A} = \int_{\mathbb{R}^{2m}} \mathrm{Tr}[\hat{A}\hat{\chi}(-\vec{\alpha})]\, \hat{\chi}(\vec{\alpha})\, d\vec{\alpha}, \tag{1.23}$$

where $\mathrm{Tr}[\hat{A}\hat{\chi}(-\vec{\alpha})]$ is the Hilbert-Schmidt inner product.

To connect these observables to actual measurement statistics we require an additional element: the quantum state. In the algebraic formulation (Petz, 1990) one treats the quantum state as a linear functional $\langle . \rangle : \mathcal{A} \to \mathbb{C}$ that maps any observable $\hat{A}$ to its expectation value $\langle \hat{A} \rangle$. The linearity of this functional can be combined with (1.23) to show that

$$\langle \hat{A} \rangle = \int_{\mathbb{R}^{2m}} \mathrm{Tr}[\hat{A}\hat{\chi}(-\vec{\alpha})]\, \langle \hat{\chi}(\vec{\alpha}) \rangle\, d\vec{\alpha}. \tag{1.24}$$

This highlights that a full knowledge of the function $\langle \hat{\chi}(\vec{\alpha}) \rangle$ for all $\vec{\alpha} \in \mathbb{R}^{2m}$ suffices to fully characterise the quantum state. One may thus simply use these functions to define states as we will do in Section 1.2.2.

In a more typical formulation of quantum mechanics one treats the algebra of observables directly as the bounded operators on a Hilbert space. The linear functionals on the space of bounded operators on Hilbert space can be shown to be isomorphic

to the space of trace-class operators on the same Hilbert space. More colloquially, this means that any state can be associated with a density matrix $\hat{\rho}$ such that

$$\langle \hat{A} \rangle = \mathrm{Tr}[\hat{\rho}\hat{A}] \quad \text{for all } \hat{A} \in \mathcal{A}. \tag{1.25}$$

This also implies that we find that (1.24) takes the form

$$\langle \hat{A} \rangle = \int_{\mathbb{R}^{2m}} \mathrm{Tr}[\hat{A}\hat{\chi}(-\vec{\alpha})]\,\mathrm{Tr}[\hat{\rho}\hat{\chi}(\vec{\alpha})]\,d\vec{\alpha}. \tag{1.26}$$

The description of states in terms of density matrices is not always convenient when dealing with infinite-dimensional systems. Yet, density matrices are ubiquitous when dealing with a finite number of photons (Flamini, Spagnolo, et al., 2018). Furthermore, they are experimentally relevant in the context of quantum state tomography (Lvovsky and Raymer, 2009). Even though this is not the main focus of this Habilitation thesis, we will briefly discuss this point of view in Section 1.2.1.

1.1.4 *Measurements*

Before we move on to study specific approaches for studying quantum states of light, there is one final key element that requires an introduction: measurements. In principle, the algebra of observables and the states that go with it are sufficient tools to mathematically describe the quantum system. In practice, any physical experiment requires measurements and generates measurement outcomes. The days in which only expectation values of observables were available are long behind us, and thus we must introduce a framework to describe how a quantum measurement device samples outcomes. This section is very loosely based on (Holevo, 2001).

The most common introduction of quantum measurements is based on the spectral theorem. When we consider an observable $\hat{A}$, we can write

$$\hat{A} = \int_{\sigma(\hat{A})} a\hat{P}_a\,da, \tag{1.27}$$

where $\sigma(\hat{A})$ denotes the spectrum of $\hat{A}$, $a \in \sigma(\hat{A})$ are the possible measurement outcomes and the elements of the spectrum, and $\hat{P}_a da$ denotes a projection-valued measure on the spectrum. Informally, a are the eigenvalues of $\hat{A}$ and $\hat{P}_a$ are the projectors on the associated eigenvectors (or eigenspaces). This also implies that $\hat{P}_a\hat{P}_{a'} = \delta(a-a')\hat{P}_a$. When we act on the observables with a state, we find that

$$\langle \hat{A} \rangle = \int_{\sigma(\hat{A})} a\langle \hat{P}_a \rangle\,da, \tag{1.28}$$

and because $\hat{P}_a da$ is a projection-valued measure, $\langle \hat{P}_a \rangle$ is a probability density. In many quantum applications, for example sampling problems, we are above all interested in

the properties of these probability densities. Thus, it is common to study the objects $\langle \hat{P}_a \rangle$ directly. Interestingly, these objects also must satisfy additional constraints:

$$\int_{\sigma(\hat{A})} \langle \hat{P}_a \rangle \, da = 1 \quad \text{(normalisation)}, \tag{1.29a}$$

$$\langle \hat{P}_a \rangle \geq 0 \, \forall a \in \sigma(\hat{A}) \quad \text{(positivity)}. \tag{1.29b}$$

The tools of Section 1.1.3 can be used to further characterise these objects.

Realistic experimental measurement devices are usually not accurately described by a projection-value measure formalism due to noise and imperfections. We therefore tend to consider the more general framework of positive operator-valued measures (POVMs). This means that we simply drop the demand that the $\hat{P}_a$ operators are projectors. We simply impose that they are operators which satisfy (1.29a) and (1.29b) for all states. Note that we can still take all measurement outcomes a and associated POVM elements $\hat{P}_a$ and use (1.27) to define a type of generalised observable (Holevo, 2001).

1.2 DISCRETE AND CONTINUOUS VARIABLES

The field of quantum optics is highly diverse and contains many different points of view to study the same fundamental object, light. Here we do not consider any type of light-matter interaction, but just focus purely on the description of light itself. Here, we typically make a distinction between discrete variables quantum optics, which focuses on the energy content of light, and continuous variable quantum optics, which is based on the field quadratures.

In Section 1.1.2, we saw that both the quadrature operators and the creation and annihilation operators generate the same algebra of observables and ultimately contain the same physical information. Yet, both are the corner stones of rather different theoretical and experimental routes to studying light. In Section 1.2.1 we introduce the Fock basis to study the behaviour of photons in a multimode system. These photons are experimentally measured with various types of photon counters. In Section 1.2.2 we will contrast this with the continuous-variable approach, where quantum states are described using the optical phase space. The measurements in this kind of experiments aim to extract field quadratures and are typically performed using homodyne or heterodyne detection. However, in Section 3 we will see that many state-of-the art quantum optics setups are actually mix elements from both approaches to create resourceful quantum states.

1.2.1 *Discrete variables and Fock space*

As mentioned before, the discrete-variable approach to quantum optics relies on the energetic properties (and measurements thereof) of the electromagnetic field. This energy is captured by the quantum Hamiltonian presented in (1.12). By using the

definition of the annihilation operator as given in (1.14), together with the commutation relation (1.15a), we can rewrite the Hamiltonian as

$$\hat{H} = 2\epsilon_0 \sum_k \mathcal{E}_k^2 \left(\hat{a}_k^\dagger \hat{a}_k + \frac{1}{2} \right), \tag{1.30}$$

where the factor $1/2$ denotes the vacuum energy contribution. The expected amount of energy in any given state is given by $\langle \hat{H} \rangle$ and is thus in practice determined by the expectation values $\langle \hat{a}_1^\dagger \hat{a}_1 \rangle, \ldots, \langle \hat{a}_m^\dagger \hat{a}_m \rangle$. The quantum state for which $\langle \hat{a}_1^\dagger \hat{a}_1 \rangle = \cdots = \langle \hat{a}_m^\dagger \hat{a}_m \rangle = 0$ is known as the vacuum state with density matrix $\hat{\rho} = |0\rangle\langle 0|$, where $|0\rangle$ is a vector that satisfies $\hat{a}_k |0\rangle = 0$ for all k.

As laid out in Section 1.1.4, to measure the energy we musk know the eigenvalues and eigenvectors of the Hamiltonian $\hat{H}$. To obtain these, we note that the Hamiltonian is a sum of commuting terms ($\hat{a}_k^\dagger \hat{a}_k$ and $\hat{a}_l^\dagger \hat{a}_l$ commute whenever $k \neq l$) which means that we can find a common eigenbasis. This basis is given by vectors of the type

$$|n_1, \ldots, n_m\rangle = \frac{\left(\hat{a}_1^\dagger\right)^{n_1} \ldots \left(\hat{a}_m^\dagger\right)^{n_m}}{\sqrt{n_1! \ldots n_m!}} |0\rangle, \tag{1.31}$$

these states are known as the Fock states. The integers n_k indicate the exact number of photons in the kth mode. The associated energy for the state $|n_1, \ldots, n_m\rangle$ is given by $\epsilon_0 \sum_k \mathcal{E}_k^2 (2n_k + 1)$. We also clearly see that the creation operator $\hat{a}_k^\dagger$ creates exactly one photon in the mode k.

The states of the type (1.31) form a basis of the Hilbert space, *i.e.* Fock space, that describes the full multimode optical system. The discrete-variable approach to quantum optics concentrates on studying states of the type $|n_1, \ldots, n_m\rangle$ and their superpositions. In addition, it is common to truncate the Hilbert space at some finite photon number N per mode, such that one effectively deals with a finite-dimensional system. This approach underlies many numerical package that simulate photonic systems, see for example (Killoran et al., 2019). In practice, this means that we often represent the state by a density matrix in the Fock basis:

$$\hat{\rho} = \sum_{\substack{n_1, \ldots, n_m \\ n_1', \ldots, n_m'}}^{N} \rho_{n_1, \ldots, n_m; n_1', \ldots, n_m'} |n_1, \ldots, n_m\rangle\langle n_1', \ldots, n_m'|. \tag{1.32}$$

To obtain such a density matrix experimentally, one can techniques based on maximum-likelihood tomography (Lvovsky, Hansen, et al., 2001; Lvovsky and Raymer, 2009; Tiunov et al., 2020) or convex optimisation (Strandberg, 2022). Ironically, these techniques often involve homodyne measurements, which measure field quadratures rather than photon numbers.

Fock states are among the few states upon which we can actually perform some form of projective measurements. Perhaps the most advanced of such device are transition-edge sensors, which are based on superconductors that are cooled just below

their critical temperature. Absorption of photons then creates enormous changes in the resistance of these materials, making it possible to directly detect up to roughly 10 photons (Fukuda et al., 2011; Gerrits et al., 2012). These devices can be pushed to more extreme regimes where they can count up to 100 photons by using more sophisticated data analysis (Eaton, Hossameldin, et al., 2022).

Many experiments rely upon different detector technologies, such as avalanche photo-diodes (APD). These have the advantage of not requiring advanced cryogenics, while being reasonably fast and cheap (at least compared to more advanced systems). However, the major downside of these devices is their lack of photon number resolution. Rather than projecting on photon-number states of the type (1.31), they implement a POVM that only contains two elements: $\{|0\rangle\langle 0|, \mathbb{1} - |0\rangle\langle 0|\}$. If we can send a single optical mode to such a detectors, while knowing that there is at most one photon present, this is still a very useful device. Even beyond this regime, a clever use of APDs can unveil many quantum properties of the light (Lachman et al., 2019; Straka, Lachman, et al., 2018; Straka, Predojević, et al., 2014). However, for more advanced multi-photon operations, we usually require different techniques.

A range of other advanced detector exist, notably those based on superconducting nano-wires provide a more efficient alternative to APDs, yet also with limited photon number resolution. Furthermore, there are more exotic types of materials that are being investigated, such as the mesoscopic detectors in (Vojetta et al., 2012). In our group we have started exploring the use of such detectors in quantum optics (Davis et al., 2021), and we intend to pursue this research in the future in collaboration with CEA Leti.

1.2.2 *Continuous variables and phase space*

In this Habilitation thesis, we focus on the continuous-variable approach rather than the discrete-variable point of view of Section 1.2.1. In the continuous-variable framework, we describe the system based on the field quadratures, which can be measured using homodyne or heterodyne detection. This means that we are effectively probing the electric field $\hat{\boldsymbol{E}}^{(+)}(\boldsymbol{r}, t)$ itself, as given by (1.13), rather than the energy content that is given by the Hamiltonian.

In Section 1.2.1 we introduced the photon number operators for the different modes as the mathematical building blocks of the discrete-variable approach. Here, this role will be taken over by the quadrature operators $\hat{q}_k$ and $\hat{p}_k$, which we more conveniently represent by the vector $\vec{\hat{x}}$ that was introduced in (1.18). The canonical commutation relations (1.11a - 1.11c) directly show that the quadrature operators cannot be trace-class (Weyl, 1927), and with a bit more effort one can also use relation (1.11a) to show that the operators cannot be bounded. As a consequence, they must have a continuous spectrum, such that, when we measure $\hat{q}_k$, we can find a continuum of possible measurement outcomes $q_k \in \mathbb{R}$ (and analogous for $\hat{p}_k$). The possible measurement outcomes for all the quadratures in $\vec{\hat{x}}$ can be represented by a vector $\vec{x} \in \mathbb{R}^{2m}$. The space of all possible

outcomes is known as the *optical phase space*. The transformation rule (1.19) for the quadrature operators imposes a similar symplectic structure on the optical phase space, with the symplectic form given by Ω.

We can use these finding to define a quadrature operator for every point in phase space $\mathbb{R}^{2m}$. The quadrature operator associated with phase space coordinate $\vec{f}$ is given by $\vec{f}^\top \vec{\hat{x}} = \vec{\hat{x}}^\top \vec{f}$. To find the complementary quadrature, it suffices to use the symplectic structure to find that is is given by $\vec{\hat{x}}^\top \Omega \vec{f} = -\vec{f}^\top \Omega \vec{\hat{x}}$. Note that in (Walschaers, 2021) we introduced quadratures in a basis independent notation

$$\hat{q}(\vec{f}) = \vec{f}^\top \vec{\hat{x}}, \tag{1.33}$$

but here we will stick to the vector notation which is more common in the literature.

We can take the role of optical phase space one step further and describe observables and states directly as functions on this space. A first step in this direction was presented in (1.23), where we clearly show that all information of the observable $\hat{A}$ is contained in the phase-space function

$$\chi_{\hat{A}}(\vec{\alpha}) = \mathrm{Tr}[\hat{A}\hat{\chi}(\alpha)]. \tag{1.34}$$

These functions are commonly known as quantum characteristic functions of the observables. Using the features of the Hilbert-Schmidt inner product, we find that they have the property that

$$\chi_{\hat{A}^\dagger}(\vec{\alpha}) = \chi^*_{\hat{A}}(-\vec{\alpha}), \tag{1.35}$$

and thus when $\hat{A} = \hat{A}^\dagger$, we find that $\chi_{\hat{A}}(-\vec{\alpha}) = \chi^*_{\hat{A}}(\vec{\alpha})$. The same functions can be defined for the state, by using the density matrix $\hat{\rho}$ to define $\chi_{\hat{\rho}}(\vec{\alpha})$. The equation (1.26) is rewritten as

$$\langle \hat{A} \rangle = \int_{\mathbb{R}^{2m}} \chi_{\hat{A}}(-\vec{\alpha}) \chi_{\hat{\rho}}(\vec{\alpha})\, d\vec{\alpha}. \tag{1.36}$$

Because quantum states must be normalized, we find that $\chi_{\hat{\rho}}(0) = 1$, but the positivity of the state is less straightforward to guarantee and relies on a quantum version of Bochner's theorem (Dangniam and Ferrie, 2015). The condition is obtained by demanding that, for any series of phase space vectors $\{\vec{f}_1, \ldots, \vec{f}_n\}$, the operator $\hat{X}^\dagger \hat{X}$, with $\hat{X} = \sum_{k=1}^n c_k \hat{\chi}(\vec{f}_k)$, is positive semi-definite. In other words, any characteristic function of a state must satisfy

$$\frac{1}{(2\pi)^m} \sum_{k,l} c_k c_l^* \chi_{\hat{\rho}}(\vec{f}_k - \vec{f}_l) e^{i\vec{f}_k \Omega \vec{f}_l} = \langle \hat{X}^\dagger \hat{X} \rangle \geq 0, \tag{1.37}$$

where we used the identity $\hat{\chi}^\dagger(\vec{f}_l)\hat{\chi}(\vec{f}_k) = \chi_{\hat{\rho}}(\vec{f}_k - \vec{f}_l) e^{i f_k \Omega \vec{f}_l}/(2\pi)^m$. The condition (1.37) is usually very hard to verify.

Beyond calculating expectation values one often needs to do algebra with observables. This too can be done entirely on phase space. It is very straightforward to use (1.34) to show that

$$\chi_{\hat{A}+\hat{B}}(\vec{\alpha}) = \chi_{\hat{A}}(\vec{\alpha}) + \chi_{\hat{B}}(\vec{\alpha}). \tag{1.38}$$

However, it can be seen from the properties of the trace that in general $\chi_{\hat{A}\hat{B}}(\vec{\alpha}) \neq \chi_{\hat{A}}(\vec{\alpha})\chi_{\hat{B}}(\vec{\alpha})$. To find the correct expression, we go back to (1.23). Let us start by writing that

$$\hat{A}\hat{B} = \int_{\mathbb{R}^{2m}} \chi_{\hat{A}\hat{B}}(-\vec{\beta})\, \hat{\chi}(\vec{\beta})\, d\vec{\beta} \tag{1.39a}$$

$$= \int_{\mathbb{R}^{2m}} \chi_{\hat{A}}(-\vec{\alpha})\chi_{\hat{B}}(-\vec{\alpha}')\, \hat{\chi}(\vec{\alpha})\hat{\chi}(\vec{\alpha}')\, d\vec{\alpha}d\vec{\alpha}' \tag{1.39b}$$

$$= \frac{1}{(2\pi)^m} \int_{\mathbb{R}^{2m}} \chi_{\hat{A}}(-\vec{\alpha})\chi_{\hat{B}}(-\vec{\alpha}')\, \hat{\chi}(\vec{\alpha}+\vec{\alpha}')e^{i\vec{\alpha}\Omega\vec{\alpha}'}\, d\vec{\alpha}d\vec{\alpha}' \tag{1.39c}$$

$$= \frac{1}{(2\pi)^m} \int_{\mathbb{R}^{2m}} \chi_{\hat{A}}(-\vec{\alpha})\chi_{\hat{B}}(\vec{\alpha}-\vec{\beta})\, \hat{\chi}(\beta)e^{i\vec{\alpha}^\top\Omega\vec{\beta}}\, d\vec{\alpha}d\vec{\beta}, \tag{1.39d}$$

which leads us to the identity

$$\chi_{\hat{A}\hat{B}}(\vec{\beta}) = \frac{1}{(2\pi)^m} \int_{\mathbb{R}^{2m}} \chi_{\hat{A}}(\vec{\alpha})\chi_{\hat{B}}(\vec{\beta}-\vec{\alpha})e^{i\vec{\beta}^\top\Omega\vec{\alpha}}\, d\vec{\alpha} \tag{1.40a}$$

$$= \chi_{\hat{A}} \circledast \chi_{\hat{B}}(\vec{\beta}). \tag{1.40b}$$

In the last line, we introduce the notation of the mathematical operation known as the *twisted convolution* (Soloviev, 2012). We have thus shown that the multiplication of operators on Hilbert space is transformed into a twisted convolution of their characteristic functions in the phase space framework.

We have introduced a phase space framework for describing observables, algebra, and expectation values, but one key ingredient is still missing: measurements. Since we are primarily interested in measurements of the quadrature operators when dealing with continuous variables, Section 1.1.4 tells us that we should find the eigenvalues and eigenvectors of operators of the type $\hat{q}_k$ and $\hat{p}_k$.[2] Each of these operators has eigenvectors given by $\hat{q}_k|q_k\rangle = q_k|q_k\rangle$ and $\hat{p}_k|p_k\rangle = p_k|p_k\rangle$. The vectors have some interesting properties:

$$\langle q_k|q_l'\rangle = \delta_{k,l}\delta(q_k - q_l') \tag{1.41a}$$

$$\langle p_k|p_l'\rangle = \delta_{k,l}\delta(p_k - p_l') \tag{1.41b}$$

$$\langle q_k|p_l\rangle = \delta_{k,l}e^{iq_kp_l} \tag{1.41c}$$

We note that the operator $\hat{q}_k$ ($\hat{p}_k$) acts only on the kth mode, which means that the notation actually is a shorthand for $\mathbb{1}\otimes\cdots\otimes\mathbb{1}\otimes\hat{q}_k\otimes\mathbb{1}\otimes\cdots\otimes\mathbb{1}$ (where every $\mathbb{1}$ acts on a single mode). This means that when we perform a projective measurement of the quadrature $\hat{q}_k$, the element of the projection-valued measure are given by $\mathbb{1}\otimes\cdots\otimes$

2 Because these operators are unbounded, the eigenvectors are not contained in the Hilbert space since they are not normalisable. We will do as physicists tend to do and just work with unnormalised states and the delta-functions that come with them.

$\mathbb{1} \otimes |q_k\rangle\langle q_k| \otimes \mathbb{1} \otimes \cdots \otimes \mathbb{1}$. This also means that we can jointly measure all the different amplitude (or phase) quadratures, which leads to projectors of the form $|q_1\rangle\langle q_1| \otimes \cdots \otimes |q_m\rangle\langle q_m|$. At the end of this section, we will discuss homodyne detection and show that this protocol is inherently mode-selective. This means that the projectors of the type $\mathbb{1} \otimes \cdots \otimes \mathbb{1} \otimes |q_k\rangle\langle q_k| \otimes \mathbb{1} \otimes \cdots \otimes \mathbb{1}$ are ubiquitous in experiments. Henceforth, whenever we write $|q_k\rangle\langle q_k|$ it is implicit that this is a single-mode operator embedded in a multimode space.

The probability density for obtaining a certain measurement outcome q_k upon the quadrature measurement of a system prepared in a state $\hat{\rho}$ is given by

$$P(q_k) = \mathrm{Tr}[\hat{\rho}|q_k\rangle\langle q_k|] = \int_{\mathbb{R}^{2m}} \chi^*_{|q_k\rangle\langle q_k|}(\vec{\alpha})\chi_{\hat{\rho}}(\vec{\alpha})\, d\vec{\alpha} \tag{1.42}$$

A quick calculation shows that

$$\chi_{|q_k\rangle\langle q_k|}(\vec{\alpha}) = \frac{1}{\sqrt{2\pi}} e^{iq_k\alpha_{2k-1}}, \tag{1.43}$$

where α_{2k-1} is the component in $\vec{\alpha}$ associated with the amplitude quadrature of the kth mode. Such that we find

$$P(q_k) = \frac{1}{\sqrt{2\pi}} \int_{\mathbb{R}^{2m}} \chi_{\hat{\rho}}(\vec{\alpha}) e^{-iq_k\alpha_{2k-1}}\, d\vec{\alpha}, \tag{1.44}$$

where we use that $d\vec{\alpha} = d\alpha_1 \ldots d\alpha_{2m}$. Equation (1.44) shows that we integrate out all coordinates except for α_{2k-1} and perform a Fourier transform of the remaining coordinate. This highlights that the quantum characteristic functions are narrowly related to the probability distributions of quadrature measurement outcomes.

It is tempting to go one step further and perform a Fourier transform on all the coordinates if the characteristic function in order to obtain a probability distributions of all the quadrature measurements. However, because amplitude and phase quadratures do not commute (1.11a), we cannot perform joint measurements of both quadratures. This means that the function

$$W_{\hat{\rho}}(\vec{x}) = \frac{1}{(2\pi)^m} \int_{\mathbb{R}^{2m}} \chi_{\hat{\rho}}(\vec{\alpha}) e^{-i\vec{\alpha}^\top \vec{x}}\, d\vec{\alpha}, \tag{1.45}$$

is not a well-defined probability distribution for all quantum states $\hat{\rho}$. The function *Wigner function* $W_{\hat{\rho}}(\vec{x})$ was introduced initially to attempt to represent quantum states on phase space in a similar fashion as in statistical mechanics (Wigner, 1932). Wigner already points out that his function can achieve negative values, which is a feature narrowly associated with non-classical behaviour (Kenfack and Życzkowski, 2004). Only very recently was it formalised that the negativity of the Wigner function is directly related to continuous variable quantum contextuality (Booth et al., 2022).

The previously introduced quantum characteristic functions can be transformed into Wigner functions through Fourier transforms. We notice first of all that by using (1.35) and (1.45), we find the identity

$$W_{\hat{A}^\dagger}(\vec{x}) = W^*_{\hat{A}}(\vec{x}). \tag{1.46}$$

This can in turn be used, together with the Parseval-Placherel theorem, to transform (1.36) into

$$\langle \hat{A} \rangle = (4\pi)^m \int_{\mathbb{R}^{2m}} W_{\hat{A}}(\vec{x}) W_{\hat{\rho}}(\vec{x})\, d\vec{x}. \tag{1.47}$$

Again, if we want to do more algebra with Wigner functions, we require additional identities. The linearity of the Fourier transform immediately leads us to

$$W_{\hat{A}+\hat{B}}(\vec{x}) = W_{\hat{A}}(\vec{x}) + W_{\hat{B}}(\vec{x}). \tag{1.48}$$

Finding the phase space representation of $\hat{A}\hat{B}$ is more intricate. To do so, let us start by Fourier transforming (1.40a). To calculate this, let us start from

$$\frac{1}{(2\pi)^m} \int \chi_{\hat{B}}(\vec{\beta} - \vec{\alpha}) e^{i\vec{\beta}^\top \Omega \vec{\alpha}} e^{-i\vec{\beta}^\top \vec{x}} d\vec{\beta} = W_{\hat{B}}(\vec{x} + \Omega\vec{\alpha}) e^{-i\vec{\alpha}^\top \vec{x}}, \tag{1.49}$$

which allows us to write

$$\begin{aligned} W_{\hat{A}\hat{B}}(\vec{x}) &= \frac{1}{(2\pi)^m} \int_{\mathbb{R}^{2m}} W_{\hat{A}}(\vec{y}) W_{\hat{B}}(\vec{x} + \Omega\vec{\alpha}) e^{-i\vec{\alpha}^\top (\vec{x} - \vec{y})} d\vec{\alpha} d\vec{y} && \text{(1.50a)} \\ &= \frac{1}{(2\pi)^m} \int_{\mathbb{R}^{2m}} W_{\hat{A}}(\vec{y}) W_{\hat{B}}(\vec{z}) e^{i(\vec{x} - \vec{z})^\top \Omega (\vec{x} - \vec{y})} d\vec{y} d\vec{z}, && \text{(1.50b)} \\ &= W_{\hat{A}} \star W_{\hat{B}}(\vec{x}) && \text{(1.50c)} \end{aligned}$$

where the second line is obtained trough a change in variables. In equation (1.50c) we introduce the *Moyal star product*, the central object of deformation quantization (Moyal, 1949). The Moyal product is more commonly presented in its differential form (Curtright et al., 1998; Hirshfeld and Henselder, 2002), but in our current presentation the integral form (Baker, 1958) appears more naturally. We can also use (1.50c) to define the Moyal bracket, as a phase space representation of the commutator:

$$\begin{aligned} \{W_{\hat{A}}, W_{\hat{B}}\}_\star(\vec{x}) &= [W_{\hat{A}} \star W_{\hat{B}}(\vec{x}) - W_{\hat{B}} \star W_{\hat{A}}(\vec{x})] && \text{(1.51a)} \\ &= \frac{2i}{(2\pi)^m} \int_{\mathbb{R}^{2m}} W_{\hat{A}}(\vec{y}) W_{\hat{B}}(\vec{z}) \sin[(\vec{x} - \vec{z})^\top \Omega (\vec{x} - \vec{y})] d\vec{y} d\vec{z}. && \text{(1.51b)} \end{aligned}$$

These brackets are useful in a range of problems, for example when considering dynamics. However, it should be noted tat integrals of the type (1.51b) can be particularly tedious to calculate.

Wigner functions are particularly suitable when it comes to representing quadratures. We find, for example, that

$$W_{\vec{f}^\top \vec{\hat{x}}}(\vec{x}) = \frac{1}{(4\pi)^m} \vec{f}^\top \vec{x} \tag{1.52}$$

After some calculations based on (1.51b), it can be shown that

$$\{W_{\vec{f}^\top \vec{\hat{x}}}, W_{\vec{g}^\top \vec{\hat{x}}}\}_\star(\vec{x}) = -2i\vec{f}^\top \Omega \vec{g}, \tag{1.53}$$

which for a specific choice of $\vec{f}$ and $\vec{g}$ reduces to $\{W_{\hat{q}_k}, W_{\hat{p}_l}\}_\star = 2i\delta_{k,l}$ such that we retrieve the canonical commutation relations. When performing quadrature measurements on the kth mode, we already found that the quantum characteristic function for the projectors on eigenvectors of $\hat{q}_k$ is given by (1.43). Through a Fourier transform, we find that

$$W_{|q_k\rangle\langle q_k|}(\vec{x}) = \frac{1}{(4\pi)^m}\delta(x_{2k-1} - q_k), \tag{1.54}$$

where x_{2k-1} is a component of $\vec{x}$, associated with the amplitude quadrature of the kth mode.

We can also choose a basis independent formulation, by considering some normalised vector in phase space $\vec{f}$ and introduce the Hilbert space elements $|q;\vec{f}\rangle$ with property

$$\vec{f}^\top \vec{\hat{x}}|q;\vec{f}\rangle = q|q;\vec{f}\rangle, \tag{1.55}$$

We now find that for these states

$$W_{|q;\vec{f}\rangle\langle q;\vec{f}|}(\vec{x}) = \frac{1}{(4\pi)^m}\delta(\vec{x}^\top \vec{f} - q), \tag{1.56}$$

when we measure the associated phase quadrature, we project on states of the type $|p;\Omega\vec{f}\rangle$.[3] As such, we find that

$$\begin{aligned}\text{Prob}(\vec{f}^\top \vec{\hat{x}} = q) &= (4\pi)^m \int_{\mathbb{R}^{2m}} W_{|q;\vec{f}\rangle\langle q;\vec{f}|}(\vec{x}) W_{\hat{\rho}}(\vec{x})\, d\vec{x} &\text{(1.57a)}\\ &= \int_{\mathbb{R}^{2m}} \delta(\vec{x}^\top \vec{f} - q) W_{\hat{\rho}}(\vec{x})\, d\vec{x}. &\text{(1.57b)}\end{aligned}$$

Which effectively shows that the marginals of the Wigner function are the probabilities distributions for quadrature measurements. In practice, these general projector on quadrature eigenvectors are very valuable objects to consider because they describe mode-selective homodyne detection (as we will see in more detail near the end of this section).

Another class of important Wigner functions are those that describe Gaussian states $\hat{\rho}_G$. These are generally of the form

$$W_{\hat{\rho}_G}(\vec{x}) = \frac{\exp\left(-\frac{1}{2}(\vec{x} - \vec{\xi})^\top V^{-1}(\vec{x} - \vec{\xi})\right)}{(2\pi)^m \sqrt{\det V}}, \tag{1.58}$$

3 Calculations with these objects quickly become a little intricate, for example. It is rather tedious to determine $\langle q;\vec{f}|q';\vec{g}\rangle$ for arbitrary phase space axes $\vec{f}$ and $\vec{g}$.

where V is the covariance matrix and ξ is the mean field. A Gaussian state is said to be *squeezed* whenever there is a normalised vector $\vec{f}$ in phase space such that $\vec{f}^\top V \vec{f} < 1$. For a general introduction into some properties of Gaussian states, we refer to Section II.D of (Walschaers, 2021), which is also included here in Section 1.3.

A particular class of interest within the Gaussian states are the *coherent states* $|\vec{\xi}\rangle\langle\vec{\xi}|$ which are fully characterised by their mean field. They are given by

$$W_{|\vec{\xi}\rangle\langle\vec{\xi}|}(\vec{x}) = \frac{\exp\left(-\frac{1}{2}\|\vec{x}-\vec{\xi}\|^2\right)}{(2\pi)^m\sqrt{\det V}}, \tag{1.59}$$

The vacuum state $\hat{\rho} = |0\rangle\langle 0|$, that was introduced in Section 1.2.1, is a special case of of the coherent states, as is it obtained for $\vec{\xi} = 0$. We can now introduce the *displacement operator*

$$\hat{D}(\vec{\xi}) = \exp\left(\frac{i}{2}\vec{\xi}^\top \Omega \vec{x}\right), \tag{1.60}$$

where we note that $\hat{D}(\vec{\xi}) = (2\pi)^m \hat{\chi}(-\Omega\vec{\xi}/2)$. The displacement operators are in a sense the generators of the coherent states:

$$\hat{D}(\vec{\xi})|0\rangle = |\vec{\xi}\rangle. \tag{1.61}$$

The coherent states have been very important for the history of quantum optics (Glauber, 1963; Sudarshan, 1963). In particular, it can be shown that the states $|\vec{\xi}\rangle$ form an overcomplete basis and that

$$\mathbb{1} = \frac{1}{(4\pi)^m}\int_{\mathbb{R}^{2m}} |\vec{\xi}\rangle\langle\vec{\xi}| d\vec{\xi}, \tag{1.62}$$

Furthermore, these states have the property of being eigenvectors of the annihilation operators $\hat{a}_{\vec{f}}$, which we define as

$$\hat{a}_{\vec{f}} = \frac{1}{2}(\vec{f}^\top \vec{x} - i\vec{f}^\top \Omega \vec{x}). \tag{1.63}$$

After a quick calculation, we can show that the following eigenvalue relation holds.

$$\hat{a}_{\vec{f}}|\vec{\xi}\rangle = \frac{1}{2}(\vec{f}^\top \vec{\xi} - i\vec{f}^\top \Omega \vec{\xi})|\vec{\xi}\rangle. \tag{1.64}$$

Invoking the spectral theorem, we find that

$$\hat{a}_{\vec{f}} = \frac{1}{(4\pi)^m}\int_{\mathbb{R}^{2m}} \frac{1}{2}\vec{f}^\top(\mathbb{1} - i\Omega)\vec{\xi}\,|\vec{\xi}\rangle\langle\vec{\xi}|\,d\vec{\xi}, \tag{1.65a}$$

$$\hat{a}^\dagger_{\vec{f}} = \frac{1}{(4\pi)^m}\int_{\mathbb{R}^{2m}} \frac{1}{2}\vec{f}^\top(\mathbb{1} + i\Omega)\vec{\xi}\,|\vec{\xi}\rangle\langle\vec{\xi}|\,d\vec{\xi}. \tag{1.65b}$$

These expression hold for any phase space vector $\vec{f}$. Note that the operators $\hat{a}_{\vec{f}}$ and $\hat{a}^\dagger_{\vec{f}}$ are generators of the algebra of observables, which means that any observable $\hat{A}$

can be approximated arbitrarily well by a polynomial built with element of the set $\{\hat{a}_{\vec{f}}, \hat{a}^\dagger_{\vec{f}} | \vec{f} \in \mathbb{R}^{2m}\}$. The spectral theorem then tells us that there is a distribution $P_{\hat{A}}(\vec{\xi})$, such that

$$\hat{A} = \frac{1}{(4\pi)^m} \int_{\mathbb{R}^{2m}} P_{\hat{A}}(\vec{\xi}) \, |\vec{\xi}\rangle\langle\vec{\xi}| \, d\vec{\xi}. \tag{1.66}$$

This distribution $P_{\hat{A}}(\vec{\xi})$ is known as the *Glauber-Sudarshan P-representation*. As always, we can now calculate the expectation value

$$\langle \hat{A} \rangle = \frac{1}{(4\pi)^m} \int_{\mathbb{R}^{2m}} P_{\hat{A}}(\vec{\xi}) \, \langle\vec{\xi}|\hat{\rho}|\vec{\xi}\rangle \, d\vec{\xi} \tag{1.67a}$$

$$= \int_{\mathbb{R}^{2m}} P_{\hat{A}}(\vec{\xi}) Q_{\hat{\rho}}(\vec{\xi}) \, d\vec{\xi}, \tag{1.67b}$$

where we have defined the Husimi Q-function (Husimi, 1940)

$$Q_{\hat{\rho}}(\vec{\xi}) = \frac{1}{(4\pi)^m} \langle\vec{\xi}|\hat{\rho}|\vec{\xi}\rangle. \tag{1.68}$$

The Q- and P-representation are said to be each other's dual, to fully characterise expectation values, one ultimately needs both. Nevertheless, a surprisingly large number of properties of quantum states can be extracted using exclusively there functions (Chabaud, Markham, et al., 2020). Generally, we mainly use the Wigner function throughout this work, but in Section 2.2, based on (Chabaud and Walschaers, 2023), we also heavily rely on the Q-function.

It is worth pointing out that (1.66) also immediately implies that

$$W_{\hat{A}}(\vec{x}) = \frac{1}{(4\pi)^m} \int_{\mathbb{R}^{2m}} P_{\hat{A}}(\vec{\xi}) \, W_{|\vec{\xi}\rangle\langle\vec{\xi}|}(\vec{x}) \, d\vec{\xi} \tag{1.69a}$$

$$= \frac{1}{(4\pi)^m} \int_{\mathbb{R}^{2m}} P_{\hat{A}}(\vec{\xi}) \, W_{|0\rangle\langle 0|}(\vec{x} - \vec{\xi}) \, d\vec{\xi} \tag{1.69b}$$

It is much less known that this result can be significantly generalised when describing quantum states (Fannes and Verbeure, 1975): we can actually consider any state $\hat{\sigma}$ and always find a distribution $F_{\hat{\rho}}(\vec{\xi})$ such that

$$W_{\hat{\rho}}(\vec{x}) = \frac{1}{(4\pi)^m} \int_{\mathbb{R}^{2m}} F_{\hat{\rho}}(\vec{\xi}) \, W_\sigma(\vec{x} - \vec{\xi}) \, d\vec{\xi}, \tag{1.70}$$

This means that, once more, we can write that

$$\langle \hat{A} \rangle = \int_{\mathbb{R}^{2m}} F_{\hat{\rho}}(\vec{\xi}) \, W_\sigma(\vec{x} - \vec{\xi}) \, W_{\hat{A}}(\vec{x}) d\vec{\xi} d\vec{x}, \tag{1.71a}$$

$$= \int_{\mathbb{R}^{2m}} F_{\hat{\rho}}(\vec{\xi}) \, G_{\hat{A}}(\vec{\xi}) d\vec{\xi}, \tag{1.71b}$$

where we defined the function

$$G_{\hat{A}}(\vec{\xi}) = \int_{\mathbb{R}^{2m}} W_{\hat{A}}(\vec{x}) W_{\sigma}(\vec{x} - \vec{\xi})\, d\vec{x} \tag{1.72a}$$

$$= \frac{1}{(4\pi)^m} \mathrm{Tr}[\hat{D}(\xi)\hat{\sigma}\hat{D}(-\xi)\hat{A}]. \tag{1.72b}$$

Even though this poorly known set of phase space representations is quite interesting from a fundamental point of view, it is not immediately clear whether there is any practical use to it.

Measurements of quadrature operators occur through homodyne detection by mixing -potentially multimode- signal, prepared in quantum state $\hat{\rho}$ on a balanced beamsplitter with a reference beam, prepared in a specific coherent state. After the beamsplitter, the two output beams are measured by a photodiode and we measure the difference between the photo currents. In practice, we have four sets of modes to describe the problem. The initial modes are given by annihilation operators $\{\hat{a}_k^{\mathrm{in}}\}$ for the signal and $\{\hat{b}_k^{\mathrm{in}}\}$ for the reference beam. After the beamsplitter they are transformed into the measured modes $\{\hat{a}_k^{\mathrm{out}}\}$ (the first output beam) and $\{\hat{b}_k^{\mathrm{out}}\}$ (the second output beam). Note that all of these beams have the same internal mode structure, given by a mode basis $\{\boldsymbol{u}_k(\boldsymbol{r}, t)\}$. The photodiodes typically do not resolve anything of the internal mode structure and we effectively measure a difference in current

$$\Delta\hat{\mathcal{I}} \propto \sum_k (\hat{a}_k^{\mathrm{out}})^\dagger \hat{a}_k^{\mathrm{out}} - (\hat{b}_k^{\mathrm{out}})^\dagger \hat{b}_k^{\mathrm{out}} = \sum_k (\hat{a}_k^{\mathrm{in}})^\dagger \hat{b}_k^{\mathrm{in}} + (\hat{b}_k^{\mathrm{in}})^\dagger \hat{a}_k^{\mathrm{in}}, \tag{1.73}$$

where in the second step we used the beamsplitter relation. Because we specially prepare the reference beam in a coherent state $|\vec{\xi}\rangle$, we typically consider this as part of the measurement, such that we actually measure

$$\Delta\hat{\mathcal{I}}_{\mathrm{signal}} = \sum_k (\hat{a}_k^{\mathrm{in}})^\dagger \langle\vec{\xi}|\hat{b}_k^{\mathrm{in}}|\vec{\xi}\rangle + \langle\vec{\xi}|(\hat{b}_k^{\mathrm{in}})|\vec{\xi}\rangle^* \hat{a}_k^{\mathrm{in}}, \tag{1.74}$$

Note that $\langle\vec{\xi}|\hat{b}_k^{\mathrm{in}}|\vec{\xi}\rangle = (\xi_{2k-1} + i\xi_{2k})/2$, and furthermore $(\hat{a}_k^{\mathrm{in}})^\dagger = (\hat{q}_k - i\hat{p}_k)/2$ and $(\hat{a}_k^{\mathrm{in}})^\dagger = (\hat{q}_k + i\hat{p}_k)/2$. This means that the reference beam effectively selects out the phase space axis (mode and phase) that are determined by the coherent state:

$$\Delta\hat{\mathcal{I}}_{\mathrm{signal}} = \frac{1}{2}\sum_k \xi_{2k-1}\hat{q}_k + \xi_{2k}\hat{p}_k = \frac{1}{2}\vec{\xi}^\top\vec{\hat{x}}. \tag{1.75}$$

Thus, homodyne detection naturally measures operators of the type $\vec{\xi}^\top\vec{\hat{x}}$. For co-propagating modes, one must prepare the coherent state in the appropriate spatial or spectral mode. For spatial modes this is typically achieved with a spatial light modulator, an optical cavity, or another mode-shaping technique (Boyer et al., 2008; Delaubert et al., 2006; Wagner et al., 2008), while for spectral modes one can use pulse shapers (Ra et al., 2020; Roslund et al., 2014).

Homodyne measurements can be used for maximum likelihood tomography (Lvovsky and Raymer, 2009), which estimates the state's density matrix in the Fock basis. For multimode systems, it is common to use multiplexed homodyne detection setups. For spatially separated modes, it is reasonably straightforward to set up a multiplexed detection scheme (X. Su et al., 2012). For co-propagating modes, more effort is required to perform multimode detection, but it has been done for spectral modes (Cai et al., 2017), and for spatial modes one can use mode-sorters of the type (Labroille et al., 2014). This allows us to measure marginals of the Wigner function.

Heterodyne detection (also known as double homodyne) is an alternative detection scheme which can be shown to project on coherent states, an elegant derivation can be found in the appendix of (Chabaud, Douce, et al., 2017). As such, this measurement device directly samples vectors that are distributed according to the Q-function (1.68). The Wigner function, on the other hand, cannot be measured directly with either one of these detectors. The reason is simply that no POVM has elements with a Wigner function that is a Dirac-delta function in phase space. However, there is a class of physical operators which have such Wigner functions: displaced parity operators (Royer, 1977). We define these operators as

$$\hat{\Pi}(\vec{\xi}) = \hat{D}^\dagger(\vec{\xi})(-\mathbb{1})^{\hat{N}}\hat{D}(\vec{\xi}), \tag{1.76}$$

where the number operator is given by $\hat{N} = \sum_k \hat{a}_k^\dagger \hat{a}_k$. It has been shown that the Wigner function of this operator take the form

$$W_{\hat{\Pi}(\vec{\xi})}(\vec{x}) = \frac{1}{(4\pi)^m}\delta(\vec{x} - \vec{\xi}). \tag{1.77}$$

Thus, the Wigner function of any state $\hat{\rho}$ in a certain point of phase space is the expectation value of a displaced parity operator

$$W_{\hat{\rho}}(\vec{x}) = \langle \hat{\Pi}(\vec{x}) \rangle. \tag{1.78}$$

This identity has been very useful in a variety of setups to reconstruct Wigner functions of continuous-variable systems (Bertet et al., 2002; Leibfried et al., 1996; Lutterbach and Davidovich, 1997; Vlastakis et al., 2013). In optics, obtaining photon-number resolution has been notoriously challenging for a long time, and it is only recently that these techniques have been adopted (Nehra et al., 2019) using the transition edge sensors that were discussed previously in Section 1.2.1.

1.3 **article:** NON-GAUSSIAN QUANTUM STATES AND WHERE TO FIND THEM

In the above sections, we presented a complementary introduction to multimode quantum optics in the general sense, without focusing too much on specific classes of states. In the joined Tutorial (Walschaers, 2021), we present a detailed introduction to

non-Gaussian quantum states, their properties, experimental realisations, and potential applications. The Tutorial also contains an introduction to quantum correlations, with a specific focus on continuous-variable systems.

Tutorial

Non-Gaussian Quantum States and Where to Find Them

Mattia Walschaers*

Laboratoire Kastler Brossel, Sorbonne Université, CNRS, ENS-Université PSL, Collège de France, 4 place Jussieu, Paris F-75252, France

(Received 2 May 2021; published 28 September 2021)

Gaussian states have played an important role in the physics of continuous-variable quantum systems. They are appealing for the experimental ease with which they can be produced, and for their compact and elegant mathematical description. Nevertheless, many proposed quantum technologies require us to go beyond the realm of Gaussian states and introduce non-Gaussian elements. In this Tutorial, we provide a roadmap for the physics of non-Gaussian quantum states. We introduce the phase-space representations as a framework to describe the different properties of quantum states in continuous-variable systems. We then use this framework in various ways to explore the structure of the state space. We explain how non-Gaussian states can be characterized not only through the negative values of their Wigner function, but also via other properties such as quantum non-Gaussianity and the related stellar rank. For multimode systems, we are naturally confronted with the question of how non-Gaussian properties behave with respect to quantum correlations. To answer this question, we first show how non-Gaussian states can be created by performing measurements on a subset of modes in a Gaussian state. Then, we highlight that these measured modes must be correlated via specific quantum correlations to the remainder of the system to create quantum non-Gaussian or Wigner-negative states. On the other hand, non-Gaussian operations are also shown to enhance or even create quantum correlations. Finally, we demonstrate that Wigner negativity is a requirement to violate Bell inequalities and to achieve a quantum computational advantage. At the end of the Tutorial, we also provide an overview of several experimental realizations of non-Gaussian quantum states in quantum optics and beyond.

DOI: 10.1103/PRXQuantum.2.030204

CONTENTS

*mattia.walschaers@lkb.upmc.fr

I. INTRODUCTION

Gaussian states have a long history in quantum physics, which dates back to Schrödinger's introduction of the coherent state as a means to study the harmonic oscillator [1]. In later times, Gaussian states rose to prominence due to their importance in the description of Bose gases [2–4] and in the theory of optical coherence [5,6]. With the advent of quantum-information theory, the elegant mathematical structure of Gaussian states made them important objects in the study of continuous-variable (CV) quantum-information theory [7–9]. In this Tutorial, we focus on bosonic systems, which means that the continuous variables of interest are field quadratures. Gaussian quantum states are then defined as the states for which measurement statistics of these field quadratures is Gaussian.

Gaussian states can be fully described by their mean field and covariance matrix, and, due to Williamson's decomposition [10], the latter can be studied using a range of tools from symplectic vector spaces. As such, one can directly relate quadrature squeezing to Gaussian entanglement via the Bloch-Messiah decomposition [11]. In the full state space of CV systems, Gaussian states are furthermore known to play a specific role: of all possible states with the same covariance matrix, the Gaussian state will always have the weakest entanglement [12] and the highest entropy [13]. From a theoretical point of view, Gaussian quantum states provide, thus, an elegant and highly relevant framework for quantum-information theory. On an experimental level, CV quantum information has long been motivated by advances in quantum optics, due to the capability of on-demand generation of ever larger entangled states using either spatial modes [14–16] or time-frequency modes [17–22]. Furthermore, Gaussian states also play a key role in the recent demonstration of a quantum advantage with Gaussian Boson sampling [23]. These developments have made the CV quantum optics an important platform for quantum computation [24].

Regardless of all the experimental and theoretical successes of Gaussian states, they have a major shortcoming in the context of quantum technologies: all Gaussian measurements of such states can be efficiently simulated [25]. In pioneering work on CV quantum computation, it is already argued that a non-Gaussian operation is necessary to implement a universal quantum computer in CV [26]. Later works that laid the groundwork for CV measurement-based quantum computing have left the question of this non-Gaussian operation somewhat in the open [27–29]. Common schemes, based on the cubic phase gate, turn out to be particularly hard to implement in realistic setups [30]. Furthermore, these protocols require highly non-Gaussian states, such as Gottesman-Kitaev-Preskill (GKP) states [31], to encode information. Even though such states could also serve as a non-Gaussian resource for implementing non-Gaussian gates [32], these states remain notoriously challenging to produce. In spite of the practical problems involved with non-Gaussian states, one is obliged to venture into non-Gaussian territory to reach a quantum computational advantage in the CV regime [33]. This emphasizes the importance of a general understanding of non-Gaussian states and their properties. In this Tutorial, we attempt to provide a roadmap to navigate within this quickly developing field.

In Sec. II, we take an unusual start to introduce CV systems. We first present some elements of many-boson physics, by treating Fock space. This mathematical environment is probably familiar to most readers to describe photons. We then explain how such a Fock space can also be described in phase space, which is the more natural framework from CV quantum optics. We introduce phase-space representations of states and observables in CV systems such as the Wigner function, and to familiarize the reader with the language of multimode systems. By first reviewing the basics of Fock space, we can make interesting connections between what is known as the discrete-variable (DV) approach and the CV approach to quantum optics. We see that there is often a shady region between these two frameworks, where techniques that are typically associated with one framework can be applied in the other. We finally argue that the main distinction lies in whether one measures photons (DV) or field quadratures (CV).

In Sec. III, we provide the reader with an introduction to some of the different structures that can be identified in the space of CV quantum states. When pure states are considered, all non-Gaussian states are known to have a nonpositive Wigner function [34,35], but this no longer holds when mixed states enter the game [36]. In the entirety of the state space, non-Gaussian states occupy such a vast territory that it is impossible to describe all of them within one single formalism. Nevertheless, there has recently been considerable progress in the classification of non-Gaussian states [37,38]. We introduce some key ideas behind quantum non-Gaussianity, the stellar rank, and Wigner negativity as tools to characterize non-Gaussian states.

Section IV introduces two main families of techniques to create non-Gaussian states starting from Gaussian inputs. The first approach concentrates on deterministic

methods, which rely on the implementation of non-Gaussian unitary transformations. We show how such transformations can be built by using a specific non-Gaussian gate. We then introduce the second class of techniques, which are probabilisitic and rely on performing non-Gaussian measurements on a Gaussian state and conditioning on a certain measurement result. We introduce our recently developed approach to describe these systems [39] and present mode-selective photon subtraction as a case study.

Then all the pieces are set to discuss the interplay between non-Gaussian effects and quantum correlations in Sec. V. First, we consider the resources that are required to conditionally prepare certain non-Gaussian states. The conditional scheme relies on performing a non-Gaussian measurement on one part of a bipartite Gaussian state, and will show that the nature of the quantum correlations in this bipartite state is essential. We show that we can only generate quantum non-Gaussian states if the initial bipartite state is entangled. Furthermore, to conditionally generate Wigner negativity we even require quantum steering. In the second part of Sec. V, we show how non-Gaussian operations can in return enhance or create quantum correlations. Finally, we show that Wigner negativity (in either the state or the measurement) is necessary to violate Bell inequalities in CV systems.

In a similar fashion, we spend most of Sec. VI explaining the result of Ref. [33], which shows that Wigner negativity is also necessary to reach a quantum advantage. To show this, we explicitly construct a protocol to efficiently simulate the measurement outcomes of a setup with states, operations, and detectors that are described by positive Wigner functions. In the remainder of the section, we provide comments on the quantum computational advantage reached with Gaussian Boson sampling.

Finally, in Sec. VII, we provide a quick overview of non-Gaussian states in CV experiments. Due to the author's background, the first half of this overview focuses on quantum optics. In the second part, we also discuss some key developments in other branches of experimental quantum physics. Readers should be warned that this is by no means an extensive review of all the relevant experimental progress. A more general conclusion and outlook on what the future may have in store is presented in Sec. VIII.

II. CONTINUOUS-VARIABLE QUANTUM STATES

Before we can start our endeavor to classify non-Gaussian states of CV systems and study their properties, we must develop some basic formalism for dealing with multimode bosonic systems. At the root of bosonic systems lies the canonical commutation relation, $[\hat{x},\hat{p}] \sim i\mathbb{1}$, which can be traced back to the early foundations of quantum mechanics. The study of the algebra of such noncommuting observables has given birth to rich branches of mathematics and mathematical physics that ponder on the subtleties of these observables and their associated states. In this Tutorial, we keep a safe distance from the representation theory of the associated C^* algebras that describe bosonic field theories in their most general sense. We do refer interested readers to a rich but technical literature [4,40–42].

In this Tutorial, we do exclusively work within the Fock representation, which implies that we consider systems with a finite expectation value for the number of particles. In quantum optics, this assumption translates to the logical requirement that energies remain finite. There are many approaches to mathematically construct such systems (luckily for us they are all equivalent [43–46]). Here, we briefly present two such approaches that nicely capture one of the key dualities on quantum physics. First we take the particle approach by introducing the Fock space that describes identical bosonic particles in Sec. A. Subsequently, in Sec. B, we take the approach that starts out from a wave picture, by concentrating on the phase-space representation of the electromagnetic field. Here we also introduce the phase-space representations of CV quantum states that proves to be crucial tools in the remainder of this Tutorial. We show how these approaches are quite naturally two sides of the same coin. In Sec. C, we briefly discuss the concept of modes and the role they play in CV quantum systems. This subsection is both intended to provide some clarification about common jargon and to eliminate common misconceptions. We finish this section by presenting a brief case study of Gaussian states in Sec. D, reviewing some key results. After all, it is difficult to appreciate the subtleties of non-Gaussian states without having a flavor from their Gaussian counterparts.

A. Fock space

In typical quantum mechanics textbooks, the story of identical particles usually starts by considering a set of n particles, which are each described by a quantum state vector in a single-particle Hilbert space $\mathcal{H}$, thus for the ith particle we ascribe a state vector $|\psi_i\rangle \in \mathcal{H}$. The joint state of these n particles is then given by the tensor product of the state vectors $|\psi_1\rangle, \ldots, |\psi_n\rangle$. However, if the particles are identical in all their internal degrees of freedom, we should be free to permute them without changing the observed physics. Formally, such permutation is implemented by a unitary operator U_σ, for the permutation $\sigma \in S_n$, which acts as

$$U_\sigma |\psi_1\rangle \otimes \cdots \otimes |\psi_n\rangle = \left|\psi_{\sigma(1)}\right\rangle \otimes \cdots \otimes \left|\psi_{\sigma(n)}\right\rangle. \quad (1)$$

Invariance of physical observables under such permutations can be achieved by either imposing the n-particle state vector to be fully symmetric (bosons) or fully antisymmetric (fermions) under these permutations of particles. In this Tutorial, we focus exclusively on bosons, and

thus the condition that must be imposed to obtain a bosonic n-particle state is

$$U_\sigma \left|\Psi^{(n)}\right\rangle = \left|\Psi^{(n)}\right\rangle. \tag{2}$$

Because these are the only states that are permitted to describe the bosonic system, we commonly use the Hilbert space $\mathcal{H}_s^{(n)}$, which is a subspace of $\mathcal{H}^{\otimes n}$ that contains only those states that fulfil Eq. (2). It is usually convenient to generate these spaces with a set of elementary tensors, known as Fock states, which we define as

$$|\psi_1\rangle \vee \cdots \vee |\psi_n\rangle := \sum_{\sigma \in S_n} \left|\psi_{\sigma(1)}\right\rangle \otimes \ldots \left|\psi_{\sigma(n)}\right\rangle, \tag{3}$$

such that

$$\mathcal{H}_s^{(n)} = \overline{\text{span}\left\{ |\psi_1\rangle \vee \cdots \vee |\psi_n\rangle \mid |\psi_i\rangle \in \mathcal{H}\right\}}, \tag{4}$$

where we refer to the Appendix for some further details on the span. This fully describes a system of n bosonic particles in what is often referred to as first quantization. It is interesting to note that these identical particles appear to be entangled with respect to the tensor product structure of $\mathcal{H}^{\otimes n}$. There is still debate on whether this is a mathematical artefact of our description or rather a genuine physical feature of identical particles. Even though there is still debate about how to exactly define entanglement between indistinguishable particles [47,48], several authors have shown how these symmetrizations can [49–52] induce useful entanglement. Furthermore, it is undeniable that this structure leads to physical interference phenomena that do not exist for distinguishable particles [53].

The name "first quantization" suggests the existence of a second quantization, which turns out to be more appropriate for this Tutorial. Second quantization finds its origins in models where particle numbers are not fixed or conserved. This formalism is largely based on creation and annihilation operators, denoted $\hat{a}^\dagger$ and $\hat{a}$, respectively, that add or remove particles. To accommodate these operators in our mathematical framework, we must equip our Hilbert space to describe a varying number of particles. Therefore, we introduce the Fock space

$$\Gamma(\mathcal{H}) := \mathcal{H}_s^{(0)} \oplus \mathcal{H}_s^{(1)} \oplus \mathcal{H}_s^{(2)} \oplus \ldots, \tag{5}$$

where the single-particle Hilbert space is given by $\mathcal{H}_s^{(1)} = \mathcal{H}$. Furthermore, we retrieve a peculiar component $\mathcal{H}_s^{(0)}$, which describes the fraction of the system that contains no particles at all. On its own, $\mathcal{H}_s^{(0)}$ is thus populated by a single state $|0\rangle$ that we refer to as the vacuum. This implies that technically $\mathcal{H}_s^{(0)} \cong \mathbb{C}$ the zero-particle Hilbert space is just described by a complex number that corresponds to the overlap of the state with the vacuum. A general pure state in Fock space $|\Psi\rangle \in \Gamma(\mathcal{H})$ can then be described using the structure, Eq. (5), as

$$|\Psi\rangle = \Psi^{(0)} \oplus \Psi^{(1)} \oplus \Psi^{(2)} \oplus \ldots, \tag{6}$$

where $\Psi^{(i)} \in \mathcal{H}_s^{(i)}$ are non-normalized vectors (and therefore we omit the $|.\rangle$) in the i-particle Hilbert space. Because $|\Psi\rangle$ is a state, we must impose the normalization condition $\|\Psi\|^2 = \sum_{i=0}^{\infty} \|\Psi^{(i)}\|^2 = 1$

We can now define a creation operator $\hat{a}^\dagger(\varphi)$ for every $\varphi \in \mathcal{H}$ [54], which acts as

$$\begin{aligned}\hat{a}^\dagger(\varphi)\,|\Psi\rangle = 0 \oplus \left(\Psi^{(0)}\,|\varphi\rangle\right) \oplus \left(|\varphi\rangle \vee \Psi^{(1)}\right) \\ \oplus \left(|\varphi\rangle \vee \Psi^{(2)}\right) \oplus \ldots\end{aligned} \tag{7}$$

In the same spirit, it is possible to provide an explicit construction of the annihilation operators $\hat{a}(\varphi)$, but here we content ourselves by just introducing the annihilation operator as the hermitian conjugate of the creation operator. Just as the creation operator that literally adds a particle to the system, the annihilation operator literally removes one. One additional property of the annihilation operators is that they destroy the vacuum state:

$$\hat{a}(\varphi)\,|0\rangle = 0. \tag{8}$$

We can now use creation and annihilation operators to build an arbitrary Fock state by creating particles on the vacuum state

$$|\psi_1\rangle \vee \cdots \vee |\psi_n\rangle = \hat{a}^\dagger(\psi_1)\hat{a}^\dagger(\psi_2)\ldots\hat{a}^\dagger(\psi_n)\,|0\rangle \tag{9}$$

and by considering superpositions of such Fock states, we can ultimately generate the entire Fock space. By considering any basis of the single-particle Hilbert space $\mathcal{H}$ and constructing all possible Fock states of all possible lengths that can be formed by generating particles in these basis vectors we construct a basis of the Fock space $\Gamma(\mathcal{H})$. We refer to this basis as the Fock basis.

The beauty of second quantization lies in the natural appearance of states, which have no fixed particle number. The most important example is the coherent state

$$|\alpha\rangle := e^{-\frac{\|\alpha\|^2}{8}} \sum_{j=0}^{\infty} \frac{[\hat{a}^\dagger(\alpha)]^j}{2^j j!}\,|0\rangle\,, \tag{10}$$

where $\alpha \in \mathcal{H}$ is a non-normalized vector in the single particle Hilbert space. One can, indeed, simply generalise (7) to non-normalized vectors in $\mathcal{H}$ which we use explicitly in Eq. (10). Second, we note that an unusual factor 2 is included to make the definition consistent with Eq. (62).

In quantum optics, these coherent states are crucial objects as they describe perfectly coherent light [5]. It is

important to remark that a coherent state is always generated by a single vector in the single-particle Hilbert space. Coherent states often provide a good approximation for the state that is produced by a single-mode laser far above threshold [55]. More generally, the study of laser light is a whole field in its own right and often the light deviates from the fully coherent approximation.

The creation and annihilation operators are not only important objects because they populate the Fock space; they are also of key importance for describing observables in a many-boson system. These operators are the generators of the algebra of observables that represents the canonical commutation relations on Fock space. This implies that any observable can ultimately be approximated by a polynomial of creation and annihilation operators. At the heart of this mathematical formalism lies the canonical commutation relation (CCR):

$$[\hat{a}(\varphi), \hat{a}^\dagger(\psi)] = \langle \varphi \mid \psi \rangle, \tag{11}$$

which describes the algebra of observables. Note that this relation holds for any vectors $|\varphi\rangle$ and $|\psi\rangle$ in the single-particle Hilbert space $\mathcal{H}$. These vectors should not form a basis, nor should they be orthogonal. When $|\varphi\rangle = |\psi\rangle$, we find that $[\hat{a}(\psi), \hat{a}^\dagger(\psi)] = 1$. On the other hand, when the single-particle states $|\varphi\rangle$ and $|\psi\rangle$ are fully orthogonal, we find that $[\hat{a}(\varphi), \hat{a}^\dagger(\psi)] = 0$. In these cases we recover the typical creation and annihilation operators for harmonic oscillators. However, by introducing the creations and annihilation operators through Eq. (7), we can also deal with more general cases. Furthermore, all definitions and the form of the CCR are still valid when φ and ψ are unnormalized vectors in $\mathcal{H}$. A more detailed discussion can be found in Ref. [56].

When we leave the realm of pure states, the description of quantum states becomes tedious. Commonly, one uses a density operator $\hat{\rho}$ with $\mathrm{tr}\,\hat{\rho} = 1$ to formally describe a state. However, we can generally think of these density operators as infinite-dimensional matrices with an infinite number of components in the Fock basis. In other words, this is not necessarily a convenient description. In an operational sense, any state is considered to be characterized when we know all the moments of all the possible observables. Because the creation and annihilation operators generate the algebra, one knows all the moments of all the observables if one knows all the correlation functions $\mathrm{tr}[\hat{\rho}\,\hat{a}^\dagger(\psi_1)\ldots\hat{a}^\dagger(\psi_n)\hat{a}(\varphi_1)\ldots\hat{a}(\varphi_m)]$, for all possible lengths n and m. Even though this might seem like an equally challenging endeavor, much of quantum statistical mechanics boils down to finding expressions of the correlation functions for relevant classes of states.

B. Phase space

In the previous subsection, we started our analysis by extending a system of one quantum particle to a system of many quantum particles. Here we follow a different route, where we start by considering the classical electric field. With some effort, we can apply such an analysis to any bosonic field, but in this Tutorial we focus on quantum optics as our main field of application. For a more extensive introduction from a quantum optics perspective we recommend Refs. [55,57,58], whereas a general introduction to quantum physics in phase space can be found in Ref. [59].

A traveling electromagnetic wave is described by a solution of Maxwell's equations. As is commonly the case in optics, we focus on the complex representation of the electric field, which is generally given by $\mathbf{E}^{(+)}(\mathbf{r}, t)$. It is related to the real-valued electric field $\mathbf{E}(\mathbf{r}, t)$ that is encountered in standard electrodynamics textbooks by $\mathbf{E}(\mathbf{r}, t) = \mathbf{E}^{(+)}(\mathbf{r}, t) + \left[\mathbf{E}^{(+)}(\mathbf{r}, t)\right]^*$. To express the electric field, it is useful to introduce an orthonormal mode basis $\{\mathbf{u}_i(\mathbf{r}, t)\}$. These modes are solutions to Maxwell's equations

$$\nabla \cdot \mathbf{u}_i(\mathbf{r}, t) = 0, \tag{12}$$

$$\left(\Delta - \frac{1}{c^2}\frac{\partial^2}{\partial t^2}\right)\mathbf{u}_i(\mathbf{r}, t) = 0. \tag{13}$$

The orthogonalization property is implemented by the following condition:

$$\frac{1}{V}\int_V \mathrm{d}^3\mathbf{r}\,[\mathbf{u}_i(\mathbf{r}, t)]^*\,\mathbf{u}_j(\mathbf{r}, t) = \delta_{i,j}, \tag{14}$$

where V is some large volume that contains the entire physical system. This assumption serves the practical purpose of allowing us to consider a discrete mode basis and on top it makes physical sense. Note that we do not integrate over t, which implies that at every instant of time t we consider a mode basis that is normalized with respect to the spatial degrees of freedom. It is practical to assume that all relevant physics can be described by a (possibly large) finite number of modes m. These modes now form a basis in which we can expand any solution to Maxwell's equations and thus we may write

$$\mathbf{E}^{(+)}(\mathbf{r}, t) = \sum_{j=1}^{m} \mathcal{E}_j\,\mathbf{u}_j(\mathbf{r}, t), \tag{15}$$

where $\mathcal{E}_i$ are a set of complex numbers, which can be written in terms of the real and imaginary parts

$$\mathcal{E}_j = E_j^{(x)} + iE_j^{(p)}. \tag{16}$$

These real and imaginary parts of the field are known as the amplitude and phase quadrature, respectively. We can interpret these quantities $\vec{E} := (E_1^{(x)}, E_1^{(p)}, \ldots, E_m^{(x)}, E_m^{(p)}) \in \mathbb{R}^{2m}$ as the coordinate in optical phase space that describes the light field.

The space of solutions of Maxwell's equations forms a Hilbert space, which we call the mode space $\mathcal{M}$ and the mode basis chosen to describe this space is far from unique. As with all Hilbert spaces, we can define unitary transformations and use them to change from one basis to another. As such, let us introduce the unitary operator U to change between bases

$$\mathbf{u}_i(\mathbf{r},t) = \sum_{j=1}^{m} U_{ji}\mathbf{v}_j(\mathbf{r},t), \tag{17}$$

$$\mathbf{v}_i(\mathbf{r},t) = \sum_{j=1}^{m} U_{ji}^{\dagger}\mathbf{u}_j(\mathbf{r},t), \tag{18}$$

where we can in principle obtain U as an infinite-dimensional matrix with

$$U_{ji} = \frac{1}{V}\int_V \mathrm{d}^3\mathbf{r}\left[\mathbf{v}_j(\mathbf{r},t)\right]^* \mathbf{u}_i(\mathbf{r},t), \tag{19}$$

which remarkably does not depend on time due to the normalization properties of the mode bases. We can analogously expand the electric field in the new mode basis

$$\mathbf{E}^{(+)}(\mathbf{r},t) = \sum_i \mathcal{E}_i'\mathbf{v}_i(\mathbf{r},t), \tag{20}$$

where $\mathcal{E}_i' = \sum_j U_{ij}\mathcal{E}_j$. This observation is of great importance when we quantize the electric field. The change of mode basis also imposes a change of coordinates in the optical phase space. Like in Eq. (16) the new components can also be divided in real and imaginary parts, which leads to a new coordinate $\vec{E}'$. Because the coordinate vectors in optical phase space are real $2m$-dimensional vectors, we obtain

$$\vec{E}' = O\vec{E}, \tag{21}$$

where O is an orthonormal transformation. However, the orthogonal transformation O on the phase space must correspond to the unitary transformation U on the modes, which imposes the constraint

$$O_{2i-1,2j-1} = \frac{1}{2}(U_{ij} + U_{ij}^*), \tag{22}$$

$$O_{2i-1,2j} = -\frac{1}{2i}(U_{ij} - U_{ij}^*), \tag{23}$$

$$O_{2i,2j-1} = \frac{1}{2i}(U_{ij} - U_{ij}^*), \tag{24}$$

$$O_{2i,2j} = \frac{1}{2}(U_{ij} + U_{ij}^*). \tag{25}$$

This imposes a symplectic structure to the transformation O such that the optical phase space, just like the phase space of analytical mechanics, can be treated as a symplectic space. The conserved symplectic structure associated with this space is given by

$$\Omega = \bigoplus_{j=1}^{m}\omega, \text{ with } \omega = \begin{pmatrix} 0 & -1 \\ 1 & 0 \end{pmatrix}, \tag{26}$$

such that $O^T\Omega O = \Omega$. Note that Ω can be interpreted as a matrix representation of the imaginary i, in the sense that it has the properties $\Omega^T = -\Omega$ and $\Omega^2 = -\mathbb{1}$ [60].

In quantum optics, the electric field of light is treated as a quantum observable $\hat{\mathbf{E}}^{(+)}(\mathbf{r},t)$. In this quantization, the modes, i.e., the normalized solutions to Maxwell's equations, remain classical objects and all the quantum features are absorbed in the coefficients. We can thus write

$$\hat{\mathbf{E}}^{(+)}(\mathbf{r},t) = \sum_i \mathcal{E}_i^{(1)}\frac{\hat{x}_i + i\hat{p}_i}{2}\mathbf{u}_i(\mathbf{r},t), \tag{27}$$

where $\mathcal{E}_i^{(1)}$ is a constant that carries the dimensions of the field, which can be interpreted as the electric field of a single photon. Glossing over many subtleties of the quantization of the electromagnetic field, we remind the reader that any system that is described on phase space can be quantized through canonical quantization. The quadrature operators $\hat{x}_j$ and $\hat{p}_k$ therefore follow the canonical commutation relations $[\hat{x}_j,\hat{p}_k] = 2i\delta_{j,k}$, such that they satisfy the Heisenberg relation $\Delta\hat{x}\Delta\hat{p} \geqslant 1$. As they are introduced above, the quadrature operators are specifically related to the specific mode basis. Indeed, $\hat{x}_j$ and $\hat{p}_j$ are the quadrature operators that describe the field in mode $\mathbf{u}_j(\mathbf{r},t)$. Thus, when we change the basis of modes, we should change the quadrature operators accordingly in line with Eq. (21). To overcome these difficulties, it is often convenient to introduce a basis-independent expression for the quadrature operators, which can be done by mapping any point in the optical phase space $\vec{f} \in \mathbb{R}^{2m}$ to an observable $\hat{q}(\vec{f})$, given by

$$\hat{q}(\vec{f}) := \sum_{j=1}^{m} f_{2j-1}\hat{x}_j + f_{2j}\hat{p}_j. \tag{28}$$

These quadrature operators follow a generalized version of the CCR, given by

$$[\hat{q}(\vec{f}_1),\hat{q}(\vec{f}_2)] = -2i\vec{f}_1{}^T\Omega\vec{f}_2, \text{ for all } \vec{f}_1,\vec{f}_2 \in \mathbb{R}^{2m}. \tag{29}$$

We highlight the particular case where $[\hat{q}(\vec{f}),\hat{q}(\Omega\vec{f})] = 2i\|\vec{f}\|^2$, such that we recover the typical form of the CCR for $\|\vec{f}\| = 1$. This highlights that Ω maps an amplitude quadrature to its associated phase quadrature. From a mathematical point of view, everything is perfectly well

defined for arbitrary $\vec{f} \in \mathbb{R}^{2m}$ and no normalization conditions have to be imposed. From Eq. (28) we can see that the norm of $\vec{f}$ can be factored out, such that it serves as a general rescaling factor of the quadrature operator. In a physical context, when a quadrature is measured, it is common to renormalize measurements to units of vacuum noise, which practically means that we set $\|\vec{f}\| = 1$. Unless explicitly stated otherwise, we assume that $\|\vec{f}\| = 1$ throughout this Tutorial. We can use these general quadrature operators to express electric field operator as

$$\hat{\mathbf{E}}^{(+)}(\mathbf{r},t) = \sum_{j=1}^{m} \mathcal{E}_j^{(1)} \frac{\hat{q}(\vec{e}_j) + i\hat{q}(\Omega\vec{e}_j)}{2} \mathbf{u}_j(\mathbf{r},t), \tag{30}$$

and we can use the basis transformation (21) to equivalently express the electric field operator in a different mode basis as

$$\hat{\mathbf{E}}^{(+)}(\mathbf{r},t) = \sum_{j=1}^{m} \mathcal{E}_j^{(1)} \frac{\hat{q}(O\vec{e}_j) + i\hat{q}(\Omega O\vec{e}_j)}{2} \mathbf{v}_j(\mathbf{r},t). \tag{31}$$

This procedure shows us that optical elements, that change the mode basis, change the associated quadrature operators accordingly.

Equation (30) shows us explicitly that quadrature operators $\hat{q}(\vec{f})$ and $\hat{q}(\Omega\vec{f})$ correspond to the same mode, regardless of the mode basis. This reflects the fact that $\vec{f}$ generates one axis in the optical phase space and $\Omega\vec{f}$ generates the second axis that corresponds to the same mode. As such, any arbitrary mode comes with an associated two-dimensional phase space that mathematically can be denoted as $\mathrm{span}(\vec{f}, \Omega\vec{f})$. Because this phase space is uniquely associated with a specific mode, we introduce the notation

$$\mathbf{f} = \mathrm{span}(\vec{f}, \Omega\vec{f}), \tag{32}$$

and we refer to this as "mode **f**." This allows us to concentrate on the multimode quantum states within this Tutorial, while the specifications of the modes can be left ambiguous. The modes can be seen as the physical implementations of the quantum system and are of major importance in the experimental setting as multimode quantum optics experiments rely on the manipulation of these modes.

Multimode quantum states define expectation values of the field, and when we consider CV quantum optics, we primarily focus on the expectation values of the quadrature operators $\hat{q}(\vec{f})$. These operators are unbounded and have a continuous spectrum. The measurement of a field quadrature thus leads to a continuum of possible outcomes and the continuous-variable approach to quantum optics implies that this characterizes quantum properties of light through the measurement of such quadrature operators.

Formally, we can again describe a quantum state on such a system by a density operator $\hat{\rho}$ but this description is rather inconvenient. It turns out that the quadrature operators $\hat{q}(\vec{f})$ generate the algebra of observables for the quantum system that is comprised within our multimode light. In other words, any observable can be approximated by a polynomial of quadrature operators. This generally implies that we can fully characterize the quantum state $\hat{\rho}$ by correlation functions of the type $\mathrm{tr}[\hat{\rho}\hat{q}(\vec{f}_1)\ldots\hat{q}(\vec{f}_n)]$. When we know these correlation functions for all lengths n and normalized vectors in phase space, we have fully characterized the state.

To go beyond the information that is contained in correlation functions, it is often convenient to consider probability distributions as a whole. For a single quadrature $\hat{q}(\vec{f})$ we can introduce the characteristic function for any $\lambda \in \mathbb{R}$ as

$$\chi(\lambda) = \mathrm{tr}[\hat{\rho}e^{i\lambda\hat{q}(\vec{f})}] = \sum_{n=0}^{\infty} \frac{(i\lambda)^n}{n!} \mathrm{tr}[\hat{\rho}\hat{q}(\vec{f})^n], \tag{33}$$

which is clearly related to the moments $\mathrm{tr}[\hat{\rho}\hat{q}(\vec{f})^n]$. The characteristic function is the Fourier transform of the probability distribution of the outcomes of observable $\hat{q}(\vec{f})$. We can thus obtain the probability distribution as

$$p(x) = \frac{1}{2\pi} \int_{\mathbb{R}} \mathrm{d}\lambda\, \chi(\lambda) e^{-ix\lambda}. \tag{34}$$

This approach can be readily generalized to the joint probability distribution for a set of commuting quadrature operators. We thus consider $\vec{f}_1, \ldots \vec{f}_n$ with $[\hat{q}(\vec{f}_j), \hat{q}(\vec{f}_k)] = 0$ for all j, k, and we define for all $\vec{\lambda} = \lambda_1\vec{f}_1 + \lambda_2\vec{f}_2 + \cdots + \lambda_n\vec{f}_n$ (note that $\vec{\lambda}$ is not normalized). We can then use the properties of the quadrature operators to construct $\hat{q}(\vec{\lambda}) = \sum_{k=1}^{n} \lambda_k \hat{q}(\vec{f}_k)$ and define the function

$$\chi(\vec{\lambda}) = \mathrm{tr}[\hat{\rho}e^{i\hat{q}(\vec{\lambda})}]. \tag{35}$$

This function generates all the correlations between observables $\hat{q}(\vec{f}_1), \ldots, \hat{q}(\vec{f}_n)$ and it can be used to obtain the multivariate probability distribution

$$p(\vec{x}) = \frac{1}{(2\pi)^n} \int_{\mathbb{R}^n} \mathrm{d}\vec{\lambda}\, \chi(\vec{\lambda}) e^{-i\vec{\lambda}^T\vec{x}}, \tag{36}$$

where $\mathrm{d}\vec{\lambda} = \mathrm{d}\lambda_1 \ldots \mathrm{d}\lambda_n$. The function $p(\vec{x})$ describes the probability density to jointly obtain $x_1, \ldots, x_n$ as measurement outcomes for the measurements of $\hat{q}(\vec{f}_1), \ldots, \hat{q}(\vec{f}_n)$, respectively. This approach relies on the fact that commuting observables can be jointly measured and what we presented to derive Eqs. (34) and (36) is ultimately just classical probability theory. However, not all quadrature operators commute such that joint measurements are not

always possible. This implies that a quantum state cannot be straightforwardly defined by a probability distribution of the optical phase space.

Intriguingly, we can carry out the same procedure for a full multimode system over a set of m modes. To this goal, let us define the quantum characteristic function

$$\chi : \mathbb{R}^{2m} \to \mathbb{C} : \vec{\lambda} \mapsto \chi(\vec{\lambda}) := \mathrm{tr}[\hat{\rho} e^{i\hat{q}(\vec{\lambda})}]. \tag{37}$$

This function, defined on the full optical phase space, can be used to generate all correlation functions between all quadrature operators. As such, it does characterize the full quantum state, but it is common practice to rather study its inverse Fourier transform, which is known as the Wigner function [61–63]

$$W(\vec{x}) := \frac{1}{(2\pi)^{2m}} \int_{\mathbb{R}^{2m}} \mathrm{d}\vec{\lambda}\ \chi(\vec{\lambda}) e^{-i\vec{\lambda}^T\vec{x}}. \tag{38}$$

This function has many appealing properties even though it is not a probability distribution but rather a quasiprobability distribution. First of all, the Wigner function is normalized, i.e., $\int_{\mathbb{R}^{2m}} \mathrm{d}\vec{x}\ W(\vec{x}) = 1$. Furthermore, its marginals consistently describe all the joint probability distributions for sets of commuting quadratures in the system. Formally, this implies that $p(\vec{x})$ of Eq. (36) can be obtained by integrating over all the phase-space axes that are not contained within $\mathrm{span}(\vec{f}_1, \ldots \vec{f}_n)$. To do so, let us introduce the n-dimensional vector $\vec{x}_M$ that is associated with the measured quadratures, and the $2m-n$ dimensional vectors $\vec{x}_c$, which describe all other axes in phase space. An arbitrary point in phase space can thus be written as $\vec{x} = \vec{x}_M \oplus \vec{x}_c$. Then we find that

$$P(\vec{x}_M) = \int_{\mathbb{R}^{2m-n}} \mathrm{d}\vec{x}_c\ W(\vec{x}_M \oplus \vec{x}_c). \tag{39}$$

Finally, the Wigner function also produces the correct expectation values

$$\int_{\mathbb{R}^{2m}} \mathrm{d}\vec{x}\ \vec{f}_1{}^T\vec{x} \ldots \vec{f}_n{}^T\vec{x} W(\vec{x}) = \mathrm{Re}\{\mathrm{tr}[\hat{\rho}\hat{q}(\vec{f}_1)\ldots\hat{q}(\vec{f}_n)]\}. \tag{40}$$

Note that considering the real part of $\mathrm{tr}[\hat{\rho}\hat{q}(\vec{f}_1)\ldots\hat{q}(\vec{f}_n)]$ is essentially equivalent to considering symmetric ordering of the operators. Regardless of these nice properties the Wigner function is by itself not a well-defined probability distribution. Due to complementarity, the function can reach negative values for some states. This Wigner negativity is consistent with the impossibility to jointly describe the measurement statistics of all quadratures while also complying with the laws of quantum physics (notably the Heisenberg relation). The profound relation between negativity of the Wigner functions and joint measurability is perhaps most strikingly illustrated by its connection to contextuality [64]. The formalism of Wigner functions can be used to construct phase-space representations of arbitrary observables by introducing

$$\chi_A(\vec{\lambda}) = \mathrm{tr}[\hat{A} e^{i\hat{q}(\vec{\lambda})}], \tag{41}$$

such that the Wigner representation is given by

$$W_A(\vec{x}) = \frac{1}{(2\pi)^{2m}} \int_{\mathbb{R}^{2m}} \mathrm{d}\vec{\lambda}\ \chi_A(\vec{\lambda}) e^{-i\vec{\lambda}^T\vec{x}}. \tag{42}$$

These Wigner representations have the appealing property that

$$\mathrm{tr}[\hat{A}\hat{\rho}] = (4\pi)^m \int_{\mathbb{R}^{2m}} \mathrm{d}\vec{x}\ W_{\hat{A}}^*(\vec{x}) W(\vec{x}). \tag{43}$$

When $\hat{A}$ is an observable and thus has $\hat{A} = \hat{A}^\dagger$, its Wigner function will be real such that $W_{\hat{A}}^*(\vec{x}) = W_{\hat{A}}(\vec{x})$. However, it may sometimes be useful to extend the formalism to more general operators. As such the entire theory of continuous-variable quantum systems can be developed using Wigner functions.

Several aspects of the phase-space representations in this section are reminiscent of earlier results in Sec. A, which was fully developed in a language of particles (also known as a discrete-variable approach). Indeed, the algebra of operators that is generated by the creation and annihilation operators is actually the same as the algebra generated by the quadrature operators. To formalize this, we must first stress that the optical phase space is isomorphic to an m-dimensional complex Hilbert space, which can equally be interpreted as the single-particle Hilbert space of a photon. Formally, this equivalence is constructed through the bijection (see also the Appendix)

$$\vec{f} \in \mathbb{R}^{2m} \mapsto \sum_j (f_{2j-1} + i f_{2j}) \left|\varphi_j\right\rangle \in \mathcal{H}, \tag{44}$$

where $\{\left|\varphi_j\right\rangle\}$ is an arbitrary basis of $\mathcal{H}$. We can introduce the operators

$$\begin{aligned} \hat{a}(\vec{f}) &= \frac{1}{2}[\hat{q}(\vec{f}) + i\hat{q}(\Omega\vec{f})], \\ \hat{a}^\dagger(\vec{f}) &= \frac{1}{2}[\hat{q}(\vec{f}) - i\hat{q}(\Omega\vec{f})]. \end{aligned} \tag{45}$$

By using Eq. (44), we can naturally associate these operators to creation and annihilation operators on the single-particle Hilbert space. We retrieve the canonical commutation relation

$$[\hat{a}(\vec{f}_1), \hat{a}^\dagger(\vec{f}_2)] = \vec{f}_1{}^T\vec{f}_2 - i\vec{f}_1{}^T\Omega\vec{f}_2, \tag{46}$$

which can be connected to the inner product on the Hilbert space $\mathcal{H}$ via Eq. (44).

The definition of creation and annihilation operators allows us to make sense of the vacuum state in our phase-space picture. The vacuum state is completely characterized by the property

$$\hat{a}(\vec{f})\,|0\rangle = 0, \text{ for all } \vec{f} \in \mathbb{R}^{2m}. \tag{47}$$

This simple fact can be used to evaluate the quantum characteristic function

$$\chi_0(\vec{\lambda}) = \mathrm{tr}(|0\rangle\langle 0|\, e^{i[\hat{a}^\dagger(\vec{\lambda})+\hat{a}(\vec{\lambda})]}) \tag{48}$$

$$= \sum_{n=0}^{\infty} \frac{i^n}{n!} \langle 0|\,[\hat{a}^\dagger(\vec{\lambda}) + \hat{a}(\vec{\lambda})]^n\,|0\rangle \tag{49}$$

$$= \sum_{n=0}^{\infty} -\frac{\|\vec{\lambda}\|^{2n}}{2^n n!} \tag{50}$$

$$= \exp\left[-\frac{\|\vec{\lambda}\|^2}{2}\right]. \tag{51}$$

To obtain Eq. (50) we need a considerable amount of combinatorics to evaluate $\langle 0|\,[\hat{a}^\dagger(\vec{\lambda}) + \hat{a}(\vec{\lambda})]^n\,|0\rangle$. In general, it can be shown that $\langle 0|\,\hat{a}^\dagger(\vec{\lambda}_1)\ldots\hat{a}^\dagger(\vec{\lambda}_k)\hat{a}(\vec{\lambda}_{k+1})\ldots\hat{a}(\vec{\lambda}_{k+l})\,|0\rangle = 0$. Thus it suffices to cast $[\hat{a}^\dagger(\vec{\lambda}) + \hat{a}(\vec{\lambda})]^n$ in normal ordering and extract the term proportional to identity. Even though straightforward, this calculation is quite cumbersome and thus we do not present the details.

From Eq. (51) the Wigner function can be obtained via an inverse Fourier transformation that leads to

$$W_0(\vec{x}) = \frac{e^{-\frac{1}{2}\|\vec{x}\|^2}}{2\pi}. \tag{52}$$

This Wigner function describes a Gaussian distribution on the phase space with unit variance along every axis. We can thus use Eq. (40) to see that the vacuum state saturates Heisenberg's inequality, i.e., $\Delta\hat{q}(\vec{f})\Delta\hat{q}(\Omega\vec{f}) = 1$.

The quadrature operators thus generate the same algebra of observables as the creation and annihilation operators. However, both sets of observables tend to cause mathematical problems because they are unbounded operators [42,65–67]. The unboundedness means that, when $|\Psi\rangle$ is contained in the Fock space, there is no guarantee that $\hat{q}(\vec{f})\,|\Psi\rangle$ will also be contained in the Fock space. One way of solving this problem explicitly is by only considering states for which $\langle\Psi|\,\hat{q}(\vec{f})^2\,|\Psi\rangle < \infty$, such that $\hat{q}(\vec{f})\,|\Psi\rangle$ is a well-defined state. Physically this assumption makes sense, as it ultimately implies that we consider only states with finite energies. However, the unboundedness of quadrature operators also disqualifies them as well-defined generators of the C^* algebra of observables (since elements of such algebras must be bounded). C^* algebras are essential tools as they allow reconstruction of the whole framework of Hilbert spaces based on representation theory of abstract algebras (which is essentially the idea of canonical quantization). A highly formal and detailed treatment that considers all these subtleties for bosonic systems is found in Ref. [41]. The key idea is to rather consider a set of bounded operators that describes the same algebra of observables [65,66] and are known as the displacement operators:

$$\hat{D}(\vec{\alpha}) = e^{-i\hat{q}(\Omega\vec{\alpha})/2}, \tag{53}$$

where $\vec{\alpha} \in \mathbb{R}^{2m}$ need not be normalized. Again, we can use the isomorphism (44) to identify the displacement operator on the quantized phase space to a displacement operator on the Fock space. These operators can be seen as generators of the quadrature operators and they act in a very natural way on them:

$$\hat{D}^\dagger(\vec{\alpha})\hat{q}(\vec{f})\hat{D}(\vec{\alpha}) = \hat{q}(\vec{f}) + \vec{\alpha}^T\vec{f}, \tag{54}$$

which means that the value $\vec{\alpha}^T\vec{f}$ is added to the measurement outcomes of $\hat{q}(\vec{f})$. The displacement operator can be combined according to the rule

$$\hat{D}(\vec{\alpha}_1)\hat{D}(\vec{\alpha}_2) = \hat{D}(\vec{\alpha}_1 + \vec{\alpha}_2)e^{\frac{i}{4}\vec{\alpha}_1^T\Omega\vec{\alpha}_2}. \tag{55}$$

This rule is yet another representation of the canonical commutation relation and it generates the same algebra of observables. This implies that any observable $\hat{A}$ can be written as a linear combination of displacement operators. We use the Hilbert-Schmidt inner product $\langle\hat{A},\hat{B}\rangle_{\mathrm{HS}} = \mathrm{tr}[\hat{A}^\dagger\hat{B}]$ to make this explicit

$$\hat{A} = \int_{\mathbb{R}^{2m}} \mathrm{d}\vec{\lambda}\,\langle\hat{D}(2\Omega\vec{\lambda}),\hat{A}\rangle_{\mathrm{HS}}\hat{D}(2\Omega\vec{\lambda}),$$

$$= \int_{\mathbb{R}^{2m}} \mathrm{d}\vec{\lambda}\,\mathrm{tr}[\hat{A}\hat{D}(-2\Omega\vec{\lambda})]\hat{D}(2\Omega\vec{\lambda}), \tag{56}$$

and we can readily identify that

$$\mathrm{tr}[\hat{A}\hat{D}(-2\Omega\vec{\lambda})] = \chi_A^*(\vec{\lambda}). \tag{57}$$

It can then directly be seen that

$$\mathrm{tr}[\hat{A}\hat{\rho}] = \int_{\mathbb{R}^{2m}} \mathrm{d}\vec{\lambda}\,\chi_A^*(\vec{\lambda})\mathrm{tr}[\hat{D}(2\Omega\vec{\lambda})\hat{\rho}], \tag{58}$$

$$= \int_{\mathbb{R}^{2m}} \mathrm{d}\vec{\lambda}\,\chi_A^*(\vec{\lambda})\chi(\vec{\lambda}). \tag{59}$$

And we immediately obtain Eq. (43) via Plancherel's theorem [67,68].

The displacement operators also implement a unitary operation on a quantum state. This unitary operation has a remarkably simple effect when it is expressed on the level

of the Wigner function. Via the property, Eq. (55), we can calculate that

$$\hat{\rho} \mapsto \hat{D}(\vec{\alpha})\hat{\rho}\hat{D}^{\dagger}(\vec{\alpha}) \implies \chi(\vec{\lambda}) \mapsto \chi(\vec{\lambda})e^{-i\vec{\alpha}^T\vec{\lambda}}. \tag{60}$$

Performing the inverse Fourier transform of these quantum characteristic functions leads to

$$W(\vec{x}) \overset{D(\vec{\alpha})}{\mapsto} W(\vec{x}-\vec{\alpha}). \tag{61}$$

The displacement operator thus literally implements a displacement of the Wigner function by a vector $\vec{\alpha} \in \mathbb{R}^{2m}$ in phase space.

Displacement operators are also well known as the generators of the coherent states that were introduced in Eq. (10). We can combine the bijection between phase space and Hilbert space, Eq. (44), the expression of creation and annihilation operators in terms of quadratures, Eq. (45), and the definition of the displacement operator, Eq. (53), to derive that

$$|\vec{\alpha}\rangle = \hat{D}(\vec{\alpha})\,|0\rangle\,. \tag{62}$$

By combining Eqs. (52) and (61), we immediately see that the Wigner function for such a coherent state is given by

$$W_{\alpha}(\vec{x}) = W_0(\vec{x}-\vec{\alpha}) = \frac{e^{-\frac{1}{2}\|\vec{x}-\vec{\alpha}\|^2}}{2\pi}. \tag{63}$$

We emphasize that there is a slight difference between the coherent states as defined here, and coherent states as sometimes introduced in the literature. The difference is a factor of 2, which appears because we normalized the shot noise to 1 rather than to 1/2. As such, our coherent states have an energy in mode **f**, which is given by

$$\langle\vec{\alpha}|\,\hat{a}^{\dagger}(\vec{f}\,)a(\vec{f}\,)\,|\vec{\alpha}\rangle = \frac{1}{4}[(\vec{\alpha}^T\vec{f}\,)^2 + (\vec{\alpha}^T\Omega\vec{f}\,)^2]. \tag{64}$$

The coherent states lead us to two other representations of quantum states and observables: the Q function and P function. The definition of the P function is related to the idea that coherent states form an overcomplete basis of Fock space. This implies, notably, that for a m-dimensional single-particle Hilbert space

$$\frac{1}{(4\pi)^m}\int_{\mathbb{R}^{2m}} \mathrm{d}\vec{\alpha}\,|\vec{\alpha}\rangle\,\langle\vec{\alpha}| = \mathbb{1}, \tag{65}$$

with $\mathbb{1}$ the identity operator. We can then show that any observable can be written as [5,6]

$$\hat{A} = \frac{1}{(4\pi)^m}\int_{\mathbb{R}^{2m}} \mathrm{d}\vec{\alpha}P_A(\vec{\alpha})\,|\vec{\alpha}\rangle\,\langle\vec{\alpha}|\,, \tag{66}$$

where we refer to $P_A(\vec{\alpha})$ as the P function of the observable $\hat{A}$. Similarly, we can represent a density of operator $\hat{\rho}$ by its P function $P(\vec{\alpha})$. The reader should be warned that P functions often have rather unpleasant mathematical properties. In particular, they often are not actual functions and can be highly singular.

The P function naturally comes with a dual representation that is known as the Q function. As often in quantum physics, what actually counts is the expectation value of an observable in a specific state. We can use the P function to write

$$\mathrm{tr}[\hat{A}\hat{\rho}] = \frac{1}{(4\pi)^m}\int_{\mathbb{R}^{2m}} \mathrm{d}\vec{\alpha}P_A(\vec{\alpha})\,\langle\vec{\alpha}|\,\hat{\rho}\,|\vec{\alpha}\rangle \tag{67}$$

$$= \frac{1}{(4\pi)^m}\int_{\mathbb{R}^{2m}} \mathrm{d}\vec{\alpha}P(\vec{\alpha})\,\langle\vec{\alpha}|\,\hat{A}\,|\vec{\alpha}\rangle\,. \tag{68}$$

This naturally introduces the Q function, given by

$$Q_A(\vec{\alpha}) = \frac{1}{(4\pi)^m}\,\langle\vec{\alpha}|\,\hat{A}\,|\vec{\alpha}\rangle\,, \tag{69}$$

and, in particular, for the quantum state $\hat{\rho}$ we find that

$$Q(\vec{\alpha}) = \frac{1}{(4\pi)^m}\,\langle\vec{\alpha}|\,\hat{\rho}\,|\vec{\alpha}\rangle\,. \tag{70}$$

The latter is of particular interest because it represents the quantum state $\hat{\rho}$ as an actual probability distribution. This leads us to the general identity that

$$\mathrm{tr}[\hat{A}\hat{B}] = \int_{\mathbb{R}^{2m}} \mathrm{d}\vec{\alpha}P_A(\vec{\alpha})Q_B(\vec{\alpha}) = \int_{\mathbb{R}^{2m}} \mathrm{d}\vec{\alpha}Q_A(\vec{\alpha})P_B(\vec{\alpha}). \tag{71}$$

Thus finishing our introduction to the various descriptions of the quantum states and observables of bosonic many-particle systems.

The Q function has a clear physical interpretation. It is directly proportional to the fidelity of the state $\hat{\rho}$ with respect to a target coherent state $|\vec{\alpha}\rangle$. Furthermore, it is always positive, which implies that it is a well-defined probability distribution. Because we can write $\langle\vec{\alpha}|\,\hat{\rho}\,|\vec{\alpha}\rangle = \mathrm{tr}[\hat{\rho}\,|\vec{\alpha}\rangle\,\langle\vec{\alpha}|]$, we can use Eqs. (43) and (52) to express the Q function in terms of the Wigner function as

$$Q(\vec{\alpha}) = \int_{\mathbb{R}^{2m}} \mathrm{d}\vec{x}\,W(\vec{x})W_0(\vec{x}-\vec{\alpha}). \tag{72}$$

To satisfy both Eqs. (43) and (71), we find that

$$W(\vec{x}) = \frac{1}{(4\pi)^m}\int_{\mathbb{R}^{2m}} \mathrm{d}\vec{\alpha}\;P(\vec{\alpha})W_0(\vec{x}-\vec{\alpha}), \tag{73}$$

$$= \frac{1}{(4\pi)^m}\int_{\mathbb{R}^{2m}} \mathrm{d}\vec{\alpha}\;P(\vec{\alpha})\frac{e^{-\frac{1}{2}\|\vec{x}-\vec{\alpha}\|^2}}{(2\pi)^m}. \tag{74}$$

In turn, this implies that

$$Q(\vec{\alpha}) = \frac{1}{(8\pi)^m} \int_{\mathbb{R}^{2m}} \mathrm{d}\vec{\beta}\, P(\vec{\beta}) \frac{e^{-\frac{1}{4}\|\vec{\beta}-\vec{\alpha}\|^2}}{(2\pi)^m}. \tag{75}$$

These results thus show that all these phase-space representations are ultimately related to one another through convolution or deconvolution with a Gaussian [recall that the Wigner function of the vacuum Eq. (52) is a Gaussian distribution on phase space]. One can now follow Ref. [69] to define a continuous family of phase-space representations $\mathcal{W}_\sigma$ for $\sigma \in [-1, 1]$

$$\mathcal{W}_\sigma(\vec{\alpha}) = \left(\frac{1}{4\pi[1-\sigma]}\right)^m \int_{\mathbb{R}^{2m}} \mathrm{d}\vec{\beta}\, P(\vec{\beta}) \frac{e^{-\frac{1}{2[1-\sigma]}\|\vec{\beta}-\vec{\alpha}\|^2}}{(2\pi)^m}, \tag{76}$$

where we convolute the P function with an ever-increasing Gaussian, smoothening its features. We can then see that

$$\mathrm{tr}[\hat{A}\hat{\rho}] = (4\pi)^m \int_{\mathbb{R}^{2m}} \mathrm{d}\vec{\alpha}\, \mathcal{W}_{A,-\sigma}(\vec{\alpha}) \mathcal{W}_\sigma(\vec{\alpha}). \tag{77}$$

We find, notably, that $W(\vec{x}) = \mathcal{W}_{\sigma=0}(\vec{x})$, $Q(\vec{\alpha}) = \mathcal{W}_{\sigma=-1}(\vec{\alpha})$, and $P(\vec{\alpha}) = (4\pi)^m \mathcal{W}_{\sigma=1}(\vec{\alpha})$. This shows that the phase-space representation becomes more regular when decreasing σ. Other generalized probability distributions have been considered in the literature [70,71], often to circumvent the unappealing properties of the P function. In this Tutorial, we mainly use the Wigner function and (to a lesser extent) the Q function, as they are suitable tools to classify non-Gaussian quantum states. The P function is often used in the literature to characterize the nonclassicality of a state, where the intuition is that classical light is a mixture of coherent states (and thus its P function is a probability distribution) [5,6].

Before we close this introductory section on the phase-space description of CV quantum systems, we introduce one final tool that often comes in handy. The Wigner function can itself be obtained as the expectation value of an operator [72]. Formally, we write

$$W(\vec{x}) = \frac{1}{(2\pi)^m} \mathrm{tr}[\hat{\rho}\hat{\Delta}(\vec{x})]. \tag{78}$$

Using linearity and Eq. (38), we obtain the special case

$$\hat{\Delta}(\vec{0}) = \frac{1}{(2\pi)^m} \int_{\mathbb{R}^{2m}} \mathrm{d}\vec{\lambda}\, e^{i\hat{q}(\vec{\lambda})}. \tag{79}$$

By using techniques based on Eqs. (54) and (55), we can show that

$$\hat{\Delta}(\vec{0})\hat{q}(\vec{f})\hat{\Delta}(\vec{0}) = -\hat{q}(\vec{f}). \tag{80}$$

This means that $\hat{\Delta}(\vec{0})$ is the parity operator. Its eigenstates are the Fock states, since

$$\hat{\Delta}(\vec{0})a^\dagger(\vec{f}_1)\ldots a^\dagger(\vec{f}_n)\,|0\rangle = (-1)^n a^\dagger(\vec{f}_1)\ldots a^\dagger(\vec{f}_n)\,|0\rangle\,. \tag{81}$$

Thus we can formally identify

$$\hat{\Delta}(\vec{0}) = (-\mathbb{1})^{\hat{N}}, \tag{82}$$

where $\hat{N}$ is the number operator. We define this operator by introducing a mode basis $\{\vec{e}_1, \Omega\vec{e}_1, \ldots, \vec{e}_m, \Omega\vec{e}_m\}$ of the optical phase space, such that $\hat{N} := \sum_{j=1}^m a^\dagger(\vec{e}_j)a(\vec{e}_j)$. This definition can be combined with the properties of the displacement operator to obtain that

$$\hat{\Delta}(\vec{x}) = \hat{D}(-\vec{x})(-\mathbb{1})^{\hat{N}}\hat{D}(\vec{x}). \tag{83}$$

Note that what we just obtained is the operator equivalent of a δ function, which becomes even more explicit when we explicitly write down its Wigner representation

$$W_{\Delta(\vec{x}')}(\vec{x}) = \frac{1}{(4\pi)^m}\delta(\vec{x}-\vec{x}'), \tag{84}$$

which follows directly from Eqs. (43) and (78).

This result may seem somewhat artificial, but it turns out to be extremely useful. The observable $\hat{\Delta}(\vec{x})$ can be measured experimentally by counting photons, which means that the combination of photon counting and displacements directly allows us to reconstruct the Wigner function of the quantum state [73]. Until recently, the lack of good photon-number-resolving detectors in the optical frequency range has long made this method unfeasible for most states. Even though there was an early demonstration of the method for coherent states [74], it is only due to recent developments in detector technologies that the method can be applied to more general states [75,76]. The idea was also applied in other settings [77], and was used in pioneering CV experiments with trapped ions, such as Ref. [78], and in cavity QED [79,80].

C. Discrete and continuous variables

In Sec. A, we have introduced a many-boson system, regardless of the physical realization of these bosons. Such a many-boson system and its Fock space are built upon the structure that is determined by the single-particle Hilbert space $\mathcal{H}$. The Fock space that is constructed accordingly has a rich structure that is further explored in the Tutorial [56]. In optics, the bosons that we consider are photons, and quantum optics can thus be seen as the theory of a many-boson system in the context of Sec. A. This approach to quantum optics is referred to as the DV approach.

In Sec. B, we contrast this with the CV approach to quantum optics. This approach relies on the measurement of the field quadratures, and can thus be seen as a bosonic quantum field theory. Therefore we started this approach by introducing the classical electric field and its modes, which we subsequently quantized through canonical quantization. We introduced the notion of optical phase space as a general way of describing CV quantum systems. The phase space is directly related to the modes of the field and manipulations of the modes also cause changes in the optical phase space. Nevertheless, any system with a phase space can be described by these techniques.

Both of these approaches are ultimately equivalent. Bosonic creation and annihilation operators describe the same algebra of observables as bosonic quadrature operators, which means that on the level of mathematical structure, both approaches can be interchanged and even mixed. This is strikingly clear when the Wigner function, i.e., the phase-space representation of quantum states and observables that is most naturally associated with field quadratures, turns out to be directly measurable by counting photons. Notably, this implies that when it comes to mathematical structures, bosonic particles such as atoms can also be described on phase space.

The real difference between CV and DV approaches is of an experimental nature. What is important is not the observables that are technically present in the quantum system, but the observables that are practically measured in the lab. For the CV approach we typically use homodyne detection to measure quadratures [7,81], whereas in DV approaches we count photons [82].

A common source of misunderstanding between the DV and CV community stems from the role they attribute to the single-particle Hilbert space and optical phase space, respectively. As we argued, both spaces are (at least for a finite-dimensional number of modes) isomorphic, see the Appendix for some additional mathematical intuition. However, the Hilbert space of a photon, which is inherently a quantum particle, is often interpreted as a quantum object. At the same time, the optical phase space represents the field quadratures of optical modes and is thus rather considered to be a classical object. The origin of this confusion lies in the fact that the optical modes, i.e., normalized solutions of Maxwell's equations, also form a Hilbert space that has its origins entirely in classical physics.

The optical modes are the vessels that contain photons much in the same way as a set of electrons contains spins. The crucial difference is that optical modes are not uniquely defined, we can manipulate them, transform them from one mode basis to another with an interferometer and thus consider new superpositions of modes. In typical experimental settings, one would not consider a superposition of two electrons a new well-defined electron.

Because creation and displacement operators always act in one specific mode (i.e., they are generated by a single vector on the single-photon Hilbert space), single-photon states and coherent states are always single-mode states. We may expand this single mode in a different mode basis, which can even be done physically by sending the state through a beam splitter, to create some form of entanglement in the quantum states. However, this entanglement is just a manifestation of the fact that we are not considering the optimal mode basis. In the CV approach, this has led to the notion of "intrinsic" properties [58], which are those properties of quantum states that are independent of the chosen mode basis. The purity and entropy of a state are notable examples, but one can also introduce a notion of "intrinsic entanglement" to refer to a state that is entangled in any possible mode basis. In the next subsection, we introduce Gaussian states, which will later be shown to never be intrinsically entangled.

D. Gaussian states

Now that we have introduced phase-space representations for states and observables of CV quantum systems, we still need one building block before we can tackle multimode non-Gaussian states: a good understanding of Gaussian states. It is not the goal of this subsection to delve deep into decades worth of research on Gaussian states. We rather highlight a few key results that set apart Gaussian quantum states from the rest of the vast states' space. For more extended reviews, we refer the reader to Refs. [8,9]. These states are also extensively studied in the mathematical physics literature under the name "quasifree states of the CCR algebra."

Gaussian states are by definition states that have a Wigner function, which is a Gaussian:

$$W_G(\vec{x}) = \frac{e^{-\frac{1}{2}(\vec{x}-\vec{\xi})^T V^{-1}(\vec{x}-\vec{\xi})}}{(2\pi)^m\sqrt{\det V}}, \tag{85}$$

where $\vec{\xi}$ is referred to as the mean field (or displacement) and V is known as the covariance matrix. With Eq. (40), we can verify that the mean field indeed corresponds to the expectation value of the field quadrature

$$\mathrm{tr}[\hat{\rho}\hat{q}(\vec{f})] = \vec{\xi}^T\vec{f}, \tag{86}$$

similarly, we find for the covariance matrix

$$\begin{aligned}&\mathrm{tr}[\hat{\rho}\hat{q}(\vec{f}_1)\hat{q}(\vec{f}_2)] - \mathrm{tr}[\hat{\rho}\hat{q}(\vec{f}_1)]\mathrm{tr}[\hat{\rho}\hat{q}(\vec{f}_2)]\\ &= \vec{f}_1^{\,T} V \vec{f}_2 - i\vec{f}_1^{\,T}\Omega\vec{f}_2.\end{aligned} \tag{87}$$

These quantities can thus be obtained for arbitrary quantum states, but for Gaussian states the covariance matrix and the mean field also determine all higher-order expectation values. The most elegant way to see this is via the

multivariate cumulants (also known as truncated correlation functions), which vanish beyond order two [4]. This fact implies that all properties of Gaussian states can ultimately be deduced from their mean field and—often more importantly—from their covariance matrix.

Hitherto, we have encountered the vacuum state $|0\rangle$ and the coherent states $|\vec{\alpha}\rangle$ as examples of Gaussian states. Both of the examples have a covariance matrix $V = \mathbb{1}$. However, there is a much larger range of possible covariance matrices available and they have to satisfy certain constraints [83]. At first instance, we note that a covariance matrix must be positive. An additional constraint is obtained by imposing that the variance $\Delta^2\hat{q}(\vec{f}) \geqslant 0$ for all $\vec{f}$ in phase space. Equation (87) then directly yields that $\vec{f}^{\,T}(V - i\Omega)\vec{f} \geqslant 0$, which implies that $V \geqslant 0$ and suggests that $(V - i\Omega) \geqslant 0$. However, the latter is not obvious, since $\vec{f}$ are real vectors, whereas $(V - i\Omega)$ is a complex matrix. We thus need an additional ingredient: the Heisenberg inequality. Formally, this inequality can be obtained through Robertson's more general inequality [84], such that we find

$$\Delta^2\hat{q}(\vec{f}_1)\Delta^2\hat{q}(\vec{f}_2) \geqslant \frac{1}{4}\left|\mathrm{tr}\{\hat{\rho}[\hat{q}(\vec{f}_1), \hat{q}(\vec{f}_2)]\}\right|^2. \tag{88}$$

We can now apply the CCR (29) to obtain the general form

$$\Delta^2\hat{q}(\vec{f}_1)\Delta^2\hat{q}(\vec{f}_2) \geqslant \left|\vec{f}_1^{\,T}\Omega\vec{f}_2\right|^2. \tag{89}$$

On the other hand, the definition (87) of the covariance matrix can be used to translate this result to

$$\vec{f}_1^{\,T}V\vec{f}_1\,\vec{f}_2^{\,T}V\vec{f}_2 \geqslant \left|\vec{f}_1^{\,T}\Omega\vec{f}_2\right|^2. \tag{90}$$

This identity can then be used to prove $(\vec{f}_1^{\,T} - i\vec{f}_2^{\,T})(V - i\Omega)(\vec{f}_1 + i\vec{f}_2) \geqslant 0$ for all $\vec{f}_1, \vec{f}_2 \in \mathbb{R}^{2m}$. As a consequence, we find that

$$V - i\Omega \geqslant 0, \tag{91}$$

an important constraint on the covariance matrix V, which can be understood as combining the positivity conditions and the Heisenberg inequality.

To further understand the structure of covariance matrices and the Gaussian states that they describe, we highlight some important results on symplectic matrices. The first of these results is Williamson's decomposition [10], which states that any positive-definite real matrix V can be diagonalized by a symplectic matrix S (i.e., a matrix with $S^T\Omega S = \Omega$):

$$V = S^T N S, \text{ with } N = \mathrm{diag}[\nu_1, \nu_1, \nu_2, \nu_2, \ldots, \nu_m, \nu_m]. \tag{92}$$

The values $\nu_1, \ldots \nu_m$ are also known as the symplectic spectrum of V. From Heisenberg's relation, we then find the additional constraint that $\nu_1, \ldots, \nu_m \geqslant 1$, in other words, the values in the symplectic spectrum are larger than shot noise. It now becomes straightforward to see the Heisenberg's relation also implies that

$$\det V \geqslant 1. \tag{93}$$

It thus becomes apparent that the Heisenberg inequality is saturated when $\det V = 1$. The states for which this is the case must have a covariance matrix $V = S^T S$.

The Gaussian states for which the Heisenberg inequality is saturated turn out to be the pure Gaussian states. Recall that the purity of a quantum state is given by $\mu = \mathrm{tr}[\hat{\rho}^2]$. This quantity can be directly calculated from the Wigner function via Eq. (43). We then find for an arbitrary Gaussian state

$$\mu_G = (4\pi)^m \int_{\mathbb{R}^{2m}} \mathrm{d}\vec{x}\, W_G(\vec{x})^2 = \frac{1}{\sqrt{\det V}}. \tag{94}$$

Alternatively, we may use the symplectic spectrum to express $\mu_G = \prod_{k=1}^m \nu_k^{-1}$. This shows us that a Gaussian state is pure if and only if its covariance matrix is a positive symplectic matrix, i.e., it can be written as $V = S^T S$.

The class of states with a covariance matrix given by $V = S^T S$ is much larger than just the vacuum and coherent states with $V = \mathbb{1}$. The additional states turn out to have asymmetric noise in their quadratures, and because the Heisenberg inequality is saturated this implies that some quadratures have less noise than the vacuum state. The states with such covariance matrices are therefore known as squeezed states. To formalize this intuition, we consider the Bloch-Messiah decomposition (which is known in mathematics and classical mechanics as Euler's decomposition) [11,85]. Any symplectic matrix S can be decomposed as follows:

$$S = O_1 K O_2, \text{ with } K = \mathrm{diag}[s_1^{1/2}, s_1^{-1/2}, \ldots, s_m^{1/2}, s_m^{-1/2}], \tag{95}$$

where O_1 and O_2 are orthogonal symplectic matrices, i.e., $O_j^T O_j = \mathbb{1}$ and $O_j^T \Omega O_j = \Omega$. We can then see that for any pure Gaussian state, we find

$$V = S^T S = O^T K^2 O. \tag{96}$$

We have already encountered orthogonal symplectic transformations in Eq. (21), where we associated them with transformations of mode bases. Thus, if we find a set of optical modes that are prepared in a pure Gaussian state, we can always find a different mode basis in which the state

is given by

$$V' = O\,VO^T = \begin{pmatrix} s_1 & & & & \\ & 1/s_1 & & & \\ & & \ddots & & \\ & & & s_m & \\ & & & & 1/s_m \end{pmatrix}. \quad (97)$$

This means that we can always find a set of symplectic eigenvectors $\{\vec{e}_1, \Omega\vec{e}_1, \ldots, \vec{e}_m, \Omega\vec{e}_m\}$ of a pure Gaussian state's covariance matrix, which have the properties that $\Delta^2\hat{q}(\vec{e}_j) = s_j$ and $\Delta^2\hat{q}(\Omega\vec{e}_j) = 1/s_j$, such that the Heisenberg relation is saturated: $\Delta^2\hat{q}(\vec{e}_j)\Delta^2\hat{q}(\Omega\vec{e}_j) = 1$. At the same time, we find that clearly either $\Delta^2\hat{q}(\vec{e}_j)$ of $\Delta^2\hat{q}(\Omega\vec{e}_j)$ is smaller than one (and thus below shot noise).

Gaussian states naturally come with the notion of Gaussian channels [86], they are the completely positive trace-preserving transformations that map Gaussian states into other Gaussian states. We have already seen that the displacement operators are unitary transformations that fulfil this condition. Because any Gaussian transformation Γ preserves the general shape of the Wigner function (85), we can simply describe the Gaussian channel Γ in terms of its actions on the mean field and the covariance matrix:

$$V \overset{\Gamma}{\mapsto} XVX^T + V_c, \quad (98)$$

$$\vec{\xi} \overset{\Gamma}{\mapsto} X\vec{\xi} + \vec{\alpha}. \quad (99)$$

The vector $\vec{\alpha}$ simply serves to displace the entire Gaussian to a different location in phase space. On the level of the covariance matrix, X transforms and reshapes the initial covariance matrix, whereas V_c describes the addition of Gaussian classical noise. Both can *a priori* be any real matrices, as long as they satisfy the constraint

$$V_c - i\Omega + iX\Omega X^T \geqslant 0. \quad (100)$$

This constraint derives from the demand that $XVX^T + V_c$ is a well-defined covariance matrix, and therefore $XVX^T + V_c - i\Omega \geqslant 0$. Because V is a well-defined covariance matrix, $X(V - i\Omega)X^T \geqslant 0$ and thus it can be seen that $XVX^T + V_c$ is also a well-defined covariance matrix whenever Eq. (100) holds. This simple argument proves Eq. (100) is a sufficient condition for Γ to transform the covariance matrix of the initial state into a new bona fide covariance matrix.

An important case is obtained when we impose that Γ conserves the purity of the state and is thus a unitary transformation. It then immediately follows that $V_c = 0$, since there cannot be any classical noise. The displacement $\vec{\alpha}$ is simply implemented by a displacement operator, and the constraint (100), combined with the demand that purity is conserved implies that X is a symplectic matrix. In other words, a Gaussian unitary transformation $\hat{U}_G$ satisfies $V \mapsto S^TVS$. Another relevant example is the case of uniform Gaussian losses, where we set $X = \sqrt{1-\eta}\mathbb{1}$, $V_c = \eta\mathbb{1}$ and $\vec{\alpha} = 0$, with the positive value $\eta \leqslant 1$ denoting the amount of loss.

More generally, the action of a Gaussian channel on an arbitrary state can be understood from its action on $\exp[i\hat{q}(\vec{\lambda})]$, which can be proven to take the form

$$\exp[i\hat{q}(\vec{\lambda})] \overset{\Gamma}{\mapsto} \exp\left[i\hat{q}(X^T\vec{\lambda}) + i\vec{\alpha}^T\vec{\lambda} - \frac{1}{2}\vec{\lambda}^T V_c\vec{\lambda}\right]. \quad (101)$$

We can then calculate the quantum characteristic function and use some properties of Fourier transforms to find that the Wigner function transforms as

$$W(\vec{x}) \overset{\Gamma}{\mapsto} \int_{\mathbb{R}^{2m}} \mathrm{d}\vec{y}\, W(X^{-1}\vec{x} - \vec{y}) \frac{e^{-\frac{1}{2}(\vec{y}-\vec{\alpha})^T V_c^{-1}(\vec{y}-\vec{\alpha})}}{(2\pi)^m\sqrt{\det V_c}}. \quad (102)$$

For Gaussian unitary transformations we find the appealing result that $W(\vec{x}) \mapsto W[S^{-1}(\vec{x} - \vec{\alpha})]$. This means that a Gaussian unitary transformation is simply a coordinate transformation on phase space.

Proving that any completely positive Gaussian channel Γ is of the form Eq. (102) with condition (100), is a challenging task. The result was first obtained in Refs. [87,88], using the language of C^* algebras. The proof is rather technical and we do not go into details here.

The paradigm of Gaussian channels is also useful to structure general Gaussian states. One may, for example, wonder which Gaussian channel would transform the vacuum state into the Gaussian state with covariance matrix V. In general, there is no unique solution to this question, but there is a straightforward route to find an answer. First, take any symplectic matrix S that satisfies $V - S^TS \geqslant 0$ (the Williamson decomposition guarantees that this is always possible). This implies that there is a positive-definite matrix V_c such that $V = S^TS + V_c$. As such, an arbitrary Gaussian state can always be decomposed as

$$W_G(\vec{x}) = \int_{\mathbb{R}^{2m}} \mathrm{d}\vec{y}\, W_0(S^{-1}\vec{x} - \vec{y}) e^{-\frac{1}{2}(\vec{y}-\vec{\alpha})^T V_c^{-1}(\vec{y}-\vec{\alpha})}. \quad (103)$$

The symplectic operation that is applied to the vacuum is known as multimode squeezing in optics. These transformations are fully equivalent to Bogoliubov transformations that are regularly used in condensed-matter physics [4,8]. Combined with a displacement, this operation provides the most general operation that maps quadrature operators into well-defined quadrature operators.

Now that we have introduced the basic concepts of Gaussian states, we are equipped to start exploring their

non-Gaussian counterparts. Several other important properties of Gaussian states will be introduced along the way to stress just how peculiar these Gaussian states are compared to the rest of state space.

III. NON-GAUSSIAN QUANTUM STATES

Contrary to Gaussian states with their elegant Wigner function and properties that can be nicely deduced from the covariance matrix, the set of non-Gaussian states is vast and wild. Literally all states with Wigner functions that are not Gaussian are contained within this class. To give an idea of the enormous variety, one can consider that highly exotic states such as Gottesman-Kitaev-Preskill states [31] and Schrödinger cat states inhabit the set of non-Gaussian states together with the states that describe single photons and even certain convex mixtures of Gaussian states. Throughout the years, there have been considerable efforts to structure the set of non-Gaussian states. We introduce the notion of quantum non-Gaussian states [89] and then extend it to a hierarchy based on stellar rank [38]. A different approach is provided by considering that the negativity of the Wigner function can be used as a genuine signature of nonclassicality [90]. However, before we attack these different measures to structure non-Gaussian quantum states, we contrast some properties of Gaussian and non-Gaussian states.

Figure 1 provides an overview that can be used as a brief guide to understand the structure of non-Gaussian states. We attempt to highlight how the different quantities used to structure the non-Gaussian part of state space are interconnected.

A. Gaussian versus Non-Gaussian

Gaussian states have many extraordinary properties that set them apart from non-Gaussian states. First of all, pure Gaussian states turn out to be the only quantum states that saturate the uncertainty relation. The easiest way to see this is by describing arbitrary pure states in terms of their wave functions. The wave functions associated with amplitude quadratures $\hat{q}(\vec{f})$ and those associated with phase quadratures $\hat{q}(\Omega\vec{f})$ are related by a Fourier transform. This fact can then be used to show that only Gaussian wave functions saturate the Heisenberg inequality. The extension to arbitrary mixed states can be achieved via Jensen's inequality, which emphasizes that no mixed states can saturate the uncertainty relation. Let us consider a mixed state $\hat{\rho} = \sum_k p_k |\Psi_k\rangle\langle\Psi_k|$ with variances $\Delta^2\hat{q}(\vec{f})$. We also introduce the variances $\Delta_k^2\hat{q}(\vec{f})$ for the pure states $|\Psi_k\rangle$. From Jensen's inequality [91], it follows that

$$\Delta^2\hat{q}(\vec{f}) \geqslant \sum_k p_k \Delta_k^2\hat{q}(\vec{f}). \tag{104}$$

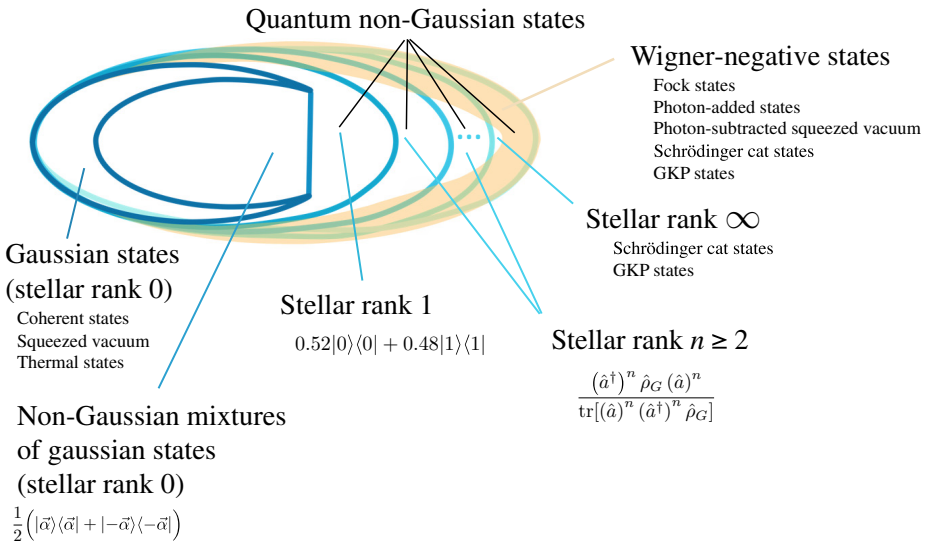

FIG. 1. Overview of the different types of non-Gaussian states that can be found in state space. The different aspects will all be considered throughout Sec. III. Here we attempt to show the stellar hierarchy and how it differentiates itself from the convex hull (mixtures) of Gaussian states. Furthermore, we emphasize that the stellar rank and Wigner negativity are different quantifiers of non-Gaussianity. It should be noted that all non-Gaussian pure states are Wigner-negative states, but we can find states that are not mixtures of Gaussian states without Wigner negativity. For all the classes, we provide examples of states that belong to this group, the Wigner functions for several of these examples are shown in Fig. 2.

For Heisenberg's inequality, we calculate

$$\Delta^2\hat{q}(\vec{f})\Delta^2\hat{q}(\Omega\vec{f}) \geqslant \sum_k p_k^2\Delta_k^2\hat{q}(\vec{f})\Delta_k^2\hat{q}(\Omega\vec{f}) + \sum_{k\neq l} p_k p_l \Delta_k^2\hat{q}(\vec{f})\Delta_l^2\hat{q}(\Omega\vec{f}) \geqslant 1. \tag{105}$$

The presence of cross terms highlights that even when all the pure states in the mixture saturate the inequality, the mixture does not. The only possible exception is the case where the state is pure.

That only pure Gaussian states saturate the Heisenberg inequality may seem like an innocent observation, but it has an important implication for non-Gaussian states. The Heisenberg inequality can be formulated entirely in terms of the covariance matrix. We showed in Eq. (92) that the inequality is saturated if and only if the covariance matrix is symplectic, i.e., $V = S^T S$. Furthermore, we showed in Eq. (94) that a Gaussian state is pure if and only if its covariance matrix is symplectic $V = S^T S$. The fact that no non-Gaussian states can saturate the inequality thus implies that non-Gaussian states can never have a symplectic covariance matrix $V = S^T S$. This is a first hint of the special role played by Gaussian states.

A more general result along these lines states that for all states $\hat{\rho}$ with the same covariance matrix V, the Gaussian state always has the highest von Neumann entropy [13]. First of all, note that entropy $-\mathrm{tr}[\hat{\rho}\log\hat{\rho}]$ is conserved under unitary transformations. Due to the Williamson decomposition (92), we can write any Gaussian state as

$$\hat{\rho}_G = \hat{U}_G \bigotimes_{j=1}^{m} \hat{\rho}_{\overline{n}_j} \hat{U}_G^\dagger, \tag{106}$$

where $\hat{\rho}_{\overline{n}_j}$ is a thermal state of the Hamiltonian $\hat{a}_j^\dagger\hat{a}_j$ with average particle number $\overline{n}_j = (\nu_j - 1)/2$. From statistical mechanics, we know that thermal states are the quantum states that maximize the von Neumann entropy for a given temperature (here fixed by the occupations $\overline{n}_j$).

It turns out that Gaussian states are limiting cases for many quantities [12]. This result shows that for a range of functionals f on the state space, we find that $f(\hat{\rho}) \geqslant f(\hat{\rho}_G)$, where $\hat{\rho}_G$ is the Gaussian state with the same covariance matrix as $\hat{\rho}$. Apart from some more technical aspects such as continuity, f must have two important features: it must be conserved under (a certain class of) unitary operations $f(\hat{U}\hat{\rho}\hat{U}^\dagger) = f(\hat{\rho})$ and it must be strongly superadditive $f(\hat{\rho}) \geqslant f(\hat{\rho}_1) + f(\hat{\rho}_2)$ (note that $\hat{\rho}_1$ and $\hat{\rho}_2$ are marginals of $\hat{\rho}$). The equality must be saturated for product states, i.e., $f(\hat{\rho}_1 \otimes \hat{\rho}_2) = f(\hat{\rho}_1) + f(\hat{\rho}_2)$. For strongly subadditive functions with $f(\hat{\rho}) \leqslant f(\hat{\rho}_1) + f(\hat{\rho}_2)$ the same result implies $f(\hat{\rho}) \leqslant f(\hat{\rho}_G)$, (after all, in that case $-f$ is a strongly superadditive function). It is clear that the von Neumann entropy fulfils the latter conditions and is maximized for Gaussian states. For superadditive entanglement measures, this result can be used to show that for all states with the same covariance matrix, Gaussian states are the least entangled ones (entanglement is much more extensively discussed in Sec. V). However, several common entanglement measures, e.g., the logarithmic negativity [92] and the entanglement of formation [93], are not superadditive.

At the heart of these extremal properties lies the central limit theorem [4,94–96]. There are many versions of the central limit theorem in quantum physics, but we stick to what is probably the simplest one. As always, we consider our optical phase space $\mathbb{R}^{2m}$, but this time, we take N copies of it, which implies that we are dealing with a phase space $\mathbb{R}^{2Nm} = \mathbb{R}^{2m} \oplus \cdots \oplus \mathbb{R}^{2m}$ for the full system. We can then embed a vector $\vec{\lambda} \in \mathbb{R}^{2m}$ in the jth of these N copies via $\vec{\lambda}_j := \vec{0} \oplus \cdots \oplus \vec{0} \oplus \vec{\lambda} \oplus \vec{0} \cdots \oplus \vec{0}$ and introduce the new averaged operator

$$\overline{q}_N(\vec{\lambda}) := \frac{1}{\sqrt{N}} \sum_{j=1}^{N} \hat{q}(\vec{\lambda}_j). \tag{107}$$

It is rather straightforward to see that these observables follow the canonical commutation relation. We can now restrict ourselves to studying the algebra that is generated entirely by such averaged quadrature operators. When we then assume that the different copies of the system are "independently and identically distributed" we must set the overall state to be $\hat{\rho}^{(N)} = \hat{\rho}^{\otimes N}$. We then find the characteristic function of the algebra of averaged observables by

$$\chi_N(\vec{\lambda}) = \mathrm{tr}[\hat{\rho}^{\otimes N} e^{i\overline{q}_N(\vec{\lambda})}]. \tag{108}$$

The following pointwise convergence can be shown:

$$\chi_N(\vec{\lambda}) \overset{N\to\infty}{\to} \chi_G(\vec{\lambda}), \tag{109}$$

where $\chi_G(\vec{\lambda})$ is the characteristic function of the Gaussian state $\hat{\rho}_G$ that has the same covariance matrix as $\hat{\rho}$. This means that the non-Gaussian features in any state $\hat{\rho}$ can be coarse grained away by averaging sufficiently many copies of the state. Note that this result considers N copies of an arbitrary m-mode state. The single-mode version of this result was proven in Ref. [94], whereas a much more general versions are derived in Refs. [95,96]. In Ref. [12] the central limit theorem is combined with invariance under local unitary transformations to prove the final extremality result, we do not review these points in detail.

The extremality of Gaussian states and the associated central limit theorem highlight why Gaussian states are important in quantum-information theory and quantum

statistical mechanics. It also shows that Gaussian states have some particular properties compared to non-Gaussian states. It thus should not come as a surprise that some of these properties can be used to measure the degree of non-Gaussianity of the state [97–99]. As we mentioned before, for a fixed covariance matrix V the von Neumann entropy is maximized by the Gaussian state. This suggest that we can use the difference in von Neumann entropy as a measure for non-Gaussianity. To formalize things, let us consider an arbitrary state $\hat{\rho}$ with covariance matrix V and mean field $\vec{\xi}$ (this quantities can be derived, respectively, for the second and first moments of the quadrature operators). We then construct a Gaussian state $\hat{\sigma}_V$, which has the same covariance matrix and the mean field. In the spirit of extremality, we then define

$$\delta(\hat{\rho}) = S(\hat{\sigma}_V) - S(\hat{\rho}), \tag{110}$$

where $S(\hat{\rho}) := -\mathrm{tr}[\hat{\rho}\log\hat{\rho}]$. Because von Neumann entropy is constant under unitary transformations, for a Gaussian state it depends only on the symplectic spectrum $\nu_1, \ldots, \nu_m$. In other words, we can calculate $S(\hat{\sigma}_V)$ directly by using the Williamson decomposition (92) on V. We find from Ref. [13] that

$$S(\hat{\sigma}_V) = \sum_{j=1}^{m}\left[\frac{\nu_j+1}{2}\log\frac{\nu_j+1}{2} - \frac{\nu_j-1}{2}\log\frac{\nu_j-1}{2}\right]. \tag{111}$$

However, it should be noted that the entropy of the non-Gaussian states $S(\hat{\rho})$ is generally harder to calculate unless we can accurately approximate the state by a finite density matrix in the Fock basis. Furthermore, if the state $\hat{\rho}$ is pure, we simply find that $\delta(\hat{\rho}) = S(\hat{\sigma}_V)$.

Due to extremality of Gaussian states it directly follows that $\delta(\hat{\rho}) \geqslant 0$, but this does not necessarily mean that $\delta(\hat{\rho})$ is a good measure for non-Gaussianity. References [13,98] establish that

$$\delta(\hat{\rho}) = S(\hat{\rho} \mid |\hat{\sigma}_V), \tag{112}$$

where $S(\hat{\rho} \mid\mid \sigma_V) := \mathrm{tr}[\hat{\rho}(\log\hat{\rho} - \log\hat{\sigma}_V)]$ is the quantum relative entropy between $\hat{\rho}$ and reference state $\hat{\sigma}_V$. The quantum relative entropy allows us to connect $\delta(\hat{\rho})$ to a range of interesting properties, as shown in Ref. [98]. For example, it directly follow that $\delta(\hat{\rho}) = 0$ if and only if $\hat{\rho} = \hat{\sigma}_V$. Furthermore, the measure $\delta(\hat{\rho})$ inherits convexity and monotonicity properties from the relative entropy. These are exactly the properties that made this measure a useful ingredient in the resource theory for quantum non-Gaussianity presented in Ref. [100].

Thus, the connection between Eq. (110) and relative entropy shows that $\delta(\hat{\rho})$ can indeed be used as a measure for non-Gaussianity in the sense that it measures "entropic distance" between $\hat{\rho}$ and $\hat{\sigma}_V$. Yet, there is one important question that remains to be answered: is σ_V indeed the closest Gaussian state to $\hat{\rho}$? An affirmative answer to this question was provided in Ref. [101], where it was shown that

$$\delta(\hat{\rho}) = \min_{\hat{\rho}_G} S(\hat{\rho} \mid |\hat{\rho}_G), \tag{113}$$

where we minimise over all possible Gaussian states $\hat{\rho}_G$. The main idea of the proof is to show that $S(\hat{\rho} \mid\mid \hat{\rho}_G) - S(\hat{\rho} \mid\mid \hat{\sigma}_V) = S(\hat{\sigma}_V \mid\mid \hat{\rho}_G) \geqslant 0$ such that the smallest relative entropy in indeed achieved for $\hat{\sigma}_V$. For the technical details, we refer the interested reader to Ref. [101]. Furthermore, we note that a similar non-Gaussianity measure was introduced by using the Wehrl entropy (based on the Q function) rather than the von Neumann entropy [102].

We have thus shown that Gaussian states are special in the sense that they minimize entanglement and maximize entropy as compared to other states with the same covariance matrix. Another profound distinction can be found when comparing pure Gaussian states to pure non-Gaussian states. In this case, there is a seminal result by Hudson [34] that was extended by Soto and Claverie to multimode systems [35], which states that a pure state can have a non-negative Wigner function if and only if the state is Gaussian. In other words, all non-Gaussian pure states exhibit Wigner negativity.

Here, we follow the approach of Ref. [103] to prove this result. First of all, we introduce the function

$$F^{\star}_{\Psi}(\vec{\alpha}) := \langle\vec{\alpha} \mid \Psi\rangle e^{\frac{1}{8}\|\vec{\alpha}\|^2}, \tag{114}$$

such that the Q function (70) of the state $|\Psi\rangle$ is given by

$$Q(\vec{\alpha}) = \frac{1}{(4\pi)^m}\left|F^{\star}_{\Psi}(\vec{\alpha})\right|^2 e^{-\frac{1}{4}\|\vec{\alpha}\|^2}. \tag{115}$$

From Eq. (114), we directly find that

$$\left|F^{\star}_{\Psi}(\vec{\alpha})\right|^2 \leqslant e^{\frac{1}{4}\|\vec{\alpha}\|^2}. \tag{116}$$

Next, we observe that a Q function that reaches zero implies a negative Wigner function, which can be seen from Eq. (72). Thus, demanding that the state has a positive Wigner function implies demanding that $Q(\vec{\alpha}) > 0$, and thus that $F^{\star}_{\Psi}(\vec{\alpha})$ has no zeros. Using the equivalence between $2m$-dimensional phase space and a complex m-dimensional Hilbert space, we can use the multidimensional but restricted version of the Hadamard theorem [35], which states that any entire function $f : \mathbb{C}^m \mapsto \mathbb{C}$ without any zeros and with order of growth [104] r is an exponential $f(z) = \exp g(z)$, where $g(z)$ is a polynomial of degree $s \leqslant r$. We then note that $F^{\star}_{\Psi}$ is an entire function of maximal growth $r = 2$ as given by Eq. (116).

Hadamard's theorem then tells us that $F^\star_\Psi(\vec{\alpha})$ is Gaussian. In other words, if a pure quantum state $|\Psi\rangle$ has a positive Wigner function $F^\star_\Psi(\vec{\alpha})$ must be Gaussian. The only states for which this is the case are Gaussian states.

In summary, we have seen that Gaussian states inherit a particular extremal behavior from the central limit theorem. This should not come as a surprise given that they are the Gibbs states of a free bosonic field at finite temperature. Thus, a non-Gaussian state can be expected to have more "exotic" features than the Gaussian state with the same covariance matrix. This also formalizes the intuition that Gaussian states are more classical states. This idea is further established by the fact that all pure Gaussian states are the only possible pure states that have a positive Wigner function.

The fact that non-Gaussian states automatically have nonpositive Wigner functions no longer holds when mixed states are considered. A simple example is that state $\hat{\rho} = [|0\rangle\langle 0| + a^\dagger(\vec{f})|0\rangle\langle 0|a(\vec{f})]/2$, which is clearly non-Gaussian but also has a positive Wigner function. There have been considerable efforts to extend Hudson's theorem in some form to mixed states [36]. However, in what follows, we see that there are many ways for a state to be non-Gaussian. This makes it particularly hard to connect a measure such as Eq. (110) to more operational interpretations. In the next section, we start by showing some examples of different non-Gaussian states to make the reader appreciate their variety.

B. Examples of non-Gaussian states

An overview of the different examples discussed in this section is shown in Fig. 2.

A first important class of non-Gaussian states are Fock states, generated by acting with creation operators $a^\dagger(\vec{f})$ on the vacuum state

$$|n_f\rangle := \frac{1}{\sqrt{n!}}[\hat{a}^\dagger(\vec{f})]^n|0\rangle, \tag{117}$$

which is a state of n photons in mode f. These states are inherently single mode, even though they can be embedded in a much larger multimode state space. The Wigner function for such states is commonly found in quantum optics textbooks, but deriving it using Eq. (38) is a good exercise. Here we simply state the result:

$$W_{n_f}(\vec{x}) = \sum_{k=0}^{n} \binom{n}{k} \frac{(-1)^{n+k}\|\vec{x}_\mathbf{f}\|^{2k}}{k!} \frac{e^{-\frac{1}{2}\|\vec{x}\|^2}}{2\pi}. \tag{118}$$

In the most general sense, we write $\vec{x}_\mathbf{f} = (\vec{f}^{\,T}\vec{x})\vec{f} + (\vec{f}^{\,T}\Omega\vec{x})\Omega\vec{f}$ as the projector of $\vec{x}$ on the phase space of mode f, but it is most practical to use the coordinate representation $\vec{x}_\mathbf{f} = (x_f, p_f)^T$ where $x_f = \vec{f}^{\,T}\vec{x}$ and $p_f = \vec{f}^{\,T}\Omega\vec{x}$ to describe the two-dimensional phase space associated with mode f.

Multimode Fock states can be obtained by acting on the vacuum with different creation operators in different modes. Even though these different modes do not necessarily have to be orthogonal [56], we here focus on the case where they are. For example, in the m-mode system, we can chose a basis $\{\vec{e}_1, \Omega\vec{e}_1, \ldots, \vec{e}_m, \Omega\vec{e}_m\}$ of the phase

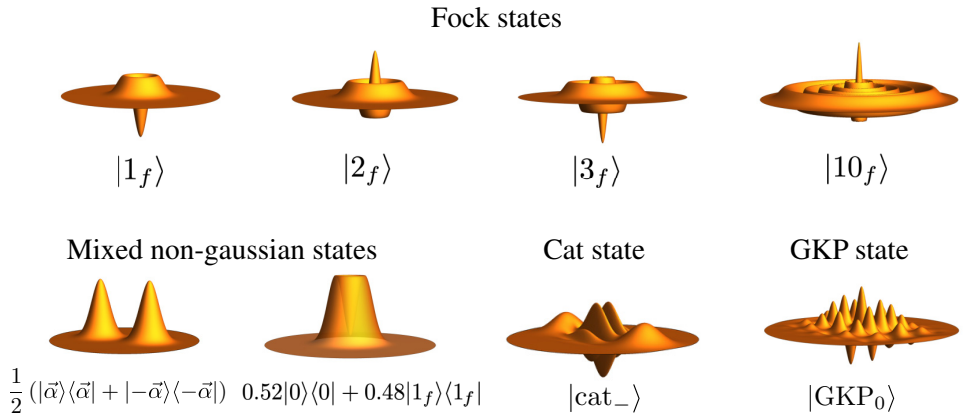

FIG. 2. Several examples of Wigner functions for single-mode non-Gaussian states. The Wigner functions for the Fock states are obtained from Eq. (118) and the mixture of a Fock state and a vacuum is given by Eq. (124). The mixture of coherent states is expressed in Eq. (122) where we set $\|\vec{\alpha}\| = 4$. The Wigner function for the cat state is given by Eq. (126) where we choose $\|\vec{\alpha}\| = 6$. Finally, for the GKP state, Eq. (130), we numerically integrated a wave-function expression of the state with $s = 2$ and $\delta = 0.3$ to obtain the Wigner function.

space $\mathbb{R}^{2m}$ and define multimode Fock states as

$$\begin{aligned}&\left|n_{e_1}\right\rangle \otimes \cdots \otimes \left|n_{e_m}\right\rangle \\ &:= \frac{1}{\sqrt{n_1! \ldots n_m!}}[\hat{a}^\dagger(\vec{e}_1)]^{n_1} \ldots [\hat{a}^\dagger(\vec{e}_m)]^{n_m} |0\rangle\,, \end{aligned} \tag{119}$$

where the kth mode in the basis contains n_k photons. Note that for $n_k = 0$ we have a vacuum mode. For the Wigner function, this implies

$$W_{n_{e_1},\ldots,n_{e_m}}(\vec{x}) = W_{n_{e_1}}(\vec{x}_{\mathbf{e}_1}) \ldots W_{n_{e_m}}(\vec{x}_{\mathbf{e_f}}). \tag{120}$$

Here we use that the phase-space point $\vec{x}$ can be expressed as $\vec{x} = \vec{x}_{\mathbf{e_1}} \oplus \cdots \oplus \vec{x}_{\mathbf{e_m}}$, where $\vec{x}_{\mathbf{e_k}}$ is the phase-space coordinate within the subspace spanned by $\vec{e}_k$ and $\Omega\vec{e}_k$. We can note $\vec{x}_{\mathbf{e_k}} = (x_k, p_k)^T$, such that we find the coordinate representation $\vec{x} = (x_1, p_1, \ldots, x_m, p_m)^T$ in the chosen basis of phase space.

Non-Gaussian states do not necessarily have to be pure, they can also come in the form of statistical mixtures. The most basic example of such as state is a non-Gaussian mixture of Gaussian states. As a simple example, let is consider a mixture of two coherent states

$$\hat{\rho} = \frac{1}{2}\left(|\vec{\alpha}\rangle\langle\vec{\alpha}| + |-\vec{\alpha}\rangle\langle-\vec{\alpha}|\right). \tag{121}$$

Even though this is a highly classical state, it is still non-Gaussian as clearly seen from its Wigner function

$$W(\vec{x}) = \frac{1}{4\pi}\left(e^{-\frac{1}{2}\|\vec{x}-\vec{\alpha}\|^2} + e^{-\frac{1}{2}\|\vec{x}+\vec{\alpha}\|^2}\right). \tag{122}$$

Another important example of a non-Gaussian mixed state is

$$\hat{\rho}_\lambda = \lambda\,|0\rangle\langle 0| + (1-\lambda)\left|1_f\right\rangle\left\langle 1_f\right|. \tag{123}$$

In the mode $\vec{f}$, the Wigner function of the state behaves as

$$W_\lambda(\vec{x}) = [(1-\lambda)\|\vec{x}_{\mathbf{f}}\|^2 + 2\lambda - 1]\frac{e^{-\frac{1}{2}\|\vec{x}\|^2}}{2\pi}. \tag{124}$$

This Wigner function reaches negative values as long as $\lambda < 1/2$ and subsequently becomes positive. Nevertheless, it will remain non-Gaussian until $\lambda = 1$. As we see in Sec. C, even when the Wigner function is positive, it is not always possible to describe this state as a mixture of Gaussian states.

Generally speaking, non-Gaussian states can come in a wide variety of shapes, which can be much more exotic than the examples discussed above. A popular class of Gaussian states is obtained by taking coherent superpositions of Gaussian states. As we see in Sec. VII, there has been a strong experimental focus on two specific types of such states: Schrödinger's cat states [105] and GKP states [31]. The former are obtained by coherently superposing two coherent states, and often are split in even $|\text{cat}_+\rangle$ and odd $|\text{cat}_-\rangle$ cat states:

$$|\text{cat}_\pm\rangle := \frac{1}{\mathcal{N}}\left(|\vec{\alpha}\rangle \pm |-\vec{\alpha}\rangle\right), \tag{125}$$

where $\mathcal{N} = \sqrt{2(1 \pm \exp[-\|\vec{\alpha}\|^2])}$ is the normalization coefficient, which depends on the displacement $\vec{\alpha}$. The latter is often referred to as "the size of the cat." The Wigner function of these states resembles that of Eq. (122) but has an additional interference term

$$W_{\text{cat}_\pm}(\vec{x}) = \frac{e^{-\frac{1}{2}\|\vec{x}-\vec{\alpha}\|^2} + e^{-\frac{1}{2}\|\vec{x}+\vec{\alpha}\|^2} \pm \cos(\sqrt{2}\,\vec{\alpha}^T\vec{x})e^{-\frac{1}{2}\|\vec{x}\|^2}}{4\pi(1 \pm e^{-\|\vec{\alpha}\|^2})}. \tag{126}$$

The appearance of these interference terms creates several regions in phase space where the Wigner function attains negative values. The term "Schrödinger's cat state" has historically grown from the idea that coherent states describe classical electromagnetic fields and can thus be considered "macroscopic," in particular, for large values of $\|\vec{\alpha}\|$. However, one should honestly admit that they fail to capture an important point of Schrödinger's thought experiment [106]: the entanglement with a microscopic quantum system (i.e., the decay event that triggers the smashing of the vial of poison). Nevertheless, the term "cat state" has established itself firmly in the CV jargon, and now also lies at the basis of derived concepts such "cat codes" for error correction [107,108].

Finally, there are the GKP states. In their idealized form, they rely on eigenvectors of the quadrature operators (sometimes also known as infinitely squeezed states). To keep notation simple, we restrict to the single mode with quadrature operators $\hat{x}$ and $\hat{p}$. The eigenvectors of these operators are then formally written as

$$\hat{x}\,|x\rangle = x\,|x\rangle, \quad \text{and} \quad \hat{p}\,|p\rangle = p\,|p\rangle. \tag{127}$$

Furthermore, we have the relations $\langle x' \mid x\rangle = \delta(x'-x)$, $\langle p' \mid p\rangle = \delta(p'-p)$, and $\langle p \mid x\rangle = e^{-ipx}/\sqrt{2\pi}$. GKP states are constructed by considering a grid of such states to create a qubit, by identifying the two following GKP vectors:

$$\left|\text{GKP}_{\tilde{0}}\right\rangle := \sum_{k\in\mathbb{Z}} \left|x = 2k\sqrt{\pi}\right\rangle, \tag{128}$$

$$\left|\text{GKP}_{\tilde{1}}\right\rangle := \sum_{k\in\mathbb{Z}} \left|x = (2k+1)\sqrt{\pi}\right\rangle. \tag{129}$$

Clearly, these states are not normalizable and not physical as they would require infinite energy to be created. Thus, it is common to construct approximate GKP states,

by replacing the states $|x\rangle$ with displaced squeezed states, and by truncating the summation by adding a Gaussian envelope:

$$|\mathrm{GKP}_0\rangle := \mathcal{N}_0 \sum_{k\in\mathbb{Z}} e^{-2\pi[k\delta]^2} \hat{D}[2k\sqrt{\pi}]\,|s\rangle\,, \tag{130}$$

$$|\mathrm{GKP}_1\rangle := \mathcal{N}_1 \sum_{k\in\mathbb{Z}} e^{-2\pi[(k+1/2)\delta]^2} \hat{D}[(2k+1)\sqrt{\pi}]\,|s\rangle\,. \tag{131}$$

Here $\mathcal{N}_{0,1}$ are normalization constants and $|s\rangle$ is a single-mode squeezed vacuum, which implies that its Wigner function is given by Eq. (85) with $\vec{\xi} = (0,0)^T$ and $V = \mathrm{diag}[1/s, s]$ for $s > 1$. To get a good GKP state for quantum error correction, we generally need that $s \gg \sqrt{\pi}$. The Wigner function of an ideal GKP state is a grid of delta functions, which again highlights that it is a nonphysical state. The more realistic states $|\mathrm{GKP}_0\rangle$ and $|\mathrm{GKP}_1\rangle$ have well-defined Wigner functions, even though they are not very insightful to write down explicitly. In Fig. 2, we plot an example that was calculated numerically by taking into account only the first few terms around $k = 0$ in the sum.

GKP states may seem a little artificial at first glance, but they have been developed with a very clear purpose: to encode a qubit in a harmonic oscillator [31]. This encoding implies a notion of fault tolerance as these states are designed to be very efficient at correcting displacement errors. The more realistic incarnations of these states, Eq. (130), are therefore often proposed as candidates for encoding the information in CV quantum computation protocols [29]. Furthermore, it was shown that these states can also be used as the sole non-Gaussian resource to implement a CV quantum computer [32]

Once we progress into the realm of multimode states, the class of non-Gaussian states becomes even more vast. In Sec. 2, we present a dedicated introduction to multimode photon-subtracted states, which is a useful state to illustrate several of the concepts treated in this Tutorial. Furthermore, these states have a particular importance in CV quantum optics experiments. As a final example, we introduce another class of multimode non-Gaussian states, which have been highly relevant for quantum metrology: $N00N$ states [109–111]. Even though these states are very promising for quantum sensing with optical setups, the general idea that underlies these states was first introduced for fermions [112] in an attempt to mimic the advantage that is provided by squeezing in optics.

$N00N$ states are two-mode entangled states defined in a pair of orthogonal modes g_1 and g_2. The state contains exactly N photons, and is a superposition of a state with all photons being mode g_1 and a state with all photons in mode g_2:

$$|N00N\rangle := \frac{1}{\sqrt{2}}\left(\left|N_{g_1}\right\rangle + \left|N_{g_2}\right\rangle\right). \tag{132}$$

Here we recall that the state $\left|N_{g_1}\right\rangle$ can be trivially embedded to the full multimode space by adding vacuum in all other modes. We study these states in more detail for $N = 2$ in our discussion of the Hong-Ou-Mandel effect surrounding Eq. (165). However, here we highlight already that the Wigner function of $|N00N\rangle$ is not simply the sum of Wigner functions of the form Eq. (118). The entanglement will create additional interference terms, just like we saw in Eq. (126). In the present case, these interferences are genuinely multimode, and thus related to quantum correlations.

Experimentally, these states have been created and analyzed using a DV approach [113]. As we highlighted in Sec. C, the distinction between DV and CV is somewhat subtle and mainly depends on what is measured. Because $N00N$ states are built from Fock states and have a well-defined total photon number, they are most natural to analyze using photon-number-resolving detectors.

C. Quantum non-Gaussianity

Non-Gaussian states come in a wide variety, which means also that some of them are more exotic than others. Non-Gaussian states that are of limited interest, are those which are convex combinations of Gaussian states. Gaussian states do not form a convex set, after all, we can immediately see that, e.g., $[W_0(\vec{x} - \vec{\alpha}_1) + W_0(\vec{x} - \vec{\alpha}_2)]/2$ is not a Gaussian function even though it is a convex combination of Gaussian states.

The fact that the set of non-Gaussian states contains mixtures of Gaussian states may lead one to suspect that any mixed state with a positive Wigner function can be written as a well-chosen mixture of Gaussian states. After all, Gaussian states are the only pure states with positive Wigner functions. This intuition turns out to be false [89], which means that the set of states with a nonpositive Wigner function is not the same as the set of states that lie outside of the convex hull of Gaussian states $\mathcal{G}$. More formally, let us define

$$\mathcal{G} := \left\{\hat{\rho} \mid \hat{\rho} = \int \mathrm{d}\gamma\, p(\gamma)\hat{\rho}_G(\gamma)\right\}, \tag{133}$$

where γ is some arbitrary way of labelling Gaussian states $\hat{\rho}_G(\gamma)$ and $p(\gamma)$ is a probability distribution on these labels. Note that Eq. (103) tells us that we can generate all Gaussian states by taking convex combinations of displaced squeezed states, and thus we can limit ourselves to $\hat{\rho}_G(\gamma) = |\Psi_G(\gamma)\rangle\langle\Psi_G(\gamma)|$ in the definition of $\mathcal{G}$.

Any quantum state $\hat{\rho}$ that is not contained in the convex hull of Gaussian states, i.e., $\hat{\rho} \notin \mathcal{G}$, is referred to

as a "quantum non-Gaussian" state. The intuition behind this terminology is that Gaussian pure states are less quantum than non-Gaussian pure states that boast a non-positive Wigner function. A mixed state that is quantum non-Gaussian may have a positive Wigner function, but it cannot be created without adding states with nonpositive Wigner functions into the pure-state decomposition. Hence, these states are more quantum than the states that are in the convex hull of Gaussian states $\mathcal{G}$.

Next, one may wonder how to differentiate between states that are quantum non-Gaussian and states which are in the convex hull $\mathcal{G}$. Throughout the last decade, many methods have been developed to answer this question. We start by introducing the main idea of Ref. [114] because it is based on the Wigner function. The key idea is that Gaussian distributions have tails, which means that we can take an arbitrary pure Gaussian state $W_0[S^{-1}(\vec{x}-\vec{\alpha})]$, and evaluate the Wigner function at to origin of phase space:

$$W_0(S^{-1}\vec{\alpha}) = \frac{e^{-\frac{1}{2}\|S^{-1}\vec{\alpha}\|^2}}{(2\pi)^2}. \tag{134}$$

Clearly, when $\|S^{-1}\vec{\alpha}\|^2 \to \infty$, we do find that $W_0(S^1\vec{\alpha}) \to 0$. This limit essentially corresponds to a system with infinite energy. It is thus natural to try to bound the value of the Wigner function in the origin by a function that depends on the energy $\overline{N}$ of the state. For an arbitrary pure Gaussian state, we find that

$$\overline{N} = \sum_{j=1}^{m} \mathrm{tr}[\hat{\rho}\hat{a}^\dagger(\vec{e}_j)\hat{a}(\vec{e}_j)] = \frac{1}{4}\left(\mathrm{tr}[S^T S - \mathbb{1}] + \|\vec{\alpha}\|^2\right). \tag{135}$$

Using the properties of the operator norm, we write $\|S^{-1}\vec{\alpha}\|^2 = \|S^{-1}O\vec{\alpha}\|^2$, where O is a symplectic orthogonal transformation. Furthermore, we note that $\|\vec{\alpha}\|^2 = \|O\vec{\alpha}\|^2$. It is then useful to explicitly write the coordinate representation of the vector $O\vec{\alpha} = (\alpha_1^{(x)}, \alpha_1^{(p)}, \ldots, \alpha_m^{(x)}, \alpha_m^{(p)})^T$, such that

$$\overline{N} = \sum_{j=1}^{m} \frac{1}{4}\left(s_j + \frac{1}{s_j} + (\alpha_j^{(x)})^2 + (\alpha_j^{(p)})^2 - 2\right) \tag{136}$$

$$= \sum_{j=1}^{m} \overline{n}_j. \tag{137}$$

At the same time, we expand

$$\|S^{-1}\vec{\alpha}\|^2 = \sum_{j=1}^{m} s_j(\alpha_j^{(x)})^2 + \frac{(\alpha_j^{(p)})^2}{s_j}, \tag{138}$$

and with a little algebra we can show that

$$\frac{1}{2}\|S^{-1}\vec{\alpha}\|^2 \leqslant \sum_{j=1}^{m} 4\overline{n}_j(2\overline{n}_j + 1) \leqslant 4\overline{N}(2\overline{N}+1), \tag{139}$$

such that

$$W_0(S^{-1}\vec{\alpha}) \geqslant \frac{1}{(2\pi)^m} e^{-4\overline{N}(2\overline{N}+1)}. \tag{140}$$

This means that the value of the Wigner function of a pure Gaussian state in the origin of phase space is bounded from below by a function of the average number of particles $\overline{N}$. However, it is not obvious that we can extend this bound to arbitrary mixtures of Gaussian states. Let us assume that $\hat{\rho} \in \mathcal{G}$, then the Wigner function in the origin is given by

$$W(\vec{0}) = \int \mathrm{d}\gamma\, p(\gamma) W_0(S_\gamma^{-1}\vec{\alpha}_\gamma), \tag{141}$$

where we saw that $W_0(S_\gamma^{-1}\vec{\alpha}_\gamma)$ is the value of a pure Gaussian state's Wigner function in the origin and γ is some arbitrary label for the Gaussian states in the mixture. Therefore we can bound the states in the convex combination

$$W(\vec{0}) \geqslant \frac{1}{(2\pi)^m} \int_0^\infty \mathrm{d}\overline{N}_\gamma \tilde{p}(\overline{N}_\gamma) e^{-4\overline{N}_\gamma(2\overline{N}_\gamma+1)}, \tag{142}$$

where we introduce a probability distribution $\tilde{p}$ on the average particle numbers of the pure Gaussian states in the mixture. The overall average number of particles in the state $\hat{\rho}$ is then given by $\overline{N} = \int_0^\infty \mathrm{d}\overline{N}_\gamma\, \tilde{p}(\overline{N}_\gamma)\overline{N}_\gamma$. The final element that we require is the fact that $\exp[-4\overline{N}_\gamma(2\overline{N}_\gamma + 1)]$ is a convex function, such that we can apply Jensen's inequality to find that

$$\hat{\rho} \in \mathcal{G} \implies W(\vec{0}) \geqslant \frac{1}{(2\pi)^m} e^{-4\overline{N}(2\overline{N}+1)}. \tag{143}$$

This means that we can simply use the total energy of the state to construct a witness for quantum non-Gaussianity. This clearly shows that there are quantum non-Gaussian states with positive Wigner functions. An explicit example can be constructed by tuning the γ in the state $[(1-\gamma)|0\rangle\langle 0| + \gamma|1_{\vec{f}}\rangle\langle 1_{\vec{f}}|]$ to $1/2 > \gamma > 1/2 - e^{-4\gamma(2\gamma+1)}$ (where we use that γ is also the average particle number in this particular state).

Nevertheless, there are many quantum non-Gaussian states that do not violate inequality (143). After all, why would the origin of phase space be the most interesting point? A first solution is provided in Ref. [114], where it is

argued that

$$\hat{\rho} \in \mathcal{G} \implies W_\Gamma(\vec{0}) \geqslant \frac{1}{(2\pi)^m} e^{-4\overline{N}_\Gamma(2\overline{N}_\Gamma+1)}, \tag{144}$$

for all Gaussian channels Γ that act on the Wigner function of $\hat{\rho}$ as $W(\vec{x}) \overset{\Gamma}{\mapsto} W_\Gamma(\vec{x})$. Recall that the action of a Gaussian channel was defined in Eq. (102). The quantity $\overline{N}_\Gamma$ then denotes the average number of particles in the state $\Gamma(\hat{\rho})$. Further generalizations of this scheme have been worked out in Ref. [115]. Moreover, Ref. [116] has considered combinations of the value of the Wigner function in several points to reach better witnesses for quantum non-Gaussianity. Further progress has been made by identifying observables that are more easily measurable with typical CV techniques [117]. Others have considered other phase-space representations of the state to identify witnesses of quantum non-Gaussianity [118,119].

Quantum non-Gaussianity has been investigated with a wide range of tools. In this Tutorial we have limited ourselves to phase-space methods in the spirit of the CV approach. However, there is also a significant body of work on quantum non-Gaussianity using techniques that are more typical in DV quantum optics. The earliest works on the subject used photon statistics to distinguish quantum non-Gaussian states from convex mixtures of Gaussian states [89]. This research line has been continued in recent years to uncover new aspects of quantum non-Gaussian states, such as the "non-Gaussian depth" [120] and techniques to differentiate different types of multiphoton states [121]. Ultimately, these photon-counting techniques were extended to develop a whole hierarchy of quantum non-Gaussian states [37]. These ideas have been further formalized and generalized through the notion of the "stellar rank" of a quantum state.

D. Stellar rank

An interesting starting point to introduce the stellar representation is the method [103] to prove Hudson's theorem. We recall the definition

$$F^\star_\Psi(\vec{\alpha}) := \langle \vec{\alpha} \mid \Psi \rangle e^{\frac{1}{8}\|\vec{\alpha}\|^2},$$

of what we henceforth refer to as the stellar function. To avoid technical complications, let us now restrict ourselves to single-mode systems such that the optical phase space is $\mathbb{R}^2$. Note that, in a single-mode system, there is only one creation operator $\hat{a}^\dagger$ with associated annihilation operators $\hat{a}$. We can then follow Ref. [38] to introduce the stellar representation of single-mode quantum states. Note that some similar ideas are also present in other works [122].

First, we develop the stellar representation for pure states, which will then be used to generalize the framework to mixed states in Eq. (148). We use the definition of the displacement operator to show that

$$|\Psi\rangle = F^\star_\Psi(\hat{a}^\dagger)\,|0\rangle\,, \tag{145}$$

which immediately implies that the stellar representation is unique. In other words, if $F^\star_\Psi = F^\star_\Phi$ it follows that $|\Psi\rangle = |\Phi\rangle$ up to a phase. In our proof of Hudson's theorem, we have already highlighted that $F^\star_\Psi$ satisfies the property (116), which means that it is an entire function with growth order $r = 2$. Because in this single-mode setting $F^\star_\Psi$ can be interpreted as a function of a single complex variable, the Hadamard-Weierstrass theorem implies that $F^\star_\Psi$ can be fully represented by its zeros (one can consider this as a generalization of the fundamental theorem of calculus). This thus implies that a single-mode state is completely determined by the zeros of the $F^\star_\Psi$, and thus by the zeros of the Q function in Eq. (115).

It is thus natural to use these zeros in order to classify pure single-mode quantum states and thus the stellar rank is introduced. Ultimately, the stellar rank is simply given by the number of zeros of $F^\star_\Psi$ or alternatively the number of zeros of the Q function. Because in practice zeros may coincide, one should also consider the multiplicity of the zeros. We thus define the stellar rank $r^\star(\Psi)$ of $|\Psi\rangle$ as the number of zeros of $F^\star_\Psi : \mathbb{C} \mapsto \mathbb{C}$ counted with multiplicity. Alternatively one may count the zeros of the Q function with multiplicity and divide by two.

The fact that a state is fully characterized by its stellar representation $F^\star_\Psi$ can be made more explicit by considering the roots $\{\vec{\alpha}_1, \ldots, \vec{\alpha}_{r^\star(\Psi)}\}$ of the Q function, which represents $|\Psi\rangle$ [note that we use (44) to interchange between phase-space representation and complex Hilbert-space representation]. The single-mode state $|\Psi\rangle$ can then be used to express

$$|\Psi\rangle = \frac{1}{\mathcal{N}} \prod_{j=1}^{r^\star(\Psi)} \hat{D}^\dagger(\vec{\alpha}_j)\hat{a}^\dagger\hat{D}(\vec{\alpha}_j)\,|\Psi_G\rangle\,, \tag{146}$$

where $|\Psi_G\rangle$ is a pure Gaussian state and $\mathcal{N}$ a normalization constant. We can then use the stellar rank to induce some further structure in the set of states by defining

$$\mathcal{R}_N := \{|\Psi\rangle \mid r^\star(\Psi) = N\}. \tag{147}$$

that groups all states of stellar rank N. Note that the Hadamard-Weierstrass theorem also considers functions with an infinite amount of zeros and the case $N = \infty$ is thus mathematically well defined. It turns out that this case is not just a pathological limit. An evaluation of the Q function shows that Gottesman-Kitaev-Preskill states and Schrödinger cat states inhabit the set $\mathcal{R}_\infty$.

Clearly, all that was introduced so far only works for pure states. We can naturally extend this result via a convex

roof construction, by defining

$$r^\star(\hat{\rho}) := \inf_{\{p(\gamma),|\Psi(\gamma)\rangle\}} \sup_{\gamma}\{r^\star[\Psi(\gamma)]\}, \tag{148}$$

where the infimum is considered of all probability distributions on the set of pure states that lead to $\hat{\rho} = \int \mathrm{d}\gamma p(\gamma)\,|\Psi(\gamma)\rangle\langle\Psi(\gamma)|$. In words, there are many ways to decompose the state $\hat{\rho}$ in pure states and we consider all of them. For each decomposition, we define the stellar rank as the highest rank of the states in the decomposition. Then we minimize these values over all possible decompositions to arrive at the stellar rank of $\hat{\rho}$.

Convex roof constructions are commonly used to treat mixed states as they are easy and natural to formally define. However, they are often much harder to calculate in practice. This is where the stellar representation unveils its most remarkable property: stellar robustness. To formalize this idea, Ref. [38] introduced the robustness as the trace distance between the state and the nearest possible state of lower stellar rank.

$$R^\star(\Psi) := \inf_{r^\star(\hat{\rho})<r^\star(\Psi)} \frac{1}{2}\mathrm{tr}\sqrt{(|\Psi\rangle\langle\Psi| - \hat{\rho})^2}. \tag{149}$$

And it can be shown that

$$R^\star(\Psi) = \sqrt{1 - \sup_{r^\star(\hat{\rho})<r^\star(\Psi)} \langle\Psi|\,\hat{\rho}\,|\Psi\rangle}, \tag{150}$$

where $\langle\Psi|\,\hat{\rho}\,|\Psi\rangle$ is the fidelity of $\hat{\rho}$ with target state $|\Psi\rangle$. Remarkably, it can be shown that $R^\star(\Psi) > 0$ when $r^\star(\Psi) < \infty$ [38]. This means that any state that is sufficiently close to a pure state of $r^\star(\Psi)$ is also of rank $r^\star(\Psi)$ or higher.

The idea of stellar robustness can be generalized [123] by introducing k robustness. For any $k < r^\star(\Psi)$, we define

$$R_k^\star(\Psi) := \inf_{r^\star(\Phi)\leqslant k} \sqrt{1 - |\langle\Phi \mid \Psi\rangle|^2}, \tag{151}$$

and show subsequently that

$$R_k^\star(\Psi) = \sqrt{1 - \sup_{r^\star(\hat{\rho})\leqslant k} \langle\Psi|\,\hat{\rho}\,|\Psi\rangle}. \tag{152}$$

The k robustness can thus be interpreted as the nearest distance from a state $|\Psi\rangle$ at which we can find any state of stellar rank k, provided $k < r^\star(\Psi)$. Beyond showing that $R_k^\star(\Psi)$ is nonzero when $|\Psi\rangle$ is of finite stellar rank, Ref. [123] also provides an explicit method to calculate $R_k^\star(\Psi)$. Thus, for whichever state $\hat{\rho}$ is available in an experiment one can attempt to find a pure target state $|\Psi\rangle$ for which $\langle\Psi|\,\hat{\rho}\,|\Psi\rangle > 1 - R_k^\star(\Psi)^2$ to prove that $\hat{\rho}$ is at least of stellar rank k.

We note that for pure states $r^\star(\Psi) = 0$ implies that the state is Gaussian (this is essentially what is proven in Hudson's theorem). From the definition (148) we can then deduce that

$$r^\star(\hat{\rho}) = 0 \iff \hat{\rho} \in \mathcal{G}, \tag{153}$$

where $\mathcal{G}$ denotes, again, the convex hull of Gaussian states. On the other hand, states for which $r^\star(\hat{\rho}) > 0$ cannot be written as a mixture of Gaussian states and are thus quantum non-Gaussian.

This idea can be extended by using the stellar k robustness, Eq. (152), as a witness of quantum non-Gaussianity. When we want to check whether $\hat{\rho}$ is quantum non-Gaussian, it suffices to find a pure target state $|\Psi\rangle$ such that $\hat{\rho}$ is closer to $|\Psi\rangle$ than the 1 robustness $R_k^\star(\Psi)$. More formally written, whenever a pure state $|\Psi\rangle$ exists with the following property:

$$\langle\Psi|\,\hat{\rho}\,|\Psi\rangle > 1 - R_1^\star(\Psi)^2 \implies \hat{\rho} \notin \mathcal{G}, \tag{154}$$

and $\hat{\rho}$ is quantum non-Gaussian. This may seem like a complicated challenge, but for a single-photon state $|\Psi\rangle = |1\rangle$ we find that $1 - R_1^\star(\Psi)^2 \approx 0.478$ [123]. This means that any state that has a fidelity of more than 0.478 with respect to a Fock state is quantum non-Gaussian. This idea can be extended to higher stellar ranks: whenever we find a target state $|\Psi\rangle$ such that $\langle\Psi|\,\hat{\rho}\,|\Psi\rangle > 1 - R_k^\star(\Psi)^2$, the state $\hat{\rho}$ is at least of stellar rank k. Note that the fidelity of an experimentally generated state $\hat{\rho}$ with any pure target state $|\Psi\rangle$ can be calculated from double homodyne measurements on $\hat{\rho}$ [123]. There is no need to experimentally create the pure state $|\Psi\rangle$, the latter is just theoretical input needed to analyze the data.

Obviously, the stellar rank imposes a lot of additional structure on the state space. It rigorously orders all states that can be achieved by combining a finite number of creation operators and Gaussian transformations. The creation operator serves as a tool to increase the stellar rank by one and the stellar rank actually corresponds to the minimal number of times the creation operator must be applied to obtain the state, together with Gaussian operations. The stellar rank remains unchanged under Gaussian unitary transformations, which makes sense for a measure of the non-Gaussian character of the state, and thus it falls within the set of intrinsic properties of a state as discussed in Sec. C. Furthermore, the class of states with infinite stellar rank can be understood as the set that contains the most exotic states. However, it is lonely at the top as it can be shown that $R_\infty^\star(\Psi) = 0$ for states of infinite rank. This means that we can find states of finite stellar rank arbitrarily close to a state of infinite stellar rank. As stressed in Ref. [38], this implies that finite-rank states are dense in the full Fock space and any state of infinite rank can be arbitrarily well approximated by finite-rank states. Whereas a finite

stellar rank k of any experimental state can be certified by achieving a sufficiently high fidelity to a target state $|\Psi\rangle$ to fall within the range given by its k robustness $R_k^\star(\Psi)$, a similar procedure is impossible for infinite stellar ranks. This means, in practice, that genuinely infinite-rank states are impossible to certify in experiments because one never achieves perfect fidelity. Nevertheless, different states of infinite rank may differ significantly in the values $R_k^\star(\Psi)$ for $k < \infty$.

Many of the results on stellar rank rely on the Hadamard-Weierstrass theorem that allows one to uniquely factorize $F_\Psi^\star(\vec{\alpha})$ as a Gaussian and a polynomial, where the roots of the polynomial are the roots of $F_\Psi^\star$ and thus also the roots of the Q function. Sadly, this theorem cannot be straightforwardly generalized to a multimode setting, which is known in mathematics as Cousin's second problem [124]. Notable progress was made in Ref. [125] where one studies multimode stellar functions, which are polynomials and it was shown that there is no straightforward generalization of Eq. (146).

E. Wigner negativity

Hudson's theorem shows us that all pure non-Gaussian states have nonpositive Wigner functions, which sets them apart from normal probability distributions of phase space. For mixed states, this no longer holds and thus we spent the previous two sections developing methods to characterize the non-Gaussian features of these states. Whether it is through quantum non-Gaussianity or the more refined stellar rank, these methods focus on characterizing the non-Gaussian resources that are required to generate a certain state. In this subsection, we change the perspective and focus rather on negative values of the Wigner function ("Wigner negativity" in short) as a resource of interest.

Wigner negativity has the advantage of being a clear quantum feature, it reflects that different quadratures in the same mode cannot be jointly measured and thus goes hand in hand with the principle of complementarity. More formally, it has even been connected to the principle of quantum contextuality [64]. Indeed, in Sec. VI we elaborate on the fact that Wigner negativity is a necessary resource for reaching a quantum advantage, i.e., performing a task that cannot be efficiently simulated by a classical computer. However, the idea of using Wigner negativity as a signature of nonclassicality was already around before it was connected to a quantum computational advantage. An important step to formalize this idea was the introduction of a measure for Wigner negativity [90], which lies at the basis of recent resource theories of Wigner negativity [100,126].

A priori, there are several natural measures than can be used for Wigner negativity. It is therefore useful to consider some desirable properties that are required for a measure of Wigner negativity. First of all, we want the measure to be zero if and only if the Wigner function is positive. It seems natural to demand that, furthermore, Wigner negativity remains unchanged under Gaussian unitary transformations. It is then tempting to simply consider the absolute value of the lowest possible value of the Wigner function, but this would have some unnatural outcomes. It would mean that a single-photon state would have more Wigner negativity than a two-photon state. We thus need to look for a different measure.

The starting point of Ref. [90] is that the normalization of the Wigner function implies that

$$\int_{\mathbb{R}^{2m}} \mathrm{d}\vec{x}\, |W(\vec{x})| \geqslant 1, \tag{155}$$

and that the inequality is strict whenever there is Wigner negativity. Furthermore, Liouville's theorem implies that integrals over phase space are unchanged by Gaussian transformations. A first possible way of measuring Wigner negativity is through the negativity volume

$$\mathcal{N}(\hat{\rho}) := \int_{\mathbb{R}^{2m}} \mathrm{d}\vec{x}\, |W(\vec{x})| - 1. \tag{156}$$

This measure has the major advantage of being convex due to the triangle inequality, which means that for $\hat{\rho} = \int \mathrm{d}\gamma p(\gamma)\hat{\rho}(\gamma)$ we find that

$$\mathcal{N}(\hat{\rho}) \leqslant \int \mathrm{d}\gamma p(\gamma)\mathcal{N}[\hat{\rho}(\gamma)]. \tag{157}$$

However, this measure is not additive, i.e., $\mathcal{N}(\hat{\rho}_1 \otimes \hat{\rho}_2) \neq \mathcal{N}(\hat{\rho}_1) + \mathcal{N}(\hat{\rho}_2)$. To circumvent this shortcoming, another measure for Wigner negativity has been introduced [100, 126,127]:

$$\mathfrak{N}(\hat{\rho}) := \log \int_{\mathbb{R}^{2m}} \mathrm{d}\vec{x}\, |W(\vec{x})|\,. \tag{158}$$

Clearly, $\mathfrak{N}(\hat{\rho}_1 \otimes \hat{\rho}_2) = \mathfrak{N}(\hat{\rho}_1) + \mathfrak{N}(\hat{\rho}_2)$ making this measure additive. However, the introduction of the logarithm destroys the convexity of the measure. Note that the two measures are closely related by $\mathfrak{N}(\hat{\rho}) = \log[\mathcal{N}(\hat{\rho}) + 1]$. Thus when $\mathcal{N}(\hat{\rho}_1) > \mathcal{N}(\hat{\rho}_2)$, we also find that $\mathfrak{N}(\hat{\rho}_1) > \mathfrak{N}(\hat{\rho}_2)$.

The single-mode examples that are considered in Ref. [90] lead to some interesting observations. First of all, they show that for Fock states Wigner negativity increases with the photon number. Furthermore, they show that for Schrödinger cat states the integral is bounded from above by a value smaller than the Wigner negativity of a two-photon state. Even though Fock states of increasing stellar rank have increasing Wigner negativity, there is no clear relation between stellar rank and Wigner negativity for more general classes of states. For example, Schrödinger

cat states are of infinite stellar rank, suggesting that they are in this regard the most exotic states, but they manifest only a limited amount of Wigner negativity.

As a case study, let us briefly concentrate on the Wigner negativity of Fock states, Eq. (117). One can now evaluate the Wigner negativity of such states to find that

$$\mathcal{N}(|1\rangle) \approx 0.426\,12 \quad \text{and} \quad \mathfrak{N}(|1\rangle) \approx 0.354\,959, \tag{159}$$

$$\mathcal{N}(|2\rangle) \approx 0.728\,99 \quad \text{and} \quad \mathfrak{N}(|2\rangle) \approx 0.547\,537, \tag{160}$$

$$\mathcal{N}(|3\rangle) \approx 0.976\,67 \quad \text{and} \quad \mathfrak{N}(|3\rangle) \approx 0.681\,415, \tag{161}$$

which shows that the negativity does not simply increase linearly with the number of photons even for the additive measure $\mathfrak{N}$. However, let us now look at a multimode n-photon state where each photon occupies a different mode, i.e., a Fock state generated by creation operators in $\vec{f}_1, \ldots, \vec{f}_n$ with $\text{span}\{\vec{f}_j, \Omega\vec{f}_j\} \neq \text{span}\{\vec{f}_k, \Omega\vec{f}_k\}$ for all $j \neq k$,

$$\hat{a}^\dagger(\vec{f}_1)\ldots\hat{a}^\dagger(\vec{f}_n)\,|0\rangle = \left|1_{f_1}\right\rangle \otimes \cdots \otimes \left|1_{f_n}\right\rangle. \tag{162}$$

The Wigner function for this state can be shown to be [showing this based on (38) is again a good exercise]

$$W_{1_{f_1},\ldots,1_{f_n}}(\vec{x}_{\mathbf{f_1}} \oplus \cdots \oplus \vec{x}_{\mathbf{f_n}}) = \prod_{k=1}^{n} W_{1_{f_k}}(\vec{x}_{\mathbf{f_k}}). \tag{163}$$

Either by explicitly using the expression of the Wigner function, or by using the additivity property, we find that

$$\mathfrak{N}\left(\left|1_{f_1}\right\rangle \otimes \cdots \otimes \left|1_{f_n}\right\rangle\right) = n\mathfrak{N}(|1\rangle). \tag{164}$$

Numerically, we can show that $n\mathfrak{N}(|1\rangle) > \mathfrak{N}(|n\rangle)$ and thus we can generally conclude that n photons in different modes hold more Wigner negativity than n photons in the same mode.

Let us now concentrate on the case where $n = 2$. We showed that two photons in different modes are more Wigner negative than two photons in the same mode, and now we combine this finding with the idea that Wigner negativity remains unchanged under Gaussian transformations. A particularly simple Gaussian transformation is a balanced beam splitter, which ultimately just implements a change in mode basis that we describe by an orthonormal transformation O_{BS}. When we mix two photons, prepared in orthogonal modes f_1 and f_2 by such a balanced beam splitter, we see the Hong-Ou-Mandel effect in action (more details can be found in Ref. [56] where a similar notation is used):

$$\left|1_{f_1}\right\rangle \otimes \left|1_{f_2}\right\rangle \overset{O_{\text{BS}}}{\mapsto} \frac{1}{\sqrt{2}}\left(\left|2_{g_1}\right\rangle - \left|2_{g_2}\right\rangle\right) := |\text{HOM}\rangle\,, \tag{165}$$

where f_1, f_2 and g_1, g_2 are the input and output modes of the beam splitter, respectively. The Hong-Ou-Mandel output state $|\text{HOM}\rangle$ is thus a superposition of two photons in mode g_1 and two photons in mode g_2. We can now use the simple fact that Wigner negativity is unchanged under Gaussian unitary transformations to show that

$$\mathfrak{N}(|\text{HOM}\rangle) = \mathfrak{N}\left(\left|1_{f_1}\right\rangle \otimes \left|1_{f_2}\right\rangle\right) = 2\mathfrak{N}(|1\rangle) > \mathfrak{N}(|2\rangle), \tag{166}$$

this then also implies that $\mathcal{N}(|\text{HOM}\rangle) > \mathcal{N}(|2\rangle)$. At first sight, this is somewhat of a peculiar finding: by taking a superposition of two states with the same Wigner negativity one finds a state with a higher Wigner negativity.

An explicit look at the Wigner function of the Hong-Ou-Mandel state $|\text{HOM}\rangle$ provides some insight. We find that this Wigner function can be written as (yet again a good exercise to show this explicitly)

$$\begin{aligned} W_{\text{HOM}}(\vec{x}_{\mathbf{g_1}} \oplus \vec{x}_{\mathbf{g_2}}) =& \frac{1}{2}[W_{2_{g_1}}(\vec{x}_{\mathbf{g_1}}) + W_{2_{g_2}}(\vec{x}_{\mathbf{g_2}})] \\ &+ W_{\text{int}}(\vec{x}_{\mathbf{g_1}} \oplus \vec{x}_{\mathbf{g_2}}), \end{aligned} \tag{167}$$

where W_{int} is the contribution to the Wigner function that contains all the interference terms that are induced by the superposition. We can calculate that

$$\mathcal{N}\left(\frac{1}{2}[W_{2_{g_1}}(\vec{x}_{\mathbf{g_1}}) + W_{2_{g_2}}(\vec{x}_{\mathbf{g_2}})]\right) \leqslant \mathcal{N}(|2\rangle), \tag{168}$$

and thus, by additionally applying the triangle inequality, we can understand that the additional negativity in the Hong-Ou-Mandel state is due to the term W_{int}.

In the Hong-Ou-Mandel effect, it is common to talk about interference between particles, but in a more general CV language this interference will be equivalent to some form of entanglement, which is exactly described by the Wigner-function contribution W_{int}. In other words, the superposition between $\left|2_{g_1}\right\rangle$ and $\left|2_{g_2}\right\rangle$ has more Wigner negativity than each of its two constituents because it creates entanglement between the modes g_1 and g_2. This is a first indication that there is a connection between quantum correlations and non-Gaussian features of the Wigner function. We explore this connection in further detail in Sec. V.

Even though Wigner negativity is an important non-Gaussian feature, it is often hard to witness [128]. The most common experimental technique is homodyne tomography [129] to fully reconstruct the quantum state. These methods come with the inconvenience that it is hard to set good error bars. Techniques to circumvent the need for a full tomography have been developed based on homodyne [130] and double-homodyne (or heterodyne) measurements [123,128]. These methods come with the advantage of permitting to put a degree of confidence on the proclaimed Wigner negativity.

IV. CREATING NON-GAUSSIAN STATES

In Sec. III we have discussed the many ways of characterizing non-Gaussian quantum states and their properties. In this section, we explore the different theoretical frameworks for creating these states. An overview of some important experimental advances to put these theoretical techniques into practice is left for Sec. VII.

Gaussian quantum states can in some sense be understood as naturally occurring states. The foundational work of Planck that lies at the basis of all of quantum mechanics provides a first description of the thermal states of light that describe black-body radiation. In a more modern language, we refer to this as the thermal states of an ensemble of quantum harmonic oscillators or a free bosonic field. It has long been understood that these states are Gaussian [2–4]. Creating this kind of Gaussian states of light is thus literally as simple as switching on a light bulb.

When we turn towards more sophisticated light sources such as lasers, we can encounter coherent light that is described by coherent states [5,6]. Generating squeezed light becomes much harder and typically requires nonlinear optics [131]. Nevertheless, pumping a nonlinear crystal with a coherent pump generally suffices to deterministically create a squeezed state [132]. Recall from the end of Sec. D that from a theoretical point of view all these pure Gaussian states can be created by applying Gaussian unitary transformation to the vacuum state.

From an experimental point of view, the creation of non-Gaussian states is much harder than the creation of their Gaussian counterparts. Nevertheless, we start by introducing an ideal theoretical approach that is not too different from Gaussian states. In essence, it suffices to apply a non-Gaussian unitary operation to the state to create a non-Gaussian state. In Sec. A we dig deeper into the desired structure of such non-Gaussian unitary transformations that would in principle allow for the deterministic generation of non-Gaussian quantum states. In experiments (in particular, those in optics) such non-Gaussian unitary transformations are hard to come by, which is why one very often uses different preparation schemes. In Sec. B, we provide a general introduction into the conditional preparation of non-Gaussian quantum states, where one measures part of the system and conditions on a certain measurement outcome. This process projects the remainder of the system into a new non-Gaussian state.

A. Deterministic methods

To introduce some further structure in the sets of Gaussian and non-Gaussian unitary transformations, it is useful to take a quantum computation approach that is inspired by Ref. [26,133]. The central idea of this work is that Gaussian unitary transformations are always generated by "Hamiltonians" that are at most quadratic in the quadrature operators (or equivalently in the creation and annihilation operators). Let us denote that as

$$\hat{U}_G = \exp\{i\mathcal{P}_2(\hat{q})\} \tag{169}$$

where the polynomials $\mathcal{P}_2(\hat{q})$ are generated by combining terms of the types $\mathbb{1}$, $\hat{q}(\vec{f})$, and $\hat{q}(\vec{f}_1)\hat{q}(\vec{f}_2)$. A remarkable property of these three types of observables is that they are closed under the action of a commutator. Indeed, using the canonical commutation relation (29) and the general properties of commutators, we can show that

$$[\hat{q}(\vec{f}_1), \hat{q}(\vec{f}_2)] \sim \mathbb{1}, \tag{170}$$

$$[\hat{q}(\vec{f}_1), \hat{q}(\vec{f}_2)\hat{q}(\vec{f}_3)] \sim \hat{q}(\vec{f}\,'), \tag{171}$$

$$[\hat{q}(\vec{f}_1)\hat{q}(\vec{f}_2), \hat{q}(\vec{f}_3)\hat{q}(\vec{f}_4)] \sim \sum \hat{q}(\vec{f}_1{}')\hat{q}(\vec{f}_2{}'). \tag{172}$$

Thus, we can use the Baker-Campbell-Hausdorff formula to show that the combination of two Gaussian unitaries $\hat{U}_G\hat{U}'_G$ is again a Gaussian unitary.

This notion lies at the basis of universal gate sets in the CV approach. Using typical techniques from Lie groups, we can look for a minimal set of Gaussian unitaries than can be combined to generate all possible Gaussian unitary transformations. Generally, such a set is clearly not unique, but there are some natural choices. For example, we previously saw that a Gaussian unitary transformation is a combination of displacement operations and symplectic transformations. Furthermore, the Bloch-Messiah decomposition (95) shows us that any symplectic transformation can be decomposed into a combination of multimode interferometers and single-mode squeezing. In turn, interferometers can be decomposed as a combination of beam splitters and phase shifters [134]. Indeed, we can choose the set of Gaussian gates to be

$$\hat{U}_D(\vec{\lambda}) := \hat{D}(\vec{\lambda}), \tag{173}$$

$$\hat{U}_S(\vec{\lambda}) := \exp i[\hat{q}(\vec{\lambda})\hat{q}(\Omega\vec{\lambda}) + \hat{q}(\Omega\vec{\lambda})\hat{q}(\vec{\lambda})], \tag{174}$$

$$\hat{U}_P(\vec{\lambda}) := \exp i[\hat{q}(\vec{\lambda})^2 + \hat{q}(\Omega\vec{\lambda})^2], \tag{175}$$

$$\hat{U}_{\mathrm{BS}}(\vec{\lambda}_1, \vec{\lambda}_2) := \exp i[\hat{q}(\vec{\lambda}_1)\hat{q}(\vec{\lambda}_2) + \hat{q}(\Omega\vec{\lambda}_1)\hat{q}(\Omega\vec{\lambda}_2)], \tag{176}$$

where we note that $\vec{\lambda}, \vec{\lambda}_1, \vec{\lambda}_2 \in \mathbb{R}^{2m}$ are not normalized and $\vec{\lambda}_1 \perp \vec{\lambda}_2$. These unitary operators describe a displacement, a squeezer, a phase shifter, and a beam splitter, respectively. We note that all these operations act on a single mode, except for the beam splitter, which connects a pair of modes. These transformations are referred to as a Gaussian gate set; when we can implement all these gates in all the modes of some mode basis, we can generate any multimode Gaussian transformation, and thus any Gaussian state.

To generate non-Gaussian unitary transformations and thus non-Gaussian states, we need to add more unitary

gates to the Gaussian gate set. The relevant question is thus how many gates one should add and which gates are the best choices. The answer to the first question is surprising: one needs to add just one single gate [27]. The argument is simple, when we consider the operators $\hat{q}(\vec{\lambda})^3$, we find that

$$\begin{aligned}[\hat{q}(\vec{\lambda}_1)^3, \hat{q}(\vec{\lambda}_2)^n] =& \hat{q}(\vec{\lambda}_1)^2[\hat{q}(\vec{\lambda}_1), \hat{q}(\vec{\lambda}_2)^n] \\ &+ [\hat{q}(\vec{\lambda}_1), \hat{q}(\vec{\lambda}_2)^n]\hat{q}(\vec{\lambda}_1)^2 \\ &+ \hat{q}(\vec{\lambda}_1)[\hat{q}(\vec{\lambda}_1), \hat{q}(\vec{\lambda}_2)^n]\hat{q}(\vec{\lambda}_1). \quad (177)\end{aligned}$$

With the canonical commutation relations we can show that $[\hat{q}(\vec{\lambda}_1), \hat{q}(\vec{\lambda}_2)^n] \sim \hat{q}(\vec{\lambda}_2)^{n-1}$, which can be inserted into Eq. (177) to obtain

$$\begin{aligned}[\hat{q}(\vec{\lambda}_1)^3, \hat{q}(\vec{\lambda}_2)^n] \sim& \hat{q}(\vec{\lambda}_1)^2\hat{q}(\vec{\lambda}_2)^{n-1} + \hat{q}(\vec{\lambda}_2)^{n-1}\hat{q}(\vec{\lambda}_1)^2 \\ &+ \hat{q}(\vec{\lambda}_1)\hat{q}(\vec{\lambda}_2)^{n-1}\hat{q}(\vec{\lambda}_1). \quad (178)\end{aligned}$$

This calculation thus shows that commutation with the operators $\hat{q}(\vec{\lambda})^3$ increases the order of the quadrature operators. Thus, with the quadratic Hamiltonians to generate all operations that conserve the order of polynomials of quadrature operators and $\hat{q}(\vec{\lambda})^3$ to increase the order of the polynomial by one, we can ultimately generate the full algebra of observables. On the level of unitary gates, this implies that a full universal gate set is given by

$$\mathcal{U} = \{\hat{U}_D(\vec{\lambda}), \hat{U}_S(\vec{\lambda}), \hat{U}_P(\vec{\lambda}), \hat{U}_{\mathrm{BS}}(\vec{\lambda}_1, \vec{\lambda}_2), \hat{U}_C(\vec{\lambda})\}, \quad (179)$$

$$\text{with} \quad \hat{U}_C := \exp i\hat{q}(\vec{\lambda})^3. \quad (180)$$

In other words, combining sufficiently many of these gates allows us to built any arbitrary unitary transformation generated by a Hamiltonian, which is polynomial in the quadrature operators.

The non-Gaussian gate $\hat{U}_C$ is known as the cubic phase gate. The argument above shows that any experiment that can implement Gaussian transformations and a cubic phase gate can in principle generate any arbitrary non-Gaussian state. Even though many protocols have been proposed to experimentally realize a cubic phase gate [28,135–138], any convincing implementations have yet to be demonstrated. One of the key problems is that experimental imperfections and finite squeezing are detrimental for the most commonly proposed methods [30].

In principle, there is no particular reason to limit our attention to cubic phase gates. Already in the very first work on the subject it is argued that essentially any Hamiltonian of a higher than quadratic order can be used as a generator [26]. Thus, optical processes that perform photon triplet generation can also be used as a non-Gaussian gate, which can even be converted into the cubic phase gate [139]. This requires well-controlled high $\chi^{(3)}$ nonlinearities, which are generally only achieved by using exotic nonlinear crystals or well-controlled individual atoms. Handling such setups with a sufficient degree of control to actually implement a quantum gate is extremely challenging.

Other CV systems are more appropriate for the implementation of non-Gaussian unitary transformations. In particular, the systems used in circuit QED have such non-Gaussian contributions in their Hamiltonians [140,141], which suggests that they may be more capable of deterministically generating non-Gaussian states than their optical counterparts. Still, the characterization, detection, and control of such states is expected to be challenging. Recently, some important progress was made by demonstrating triplet generation in these systems [142].

B. Conditional methods

The experimental difficulties that are encountered when trying to implement non-Gaussian unitary transformations can be circumvented by abandoning the demand of unitarity. This implies that we no longer consider operations that can be implemented deterministically, but rather resort to what can be broadly referred to as conditional operations. This idea was formalized by Kraus when characterizing the most general ways of manipulating quantum states [143].

In the most general sense, we can implement a conditional operation by taking a set of linear operators on Fock space $\hat{X}_1, \hat{X}_2, \ldots$ and acting on the state in the following way:

$$\hat{\rho} \mapsto \frac{\sum_j \hat{X}_j \hat{\rho} \hat{X}_j^\dagger}{\mathrm{tr}[\hat{\rho} \sum_j \hat{X}_j^\dagger \hat{X}_j]}. \quad (181)$$

This formalism is typically implemented by performing some form of generalized measurement on the state $\hat{\rho}$ [144]. When $\hat{\rho}$ is a deterministically generated Gaussian state, the action of a well-chosen set of operators $\hat{X}_1, \hat{X}_2, \ldots$ can turn it into a non-Gaussian state. In optics, two of the most well-known examples of this technique are single-photon addition and subtraction. In both cases, there is only a single operator $\hat{X}_1$. For photon addition, we implement $\hat{X}_1 = \hat{a}^\dagger(\vec{f})$, whereas photon subtraction requires the realization of a case where $\hat{X}_1 = \hat{a}(\vec{f})$.

In many physical setups, and, in particular, in optics, the problem is that measurements are destructive and a measurement effectively removes the measured mode from the system. Therefore, it is common to prepare large multimode Gaussian states of which a subset of modes is measured in order to conditionally prepare a non-Gaussian state in the remaining modes. We now introduce a general framework to describe the non-Gaussian Wigner functions that are created accordingly [39].

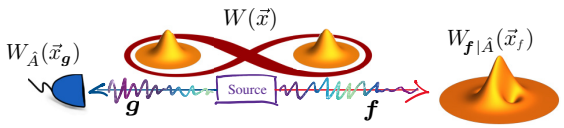

FIG. 3. Sketch representation of the conditional preparation scheme for creating the non-Gaussian states described by Eq. (190). Note that both **f** and **g** can be highly multimode. The Wigner function shown on the right is obtained by a conditional protocol shown in Ref. [39].

1. General framework

First of all, let us consider a general multimode phase space and separate it into two subsystems, i.e., $\mathbb{R}^{2m} = \mathbb{R}^{2l} \oplus \mathbb{R}^{2l'}$, where we perform some generalized measurement on the l' modes and leave the remaining l modes untouched. This introduces a general structure in the points of phase space $\vec{x} \in \mathbb{R}^{2m}$, which can now be written as $\vec{x} = \vec{x}_{\mathbf{f}} \oplus \vec{x}_{\mathbf{g}}$ with $\vec{x}_{\mathbf{f}} \in \mathbb{R}^{2l}$ and $\vec{x}_{\mathbf{g}} \in \mathbb{R}^{2l'}$. The general procedure is schematically outlined in Fig. 3 and we present the details step by step.

Any state $\hat{\rho}$ on this system then comes with a Wigner function $W(\vec{x}) = W(\vec{x}_{\mathbf{f}} \oplus \vec{x}_{\mathbf{g}})$ that is defined on the global phase space. This state can be reduced to one of the two subsystems by tracing out the other subsystem, which can be described on the level of the Wigner function by the following integrals:

$$W_{\mathbf{f}}(\vec{x}_{\mathbf{f}}) := \int_{\mathbb{R}^{2l'}} \mathrm{d}\vec{x}_{\mathbf{g}} W(\vec{x}_{\mathbf{f}} \oplus \vec{x}_{\mathbf{g}}), \tag{182}$$

$$W_{\mathbf{g}}(\vec{x}_{\mathbf{g}}) := \int_{\mathbb{R}^{2l}} \mathrm{d}\vec{x}_{\mathbf{f}} W(\vec{x}_{\mathbf{f}} \oplus \vec{x}_{\mathbf{g}}). \tag{183}$$

When the state is Gaussian and the Wigner function is given by Eq. (85), the structure of the phase space is reflected in the mean field vector $\vec{\xi}$ and in the covariance matrix V:

$$\vec{\xi} = \vec{\xi}_{\mathbf{f}} \oplus \vec{\xi}_{\mathbf{g}}, \tag{184}$$

$$V = \begin{pmatrix} V_{\mathbf{f}} & V_{\mathbf{fg}} \\ V_{\mathbf{gf}} & V_{\mathbf{g}} \end{pmatrix}, \tag{185}$$

with $V_{\mathbf{fg}} = V_{\mathbf{gf}}^T$. The matrices $V_{\mathbf{f}}$ and $V_{\mathbf{g}}$ describe all the variances and correlations of the modes within $\mathbb{R}^{2l}$ and $\mathbb{R}^{2l'}$, respectively. In addition, the submatrix $V_{\mathbf{gf}}$ contains all the correlations between the modes in the different subspaces, which will be important for conditional state preparation. One can show that for such Gaussian states, the reduced states are also Gaussian, for the modes in $\mathbb{R}^{2l}$ given by

$$W_{\mathbf{f}}(\vec{x}_{\mathbf{f}}) = \frac{e^{-\frac{1}{2}(\vec{x}_{\mathbf{f}} - \vec{\xi}_{\mathbf{f}})^T V_{\mathbf{f}}^{-1} (\vec{x}_{\mathbf{f}} - \vec{\xi}_{\mathbf{f}})}}{(2\pi)^m \sqrt{\det V_{\mathbf{f}}}}, \tag{186}$$

and analogously for the modes in $\mathbb{R}^{2l'}$. As Gaussian states are the states that are least challenging to produce, they form the starting point of the conditional state preparation scheme.

As a next step, we must implement some form of operation on the modes that correspond to the phase space $\mathbb{R}^{2l'}$. To do so, we consider the action of a general positive operator-valued measure (POVM) element $\hat{A} \geqslant 0$ that corresponds to a specific measurement outcome. We can then obtain a conditional state via

$$\hat{\rho}_{\mathbf{f}|\mathbf{A}} := \frac{\mathrm{tr}_{\mathbf{g}}[\hat{A}\hat{\rho}]}{\mathrm{tr}[\hat{A}\hat{\rho}]}. \tag{187}$$

The partial trace $\mathrm{tr}_{\mathbf{g}}[\hat{A}\hat{\rho}]$ runs only over the modes in $\mathbb{R}^{2l'}$ because the other modes are left untouched. The denominator $\mathrm{tr}[\hat{A}\hat{\rho}]$ renormalizes the state and gives the probability of actually obtaining the measurement result that corresponds to $\hat{A}$. In an actual experiment, this operation is implemented by many repeated measurements of the modes in $\mathbb{R}^{2l'}$ and $\hat{A}$ corresponds to a specific detector output of these measurements. The nonmeasured part of the state is only used when the detector indicates this specific output, otherwise it is simply discarded. This conditional selection of the state significantly changes the properties of the state in a way that is strongly influenced by $\hat{A}$.

As we described in Eq. (42), the operator $\hat{A}$ comes with an associated phase-space representation $W_A(\vec{x}_{\mathbf{g}})$, which can be used to formally describe the phase-space representation of $\hat{\rho}_{\mathbf{f}|\mathbf{A}}$:

$$W_{\mathbf{f}|\mathbf{A}}(\vec{x}_{\mathbf{f}}) = \frac{\int_{\mathbb{R}^{2l'}} \mathrm{d}\vec{x}_{\mathbf{g}} W_A(\vec{x}_{\mathbf{g}}) W(\vec{x}_{\mathbf{f}} \oplus \vec{x}_{\mathbf{g}})}{\int_{\mathbb{R}^{2l'}} \mathrm{d}\vec{x}_{\mathbf{g}} W_A(\vec{x}_{\mathbf{g}}) W_{\mathbf{g}}(\vec{x}_{\mathbf{g}})}. \tag{188}$$

There is a more practical way of expressing this Wigner function by exploiting the fact that the initial multimode Wigner function $W(\vec{x}_{\mathbf{f}} \oplus \vec{x}_{\mathbf{g}})$ is positive and therefore describes a well-defined probability distribution on phase space. This implies that the conditional probability distribution

$$W(\vec{x}_{\mathbf{g}} \mid \vec{x}_{\mathbf{f}}) := \frac{W(\vec{x}_{\mathbf{f}} \oplus \vec{x}_{\mathbf{g}})}{W_{\mathbf{f}}(\vec{x}_{\mathbf{f}})}, \tag{189}$$

is also a well-defined probability distribution, which is obtained when we fix one point in phase space $\vec{x}_{\mathbf{f}} \in \mathbb{R}^{2l}$ and look at the probability distribution for the remaining modes in $\mathbb{R}^{2l'}$. We can then use this conditional probability distribution to write $W(\vec{x}_{\mathbf{f}} \oplus \vec{x}_{\mathbf{g}}) = W(\vec{x}_{\mathbf{g}} \mid \vec{x}_{\mathbf{f}}) W_{\mathbf{f}}(\vec{x}_{\mathbf{f}})$, which can be inserted in Eq. (188) to find

$$W_{\mathbf{f}|\mathbf{A}}(\vec{x}_{\mathbf{f}}) = \frac{\langle \hat{A} \rangle_{\mathbf{g}|\vec{x}_{\mathbf{f}}}}{\langle \hat{A} \rangle} W_{\mathbf{f}}(\vec{x}_{\mathbf{f}}), \tag{190}$$

where we define

$$\langle \hat{A} \rangle := (4\pi)^{l'} \int_{\mathbb{R}^{2l'}} \mathrm{d}\vec{x}_{\mathbf{g}} W_A(\vec{x}_{\mathbf{g}}) W_{\mathbf{g}}(\vec{x}_{\mathbf{g}}), \tag{191}$$

$$\langle \hat{A} \rangle_{\mathbf{g}|\vec{x}_{\mathbf{f}}} := (4\pi)^{l'} \int_{\mathbb{R}^{2l'}} \mathrm{d}\vec{x}_{\mathbf{g}} W_A(\vec{x}_{\mathbf{g}}) W(\vec{x}_{\mathbf{g}} \mid \vec{x}_{\mathbf{f}}). \tag{192}$$

The quantity $\langle \hat{A} \rangle$ is simply the expectation value of the observable $\hat{A}$ in the state $\hat{\rho}$. $\langle \hat{A} \rangle_{\mathbf{g}|\vec{x}_{\mathbf{f}}}$, on the other hand, is the expectation value of the function $W_A(\vec{x}_{\mathbf{g}})$ where $\vec{x}_{\mathbf{g}}$ is distributed according to the distribution $W(\vec{x}_{\mathbf{g}} \mid \vec{x}_{\mathbf{f}})$, which makes $\langle \hat{A} \rangle_{\mathbf{g}|\vec{x}_{\mathbf{f}}}$ a function of the selected phase-space point $\vec{x}_{\mathbf{f}}$. However, even though $W(\vec{x}_{\mathbf{g}} \mid \vec{x}_{\mathbf{f}})$ is a well-defined probability distribution on phase space, it does not necessarily correspond to a quantum state. Indeed, $W(\vec{x}_{\mathbf{g}} \mid \vec{x}_{\mathbf{f}})$ may violate the Heisenberg inequality, which will be of vital importance in Sec. V as it is narrowly connected to quantum steering.

In the specific case where $W(\vec{x}_{\mathbf{f}} \oplus \vec{x}_{\mathbf{g}})$ is Gaussian, we find that $W(\vec{x}_{\mathbf{g}} \mid \vec{x}_{\mathbf{f}})$ is also a Gaussian probability distribution, given by

$$W(\vec{x}_{\mathbf{g}} \mid \vec{x}_{\mathbf{f}}) = \frac{\exp\left[-\frac{1}{2}(\vec{x}_{\mathbf{g}} - \vec{\xi}_{\mathbf{g}|\vec{x}_{\mathbf{f}}})^T V_{\mathbf{g}|\vec{x}_{\mathbf{f}}}^{-1} (\vec{x}_{\mathbf{g}} - \vec{\xi}_{\mathbf{g}|\vec{x}_{\mathbf{f}}})\right]}{(2\pi)^{l'} \sqrt{\det V_{\mathbf{g}|\vec{x}_{\mathbf{f}}}}}. \tag{193}$$

Using the notation of Eq. (185), we express its covariance matrix

$$V_{\mathbf{g}|\vec{x}_{\mathbf{f}}} = V_{\mathbf{g}} - V_{\mathbf{gf}} V_{\mathbf{f}}^{-1} V_{\mathbf{gf}}^T, \tag{194}$$

and mean field vector

$$\vec{\xi}_{\mathbf{g}|\vec{x}_{\mathbf{f}}} = \vec{\xi}_{\mathbf{g}} + V_{\mathbf{gf}} V_{\mathbf{f}}^{-1} (\vec{x}_{\mathbf{f}} - \vec{\xi}_{\mathbf{f}}). \tag{195}$$

The covariance matrix $V_{\mathbf{g}|\vec{x}_{\mathbf{f}}}$ is known in the mathematics literature [145] as the Schur complement of V. The Schur complement has interesting properties, for example, V is a positive matrix if and only if the same holds for the Schur complement $V_{\mathbf{g}|\vec{x}_{\mathbf{f}}}$. This immediately implies that the Gaussian probability distribution in Eq. (193) is well defined. Furthermore, the Schur complement also plays an important role in the theory of Gaussian quantum correlations [146]. It should be noted that $V_{\mathbf{g}|\vec{x}_{\mathbf{f}}}$ does not actually depend on the chosen value for $\vec{x}_{\mathbf{f}}$. Thus, the conditional expectation value $\langle \hat{A} \rangle_{\mathbf{g}|\vec{x}_{\mathbf{f}}}$ depends only on the phase-space point $\vec{x}_{\mathbf{f}}$ through the displacement $\vec{\xi}_{\mathbf{g}|\vec{x}_{\mathbf{f}}}$. This is a particular feature of Gaussian states.

Finally, remark that the derivation of Eq. (190) holds true for all initial states with a positive Wigner function. Whenever the initial multimode Wigner function $W(\vec{x}_{\mathbf{f}} \oplus \vec{x}_{\mathbf{g}})$ is positive, it follows that $W_{\mathbf{f}}(\vec{x}_{\mathbf{f}})$ is also positive. Furthermore, given that $\langle \hat{A} \rangle$ is the quantum expectation value of a positive semidefinite operator it clearly also is a positive quantity. Hence, Wigner negativity is entirely contained with $\langle \hat{A} \rangle_{\mathbf{g}|\vec{x}_{\mathbf{f}}}$. The fact that $\langle \hat{A} \rangle_{\mathbf{g}|\vec{x}_{\mathbf{f}}}$ can take negative values is exactly due to $W(\vec{x}_{\mathbf{g}} \mid \vec{x}_{\mathbf{f}})$ not being the Wigner function of a quantum state. Furthermore, Eq. (192) teaches us that the conditionally generated Wigner function $W_{\mathbf{f}|\mathbf{A}}(\vec{x}_{\mathbf{f}})$ can only achieve negative value when $W_A(\vec{x}_{\mathbf{g}})$ is nonpositive.

Thus, in order to conditionally prepare a state with Wigner negativity, one faces strict requirements, on both the POVM element $\hat{A}$ that is conditioned upon and on the conditional probability distribution $W(\vec{x}_{\mathbf{g}} \mid \vec{x}_{\mathbf{f}})$ that is obtained from the initial multimode state. We discuss this point in greater detail in Sec. B. For a more experimentally inclined perspective on the production of non-Gaussian states, we refer to Ref. [81].

Before we move on to consider photon subtraction as an example of conditional creation of non-Gaussian states, let us take for a moment the opposite process: Gaussification. The authors of Ref. [147] consider several copies of an initial non-Gaussian state, which are mixed through linear optics and subsequently some output modes are measured with on-off detectors. The conditioning is done of the events where no photons are detected, and such that we can interpret $\hat{A}$ as a projector in vacuum. By repeating several iterations of this scheme (assuming many successful conditioning events), the initial non-Gaussian state is converted into a Gaussian state. The Gaussification process thus relies on starting from a non-Gaussian state and conditioning by projecting on a Gaussian state: the vacuum. This point of view nicely complements our approach to create non-Gaussian states.

2. An example: photon subtraction

Single-photon subtracted states are theoretically obtained by acting with an annihilation operator on the state. Their density matrices are given by

$$\hat{\rho}^- = \frac{\hat{a}(\vec{b})\hat{\rho}\hat{a}^\dagger(\vec{b})}{\mathrm{tr}[\hat{a}^\dagger(\vec{b})\hat{a}(\vec{b})\hat{\rho}]}, \tag{196}$$

if the photon is subtracted in one specific mode **b**. In practice [129,148,149], we can implement this operation on the state $\hat{\rho}$ through a mode-selective beam splitter $\hat{U} = \exp\{\theta[\hat{a}^\dagger(\vec{g})\hat{a}(\vec{b}) - \hat{a}^\dagger(\vec{b})\hat{a}(\vec{g})]\}$, that couples the mode **b** to an auxiliary mode **g**, which is prepared in a vacuum state. We thus describe the action of the beam splitter on the system of interest and the auxiliary mode as $\hat{U}(\hat{\rho} \otimes |0\rangle\langle 0|)\hat{U}^\dagger$. As a next step, we mount a photon detector on one of the output modes of the beam splitter. This detector is crucial to make sure that no information is lost, without it we would effectively trace out the mode and the beam splitter would simply induce losses. In contrast, we condition on the specific events where the detector counts a single

photon, we generate the state

$$\hat{\rho}_\theta^- = \frac{\mathrm{tr}_{\mathbf{g}}[\hat{U}(\hat{\rho}\otimes|0\rangle\langle 0|)\hat{U}^\dagger(\mathbb{1}\otimes|1\rangle\langle 1|)]}{\mathrm{tr}[\hat{U}(\hat{\rho}\otimes|0\rangle\langle 0|)\hat{U}^\dagger(\mathbb{1}\otimes|1\rangle\langle 1|)]}. \tag{197}$$

The reader can now recognize Eq. (187). As a next step, we assume that the beam splitter is transmitting nearly all the incoming light, such that $\theta \to 0$. We can then approximate $\hat{U} \approx \mathbb{1} + \theta[\hat{a}^\dagger(\vec{g})\hat{a}(\vec{b}) - \hat{a}^\dagger(\vec{b})\hat{a}(\vec{g})]$. Then, when we insert this approximation in the expression for $\hat{\rho}_\theta^-$, we find that only the terms proportional to θ^2 survive such that

$$\hat{\rho}^- = \lim_{\theta\to 0}\hat{\rho}_\theta^- = \frac{\hat{a}(\vec{b})\hat{\rho}\hat{a}^\dagger(\vec{b})}{\mathrm{tr}[\hat{a}^\dagger(\vec{b})\hat{a}(\vec{b})\hat{\rho}]}. \tag{198}$$

A much more detailed analysis of multimode photon subtraction with imperfect mode selectivity can be found in Ref. [150]. We note that through this approach, photon subtraction can be understood as a weak measurement of the number of photons [151].

We can now derive the Wigner function of a single-photon-subtracted state through Eq. (193) by following the idea of Eq. (197). We initially start from a Gaussian state with covariance matrix $V_{\mathbf{f}}$ and one auxiliary mode that is prepared in the vacuum

$$V_{\mathrm{ini}} = \begin{pmatrix} V_{\mathbf{f}} & 0 \\ 0 & \mathbb{1} \end{pmatrix}. \tag{199}$$

We then implement a mode-selective beam splitter that mixes one specific mode **b** with the auxiliary vacuum mode, following the scheme outlined in Fig. 4. An effective way to describe such a transformation is by designing a new mode basis $\mathcal{B}$, which has **b** as one of the modes in the mode basis. We complete the basis with complementary modes $b_1^c, \ldots b_{m-1}^c$, such that the modes basis of phase space is given by $\mathcal{B} = \{\vec{b}_1^c, \Omega\vec{b}_1^c, \ldots, \vec{b}_{m-1}^c, \Omega\vec{b}_{m-1}^c, \vec{b}, \Omega\vec{b}\}$. Thus, we can perform such a basis change as

$$\begin{pmatrix} V_{\mathbf{f}} & 0 \\ 0 & \mathbb{1} \end{pmatrix} \mapsto \begin{pmatrix} O_{\mathcal{B}}^T & 0 \\ 0 & \mathbb{1} \end{pmatrix}\begin{pmatrix} V_{\mathbf{f}} & 0 \\ 0 & \mathbb{1} \end{pmatrix}\begin{pmatrix} O_{\mathcal{B}} & 0 \\ 0 & \mathbb{1} \end{pmatrix}, \tag{200}$$

where the matrix of basis change is given by

$$O_{\mathcal{B}} = \begin{pmatrix} | & | & & | & | & | \\ \vec{b}_1^c & \Omega\vec{b}_1^c & \ldots & \vec{b}_{m-1}^c & \Omega\vec{b}_{m-1}^c & \vec{b} & \Omega\vec{b} \\ | & | & & | & | & | \end{pmatrix}. \tag{201}$$

It is now instructive to explicitly write the rows and columns corresponding to mode b:

$$O_{\mathcal{B}}^T V_{\mathbf{f}} O_{\mathcal{B}} = \begin{pmatrix} V_{\mathbf{f}}^c & V_{\mathbf{f}}^{cb} \\ V_{\mathbf{f}}^{bc} & V_{\mathbf{f}}^b \end{pmatrix}. \tag{202}$$

Note that $V_{\mathbf{f}}^b$ is the 2×2 matrix that describes the initial state covariances of mode b, while $V_{\mathbf{f}}^c$ is the $(m-1)\times(m-1)$ that describes all the covariances in the complementary modes. The rectangular matrices $V_{\mathbf{f}}^{cb}$ and $V_{\mathbf{f}}^{bc}$ contain all the correlations between the mode b and the complementary modes in the basis. Now, we mix the mode b and the auxiliary vacuum mode on a beam splitter. This beam splitter is implemented by the transformation

$$V_{\mathrm{BS}}^{(\mathcal{B})} = O_{\mathrm{BS}}^{(\mathcal{B})}\begin{pmatrix} V_{\mathbf{f}}^c & V_{\mathbf{f}}^{cb} & 0 \\ V_{\mathbf{f}}^{bc} & V_{\mathbf{f}}^b & 0 \\ 0 & 0 & \mathbb{1} \end{pmatrix} O_{\mathrm{BS}}^{(\mathcal{B})\,T}, \tag{203}$$

where $O_{\mathrm{BS}}^{(\mathcal{B})}$ is given by

$$O_{\mathrm{BS}}^{(\mathcal{B})} = \begin{pmatrix} \mathbb{1} & 0 & 0 \\ 0 & \cos\theta\mathbb{1} & -\sin\theta\mathbb{1} \\ 0 & \sin\theta\mathbb{1} & \cos\theta\mathbb{1} \end{pmatrix}. \tag{204}$$

As a final step, we change the basis back to the original basis, such that the final state's covariance matrix becomes

$$V = \begin{pmatrix} O_{\mathcal{B}} & 0 \\ 0 & \mathbb{1} \end{pmatrix} V_{\mathrm{BS}}^{(\mathcal{B})}\begin{pmatrix} O_{\mathcal{B}}^T & 0 \\ 0 & \mathbb{1} \end{pmatrix}. \tag{205}$$

We can now rewrite this entire transformation such that the matrix V in Eq. (185) is given by

$$V = O_{\mathrm{BS}} V_{\mathrm{ini}} O_{\mathrm{BS}}^T, \tag{206}$$

with

$$\begin{aligned} O_{\mathrm{BS}} &= \begin{pmatrix} O_{\mathcal{B}} & 0 \\ 0 & \mathbb{1} \end{pmatrix} O_{\mathrm{BS}}^{(\mathcal{B})}\begin{pmatrix} O_{\mathcal{B}}^T & 0 \\ 0 & \mathbb{1} \end{pmatrix} \\ &= \begin{pmatrix} (\cos\theta - 1)\,BB^T + \mathbb{1} & \sin\theta\, B \\ -\sin\theta\, B^T & \cos\theta\mathbb{1} \end{pmatrix}. \end{aligned} \tag{207}$$

We introduce the $2m\times 2$ matrix B, which implements the mode selectivity of the beam splitter in mode b and is defined as

$$B = \begin{pmatrix} | & | \\ \vec{b} & \Omega\vec{b} \\ | & | \end{pmatrix}. \tag{208}$$

Hence, we can simply use O_{BS} as a mode-selective beam splitter that mixes one specific mode of a multimode state with the auxiliary mode. We should highlight that O_{BS} ultimately turns out to be independent of the complementary modes $b_1^c, \ldots b_{m-1}^c$. This means that the finer details of the interferometer $O_{\mathcal{B}}$ are not important for the final O_{BS}, the key point is that $O_{\mathcal{B}}$ changes towards a mode basis in which $\vec{b}$ and $\Omega\vec{b}$ are basis vectors of the phase space.

For the particular case of photon subtraction, we consider a very weak beam splitter, such that we consider the limit $\theta \to 0$. In this case, we can express the conditional

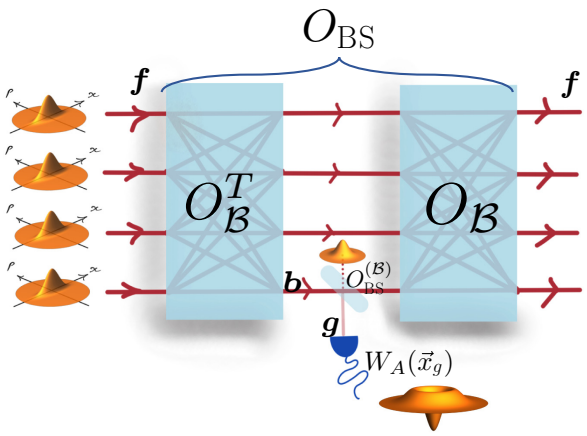

FIG. 4. Schematic representation of an implementation of mode-selective photon subtraction. See main text for details. For illustration, the initial state on the left is a product of single-mode squeezed vacuum states, but the protocol can in principle be applied to any Gaussian state.

mean field, Eq. (195), and covariance matrix, Eq. (194), of the auxiliary mode **g** by

$$\begin{aligned}\vec{\xi}_{\mathbf{g}|\vec{x}_\mathbf{f}} &\approx \theta(V_{\mathbf{bf}} - B^T)V_\mathbf{f}^{-1}(\vec{x}_\mathbf{f} - \vec{\xi}_\mathbf{f}) + \theta\vec{\xi}_\mathbf{b} \\ &= \theta B^T(\mathbb{1} - V_\mathbf{f}^{-1})(\vec{x}_\mathbf{f} - \vec{\xi}_\mathbf{f}) + \theta\vec{\xi}_\mathbf{b} \qquad (209)\\ V_{\mathbf{g}|\vec{x}_\mathbf{f}} &\approx \mathbb{1} + \theta^2\left[V_\mathbf{b} - \mathbb{1} - (V_\mathbf{bf} - B^T)V_\mathbf{f}^{-1}(V_\mathbf{fb} - B)\right], \\ &= \mathbb{1} + \theta^2\left(\mathbb{1} - B^T V_\mathbf{f}^{-1}B\right), \qquad (210)\end{aligned}$$

where we introduce the matrices $V_\mathbf{b} = B^T V_\mathbf{f} B$, $V_{\mathbf{b}\,\mathbf{f}} = B^T V_\mathbf{f}$, and $V_\mathbf{fb} = V_\mathbf{f} B$ as well as the vector $\vec{\xi}_\mathbf{b} = B^T\vec{\xi}_\mathbf{f}$. We can then use these quantities to evaluate that

$$\begin{aligned}W(\vec{x}_\mathbf{g} \mid \vec{x}_\mathbf{f}) \approx \frac{e^{-\frac{1}{2}\|\vec{x}_\mathbf{g}\|}}{(2\pi)^m}\Big(1 &+ \theta\,\vec{x}_\mathbf{g}^T\cdot B^T(\mathbb{1} - V_\mathbf{f}^{-1})(\vec{x}_\mathbf{f} - \vec{\xi}_\mathbf{f}) \\ &+ \theta\vec{x}_\mathbf{g}^T\cdot\vec{\xi}_\mathbf{b} + \frac{\theta^2}{2}\big[(\vec{x}_\mathbf{g}^T\cdot B^T(\mathbb{1} - V_\mathbf{f}^{-1})(\vec{x}_\mathbf{f} - \vec{\xi}_\mathbf{f}) \\ &+ \vec{x}_\mathbf{g}^T\cdot\vec{\xi}_\mathbf{b})^2 - \|B^T(\mathbb{1} - V_\mathbf{f}^{-1})(\vec{x}_\mathbf{f} - \vec{\xi}_\mathbf{f}) + \vec{\xi}_\mathbf{b}\|^2 \\ &+ \vec{x}_\mathbf{g}^T\left(\mathbb{1} - B^T V_\mathbf{f}^{-1}B\right)\vec{x}_\mathbf{g}\big] + \mathcal{O}(\theta^3)\Big). \qquad (211)\end{aligned}$$

As a next step, we must choose a POVM element $\hat{A}$ to measure. In the case of photon subtraction, we mount a photon counter on the auxiliary mode and for single-photon subtraction we condition on the event where this detector detects exactly one photon. Because we use a very weakly reflective beam splitter, the probability of obtaining such an event is small but when it occurs, we have created a photon subtracted state on the remaining modes.

On a theoretical level, mounting a photon counter and conditioning on a single photon is translated to choosing $\hat{A} = |1_g\rangle\langle 1_g|$. We already encountered the corresponding Wigner function in Eq. (118), and thus we can combine this with Eq. (211) to obtain

$$\begin{aligned}\langle\hat{A}\rangle_{\mathbf{g}|\vec{x}_\mathbf{f}} &= 4\pi\int_{\mathbb{R}^2} \mathrm{d}\vec{x}_\mathbf{g} W_{1_{\vec{g}}}(\vec{x}_\mathbf{g})W(\vec{x}_\mathbf{g} \mid \vec{x}_\mathbf{f}) \\ &\approx \frac{\theta^2}{2}\Big(\|B^T(\mathbb{1} - V_\mathbf{f}^{-1})(\vec{x}_\mathbf{f} - \vec{\xi}_\mathbf{f}) + \vec{\xi}_\mathbf{b}\|^2 \\ &\quad + \mathrm{tr}\left[\mathbb{1} - B^T V_\mathbf{f}^{-1}B\right]\Big) + \mathcal{O}(\theta^3), \qquad (212)\end{aligned}$$

and in a similar fashion we find that

$$\begin{aligned}0\langle\hat{A}\rangle &= 4\pi\int_{\mathbb{R}^2} \mathrm{d}\vec{x}_\mathbf{g} W_{1_{\vec{g}}}(\vec{x}_\mathbf{g})W_\mathbf{g}(\vec{x}_\mathbf{g}) \\ &\approx \frac{\theta^2}{2}\left(\mathrm{tr}\left[V_\mathbf{b} - \mathbb{1}\right] + \|\vec{\xi}_\mathbf{b}\|^2\right) + \mathcal{O}(\theta^3). \qquad (213)\end{aligned}$$

The actual evaluation of these integrals is not completely straightforward. As a key idea, we use that the integral takes the form of a polynomial multiplied by a Gaussian. We can thus evaluate the expectation value of the polynomial with respect to this Gaussian distribution. In essence, this boils down to calculating a set of moments of a Gaussian probability distribution. We see rather quickly that the lowest orders in θ vanish, such that the leading order is θ^2. Putting everything together, we find that

$$\begin{aligned}\lim_{\theta\to 0} W_{\mathbf{f}|\mathbf{A}}(\vec{x}_\mathbf{f}) &= \lim_{\theta\to 0}\frac{\langle\hat{A}\rangle_{\mathbf{g}|\vec{x}_\mathbf{f}}}{\langle\hat{A}\rangle}W_\mathbf{f}(\vec{x}_\mathbf{f}) \\ &= \frac{\|B^T(\mathbb{1} - V_\mathbf{f}^{-1})(\vec{x}_\mathbf{f} - \vec{\xi}_\mathbf{f}) + \vec{\xi}_\mathbf{b}\|^2 + \mathrm{tr}\left[\mathbb{1} - B^T V_\mathbf{f}^{-1}B\right]}{\mathrm{tr}\,(V_\mathbf{b} - \mathbb{1}) + \|\vec{\xi}_\mathbf{b}\|^2} \\ &\quad W_\mathbf{f}(\vec{x}_\mathbf{f}). \qquad (214)\end{aligned}$$

As such, we obtain the Wigner function for a multimode photon-subtracted state. This Wigner function can be obtained using several different methods, ranging from algebraic [152,153] to analytical [154]. The difference between those approaches and our method here is that we do not directly use the properties of the annihilation operator, but rather model the exact experimental setup, while relying entirely on phase-space representations.

The methods presented here for treating photon-subtracted states can straightforwardly be extended to the subtraction of multiple photons in different modes and we can easily replace photon-number-resolving detection with an on-off detector by setting $\hat{A} = \mathbb{1} - |0\rangle\langle 0|$. The techniques used in the calculations remain essentially the same and it yields the same result in the $\theta \to 0$ limit (doing this calculation may prove to be a good exercise for the motivated reader). However, any real implementation of a photon-subtraction experiment will use a beam splitter with finite reflectivity, such that there will be a

difference between on-off detectors and photon-number-resolving detectors due to the small contributions of higher order terms in θ. In practice, one chooses the reflectivity of the beam splitter with respect to the energy content of the initial state to effectively suppress all higher-order terms in Eq. (211). In the single-mode case, an early thorough analysis of the implementation of photon subtraction can be found in Ref. [155]. There are also proposals in the literature to use a photon-subtraction setup with larger values of θ to gain an additional advantage in quantum state preparation [156–158].

As a final note, we point out that a similar treatment can be used to describe photon-added states, which are also relevant in experiments [159,160]. It is perhaps surprising that such a state can be obtained by performing a measurement on a part of a Gaussian state, but it suffices to replace the beam splitter in Eq. (197) with a two-mode squeezer. In other words, we set $\hat{U} = \exp\{\theta[\hat{a}^\dagger(\vec{g})\hat{a}^\dagger(\vec{b}) - \hat{a}(\vec{b})\hat{a}(\vec{g})]\}$, and consider again the limit where the parameter θ is small, i.e., weak squeezing. Even though this is a simple step in theory, it is much harder in an actual experimental setting. Photon subtraction can be implemented with a passive linear optics element, while photon addition always requires squeezing and thus a nonlinear optics implementation.

V. NON-GAUSSIAN STATES AND QUANTUM CORRELATIONS

In this section, we explore the interplay between non-Gaussian effects and quantum correlations. First, in Sec. A, we provide a crash course to introduce the unfamiliar reader to the most important types of quantum correlations: entanglement, steering, and Bell nonlocality. In Sec. B we subsequently highlight how certain types of quantum correlations can be used to create certain types of non-Gaussian states via the methods of Sec. B. In Sec. C, we then explore how non-Gaussian operations can create or enhance quantum correlations by focusing on photon-subtracted states. Finally, we explore the role that is played by non-Gaussian states in Bell inequalities in Sec. D.

A. Quantum correlations: a crash course

We start by giving a quick introduction to the different kinds of common quantum correlations. Readers who want to get a more thorough overview on these subjects are referred to Refs. [161–163] as natural starting points.

In this Tutorial, we solely consider bipartite quantum correlations. This implies that we structure the system in a similar way as in Sec. B and divide the m-mode system in two parts, each with their own phase space, i.e., $\mathbb{R}^{2m} = \mathbb{R}^{2l} \oplus \mathbb{R}^{2l'}$. It is noteworthy that the corresponding Fock space takes the structure $\Gamma(\mathcal{H}_m) = \Gamma(\mathcal{H}_l) \otimes \Gamma(\mathcal{H}_{l'})$, where we again use the mapping, Eq. (44), between the phase space $\mathbb{R}^{2k}$ and the k-dimension Hilbert space $\mathcal{H}_k$. These structures are crucial to understand quantum correlations.

1. Correlations

To better understand quantum correlations, it is useful to start by generally defining what a correlations is. In a statistical sense, two stochastic variables X and Y are correlated when the expectation values have the following property:

$$\mathbb{E}(XY) \neq \mathbb{E}(X)\mathbb{E}(Y). \tag{215}$$

This can be translated to the level of probability distributions by stating that the joint probability distribution for outcomes $X = x$ and $Y = y$ is not the product of the marginals

$$P(x,y) \neq P(x)P(y), \tag{216}$$

where

$$P(x) = \int_{\mathcal{Y}} \mathrm{d}y\, P(x,y), \text{ and } P(y) = \int_{\mathcal{X}} \mathrm{d}x\, P(x,y). \tag{217}$$

Here, $\mathcal{X}$ and $\mathcal{Y}$ denote the possible outcomes of the stochastic variables X and Y, respectively [164].

When we talk about quantum systems, there are generally many observables that can be considered. When we consider a global multimode system with phase space $\mathbb{R}^{2m}$ and two subsystems with phase spaces $\mathbb{R}^{2l}$ and $\mathbb{R}^{2l'}$, there is a whole algebra of observables involved. The role of the stochastic observables X and Y will be taken up by local observables $\hat{X}$ and $\hat{Y}$ that are contained in the observable algebra generated by, respectively, $\hat{q}(\vec{f})$ and $\hat{q}(\vec{g})$, with $\vec{f} \in \mathbb{R}^{2l}$ and $\vec{g} \in \mathbb{R}^{2l'}$. These local observables are correlated when

$$\mathrm{tr}(\hat{X} \otimes \hat{Y}\hat{\rho}) \neq \mathrm{tr}(\hat{X}\hat{\rho}_{\mathbf{f}})\mathrm{tr}(\hat{Y}\hat{\rho}_{\mathbf{g}}), \tag{218}$$

where $\hat{\rho}_{\mathbf{f}}$ and $\hat{\rho}_{\mathbf{g}}$ are the marginals (or reduced states) of $\hat{\rho}$ for the subsystems $\mathbb{R}^{2l}$ and $\mathbb{R}^{2l'}$.

When we talk about correlated systems rather than correlated observables, we consider that there exists a pair of local observables such that Eq. (218) holds. Thus, if two systems are not correlated, it follows that for all possible observables $\mathrm{tr}(\hat{X} \otimes \hat{Y}\hat{\rho}) = \mathrm{tr}(\hat{X}\hat{\rho}_{\mathbf{f}})\mathrm{tr}(\hat{Y}\hat{\rho}_{\mathbf{g}})$. This lack of correlations can be expressed on the level of the quantum state by the identity $\hat{\rho} = \hat{\rho}_{\mathbf{f}} \otimes \hat{\rho}_{\mathbf{g}}$. On the level of Wigner functions, we can therefore say that a state contains correlations if the Wigner function satisfies

$$W(\vec{x}_{\mathbf{f}} \oplus \vec{x}_{\mathbf{g}}) \neq W_{\mathbf{f}}(\vec{x}_{\mathbf{f}})W_{\mathbf{g}}(\vec{x}_{\mathbf{g}}), \tag{219}$$

where the marginal Wigner functions are defined as in Eqs. (182), (183).

It is clear that correlations between systems can occur, both, in the context of classical probability theory and in quantum theory. However, we already established that quantum physics imposes additional constraints on the statistics of observables, which ultimately make it impossible to describe CV quantum systems in terms of probability distributions on phase space. Similarly, quantum physics leads to new features for the correlations of subsystems. Thus, in our study of quantum correlations we explore correlated systems, in the sense of Eq. (219), and we seek to differentiate between correlations that are of classical origin and those that can be attributed to a quantum origin.

2. Quantum entanglement

Quantum entanglement is probably the most well-known type of quantum correlation. The notion of entanglement derives directly from the structure of the quantum state space and is related to the contrast between pure states in classical and quantum physics.

To understand this contrast, we loosely follow the idea of Ref. [165]. Let us be a bit more precise as to what is meant with pure states in classical physics in the context of CV systems. Classically, in a context of statistical mechanics, any CV system can be described by a probability distribution on phase space. From a mathematical point of view, this means that the space containing all the possible classical states is a convex set because any convex combination of two probability distributions is again a probability distribution. Pure states are formally defined as the extreme points of the convex set, i.e., the states that cannot be decomposed as being a convex combination of two other states. In a classical theory, where states can unambiguously be represented by probability distributions on phase space, the pure states are delta functions centered on the different points of phase space. From a physical point of view, this corresponds to the intuition that pure states are "the least noisy" states, which simply corresponds to a single point in phase space.

For our phase space $\mathbb{R}^{2m} = \mathbb{R}^{2l} \oplus \mathbb{R}^{2l'}$ these delta functions factorize with respect to the subsystems, i.e., $\delta(\vec{x} - \vec{x}') = \delta(\vec{x}_{\mathbf{f}} - \vec{x}'_{\mathbf{f}})\delta(\vec{x}_{\mathbf{g}} - \vec{x}'_{\mathbf{g}})$, with $\vec{x}, \vec{x}' \in \mathbb{R}^{2m}$, $\vec{x}_{\mathbf{f}}, \vec{x}'_{\mathbf{f}} \in \mathbb{R}^{2l}$, and $\vec{x}_{\mathbf{g}}, \vec{x}'_{\mathbf{g}} \in \mathbb{R}^{2l'}$. In the light of Eq. (216) we thus conclude that pure states of classical systems are always uncorrelated [166]. Any correlations that are present in classical states are thus obtained by taking a convex combination of uncorrelated pure states.

In quantum systems, pure states are represented by state vectors in a Hilbert space (in our case Fock space). They also can be seen as the extreme points of a convex set of states that contains all density matrices $\hat{\rho}$. As we saw in the example where we discussed the Hong-Ou-Mandel state $|\mathrm{HOM}\rangle$ in Eq. (165), pure quantum states can actually be correlated in the sense of Eq. (219). This crucial difference between classical and quantum pure states lies at the basis of quantum entanglement.

The notion of entanglement derives directly from the structure of the quantum state and is defined as the opposite of a separable state. For pure states, separable states $|\Psi\rangle \in \Gamma(\mathcal{H}_m)$ are the pure states that are uncorrelated and can thus be written as $|\Psi\rangle = |\Psi_l\rangle \otimes |\Psi_{l'}\rangle$ with $|\Psi_l\rangle \in \Gamma(\mathcal{H}_l)$ and $|\Psi_{l'}\rangle \in \Gamma(\mathcal{H}_{l'})$. All other pure states are said to be entangled. They possess correlations that are not due to some type of convex combination of uncorrelated states, something which is impossible for classical pure states.

The situation is more subtle when considering mixed states, i.e., convex combinations of pure states. Convex mixtures of classical pure states can also show correlations, and it is therefore crucial to make a distinction between this type of classical correlations and quantum correlations. Due to the structure of classical pure states, we find that any classical joint probability distribution on phase space can be written as a convex combination of local probability distributions

$$P(\vec{x}_{\mathbf{f}} \oplus \vec{x}_{\mathbf{g}}) = \int \mathrm{d}\gamma\, p(\gamma) P^{(\gamma)}(\vec{x}_{\mathbf{f}}) P^{(\gamma)}(\vec{x}_{\mathbf{g}}), \tag{220}$$

where γ is some arbitrary way of labeling states, distributed according to distribution $p(\gamma)$. This notion of classical correlations can directly be generalized to quantum states [167], and thus a mixed state is said to be separable when all of its correlations are classical, i.e., when it is a convex mixture of product states

$$\hat{\rho} = \int \mathrm{d}\gamma\; p(\gamma) \hat{\rho}^{(\gamma)}_{\mathbf{f}} \otimes \hat{\rho}^{(\gamma)}_{\mathbf{g}}. \tag{221}$$

In the language of Wigner functions, the separability condition translates to

$$W(\vec{x}_{\mathbf{f}} \oplus \vec{x}_{\mathbf{g}}) = \int \mathrm{d}\gamma\, p(\gamma) W^{(\gamma)}_{\mathbf{f}}(\vec{x}_{\mathbf{f}}) W^{(\gamma)}_{\mathbf{g}}(\vec{x}_{\mathbf{g}}), \tag{222}$$

where we again use the definitions of Eqs. (182), (183). Quantum states that cannot be described by a Wigner function of the form Eq. (222) are not separable and are said to be entangled.

Hence, quantum entanglement describes the origin of the quantum correlations rather than their properties. Nevertheless, the set of separable states is a convex set and thus the Hahn-Banach separation theorem [168,169] teaches us that it is in principle possible to use observables to distinguish between separable and entangled states. In this sense the difference between entangled and separable states is measurable. For the sake of uniformity, we highlight that separable states lead to the following measurement

statistics of local observables $\hat{X}$ and $\hat{Y}$:

$$P(x,y) = \int \mathrm{d}\gamma p(\gamma) P^{(\gamma)}_{\hat{\rho}}(x) P^{(\gamma)}_{\hat{\rho}}(y). \tag{223}$$

It is crucial to emphasize that the distributions of measurement outcomes $P^{(\gamma)}_{\hat{\rho}}(x)$ and $P^{(\gamma)}_{\hat{\rho}}(y)$ are governed by the laws of quantum physics. Formally, we can use the spectral theorem to write

$$\hat{X} = \int_{\mathcal{X}} \mathrm{d}x\, x \hat{E}_x, \quad \text{and} \quad \hat{Y} = \int_{\mathcal{Y}} \mathrm{d}y\, y \hat{E}_y, \tag{224}$$

such that $\hat{E}_x$ and $\hat{E}_y$ are the POVM elements that correspond to the measurement outcomes x and y for the measurement of the (generalized) observables $\hat{X}$ and $\hat{Y}$, respectively. The probability distribution $P^{(\gamma)}_{\hat{\rho}}(x)$ is then given by

$$P^{(\gamma)}_{\hat{\rho}}(x) = \mathrm{tr}[\hat{E}_x \hat{\rho}^{(\gamma)}_{\mathbf{f}}] = (4\pi)^l \int_{\mathbb{R}^{2l}} \mathrm{d}\vec{x}_{\mathbf{f}}\, W_{E_x}(\vec{x}_{\mathbf{f}}) W_{\mathbf{f}}(\vec{x}_{\mathbf{f}}), \tag{225}$$

and analogously for $P^{(\gamma)}_{\hat{\rho}}(y)$.

For separable states, Eq. (223) with local probability distribution given by Eq. (225) holds for any arbitrary pair of local observables. The model that is described by these equations is known as a local hidden variable model for quantum entanglement, where γ is the hidden variable. We may not necessarily know the origins and behavior of γ, but the model generally captures two important elements. First, all correlations are induced by the common variable γ that governs the convex mixture. Second, the local probability distributions $P^{(\gamma)}_{\hat{\rho}}(x)$ and $P^{(\gamma)}_{\hat{\rho}}(y)$ have a quantum origin. For CV systems the latter point, for example, implies that these local probability distributions must satisfy the Heisenberg inequality. These quantum constraints on the local probability distributions $P^{(\gamma)}_{\hat{\rho}}(x)$ and $P^{(\gamma)}_{\hat{\rho}}(y)$ are typically useful for the falsification of the local hidden variable model, Eq. (223), and thus prove the presence of quantum entanglement [170,171].

3. Quantum steering

In a formal sense, quantum steering is a rather recent addition to the family of quantum correlations. Nevertheless, it is exactly this phenomenon that lies at the basis of the Einstein-Podolsky-Rosen (EPR) paradox [172]. Schrödinger's response to the EPR paper [173,174] lies at the basis of what we now call quantum steering, but the broader implications of these results were only sporadically discovered and formalized [175,176].

Just like for quantum entanglement, a system is said to be steerable if the measurement statistics cannot be explained in terms of a local hidden variable model. A peculiarity of quantum steering is that it involves a certain directionality, where one of the subsystems is said to "steer" the other subsystem. This asymmetry is represented in the local hidden variable model, which takes the following form:

$$P(x,y) = \int \mathrm{d}\gamma p(\gamma) P^{(\gamma)}(x) P^{(\gamma)}_{\hat{\rho}}(y), \tag{226}$$

where we emphasize the striking resemblance to Eq. (223). Note that, contrary to the case of quantum entanglement, we now allow the probability distribution $P^{(\gamma)}(x)$ for the first subsystem to be arbitrary and thus do not impose any constraints of quantum theory on it. If there exist observables $\hat{X}$ and $\hat{Y}$ for which the probability distribution is not consistent with the model, Eq. (226), the subsystems with phase space $\mathbb{R}^{2l}$ is able to steer the subsystem with phase space $\mathbb{R}^{2l'}$.

Quantum steering is perhaps most logically explained in terms of conditional states and probability distributions. For nonsteerable states, the local hidden variable model, Eq. (226), must hold for all observables, which in turn imposes conditions on the level of states. Here these conditions manifest on the level of conditional states of the type Eq. (187). To see this, we consider the conditional probability distribution associated with Eq. (226):

$$P(y \mid x) = \frac{\int \mathrm{d}\gamma p(\gamma) P^{(\gamma)}(x) P^{(\gamma)}_{\hat{\rho}}(y)}{P(x)}, \tag{227}$$

where the probability to obtain a certain outcome $\hat{X} = x$ is given by

$$P(x) = \int \mathrm{d}\gamma p(\gamma) P^{(\gamma)}(x). \tag{228}$$

Note that for any x the function

$$\tilde{P}(\gamma \mid x) := \frac{p(\gamma) P^{(\gamma)}(x)}{P(x)} \tag{229}$$

is a well-defined probability distribution. Furthermore, if we demand that Eq. (227) holds for all observables $\hat{Y}$, we find the following condition for the conditional state:

$$\hat{\rho}_{\mathbf{g}|\hat{X}=x} = \int \mathrm{d}\gamma\, \tilde{P}(\gamma \mid x) \hat{\rho}^{(\gamma)}_{\mathbf{g}}. \tag{230}$$

Because quantum steering is a property of the state, we again require Eq. (230) to hold for all observables $\hat{X}$ for a state to not be steerable.

The local hidden variable model, Eq. (226), and the consequence for the conditional state, Eq. (230), may seem stringent, but it is often intricate to formally prove that such a model cannot explain observed data. It turns out

that computational methods based on semidefinite programming [177] are well suited to prove that the set of all possible conditional states is inconsistent with Eq. (230). A more physical point of view is based on developing steering inequalities [178]. As a notable example, one can derive a type of conditional Heisenberg inequality for states of the form Eq. (230). The local hidden variable model, Eq. (226), assumes that the laws of quantum physics constrain the measurement statistics in the second subsystem. We can then define the conditional variance of an arbitrary observable $\hat{Y}$

$$\Delta^2(\hat{Y} \mid \hat{X} = x) := \mathrm{tr}[\hat{Y}^2 \hat{\rho}_{\mathbf{g}|\hat{X}=x}] - \mathrm{tr}[\hat{Y}\hat{\rho}_{\mathbf{g}|\hat{X}=x}]^2, \quad (231)$$

which leads to the "average inference variance"

$$\Delta^2_{\mathrm{inf}}(\hat{Y}) := \int_{\mathcal{X}} \mathrm{d}x P(x) \Delta^2(\hat{Y} \mid \hat{X} = x), \quad (232)$$

that characterizes the precision with which we can infer the measurement outcome of $\hat{Y}$, given a measurement outcome of $\hat{X}$. Under the assumption that Eq. (230) holds, we can than prove the inference Heisenberg inequality [178]

$$\Delta^2_{\mathrm{inf}}(\hat{Y}_1)\Delta^2_{\mathrm{inf}}(\hat{Y}_2) \geqslant \frac{1}{2}\int_{\mathcal{X}_3} \mathrm{d}x P(x) \left|\mathrm{tr}\left([\hat{Y}_1, \hat{Y}_2]\hat{\rho}_{\mathbf{g}|\hat{X}_3=x}\right)\right|^2, \quad (233)$$

where $\Delta^2_{\mathrm{inf}}(\hat{Y}_1)$ and $\Delta^2_{\mathrm{inf}}(\hat{Y}_2)$ can be conditioned on any observables $\hat{X}_1$ and $\hat{X}_2$, respectively.

Thus, whenever one performs a series of conditional measurements that violate the inference Heisenberg inequality (233), the assumption (230) cannot hold and thus the measurements in the subsystem with phase space $\mathbb{R}^{2l}$ have steered those in the subsystem with phase space $\mathbb{R}^{2l'}$. In more colloquial terms, the inequality (233) sets a limit on the precision with which classical correlations between observables can be used to infer measurement outcomes of one quantum subsystem, based on measurement outcome of the other subsystem (regardless of whether it is quantum or not). Quantum correlations allow us to outperform these bounds and provide better inference than classically possible, and this phenomenon is the essence of quantum steering.

Now let us now express Eq. (233) for quadrature operators:

$$\Delta^2_{\mathrm{inf}}[\hat{q}(\vec{g}_1)]\Delta^2_{\mathrm{inf}}[\hat{q}(\vec{g}_2)] \geqslant \left|\vec{g}_1^T \Omega \vec{g}_2\right|^2, \quad (234)$$

where $\vec{g}_1, \vec{g}_2 \in \mathbb{R}^{2l'}$. As a next step, we must understand the properties of the average inference variance $\Delta^2_{\mathrm{inf}}[\hat{q}(\vec{g}_1)]$, which we obtain by conditioning on a quadrature observable in the other subsystem's phase space $\mathbb{R}^{2l}$. More specifically let us assume that we condition on measurements of $\hat{q}(\vec{f}_1)$, such that we must evaluate the conditional variance $\Delta^2[\hat{q}(\vec{g}_1) \mid \hat{q}(\vec{f}_1) = x]$. The conditional variance $\Delta^2[\hat{q}(\vec{g}_1) \mid \hat{q}(\vec{f}_1) = x]$ is then given by the matrix element of the covariance matrix that describes $W(\vec{x}_{\mathbf{g}} \mid x\vec{f}_1)$ as defined in Eq. (193):

$$\Delta^2[\hat{q}(\vec{g}_1) \mid \hat{q}(\vec{f}_1) = x] = \vec{g}_1^T \left[V_{\mathbf{g}} - \frac{V_{\mathbf{gf}}\vec{f}_1\vec{f}_1^T V_{\mathbf{fg}}}{\vec{f}_1^T V_{\mathbf{f}} \vec{f}_1}\right]\vec{g}_1, \quad (235)$$

because the quantity does not depend on the actual outcome that is postselected upon, we find that

$$\Delta^2_{\mathrm{inf}}[\hat{q}(\vec{g}_1)] = \vec{g}_1^T \left[V_{\mathbf{g}} - \frac{V_{\mathbf{gf}}\vec{f}_1\vec{f}_1^T V_{\mathbf{fg}}}{\vec{f}_1^T V_{\mathbf{f}} \vec{f}_1}\right]\vec{g}_1, \quad (236)$$

$$\Delta^2_{\mathrm{inf}}[\hat{q}(\vec{g}_2)] = \vec{g}_2^T \left[V_{\mathbf{g}} - \frac{V_{\mathbf{gf}}\vec{f}_2\vec{f}_2^T V_{\mathbf{fg}}}{\vec{f}_2^T V_{\mathbf{f}} \vec{f}_2}\right]\vec{g}_2. \quad (237)$$

From Eqs. (236) and (237) we can deduce that $\Delta^2_{\mathrm{inf}}[\hat{q}(\vec{g})] \geqslant \vec{g}^T V_{\mathbf{g}|\vec{x}_{\mathbf{f}}}\vec{g}$ for all $\vec{g} \in \mathbb{R}^{2l'}$ regardless of the $\hat{q}(\vec{f})$ that is conditioned upon. Thus, if $V_{\mathbf{g}|\vec{x}_{\mathbf{f}}}$ satisfies the Heisenberg inequality the inference Heisenberg inequality (234) is also satisfied.

The setting with homodyne measurements, or more general Gaussian measurements, is close to the system that is discussed in Ref. [172]. For this reason, we refer to quantum steering with Gaussian measurements as EPR steering in contrast to more general quantum steering. This type of steering has been studied extensively in the literature, e.g., [176,179–181] and will be a key element in Sec. 2.

Note that both subsystems clearly play a very different role in this setting. The first subsystem simply produces measurement results of different observables. The information of these measurements in the first subsystem is then used to infer measurement results in the second subsystem, which is assumed to be a quantum system. In a quantum communication context, this asymmetry corresponds to a level of trust: we position ourselves in the steered system and trust that our system is a well-behaved quantum system, but we do not trust the party that controls the other subsystem (up to a point where we do not even want to assume that the data that are communicated to us come from an actual quantum system). The violation of a steering inequality practically allows verification in such a setting that there is indeed a quantum correlation between the two subsystems [182].

The inference Heisenberg inequality (233) shows that quantum steering describes certain properties of the quantum correlations. States that can perform quantum steering thus possess correlations that can be used to infer measurement outcomes better than any classical correlations

could. These correlations cannot be described by a hidden variable model of the form Eq. (226), which is more general than the model, Eq. (223). Thus, all states that produce statistics consistent with Eq. (223) are also consistent with Eq. (226) such that states that can perform steering must be entangled. However, there are states that produce statistics that is consistent with Eq. (226), but inconsistent with Eq. (223). In other words, not all entangled states can be used to perform quantum steering. In this sense, quantum steering can be said to be "stronger" than quantum entanglement.

4. Bell nonlocality

To date, the seminal work of John S. Bell on the Einstein-Podolsky-Rosen paradox [183] is probably one of the most remarkable findings on the foundations of quantum physics. What most had long taken for granted, the existence of local hidden variables to explain the probabilistic nature of quantum physics, turned out to be inconsistent with the theoretical quantum formalism. It is here that we find the real historical origin of the concept of quantum correlations as something fundamentally different from classical ones.

As for quantum entanglement and steering, the story of Bell nonlocality starts from a local hidden variable model that bears a strong resemblance to Eqs. (223) and (226). In this case, the model attempts to describe the joint measurement statistics of $\hat{X}$ and $\hat{Y}$ as

$$P(x,y) = \int \mathrm{d}\gamma p(\gamma) P^{(\gamma)}(x) P^{(\gamma)}(y). \tag{238}$$

The key observation is that now all the quantum constraints on the probability distributions have been dropped and both the $P^{(\gamma)}(x)$ and $P^{(\gamma)}(y)$ can be any mathematically well-defined probability distributions. Even though the difference between Eqs. (223) and (226) on the one hand, and Eq. (238) on the other hand, may appear small, the impact of dropping the constraints on the local distributions is enormous. Think, for example, of the Hahn-Banach separation theorem that is invoked to define entanglement witnesses, this crucially relies on the Hilbert-space structure of the state space. Think for example of (233) which crucially depends on the fact that quantum probabilities are constrained by the Heisenberg inequality. Abandoning all connections that tie probabilities to operator algebras on Hilbert spaces deprives quantum mechanics of their toolbox. Nevertheless, it turns out that some quantum states induce statistics that is inconsistent with Eq. (238).

Again, we note that states that can be described by the models, Eqs. (223) or (226), can also be described by the model, Eq. (238). Bell's local hidden variable model, Eq. (238), is thus the most general one and the class of states that lead to measurement statistics that cannot be described by it is the smallest. Therefore, we say that the correlations that lead to a violation of the mode, Eq. (238), also known as Bell nonlocality, are the strongest types of quantum correlations.

The key insight of Bell's work [183,184] is that Eq. (238) puts constraints on the correlations of different combinations of observables in the subsystems. These constraints, cast in the form of Bell inequalities can be violated by certain quantum states. The inconsistency of quantum physics with the model, Eq. (238), can in itself be seen as a special case of contextuality [185]. Over the decades, many different kinds of Bell inequalities have been derived (see, for example, Ref. [186]). Here we restrict to presenting one of the most commonly used incarnations: the Clauser-Horne-Shimony-Holt (CHSH) inequality [187]. This inequality relies on the measurement of four observables: $\hat{X}$ and $\hat{X}'$ on the first subsystem and $\hat{Y}$ and $\hat{Y}'$ on the second subsystem. Furthermore, we consider that the observables can take two possible values: -1 or 1. Assuming the model in Eq. (238) it is then possible to derive

$$\left|\langle \hat{X}\hat{Y}\rangle - \langle \hat{X}\hat{Y}'\rangle + \langle \hat{X}'\hat{Y}\rangle + \langle \hat{X}'\hat{Y}'\rangle\right| \leqslant 2, \tag{239}$$

where $\langle . \rangle$ denotes the expectation value. In this Tutorial we skip the derivation of this result, but the interested reader is referred to Ref. [188] for a detailed discussion. Remarkably, certain highly entangled states can violate this inequality.

The experimental violation of Bell's inequalities formally shows that quantum correlations are profoundly different than classical correlations [189–192]. However, one needs clever combinations of several observables in both subsystems to actually observe the difference. With most experimental loopholes now closed [193–197], Bell inequalities can now in principle be used to impose a device-independent level of security on various quantum protocols [198].

As a concluding remark, it is interesting to highlight the existence of a semidevice-independent framework for testing quantum correlations [199,200]. The key idea is that nothing is assumed about the measurement devices nor about the states, much like in the scenario of Bell inequalities. Yet, in the framework of Refs. [199,200] one does add an additional level of trust in the sense that one assumes that the inputs of the measurement device can be controlled and trusted. In a way, this additional intermediate level of trust is somewhat reminiscent of quantum steering. This framework was very recently extended to the CV setting [201].

B. Non-Gaussianity through quantum correlations

In Sec. B, we explained how conditional operations can be used to create non-Gaussian quantum states. The presence of correlations plays an essential role in this

framework. Indeed, in the absence of correlations the combination of Eqs. (222) and (189) implies that $W(\vec{x}_{\mathbf{g}} \mid \vec{x}_{\mathbf{f}}) = W_{\mathbf{g}}(\vec{x}_{\mathbf{g}})$. As a consequence, we see from Eq. (192) for the conditional expectation value $\langle \hat{A} \rangle_{\mathbf{g}|\vec{x}_{\mathbf{f}}} = \langle \hat{A} \rangle$, and thus from Eq. (190) that $W_{\mathbf{f}|\hat{A}}(\vec{x}_{\mathbf{f}}) = W_{\mathbf{f}}(\vec{x}_{\mathbf{f}})$. In other words, the conditional operation has no effect whatsoever and gives the same result as tracing out the modes in $\mathbb{R}^{2l'}$.

A closer look at the explicit expressions

$$W_{\mathbf{f}|\mathbf{A}}(\vec{x}_{\mathbf{f}}) = \frac{\langle \hat{A} \rangle_{\mathbf{g}|\vec{x}_{\mathbf{f}}}}{\langle \hat{A} \rangle} W_{\mathbf{f}}(\vec{x}_{\mathbf{f}}),$$

and

$$\langle \hat{A} \rangle_{\mathbf{g}|\vec{x}_{\mathbf{f}}} := (4\pi)^{l'} \int_{\mathbb{R}^{2l'}} \mathrm{d}\vec{x}_{\mathbf{g}} W_A(\vec{x}_{\mathbf{g}}) W(\vec{x}_{\mathbf{g}} \mid \vec{x}_{\mathbf{f}}),$$

shows that whenever there are correlations, and thus $\langle \hat{A} \rangle_{\mathbf{g}|\vec{x}_{\mathbf{f}}} \neq \langle \hat{A} \rangle$, the conditional Wigner function is *a priori* non-Gaussian. When we use explicitly that the initial state is Gaussian and thus that $W(\vec{x}_{\mathbf{g}} \mid \vec{x}_{\mathbf{f}})$ is given by Eq. (193), this condition can be translated to the existence of nonzero components in $V_{\mathbf{gf}}$ in Eq. (185). The precise properties of the resulting non-Gaussian quantum state depend on the conditional expectation value $\langle \hat{A} \rangle_{\mathbf{g}|\vec{x}_{\mathbf{f}}}$.

In the literature, some attention has been devoted to proposing different types of measurements for such heralding procedures. One may think of using on-off detectors [202], photon-number-resolving detectors [156], parity detectors [203], and more exotic multimode setups [204,205]. However, these works usually assume that the initial quantum state is a pure Gaussian state obtained by an idealized source of multimode squeezed vacuum states. As we saw in Sec. 2, for pure-state correlations automatically imply entanglement, and it even turns out that all correlated pure states violate a Bell inequality [206]. In other words, for pure states all correlations are quantum correlations and all these quantum correlations are of the strongest type. When we no longer make such assumptions on the initial multimode Gaussian state, we see that $\langle \hat{A} \rangle_{\mathbf{g}|\vec{x}_{\mathbf{f}}}$ will not only depend on the chosen POVM $\hat{A}$, but also on the properties of $W(\vec{x}_{\mathbf{g}} \mid \vec{x}_{\mathbf{f}})$. In Secs. 1 and 2, we explain that certain types of non-Gaussian features can only be achieved through certain types of quantum correlations in the initial Gaussian state. An overview of the results of this section is provided in Fig. 5.

1. Quantum non-Gaussianity and entanglement

To understand the role of quantum entanglement in a conditional preparation scheme, we contrast it to a system with only classical correlations. In that regard, let us suppose that the initial quantum state is separable such that its Wigner function can be cast in the form Eq. (222). By inserting this form in Eq. (188), we find that

$$W_{\mathbf{f}|\mathbf{A}}(\vec{x}_{\mathbf{f}}) = \int \mathrm{d}\gamma p(\gamma) \frac{\int_{\mathbb{R}^{2l'}} \mathrm{d}\vec{x}_{\mathbf{g}} W_A(\vec{x}_{\mathbf{g}}) W_{\mathbf{g}}^{(\gamma)}(\vec{x}_{\mathbf{g}})}{\int_{\mathbb{R}^{2l'}} \mathrm{d}\vec{x}_{\mathbf{g}} W_A(\vec{x}_{\mathbf{g}}) W_{\mathbf{g}}(\vec{x}_{\mathbf{g}})} W_{\mathbf{f}}^{(\gamma)}(\vec{x}_{\mathbf{f}}). \tag{240}$$

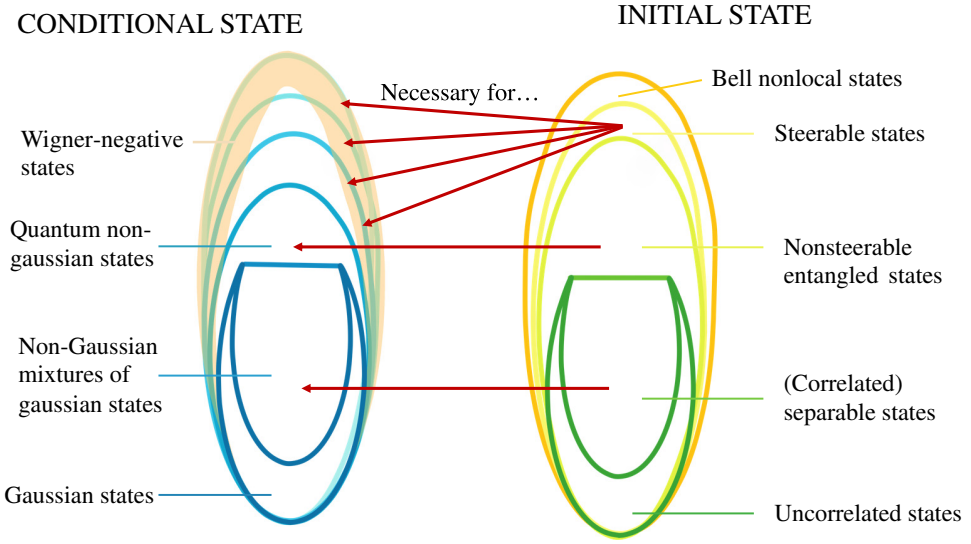

FIG. 5. Different types of quantum correlations are required to be present in the initial Gaussian state $W(\vec{x})$ to create conditional states $W_{\mathbf{f}|\mathbf{A}}(\vec{x}_{\mathbf{f}})$, as described in Eq. (190), that belong to a certain class. We thus show how the typical hierarchy of quantum correlations (right) can be connected to the structure of the CV state space that was introduced previously in Fig. 1. Throughout Sec. B, we prove that these different types of quantum correlations are necessary resources to achieve different types of states.

As a next step, we define

$$\tilde{p}_A(\gamma) := p(\gamma)\frac{\int_{\mathbb{R}^{2l'}} \mathrm{d}\vec{x}_{\mathbf{g}} W_A(\vec{x}_{\mathbf{g}}) W^{(\gamma)}_{\mathbf{g}}(\vec{x}_{\mathbf{g}})}{\int_{\mathbb{R}^{2l'}} \mathrm{d}\vec{x}_{\mathbf{g}} W_A(\vec{x}_{\mathbf{g}}) W_{\mathbf{g}}(\vec{x}_{\mathbf{g}})}, \tag{241}$$

and show that $\tilde{p}_A(\gamma)$ is a well-defined probability distribution. First, we use the definition of the reduced state

$$W_{\mathbf{g}}(\vec{x}_{\mathbf{g}}) = \int_{\mathbb{R}^{2l}} \mathrm{d}\vec{x}_{\mathbf{f}} W(\vec{x}_{\mathbf{f}} \oplus \vec{x}_{\mathbf{g}}) \tag{242}$$

$$= \int \mathrm{d}\gamma p(\gamma) W^{(\gamma)}_{\mathbf{g}}(\vec{x}_{\mathbf{g}}), \tag{243}$$

and thus we immediately find that $\int \mathrm{d}\gamma \tilde{p}_A(\gamma) = 1$. Furthermore, we note that $W^{(\gamma)}_{\mathbf{g}}(\vec{x}_{\mathbf{g}})$ is the Wigner function of a well-defined quantum state $\hat{\rho}^{(\gamma)}_{\mathbf{g}}$ and thus

$$\int_{\mathbb{R}^{2l'}} \mathrm{d}\vec{x}_{\mathbf{g}} W_A(\vec{x}_{\mathbf{g}}) W^{(\gamma)}_{\mathbf{g}}(\vec{x}_{\mathbf{g}}) = \mathrm{tr}[\hat{\rho}^{(\gamma)}_{\mathbf{g}} \hat{A}] \geqslant 0. \tag{244}$$

The final inequality follows from the fact that $\hat{A}$ is a positive semidefinite operator. As a consequence, we find that $\tilde{p}_A(\gamma) \geqslant 0$ for every possible γ. Thus, we find that for a separable initial state

$$W_{\mathbf{f}|\mathbf{A}}(\vec{x}_{\mathbf{f}}) = \int \mathrm{d}\gamma \tilde{p}_A(\gamma) W^{(\gamma)}_{\mathbf{f}}(\vec{x}_{\mathbf{f}}). \tag{245}$$

Up to this point, we assumed only that the initial state is separable. As we saw in Sec. C, a mixed quantum state with a positive Wigner function cannot necessarily be decomposed in states with positive Wigner functions. Therefore, we can generally not infer much about the properties of the Wigner function $W^{(\gamma)}_{\mathbf{f}}(\vec{x}_{\mathbf{f}})$ in Eq. (245).

As a next step, we use the fact that the initial state is also a Gaussian state. Recall from Eq. (103) that any mixed Gaussian state can be decomposed as a mixture of pure Gaussian states. *A priori*, however, it is not trivial that this decomposition is consistent with decomposition in separable states, Eq. (222). Thus, it remains to show that for Gaussian separable states the Wigner functions $W^{(\gamma)}_{\mathbf{f}}(\vec{x}_{\mathbf{f}})$ and $W^{(\gamma)}_{\mathbf{g}}(\vec{x}_{\mathbf{g}})$ in Eq. (222) are also Gaussian.

We start from a crucial observation on covariance matrices that was made in Ref. [207]: whenever an m-mode state with covariance matrix V is separable, there are covariance matrices $V'_{\mathbf{f}}$ and $V'_{\mathbf{g}}$ such that

$$V \geqslant \begin{pmatrix} V'_{\mathbf{f}} & 0 \\ 0 & V'_{\mathbf{g}} \end{pmatrix} = V'_{\mathbf{f}} \oplus V'_{\mathbf{g}}. \tag{246}$$

Note that $V'_{\mathbf{f}}$ and $V'_{\mathbf{g}}$ are covariance matrices on the phase spaces $\mathbb{R}^{2l}$ and $\mathbb{R}^{2l'}$, respectively. Nevertheless, $V'_{\mathbf{f}}$ and $V'_{\mathbf{g}}$ are generally not the same as the covariance matrices $V_{\mathbf{f}}$ and $V_{\mathbf{g}}$ of Eq. (185) that describe the marginal distributions. We should emphasize that the Williamson, Eq. (92), and Bloch-Messiah, Eq. (95), decompositions offer the necessary tools to explicitly construct $V'_{\mathbf{f}}$ and $V'_{\mathbf{g}}$ (we come back to this point in Sec. C). This allows us to use similar techniques as in Eq. (103). Let us first define

$$W'_{\mathbf{f}}(\vec{x}_{\mathbf{f}}) := \frac{e^{-\frac{1}{2}\vec{x}_{\mathbf{f}}^T V'^{-1}_{\mathbf{f}} \vec{x}_{\mathbf{f}}}}{(2\pi)^m \sqrt{\det V'_{\mathbf{f}}}}, \tag{247}$$

$$W'_{\mathbf{g}}(\vec{x}_{\mathbf{g}}) := \frac{e^{-\frac{1}{2}\vec{x}_{\mathbf{g}}^T V'^{-1}_{\mathbf{g}} \vec{x}_{\mathbf{g}}}}{(2\pi)^m \sqrt{\det V'_{\mathbf{g}}}}. \tag{248}$$

We can then use Eq. (246) to define a positive definite matrix $V_c := V - V'_{\mathbf{f}} \oplus V'_{\mathbf{g}}$, such that a decomposition of the type Eq. (103) gives us

$$W(\vec{x}_{\mathbf{f}} \oplus \vec{x}_{\mathbf{g}}) = \int_{\mathbb{R}^{2m}} \mathrm{d}\vec{y}\ W'_{\mathbf{f}}(\vec{x}_{\mathbf{f}} - \vec{y}_{\mathbf{f}}) W'_{\mathbf{g}}(\vec{x}_{\mathbf{g}} - \vec{y}_{\mathbf{g}}) \times \frac{e^{-\frac{1}{2}(\vec{y}-\vec{\xi})^T V_c^{-1}(\vec{y}-\vec{\xi})}}{(2\pi)^m \sqrt{\det V_c}}, \tag{249}$$

where we again impose the structure of the bipartition on $\vec{y} = \vec{y}_{\mathbf{f}} \oplus \vec{y}_{\mathbf{g}}$, with $\vec{y}_{\mathbf{f}} \in \mathbb{R}^{2l}$ and $\vec{y}_{\mathbf{g}} \in \mathbb{R}^{2l'}$. Furthermore, recall that $\vec{\xi}$ is the mean field of the initial Gaussian state $W(\vec{x}_{\mathbf{f}} \oplus \vec{x}_{\mathbf{g}})$. The structure we obtain in Eq. (249) exactly corresponds to Eq. (222), where $\vec{y}$ now labels the states and thus plays the role of the abstract variable γ.

We can then use the structure Eq. (249) in the derivation Eq. (245) and then we find that

$$W_{\mathbf{f}|\mathbf{A}}(\vec{x}_{\mathbf{f}}) = \int_{\mathbb{R}^{2l}} \mathrm{d}\vec{y}_{\mathbf{f}} W'_{\mathbf{f}}(\vec{x}_{\mathbf{f}} - \vec{y}_{\mathbf{f}}) \tilde{p}_A(\vec{y}_{\mathbf{f}}). \tag{250}$$

In any concrete choice of $\hat{A}$, one can use Eq. (241) to derive an explicit expression for $\tilde{p}_A(\vec{y}_{\mathbf{f}})$, which will generally be a non-Gaussian probability distribution, such that $W_{\mathbf{f}|\mathbf{A}}(\vec{x}_{\mathbf{f}})$ describes a non-Gaussian state. However, the resulting conditional state, Eq. (250), is clearly a statistical mixture of Gaussian states and thus lies in the convex hull of Gaussian states. In the language of Sec. C this means that the conditional state is non-Gaussian but not quantum non-Gaussian and has a stellar rank 0.

In summary, we have assumed that our initial state with Wigner function $W(\vec{x}_{\mathbf{f}} \oplus \vec{x}_{\mathbf{g}})$ is a separable Gaussian state. Without making any assumptions on the POVM element $\hat{A}$ of the conditional operation, we retrieve that the conditional state always is a convex combination of Gaussian states, given by Eq. (250). Thus, when the initial state is Gaussian, entanglement is a necessary resource to produce quantum non-Gaussian states via conditional operations.

2. Wigner negativity and Einstein-Podolsky-Rosen steering

In Sec. E, we explained that Wigner negativity is a "stronger" non-Gaussian feature than quantum non-Gaussianity. Here, we show that also stronger types of quantum correlations are required to conditionally create Wigner negativity. To understand how Wigner negativity can be achieved through a conditional preparation scheme, it suffices to understand when the conditional expectation value $\langle\hat{A}\rangle_{\mathbf{g}|\vec{x}_\mathbf{f}}$ in Eq. (192) reaches negative values.

Regardless of the chosen POVM, $W_A(\vec{x}_\mathbf{g})$ is the Wigner function of a positive semidefinite operator $\hat{A}$ as defined by Eq. (42). Thus, whenever there is a quantum state $\hat{\rho}'$ that has $W(\vec{x}_\mathbf{g} \mid \vec{x}_\mathbf{f})$ as associated Wigner function, Eq. (43) implies that $\langle\hat{A}\rangle_{\mathbf{g}|\vec{x}_\mathbf{f}} = \mathrm{tr}[\hat{\rho}'\hat{A}] \geqslant 0$. Hence, to conditionally create a nonpositive Wigner function (190) the conditional probability distribution $W(\vec{x}_\mathbf{g} \mid \vec{x}_\mathbf{f})$ cannot be a well-defined Wigner function. This observation holds whenever the initial state has a positive Wigner function.

When in addition we assume that the initial state is Gaussian, we find that $W(\vec{x}_\mathbf{g} \mid \vec{x}_\mathbf{f})$ is a Gaussian distribution (193). Whether the conditional probability distribution Eq. $W(\vec{x}_\mathbf{g} \mid \vec{x}_\mathbf{f})$ describes a Gaussian quantum state depends entirely in the properties of its covariance matrix, i.e., the Schur complement $V_{\mathbf{g}|\vec{x}_\mathbf{f}}$. Indeed, $W(\vec{x}_\mathbf{g} \mid \vec{x}_\mathbf{f})$ describes a quantum state if and only if $V_{\mathbf{g}|\vec{x}_\mathbf{f}}$ satisfies the Heisenberg inequality. Because $V_{\mathbf{g}|\vec{x}_\mathbf{f}}$ does not depend on the choice $\vec{x}_\mathbf{f} \in \mathbb{R}^{2l}$, it follows that $W(\vec{x}_\mathbf{g} \mid \vec{x}_\mathbf{f})$ corresponds to a quantum state either for all $\vec{x}_\mathbf{f} \in \mathbb{R}^{2l}$ [if the Schur complement Eq. (194) satisfies the Heisenberg inequality] or for none of the $\vec{x}_\mathbf{f} \in \mathbb{R}^{2l}$ [if the Schur complement Eq. (194) violates the Heisenberg inequality].

If $V_{\mathbf{g}|\vec{x}_\mathbf{f}}$ satisfies the Heisenberg inequality, the conditional state's Wigner function $W_{\mathbf{f}|\mathbf{A}}(\vec{x}_\mathbf{f})$ must thus be positive. To better understand the physical resources required to conditionally create Wigner negativity, one must comprehend what it means for $V_{\mathbf{g}|\vec{x}_\mathbf{f}}$ to violate Heisenberg's inequality in terms of quantum correlations. It turns out that this condition is closely related to the original argument of the EPR paper [172]. The violation of Heisenberg's inequality by the Schur complement $V_{\mathbf{g}|\vec{x}_\mathbf{f}}$ corresponds to Gaussian quantum steering in the state $W(\vec{x}_\mathbf{g} \oplus \vec{x}_\mathbf{f})$.

To understand the connection between the conditional covariance matrix $V_{\mathbf{g}|\vec{x}_\mathbf{f}}$ and quantum steering, we first express the Wigner function obtained by conditioning on a Gaussian measurement, such that the associated POVM element has a Wigner function $W_G(\vec{x}_\mathbf{f})$:

$$W_{\mathbf{g}|G}(\vec{x}_\mathbf{g}) = \frac{\int_{\mathbb{R}^{2l}} \mathrm{d}\vec{x}_\mathbf{f} W_G(\vec{x}_\mathbf{f}) W(\vec{x}_\mathbf{f} \mid \vec{x}_\mathbf{g})}{\int_{\mathbb{R}^{2l}} \mathrm{d}\vec{x}_\mathbf{f} W_G(\vec{x}_\mathbf{f}) W_\mathbf{f}(\vec{x}_\mathbf{f})} W_\mathbf{g}(\vec{x}_\mathbf{g}). \tag{251}$$

In a very similar way, we can also show that

$$W_{\mathbf{g}|G}(\vec{x}_\mathbf{g}) = \int_{\mathbb{R}^{2l}} \mathrm{d}\vec{x}_\mathbf{f} \frac{W_G(\vec{x}_\mathbf{f}) W_\mathbf{f}(\vec{x}_\mathbf{f})}{\int_{\mathbb{R}^{2l}} \mathrm{d}\vec{x}_\mathbf{f} W_G(\vec{x}_\mathbf{f}) W_\mathbf{f}(\vec{x}_\mathbf{f})} W(\vec{x}_\mathbf{g} \mid \vec{x}_\mathbf{f}). \tag{252}$$

Hence, when $W(\vec{x}_\mathbf{g} \mid \vec{x}_\mathbf{f})$ is a bona fide Wigner function for every $\vec{x}_\mathbf{f}$ this expression is an explicit manifestation of the local hidden variable model Eq. (230). In other words, whenever $W(\vec{x}_\mathbf{g} \mid \vec{x}_\mathbf{f})$ describes a quantum state, the modes in $\mathbf{g}$ cannot be steered by Gaussian measurements on the modes $\mathbf{f}$. Note that we can generalize Gaussian measurements to any measurement with a positive Wigner function.

The remarkable feature of EPR steering is that the inverse statement also holds: when $W(\vec{x}_\mathbf{g} \mid \vec{x}_\mathbf{f})$ is not a bona fide Wigner function Gaussian measurements can steer the state. Let us assume that Eq. (230) holds for Gaussian measurements. It then follows that a well-defined covariance matrix U exists such that the covariance matrix $V_{\mathbf{g}|G}$ of the conditional state $W_{\mathbf{g}|G}(\vec{x}_\mathbf{g})$ satisfies $V_{\mathbf{g}|G} \geqslant U$ for all Gaussian measurements. Furthermore, U is physical and satisfies the Heisenberg inequality. Reference [176] shows that the existence of such a U implies that the full covariance matrix of the system satisfies $V + 0_\mathbf{f} \oplus i\Omega_\mathbf{g} \geqslant 0$, which in turn implies that $V_{\mathbf{g}|\vec{x}_\mathbf{f}}$, the Schur complement of V, satisfies the Heisenberg inequality.

This shows that we can only generate Wigner negativity through Eq. (190) if the initial state can be steered by Gaussian measurements on the subsystem associated with phase space $\mathbb{R}^{2l}$. Note that the creation of Wigner negativity occurs in the opposite direction to the steering: We can produce Wigner negativity in the modes $\mathbf{f}$ by performing a measurement on the modes $\mathbf{g}$ if the modes $\mathbf{g}$ can be steered by performing Gaussian measurements on the modes $\mathbf{f}$. Somewhat counterintuitively, it turns out that the created Wigner negativity volume, Eq. (156), is not directly proportional to the strength of EPR steering [208].

As a final remark, we note that, in a multimode context, EPR steering is constrained by monogamy relations [209–211]. Notably, this implies that when a single mode g can be steered by a single other mode f, it is impossible for any other mode to also steer g. This naturally has profound consequences for the conditional generation of Wigner negativity that we discussed in this section. The monogamy relations for quantum steering can be used to derive similar monogamy relations [208] for the created Wigner negativity volume (156).

C. Quantum correlations through non-Gaussianity

In Sec. B, we extensively considered the use of quantum correlations as a resource to create non-Gaussian effects. In this subsection, we focus on the opposite idea where non-Gaussian operations increase or even create quantum

correlations. The subject of entanglement in non-Gaussian states is generally difficult to study, for some states it may be sufficient to evaluate lower-order moments [212] and when the density matrix in the Fock representation is available one can apply DV approaches to characterize entanglement [213]. However, these methods cannot always be applied and there are no universally applicable entanglement criteria that are practical to evaluate for arbitrary CV quantum states.

1. Entanglement measures on phase space

In Sec. 2, we argued that any pure state that manifests correlations between subsystems contains entanglement. Measuring entanglement in this case becomes equivalent to measuring the amount of correlation within the pure state. In particular, for pure states, one finds a wide range of entanglement measures in the literature [161]. In the case of CV systems, some measures are more appropriate than others, and here we focus on one particularly intuitive measure that is based on purity.

When we consider an arbitrary bipartite pure quantum state with Wigner function $W(\vec{x}_{\mathbf{f}} \oplus \vec{x}_{\mathbf{g}})$ (with $\vec{x}_{\mathbf{f}} \in \mathbb{R}^{2l}$ and $\vec{x}_{\mathbf{g}} \in \mathbb{R}^{2l'}$), we find that its purity is $\mu = 1$ by definition. However, this is not necessarily true for the subsystems **f** and **g**. We can use Eq. (94) to evaluate the purity of any state based on its Wigner function, and we define

$$\mu_{\mathbf{f}} = \int_{\mathbb{R}^{2l}} \mathrm{d}\vec{x}_{\mathbf{f}} [W_{\mathbf{f}}(\vec{x}_{\mathbf{f}})]^2, \text{ and } \quad \mu_{\mathbf{g}} = \int_{\mathbb{R}^{2l'}} \mathrm{d}\vec{x}_{\mathbf{g}} [W_{\mathbf{g}}(\vec{x}_{\mathbf{g}})]^2, \tag{253}$$

where we again use the definitions (182), (183). Because the global state with Wigner function $W(\vec{x}_{\mathbf{f}} \oplus \vec{x}_{\mathbf{g}})$ is pure, we always find that $\mu_{\mathbf{f}} = \mu_{\mathbf{g}}$ (this is a general consequence of the existence of a Schmidt decomposition for pure states). Furthermore, if the pure state is separable, we find $W(\vec{x}_{\mathbf{f}} \oplus \vec{x}_{\mathbf{g}}) = W_{\mathbf{f}}(\vec{x}_{\mathbf{f}}) W_{\mathbf{g}}(\vec{x}_{\mathbf{g}})$ and as a consequence we obtain that $\mu_{\mathbf{f}} = \mu_{\mathbf{g}} = 1$. However, when $\mu_{\mathbf{f}} = \mu_{\mathbf{g}} < 1$ there must be correlations between the subsystems **f** and **g** and the smaller the purity of the subsystems, the stronger these correlations are. Without delving into the details, we stress that the opposite notion also holds: when there is a correlation between the subsystems, the purity of the subsystems is smaller than one.

To convert this quantity into an entanglement measure [214], it is useful to define the Rényi-2 entropy for subsystem **f**

$$S_R := -\log \mu_{\mathbf{f}}. \tag{254}$$

We then find that $S_R \geqslant 0$ and $S_R = 0$ if and only if the state is separable. Furthermore, it should be clear that S_R cannot be increased by local unitary operations on the subsystems **f** and **g**. We can thus define an entanglement measure for the pure state $|\Psi\rangle$ with Wigner function $W(\vec{x}_{\mathbf{f}} \oplus \vec{x}_{\mathbf{g}})$ by setting

$$\mathcal{E}_R(|\Psi\rangle) := S_R. \tag{255}$$

This constitutes a well-defined entanglement measure for any chosen bipartition and any pure state on the phase space.

To extend this measure to mixed states, we follow Ref. [214] and construct a convex roof. Any mixed state $\hat{\rho}$ can be decomposed in pure states as $\hat{\rho} = \int \mathrm{d}\gamma\, p(\gamma) \left|\Psi^{(\gamma)}\right\rangle\!\left\langle\Psi^{(\gamma)}\right|$, we abbreviate this decomposition as the ensemble $\{p(\gamma), \left|\Psi^{(\gamma)}\right\rangle\}$. For each pure state in this ensemble, we can evaluate the entanglement $\mathcal{E}_R(\left|\Psi^{(\gamma)}\right\rangle)$ and subsequently average all of these values according to $p(\gamma)$. However, the decomposition of $\hat{\rho}$ in pure states is far from unique and different ensembles $\{p(\gamma), \left|\Psi^{(\gamma)}\right\rangle\}$ generally lead to a different value of entanglement even though they are all constrained to produce the same state $\hat{\rho}$. Therefore, it is common to define

$$\mathcal{E}_R(\hat{\rho}) := \inf_{\{p(\gamma), \left|\Psi^{(\gamma)}\right\rangle\}} \int \mathrm{d}\gamma\, p(\gamma) \mathcal{E}_R\left(\left|\Psi^{(\gamma)}\right\rangle\right) \tag{256}$$

as the general "Rényi-2 entanglement" of the state $\hat{\rho}$.

Formally, this is an elegant definition that can in principle be calculated directly from the Wigner function. However, in practice it is nearly impossible to actually identify all possible decompositions $\{p(\gamma), \left|\Psi^{(\gamma)}\right\rangle\}$, which makes this measure notoriously hard to evaluate for mixed states. This has sparked some alternative definitions of entanglement measures for Gaussian states, where any Gaussian state can be decomposed in an ensemble of Gaussian states, Eq. (103). Thus, one can define "Gaussian Rényi-2 entanglement" by restricting Eq. (256) to only Gaussian decompositions [215]. In this sense, Gaussian Rényi-2 entanglement is by construction an upper bound to the general Rényi-2 entanglement.

As an alternative to entanglement measures, it is common to use entanglement witnesses. These have been particularly successful for Gaussian states [146,216–220], where one commonly applies methods based on the covariance matrix of the state. Due to the extremality of Gaussian states [12] these results also provide witnesses for entanglement if the state is non-Gaussian. However, there are several examples of non-Gaussian entangled states for which no entanglement can be detected from the covariance matrix. Notable progress was made by developing entanglement witnesses for non-Gaussian states with specific structure in their Wigner function [221].

It is noteworthy to emphasize that the positive-partial transpose (PPT) criterion of Ref. [216] can in principle be implemented on the level of Wigner functions. To make this apparent, let us first define the transposition operator T that implements $\hat{\rho} \mapsto \hat{\rho}^T$. When $W(\vec{x})$ with $\vec{x} \in \mathbb{R}^{2m}$

denotes the Wigner function of the state $\hat{\rho}$, we can write the Wigner function of $\hat{\rho}^T$ as $W(T\vec{x})$. The matrix T can be written as

$$T = \bigoplus^{m} \begin{pmatrix} 1 & 0 \\ 0 & -1 \end{pmatrix}, \tag{257}$$

which can be derived from the definition of the Wigner function [222]. The concept of partial transposition in entanglement theory relies on the simple idea that one can apply a transpose only on one of the two subsystems in the bipartition. In our context, this means that the Wigner function changes as $W(\vec{x}_{\mathbf{f}} \oplus \vec{x}_{\mathbf{g}}) \mapsto W(\vec{x}_{\mathbf{f}} \oplus T\vec{x}_{\mathbf{g}})$ (where T is now taken only on the l' modes of subsystem **g**). The PPT criterion is based on the idea that, in absence of entanglement, the function $W(\vec{x}_{\mathbf{f}} \oplus T\vec{x}_{\mathbf{g}})$ still gives a well-defined Wigner function of a quantum state. However, there are entangled states for which this is no longer true and $W(\vec{x}_{\mathbf{f}} \oplus T\vec{x}_{\mathbf{g}})$ becomes unphysical. This lack of physicality is expressed by the fact there exist positive semidefinite operators $\hat{A}$ for which

$$(4\pi)^m \int_{\mathbb{R}^{2m}} \mathrm{d}\vec{x}\, W_A(\vec{x}) W(\vec{x}_{\mathbf{f}} \oplus T\vec{x}_{\mathbf{g}}) < 0. \tag{258}$$

Finding such observables $\hat{A} \geqslant 0$ for a non-Gaussian state $W(\vec{x}_{\mathbf{f}} \oplus \vec{x}_{\mathbf{g}})$ is generally a very hard task. For Gaussian states, on the other hand, the physicality of $W(\vec{x}_{\mathbf{f}} \oplus T\vec{x}_{\mathbf{g}})$ is simply checked through Heisenberg's inequality. For more general non-Gaussian states, this is insufficient and one should check a full hierarchy of inequalities instead [212]. Nevertheless, one may yet uncover more direct methods to check the properties of $W(\vec{x}_{\mathbf{f}} \oplus T\vec{x}_{\mathbf{g}})$.

2. Entanglement increase

One of the most well-known protocols for increasing entanglement is entanglement distillation. In this protocol, one acts with local operations on a large number of mixed entangled states that are shared by two parties and concentrates the entanglement in a smaller number of maximally entangled pairs [223]. When the initial states are pure and the local operation serves only to increase the entanglement and not the purity, we speak of entanglement concentration [224]. Conditional operations play an important role in these protocols, and we can alternatively think of entanglement distillation as the idea that a conditional operation can increase the entanglement of a state. For Gaussian quantum states, there is a notorious no-go theorem that states that Gaussian measurements (or Gaussian operations in general) cannot increase bipartite entanglement [225–227]. It was quickly realized that these no-go results can be circumvented by even the most basics non-Gaussian states: those created through a non-Gaussian noise process [228,229]. On the other hand, if one wants to distill entanglement in a CV system starting from initial Gaussian states one really requires non-Gaussian operations. One such example is given in Refs. [230,231], where the authors propose to use a Kerr nonlinearity to distill entanglement for mixed Gaussian states. In contrast, conditional schemes have also been proposed [147,232,233], avoiding the need for optical nonlinearities. In those protocols, one first uses conditional operations to create non-Gaussian states and subsequently uses Gaussification to obtain states with higher entanglement. A narrowly related protocol [234] relies on the implementation of noiseless linear amplification [235], where the non-Gaussian element is injected in the form of auxiliary Fock states.

The realization that photon subtraction and addition can be used to increase the entanglement of a Gaussian input state was developed reasonably early [236–238] and was further formalized in works such as Refs. [239–241]. Remarkably, all of these works explicitly assume that the initial state under consideration is a two-mode squeezed state and the approach strongly relies on the structure of this type of state in the Fock basis. Beyond the two mode setting, the class of CV graph states has also been studied in the context of entanglement increase [242,243]. Here we provide an alternative approach, based on phase-space representations to understand entanglement increase due to the subtraction of a single photon.

Our approach relies on the fact that we can easily apply the entanglement measure (256) when the global state is pure. This means that we are focusing on a context of entanglement concentration. Furthermore, when we perform photon subtraction on a pure Gaussian state, the resulting photon-subtracted state is also pure, as we saw in Sec. 2. The starting point is the Wigner function of the photon-subtracted state, Eq. (214), which we rewrite as

$$W^-(\vec{x}) = \frac{W(\vec{x})}{\mathrm{tr}\,(V_{\mathbf{b}} - \mathbb{1}) + \|\vec{\xi}_{\mathbf{b}}\|^2} \Big(\|B^T(\mathbb{1} - V^{-1})(\vec{x} - \vec{\xi}) + \vec{\xi}_{\mathbf{b}}\|^2 + \mathrm{tr}\left[\mathbb{1} - B^T V^{-1} B\right] \Big). \tag{259}$$

The state $W^-(\vec{x})$ is thus obtained by subtracting a photon from the Gaussian state $W(\vec{x})$. As we consider a pure two-mode state we assume that the state has a 4×4 covariance matrix of the form $V = S^T S$, where S is a symplectic matrix. We assume that the photon is locally subtracted in one of the modes of the mode basis, such that

$$B = \begin{pmatrix} 0 & 0 \\ 0 & 0 \\ 1 & 0 \\ 0 & 1 \end{pmatrix}. \tag{260}$$

However, to assess the entanglement in the system, we must obtain the Wigner function for the reduced state associated to either of the two modes. When we focus on mode

b where the photon is subtracted, we can simply obtain the reduced photon subtracted state $W_{\mathbf{b}}^{-}(\vec{x}_{\mathbf{b}})$ by subtracting a photon from the reduced Gaussian state $W_{\mathbf{b}}(\vec{x}_{\mathbf{b}})$. As such, we obtain

$$W_{\mathbf{b}}^{-}(\vec{x}_{\mathbf{b}}) = \frac{\|(\mathbb{1} - V_{\mathbf{b}}^{-1})\vec{x}_{\mathbf{b}} + V_{\mathbf{b}}^{-1}\vec{\xi}_{\mathbf{b}}\|^2 + \mathrm{tr}\left[\mathbb{1} - V_{\mathbf{b}}^{-1}\right]}{\mathrm{tr}\,(V_{\mathbf{b}} - \mathbb{1}) + \|\vec{\xi}_{\mathbf{b}}\|^2} W_{\mathbf{b}}(\vec{x}_{\mathbf{b}}). \tag{261}$$

This is now a single-mode photon subtracted state, but it is no longer pure. This lack of purity is notably reflected by $V_{\mathbf{b}}$, which is no longer symplectic. Nevertheless, we can use the Williamson decomposition, Eq. (92), and write

$$V_{\mathbf{b}} = \nu \begin{pmatrix} r & 0 \\ 0 & r^{-1} \end{pmatrix}, \tag{262}$$

where we set the phase such that the squeezing coincides with one of the axes of phase space. What remains is for us to calculate the purity

$$\mu_{\mathbf{b}}^{-} = 4\pi \int_{\mathbb{R}^2} \mathrm{d}\vec{x}_{\mathbf{b}} [W_{\mathbf{b}}^{-}(\vec{x}_{\mathbf{b}})]^2. \tag{263}$$

The final expression for the purity is not very insightful. When on top we use that the purity $\mu_{\mathbf{b}}$ of the Gaussian state $W_{\mathbf{b}}(\vec{x}_{\mathbf{b}})$ is given by $\mu_{\mathbf{b}} = 1/\nu$, an explicit calculation of $\mu_{\mathbf{b}}^{-}$ makes it possible to prove (the motivated reader can use a combination of patience and software for symbolic algebra to do so) that

$$\frac{\mu_{\mathbf{b}}^{-}}{\mu_{\mathbf{b}}} \leqslant \frac{1}{2}. \tag{264}$$

In other words, photon subtraction reduces the purity at most by a factor of 2.

When we use Eq. (256) to define the entanglement of the two-mode photon-subtracted state, Eq. (259), we find that it is given by

$$\mathcal{E}_R(|\Psi^{-}\rangle) = -\log \mu_{\mathbf{b}}^{-}, \tag{265}$$

because the two-mode state is pure. The entanglement of the initial Gaussian state is given by $\mathcal{E}_R(|\Psi_G\rangle) = -\log \mu_{\mathbf{b}}$, such that we can use Eq. (264) to find that

$$\Delta\mathcal{E}_R := \mathcal{E}_R(|\Psi^{-}\rangle) - \mathcal{E}_R(|\Psi_G\rangle) \leqslant \log 2. \tag{266}$$

In other words, photon subtraction can increase the Rényi-2 entanglement of an arbitrary Gaussian state, but at most by an amount $\log 2$. It turns out that this result can be generalized to all bipartitions of Gaussian pure states of an arbitrary number of modes [244]. Furthermore, the same work shows that when the entanglement measure $\mathcal{E}_R(|\Psi_G\rangle)$ is replaced with the Gaussian Rényi-2 entropy of Ref. [215], the result holds for all bipartitions of all Gaussian states (including mixed ones).

For the particular case of a two-mode pure Gaussian state, we can directly evaluate $\Delta\mathcal{E}_R$ for some important examples. Say, for example, that we consider the EPR state that is obtained by mixing two oppositely squeezed vacuum states on a balanced beam splitter. In this case $\vec{\xi} = 0$ and V is given by

$$\begin{aligned} V &= \frac{1}{2}\begin{pmatrix} 1 & 0 & 1 & 0 \\ 0 & 1 & 0 & 1 \\ -1 & 0 & 1 & 0 \\ 0 & -1 & 0 & 1 \end{pmatrix}^T \begin{pmatrix} s & & & \\ & s^{-1} & & \\ & & s^{-1} & \\ & & & s \end{pmatrix} \\ &\quad \times \begin{pmatrix} 1 & 0 & 1 & 0 \\ 0 & 1 & 0 & 1 \\ -1 & 0 & 1 & 0 \\ 0 & -1 & 0 & 1 \end{pmatrix} \\ &= \frac{1}{2s}\begin{pmatrix} s^2+1 & 0 & s^2-1 & 0 \\ 0 & s^2+1 & 0 & 1-s^2 \\ s^2-1 & 0 & s^2+1 & 0 \\ 0 & 1-s^2 & 0 & s^2+1 \end{pmatrix}. \end{aligned} \tag{267}$$

We then extract directly that

$$V_{\mathbf{b}} = \frac{s^2+1}{2s}\,\mathbb{1}, \tag{268}$$

such that we find that the parameters in Eq. (262) are set to $r = 1$ and $\nu = (s^2+1)/(2s)$. And thus we directly obtain

$$\Delta\mathcal{E}_R = \log(2) - \log\left(\frac{s^4 + 6s^2 + 1}{(s^2+1)^2}\right). \tag{269}$$

We clearly see that the entanglement increase vanishes in absence of squeezing, whereas we achieve the $\log(2)$ limit for $s \to \infty$. Adding a mean field with $\vec{\xi}_{\mathbf{b}} \neq 0$ immediately complicates the problem. As can be seen in Fig. 6, where we plot the case $\vec{\xi}_{\mathbf{b}} = (0,1)^T$, the presence of a mean field in the mode of photon subtraction lowers the entanglement increase $\Delta\mathcal{E}_R$. Nevertheless, in the limit $s \to \infty$ we reach the limit $\log(2)$ regardless of the displacement.

This example clearly shows that photon subtraction can be used as a tool to increase entanglement. The setting corresponds to the case that is typically studied in most works on CV entanglement distillation such as Refs. [239–241]. It turns out that one can further increase entanglement in such systems by subtracting more photons. Furthermore, photon addition and the combination of addition and subtraction on both modes have also been considered. The methods we use in this Tutorial are not easily generalized to the subtraction and addition of many photons, but in return they can be applied to a much wider class of initial Gaussian states.

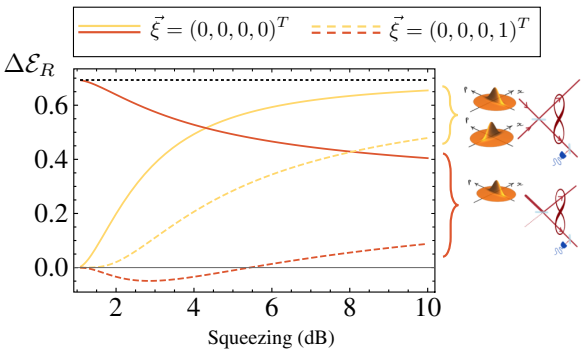

FIG. 6. Entanglement increase, Eq. (266), through photon subtraction in one mode of a pair of entangled modes. The initial Gaussian states are obtained by mixing either two equally squeezed modes (yellow curves) or one squeezed mode and one vacuum mode (red curves) on a beam splitter (see also sketches on the right). We show how a variation of squeezing (in dB compared to shot noise level) in these initial squeezed vacuum states influences the entanglement increase due to photon subtraction. We consider cases without mean field (solid curves) and with a mean field $\vec{\xi} = (0,0,0,1)^T$ (dashed curves).

As a second example, we consider a single-mode squeezed state that is split in two on a balanced beam splitter. This means that the Gaussian state is given by

$$V = \frac{1}{2}\begin{pmatrix} 1 & 0 & 1 & 0 \\ 0 & 1 & 0 & 1 \\ -1 & 0 & 1 & 0 \\ 0 & -1 & 0 & 1 \end{pmatrix}^T \begin{pmatrix} s & & & \\ & s^{-1} & & \\ & & 1 & \\ & & & 1 \end{pmatrix} \times \begin{pmatrix} 1 & 0 & 1 & 0 \\ 0 & 1 & 0 & 1 \\ -1 & 0 & 1 & 0 \\ 0 & -1 & 0 & 1 \end{pmatrix} = \frac{1}{2}\begin{pmatrix} s+1 & 0 & s-1 & 0 \\ 0 & \frac{s+1}{s} & 0 & \frac{1}{s}-1 \\ s-1 & 0 & s+1 & 0 \\ 0 & \frac{1}{s}-1 & 0 & \frac{s+1}{s} \end{pmatrix}, \tag{270}$$

such that we get

$$V_{\mathbf{b}} = \frac{1}{2}\begin{pmatrix} s+1 & 0 \\ 0 & \frac{s+1}{s} \end{pmatrix}, \tag{271}$$

such that we find that we identify the parameters of Eq. (262) as $\nu = \sqrt{2+s+s^{-1}}/2$ and $r = (1+s)/\sqrt{2+s+s^{-1}}$. In absence of any mean field, i.e., with $\vec{\xi} = 0$, we then find an entanglement gain given by

$$\Delta\mathcal{E}_R = \log(2) - \log\left(\frac{3+2s+3s^2}{2(s+1)^2}\right). \tag{272}$$

Interestingly, in this case we reach the maximal entanglement gain for vanishing squeezing $s \to 1$, where we reach $\Delta\mathcal{E}_R \to \log(2)$. This case may seem somewhat counterintuitive, but it should be emphasized that the success probability of photon subtraction also vanishes in this case. Yet, our conditional approach assumes that we are in the scenario where a photon was subtracted and the negligible fraction of the state that is not in vacuum is enhanced. In the limit of vanishing squeezing, the photon subtracted state converges to the Bell state $(|1,0\rangle + |0,1\rangle)/\sqrt{2}$. On the other hand, in the limit where squeezing is high we still find a finite entanglement increase as $\Delta\mathcal{E}_R \to \log(4/3)$.

When we add a mean field given by $\vec{\xi}_{\mathbf{b}} \neq 0$, there is an importance of the phase because our state locally has some remaining asymmetry (which can be seen from $r \neq 1$). In Fig. 6 we particularly show the case where $\vec{\xi}_{\mathbf{b}} = (0,1)^T$ such that the direction of the displacement coincides with the quadrature where the noise is minimal. In this case we observe that for some values of initial squeezing, the entanglement decreases due to photon subtraction. Note that this quite remarkably implies that in some cases photon subtraction can actually be used to increase the purity of a state.

We thus showed that photon subtraction is a useful non-Gaussian operation to increase entanglement. However, in the presence of a mean field in the subtraction mode, it is also possible to decrease entanglement. Even though this subject has been studied for nearly two decades, for arbitrary Gaussian input states, there are still many open questions. Notably, there has not been much work on the effect of photon subtraction on multipartite entanglement, nor on stronger types of quantum correlations. Our discussion in Sec. 2 suggests an important interplay between EPR steering and Wigner negativity, and thus it is intriguing to wonder whether well-chosen non-Gaussian operations can increase quantum steering. Since all steerable states are also entangled, it is a reasonable conjecture that some of the protocols that can increase quantum entanglement should also increase quantum steering.

We have followed the terminology found in the literature and referred to this process as entanglement distillation, because our conditional operation has only a finite success probability. This implies that we can use a large number of Gaussian entangled states and use photon subtraction to obtain a much smaller number of more entangled states. Yet, it must be stressed that there is a more subtle process happening: the entanglement is increased by adding non-Gaussian entanglement on top of the existing Gaussian entanglement. To get a better grasp of this non-Gaussian entanglement, it is useful to go to a setting where no other type of entanglement is present as we do in Sec. 3.

3. Purely non-Gaussian quantum entanglement

In this subsection, we explore an idea that is in many ways complementary to the previous subsection: rather

than using a local non-Gaussian operation to increase already existing entanglement, we now use a nonlocal non-Gaussian operation to create entanglement between unentangled modes.

Let us again assume that our state is initially Gaussian as described by Eq. (85), and we induce the non-Gaussian features through the conditional methods of Sec. B. The mean field of the initial state is given by $\vec{\xi} = \vec{\xi}_{\mathbf{f}} \oplus \vec{\xi}_{\mathbf{g}}$, and

$$V = \begin{pmatrix} V_{\mathbf{f}} & V_{\mathbf{fg}} \\ V_{\mathbf{gf}} & V_{\mathbf{g}} \end{pmatrix}, \quad \text{with} \quad V_{\mathbf{f}} = V_{\mathbf{f_1}} \oplus V_{\mathbf{f_2}}. \tag{273}$$

Here, we have introduced the modes of interest, labeled by $\mathbf{f}$ and a set of auxiliary modes $\mathbf{g}$ upon which a measurement will be performed to induce non-Gaussian features in the modes $\mathbf{f}$. In the initial state, we consider a bipartition in the modes $\mathbf{f}$ without any direct correlations, hence $V_{\mathbf{f}} = V_{\mathbf{f_1}} \oplus V_{\mathbf{f_2}}$. In other words, the modes in $\mathbf{f_1}$ are completely uncorrelated to the modes in $\mathbf{f_2}$.

To induce non-Gaussian effects, we resort to the conditional framework by acting with a POVM element $\hat{A}$ upon the auxiliary modes $\mathbf{g}$, and we rewrite Eq. (190) as

$$W_{\mathbf{f}|\mathbf{A}}(\vec{x}_{\mathbf{f_1}} \oplus \vec{x}_{\mathbf{f_2}}) = \frac{\langle \hat{A} \rangle_{\mathbf{g}|\vec{x}_{\mathbf{f_1}} \oplus \vec{x}_{\mathbf{f_2}}}}{\langle \hat{A} \rangle} W_{\mathbf{f_1}}(\vec{x}_{\mathbf{f_1}}) W_{\mathbf{f_2}}(\vec{x}_{\mathbf{f_2}}), \tag{274}$$

and the conditional expectation value $\langle \hat{A} \rangle_{\mathbf{g}|\vec{x}_{\mathbf{f_1}} \oplus \vec{x}_{\mathbf{f_2}}}$ is again given by Eq. (192). The entanglement in the resulting state thus crucially depends on the exact properties of $\langle \hat{A} \rangle_{\mathbf{g}|\vec{x}_{\mathbf{f_1}} \oplus \vec{x}_{\mathbf{f_2}}}$.

First of all, note that $W_{\mathbf{f_1}}(\vec{x}_{\mathbf{f_1}})$ and $W_{\mathbf{f_2}}(\vec{x}_{\mathbf{f_2}})$ are generally not pure states and as a consequence $W_{\mathbf{f}|\mathbf{A}}(\vec{x}_{\mathbf{f_1}} \oplus \vec{x}_{\mathbf{f_2}})$ is not a pure state either. Even though the specific structure of the Wigner function makes it a suitable case to apply the methods of Ref. [221], we follow a different route in this Tutorial by focusing on a particular example for which we can assume that $W_{\mathbf{f_1}}(\vec{x}_{\mathbf{f_1}})$ and $W_{\mathbf{f_2}}(\vec{x}_{\mathbf{f_2}})$ are pure.

Just as in Sec. 2, we concentrate on photon subtraction. To get a conceptual idea of such a setup in this specific scenario, we present two equivalent schemes in (a) and (b) of Fig. 7. Note that the equivalence stems from the fact that the beam splitters that subtract the light from the signal beams to send it to the photodetector are of extremely low reflectivity. In this limit, we can be sure that there is at most one photon in the path and when it is detected, we herald a single-photon-subtracted state. In Fig. 7(a), the combination of this heralding process and the presence of at most one photon avoids that the unmeasured output causes any losses or impurities. Nevertheless, the unmeasured output will practically change the success probability of the heralding process, such that for practical implementations Fig. 7(b) may be the preferential setup. Recall that the Wigner function for a state with a photon subtracted in a particular mode $\mathbf{b}$ was given by Eq. (259), which here becomes

$$\begin{aligned} W^{-}(\vec{x}_{\mathbf{f_1}} \oplus \vec{x}_{\mathbf{f_2}}) = & \frac{W_{\mathbf{f_1}}(\vec{x}_{\mathbf{f_1}}) W_{\mathbf{f_2}}(\vec{x}_{\mathbf{f_2}})}{\mathrm{tr}\,(V_{\mathbf{b}} - \mathbb{1}) + \|\vec{\xi}_{\mathbf{b}}\|^2} \\ & \times \Big(\|B^T(\mathbb{1} - V_{\mathbf{f_1}}^{-1} \oplus V_{\mathbf{f_2}}^{-1})(\vec{x}_{\mathbf{f_1}} \oplus \vec{x}_{\mathbf{f_2}} \\ & - \vec{\xi}_1 \oplus \vec{\xi}_2) + \vec{\xi}_{\mathbf{b}} \|^2 \\ & + \mathrm{tr}\Big[\mathbb{1} - B^T(V_{\mathbf{f_1}}^{-1} \oplus V_{\mathbf{f_2}}^{-1}) B \Big] \Big). \end{aligned} \tag{275}$$

Because we consider a limit where the state is completely transmitted by the beam splitter and only a negligible amount is sent to the photon counter to subtract the photon, we can indeed assume that the state is pure. For simplicity, we also assume that $\mathbf{f_1}$ and $\mathbf{f_2}$ are single modes. As we did before, we now calculate the reduced state

$$W_1^{-}(\vec{x}_{\mathbf{f_1}}) = \int_{\mathbb{R}^2} \mathrm{d}\vec{x}_{\mathbf{f_2}} W^{-}(\vec{x}_{\mathbf{f_1}} \oplus \vec{x}_{\mathbf{f_2}}). \tag{276}$$

The integral is rather tedious to evaluate, therefore we immediately jump to the result (see Ref. [153] for an alternative method that circumvents the explicit calculation of integrals):

$$\begin{aligned} W_1^{-}(\vec{x}_{\mathbf{f_1}}) = & \frac{W_{\mathbf{f_1}}(\vec{x}_{\mathbf{f_1}})}{\mathrm{tr}\,(V_{\mathbf{b}} - \mathbb{1}) + \|\vec{\xi}_{\mathbf{b}}\|^2} \Big(\|B^T F_1 (\mathbb{1} - V_{\mathbf{f_1}}^{-1})(\vec{x}_{\mathbf{f_1}} - \vec{\xi}_1) \\ & + \vec{\xi}_{\mathbf{b}} \|^2 + \mathrm{tr}\Big[B^T F_1 (\mathbb{1} - V_{\mathbf{f_1}}^{-1}) F_1^T B \Big] \\ & + \mathrm{tr}\left[B^T F_2 (V_{\mathbf{f_2}} - \mathbb{1}) F_2^T B \right] \Big), \end{aligned} \tag{277}$$

where we introduce the matrices F_k, given by

$$F_k = \begin{pmatrix} | & | \\ \vec{f}_k & \Omega \vec{f}_k \\ | & | \end{pmatrix}, \tag{278}$$

such that we can use the properties of the symplectic form Ω to obtain

$$B^T F_k = \begin{pmatrix} \vec{b}^T \vec{f}_k & \vec{b}^T \Omega \vec{f}_k \\ -\vec{b}^T \Omega \vec{f}_k & \vec{b}^T \vec{f}_k \end{pmatrix}. \tag{279}$$

If mode $\mathbf{b}$ is orthogonal to mode $\mathbf{f}_1$, we find that $B^T F_1 = 0$ such that $W_1^{-}(\vec{x}_{\mathbf{f_1}}) = W_{\mathbf{f_1}}(\vec{x}_{\mathbf{f_1}})$. On the other hand, when mode $\mathbf{b}$ is exactly the same as $\mathbf{f}_1$ we find that $B^T F_1 = \mathbb{1}$ such that the photon is only subtracted there. In this case $W_1^{-}(\vec{x}_{\mathbf{f_1}})$ is a pure state and no entanglement is created. In this case, one can check that $W_2^{-}(\vec{x}_{\mathbf{f_2}}) = W_2(\vec{x}_{\mathbf{f_2}})$.

To create entanglement, we are thus interested in the case where $\mathbf{b}$ is a superposition of the two modes $\mathbf{f}_1$ and $\mathbf{f}_2$. To keep things simple, let us assume that $\vec{b} = \cos\theta\, \vec{f}_1 +$

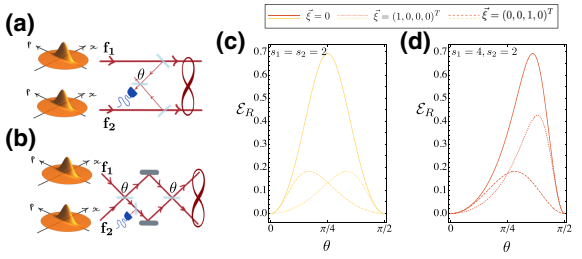

FIG. 7. Entanglement creation through photon subtraction in a superposition of uncorrelated modes $\mathbf{f_1}$ and $\mathbf{f_2}$. (a),(b) Sketches of two equivalent setups to implement a photon subtraction in the mode $\mathbf{b}$, with $\vec{b} = \cos\theta\vec{f}_1 + \sin\theta\vec{f}_2$. In (c),(d), we show the created entanglement, as measure through the Rényi entropy, Eq. (256), for varying values of θ. The initial Gaussian states are pure, with covariance matrices $V_{\mathbf{f_1}} = \mathrm{diag}[s_1, 1/s_1]$ and $V_{\mathbf{f_2}} = \mathrm{diag}[s_2, 1/s_2]$ for modes $\mathbf{f_1}$ and $\mathbf{f_2}$, respectively. The global mean field, i.e., displacement, is varied $\vec{\xi} = 0$ (solid curves), $\vec{\xi} = (1,0,0,0)^T$ (dotted curves), and $\vec{\xi} = (0,0,1,0)^T$ (dotted curves). (c) The particular case where the squeezing is balanced, i.e., $s_1 = s_2 = 2$. (d) An unbalanced example where $s_1 = 4$ and $s_2 = 2$. All squeezing values s_1 and s_2 are measured in units of vacuum noise.

$\sin\theta\vec{f}_2$. Because the modes $\mathbf{f}_1$ and $\mathbf{f}_2$ are orthogonal, we can use that $\vec{f}_1^{\,T}\vec{f}_2 = 0$ and thus we find that $B^T F_1 = \cos\theta\,\mathbb{1}$ and $B^T F_2 = \sin\theta\,\mathbb{1}$. Nevertheless, the general expression for $W_1^-(\vec{x}_{\mathbf{f_1}})$ does not simplify much.

To acquire additional insight, let us now assume that both modes $\mathbf{f_1}$ and $\mathbf{f_2}$ have exactly the same squeezing in the same quadrature:

$$V_{\mathbf{f_1}} = V_{\mathbf{f_2}} = \begin{pmatrix} s & 0 \\ 0 & \frac{1}{s} \end{pmatrix}. \tag{280}$$

Furthermore, let us assume that there is no mean field, such that $\vec{\xi} = 0$. In this particular case, we find the expression

$$W_1^-(x_{\mathbf{f_1}}, p_{\mathbf{f_1}}) = W_1(x_{\mathbf{f_1}}, p_{\mathbf{f_1}}) \times \left[p_{\mathbf{f_1}}^2 s + \frac{x_{\mathbf{f_1}}^2}{s} + \cos(2\theta)\left(p_{\mathbf{f_1}}^2 s + \frac{x_{\mathbf{f_1}}^2}{s} - 2 \right) \right]. \tag{281}$$

In particular, it turns out that the purity takes a simple form, such that we can quantify the entanglement for this state as

$$\mathcal{E}_R = \log(2) - \log\left(\frac{\cos(4\theta) + 3}{2} \right). \tag{282}$$

This shows that the maximal entanglement is reached for $\theta = \pi/4$ and—as expected—the entanglement vanishes when $\theta = 0$ and $\theta = \pi/2$, i.e., when we subtract entirely in either mode $\mathbf{f_1}$ and $\mathbf{f_2}$.

More general settings are shown in Fig. 7, where we show the entanglement creation for unbalanced squeezing, by setting

$$V_{\mathbf{f_1}} = \begin{pmatrix} s_1 & 0 \\ 0 & \frac{1}{s_1} \end{pmatrix}, \quad \text{and} \quad V_{\mathbf{f_2}} = \begin{pmatrix} s_2 & 0 \\ 0 & \frac{1}{s_2} \end{pmatrix}. \tag{283}$$

We compare the case with $s_1 = s_2$ to the case with $s_1 \neq s_2$ and find that in absence of a mean field one can reach the same maximal amount of entanglement. However, the maximum is attained at a different value of θ when the squeezing is unbalanced. From Eq. (282) we know that in absence of a mean field, the curve for $s_1 = s_2$ does not depend on the actual value of squeezing.

Figure 7 also shows the effect of an existing mean field, by probing a mean field in mode $\mathbf{f_1}$ with $\vec{\xi} = (1,0,0,0)^T$ and in mode $\mathbf{f_2}$ with $\vec{\xi} = (0,0,1,0)^T$. Generally speaking, we observe that the mean field reduces the created entanglement. Nevertheless, the unbalance of squeezing ($s_1 \neq s_2$) also unbalances the effect of the mean field. The higher squeezing in mode $\mathbf{f_1}$ makes the entanglement creation more resilient to displacements, but a mean field in mode $\mathbf{f_2}$ will reduce the maximal attainable amount of entanglement to the same level as in the balanced case [because in both (c) and (d) mode $\mathbf{f_2}$ is squeezed with $s_2 = 2$]. In the presence of a mean field, we also find that unbalanced squeezing shifts the value θ for which most entanglement is created. In other words, to achieve maximal entanglement upon photon subtraction in two modes with unequal squeezing, one must subtract in an unbalanced superposition of these modes.

Through this example, we showed that entanglement between previously uncorrelated Gaussian states can be created by a non-Gaussian operation. This entanglement has some additional peculiarities. For example, a quick glance at how this procedure affects Eq. (190) shows that we can split the state in a Gaussian, i.e., $W_{\mathbf{f}}(\vec{x}_{\mathbf{f}})$, and a non-Gaussian part, i.e., $\langle\hat{A}\rangle_{\mathbf{g}|\vec{x}_{\mathbf{f}}}/\langle\hat{A}\rangle$. In this case of Eq. (259) the Gaussian part of the state clearly remains fully separable. This means that, in this representation, all entanglement is originating from the non-Gaussian part of the state. Nevertheless, the decomposition, Eq. (190), of the state into a Gaussian and a non-Gaussian part most probably is not unique for mixed states, making it challenging to study such non-Gaussian entanglement in its most general sense.

Yet, common tools that rely on the covariance matrix, such as Refs. [216,217], to characterize entanglement in the photon subtracted states, Eq. (259), are doomed to fail. In Ref. [152] it is explicitly shown that the covariance matrix of a photon-subtracted state is given by the covariance matrix of the initial Gaussian state with a positive matrix added to it. This means that photon subtraction just adds correlated noise to the covariance matrix and if we consider a Gaussian state that has exactly this covariance matrix we can decompose it using Eq. (103). In other

words, when there is no entanglement visible in the covariance matrix of the initial Gaussian state, we do not witness any entanglement based on the covariance matrix of the photon-subtracted state. In this case, the non-Gaussian entanglement is thus genuinely non-Gaussian in the sense that it cannot be detected through Gaussian witnesses. Hence, rather than decomposing the states in a Gaussian and non-Gaussian part, as was done in Eq. (190), it may be more fruitful to define non-Gaussian entanglement as any entanglement that cannot be witnessed based solely on the covariance matrix of the state. This approach also offers a natural connection to the framework of Gaussian passivity on quantum thermodynamics [245].

Another peculiarity that was presented in Refs. [152, 153] is the intrinsic nature of this non-Gaussian entanglement. When we transform the system into a different mode basis, there will still be entanglement in the system. The entanglement is said to be intrinsic because the state is entangled in every possible mode basis. As we saw in Eq. (249) Gaussian entanglement is never intrinsic as there always exists a basis in which a Gaussian state is separable.

Figure 7(b) gives a rather interesting approach to understanding the intrinsic nature of non-Gaussian entanglement. In this sketch, the second beam splitter is intended to undo the superposition θ and return to the initial mode basis with modes $\mathbf{f_1}$ and $\mathbf{f_2}$. Changing this beam splitter thus implies a basis change. If we remove this beam splitter entirely, we find ourselves in the entanglement distillation scenario of Sec. 2. In this case, the photon subtraction is fully local, but it happens on a state with Gaussian entanglement. The photon subtraction can then increase the Rényi entanglement by a maximal amount of $\log 2$. When we change to a mode basis where there is no Gaussian entanglement and the entanglement is created through a nonlocal photon subtraction, we create a maximal amount of Rényi entanglement given by $\log 2$. Changing the mode basis in a different way will combine the physics of these two extreme cases such that there will always be entanglement, regardless of the basis.

Extending these ideas to more general non-Gaussian operations on more general Gaussian mixed states is a hard and currently open problem. This reflects the general status of entanglement theory in CV systems: we lack a structured theoretical understanding of this phenomenon and as a consequence we also lack good tools to detect it.

D. Non-Gaussianity and Bell inequalities

In this final subsection of our study of quantum correlations in non-Gaussian states, we study Bell inequalities. First of all, we argue that it is impossible to violate Bell inequalities when both of the states and all the measurements involved can be described by positive Wigner functions. Then, we show that the Wigner function of the state can itself be used to formulate a Bell inequality when we allow for nonpositive Wigner functions.

The general setup for studying nonlocality in CV revolves around a multimode state with Wigner function $W(\vec{x}_{\mathbf{f}} \oplus \vec{x}_{\mathbf{g}})$ defined on a phase space $\mathbb{R}^{2m} = \mathbb{R}^{2l} \oplus \mathbb{R}^{2l'}$. Bell nonlocality entails that some measurements on this state cannot be described by a local hidden variable model of the type, Eq. (238). In a quantum framework, the local measurements with POVM elements $\{\hat{A}_j\}$ (on the modes in $\mathbf{f}$) and $\{\hat{B}_j\}$ (on the modes in $\mathbf{g}$) can also be described by Wigner functions $W_{A_j}(\vec{x}_{\mathbf{f}})$ and $W_{B_j}(\vec{x}_{\mathbf{g}})$. Because we are dealing with a POVM, we find that

$$(4\pi)^l \sum_j W_{A_j}(\vec{x}_{\mathbf{f}}) = (4\pi)^{l'} \sum_j W_{B_j}(\vec{x}_{\mathbf{g}}) = 1. \tag{284}$$

Note that this equality holds for all possible coordinates $\vec{x}_{\mathbf{f}}$ and $\vec{x}_{\mathbf{g}}$. Here we assume that the measurement outcomes A_j and B_j are discrete, but by correctly defining resolutions of the identity we can also deal with more general probability distributions, e.g., homodyne measurements.

The probability to get the joint measurement result (A_j, B_k) is given by

$$P(A_j, B_k) = (4\pi)^m \int_{\mathbb{R}^{2l}} \int_{\mathbb{R}^{2l'}} \mathrm{d}\vec{x}_{\mathbf{f}} \mathrm{d}\vec{x}_{\mathbf{g}} W(\vec{x}_{\mathbf{f}} \oplus \vec{x}_{\mathbf{g}}) W_{A_j}(\vec{x}_{\mathbf{f}}) W_{B_k}(\vec{x}_{\mathbf{g}}). \tag{285}$$

Now let us assume that all these Wigner functions are positive. Because they are normalized, this implies that $W(\vec{x}_{\mathbf{f}} \oplus \vec{x}_{\mathbf{g}})$ is a probability distribution on the entire phase space $\mathbb{R}^{2m}$, and $W_{A_j}(\vec{x}_{\mathbf{f}})$ and $W_{B_j}(\vec{x}_{\mathbf{g}})$ are probability distributions on the reduced phase spaces $\mathbb{R}^{2l}$ and $\mathbb{R}^{2l'}$, respectively. However, the model, Eq. (238), does not require probability distributions on phase space, but rather on the possible measurement outcomes.

This is where Eq. (284) comes into play. Because $W_{A_j}(\vec{x}_{\mathbf{f}})$ and $W_{B_j}(\vec{x}_{\mathbf{g}})$ are positive, more than just treat them as probability distributions in phase space we can also consider $P_{\vec{x}_{\mathbf{f}}}(A_j) = (4\pi)^l W_{A_j}(\vec{x}_{\mathbf{f}})$ and $P_{\vec{x}_{\mathbf{g}}}(B_j) = (4\pi)^{l'} W_{B_j}(\vec{x}_{\mathbf{g}})$ as the probability of getting the measurement outcomes A_j and B_k, respectively. Because of Eq. (284) we find that these probabilities are correctly normalized

$$\sum_j P_{\vec{x}_{\mathbf{f}}}(A_j) = \sum_j P_{\vec{x}_{\mathbf{g}}}(B_j) = 1, \tag{286}$$

and because the Wigner functions are positive, we also find that $P_{\vec{x}_{\mathbf{f}}}(A_j), P_{\vec{x}_{\mathbf{g}}}(B_j) \geqslant 0$. Note that the phase-space coordinates $\vec{x}_{\mathbf{f}}$ and $\vec{x}_{\mathbf{g}}$ are no longer treated as the variable, but rather as a label. The set $\{P_{\vec{x}_{\mathbf{f}}}(A_j) \mid \vec{x}_{\mathbf{f}} \in \mathbb{R}^{2l}\}$ denotes a family of different probability distributions on

the space of measurement outcomes $\{A_1, A_2, \dots\}$. The set $\{P_{\vec{x}_\mathbf{g}}(B_j) \mid \vec{x}_\mathbf{g} \in \mathbb{R}^{2l'}\}$ can be interpreted analogously.

We can thus recast Eq. (285) in the following form:

$$P(A_j, B_k) = \int \mathrm{d}\vec{x}_\mathbf{f}\mathrm{d}\vec{x}_\mathbf{g} W(\vec{x}_\mathbf{f} \oplus \vec{x}_\mathbf{g}) P_{\vec{x}_\mathbf{f}}(A_j) P_{\vec{x}_\mathbf{g}}(B_k). \quad (287)$$

Because $W(\vec{x}_\mathbf{f} \oplus \vec{x}_\mathbf{g})$ is a positive and normalized Wigner function, it is a joint probability distribution on the coordinates $\vec{x}_\mathbf{f}$ and $\vec{x}_\mathbf{g}$. These coordinates label families of probability distributions $\{P_{\vec{x}_\mathbf{f}}(A_j) \mid \vec{x}_\mathbf{f} \in \mathbb{R}^{2l}\}$ and $\{P_{\vec{x}_\mathbf{g}}(B_j) \mid \vec{x}_\mathbf{g} \in \mathbb{R}^{2l'}\}$ for the measurement outcomes. The expression (287) is thus fully consistent with Bell's local hidden variable model, Eq. (238). As a consequence, we cannot violate any Bell inequalities when the system is prepared in a state with a positive Wigner function and when we only have access to POVM that have Wigner representations with positive Wigner functions.

Let us emphasize that there is generally no reason to assume that the probabilities $P_{\vec{x}_\mathbf{f}}(A_j)$ and $P_{\vec{x}_\mathbf{g}}(B_j)$ are also consistent with quantum mechanics. In other words, there is not necessarily any state $\hat{\rho}$ such that $P_{\vec{x}_\mathbf{f}}(A_j) = \mathrm{tr}[\hat{\rho}\hat{A}_j]$. However, because we are dealing with Bell nonlocality, we do not need this to be the case, since Eq. (238) allows for arbitrary local probability distributions.

To make a long story short, we have shown that Wigner negativity is necessary for witnessing Bell nonlocality. The interested reader can consult works such as Ref. [64] that relate Wigner negativity to the more general concept of quantum contextuality. However, the topic of contextuality in CV systems is still a matter of scientific debate [246].

There has been a significant body of work about the violation of Bell inequalities in CV setups [247–249]. It is evident that this is an arduous task once one approaches a realistic experimental setting [250]. Here, we focus on one particular suggestion to test Bell nonlocality based on a state's Wigner function [251,252].

The starting point of this approach is the CHSH inequality

$$\left|\langle \hat{X}\hat{Y}\rangle - \langle \hat{X}\hat{Y}'\rangle + \langle \hat{X}'\hat{Y}\rangle + \langle \hat{X}'\hat{Y}'\rangle\right| \leqslant 2.$$

As we discussed in Sec. 4, this inequality relies on some assumptions for the observables X, X', Y, and Y'. In particular, we must assume that the measurement outcomes are either -1 or 1. In a CV setting, where we generally deal with a continuum of possible measurement outcomes, this seems like a serious constraint. Nevertheless, we have already encountered some natural examples during this Tutorial. For example, photon counters yield a discrete number of possible measurement outcomes. Here, we choose a related observable that takes us all the way back to Sec. B, where we encountered the observable

$$\hat{\Delta}(\vec{x}) = \hat{D}(-\vec{x})(-\mathbb{1})^{\hat{N}}\hat{D}(\vec{x}).$$

This displaced parity operator has a rich structure, but when it comes to actual measurement outcomes is will return either -1 or 1. This means that we can choose X, X', Y, and Y' to be parity operators. First of all, let us note that

$$\hat{\Delta}(\vec{x}_\mathbf{f} \oplus \vec{x}_\mathbf{g}) = \hat{\Delta}(\vec{x}_\mathbf{f}) \otimes \hat{\Delta}(\vec{x}_\mathbf{g}). \quad (288)$$

To see this, one can first show that $(-\mathbb{1})^{\hat{N}_m} = (-\mathbb{1})^{\hat{N}_l + \hat{N}_{l'}} = (-\mathbb{1})^{\hat{N}_l} \otimes (-\mathbb{1})^{\hat{N}_{l'}}$ and subsequently use $\hat{D}(\vec{x}_\mathbf{f} \oplus \vec{x}_\mathbf{g}) = \hat{D}(\vec{x}_\mathbf{f}) \otimes \hat{D}(\vec{x}_\mathbf{g})$ (displacements in different modes are independent from each other).

Now we can identify the observables as follows:

$$\begin{aligned} X &= \hat{\Delta}(\vec{x}_\mathbf{f}), \quad X' = \hat{\Delta}(\vec{x}'_\mathbf{f}), \\ Y &= \hat{\Delta}(\vec{x}_\mathbf{g}), \quad Y' = \hat{\Delta}(\vec{x}'_\mathbf{g}), \end{aligned} \quad (289)$$

and therefore the CHSH inequality is transformed into

$$\left|\langle \hat{\Delta}(\vec{x}_\mathbf{f} \oplus \vec{x}_\mathbf{g})\rangle - \langle \hat{\Delta}(\vec{x}_\mathbf{f} \oplus \vec{x}'_\mathbf{g})\rangle + \langle \hat{\Delta}(\vec{x}'_\mathbf{f} \oplus \vec{x}_\mathbf{g})\rangle + \langle \hat{\Delta}(\vec{x}'_\mathbf{f} \oplus \vec{x}'_\mathbf{g})\rangle\right| \leqslant 2. \quad (290)$$

As a next step, we use Eq. (78) to write

$$\langle \hat{\Delta}(\vec{x}_\mathbf{f} \oplus \vec{x}_\mathbf{g})\rangle = (2\pi)^m W(\vec{x}_\mathbf{f} \oplus \vec{x}_\mathbf{g}), \quad (291)$$

such that the inequality (290) can be recast as

$$\left|W(\vec{x}_\mathbf{f} \oplus \vec{x}_\mathbf{g}) - W(\vec{x}_\mathbf{f} \oplus \vec{x}'_\mathbf{g}) + W(\vec{x}'_\mathbf{f} \oplus \vec{x}_\mathbf{g}) + W(\vec{x}'_\mathbf{f} \oplus \vec{x}'_\mathbf{g})\right| \leqslant \frac{2}{(2\pi)^m}. \quad (292)$$

Any state with a Wigner function that violates this inequality for some choice of coordinates $\vec{x}_\mathbf{f}, \vec{x}'_\mathbf{f}, \vec{x}_\mathbf{g}$, and $\vec{x}'_\mathbf{g}$ possesses some form of Bell nonlocality. In Refs. [251,252] it is argued that the inequality (292) can be violated by sending a single photon through a beam splitter, but also by an EPR state. The fact that a Gaussian Wigner function suffices to violate Eq. (292) sometimes comes as a surprise, because we previously argued that one needs Wigner negativity to violate Bell inequalities. The reason why one can detect Bell nonlocality with this inequality even when the Wigner function is positive stems from our choice of observable $\hat{\Delta}(\vec{x}_\mathbf{f} \oplus \vec{x}_\mathbf{g})$. The POVM elements that correspond to the measurement outcomes 1 and -1 have Wigner functions that are strongly Wigner negative. As a consequence the necessary Wigner negativity is baked into Eq. (292) by construction.

In practice, the inequality (292) is highly sensitive to impurities and can often be hard to violate with experimentally reconstructed Wigner functions. The hunt for good new techniques to show Bell nonlocality in CV systems

is therefore still open. However, this subsection clearly showed us that Wigner negativity is necessary to observe one of the most exotic features in quantum physics. This negativity might be baked into the state, but it could just as well be induced by measurements. The conditional methods of Sec. B also highlight this duality, where Wigner negativity in the measurement is used to induce Wigner negativity in the state. It should come as no surprise that Wigner negativity is also a necessary ingredient for the most exotic quantum protocols. However, it should also be highlighted that even with a little extra trust, it is possible to design protocols that do not require Wigner negativity to witness quantum correlations [201]. In the next section, we discuss its importance for reaching a quantum advantage with CV systems.

VI. NON-GAUSSIAN QUANTUM ADVANTAGES

It has been long known that systems that are entirely built with Gaussian building blocks are easy to simulate [25]. It should perhaps not come as a surprise that efficient numerical tools exist to sample numbers from a multivariate Gaussian distribution. The discrete variable analog of this result comes across as less intuitive and goes by the name "Gottesman-Knill theorem" [253]. Yet, it turns out that something stronger than mere non-Gaussian elements is required to render a system hard to simulate.

In Sec. D, we encountered the power of Wigner negativity by realizing that it is a necessary requirement for Bell nonlocality. This connection between Wigner negativity and the most exotic types of quantum correlations shows us that Wigner negativity is key to giving CV systems their most prominent quantum features. It is then perhaps not a surprise that such Wigner negativity is also a necessary requirement for implementing any type of protocol that cannot be efficiently simulated by a classical computer [33,254,255]. We thus start our discussion of quantum advantages by explaining the result of Ref. [33]. To show the necessity of Wigner negativity, we show an explicit simulation algorithm for general quantum protocols without Wigner negativity.

Any quantum protocol ultimately relies on the measurement of a certain set of measurement operators $\{\hat{E}_j\}$ (typically a POVM) of a system prepared on a state $\hat{\rho}$. In a Wigner function formalism, we then find

$$p_j = (4\pi)^m \int_{\mathbb{R}^{2m}} \mathrm{d}\vec{x}\; W_{E_j}(\vec{x}) W(\vec{x}). \tag{293}$$

Furthermore, the fact that the set $\{\hat{E}_j\}$ forms a POVM implies that

$$(4\pi)^m \sum_j W_{E_j}(\vec{x}) = 1. \tag{294}$$

As we already discussed in Sec. D, surrounding Eq. (284), it is crucial that the normalization condition (294) holds for any phase-space coordinate $\vec{x}$. In the present context, we want to show that there is an efficient method for a classical device to sample values from the probability distribution $\{p_j\}$ when all involved Wigner functions are positive.

Let us start by assuming that the Wigner functions that describe the POVM elements are all positive. When combined with the POVM condition (294), this implies that we can identify a set of probabilities $P_{\vec{x}}(e_j) = (4\pi)^m W_{E_j}(\vec{x})$ as the probability to obtain the measurement outcome e_j, associated with the POVM element $\hat{E}_j$. These $P_{\vec{x}}(e_j)$ depend on a parameter $\vec{x}$, we can thus form a family of probability distributions $\{P_{\vec{x}}(e_j) \mid \vec{x} \in \mathbb{R}^{2m}\}$ that describe the probability of obtaining the different results e_j, depending on a chosen phase-space point. The normalization condition (294) now states that $\sum_j P_{\vec{x}}(e_j) = 1$ for all $\vec{x}$. Let us emphasize that this family of probabilities would not be well defined if $W_{E_j}(\vec{x})$ were not positive Wigner functions, as some of the probabilities would be negative.

Going back to the initial Eq. (293), we now find that

$$p_j = \int_{\mathbb{R}^{2m}} \mathrm{d}\vec{x}\; P_{\vec{x}}(e_j) W(\vec{x}). \tag{295}$$

To find the actual probability of getting the jth outcome is thus given by "averaging" the probabilities $P_{\vec{x}}(e_j)$ over the different phase-space coordinates. Generally speaking, this is not a real average, unless the Wigner function $W(\vec{x})$ of the state is an actual probability distribution on phase space. The latter is exactly the case when $W(\vec{x})$ is positive. Then, we can simply think of the probability p_j for obtaining event e_j as $p_j = \mathbb{E}_W[P_{\vec{x}}(e_j)]$, where $\mathbb{E}_W$ is the expectation value over the probability distribution $W(\vec{x})$.

Hence, when all Wigner functions are positive, the algorithm to simulate our relevant quantum process can simply be expressed by the following steps:

1. Sample a phase-space coordinate $\vec{x}$ from the probability distribution $W(\vec{x})$.
2. Construct the probability distribution $P_{\vec{x}}(e_j)$ for the sampled value $\vec{x}$.
3. Sample an outcome e_j from the probability distribution $P_{\vec{x}}(e_j)$.

Even though this is the general idea behind our sampling protocol, there are some major hidden assumptions. First, we assume here that the Wigner function for the state and the measurement are known. Furthermore, we also assume that we can simply sample points from any distribution on phase space and from any distribution of measurement outcomes $P_{\vec{x}}(e_j)$. In particular, for the sampling aspects it is not at all clear that these are reasonable assumptions to make. Standard sampling protocols for multivariate probability distributions tend to get highly inefficient once the

probability distributions become too exotic such that it is dangerous to assume that we can "just sample."

To address this point Ref. [33] makes more assumptions on the exact setup we are trying to simulate. First, we assume that the detection is done by a series of single-mode detectors, such that our label j now become a tuple $\mathbf{j} = (j_1, j_2, \ldots, j_m)$ where j_k denotes the outcome $e_{j_k}^{(k)}$ for the detector on the kth mode. We can thus write the POVM element as $\hat{E}_{\mathbf{j}} = \hat{E}_{j_1}^{(1)} \otimes \cdots \otimes \hat{E}_{j_m}^{(m)}$, such that

$$W_{E_{\mathbf{j}}}(\vec{x}) = W_{E_{j_1}^{(1)}}(x_1, p_1) W_{E_{j_2}^{(2)}}(x_2, p_2) \ldots W_{E_{j_m}^{(m)}}(x_m, p_m). \tag{296}$$

We assume that each detector has been accurately calibrated, such that all the individual Wigner functions are known. This implies that for a given point in phase space $\vec{x} = (x_1, p_1, \ldots, x_m, p_m)^T$, we can simply evaluate the probabilities for each detector to produce a certain outcome. Thus, we calculate the probability distributions $P_{(x_k,p_k)}(e_j^{(k)}) = 4\pi W_{E_j^{(k)}}(x_k, p_k)$ for all the possible measurement outcomes for that specific mode. We assume that sampling outcomes $e_j^{(k)}$ from these probability distributions $P_{(x_k,p_k)}(e_j^{(k)})$ is a feasible task. For typical detectors in quantum optics experiments this is a very reasonable assumption.

The Wigner function $W(\vec{x})$ that describes the state is more subtle as it also includes all correlations between modes. If the state is Gaussian, a measurement of the covariance matrix would be sufficient to know the full Wigner function. Because of its Gaussian features, there are efficient tools to directly sample phase-space points. Yet, for more general non-Gaussian positive Wigner functions this sampling may be much harder. Therefore, Ref. [33] makes an essential assumption: it assumes that we know a protocol that combines local operations to design the state $W(\vec{x})$ from a known initial state with no correlations between the modes. The notion of "locality" should here be understood in the sense of acting on a small set of modes while leaving the others fully untouched. These local operations are also supposed to be represented by positive Wigner functions, which depend only on the phase-space coordinates of the subset of modes on which they act.

Generally speaking, such Wigner positive operations $\Xi : \mathcal{H}^{\text{in}} \to \mathcal{H}^{\text{out}}$ map a state $\hat{\rho}$ to a new state $\Xi[\hat{\rho}]$. In Ref. [33], the Choi representation [256,257] is used to represent Ξ as a state on a larger Hilbert space $\mathcal{H}^{\text{in}} \otimes \mathcal{H}^{\text{out}}$. This becomes particularly appealing when we go to a Wigner representation, where the Choi representation of Ξ is given by a Wigner function $W_\Xi(\vec{x}^{\,\text{in}} \oplus \vec{x}^{\,\text{out}})$. The action of Ξ on a state with Wigner function $W(\vec{x}^{\,\text{in}})$ is then given by

$$W_{\text{out}}(\vec{x}^{\,\text{out}}) = (4\pi)^m \int_{\mathbb{R}^{2m}} \mathrm{d}\vec{x}^{\,\text{in}}\, W_\Xi(\vec{x}^{\,\text{in}} \oplus T\vec{x}^{\,\text{out}}) W(\vec{x}^{\,\text{in}}), \tag{297}$$

where m is the number of modes of the input state. For technical reasons, we must include the transposition operator T, Eq. (257), in the action of the channel. Because this operation must be trace preserving, we on top get the property that

$$(4\pi)^m \int_{\mathbb{R}^{2m}} \mathrm{d}\vec{x}^{\,\text{out}}\, W_\Xi(\vec{x}^{\,\text{in}} \oplus T\vec{x}^{\,\text{out}}) = 1. \tag{298}$$

When we now assume that the operation Ξ has a Wigner-Choi representation $W_\Xi(\vec{x}^{\,\text{in}} \oplus \vec{x}^{\,\text{out}})$, which is a positive function, it immediately follows that the operation Ξ turns a Wigner positive initial state $W(\vec{x}^{\,\text{in}})$ into a Wigner positive output state $W_{\text{out}}(\vec{x}^{\,\text{out}})$.

It is useful to note that such operations, Eq. (297), can be trivially embedded in a larger space. Let us assume that we consider a state $W(\vec{x}_{\mathbf{f}} \oplus \vec{x}_{\mathbf{g}})$, we can simply let the operation act on the modes $\mathbf{g}$ by taking

$$W_{\text{out}}(\vec{x}_{\mathbf{f}} \oplus \vec{x}_{\mathbf{g}}^{\,\text{out}}) = (4\pi)^{l'} \int_{\mathbb{R}^{2l'}} \mathrm{d}\vec{x}_{\mathbf{g}}^{\,\text{in}}\, W_\Xi(\vec{x}_{\mathbf{g}}^{\,\text{in}} \oplus T\vec{x}_{\mathbf{g}}^{\,\text{out}}) \times W(\vec{x}_{\mathbf{f}} \oplus \vec{x}_{\mathbf{g}}^{\,\text{in}}). \tag{299}$$

Notationally, this may seem a little complicated, but, in essence, we just carry out the integration over a subset of the full phase space. We call these operations local Wigner positive operations.

In our simulation protocol, we thus assume that $W(\vec{x})$ is created by a series of such local Wigner positive operations of $\Xi_1, \ldots, \Xi_t$ on a noncorrelated input state $W_{\text{in}}(\vec{x}_{\text{in}}) = W_{\text{in}}^{(1)}(x_1, p_1) W_{\text{in}}^{(2)}(x_2, p_2) \ldots W_{\text{in}}^{(m)}(x_m, p_m)$.

$$W(\vec{x}) = (4\pi)^{mt} \int_{\mathrm{R}^{2m}} \mathrm{d}\vec{x}_t \ldots \int_{\mathrm{R}^{2l}} \mathrm{d}\vec{x}_t W_{\Xi_t}(\vec{x}_t \oplus T\vec{x}) \ldots \times W_{\Xi_2}(\vec{x}_1 \oplus T\vec{x}_2) W_{\Xi_1}(\vec{x}_{\text{in}} \oplus T\vec{x}_1) \times W_{\text{in}}(\vec{x}_{\text{in}}). \tag{300}$$

We assume on top that each operation is local over a small number of modes $l \ll m$. To model this with Eq. (299), it suffices to split $\vec{x}_{t_{k-1}} = \vec{x}^{\,l}_{t_{k-1}} \oplus \vec{x}^{\,l'}_{t_{k-1}}$ and $\vec{x}_{t_k} = \vec{x}^{\,l}_{t_k} \oplus \vec{x}^{\,l'}_{t_k}$, such that

$$(4\pi)^m W_{\Xi_{t_k}}(\vec{x}_{t_{k-1}} \oplus T\vec{x}_{t_k}) = (4\pi)^l W_{\Xi_{t_k}}(\vec{x}^{\,l}_{t_{k-1}} \oplus T\vec{x}^{\,l}_{t_k}) \delta(\vec{x}^{\,l'}_{t_{k-1}} - \vec{x}^{\,l'}_{t_k}). \tag{301}$$

Even though the notation is complicated, it simply describes that we act on an l-mode subspace with the operation Ξ_{t_k} and leave the other l' modes untouched.

The normalization condition (298) now has an important consequence, since it allows us to identify a probability distribution on phase space $P_{\vec{x}_{t_{k-1}}}(\vec{x}_{t_k}) = (4\pi)^m W_{\Xi_{t_k}}(\vec{x}_{t_{k-1}} \oplus T\vec{x}_{t_k})$. It gives us the probability of choosing a phase space value $\vec{x}_{t_k}$, given that we know $\vec{x}_{t_{k-1}}$. Because the operations are local, Eq. (301) allows us to keep most of the phase-space coordinates constant from step to step. Furthermore, the first step is simple. Every pair (x_k, p_k) of the initial coordinate $\vec{x}_{\text{in}}$ can be sampled independently because $W_{\text{in}}(\vec{x}_{\text{in}})$ factorizes. This now gives us the following new algorithm:

1. Take the initial Wigner function $W_{\text{in}}(\vec{x}^{\,\text{in}}) = W_{\text{in}}^{(1)}(x_1,p_1)W_{\text{in}}^{(2)}(x_2,p_2)\ldots W_{\text{in}}^{(m)}(x_m,p_m)$ and sample a pair (x_k,p_k) from every single-mode probability distribution $W_{\text{in}}^{(k)}(x_k,p_k)$. Put all these pairs together to obtain $\vec{x}^{\,\text{in}} = (x_1,p_1,\ldots,x_m,p_m)$.
2. Update the coordinate by sampling new coordinates based on $P_{\vec{x}_{t_{k-1}}}(\vec{x}_{t_k}) = (4\pi)^m W_{\Xi_{t_k}}(\vec{x}_{t_{k-1}} \oplus T\vec{x}_{t_k})$. Because Ξ_{t_k} are local operations, it suffices to only locally update coordinates. Let us make this clear through an example. Say we have $\vec{x}_{t_{k-1}} = (x_1^{(k-1)},p_1^{(k-1)},\ldots,x_m^{(k-1)},p_m^{(k-1)})^T$ and operation Ξ_{t_k} acts locally on modes with labels $2, 5$, and 7. Take $\vec{x}^{\,l}_{t_{k-1}} = (x_2^{(k-1)},p_2^{(k-1)},x_5^{(k-1)},p_5^{(k-1)},x_7^{(k-1)},p_7^{(k-1)})$ and use it to evaluate $P_{\vec{x}_{t_{k-1}}}(\vec{x}^{\,l}_{t_k}) = (4\pi)^l W_{\Xi_{t_k}}(\vec{x}^{\,l}_{t_{k-1}} \oplus T\vec{x}^{\,l}_{t_k})$. Now sample a new vector $\vec{x}^{\,l}_{t_k} = (x_2^{(k)},p_2^{(k)},x_5^{(k)},p_5^{(k)},x_7^{(k)},p_7^{(k)})$ from this probability distribution. Then construct the new vector $\vec{x}_{t_k}$ by taking $\vec{x}_{t_{k-1}}$ and updating the coordinates associated to modes $2, 5$, and 7 to the newly sampled coordinates
3. After the operations $\Xi_1,\ldots,\Xi_t$ have been implemented by updating the phase-space coordinate, take the final phase-space coordinate $\vec{x} = (x_1,p_1,\ldots,x_m,p_m)^T$ and the Wigner function describing the detectors $W_{E_\mathbf{j}}(\vec{x}) = W_{E_{j_1}^{(1)}}(x_1,p_1)W_{E_{j_2}^{(2)}}(x_2,p_2)\ldots W_{E_{j_m}^{(m)}}(x_m,p_m)$. For each detector k, use the phase-space coordinate $\vec{x}$ to generate the probability distribution $P_{(x_k,p_k)}(e_j^{(k)}) = W_{E_j^{(k)}}(x_k,p_k)$.
4. Sample an outcome $e_j^{(k)}$ from the distribution $P_{(x_k,p_k)}(e_j^{(k)})$ for every detector.

Sampling the final phase-space coordinate $\vec{x}$ by using a Monte-Carlo-style update rule is time consuming, but if the operations are local it can be done efficiently. This procedure implicitly assumes that we do not just know the state we are sampling from, but that we know the circuit of local operations that is used to create the state from local resources. Ultimately, when one considers the circuit representation of quantum algorithms, this is also how a quantum algorithm works. For example, Sec. A exactly shows that any unitary CV circuit can be built with single- and two-mode gates. The algorithm outlined in this section shows that we can efficiently simulate any protocol where the local input state, the circuit's operations, and the measurements are described by positive Wigner functions.

One may wonder whether any positive Wigner function $W(\vec{x})$ can be constructed through such a circuit and, if so, whether there is an efficient way to design such a circuit when we know the Wigner function. If we assume that not only the state $W(\vec{x})$ but also all its marginals are known, it is possible to construct a stepwise sampling procedure through the chain rule of probability theory:

$$W(\vec{x}) = W(x_m,p_m \mid x_{m-1},p_{m-1},\ldots x_1,p_1) \times \ldots \\ W(x_3,p_3 \mid x_2,p_2,x_1,p_1)W(x_2,p_2 \mid x_1,p_1)W(x_1,p_1). \tag{302}$$

This process effectively executes a type of random walk with memory. In each step of this walk, we then sample the phase-space coordinates for one mode. Nevertheless, this process only works when we have access to all these conditional probabilities, which practically implies having access to all the marginals of the distribution. In practical setups, this will often not be the case. Nevertheless, it is quickly seen that this setup can be efficiently used to sample from Gaussian Wigner functions where these conditional distributions have a particularly simple form.

Thus, we have shown that it is impossible to obtain a quantum computational advantage by using only local states, measurements, and operations with positive Wigner functions. This means that Wigner negativity is necessary to reach a quantum advantage in such setups. However, Wigner negativity is certainly not sufficient since there are many setups of quantum systems that involve negative Wigner functions that can be efficiently simulated [258]. It is thus interesting to take the opposite approach and explore a setup that is known to lead to a quantum advantage. In the spirit of CV setups, the most logical choice for such a discussion is Gaussian boson sampling [259]. In the literature, this setup has been studied mainly from the point of view of complexity theory [260,261], but here we rather focus on its physical building blocks.

Boson sampling [262] is a problem in which one injects a set of N bosons (generally photons) into an m-mode interferometer. On the output ports of this interferometer, photodetectors are mounted to count the particles at the output. Simulating this type of quantum Galton board is a computationally hard task, implying that a quantum advantage could be reached by implementing the setup in a quantum optics experiment. On the other hand, it turns out that the required number of photons to implement such an experiment is also hard to come by. This was the motivation for developing a new approach, where the input photons are replaced by squeezed states that are injected

in each of the interferometer inputs. Because an interferometer, built out of phase shifters and beam splitters, is a Gaussian transformation the output state will remain Gaussian. We can thus effectively say that we are sampling photons from a state with Wigner function $W_G(\vec{x})$. In addition, there is no mean field in the setup such that the entire state is characterized by its covariance matrix V.

When we assume that the detectors resolve photon numbers, the probability to detect a string of counts $\mathbf{n} = (n_1, \ldots, n_m)$ can we written as

$$P(\mathbf{n}) = (4\pi)^m \int_{\mathbb{R}^{2m}} \mathrm{d}\vec{x}\; W_{\mathbf{n}}(\vec{x}) W_G(\vec{x}). \tag{303}$$

We can then use Eq. (118) to write

$$W_{\mathbf{n}}(\vec{x}) = W_{n_1}(x_1, p_1) \ldots W_{n_m}(x_m, p_m). \tag{304}$$

Even though the integral (303) is hard to compute, it is insightful in the light of Eq. (295) and our discussion regarding the necessity of Wigner negativity. Indeed, we see immediately that the detectors form a crucial element in rendering the setup hard to simulate. The same holds when we replace the number-resolving detectors with their on-off counterparts [263] such that $n_k = \{0, 1\}$ and the Wigner functions are given by $W_{n_k}(x_k, p_k) = \{1 - 2\exp[-(x_k^2 + p_k^2)/2]\}/(4\pi)$.

When we stick with number-resolving detectors that project on Fock states, it is practical to reformulate the problem in terms of P functions and Q functions, such that

$$P(\mathbf{n}) = \int_{\mathbb{R}^{2m}} \mathrm{d}\vec{x}\; P_{\mathbf{n}}(\vec{x}) Q_G(\vec{x}). \tag{305}$$

For the detailed calculation, we refer to Ref. [259]. It turns out that the probabilities $P(\mathbf{n})$ can be expressed in terms of the Hafnian of a matrix [264], which establishes a connection to the problem of finding perfect matchings in graph theory. This connection has led to several suggested applications for Gaussian Boson sampling [265–267].

In the light of this Tutorial, the most interesting application of Gaussian Boson sampling is its potential role in quantum state engineering [205]. When only a subset of modes are measured, we can see Gaussian Boson sampling as a generalization of photon subtraction (and even as a generalization of "generalized photon subtraction" [157]). The idea is reasonably simply explained in the light of Sec. B: when we split the system in two parts $\mathbb{R}^{2m} = \mathbb{R}^{2l} \oplus \mathbb{R}^{2l'}$, such that the Gaussian state that comes out of the interferometer now takes the form $W_G(\vec{x}_{\mathbf{f}} \oplus \vec{x}_{\mathbf{g}})$, we can postselect on a measurement outcome $\mathbf{n} = (n_1, \ldots n_{l'})$ for the second subsystem. We thus project on a state $W_{\mathbf{n}}(\vec{x}_{\mathbf{g}})$, which is a product of l' Fock states, and from Eq. (190), we obtain that the conditional state on the remaining modes is given by

$$W_{\mathbf{f}|\mathbf{n}}(\vec{x}_{\mathbf{f}}) = \frac{\langle [|n_1\rangle \langle n_1| \otimes \cdots \otimes |n_{l'}\rangle \langle n_{l'}|] \rangle_{\mathbf{g}|\vec{x}_{\mathbf{f}}}}{\langle [|n_1\rangle \langle n_1| \otimes \cdots \otimes |n_{l'}\rangle \langle n_{l'}|] \rangle} W_{\mathbf{f}}(\vec{x}_{\mathbf{f}}), \tag{306}$$

with $W_{\mathbf{f}}(\vec{x}_{\mathbf{f}})$ defined by Eq. (182). From Eq. (192) we recall the expression

$$\begin{aligned} &\langle [|n_1\rangle \langle n_1| \otimes \cdots \otimes |n_{l'}\rangle \langle n_{l'}|] \rangle_{\mathbf{g}|\vec{x}_{\mathbf{f}}} \\ &= (4\pi)^{l'} \int_{\mathbb{R}^{2l'}} \mathrm{d}\vec{x}_{\mathbf{g}}\; W_{\mathbf{n}}(\vec{x}_{\mathbf{g}}) W_G(\vec{x}_{\mathbf{g}} \mid \vec{x}_{\mathbf{f}}), \end{aligned} \tag{307}$$

and because the initial state $W_G(\vec{x}_{\mathbf{f}} \oplus \vec{x}_{\mathbf{g}})$ is Gaussian, we find that the conditional probability distribution $W_G(\vec{x}_{\mathbf{g}} \mid \vec{x}_{\mathbf{f}})$ is given by Eq. (193). Ironically, to evaluate $\langle [|n_1\rangle \langle n_1| \otimes \cdots \otimes |n_{l'}\rangle \langle n_{l'}|] \rangle_{\mathbf{g}|\vec{x}_{\mathbf{f}}}$ and $\langle [|n_1\rangle \langle n_1| \otimes \cdots \otimes |n_{l'}\rangle \langle n_{l'}|] \rangle$ we must essentially solve the same hard problem as for the implementation of Gaussian Boson sampling itself. Therefore, the exact description of the resulting states is generally complicated.

Nevertheless, in idealized scenarios, even small Gaussian Boson sampling circuits can be used to prepare interesting non-Gaussian states [205]. In particular, the capacity of Gaussian Boson sampling to produce GKP states has taken up a prominent place in a recent blueprint for photonic quantum computation [24]. Furthermore, the results in Sec. C suggest that states created by performing Gaussian Boson sampling on a subset of modes can have additional non-Gaussian entanglement. Yet, to be able to use this procedure to produce highly resourceful Wigner negative states, Sec. 2 highlights that the initial Gaussian state needs to be such that the modes in **f** can steer the modes in **g**. This condition can be seen as a basic quality requirement for the Gaussian Boson samplers that are used in Ref. [24].

Finally, the experimental imperfections are also detrimental for the quantum advantage that is produced in Gaussian Boson sampling. Clearly, when the Gaussian state $W_G(\vec{x})$ can be written as a Gaussian mixture of coherent states (meaning that no mode basis exists in which the quadrature noise is below vacuum noise), the sampling can be simulated efficiently. Because multimode coherent states are always just a tensor product of single-mode coherent states, it suffices to sample a coherent state from the mixture, calculate all the individual probabilities for the output detectors, and sample independent detector outputs according to these probabilities. The presence of entanglement in the Gaussian state from which we sample is thus crucial. In addition, detector efficiencies must be sufficiently high such that their Wigner functions remain nonpositive, otherwise the protocol of Ref. [33] renders the setup easy to simulate (as explained in the first part

of this section). A more thorough analysis of how different experimental imperfections render Gaussian Boson sampling easier to simulate can be found in Ref. [268].

There are clearly still many aspects of the relation between non-Gaussian features of quantum states on the one hand, and the ability to achieve a quantum computational advantage on the other hand, that are not yet fully understood. The Gaussian Boson sampling setup clearly emphasizes the importance of entanglement in combination with Wigner negativity. Furthermore, there is the implicit fact that a simulation scheme such as Ref. [33] requires knowledge of the actual circuit of local operations that was used to create the state. It does make sense to assume that we actually have some ideas of the quantum protocol that we are attempting to simulate, but yet one may wonder whether there could be a reasonable setting (in the sense that we are actually implementing a well-controlled protocol) in which the assumptions of Ref. [33] do not hold. This clearly shows that many fundamental theoretical aspects of CV quantum computation remain to be uncovered.

VII. EXPERIMENTAL REALIZATIONS

Now that we have provided an overview of some theoretical aspects of non-Gaussian quantum states, we interpret the "where to find them" part of the title in a very literal sense. Non-Gaussian states are generally rather fragile, as one should expect from quantum central limit theorem and the fact that thermal states in free bosonic theories are Gaussian. Producing and analyzing non-Gaussian states in a laboratory setting is indeed challenging, but nevertheless it has been done numerous times. Our main focus in Sec. A is quantum optics, which is the historical testbed for CV quantum physics. However, in recent years there has been increased attention for CV approaches in other setting such as optomechanics, superconducting circuits, and trapped ions.

A. Quantum optics experiments

This section provides an overview of some of the most important milestones in the generation of non-Gaussian states in optics. For more details, we refer the reader to a specialized review [81].

Historically, one might argue that the first experimental realizations of non-Gaussian states in optical setups relied on sufficiently sensitive photon detectors. Initial demonstrations primarily used photoemission of atoms [269,270], which are prepared in excited states (e.g., by electron bombardment) or via resonance fluorescence in ions [271]. The development of spontaneous parametric down-conversion (SPDC) made it possible to create a single-photon state using only bulk optical elements [202]. However, all these early non-Gaussian states were characterized through counting statistics, which means that we generally classify them as DV experiments.

It is perhaps intriguing to note that SPDC is also the process that lies at the basis of the creation of squeezed states of light [272], which are Gaussian. These states play a key role in the generation of single-photon states, simply because a weakly squeezed vacuum is mainly a superposition of vacuum and a photon pair. By detecting one photon of the pair, the presence of the second photon is heralded. Hence, the approach of Ref. [202] is a basic implementation of a conditional scheme for the generation of non-Gaussian states as presented in Sec. B.

A genuine CV treatment of such non-Gaussian states would only be achieved much later in a work that presents the first tomographic reconstruction of a state with Wigner negativity in optics [273]. Due to the developments of an easily implementable maximum-likelihood algorithm for state reconstruction, homodyne tomography became one of the main tools to study non-Gaussian states in CV quantum optics [274]. It did not take long before this also led to the reconstruction of a displaced single-photon Fock state [275] and a two-photon Fock state [276]. The combination of increased squeezing with type-II SPDC and an array of photon detectors to increase the number of heralded photons more recently made it possible to resolve the Wigner function of a three-photon Fock state [277]. Similar ideas of multiplexed photon detection have also been used to generate superpositions of Fock states [278].

For non-Gaussian states beyond Fock states, photon subtraction, as described in Sec. 2, is a common experimental tool. Its first experimental implementation successfully showed the capability of generating non-Gaussian statistics in the homodyne measurements, but it failed to demonstrate Wigner negativity [148]. Later experiments improved the quality of the generated states, demonstrating Wigner negativity and creating so-called "Schrödinger kittens" [129,279,280]. The terminology is chosen because these states resemble cat states proportional to $|\alpha\rangle - |-\alpha\rangle$ for small values of the mean field α. Even though such Schrödinger kittens are ultimately not very different from squeezed single-photon states, the nomenclature makes more sense in the context of experiments that "breed" cat states [281]. Here, one mixes two Schrödinger kittens on a beam splitter and performs homodyne detection on one output port. By conditioning on instances where this homodyne detector registers values close to zero, one effectively heralds a larger cat state (the value of α has increased). A variation of photon subtraction has also been used to create a type of CV qubit [282].

As an alternative to photon subtraction, one can also add a photon [159]. Even though this operation theoretically equates to applying a creation operator on the state, it is experimentally much harder to implement than photon subtraction as it requires nonlinear optics. However, photon subtraction can only produce Wigner negativity

when the initial state is squeezed. Photon addition, on the other hand, provides the advantage of always creating a Wigner negative state. A simple way to see this is by applying a creation operator to the state and evaluating the Q function (70). When a photon is added to the mode g, the Q function after photon addition has the property $Q^{+}(\vec{\alpha}) \sim (\vec{\alpha}^{T}\vec{g})^{2} Q_{G}(\vec{\alpha})$, where $Q_{G}(\vec{\alpha})$ is the Q function of the initial Gaussian state. This relation implies automatically that the Q function will be exactly zero for $\vec{\alpha} = \vec{0}$, and a zero of the Q function implies Wigner negativity. This means that one can apply photon addition to highly classical states, such as a coherent state or a thermal state, and still end up creating Wigner negativity. Such photon-added coherent states were also used to experimentally measure [283] non-Gaussianity $\delta(\hat{\rho})$ as defined in Eq. (110). Remarkably, combining photon addition and photon subtraction operations in both possible orders provides a way to experimentally verify the canonical commutation relations $[\hat{a}, \hat{a}^{\dagger}] = 1$, as was shown in Ref. [160].

The above methods are all based on Gaussian states as initial resources to generate non-Gaussian states. The non-Gaussian states that are created as such can in turn serve as useful resources to create more intricate non-Gaussian states. Fock states are a commonly used type of input state, for example, in the first demonstration of a large Schrödinger's cat state [284]. Intriguingly, by using non-Gaussian initial states, it suffices to use homodyne detection as the conditional operation. This setup can then be extended to a cat breeding scheme [285]. Another method to create large cat states in optics relies on making the light field interact with an atom [286]. The presence of entanglement between the "macroscopic" coherent state and the "microscopic" atomic degrees of freedom make for an experiment that resembles Schrödinger's original though experiment [106]. Once the atom and the coherent light are entangled, a spin rotation of the atom is followed by a measurement to project the state of the light field in either an even or an odd cat state. This reflects the general idea that atoms still induce much larger nonlinearities than nonlinear crystals. These nonlinearities are the direct source of non-Gaussian effect, but they are also much harder to control. At present, experiments that rely on such higher-order nonlinearities to create non-Gaussian states remain rare in the optical regime.

The above methods all focus on the creation of single-mode non-Gaussian states. For multimode systems, much of the experimental progress has concentrated on two-mode systems. As we extensively discussed throughout this tutorial, an important feature in such multimode systems are quantum correlations. Some of the first experimental demonstrations of non-Gaussian quantum correlations were based on the Bell inequality (292). Homodyne tomography and a single photon, delocalized over two modes by a beam splitter, suffices to violate the inequality [287,288]. However, these works also teach us that extreme high purities are required to do so.

Motivated by photon-subtraction experiments and challenged by the no-go theorem of [225–227], entanglement distillation soon became a new focus for non-Gaussian quantum optics experiments. Some of these experiments have focused on adding some form of non-Gaussian noise on the initial state to circumvent the no-go theorem [228, 229]. Entanglement distillation through local photon subtraction from the entangled modes of a Gaussian input state would later be demonstrated in Ref. [289]. Earlier, it had already been shown that Gaussian entanglement can be increased by photon subtraction in a superposition of the entangled mode [290]. Interestingly, in the latter case, the photon is effectively subtracted in a nonentangled mode such that the setup is essentially equivalent to mixing a squeezed vacuum and a photon-subtracted squeezed vacuum on a beam splitter. A similar photon subtraction in a coherent superposition of modes was later carried out to entangle two Schrödinger kittens [291]. This can probably be seen as the first realizations of purely non-Gaussian entanglement in CV.

Photon addition has also been considered as a tool for creating entanglement between pairs of previously uncorrelated modes [292]. The resulting state can be seen as a hybrid entangled state proportional to $|0\rangle|\alpha\rangle + |1\rangle|-\alpha\rangle$, such states have also been produced using techniques similar to photon subtraction [293]. For two modes, photon addition can be implemented in a mode-selective way [294]. This setup is particularly useful to create entanglement between coherent states by adding a photon in a superposition of displaced modes.

Going beyond two modes has always remained a challenging task. For mode-selective photon subtraction from a multimode field, one must abandon the typical implementation based on a beam splitter. For two modes, such an alternative photon subtraction scheme was, for example, realized in the time-frequency domain, by subtracting a photon from a sideband [295]. Yet, going to a genuine multimode scenario required the design of a whole new photon subtractor based on sum-frequency generation [296,297]. This finally permitted the first demonstration of multimode non-Gaussian state in a CV setting, demonstrating non-Gaussian features in up to four entangled modes [298].

Such highly multimode states of more than two modes are confronted with a considerable problem: the exponential scaling of the required number of measurements for a full state tomography. This makes it highly challenging to demonstrate non-Gaussian features such as Wigner negativity in multimode non-Gaussian states. For single-photon-subtracted states, it has been pointed out that good analytical models can be used to train machine-learning

algorithms to recognize Wigner negativity based on single-mode measurements [299]. Furthermore, the techniques of Ref. [128] combined with Ref. [300] should also make it possible to use multiplexed double homodyne detection to witness Wigner negativity in certain classes of multimode states.

In multimode systems, we are confronted with the limitations of homodyne tomography. Recently, it has been shown that machine-learning techniques can be used to implement an improved form of CV tomography based on homodyne measurements [301]. Even though this setup is computationally heavy in single-mode setups, it uses a smaller set of states as a basis for state reconstruction, which might make multimode versions of the protocol more scalable. Alternatively, one can also bypass homodyne measurements all together. Photon-number-resolving detectors such as transition edge sensors [302] make it possible to use the identity, Eq. (78), to directly measure the Wigner function [76]. Intriguingly, this implies that a photon-number-resolving detector and a setup to generate displacements of the state in arbitrary modes makes it possible to directly measure the full multimode Wigner function. Nevertheless, such a multimode protocol has so far not been realized in any experiment.

B. Other experimental setups

Given all the experimental work in CV quantum optics, it is perhaps surprising that the first experimental demonstrations of quantum states with Wigner negativity happened in different fields. The very first realization of such a state was achieved with trapped ions. Even though one often uses the atomic transitions in these systems to isolate qubits for potential quantum computers, trapped ions also have interesting motional degrees of freedom. By exploiting a Jaynes-Cummings type interaction between the atom and the trapping field, it is possible to use the ions' internal atomic degrees of freedom to create well-controlled non-Gaussian states such as a Fock state [78] and a Schrödinger's cat state [303] in the motional degrees of freedom.

Mathematically, this setup is equivalent to cavity QED, where it was shown that photons in a cavity can be manipulated through interactions with atoms [304] and the Rabi oscillations of the injected Rydberg atoms can in turn be used to probe the field within the cavity [305]. These methods would then be combined to experimentally generate a single-photon Fock state of the microwave field in a cavity [306], confirm its Wigner negativity [79], and probe its full Wigner function [80]. A few years later, similar techniques were used to finally generate Schrödinger cat states and higher-order Fock states [307].

A third setup with very similar physics is found in circuit QED. In this field, the macroscopic microwave cavities are replaced by superconducting circuits, and nonlinearities are induced by Josephson junctions rather than atoms [140]. Even though these setups are often used in a DV approach, the microwave fields involved can equally be treated in a CV approach. The large nonlinearities rather naturally create non-Gaussian states, but getting a good sense of control over them can be challenging. Nevertheless, a wide range of non-Gaussian states such as Fock state [308] and large Schrödinger cat states [309] have been experimentally realized. The latter have furthermore been stabiized by engineering the decoherence processes in the system [310]. Very recently these systems have also been used to demonstrate the deterministic generation of photon triplets [142].

In recent years, both, trapped ions [311] and superconducting circuits [312] were used to achieve another important milestone in CV quantum computing: the experimental generation of a GKP state. These highly non-Gaussian states are useful for encoding a fault-tolerant qubit in a CV degree of freedom. By exploiting the redundancy that is offered by the infinite dimension Hilbert space of a CV system, one can create a qubit with a certain degree of robustness. This effectively makes it possible to implement error-correction routines, as shown in Ref. [312]. In other words, these systems have managed to generate CV states that are so non-Gaussian that they can be effectively used as fault-tolerant DV states.

A final field that has shown much potential over the last decades is cavity optomechanics. Here, an optical field is injected into a cavity with one moving mirror (more generally also other types of "dynamic cavities" can be used). The goal is to cool this mirror to its ground state to observe its quantum features. This way, one hopes to create nonclassical states of motion in reasonably large objects. A wide variety of such optomechanical devices exist [313]. Several theoretical schemes have been proposed to generate non-Gaussian states in such an optomechanical setup [314,315]. Even though quantum features such as photon-phonon entanglement have been demonstrated in such systems [316,317], it remains highly challenging to obtain good experimental control over the motional quantum state. Nevertheless, some CV non-Gaussian states states in the form of superpositions between vacuum and a single-phonon Fock state have been experimentally realized [318].

A common problem in these setups is the creation of entanglement between the CV degrees of freedom in different modes. Some degree of such CV entanglement has been experimentally achieved in trapped ion [319] and circuit QED setups [320]. However, the number of entangled modes is much lower than what has been achieved in optics [18–21,220], where even non-Gaussian entangled states of more than two modes have been created [298]. This shows clearly how different experimental setups have different strengths and weaknesses. Optics comes with the advantage of spatial, temporal, and spectral mode

manipulations, which allows the creation of large entangled states. However, the resilience of optical setups to decoherence is due to limited interaction with the environment. The latter implies that it is also difficult to find controlled ways to make these systems strongly non-Gaussian. On the other hand, the other setups, which we discussed, require much more significant shielding from environmental degrees of freedom. When this coupling to other degrees of freedom can be controlled, it provides the means to create non-Gaussian quantum states. In this context, it is appealing to combine the advantages of different regimes. Optomechanics offers a potential pathway to achieve this by converting between microwave and optical degrees of freedom [321,322].

As a last remark, it is interesting to mention that phase-space descriptions and non-Gaussian states also appear in atomic ensembles. This framework relies on the fact that an ensemble of a large number of atoms can be described by collective observables that behave very similar to bosonic systems. The associated phase space behaves differently from the optical phase space, in the sense that it is compact. More specifically, the phase space will cover a sphere and the radius of this sphere will depend on the number of atoms. Effectively, we would recover a bosonic system in the limit of an infinite number of atoms. However, the compactness of phase space for a finite ensemble comes with interesting side effects: a sufficiently high amount of spin squeezing can create non-Gaussian states. We do not go into details for these systems, but it should nevertheless be highlighted that non-Gaussian spin states have received considerable attention in the literature [323] and have been produced in a range of experiments [324–327].

VIII. CONCLUSIONS AND OUTLOOK

In this Tutorial, we have presented a framework based on phase-space representations to study continuous-variable quantum systems. We then focused on the various aspects of non-Gaussian states, where we first represented different ways to structure the space of continuous-variable states in a single mode in Fig. 1. Whenever possible, we generalized results from the literature to a multimode setting. However, for certain properties such as the stellar rank, these generalizations become insufficient to classify all possible quantum states.

We introduced two paradigms to create non-Gaussian states, where one is a deterministic approach based on unitary transformations, reminiscent of the circuit approach for quantum-information processing. The second approach is conditional, in the sense that it relies on conditioning one part of a state on measurement outcomes for another part of a state, which is more narrowly related to a measurement-based approach to quantum protocols. Throughout the remainder of the Tutorial, we have largely focused on conditional operations, since it is the most commonly used approach in experiments. It also provides a natural avenue to start studying the relation between quantum correlations and non-Gaussian features. We show how the conditional approach requires certain correlations in the initial Gaussian state to be able to induce certain type of non-Gaussianity in the conditional state, as summarized in Fig. 5.

On the other hand, non-Gaussian operations can also create a type of non-Gaussian entanglement as introduced in Sec. C. This kind of entanglement is particular as it can not be identified with typical techniques that rely on the state's covariance matrix. Nevertheless, we use Rényi-2 entanglement as a measure to illustrate the existence of such purely non-Gaussian quantum correlations in photon-subtracted states. Even though its existence is known from pure-state examples, it has only received limited attention in both theoretical and experimental work. One possible reason is the difficulty of studying this type of entanglement for mixed states, since convex roof constructions tend to become highly intractable for non-Gaussian states.

As a final theoretical aspect of the Tutorial, we highlight the need of Wigner negativity to achieve some of the most striking features in quantum technologies. On the one hand, we show that Wigner negativity in either the state or the measurement is necessary to violate a Bell inequality. This observation can be understood in the broader context of nonlocality and contextuality: Wigner negativity is often seen as a manifestation of the contextual behavior of quantum systems, and nonlocality can be understood as a type of contextuality of measurements on different subsystems. On the other hand, we also present results that show how Wigner negativity is a requirement to achieve a quantum computational advantage. Intuitively, it is perhaps not surprising that states, operations, and measurements that can all be described by probability distributions on phase space can be efficiently simulated on a classical computer. However, as we showed in Sec. VI, the actual simulations protocol contains many subtle points. Here, too, we conclude that there are still many open questions surrounding the physics of quantum computational advantages in continuous-variable setups.

As a last step of this Tutorial, we provided an overview of the experimental realizations of non-Gaussian states with continuous variables. Quantum states of light are indeed the usual suspects for continuous-variable quantum-information processing, but it turns out to be remarkably challenging to engineer highly non-Gaussian states in such setups. We highlighted how trapped ions, cavity QED, and circuit QED have proven to be better equipped for this task, but in return they are confronted with other problems. Optomechanics presents itself as an ideal translator between these two regimes, which may soon make it possible to combine the scalability of

optical setups with the high nonlinearities of the microwave domain.

In a more general sense, there are definitely many open question to be resolved in the domain of continuous-variable quantum physics. In this Tutorial, we have focused extensively on questions related to non-Gaussian features, notably in multimode systems. In the greater scheme of things, this is only one of the many challenges in the field. The recent demonstration of a quantum computational advantage with Gaussian Boson sampling has set an important milestone for continuous-variable quantum technologies [23], but we are still far away from useful computational protocols as set out in the roadmap of Ref. [24]. Even though the quest for a Gottesman-Kitaev-Preskill state [31] is one of the main experimental priorities, there are still many open challenges in designing the Gaussian operations that form the basis of such a setup [328,329].

Beyond universal fault-tolerant quantum computers, there are many other potential applications for continuous-variable systems. They are widely used in quantum communications for quantum key distribution [330] and and secret sharing [331]. These protocols are largely based on Gaussian states and measurements, such that also the best possible attacks to these systems are Gaussian [332]. Nevertheless, non-Gaussian protocols for quantum key distribution, based on photon subtraction, have been proposed [333]. Such non-Gaussian quantum computation protocols and their security still involve many open questions.

Continuous-variable systems also provide a natural link to other bosonic systems, which is why they have been suggested as a platform to simulate molecular vibronic spectra [334]. The continuous-variable approach also plays an important role in quantum algorithms for other chemistry-related problems such as drug discovery through molecular docking [335] and the simulation of electron transport [336].

Furthermore, the continuous-variable setting is also suitable to implement certain elements for quantum machine learning such as quantum neural networks [337]. Even though this is a promising platform for tackling a wide range of problems, the proposal is highly ambitious on several points. In the context of this Tutorial, we emphasize the need of non-Gaussian unitary transformations. In principle, neural networks require linear couplings between different "neurons," which each implement some form of nonlinear operation. Non-Gaussian operations play the role of this nonlinear element, making them a crucial step in the scheme. To implement such continuous-variable neural networks we thus require either new developments on the implementation of non-Gaussian operations, or theoretical modifications in the protocol to make it fit for implementable conditional non-Gaussian operations. It should be highlighted that other machine-learning approaches exist, such as reservoir computing, which can be entirely based on Gaussian states [338].

A final quantum technology that may benefit from the use of non-Gaussian states is quantum metrology, as was recently demonstrated with motional Fock states of trapped ions [339]. Even though early work has shown that there is no clear benefit in using non-Gaussian operations such as photon subtraction for parameter estimation [154], there may still be other settings where such states are beneficial. Non-Gaussian entanglement could, for example, have a formal metrological advantage that is reflected in the quantum Fisher information [340]. On the other hand, ideas from quantum metrology also provide a possible approach for measuring non-Gaussian quantum steering [341]. The effects of non-Gaussian features on the sensitivity of the state can in principle be captured by higher moments of the quadrature operators [342]. It was recently shown that postselected measurements could, indeed, offer a quantum advantage for metrology [343]. This result is narrowly connected to the field of weak measurements and makes a connection to yet another phase-space representation: the Kirkwood-Dirac distribution [70,344]. Hence, we circle back to the fundamental physics of continuous-variable systems and conclude that there are still many connections to be made.

Beyond the technological applications that continuous-variable systems may have to offer, there is an important down-to-earth perspective that must be emphasized. With the improvement of detectors throughout the years, we have reached a point where theory and experiment can be considered mature to tackle single-mode problems. In multimode systems, the same cannot be said. With the exponential scaling of standard homodyne tomography, experimental tools for studying large multimode states beyond the Gaussian regime are limited. We may have to accept that the full quantum state is out of reach for experimental measurements. Even theoretically, highly multimode Wigner functions quickly become cumbersome to handle. Treating them with numerical integration techniques becomes a near-impossible task, once the number of modes is drastically increased. This makes even numerical simulations challenging. How then can we understand and even detect the non-Gaussian features of these systems?

One clear and important future research goal in this field is to provide an answer to this question. For quantum technologies, this may provide us with new ways to benchmark our systems, but more fundamentally it might teach us something new about the physics of these systems. One place where one might look for inspiration is the field of statistical mechanics, where statistical methods show that even highly complex systems can produce clear emergent signatures. We recently took a first step in exploring such ideas by looking at emergent network structures for continuous-variable non-Gaussian states [345]. The most exciting lesson from such preliminary work is that there

is still much to be learned about non-Gaussian quantum states.

ACKNOWLEDGMENTS

First, I want to express sincere gratitude to the anonymous referees for providing very thorough reports and many useful suggestions that significantly improved the clarity and completeness of this Tutorial. I also thank M. Genoni for several useful suggestions. More generally speaking, the content of this text was influenced by stimulating discussions throughout the years with many colleagues, notably F. Grosshans, R. Filip, Q. He, M. Gessner, and G. Ferrini. Furthermore, I am very grateful to M. Fannes for teaching me the mathematical foundations that lie at the basis bosonic quantum systems. This point of view was complemented by colleagues in the multimode quantum optics group of the Laboratoire Kastler Brossel, V. Parigi, N. Treps, and C. Fabre, who have introduced me to the wonderful world of experimental quantum optics. Still, the main source of inspiration for this Tutorial are the many excellent students and postdocs that I have worked with in the last few years. Their questions and struggles have been essential to highlight the barriers that I try to overcome in this Tutorial. Among these students and postdocs, I want to express explicit gratitude to U. Chabaud, G. Sorelli, and D. Barral for their careful and detailed reading of the Tutorial and for their useful comments. I also acknowledge the many useful discussions with K. Zhang, who notably made me aware of the possibility of reducing entanglement through photon subtraction (here shown in Fig. 7). Last but not least, I want to express special thanks to C. Lopetegui, who started reading this Tutorial as a newcomer to the field of CV quantum optics and thus had the perfect point of view to help fine tune the content.

APPENDIX: MATHEMATICAL REMARKS

Here we present some important well-known mathematical concepts that are regularly used in the Tutorial to make the text more self-contained. The comments and definitions given here are not very rigorous and mainly aim at giving the reader an intuitive understanding, for a more formal introduction one should consult a standard textbook [41,346,347].

1. Topological vector spaces

Throughout this Tutorial, we often deal implicitly with topological vector spaces. Vector spaces are well known from linear algebra and can be thought of as sets of mathematical objects called vectors, which can be added together in a commutative way and multiplied by scalars. When we consider a vector space $\mathcal{V}$ on a field $\mathcal{F}$, this means that for any $\vec{v}_1, \vec{v}_2 \in \mathcal{V}$ and any $\alpha_1, \alpha_2 \in \mathcal{F}$ the object $\alpha_1\vec{v}_1 + \alpha_2\vec{v}_2 \in \mathcal{V}$. This means that the vector space is closed under addition and scalar multiplication. In this Tutorial, the field $\mathcal{F}$ is either identified as $\mathbb{R}$ (for phase space) or $\mathbb{C}$ (for Hilbert spaces).

The spaces that are considered in the Tutorial have much more structure than what is given by the vector space. First of all, we generally deal with normed spaces, which means that our vector spaces are topological vector spaces in the sense that there is a notion of distance defined upon them. Generally speaking, topological vector spaces can be equipped with exotic topologies, but here we simply deal with norms. On top, we again add an additional structure when we assume that these norms are generated by inner products (depending on exact properties, these inner products go by different names such as "positive-definite sesquilinear form", which is what we typically consider in quantum mechanics).

As we deal with infinite-dimensional spaces to describe bosonic quantum states and Fock space, it is important to set some terminology straight. When we talk about a Hilbert space, there is the assumption that the space is complete. In an infinite-dimensional inner-product space, we can define sequences of elements in $\mathcal{V}$. If we consider a sequence $(\vec{v}_j)_{j\in\mathbb{N}}$ such that for any ϵ we can find a value $N > 0$ such that $\|\vec{v}_j - \vec{v}_k\| < \epsilon$ for all $j, k > N$, we call the sequence a Cauchy sequence. In other words, the distance between elements in the Cauchy sequence shrinks as we proceed further into the sequence. The fact that a Hilbert space is closed means that all Cauchy sequences converge in the sense that $\lim_{j\to\infty} \vec{v}_j = \vec{v} \in \mathcal{V}$. Finite-dimensional inner-product spaces automatically have this property, but for infinite-dimensional spaces it must be imposed explicitly.

Another class of structured vector space, that is often encountered in the Tutorial, is a real symplectic space. These spaces appear when we consider phase space, and they are given by a real vector space with an additional symplectic form σ instead of the usual inner product. In the mathematical literature, one often encounters the notation $(\mathcal{V}, \sigma)$ for a symplectic space, where the symplectic form has the following properties: we consider $\vec{v}_1.\vec{v}_2 \in \mathcal{V}$ and find that $\sigma(\vec{v}_1, \vec{v}_2) \in \mathbb{R}$, σ is bilinear, and $\sigma(\vec{v}_1, \vec{v}_2) = -\sigma(\vec{v}_2, \vec{v}_1)$. In all cases in this Tutorial, we also consider that σ is nondegenerate, which means that $\sigma(\vec{v}_1, \vec{v}_2) = 0$ for all $\vec{v}_1 \in \mathcal{V}$ if and only if $\vec{v}_2 = \vec{0}$. When the symplectic space is finite dimensional, it is often practical to represent the symplectic form in terms of a matrix. In the Tutorial this is done by associating $\sigma(\vec{v}_1, \vec{v}_2) = \vec{v}_1^T \Omega \vec{v}_2$.

In principle, a real symplectic space is all that is needed to develop the mathematical framework of the CCR algebra. However, it is often natural when dealing with bosonic systems to include an additional structure in the form of an inner product. In the Tutorial, this is done implicitly by also using the standard inner product $\vec{v}_1^T\vec{v}_2$ on phase space. This allows us to ultimately get the isomorphism (44). In the quantum statistical mechanics literature, it is common to

see references to a "pre-Hilbert space", rather than a phase space or a symplectic space. When we refer to a pre-Hilbert space, we consider an inner-product space, which is not necessarily complete and one must consider the closure to be guaranteed to obtain a full Hilbert space. The reason is that phase space, as a real vector space $\mathcal{V}$ with an inner product, given by a bilinear form $s(.,.)$, and a symplectic form $\sigma(.,.)$ is equivalent to a complex pre-Hilbert space $\mathcal{H}$. For finite-dimensional spaces, the equivalence between the vector spaces is obtained via isomorphism (44):

$$\vec{f} \in \mathcal{V} \mapsto |\psi_f\rangle = \sum_j (f_{2j-1} + if_{2j}) |\varphi_j\rangle \in \mathcal{H}, \tag{A1}$$

where $|\varphi_j\rangle$ for a basis of $\mathcal{H}$. As we are talking about an isomorphism between structured vectors spaces, we also need an identity between additional structures, which is given by

$$\langle \psi_{f_1} \mid \psi_{f_2} \rangle = s(\vec{f}_1, \vec{f}_2) - i\sigma(\vec{f}_1, \vec{f}_2). \tag{A2}$$

This isomorphism holds very generally and can be extended to infinite-dimensional spaces. It provides a very formal connection between the single-particle Hilbert space for a many-boson system and its phase space associated with the modes of the bosonic field. Technically, we note that the phase space is equivalent to a pre-Hilbert space, and the closure of this space is the single-particle Hilbert space. Whenever the phase space (and thus the single-particle Hilbert space) is finite dimensional, the pre-Hilbert space is closed such that phase space and single-particle Hilbert space really are equivalent. For a very rigorous treatment on all these points, we refer to Ref. [42].

2. Span

Throughout the Tutorial, we often refer to the "span" of a certain set of vectors. These vectors can be members of a vector space, symplectic space, topological vectors space, pre-Hilbert space, or Hilbert space, the definition of the span is always the same. Let us here assume that $\mathcal{V}$ denotes any type of vector space over a field $\mathcal{F}$ and consider a set $\vec{v}_1, \ldots \vec{v}_n \in \mathcal{V}$. We can now define the span of this set of vectors as the set of all linear combinations that can be made with these vectors

$$\text{span}\{\vec{v}_1, \ldots \vec{v}_n\} := \{\alpha_1 \vec{v}_1 + \cdots + \alpha_n \vec{v}_n \mid \alpha_1, \ldots, \alpha_n \in \mathcal{F}\}. \tag{A3}$$

We emphasize that there is no need for the set $\vec{v}_1, \ldots \vec{v}_n$ to form a basis, nor for the vectors to be linearly independent, nor for the vectors to be normalized, nor for the vectors to be orthogonal to one another.

Throughout the Tutorial, the vector spaces we encounter are either real (in the case of phase space) such that $\mathcal{F} = \mathbb{R}$ or complex (in the case of Hilbert spaces for quantum systems) such that $\mathcal{F} = \mathbb{C}$. In the case where the vector spaces have some topological structure (which we can colloquially understand as a mathematical sense of distance that allows limits to be defined), it can make sense to consider the closure of a span, denoted by

$$\overline{\text{span}\{\vec{v}_1, \ldots \vec{v}_n\}}, \tag{A4}$$

such that any convergent sequence built with elements of the span has its limit also included in the closure.

[1] E. Schrödinger, Der stetige übergang von der mikro- zur makromechanik, Naturwissenschaften **14**, 664 (1926).

[2] H. Araki and E. J. Woods, Representations of the canonical commutation relations describing a nonrelativistic infinite free bose gas, J. Math. Phys. **4**, 637 (1963).

[3] D. W. Robinson, The ground state of the Bose gas, Commun.Math. Phys. **1**, 159 (1965).

[4] A. Verbeure, *Many-Body Boson Systems: Half a Century Later*, Theoretical and mathematical physics (Springer, London ; New York, 2011).

[5] R. J. Glauber, Coherent and incoherent states of the radiation field, Phys. Rev. **131**, 2766 (1963).

[6] E. C. G. Sudarshan, Equivalence of Semiclassical and Quantum Mechanical Descriptions of Statistical Light Beams, Phys. Rev. Lett. **10**, 277 (1963).

[7] S. L. Braunstein and P. van Loock, Quantum information with continuous variables, Rev. Mod. Phys. **77**, 513 (2005).

[8] C. Weedbrook, S. Pirandola, R. García-Patrón, N. J. Cerf, T. C. Ralph, J. H. Shapiro, and S. Lloyd, Gaussian quantum information, Rev. Mod. Phys. **84**, 621 (2012).

[9] G. Adesso, S. Ragy, and A. R. Lee, Continuous variable quantum information: Gaussian states and beyond, Open Syst. Inf. Dynamics **21**, 1440001 (2014).

[10] J. Williamson, On the algebraic problem concerning the normal forms of linear dynamical systems, American J. Math. **58**, 141 (1936).

[11] S. L. Braunstein, Squeezing as an irreducible resource, Phys. Rev. A **71**, 055801 (2005).

[12] M. M. Wolf, G. Giedke, and J. I. Cirac, Extremality of Gaussian Quantum States, Phys. Rev. Lett. **96**, 080502 (2006).

[13] A. S. Holevo, M. Sohma, and O. Hirota, Capacity of quantum gaussian channels, Phys. Rev. A **59**, 1820 (1999).

[14] M. Yukawa, R. Ukai, P. van Loock, and A. Furusawa, Experimental generation of four-mode continuous-variable cluster states, Phys. Rev. A **78**, 012301 (2008).

[15] X. Su, Y. Zhao, S. Hao, X. Jia, C. Xie, and K. Peng, Experimental preparation of eight-partite cluster state for photonic qumodes, Opt. Lett. **37**, 5178 (2012).

[16] D. Barral, M. Walschaers, K. Bencheikh, V. Parigi, J. A. Levenson, N. Treps, and N. Belabas, Versatile Photonic Entanglement Synthesizer in the Spatial Domain, Phys. Rev. Appl. **14**, 044025 (2020).

[17] J. Roslund, R. M. de Araújo, S. Jiang, C. Fabre, and N. Treps, Wavelength-multiplexed quantum networks with ultrafast frequency combs, Nat Photon **8**, 109 (2014).

[18] M. Chen, N. C. Menicucci, and O. Pfister, Experimental Realization of Multipartite Entanglement of 60 Modes of a Quantum Optical Frequency Comb, Phys. Rev. Lett. **112**, 120505 (2014).

[19] Y. Cai, J. Roslund, G. Ferrini, F. Arzani, X. Xu, C. Fabre, and N. Treps, Multimode entanglement in reconfigurable graph states using optical frequency combs, Nat. Commun. **8**, 15645 (2017).

[20] W. Asavanant, Y. Shiozawa, S. Yokoyama, B. Charoensombutamon, H. Emura, R. N. Alexander, S. Takeda, J.-i. Yoshikawa, N. C. Menicucci, H. Yonezawa, and A. Furusawa, Generation of time-domain-multiplexed two-dimensional cluster state, Science **366**, 373 (2019).

[21] M. V. Larsen, X. Guo, C. R. Breum, J. S. Neergaard-Nielsen, and U. L. Andersen, Deterministic generation of a two-dimensional cluster state, Science **366**, 369 (2019).

[22] Z. Yang, M. Jahanbozorgi, D. Jeong, S. Sun, O. Pfister, H. Lee, and X. Yi, A squeezed quantum microcomb on a chip, arXiv:2103.03380 [physics.optics] (2021).

[23] H.-S. Zhong *et al.*, Quantum computational advantage using photons, Science 370, 1460 (2020), https://science.sciencemag.org/content/370/6523/1460.full.pdf.

[24] J. E. Bourassa, R. N. Alexander, M. Vasmer, A. Patil, I. Tzitrin, T. Matsuura, D. Su, B. Q. Baragiola, S. Guha, G. Dauphinais, K. K. Sabapathy, N. C. Menicucci, and I. Dhand, Blueprint for a scalable photonic fault-tolerant quantum computer, Quantum **5**, 392 (2021).

[25] S. D. Bartlett, B. C. Sanders, S. L. Braunstein, and K. Nemoto, Efficient Classical Simulation of Continuous Variable Quantum Information Processes, Phys. Rev. Lett. **88**, 097904 (2002).

[26] S. Lloyd and S. L. Braunstein, Quantum Computation Over Continuous Variables, Phys. Rev. Lett. **82**, 1784 (1999).

[27] N. C. Menicucci, P. van Loock, M. Gu, C. Weedbrook, T. C. Ralph, and M. A. Nielsen, Universal Quantum Computation with Continuous-Variable Cluster States, Phys. Rev. Lett. **97**, 110501 (2006).

[28] M. Gu, C. Weedbrook, N. C. Menicucci, T. C. Ralph, and P. van Loock, Quantum computing with continuous-variable clusters, Phys. Rev. A **79**, 062318 (2009).

[29] N. C. Menicucci, Fault-Tolerant Measurement-Based Quantum Computing with Continuous-Variable Cluster States, Phys. Rev. Lett. **112**, 120504 (2014).

[30] F. Arzani, N. Treps, and G. Ferrini, Polynomial approximation of non-gaussian unitaries by counting one photon at a time, Phys. Rev. A **95**, 052352 (2017).

[31] D. Gottesman, A. Kitaev, and J. Preskill, Encoding a qubit in an oscillator, Phys. Rev. A **64**, 012310 (2001).

[32] B. Q. Baragiola, G. Pantaleoni, R. N. Alexander, A. Karanjai, and N. C. Menicucci, All-Gaussian Universality and Fault Tolerance with the Gottesman-Kitaev-Preskill Code, Phys. Rev. Lett. **123**, 200502 (2019).

[33] A. Mari and J. Eisert, Positive Wigner Functions Render Classical Simulation of Quantum Computation Efficient, Phys. Rev. Lett. **109**, 230503 (2012).

[34] R. Hudson, When is the Wigner quasi-probability density non-negative?, Rep. Math. Phys. **6**, 249 (1974).

[35] F. Soto and P. Claverie, When is the Wigner function of multidimensional systems nonnegative?, J. Math. Phys. **24**, 97 (1983).

[36] A. Mandilara, E. Karpov, and N. J. Cerf, Extending Hudson's theorem to mixed quantum states, Phys. Rev. A **79**, 062302 (2009).

[37] L. c. v. Lachman, I. Straka, J. Hloušek, M. Ježek, and R. Filip, Faithful Hierarchy of Genuine *n*-Photon Quantum Non-Gaussian Light, Phys. Rev. Lett. **123**, 043601 (2019).

[38] U. Chabaud, D. Markham, and F. Grosshans, Stellar Representation of Non-Gaussian Quantum States, Phys. Rev. Lett. **124**, 063605 (2020).

[39] M. Walschaers, V. Parigi, and N. Treps, Practical framework for conditional non-gaussian quantum state preparation, PRX Quantum **1**, 020305 (2020).

[40] D. Petz, *An Invitation to the Algebra of Canonical Comutation Relations*, Leuven notes in mathematical and theoretical physics Series A No. 2 (Leuven Univ. Press, Leuven, 1990).

[41] O. Bratteli and D. W. Robinson, *Operator Algebras and Quantum Statistical Mechanics 1* (Springer Berlin Heidelberg, Berlin, Heidelberg, 1987).

[42] O. Bratteli and D. W. Robinson, *Operator Algebras and Quantum Statistical Mechanics Equilibrium States. Models in Quantum Statistical Mechanics* (Springer, Berlin, 1997).

[43] M. H. Stone, Linear transformations in Hilbert space: III. Operational methods and group theory, PNAS **16**, 172 (1930).

[44] J. von Neumann, Die eindeutigkeit der Schrödingerschen operatoren, Math. Ann. **104**, 570 (1931).

[45] M. H. Stone, On one-parameter unitary groups in Hilbert space, Ann. Math. **33**, 643 (1932).

[46] J. von Neumann, Über einen satz von herrn M. H. Stone, Ann. Math. **33**, 567 (1932).

[47] M. C. Tichy, F. Mintert, and A. Buchleitner, Essential entanglement for atomic and molecular physics, J. Phys. B: At. Mol. Opt. Phys. **44**, 192001 (2011).

[48] F. Benatti, R. Floreanini, F. Franchini, and U. Marzolino, Entanglement in indistinguishable particle systems, Phys. Rep. **878**, 1 (2020), entanglement in indistinguishable particle systems.

[49] N. Killoran, M. Cramer, and M. B. Plenio, Extracting Entanglement from Identical Particles, Phys. Rev. Lett. **112**, 150501 (2014).

[50] N. Killoran, F. E. S. Steinhoff, and M. B. Plenio, Converting Nonclassicality Into Entanglement, Phys. Rev. Lett. **116**, 080402 (2016).

[51] R. Lo Franco and G. Compagno, Indistinguishability of Elementary Systems as a Resource for Quantum Information Processing, Phys. Rev. Lett. **120**, 240403 (2018).

[52] B. Morris, B. Yadin, M. Fadel, T. Zibold, P. Treutlein, and G. Adesso, Entanglement between Identical Particles is a Useful and Consistent Resource, Phys. Rev. X **10**, 041012 (2020).

[53] M. C. Tichy, Interference of identical particles from entanglement to boson-sampling, J. Phys. B: At. Mol. Opt. Phys. **47**, 103001 (2014).

[54] Note that the notation is not a coincidence, we can indeed construct a formal linear map from the single-particle Hilbert space into the operator algebra of linear operators on the Fock space. This mapping takes single-particle state vectors $\psi \in \mathcal{H}$ and maps them to a creation operators. The mapping is linear in the sense that $\hat{a}^\dagger(x\psi + y\varphi) = x\hat{a}^\dagger(\psi) + y\hat{a}^\dagger(\varphi)$, for all $x, y \in \mathbb{C}$.

[55] L. Mandel and E. Wolf, *Optical Coherence and Quantum Optics* (Cambridge University Press, Cambridge, 1995).

[56] M. Walschaers, Signatures of many-particle interference, J. Phys. B: At. Mol. Opt. Phys. **53**, 043001 (2020).

[57] W. P. Schleich, *Quantum Optics in Phase Space* (Wiley VCH, Berlin, 2001).

[58] C. Fabre and N. Treps, Modes and states in quantum optics, Rev. Mod. Phys. **92**, 035005 (2020).

[59] A. M. O. de Almeida, The weyl representation in classical and quantum mechanics, Phys. Rep. **295**, 265 (1998).

[60] In the literature, one will encounter various different choices for the symplectic structure, which correspond to different forms of ordering the amplitude and phase quadratures. In general, any matrix J that satisfies the conditions $J^T = -J$ and $J^2 = -\mathbb{1}$ defines a symplectic structure. A popular alternative to the ordering $(E_1^{(x)}, E_1^{(p)}, \ldots, E_m^{(x)}, E_m^{(p)})$ that we follow in this Tutorial is the ordering $(E_1^{(x)}, \ldots, E_m^{(x)}, E_1^{(p)}, \ldots, E_m^{(p)})$. The choice in this Tutorial is motivated by the study of entanglement, where it is more convenient to group the quadratures that correspond to the same modes together.

[61] E. Wigner, On the quantum correction for thermodynamic equilibrium, Phys. Rev. **40**, 749 (1932).

[62] M. Hillery, R. O'Connell, M. Scully, and E. Wigner, Distribution functions in physics: Fundamentals, Phys. Rep. **106**, 121 (1984).

[63] W. P. Schleich, in *Quantum Optics in Phase Space* (John Wiley and Sons, Ltd, 2001), Chap. 3, p. 67.

[64] R. W. Spekkens, Negativity and Contextuality are Equivalent Notions of Nonclassicality, Phys. Rev. Lett. **101**, 020401 (2008).

[65] J. von Neumann, *Mathematical Foundations of Quantum Mechanics* (Princeton University Press, Berlin, Heidelberg, 1955).

[66] H. Weyl, Quantenmechanik und gruppentheorie, Zeitschrift für Physik **46**, 1 (1927).

[67] J. B. Conway, in *A Course in Functional Analysis* (Springer New York, New York, NY, 1985), p. 310.

[68] M. Plancherel, Contribution à l'étude de la représentation d'une fonction arbitraire par des intégrales définies, Rendiconti del Circolo Matematico di Palermo (1884-1940) **30**, 289 (1910).

[69] K. E. Cahill and R. J. Glauber, Density operators and quasiprobability distributions, Phys. Rev. **177**, 1882 (1969).

[70] P. A. M. Dirac, On the analogy between classical and quantum mechanics, Rev. Mod. Phys. **17**, 195 (1945).

[71] J. Sperling and W. Vogel, Quasiprobability distributions for quantum-optical coherence and beyond, Physica Scripta **95**, 034007 (2020).

[72] A. Royer, Wigner function as the expectation value of a parity operator, Phys. Rev. A **15**, 449 (1977).

[73] K. Banaszek and K. Wódkiewicz, Direct Probing of Quantum Phase Space by Photon Counting, Phys. Rev. Lett. **76**, 4344 (1996).

[74] K. Banaszek, C. Radzewicz, K. Wódkiewicz, and J. S. Krasiński, Direct measurement of the wigner function by photon counting, Phys. Rev. A **60**, 674 (1999).

[75] K. Laiho, K. N. Cassemiro, D. Gross, and C. Silberhorn, Probing the Negative Wigner Function of a Pulsed Single Photon Point by Point, Phys. Rev. Lett. **105**, 253603 (2010).

[76] R. Nehra, A. Win, M. Eaton, R. Shahrokhshahi, N. Sridhar, T. Gerrits, A. Lita, S. W. Nam, and O. Pfister, State-independent quantum state tomography by photon-number-resolving measurements, Optica **6**, 1356 (2019).

[77] L. G. Lutterbach and L. Davidovich, Method for Direct Measurement of the Wigner Function in Cavity qed and ion Traps, Phys. Rev. Lett. **78**, 2547 (1997).

[78] D. Leibfried, D. M. Meekhof, B. E. King, C. Monroe, W. M. Itano, and D. J. Wineland, Experimental Determination of the Motional Quantum State of a Trapped Atom, Phys. Rev. Lett. **77**, 4281 (1996).

[79] G. Nogues, A. Rauschenbeutel, S. Osnaghi, P. Bertet, M. Brune, J. M. Raimond, S. Haroche, L. G. Lutterbach, and L. Davidovich, Measurement of a negative value for the wigner function of radiation, Phys. Rev. A **62**, 054101 (2000).

[80] P. Bertet, A. Auffeves, P. Maioli, S. Osnaghi, T. Meunier, M. Brune, J. M. Raimond, and S. Haroche, Direct Measurement of the Wigner Function of a One-Photon Fock State in a Cavity, Phys. Rev. Lett. **89**, 200402 (2002).

[81] A. I. Lvovsky, P. Grangier, A. Ourjoumtsev, V. Parigi, M. Sasaki, and R. Tualle-Brouri, Production and applications of non-gaussian quantum states of light, arXiv:2006.16985 [quant-ph] (2020).

[82] F. Flamini, N. Spagnolo, and F. Sciarrino, Photonic quantum information processing: A review, Rep. Prog. Phys. **82**, 016001 (2018).

[83] R. Simon, N. Mukunda, and B. Dutta, Quantum-noise matrix for multimode systems: U(n) invariance, squeezing, and normal forms, Phys. Rev. A **49**, 1567 (1994).

[84] H. P. Robertson, The uncertainty principle, Phys. Rev. **34**, 163 (1929).

[85] Arvind, B. Dutta, N. Mukunda, and R. Simon, The real symplectic groups in quantum mechanics and optics, Pramana **45**, 471 (1995).

[86] J. Eisert and M. M. Wolf, in *Quantum Information with Continuous Variables of Atoms and Light* (World Scientific, 2007), p. 23.

[87] B. Demoen, P. Vanheuverzwijn, and A. Verbeure, Completely positive maps on the CCR-algebra, Lett Math Phys **2**, 161 (1977).

[88] B. Demoen, P. Vanheuverzwijn, and A. Verbeure, Completely positive quasi-free maps of the CCR-algebra, Rep. Math. Phys. **15**, 27 (1979).

[89] R. Filip and L. Mišta, Detecting Quantum States with a Positive Wigner Function beyond Mixtures of Gaussian States, Phys. Rev. Lett. **106**, 200401 (2011).

[90] A. Kenfack and K. Życzkowski, Negativity of the wigner function as an indicator of non-classicality, J. Opt. B: Quantum Semiclassical Opt. **6**, 396 (2004).

[91] J. L. W. V. Jensen, Sur les fonctions convexes et les inégalités entre les valeurs moyennes, Acta Math. **30**, 175 (1906).

[92] G. Vidal and R. F. Werner, Computable measure of entanglement, Phys. Rev. A **65**, 032314 (2002).

[93] M. B. Hastings, Superadditivity of communication capacity using entangled inputs, Nat. Phys. **5**, 255 (2009).

[94] C. D. Cushen and R. L. Hudson, A quantum-mechanical central limit theorem, J. Appl. Probab. **8**, 454 (1971).

[95] J. Quaegebeur, A noncommutative central limit theorem for ccr-algebras, J. Funct. Anal. **57**, 1 (1984).

[96] D. Goderis, A. Verbeure, and P. Vets, Non-commutative central limits, Probab. Theory Relat. Fields **82**, 527 (1989).

[97] M. G. Genoni, M. G. A. Paris, and K. Banaszek, Measure of the non-gaussian character of a quantum state, Phys. Rev. A **76**, 042327 (2007).

[98] M. G. Genoni, M. G. A. Paris, and K. Banaszek, Quantifying the non-gaussian character of a quantum state by quantum relative entropy, Phys. Rev. A **78**, 060303 (2008).

[99] M. G. Genoni and M. G. A. Paris, Quantifying non-gaussianity for quantum information, Phys. Rev. A **82**, 052341 (2010).

[100] F. Albarelli, M. G. Genoni, M. G. A. Paris, and A. Ferraro, Resource theory of quantum non-gaussianity and wigner negativity, Phys. Rev. A **98**, 052350 (2018).

[101] P. Marian and T. A. Marian, Relative entropy is an exact measure of non-gaussianity, Phys. Rev. A **88**, 012322 (2013).

[102] J. S. Ivan, M. S. Kumar, and R. Simon, A measure of non-gaussianity for quantum states, Quantum Inf. Process. **11**, 853 (2012).

[103] N. Lütkenhaus and S. M. Barnett, Nonclassical effects in phase space, Phys. Rev. A **51**, 3340 (1995).

[104] A function f is said to have an order of growth r when there are constant $a, b \in \mathbb{C}$ such that $|f(z)| \leqslant a\, e\, xp(b|z|^r)$ for all $z \in \mathbb{C}$.

[105] B. Yurke and D. Stoler, Generating Quantum Mechanical Superpositions of Macroscopically Distinguishable States via Amplitude Dispersion, Phys. Rev. Lett. **57**, 13 (1986).

[106] E. Schrödinger, Die gegenwärtige situation in der quantenmechanik, Naturwissenschaften **23**, 807 (1935).

[107] P. T. Cochrane, G. J. Milburn, and W. J. Munro, Macroscopically distinct quantum-superposition states as a bosonic code for amplitude damping, Phys. Rev. A **59**, 2631 (1999).

[108] Z. Leghtas, G. Kirchmair, B. Vlastakis, R. J. Schoelkopf, M. H. Devoret, and M. Mirrahimi, Hardware-Efficient Autonomous Quantum Memory Protection, Phys. Rev. Lett. **111**, 120501 (2013).

[109] B. C. Sanders, Quantum dynamics of the nonlinear rotator and the effects of continual spin measurement, Phys. Rev. A **40**, 2417 (1989).

[110] A. N. Boto, P. Kok, D. S. Abrams, S. L. Braunstein, C. P. Williams, and J. P. Dowling, Quantum Interferometric Optical Lithography: Exploiting Entanglement to Beat the Diffraction Limit, Phys. Rev. Lett. **85**, 2733 (2000).

[111] H. Lee, P. Kok, and J. P. Dowling, A quantum rosetta stone for interferometry, J. Mod. Opt. **49**, 2325 (2002).

[112] B. Yurke, Input States for Enhancement of Fermion Interferometer Sensitivity, Phys. Rev. Lett. **56**, 1515 (1986).

[113] Y. Israel, I. Afek, S. Rosen, O. Ambar, and Y. Silberberg, Experimental tomography of noon states with large photon numbers, Phys. Rev. A **85**, 022115 (2012).

[114] M. G. Genoni, M. L. Palma, T. Tufarelli, S. Olivares, M. S. Kim, and M. G. A. Paris, Detecting quantum non-Gaussianity via the Wigner function, Phys. Rev. A **87**, 062104 (2013).

[115] C. Hughes, M. G. Genoni, T. Tufarelli, M. G. A. Paris, and M. S. Kim, Quantum non-Gaussianity witnesses in phase space, Phys. Rev. A **90**, 013810 (2014).

[116] J. Park, J. Zhang, J. Lee, S.-W. Ji, M. Um, D. Lv, K. Kim, and H. Nha, Testing Nonclassicality and Non-Gaussianity in Phase Space, Phys. Rev. Lett. **114**, 190402 (2015).

[117] L. Happ, M. A. Efremov, H. Nha, and W. P. Schleich, Sufficient condition for a quantum state to be genuinely quantum non-Gaussian, New J. Phys. **20**, 023046 (2018).

[118] B. Kühn and W. Vogel, Quantum non-Gaussianity and quantification of nonclassicality, Phys. Rev. A **97**, 053823 (2018).

[119] M. Bohmann, E. Agudelo, and J. Sperling, Probing nonclassicality with matrices of phase-space distributions, Quantum **4**, 343 (2020).

[120] I. Straka, A. Predojević, T. Huber, L. c. v. Lachman, L. Butschek, M. Miková, M. Mičuda, G. S. Solomon, G. Weihs, M. Ježek, and R. Filip, Quantum Non-Gaussian Depth of Single-Photon States, Phys. Rev. Lett. **113**, 223603 (2014).

[121] I. Straka, L. Lachman, J. Hloušek, M. Miková, M. Mičuda, M. Ježek, and R. Filip, Quantum non-Gaussian multiphoton light, Npj Quantum Inf. **4**, 4 (2018).

[122] C. N. Gagatsos and S. Guha, Efficient representation of Gaussian states for multimode non-Gaussian quantum state engineering via subtraction of arbitrary number of photons, Phys. Rev. A **99**, 053816 (2019).

[123] U. Chabaud, G. Roeland, M. Walschaers, F. Grosshans, V. Parigi, D. Markham, and N. Treps, Certification of non-Gaussian states with operational measurements, PRX Quantum **2**, 020333 (2021).

[124] P. Lelong and L. Gruman, *Entire Functions of Several Complex Variables* (Springer-Verlag Berlin Heidelberg, 1986).

[125] U. Chabaud, G. Ferrini, F. Grosshans, and D. Markham, Classical simulation of Gaussian quantum circuits with non-Gaussian input states, Phys. Rev. Res. **3**, 033018 (2021).

[126] R. Takagi and Q. Zhuang, Convex resource theory of non-Gaussianity, Phys. Rev. A **97**, 062337 (2018).

[127] V. Veitch, S. A. H. Mousavian, D. Gottesman, and J. Emerson, The resource theory of stabilizer quantum computation, New J. Phys. **16**, 013009 (2014).

[128] U. Chabaud, P.-E. Emeriau, and F. Grosshans, Witnessing Wigner negativity, Quantum **5**, 471 (2021).

[129] A. Ourjoumtsev, R. Tualle-Brouri, J. Laurat, and P. Grangier, Generating optical Schrödinger kittens for quantum information processing, Science **312**, 83 (2006).

[130] A. Mari, K. Kieling, B. M. Nielsen, E. S. Polzik, and J. Eisert, Directly Estimating Nonclassicality, Phys. Rev. Lett. **106**, 010403 (2011).
[131] R. Loudon and P. Knight, Squeezed light, J. Mod. Opt. **34**, 709 (1987).
[132] L.-A. Wu, H. J. Kimble, J. L. Hall, and H. Wu, Generation of Squeezed States by Parametric Down Conversion, Phys. Rev. Lett. **57**, 2520 (1986).
[133] D. P. DiVincenzo, Quantum computation, Science **270**, 255 (1995).
[134] M. Reck, A. Zeilinger, H. J. Bernstein, and P. Bertani, Experimental Realization of any Discrete Unitary Operator, Phys. Rev. Lett. **73**, 58 (1994).
[135] P. Marek, R. Filip, and A. Furusawa, Deterministic implementation of weak quantum cubic nonlinearity, Phys. Rev. A **84**, 053802 (2011).
[136] K. Marshall, R. Pooser, G. Siopsis, and C. Weedbrook, Repeat-until-success cubic phase gate for universal continuous-variable quantum computation, Phys. Rev. A **91**, 032321 (2015).
[137] K. Miyata, H. Ogawa, P. Marek, R. Filip, H. Yonezawa, J.-i. Yoshikawa, and A. Furusawa, Implementation of a quantum cubic gate by an adaptive non-Gaussian measurement, Phys. Rev. A **93**, 022301 (2016).
[138] R. Yanagimoto, T. Onodera, E. Ng, L. G. Wright, P. L. McMahon, and H. Mabuchi, Engineering a Kerr-Based Deterministic Cubic Phase Gate via Gaussian Operations, Phys. Rev. Lett. **124**, 240503 (2020).
[139] Y. Zheng, O. Hahn, P. Stadler, P. Holmvall, F. Quijandría, A. Ferraro, and G. Ferrini, Gaussian conversion protocols for cubic phase state generation, PRX Quantum **2**, 010327 (2021).
[140] D. Vion, A. Aassime, A. Cottet, P. Joyez, H. Pothier, C. Urbina, D. Esteve, and M. H. Devoret, Manipulating the quantum state of an electrical circuit, Science **296**, 886 (2002).
[141] M. H. Devoret and R. J. Schoelkopf, Superconducting circuits for quantum information: An outlook, Science **339**, 1169 (2013).
[142] C. W. S. Chang, C. Sabín, P. Forn-Díaz, F. Quijandría, A. M. Vadiraj, I. Nsanzineza, G. Johansson, and C. M. Wilson, Observation of Three-Photon Spontaneous Parametric Down-Conversion in a Superconducting Parametric Cavity, Phys. Rev. X **10**, 011011 (2020).
[143] K. Kraus, General state changes in quantum theory, Ann. Phys. (N. Y) **64**, 311 (1971).
[144] Statistics of quantum measurements, in *Statistical Structure of Quantum Theory* (Springer Berlin Heidelberg, Berlin, Heidelberg, 2001) p. 39.
[145] R. A. Horn and C. R. Johnson, *Matrix Analysis* (Cambridge University Press, New York, NY, 2017), 2nd ed. corrected reprint ed.
[146] L. Lami, A. Serafini, and G. Adesso, Gaussian entanglement revisited, New J. Phys. **20**, 023030 (2018).
[147] D. E. Browne, J. Eisert, S. Scheel, and M. B. Plenio, Driving non-Gaussian to Gaussian states with linear optics, Phys. Rev. A **67**, 062320 (2003).
[148] J. Wenger, R. Tualle-Brouri, and P. Grangier, Non-Gaussian Statistics from Individual Pulses of Squeezed Light, Phys. Rev. Lett. **92**, 153601 (2004).
[149] A. Zavatta, V. Parigi, M. S. Kim, and M. Bellini, Subtracting photons from arbitrary light fields: Experimental test of coherent state invariance by single-photon annihilation, New J. Phys. **10**, 123006 (2008).
[150] V. Averchenko, C. Jacquard, V. Thiel, C. Fabre, and N. Treps, Multimode theory of single-photon subtraction, New J. Phys. **18**, 083042 (2016).
[151] H. M. Wiseman and G. J. Milburn, *Quantum Measurement and Control* (Cambridge University Press, Cambridge, 2009).
[152] M. Walschaers, C. Fabre, V. Parigi, and N. Treps, Entanglement and Wigner Function Negativity of Multimode Non-Gaussian States, Phys. Rev. Lett. **119**, 183601 (2017).
[153] M. Walschaers, C. Fabre, V. Parigi, and N. Treps, Statistical signatures of multimode single-photon-added and -subtracted states of light, Phys. Rev. A **96**, 053835 (2017).
[154] D. Braun, P. Jian, O. Pinel, and N. Treps, Precision measurements with photon-subtracted or photon-added gaussian states, Phys. Rev. A **90**, 013821 (2014).
[155] K. Mølmer, Non-Gaussian states from continuous-wave Gaussian light sources, Phys. Rev. A **73**, 063804 (2006).
[156] M. Dakna, T. Anhut, T. Opatrný, L. Knöll, and D.-G. Welsch, Generating Schrödinger-cat-like states by means of conditional measurements on a beam splitter, Phys. Rev. A **55**, 3184 (1997).
[157] K. Takase, J.-i. Yoshikawa, W. Asavanant, M. Endo, and A. Furusawa, Generation of optical Schrödinger cat states by generalized photon subtraction, Phys. Rev. A **103**, 013710 (2021).
[158] A. O. C. Davis, M. Walschaers, V. Parigi, and N. Treps, Conditional preparation of non-Gaussian quantum optical states by mesoscopic measurement, New J. Phys. **23**, 063039 (2021).
[159] A. Zavatta, S. Viciani, and M. Bellini, Quantum-to-classical transition with single-photon-added coherent states of light, Science **306**, 660 (2004).
[160] V. Parigi, A. Zavatta, M. Kim, and M. Bellini, Probing quantum commutation rules by addition and subtraction of single photons to/from a light field, Science **317**, 1890 (2007).
[161] R. Horodecki, P. Horodecki, M. Horodecki, and K. Horodecki, Quantum entanglement, Rev. Mod. Phys. **81**, 865 (2009).
[162] R. Uola, A. C. S. Costa, H. C. Nguyen, and O. Gühne, Quantum steering, Rev. Mod. Phys. **92**, 015001 (2020).
[163] N. Brunner, D. Cavalcanti, S. Pironio, V. Scarani, and S. Wehner, Bell nonlocality, Rev. Mod. Phys. **86**, 419 (2014).
[164] One could introduce more general and rigorous notation based on measure theory, but here we restrict to a simpler, though less general, formulation for pedagogical purposes.
[165] R. Jozsa, Quantum effects in algorithms, Chaos, Solitons Fractals **10**, 1657 (1999).
[166] This is true for general "states" in classical probability theory, but in the CV context of this Tutorial it is appealing to

phrase the argument in terms of probability distributions of phase space.
[167] R. F. Werner, Quantum states with einstein-podolsky-rosen correlations admitting a hidden-variable model, Phys. Rev. A **40**, 4277 (1989).
[168] J. B. Conway, in *A Course in Functional Analysis* (Springer New York, New York, NY, 2007), p. 63.
[169] Sohail and U. Sen, Witnessing nonseparability of bipartite quantum operations, Phys. Lett. A **404**, 127411 (2021).
[170] H. F. Hofmann and S. Takeuchi, Violation of local uncertainty relations as a signature of entanglement, Phys. Rev. A **68**, 032103 (2003).
[171] O. Gittsovich, O. Gühne, P. Hyllus, and J. Eisert, Unifying several separability conditions using the covariance matrix criterion, Phys. Rev. A **78**, 052319 (2008).
[172] A. Einstein, B. Podolsky, and N. Rosen, Can quantum-mechanical description of physical reality be considered complete?, Phys. Rev. **47**, 777 (1935).
[173] E. Schrödinger, Discussion of probability relations between separated systems, Math. Proc. Cambridge Philosophical Soc. **31**, 555 (1935).
[174] E. Schrödinger, Probability relations between separated systems, Math. Proc. Cambridge Philosophical Soc. **32**, 446 (1936).
[175] M. D. Reid, Demonstration of the einstein-podolsky-rosen paradox using nondegenerate parametric amplification, Phys. Rev. A **40**, 913 (1989).
[176] H. M. Wiseman, S. J. Jones, and A. C. Doherty, Steering, Entanglement, Nonlocality, and the Einstein-Podolsky-Rosen Paradox, Phys. Rev. Lett. **98**, 140402 (2007).
[177] D. Cavalcanti and P. Skrzypczyk, Quantum steering: A review with focus on semidefinite programming, Rep. Prog. Phys. **80**, 024001 (2017).
[178] E. G. Cavalcanti, S. J. Jones, H. M. Wiseman, and M. D. Reid, Experimental criteria for steering and the einstein-podolsky-rosen paradox, Phys. Rev. A **80**, 032112 (2009).
[179] I. Kogias, A. R. Lee, S. Ragy, and G. Adesso, Quantification of Gaussian Quantum Steering, Phys. Rev. Lett. **114**, 060403 (2015).
[180] Q. Y. He, Q. H. Gong, and M. D. Reid, Classifying Directional Gaussian Entanglement, Einstein-Podolsky-Rosen Steering, and Discord, Phys. Rev. Lett. **114**, 060402 (2015).
[181] X. Deng, Y. Xiang, C. Tian, G. Adesso, Q. He, Q. Gong, X. Su, C. Xie, and K. Peng, Demonstration of Monogamy Relations for Einstein-Podolsky-Rosen Steering in Gaussian Cluster States, Phys. Rev. Lett. **118**, 230501 (2017).
[182] C. Branciard, E. G. Cavalcanti, S. P. Walborn, V. Scarani, and H. M. Wiseman, One-sided device-independent quantum key distribution: Security, feasibility, and the connection with steering, Phys. Rev. A **85**, 010301 (2012).
[183] J. S. Bell, On the einstein podolsky rosen paradox, Physics Physique Fizika **1**, 195 (1964).
[184] J. S. BELL, On the problem of hidden variables in quantum mechanics, Rev. Mod. Phys. **38**, 447 (1966).
[185] N. D. Mermin, Hidden variables and the two theorems of john bell, Rev. Mod. Phys. **65**, 803 (1993).
[186] A. Peres, All the bell inequalities, Found. Phys. **29**, 589 (1999).
[187] J. F. Clauser, M. A. Horne, A. Shimony, and R. A. Holt, Proposed Experiment to Test Local Hidden-Variable Theories, Phys. Rev. Lett. **23**, 880 (1969).
[188] J. F. Clauser and M. A. Horne, Experimental consequences of objective local theories, Phys. Rev. D **10**, 526 (1974).
[189] S. J. Freedman and J. F. Clauser, Experimental Test of Local Hidden-Variable Theories, Phys. Rev. Lett. **28**, 938 (1972).
[190] A. Aspect, P. Grangier, and G. Roger, Experimental Tests of Realistic Local Theories via Bell's Theorem, Phys. Rev. Lett. **47**, 460 (1981).
[191] A. Aspect, J. Dalibard, and G. Roger, Experimental Test of Bell's Inequalities Using Time-Varying Analyzers, Phys. Rev. Lett. **49**, 1804 (1982).
[192] G. Weihs, T. Jennewein, C. Simon, H. Weinfurter, and A. Zeilinger, Violation of Bell's Inequality under Strict Einstein Locality Conditions, Phys. Rev. Lett. **81**, 5039 (1998).
[193] B. Hensen, H. Bernien, A. E. Dréau, A. Reiserer, N. Kalb, M. S. Blok, J. Ruitenberg, R. F. L. Vermeulen, R. N. Schouten, C. Abellán, W. Amaya, V. Pruneri, M. W. Mitchell, M. Markham, D. J. Twitchen, D. Elkouss, S. Wehner, T. H. Taminiau, and R. Hanson, Loophole-free bell inequality violation using electron spins separated by 1.3 kilometres, Nature **526**, 682 (2015).
[194] M. Giustina *et al.*, Significant-Loophole-Free Test of Bell's Theorem with Entangled Photons, Phys. Rev. Lett. **115**, 250401 (2015).
[195] L. K. Shalm *et al.*, Strong Loophole-Free Test of Local Realism, Phys. Rev. Lett. **115**, 250402 (2015).
[196] C. Abellán *et al.*, T. B. B. T. Collaboration, Challenging local realism with human choices, Nature **557**, 212 (2018).
[197] D. Rauch, J. Handsteiner, A. Hochrainer, J. Gallicchio, A. S. Friedman, C. Leung, B. Liu, L. Bulla, S. Ecker, F. Steinlechner, R. Ursin, B. Hu, D. Leon, C. Benn, A. Ghedina, M. Cecconi, A. H. Guth, D. I. Kaiser, T. Scheidl, and A. Zeilinger, Cosmic Bell Test Using Random Measurement Settings from High-Redshift Quasars, Phys. Rev. Lett. **121**, 080403 (2018).
[198] A. Acín, N. Brunner, N. Gisin, S. Massar, S. Pironio, and V. Scarani, Device-Independent Security of Quantum Cryptography against Collective Attacks, Phys. Rev. Lett. **98**, 230501 (2007).
[199] F. Buscemi, All Entangled Quantum States are Nonlocal, Phys. Rev. Lett. **108**, 200401 (2012).
[200] C. Branciard, D. Rosset, Y.-C. Liang, and N. Gisin, Measurement-Device-Independent Entanglement Witnesses for all Entangled Quantum States, Phys. Rev. Lett. **110**, 060405 (2013).
[201] P. Abiuso, S. Bäuml, D. Cavalcanti, and A. Acín, Measurement-Device-Independent Entanglement Detection for Continuous-Variable Systems, Phys. Rev. Lett. **126**, 190502 (2021).
[202] C. K. Hong and L. Mandel, Experimental Realization of a Localized One-Photon State, Phys. Rev. Lett. **56**, 58 (1986).
[203] G. S. Thekkadath, B. A. Bell, I. A. Walmsley, and A. I., Engineering Schrödinger cat states with a photonic even-parity detector, Quantum **4**, 239 (2020).

[204] M. Eaton, R. Nehra, and O. Pfister, Non-gaussian and gottesman–kitaev–preskill state preparation by photon catalysis, New J. Phys. **21**, 113034 (2019).
[205] D. Su, C. R. Myers, and K. K. Sabapathy, Conversion of gaussian states to non-gaussian states using photon-number-resolving detectors, Phys. Rev. A **100**, 052301 (2019).
[206] S. Yu, Q. Chen, C. Zhang, C. H. Lai, and C. H. Oh, All Entangled Pure States Violate a Single Bell's Inequality, Phys. Rev. Lett. **109**, 120402 (2012).
[207] R. F. Werner and M. M. Wolf, Bound Entangled Gaussian States, Phys. Rev. Lett. **86**, 3658 (2001).
[208] Y. Xiang, S. Liu, J. Guo, Q. Gong, N. Treps, Q. He, and M. Walschaers, Quantification of wigner negativity remotely generated via einstein-podolsky-rosen steering, arXiv:2104.00451 [quant-ph] (2021).
[209] M. D. Reid, Monogamy inequalities for the einstein-podolsky-rosen paradox and quantum steering, Phys. Rev. A **88**, 062108 (2013).
[210] S.-W. Ji, M. S. Kim, and H. Nha, Quantum steering of multimode gaussian states by gaussian measurements: monogamy relations and the peres conjecture, J. Phys. A: Math. Theor. **48**, 135301 (2015).
[211] X. Deng, Y. Xiang, C. Tian, G. Adesso, Q. He, Q. Gong, X. Su, C. Xie, and K. Peng, Demonstration of Monogamy Relations for Einstein-Podolsky-Rosen Steering in Gaussian Cluster States, Phys. Rev. Lett. **118**, 230501 (2017).
[212] E. Shchukin and W. Vogel, Inseparability Criteria for Continuous Bipartite Quantum States, Phys. Rev. Lett. **95**, 230502 (2005).
[213] J. Sperling and W. Vogel, Verifying continuous-variable entanglement in finite spaces, Phys. Rev. A **79**, 052313 (2009).
[214] J. S. Kim and B. C. Sanders, Monogamy of multi-qubit entanglement using rényi entropy, J. Phys. A: Math. Theor. **43**, 445305 (2010).
[215] G. Adesso, D. Girolami, and A. Serafini, Measuring Gaussian Quantum Information and Correlations Using the rényi Entropy of Order 2, Phys. Rev. Lett. **109**, 190502 (2012).
[216] R. Simon, Peres-Horodecki Separability Criterion for Continuous Variable Systems, Phys. Rev. Lett. **84**, 2726 (2000).
[217] L.-M. Duan, G. Giedke, J. I. Cirac, and P. Zoller, Inseparability Criterion for Continuous Variable Systems, Phys. Rev. Lett. **84**, 2722 (2000).
[218] P. van Loock and A. Furusawa, Detecting genuine multipartite continuous-variable entanglement, Phys. Rev. A **67**, 052315 (2003).
[219] P. Hyllus and J. Eisert, Optimal entanglement witnesses for continuous-variable systems, New J. Phys. **8**, 51 (2006).
[220] S. Gerke, J. Sperling, W. Vogel, Y. Cai, J. Roslund, N. Treps, and C. Fabre, Full Multipartite Entanglement of Frequency-Comb Gaussian States, Phys. Rev. Lett. **114**, 050501 (2015).
[221] A. A. Valido, F. Levi, and F. Mintert, Hierarchies of multipartite entanglement for continuous-variable states, Phys. Rev. A **90**, 052321 (2014).
[222] Note that there is also a more profound connection between the transpose and time reversal through Wigner's theorem. The latter is here effectively implemented by changing the sign of the momentum variables. However, this connection is beyond the scope of this Tutorial and interested readers are invited to indulge in the literature on quantum chaos instead.
[223] C. H. Bennett, G. Brassard, S. Popescu, B. Schumacher, J. A. Smolin, and W. K. Wootters, Purification of Noisy Entanglement and Faithful Teleportation via Noisy Channels, Phys. Rev. Lett. **76**, 722 (1996).
[224] C. H. Bennett, H. J. Bernstein, S. Popescu, and B. Schumacher, Concentrating partial entanglement by local operations, Phys. Rev. A **53**, 2046 (1996).
[225] J. Eisert, S. Scheel, and M. B. Plenio, Distilling Gaussian States with Gaussian Operations is Impossible, Phys. Rev. Lett. **89**, 137903 (2002).
[226] J. Fiurášek, Gaussian Transformations and Distillation of Entangled Gaussian States, Phys. Rev. Lett. **89**, 137904 (2002).
[227] G. Giedke and J. Ignacio Cirac, Characterization of gaussian operations and distillation of gaussian states, Phys. Rev. A **66**, 032316 (2002).
[228] R. Dong, M. Lassen, J. Heersink, C. Marquardt, R. Filip, G. Leuchs, and U. L. Andersen, Experimental entanglement distillation of mesoscopic quantum states, Nat. Phys. **4**, 919 (2008).
[229] B. Hage, A. Samblowski, J. DiGuglielmo, A. Franzen, J. Fiurášek, and R. Schnabel, Preparation of distilled and purified continuous-variable entangled states, Nat. Phys. **4**, 915 (2008).
[230] L.-M. Duan, G. Giedke, J. I. Cirac, and P. Zoller, Entanglement Purification of Gaussian Continuous Variable Quantum States, Phys. Rev. Lett. **84**, 4002 (2000).
[231] L.-M. Duan, G. Giedke, J. I. Cirac, and P. Zoller, Physical implementation for entanglement purification of gaussian continuous-variable quantum states, Phys. Rev. A **62**, 032304 (2000).
[232] J. Fiurášek, Distillation and purification of symmetric entangled gaussian states, Phys. Rev. A **82**, 042331 (2010).
[233] E. T. Campbell, M. G. Genoni, and J. Eisert, Continuous-variable entanglement distillation and noncommutative central limit theorems, Phys. Rev. A **87**, 042330 (2013).
[234] J. Dias and T. C. Ralph, Quantum repeaters using continuous-variable teleportation, Phys. Rev. A **95**, 022312 (2017).
[235] G. Y. Xiang, T. C. Ralph, A. P. Lund, N. Walk, and G. J. Pryde, Heralded noiseless linear amplification and distillation of entanglement, Nat. Photonics **4**, 316 (2010).
[236] T. Opatrný, G. Kurizki, and D.-G. Welsch, Improvement on teleportation of continuous variables by photon subtraction via conditional measurement, Phys. Rev. A **61**, 032302 (2000).
[237] P. T. Cochrane, T. C. Ralph, and G. J. Milburn, Teleportation improvement by conditional measurements on the two-mode squeezed vacuum, Phys. Rev. A **65**, 062306 (2002).

[238] S. Olivares, M. G. A. Paris, and R. Bonifacio, Teleportation improvement by inconclusive photon subtraction, Phys. Rev. A **67**, 032314 (2003).
[239] A. Kitagawa, M. Takeoka, M. Sasaki, and A. Chefles, Entanglement evaluation of non-gaussian states generated by photon subtraction from squeezed states, Phys. Rev. A **73**, 042310 (2006).
[240] Y. Yang and F.-L. Li, Entanglement properties of non-gaussian resources generated via photon subtraction and addition and continuous-variable quantum-teleportation improvement, Phys. Rev. A **80**, 022315 (2009).
[241] C. Navarrete-Benlloch, R. García-Patrón, J. H. Shapiro, and N. J. Cerf, Enhancing quantum entanglement by photon addition and subtraction, Phys. Rev. A **86**, 012328 (2012).
[242] T. Das, R. Prabhu, A. Sen(De), and U. Sen, Superiority of photon subtraction to addition for entanglement in a multimode squeezed vacuum, Phys. Rev. A **93**, 052313 (2016).
[243] M. Walschaers, S. Sarkar, V. Parigi, and N. Treps, Tailoring Non-Gaussian Continuous-Variable Graph States, Phys. Rev. Lett. **121**, 220501 (2018).
[244] K. Zhang, J. Jing, N. Treps, and M. Walschaers, Maximal entanglement distillation with single-photon subtraction, arXiv:2103.09197 [quant-ph] (2021).
[245] E. G. Brown, N. Friis, and M. Huber, Passivity and practical work extraction using gaussian operations, New J. Phys. **18**, 113028 (2016).
[246] R. S. Barbosa, T. Douce, P.-E. Emeriau, E. Kashefi, and S. Mansfield, Continuous-variable nonlocality and contextuality, arXiv:1905.08267 [quant-ph] (2019).
[247] A. Acín, N. J. Cerf, A. Ferraro, and J. Niset, Tests of multimode quantum nonlocality with homodyne measurements, Phys. Rev. A **79**, 012112 (2009).
[248] R. García-Patrón, J. Fiurášek, N. J. Cerf, J. Wenger, R. Tualle-Brouri, and P. Grangier, Proposal for a Loophole-Free Bell Test Using Homodyne Detection, Phys. Rev. Lett. **93**, 130409 (2004).
[249] D. Klyshko, The bell and ghz theorems: A possible three-photon interference experiment and the question of nonlocality, Phys. Lett. A **172**, 399 (1993).
[250] W. N. Plick, F. Arzani, N. Treps, E. Diamanti, and D. Markham, Violating bell inequalities with entangled optical frequency combs and multipixel homodyne detection, Phys. Rev. A **98**, 062101 (2018).
[251] K. Banaszek and K. Wódkiewicz, Nonlocality of the einstein-podolsky-rosen state in the wigner representation, Phys. Rev. A **58**, 4345 (1998).
[252] K. Banaszek and K. Wódkiewicz, Testing Quantum Nonlocality in Phase Space, Phys. Rev. Lett. **82**, 2009 (1999).
[253] S. Aaronson and D. Gottesman, Improved simulation of stabilizer circuits, Phys. Rev. A **70**, 052328 (2004).
[254] V. Veitch, N. Wiebe, C. Ferrie, and J. Emerson, Efficient simulation scheme for a class of quantum optics experiments with non-negative wigner representation, New J. Phys. **15**, 013037 (2013).
[255] S. Rahimi-Keshari, T. C. Ralph, and C. M. Caves, Sufficient Conditions for Efficient Classical Simulation of Quantum Optics, Phys. Rev. X **6**, 021039 (2016).
[256] M.-D. Choi, Completely positive linear maps on complex matrices, Linear Algebra Appl. **10**, 285 (1975).
[257] A. S. Holevo, The choi–jamiolkowski forms of quantum gaussian channels, J. Math. Phys. **52**, 042202 (2011).
[258] L. García-Álvarez, C. Calcluth, A. Ferraro, and G. Ferrini, Efficient simulatability of continuous-variable circuits with large wigner negativity, Phys. Rev. Res. **2**, 043322 (2020).
[259] C. S. Hamilton, R. Kruse, L. Sansoni, S. Barkhofen, C. Silberhorn, and I. Jex, Gaussian Boson Sampling, Phys. Rev. Lett. **119**, 170501 (2017).
[260] R. Kruse, C. S. Hamilton, L. Sansoni, S. Barkhofen, C. Silberhorn, and I. Jex, Detailed study of gaussian boson sampling, Phys. Rev. A **100**, 032326 (2019).
[261] A. Deshpande, A. Mehta, T. Vincent, N. Quesada, M. Hinsche, M. Ioannou, L. Madsen, J. Lavoie, H. Qi, J. Eisert, D. Hangleiter, B. Fefferman, and I. Dhand, Quantum computational supremacy via high-dimensional gaussian boson sampling, arXiv:2102.12474 [quant-ph] (2021).
[262] S. Aaronson and A. Arkhipov, The computational complexity of linear optics, Theory of Computing **9**, 143 (2013).
[263] N. Quesada, J. M. Arrazola, and N. Killoran, Gaussian boson sampling using threshold detectors, Phys. Rev. A **98**, 062322 (2018).
[264] E. R. Caianiello, On quantum field theory —i: Explicit solution of dyson's equation in electrodynamics without use of feynman graphs, Il Nuovo Cimento (1943-1954) **10**, 1634 (1953).
[265] K. Brádler, P.-L. Dallaire-Demers, P. Rebentrost, D. Su, and C. Weedbrook, Gaussian boson sampling for perfect matchings of arbitrary graphs, Phys. Rev. A **98**, 032310 (2018).
[266] M. Schuld, K. Brádler, R. Israel, D. Su, and B. Gupt, Measuring the similarity of graphs with a gaussian boson sampler, Phys. Rev. A **101**, 032314 (2020).
[267] T. R. Bromley, J. M. Arrazola, S. Jahangiri, J. Izaac, N. Quesada, A. D. Gran, M. Schuld, J. Swinarton, Z. Zabaneh, and N. Killoran, Applications of near-term photonic quantum computers: Software and algorithms, Quantum Sci. Technol. **5**, 034010 (2020).
[268] H. Qi, D. J. Brod, N. Quesada, and R. García-Patrón, Regimes of Classical Simulability for Noisy Gaussian Boson Sampling, Phys. Rev. Lett. **124**, 100502 (2020).
[269] J. F. Clauser, Experimental distinction between the quantum and classical field-theoretic predictions for the photoelectric effect, Phys. Rev. D **9**, 853 (1974).
[270] H. J. Kimble, M. Dagenais, and L. Mandel, Photon Antibunching in Resonance Fluorescence, Phys. Rev. Lett. **39**, 691 (1977).
[271] F. Diedrich and H. Walther, Nonclassical Radiation of a Single Stored ion, Phys. Rev. Lett. **58**, 203 (1987).
[272] R. Schnabel, Squeezed states of light and their applications in laser interferometers, Phys. Rep. **684**, 1 (2017).
[273] A. I. Lvovsky, H. Hansen, T. Aichele, O. Benson, J. Mlynek, and S. Schiller, Quantum State Reconstruction of the Single-Photon Fock State, Phys. Rev. Lett. **87**, 050402 (2001).

[274] A. I. Lvovsky and M. G. Raymer, Continuous-variable optical quantum-state tomography, Rev. Mod. Phys. **81**, 299 (2009).
[275] A. I. Lvovsky and S. A. Babichev, Synthesis and tomographic characterization of the displaced fock state of light, Phys. Rev. A **66**, 011801 (2002).
[276] A. Ourjoumtsev, R. Tualle-Brouri, and P. Grangier, Quantum Homodyne Tomography of a Two-Photon Fock State, Phys. Rev. Lett. **96**, 213601 (2006).
[277] M. Cooper, L. J. Wright, C. Söller, and B. J. Smith, Experimental generation of multi-photon fock states, Opt. Express **21**, 5309 (2013).
[278] M. Yukawa, K. Miyata, T. Mizuta, H. Yonezawa, P. Marek, R. Filip, and A. Furusawa, Generating superposition of up-to three photons for continuous variable quantum information processing, Opt. Express **21**, 5529 (2013).
[279] J. S. Neergaard-Nielsen, B. M. Nielsen, C. Hettich, K. Mølmer, and E. S. Polzik, Generation of a Superposition of odd Photon Number States for Quantum Information Networks, Phys. Rev. Lett. **97**, 083604 (2006).
[280] K. Wakui, H. Takahashi, A. Furusawa, and M. Sasaki, Photon subtracted squeezed states generated with periodically poled ktiopo4, Opt. Express **15**, 3568 (2007).
[281] D. V. Sychev, A. E. Ulanov, A. A. Pushkina, M. W. Richards, I. A. Fedorov, and A. I. Lvovsky, Enlargement of optical schrödinger's cat states, Nat. Photonics **11**, 379 (2017).
[282] J. S. Neergaard-Nielsen, M. Takeuchi, K. Wakui, H. Takahashi, K. Hayasaka, M. Takeoka, and M. Sasaki, Optical Continuous-Variable Qubit, Phys. Rev. Lett. **105**, 053602 (2010).
[283] M. Barbieri, N. Spagnolo, M. G. Genoni, F. Ferreyrol, R. Blandino, M. G. A. Paris, P. Grangier, and R. Tualle-Brouri, Non-gaussianity of quantum states: An experimental test on single-photon-added coherent states, Phys. Rev. A **82**, 063833 (2010).
[284] A. Ourjoumtsev, H. Jeong, R. Tualle-Brouri, and P. Grangier, Generation of optical 'schrödinger cats'from photon number states, Nature **448**, 784 (2007).
[285] J. Etesse, M. Bouillard, B. Kanseri, and R. Tualle-Brouri, Experimental Generation of Squeezed cat States with an Operation Allowing Iterative Growth, Phys. Rev. Lett. **114**, 193602 (2015).
[286] B. Hacker, S. Welte, S. Daiss, A. Shaukat, S. Ritter, L. Li, and G. Rempe, Deterministic creation of entangled atom–light schrödinger-cat states, Nat. Photonics **13**, 110 (2019).
[287] S. A. Babichev, J. Appel, and A. I. Lvovsky, Homodyne Tomography Characterization and Nonlocality of a Dual-Mode Optical Qubit, Phys. Rev. Lett. **92**, 193601 (2004).
[288] M. D'Angelo, A. Zavatta, V. Parigi, and M. Bellini, Tomographic test of bell's inequality for a time-delocalized single photon, Phys. Rev. A **74**, 052114 (2006).
[289] H. Takahashi, J. S. Neergaard-Nielsen, M. Takeuchi, M. Takeoka, K. Hayasaka, A. Furusawa, and M. Sasaki, Entanglement distillation from Gaussian input states, Nat. Photon **4**, 178 (2010).
[290] A. Ourjoumtsev, A. Dantan, R. Tualle-Brouri, and P. Grangier, Increasing Entanglement between Gaussian States by Coherent Photon Subtraction, Phys. Rev. Lett. **98**, 030502 (2007).
[291] A. Ourjoumtsev, F. Ferreyrol, R. Tualle-Brouri, and P. Grangier, Preparation of non-local superpositions of quasi-classical light states, Nat. Phys. **5**, 189 (2009).
[292] H. Jeong, A. Zavatta, M. Kang, S.-W. Lee, L. S. Costanzo, S. Grandi, T. C. Ralph, and M. Bellini, Generation of hybrid entanglement of light, Nat. Photonics **8**, 564 (2014).
[293] O. Morin, K. Huang, J. Liu, H. Le Jeannic, C. Fabre, and J. Laurat, Remote creation of hybrid entanglement between particle-like and wave-like optical qubits, Nat. Photonics **8**, 570 (2014).
[294] N. Biagi, L. S. Costanzo, M. Bellini, and A. Zavatta, Entangling Macroscopic Light States by Delocalized Photon Addition, Phys. Rev. Lett. **124**, 033604 (2020).
[295] T. Serikawa, J.-i. Yoshikawa, S. Takeda, H. Yonezawa, T. C. Ralph, E. H. Huntington, and A. Furusawa, Generation of a cat State in an Optical Sideband, Phys. Rev. Lett. **121**, 143602 (2018).
[296] V. A. Averchenko, V. Thiel, and N. Treps, Nonlinear photon subtraction from a multimode quantum field, Phys. Rev. A **89**, 063808 (2014).
[297] Y.-S. Ra, C. Jacquard, A. Dufour, C. Fabre, and N. Treps, Tomography of a Mode-Tunable Coherent Single-Photon Subtractor, Phys. Rev. X **7**, 031012 (2017).
[298] Y.-S. Ra, A. Dufour, M. Walschaers, C. Jacquard, T. Michel, C. Fabre, and N. Treps, Non-gaussian quantum states of a multimode light field, Nat. Phys. **16**, 144 (2020).
[299] V. Cimini, M. Barbieri, N. Treps, M. Walschaers, and V. Parigi, Neural Networks for Detecting Multimode Wigner Negativity, Phys. Rev. Lett. **125**, 160504 (2020).
[300] U. Chabaud, F. Grosshans, E. Kashefi, and D. Markham, Efficient verification of boson sampling, arXiv:2006.03520 [quant-ph] (2021).
[301] E. S. Tiunov, V. V. T. (Vyborova), A. E. Ulanov, A. I. Lvovsky, and A. K. Fedorov, Experimental quantum homodyne tomography via machine learning, Optica **7**, 448 (2020).
[302] A. E. Lita, A. J. Miller, and S. W. Nam, Counting near-infrared single-photons with 95% efficiency, Opt. Express **16**, 3032 (2008).
[303] C. Monroe, D. M. Meekhof, B. E. King, and D. J. Wineland, A "schrödinger cat" superposition state of an atom, Science **272**, 1131 (1996).
[304] M. Brune, S. Haroche, J. M. Raimond, L. Davidovich, and N. Zagury, Manipulation of photons in a cavity by dispersive atom-field coupling: Quantum-nondemolition measurements and generation of "Schrödinger cat" states, Phys. Rev. A **45**, 5193 (1992).
[305] M. Brune, F. Schmidt-Kaler, A. Maali, J. Dreyer, E. Hagley, J. M. Raimond, and S. Haroche, Quantum Rabi Oscillation: A Direct Test of Field Quantization in a Cavity, Phys. Rev. Lett. **76**, 1800 (1996).
[306] G. Nogues, A. Rauschenbeutel, S. Osnaghi, M. Brune, J. M. Raimond, and S. Haroche, Seeing a single photon without destroying it, Nature **400**, 239 (1999).

[307] S. Deléglise, I. Dotsenko, C. Sayrin, J. Bernu, M. Brune, J.-M. Raimond, and S. Haroche, Reconstruction of non-classical cavity field states with snapshots of their decoherence, Nature **455**, 510 (2008).
[308] M. Hofheinz, E. M. Weig, M. Ansmann, R. C. Bialczak, E. Lucero, M. Neeley, A. D. O'Connell, H. Wang, J. M. Martinis, and A. N. Cleland, Generation of Fock states in a superconducting quantum circuit, Nature **454**, 310 (2008).
[309] B. Vlastakis, G. Kirchmair, Z. Leghtas, S. E. Nigg, L. Frunzio, S. M. Girvin, M. Mirrahimi, M. H. Devoret, and R. J. Schoelkopf, Deterministically encoding quantum information using 100-photon Schrödinger cat states, Science **342**, 607 (2013).
[310] Z. Leghtas, S. Touzard, I. M. Pop, A. Kou, B. Vlastakis, A. Petrenko, K. M. Sliwa, A. Narla, S. Shankar, M. J. Hatridge, M. Reagor, L. Frunzio, R. J. Schoelkopf, M. Mirrahimi, and M. H. Devoret, Confining the state of light to a quantum manifold by engineered two-photon loss, Science **347**, 853 (2015).
[311] C. Flühmann, T. L. Nguyen, M. Marinelli, V. Negnevitsky, K. Mehta, and J. P. Home, Encoding a qubit in a trapped-ion mechanical oscillator, Nature **566**, 513 (2019).
[312] P. Campagne-Ibarcq, A. Eickbusch, S. Touzard, E. Zalys-Geller, N. E. Frattini, V. V. Sivak, P. Reinhold, S. Puri, S. Shankar, R. J. Schoelkopf, L. Frunzio, M. Mirrahimi, and M. H. Devoret, Quantum error correction of a qubit encoded in grid states of an oscillator, Nature **584**, 368 (2020).
[313] M. Aspelmeyer, T. J. Kippenberg, and F. Marquardt, Cavity optomechanics, Rev. Mod. Phys. **86**, 1391 (2014).
[314] U. B. Hoff, J. Kollath-Bönig, J. S. Neergaard-Nielsen, and U. L. Andersen, Measurement-Induced Macroscopic Superposition States in Cavity Optomechanics, Phys. Rev. Lett. **117**, 143601 (2016).
[315] M. Brunelli, O. Houhou, D. W. Moore, A. Nunnenkamp, M. Paternostro, and A. Ferraro, Unconditional preparation of nonclassical states via linear-and-quadratic optomechanics, Phys. Rev. A **98**, 063801 (2018).
[316] T. A. Palomaki, J. D. Teufel, R. W. Simmonds, and K. W. Lehnert, Entangling mechanical motion with microwave fields, Science **342**, 710 (2013).
[317] R. Riedinger, S. Hong, R. A. Norte, J. A. Slater, J. Shang, A. G. Krause, V. Anant, M. Aspelmeyer, and S. Gröblacher, Non-classical correlations between single photons and phonons from a mechanical oscillator, Nature **530**, 313 (2016).
[318] A. P. Reed, K. H. Mayer, J. D. Teufel, L. D. Burkhart, W. Pfaff, M. Reagor, L. Sletten, X. Ma, R. J. Schoelkopf, E. Knill, and K. W. Lehnert, Faithful conversion of propagating quantum information to mechanical motion, Nat. Phys. **13**, 1163 (2017).
[319] J. D. Jost, J. P. Home, J. M. Amini, D. Hanneke, R. Ozeri, C. Langer, J. J. Bollinger, D. Leibfried, and D. J. Wineland, Entangled mechanical oscillators, Nature **459**, 683 (2009).
[320] E. Flurin, N. Roch, F. Mallet, M. H. Devoret, and B. Huard, Generating Entangled Microwave Radiation Over two Transmission Lines, Phys. Rev. Lett. **109**, 183901 (2012).
[321] M. Forsch, R. Stockill, A. Wallucks, I. Marinković, C. Gärtner, R. A. Norte, F. van Otten, A. Fiore, K. Srinivasan, and S. Gröblacher, Microwave-to-optics conversion using a mechanical oscillator in its quantum ground state, Nat. Phys. **16**, 69 (2020).
[322] R. Lescanne, S. Deléglise, E. Albertinale, U. Réglade, T. Capelle, E. Ivanov, T. Jacqmin, Z. Leghtas, and E. Flurin, Irreversible Qubit-Photon Coupling for the Detection of Itinerant Microwave Photons, Phys. Rev. X **10**, 021038 (2020).
[323] L. Pezzè, A. Smerzi, M. K. Oberthaler, R. Schmied, and P. Treutlein, Quantum metrology with nonclassical states of atomic ensembles, Rev. Mod. Phys. **90**, 035005 (2018).
[324] B. Dubost, M. Koschorreck, M. Napolitano, N. Behbood, R. J. Sewell, and M. W. Mitchell, Efficient Quantification of Non-Gaussian Spin Distributions, Phys. Rev. Lett. **108**, 183602 (2012).
[325] F. Haas, J. Volz, R. Gehr, J. Reichel, and J. Estève, Entangled states of more than 40 atoms in an optical fiber cavity, Science **344**, 180 (2014).
[326] H. Strobel, W. Muessel, D. Linnemann, T. Zibold, D. B. Hume, L. Pezzè, A. Smerzi, and M. K. Oberthaler, Fisher information and entanglement of non-Gaussian spin states, Science **345**, 424 (2014).
[327] R. McConnell, H. Zhang, J. Hu, S. Ćuk, and V. Vuletić, Entanglement with negative Wigner function of almost 3,000 atoms heralded by one photon, Nature **519**, 439 (2015).
[328] M. V. Larsen, X. Guo, C. R. Breum, J. S. Neergaard-Nielsen, and U. L. Andersen, Deterministic multi-mode gates on a scalable photonic quantum computing platform, arXiv:2010.14422 [quant-ph] (2020).
[329] J. M. Arrazola *et al.*, Quantum circuits with many photons on a programmable nanophotonic chip, Nature **591**, 54 (2021).
[330] P. Jouguet, S. Kunz-Jacques, A. Leverrier, P. Grangier, and E. Diamanti, Experimental demonstration of long-distance continuous-variable quantum key distribution, Nat. Photonics **7**, 378 (2013).
[331] B. A. Bell, D. Markham, D. A. Herrera-Martí, A. Marin, W. J. Wadsworth, J. G. Rarity, and M. S. Tame, Experimental demonstration of graph-state quantum secret sharing, Nat. Commun. **5**, 5480 (2014).
[332] M. Navascués, F. Grosshans, and A. Acín, Optimality of Gaussian Attacks in Continuous-Variable Quantum Cryptography, Phys. Rev. Lett. **97**, 190502 (2006).
[333] Y. Guo, Q. Liao, Y. Wang, D. Huang, P. Huang, and G. Zeng, Performance improvement of continuous-variable quantum key distribution with an entangled source in the middle via photon subtraction, Phys. Rev. A **95**, 032304 (2017).
[334] J. Huh, G. G. Guerreschi, B. Peropadre, J. R. McClean, and A. Aspuru-Guzik, Boson sampling for molecular vibronic spectra, Nat. Photonics **9**, 615 (2015).
[335] L. Banchi, M. Fingerhuth, T. Babej, C. Ing, and J. M. Arrazola, Molecular docking with Gaussian Boson sampling, Sci. Adv. **6** (2020).
[336] S. Jahangiri, J. M. Arrazola, and A. Delgado, Quantum algorithm for simulating single-molecule electron transport, *The Journal of Physical Chemistry Letters*, J. Phys. Chem. Lett. **12**, 1256 (2021).
[337] N. Killoran, T. R. Bromley, J. M. Arrazola, M. Schuld, N. Quesada, and S. Lloyd, Continuous-variable

quantum neural networks, Phys. Rev. Res. **1**, 033063 (2019).

[338] J. Nokkala, R. Martínez-Peña, G. L. Giorgi, V. Parigi, M. C. Soriano, and R. Zambrini, Gaussian states of continuous-variable quantum systems provide universal and versatile reservoir computing, Commun. Physics **4**, 53 (2021).

[339] F. Wolf, C. Shi, J. C. Heip, M. Gessner, L. Pezzè, A. Smerzi, M. Schulte, K. Hammerer, and P. O. Schmidt, Motional Fock states for quantum-enhanced amplitude and phase measurements with trapped ions, Nat. Commun. **10**, 2929 (2019).

[340] M. Gessner, L. Pezzè, and A. Smerzi, Entanglement and squeezing in continuous-variable systems, Quantum **1**, 17 (2017).

[341] B. Yadin, M. Fadel, and M. Gessner, Metrological complementarity reveals the Einstein-Podolsky-Rosen paradox, Nat. Commun. **12**, 2410 (2021).

[342] M. Gessner, A. Smerzi, and L. Pezzè, Metrological Nonlinear Squeezing Parameter, Phys. Rev. Lett. **122**, 090503 (2019).

[343] D. R. M. Arvidsson-Shukur, N. Yunger Halpern, H. V. Lepage, A. A. Lasek, C. H. W. Barnes, and S. Lloyd, Quantum advantage in postselected metrology, Nat. Commun. **11**, 3775 (2020).

[344] J. G. Kirkwood, Quantum statistics of almost classical assemblies, Phys. Rev. **44**, 31 (1933).

[345] M. Walschaers, N. Treps, B. Sundar, L. D. Carr, and V. Parigi, Emergent complex quantum networks in continuous-variables non-gaussian states, arXiv:2012.15608 [quant-ph] (2021).

[346] H. H. Schaefer, *Topological Vector Spaces* (Springer New York, New York, NY, 1971).

[347] J. B. Conway, *A Course in Functional Analysis* (Springer New York, New York, NY, 2007).

2

REACHING A QUANTUM COMPUTATIONAL ADVANTAGE

LIST OF ARTICLES

1. **M. Walschaers**, J. Kuipers, J.-D. Urbina, K. Mayer, M. C. Tichy, K. Richter, and A. Buchleitner, *Statistical Benchmark for BosonSampling*, New J. Phys. **18**, 032001 (2016).
2. **M. Walschaers**, J. Kuipers, and A. Buchleitner, *From Many-Particle Interference to Correlation Spectroscopy*, Phys. Rev. A **94**(R), 020104 (2016).
3. T. Giordani, F. Flamini, M. Pompili, N. Viggianiello, N. Spagnolo, A. Crespi, R. Osellame, N. Wiebe, **M. Walschaers**, A. Buchleitner, and F. Sciarrino, *Experimental statistical signature of many-body quantum interference*, Nat. Photonics **12**, 173-178 (2018).
4. C. Dittel, G. Dufour, **M. Walschaers**, G. Weihs, A. Buchleitner, and R. Keil, *Totally destructive many-particle interference*, Phys. Rev. Lett. **120**, 240404 (2018).
5. C. Dittel, G. Dufour, **M. Walschaers**, G. Weihs, A. Buchleitner, and R. Keil, *Totally destructive interference for permutation-symmetric many-particle states*, Phys. Rev. A **97**, 062116 (2018).
6. D. S. Phillips, **M. Walschaers**, J. J. Renema, I. A. Walmsley, N. Treps, J. Sperling, *Benchmarking of Gaussian boson sampling using two-point correlators*, Phys. Rev. A **99**, 023836 (2019).
7. **M. Walschaers**, *Signatures of Many-Particle Interference*, J. Phys. B: At. Mol. Opt. Phys. **53** 043001 (2020).
8. F. Flamini, **M. Walschaers**, N. Spagnolo, N. Wiebe, A. Buchleitner, F. Sciarrino, *Validating multi-photon quantum interference with finite data*, Quantum Sci. Technol. **5** 045005 (2020).
9. **M. Walschaers**, *Non-Gaussian Quantum States and Where to Find Them*, PRX Quantum **2**, 030204 (2021).
10. U. Chabaud and **M. Walschaers**, *Resources for bosonic quantum computational advantage*, Phys. Rev. Lett. **130**, 090602 (2023)

2.1 BENCHMARKING BOSON SAMPLING

Quantum computing is often seen as a sort of holy grail among quantum technologies because it promises to solve some problems much faster than what could be achieved on classical hardware. Initially, the study of quantum speedups focused on specific algorithms, such as (Shor, 1994), where one compares a quantum algorithm to the best known classical algorithm for solving the same problem. The problem with this approach is that one does not necessarily know whether the best *known* classical algorithm is also the best *possible* classical algorithm. Roughly a decade ago, several seminal results (Aaronson and Arkhipov, 2011; Bremner et al., 2010) changed this perspective by developing protocols which are (to some extent) provably hard to run on a classical device.

Among these protocols, Boson Sampling had a major impact on the quantum optics community because all one needs for an experimental implementation are Fock states and passive linear optics. It did not take long before we saw the first proof-of-principle Boson Samplers (Broome et al., 2013; Crespi, Osellame, Ramponi, Brod, et al., 2013; Spring et al., 2013; Tillmann et al., 2013). However, scaling up to a significant number of photons and modes to achieve a genuine quantum computational advantage was an enormous challenge for a variety of reasons. Throughout the years, it became clear that experimental imperfections can profoundly impact the many-particle interference that underlies the Boson Sampling protocol (V. S. Shchesnovich, 2015; Tichy, 2015). This effect was shown to be highly detrimental for the computational complexity of the protocol (García-Patrón et al., 2019; Moylett et al., 2019; Renema et al., 2018).

In parallel, there were debates in the context of complexity theory on whether or not Boson Sampling could be distinguished from much simpler probability distributions (Aaronson and Arkhipov, 2014; Gogolin et al., 2013). This debate imposed a crucial question: *how does one certify a Boson Sampler?* In absolute terms, this task has been proven to be impossible (Hangleiter et al., 2019). However, when one is willing to make some assumptions, there are still ample possibilities to benchmark such experiments. Crucially, the perspective changes when one abandons the rigid setting with malicious adversaries that is common in computer science and accepts a paradigm in which a well-intending experimental physicist wants to test whether an experimental setups works as it is supposed to. This approach was pioneered in works such as (Carolan et al., 2014; Spagnolo et al., 2014).

In my own research, I worked on several techniques for benchmarking Boson Sampling, a detailed overview of which can be found in Walschaers, 2020. In general, we can identify two main approaches to which I contributed: suppression laws and statistical benchmarking. The former builds upon a generalisation of the Hong-Ou-Mandel effect (Hong et al., 1987) to a multimode context for specific interferometers (Tichy, Tiersch, et al., 2010), which was later transformed into a validation protocol for Boson Sampling (Tichy, Mayer, et al., 2014). This protocol was successfully implemented

(Crespi, Osellame, Ramponi, Bentivegna, et al., 2016), showing that it is indeed possible to test whether the input photons are of sufficient quality to achieve multi-photon interference. I later contributed to a generalisation of such suppression laws (Dittel et al., 2018a,b). We used permutation symmetries to derive a general recipe to design interferometers that lead to total destructive interference for some output events, *i.e.*, a suppression law. Very recently, it was shown that even more general families of suppression laws can be derived (Bezerra and V. Shchesnovich, 2023).

Suppression laws have the advantage of being extremely sensitive probes for many-particle interference, and thus the indistinguishability of the photons. However, the disadvantage of such a setup is that it relies on specifically designed interferometers. This means that we are only testing a part of the full Boson Sampling setup. Other techniques, such as (Chabaud, Grosshans, et al., 2021), which rely on interchanging photon counters with another type of detector suffer from a similar problem. Thus, our goal when designing the *statistical benchmark* (Walschaers, Kuipers, Urbina, et al., 2016) was to find a way of testing the functioning of our boson sampler by directly using its output data. The core idea of the approach is to study correlations

$$C_{kl} = \langle \hat{a}_k^\dagger \hat{a}_k \hat{a}_l^\dagger \hat{a}_l \rangle - \langle \hat{a}_k^\dagger \hat{a}_k \rangle \langle \hat{a}_l^\dagger \hat{a}_l \rangle \tag{2.1}$$

between output modes k and l. Not that, as discussed in Section 1.2.1, these correlators can directly be extracted from measurements using photon-number resolving detectors. Because Boson Sampling is supposed to be implemented with photonic circuits that are described by a unitary matrix that is chosen according to the Haar measure, we used random matrix theory to analyse the typical properties of C_{kl}. In later work, we also showed that these correlations are extremely sensitive to partial distinguishability of the input photons (Walschaers, Kuipers, and Buchleitner, 2016). Finally, we combined the ideas of the statistical benchmark with machine learning to reach a highly versatile experimental technique for testing Boson Samplers (Flamini, Walschaers, et al., 2020; Giordani et al., 2018).

The statistical benchmark has seen various extensions (Brunner et al., 2022; Heurtel et al., 2022; Meer et al., 2021; Mezher and Mansfield, 2022; Rigovacca et al., 2018; Seron et al., 2022) and the role of low-order correlation functions in understanding different degrees of many-particle interference is still being explored. My own contribution to extending the statistical benchmark was limited to translating it to the framework of Gaussian Boson Sampling (Phillips et al., 2019). Gaussian Boson Sampling was initially proposed in (Hamilton et al., 2016), as an attempt to bypass the problem of generating sufficiently many photons for the input of the Boson Sampler. The simulation protocol of (P. Clifford and R. Clifford, 2018) drastically increased the number of photons that were required to build a Boson Sampler that could not be simulated with a classical computer, whereas (Renema et al., 2018) sets very stringent demands on the quality of these photons. Hence, the alternative route of Gaussian Boson Sampling, *i.e.*, replacing the input states with squeezed vacuum, was very appealing and ultimately led to large-

scale devices that claimed to achieve a quantum computational advantage (Madsen et al., 2022; Zhong, Deng, et al., 2021; Zhong, Wang, et al., 2020). The statistical benchmark, developed in (Phillips et al., 2019; Walschaers, Kuipers, Urbina, et al., 2016), was one of the tools used to validate these setups.

2.2 RESOURCES FOR BOSONIC SAMPLING PROBLEMS

The benchmarking schemes presented in Section 2.1 do not attempt to verify whether the obtained measurement outcomes were sampled from the exact probability distribution associated with the Boson Sampler. Instead, they strive to test whether the samples originate from a probability distribution with the right properties. Boson Sampling is in principle generalisation of Hong-Ou-Mandel interference to many particles, which we refer to as *many-particle interference* (Tichy, 2014; Walschaers, 2020). This interference effect and its description in terms of permanents lie at the heart of the hardness of Boson Sampling (Aaronson and Arkhipov, 2011). Most of the benchmarking schemes discussed in Section 2.1 are designed to identify a signature of many-particle interference in the sampling data. Benchmarking Boson Sampling thus boils down to gathering evidence for many-particle interference. Even though the Boson Sampler may not work exactly as it ideally should, we still have evidence that the data are hard to simulate.

On a more abstract level, we consider many-particle interference as a resource for reaching a quantum computational advantage with Boson Sampling. In a more general sense, when we benchmark quantum devices, we actually test whether these devices contain the necessary quantum resources (Eisert et al., 2020). There is one important caveat in this approach: one must know that physical resources to look for.

Understanding the required physical resources for reaching a quantum computational advantage is a challenging task. The most direct approach for gaining insights is by understanding with quantum setups can be efficiently simulated on classical hardware. When we focus only on bosonic systems, a considerable body of work has already been done. Looking back at equation (1.47), it should not come as a surprise that we require a non-Gaussian element at some point in the setup. If all the Wigner functions involved in the sampling protocol are Gaussian, it is reasonably straightforward to develop a sampling protocol based on Gaussian probability distributions to simulate the device. This result is effectively proven in (Bartlett et al., 2002) through very different techniques. Later, it was shown that one actually needs not just non-Gaussian elements, but Wigner-negative ones (Mari and Eisert, 2012; Veitch et al., 2013). For pure states non-Gaussianity and Wigner negativity are equivalent (Hudson, 1974; Soto and Claverie, 1983), but for mixed states this is certainly not the case. The proof of (Mari and Eisert, 2012) relies on Wigner functions and effectively constructs a simulation algorithm based on a type of Markov chain (the protocol is also described in Section VI

of the included Article 1.3). The creation of Wigner-negative states is therefore one of the main goals of many quantum-state engineering protocols discussed in Chapter 3.

Finding necessary resources, such as Wigner negativity, by constructing explicit simulation algorithms leaves much to be desired. We are lacking a quantitative connection between Wigner negativity and computational complexity. While there is a full fledged resource theory for Wigner negativity (Albarelli et al., 2018; Takagi and Zhuang, 2018), it is not clear whether and how the amount of Wigner negativity related to computational hardness. As a matter of fact, there are quantum circuits with large Wigner negativity that can be simulated efficiently on classical hardware (García-Álvarez et al., 2020). This also emphasises that Wigner negativity is not a sufficient resource for reaching a quantum computational advantage, it must be combined with something more.

Our recent work (Chabaud and Walschaers, 2023), which is included here as Article 2.4, provides some additional pieces to solve this puzzle. Rather than focusing on Wigner negativity, this work uses the stellar representation of (Chabaud, Markham, et al., 2020), which is presented in Section III.D of Article 1.3, as a starting point. By using quantum optics techniques based of photon addition and subtraction (see Section 3.1), we manage to develop an algorithm that can simulate any bosonic sampling setup, *i.e.*, any set of single mode measurements on a multimode bosonic system. Crucially, the complexity of this simulation algorithm scales exponentially in the *stellar rank* of the global system (state + measurements). The generality of our approach comes at a prize. Our simulation method is far from optimal for any known system. For example, in the cases of Boson Sampling and Gaussian Boson Sampling one can find much more efficient simulation algorithms. We can therefore say that our approach is a worst-case scenario, and it again establishes a high stellar rank as a necessary requirement. Note, however, that our result is quantitative and given any sampling setup and a given amount of classical computational power, we can provide a minimal required stellar rank starting from which the setup cannot be simulated within any reasonable time.

At the core of our work lies the identity (5) of (Chabaud and Walschaers, 2023), which effectively connects a bosonic sampling setup to a family of Q-functions [see equation (1.68)] on larger mode spaces (see Figure 1 in the article). In general, every outcome of the bosonic sampler is mapped onto a different Q-function. The framework of Q-functions allows us to exploit some additional quantum optics insight. When $\hat{U}$ is a unitary transformation on the quantum states that corresponds to a mode basis change (1.5), we can use the properties of coherent states to show that $\hat{U}|\vec{\xi}\rangle = |O\vec{\xi}\rangle$, with O given by (1.19). We can then directly show that

$$Q_{\hat{U}\hat{\rho}\hat{U}^\dagger}(\vec{\xi}) = Q_{\hat{\rho}}(O^\top \vec{\xi}), \tag{2.2}$$

which means that if we can calculate the Q-function, we can easily translate it to any mode basis. Or in other words, we can implement of undo any passive linear optics transformation with negligible overhead. This means that any entanglement in

the state $\hat{\rho}$ that can be undone with passive linear optics is cannot contribute to the computational complexity of a sampling problem based on the Q-function.

In (Walschaers, Fabre, et al., 2017a,b) we introduced the notion of passive separability to describe a state that can be disentangled through a mode-basis change. We also showed that any Gaussian state is passively separable. This means that states that are not passively separable are entangled in a profoundly non-Gaussian way. The work (Chabaud and Walschaers, 2023), included as Article 2.4, establishes that this kind of entanglement must be present in the state $\hat{\rho}_{\text{total}}$ for the sampling problem to be hard to simulate. Effectively, the lack of passive separability means that many different non-classical resources must be combined in a particular way to lead to a high computational complexity. Details of non-Gaussian entanglement are left for Chapter 5.

2.3 OUTLOOK

Our recent result (Chabaud and Walschaers, 2023) appears to offer an entirely new toolbox, based on the stellar representation and Q-functions, for studying sampling problems and their computational complexity. It has already put forth the stellar rank and the notion of non-Gaussian entanglement (in the sense of not being passively separable) as crucial resources for reaching a quantum computational advantage. However, this hardly seems like the end of the story.

A stellar rank of one or more implies that a state is quantum non-Gaussian (Filip and Mišta, 2011; Genoni et al., 2013), but not all quantum non-Gaussian states are Wigner-negative. This means that the connection to the stellar rank is not equivalent to results of (Mari and Eisert, 2012; Veitch et al., 2013) on Wigner-negativity. It thus remains an open question how Wigner negativity fits in our approach (Chabaud and Walschaers, 2023). Perhaps there is a fundamental connection between Wigner negativity and a lack of passive separability or perhaps there are other resources that remain to be unveiled. To answer that question, it may be fruitful to develop a type of Markov chain algorithm like in (Mari and Eisert, 2012) for Q-functions.

Finally, our results highlight the need for new resource theories of stellar rank, and of various types of non-Gaussian entanglement. Since many of these resources need to work together in a specific way to effectively reach a quantum computational advantage, a multi-resource theory may be required.

2.4 **article:** RESOURCES FOR BOSONIC QUANTUM COMPUTATIONAL ADVANTAGE

Resources for Bosonic Quantum Computational Advantage

Ulysse Chabaud[1,2,*] and Mattia Walschaers[3,†]
[1]DIENS, École normale supérieure, PSL University, CNRS, INRIA, 45 rue d'Ulm, Paris 75005, France
[2]Institute for Quantum Information and Matter, Caltech, Pasadena, California 91125, USA
[3]Laboratoire Kastler Brossel, Sorbonne Université, CNRS, ENS-Université PSL, Collège de France, 4 place Jussieu, F-75252 Paris, France

(Received 2 August 2022; accepted 23 January 2023; published 2 March 2023)

Quantum computers promise to dramatically outperform their classical counterparts. However, the nonclassical resources enabling such computational advantages are challenging to pinpoint, as it is not a single resource but the subtle interplay of many that can be held responsible for these potential advantages. In this Letter, we show that every bosonic quantum computation can be recast into a continuous-variable sampling computation where all computational resources are contained in the input state. Using this reduction, we derive a general classical algorithm for the strong simulation of bosonic computations, whose complexity scales with the non-Gaussian stellar rank of both the input state and the measurement setup. We further study the conditions for an efficient classical simulation of the associated continuous-variable sampling computations and identify an operational notion of non-Gaussian entanglement based on the lack of passive separability, thus clarifying the interplay of bosonic quantum computational resources such as squeezing, non-Gaussianity, and entanglement.

DOI: 10.1103/PhysRevLett.130.090602

Introduction.—Ever since the earliest quantum algorithms [1–3], it has been clear that quantum computing holds the potential of reaching exponential speedups as compared to classical computers—be it for very specific problems. The computational advantage [4] of quantum computers was more rigorously established by connecting the classical simulation of certain quantum sampling problems to the collapse of the polynomial hierarchy of complexity classes [5,6]. Boson sampling, in particular, has drawn the attention of a part of the physics community, because the protocol is naturally implemented with indistinguishable photons and linear optics. These sampling problems also lie at the basis of the random circuit sampling protocol [7], which would lead to the first experimental claim of a quantum computational advantage [8]. However, in a game of constantly shifting goal posts, this claim has already been challenged [9].

At the same time, the development of building blocks for potential quantum computing hardware has drastically accelerated during the last decade. Even though platforms such as superconducting circuits and trapped ions have booked great successes, the present work mainly focuses on optical implementations. The Knill-Laflamme-Milburn scheme [10] provided the first proposal for a universal photonic quantum computer, which to this day remains extremely challenging to implement. Even though boson sampling [6] renewed the interest in photonic quantum computing, generating, controlling, and detecting sufficiently many indistinguishable photons is still very challenging.

To circumvent the difficulties of dealing with single photons and conserve the advantages that optics can provide for quantum information processing, such as intrinsic resilience against decoherence, several research groups have explored continuous-variable (CV) quantum optics as an alternative. Rather than detecting photons, this approach encodes information in the quadratures of the electromagnetic field, which can be detected through either homodyne or double homodyne (sometimes called heterodyne) measurements [11]. Equipped with its own framework for quantum computing in infinite-dimensional Hilbert spaces [12], the CV approach has the advantage of deterministic generation of large entangled states, over millions of subsystems [13–17]. By now, CV quantum optics is considered a promising platform for quantum computing [18]. Several sampling problems have also been translated to an infinite-dimensional context [19–23]. Among these proposals, Gaussian boson sampling in particular attracted much attention, which led ultimately to experimental realizations beyond the reach of classical computers [24–26].

From a complexity-theoretic point of view, it is well understood why some of these specific sampling problems cannot be efficiently simulated by a classical computer [27]. From a physical point of view, several groups have explored the required resources for reaching a quantum computational advantage. Such endeavors typically aim to identify a physical property without which a setup can be efficiently simulated classically. Phase-space descriptions of quantum computations, such as the Wigner

function [28,29], are particularly useful in that respect. For example, it has been shown that negativity of the Wigner function is one of such necessary resources [30,31], albeit not sufficient [32]. More recently, it became clear that squeezing and entanglement also play an important role in the hardness of some sampling problems, but only when combined in the right way [33,34]. In Gaussian boson sampling, for example, the state at hand is an entangled Gaussian state, which can be described using a positive Wigner function, while negativity of the Wigner function is provided by the non-Gaussian photon detectors. This potential resourcefulness of the measurements is one reason why sampling problems are complicated to analyze.

In this Letter, we address this problem by introducing a new paradigm for studying resources for bosonic computations. Our contribution is threefold: First, we show that every bosonic sampling computation has a dual CV sampling setup, where the measurement is performed using double homodyne detection, which can be understood as quasiclassical and thus nonresourceful. This means that, in this dual sampling setup, all computational resources are ingrained in the measured state. Second, using this construction, we obtain a classical algorithm for strongly simulating bosonic computations, whose complexity scales with the stellar rank, a discrete non-Gaussian measure [35], of both the input state and the measurement setup of the original computation. Our algorithm is a generalization of that of [36]—which applies only to a restricted set of bosonic computations—to essentially any bosonic computation. Our result thus establishes the stellar rank as a necessary non-Gaussian resource for reaching a quantum computational advantage with bosonic information processing. Third, we further show that the associated CV sampling setup can also be efficiently simulated classically whenever its corresponding input state is passively separable. We explain that states that are not passively separable possess non-Gaussian entanglement, thus showing that this type of entanglement is necessary for reaching a quantum computational advantage. Our results allow us to clarify the role played by different nonclassical resources in enabling quantum computational advantage, which we illustrate with the example of boson sampling.

Sampling tasks.—Our starting point is that of a general sampling setup, where a quantum state $\hat{\rho}$ over m subsystems, or modes, is measured by a series of m local detectors. We assume that the kth detector measures an observable $\hat{Y}_k$ with a spectral decomposition $\hat{Y}_k = \int_{\mathcal{Y}_k} y \hat{P}_{k;y_k} dy$, where $\mathcal{Y}_k$ is the spectrum of $\hat{Y}_k$. Here, we limit ourselves to projective measurements, but our results can be extended to more general positive operator-valued measures through Naimark's dilation theorem.

In a sampling setup, our goal is to sample detector outcomes with respect to the probability distribution given by the Born rule: $P(y_1, \ldots, y_m|\hat{\rho}) \coloneqq \mathrm{Tr}[\hat{\rho} \bigotimes_{k=1}^{m} \hat{P}_{k;y_k}]$. For simplicity, we can assume that the projectors are rank 1, such that $\hat{P}_{k;y_k} = |y_k\rangle\langle y_k|$. The measurement can thus be resourceful if $|y_k\rangle$ has a negative Wigner function or if it contains squeezing. *A priori*, the state $\hat{\rho}$ can be any multimode mixed state, but in a typical sampling setup it would be generated by applying a series of few-mode gates to a set of single-mode input states.

Stellar hierarchy.—Hereafter, we describe bosonic states using the stellar hierarchy [35] (see the Supplemental Material [37] for a concise review). This formalism associates to each m-mode pure state $|\boldsymbol{\psi}\rangle = \sum_{\boldsymbol{n}\geq \boldsymbol{0}} \psi_{\boldsymbol{n}} |\boldsymbol{n}\rangle$ its stellar (or Bargmann) function $F^{\star}_{\boldsymbol{\psi}}(z) = \sum_{\boldsymbol{n}\geq \boldsymbol{0}} (\psi_{\boldsymbol{n}}/\sqrt{\boldsymbol{n}!}) z^{\boldsymbol{n}}$, for all $z \in \mathbb{C}^m$, and classifies bosonic states according to their stellar rank: pure states of finite stellar rank $r^{\star}$ are those states whose stellar function is of the form $F^{\star}(z) = P(z)G(z)$, where P is a multivariate polynomial of degree $r^{\star}$ and G is a multivariate Gaussian. Such states can be decomposed as $\hat{G}|\boldsymbol{C}\rangle$, where $\hat{G}$ is a Gaussian unitary and $|\boldsymbol{C}\rangle$ is a core state, i.e., a finite superposition of Fock states. The number of nonzero coefficients of $|\boldsymbol{C}\rangle$ is called the core state support size. For mixed states, the stellar rank is defined by a convex roof construction: $r^{\star}(\hat{\rho}) = \inf_{p_i, \boldsymbol{\psi}_i} \sup r^{\star}(\boldsymbol{\psi}_i)$, where the infimum is over the decompositions $\hat{\rho} = \sum_i p_i |\boldsymbol{\psi}_i\rangle\langle\boldsymbol{\psi}_i|$. The stellar rank is a faithful and operational non-Gaussian measure [34], as it is invariant under Gaussian unitaries, nonincreasing under Gaussian maps, and it lower bounds the minimal number of non-Gaussian operations (such as photon additions or photon subtractions) necessary to prepare a bosonic state from the vacuum, together with Gaussian unitary operations. Moreover, any state can be approximated arbitrarily well in trace distance by states of finite stellar rank, and an optimal approximating state of a given stellar rank can be found efficiently [47].

To establish the duality between sampling an outcome from the distribution $P(y_1, \ldots, y_m)$ and double homodyne sampling, we must analyze the pure states $|y_k\rangle$. It is convenient to use the stellar hierarchy to describe them: we can represent any single-mode state $|y_k\rangle$ of finite stellar rank as [35]

$$|y_k\rangle = \frac{1}{\sqrt{\mathcal{N}_k}} \left[\prod_{j=1}^{r^{\star}(y_k)} \hat{D}(\beta_{k;j}) \hat{a}_k^{\dagger} \hat{D}^{\dagger}(\beta_{k;j}) \right] |G_k\rangle, \qquad (1)$$

where $r^{\star}(y_k) \in \mathbb{N}$ denotes the stellar rank of the state $|y_k\rangle$, $|G_k\rangle$ is a Gaussian state, $\hat{D}(\beta_{k;j})$ is a displacement operator that acts on mode k with $\beta_{k;j} \in \mathbb{C}$, $\hat{a}_k^{\dagger}$ is the creation operator in mode k, and $\mathcal{N}_k$ is a normalization factor. In this case, we can interpret $|y_k\rangle$ as an $r^{\star}(y_k)$-photon-added Gaussian state [when $r^{\star}(y_k) = 0$, the empty product is the identity operator by convention]. Furthermore, since we can approximate any state $|y_k\rangle$ by a finite-rank state to arbitrary precision in trace distance, we assume that all $|y_k\rangle$ have a—possibly high—finite stellar rank.

The single-mode Gaussian states $|G_k\rangle$ can always be obtained from the vacuum with squeezing and displacement operations. This allows us to write $|G_k\rangle = \hat{S}_k|\alpha_k\rangle$, where $\hat{S}_k$ is a suitably chosen squeezing operation and $|\alpha_k\rangle = \hat{D}(\alpha_k)|0\rangle_{\text{vac}}$ is a coherent state. Combining this with Eq. (1), we can now recast

$$P(y_1,\ldots,y_m|\hat{\rho}) = \frac{1}{\mathcal{N}}\text{Tr}\left[\hat{\boldsymbol{S}}^\dagger\hat{\rho}^-\hat{\boldsymbol{S}}\bigotimes_{k=1}^{m}|\alpha_k\rangle\langle\alpha_k|\right], \quad (2)$$

where $\hat{\boldsymbol{S}} \coloneqq \bigotimes_k \hat{S}_k$ and $\hat{\rho}^-$ is a non-normalized photon-subtracted state, given by $\hat{\rho}^- \coloneqq \hat{\boldsymbol{A}}\hat{\rho}\hat{\boldsymbol{A}}^\dagger$, with a photon-subtraction operator $\hat{\boldsymbol{A}} \coloneqq \bigotimes_{k=1}^m \prod_{n=1}^{r^\star(y_k)} \hat{D}(\beta_{k;n})\hat{a}_k\hat{D}^\dagger(\beta_{k;n})$. The normalization factor $\mathcal{N}$ in Eq. (2) is directly related to the detectors we use, thus we assume it to be known *a priori*.

Coherent state samplers.—Double homodyne measurement corresponds to a (subnormalized) projection onto coherent states [11]. Hence, the expression in Eq. (2) shows that sampling measurement outcomes $y_1,\ldots,y_m$ can always be connected to performing double homodyne measurements on a state that is obtained by squeezing and subtracting photons from the initial state $\hat{\rho}$. The implementation of photon subtraction generally requires measurements on auxiliary modes. The most common implementation involves a photon-counting measurement [48], but this is not compatible with our aim of not having any resources at the level of the measurement, since these measurements are represented by negative Wigner functions. Thus, we introduce a more unusual construction inspired by sum-frequency generation [49].

To subtract a photon in a mode k from a state $\hat{\rho}$, we attach an auxiliary mode to our system, containing exactly one photon. This state is injected in a very weak two-mode squeezer, given by a unitary $\hat{U}(\xi) = \exp[i\xi(\hat{a}_k^\dagger\hat{a}_{\text{aux}}^\dagger + \hat{a}_k\hat{a}_{\text{aux}})]$ (acting as identity on all except the kth and the auxiliary modes). After having applied $\hat{U}(\xi)$, we project the auxiliary mode on the vacuum state to find $\text{Tr}_{\text{aux}}\{\hat{U}(\xi)[\hat{\rho}\otimes|1\rangle\langle 1|]\hat{U}^\dagger(\xi)[\hat{\mathbb{1}}\otimes|0\rangle\langle 0|]\} \approx \xi^2\hat{a}_k\hat{\rho}\hat{a}_k^\dagger$, where the approximation becomes exact when the approximation parameter ξ goes to zero (see Supplemental Material [37]). Replacing each photon subtraction in Eq. (2) by the above construction, we show in the Supplemental Material that, for any $\epsilon > 0$, one can pick approximation parameters $\xi_{k;j} = \text{poly}[\epsilon,(1/m)]$ for all $k \in \{1,\ldots,m\}$ and all $j \in \{1,\ldots,r^\star(y_k)\}$, such that

$$P(y_1,\ldots,y_m|\hat{\rho}) = \frac{1}{\mathcal{N}\prod_{k=1}^m\prod_{j=1}^{r^\star(y_k)}\xi_{k;j}^2} \times \text{Tr}\left[\hat{\rho}_{\text{total}}\left(\bigotimes_{k=1}^{m}|\alpha_k\rangle\langle\alpha_k|\otimes|0\rangle\langle 0|^{\otimes n}\right)\right] + O(\epsilon), \quad (3)$$

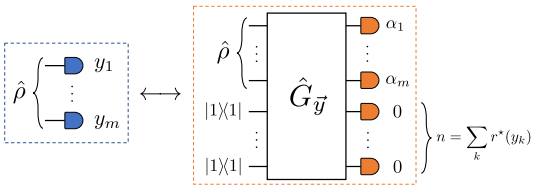

FIG. 1. To any bosonic computation (left, in blue) is associated a coherent state sampling setup (right, in orange), which takes as input the same state $\hat{\rho}$, together with auxiliary single-photon Fock states, and whose output probability density approximates to arbitrary precision the output probability of a given outcome up to normalization, i.e., $P(\alpha_1,\ldots,\alpha_m,0,\ldots,0) \approx (1/\mathcal{N}')P(y_1,\ldots,y_m)$. The number of auxiliary Fock states n is the sum of the stellar ranks of the projectors associated with the outcomes $y_1,\ldots,y_m$.

where we have set $n \coloneqq \sum_{k=1}^m r^\star(y_k)$, and where the state $\hat{\rho}_{\text{total}}$ is defined on the full Hilbert space, including all the auxiliary modes, and is given by

$$\hat{\rho}_{\text{total}} \coloneqq (\hat{\boldsymbol{S}}^\dagger\otimes\hat{\mathbb{1}}_{\text{aux}})\hat{\boldsymbol{\mathcal{U}}}^\dagger(\hat{\rho}\otimes|1\rangle\langle 1|^{\otimes n})\hat{\boldsymbol{\mathcal{U}}}(\hat{\boldsymbol{S}}\otimes\hat{\mathbb{1}}_{\text{aux}}), \quad (4)$$

with $\hat{\boldsymbol{\mathcal{U}}}$ given by $\hat{\boldsymbol{\mathcal{U}}} \coloneqq \bigotimes_{k=1}^m\prod_{j=1}^{r^\star(y_k)}\hat{D}(\beta_{k;j})\hat{U}^\dagger(\xi_{k;j})\hat{D}^\dagger(\beta_{k;j})$. We note that $\hat{U}(\xi_{k;j})$ is the two-mode squeezer that connects the kth detection mode to the auxiliary mode that implements the jth photon-subtraction operation associated with it, and thus $(\hat{\boldsymbol{S}}^\dagger\otimes\hat{\mathbb{1}}_{\text{aux}})\hat{\boldsymbol{\mathcal{U}}}^\dagger$ is a Gaussian unitary. In particular, $r^\star(\hat{\rho}_{\text{total}}) = r^\star(\hat{\rho}\otimes|1\rangle\langle 1|^{\otimes n}) = r^\star(\hat{\rho}) + \sum_{k=1}^m r^\star(y_k)$ since the stellar rank is fully additive with respect to tensor products with pure states [34].

The projection on the vacuum is consistent with double homodyne detection since $|0\rangle_{\text{vac}}$ is also a coherent state. The expression in Eq. (3) thus shows that any setup where one samples a given outcome from a bosonic state can be mapped theoretically to a larger coherent state sampling setup, whose output probability density matches to arbitrary precision the output probability of that outcome, up to a normalizing factor (see Fig. 1). Furthermore, the stellar ranks of the projection operators translate to the inclusion of additional single-photon Fock states in auxiliary modes. A similar derivation, detailed in the Supplemental Material [37], shows that the corresponding marginal probabilities are also reproduced by the marginal probability densities of coherent state samplers.

Strong simulation of bosonic computations.—These results highlight that coherent state samplers can be very generally used to simulate other sampling setups using similar techniques as in [36]. Strong simulation, in particular, refers to the evaluation of any output probability of a computation or any of its marginal probabilities. Hereafter, we rely on the following notion of approximate strong simulation: let P be a probability distribution (density); for $\epsilon > 0$, approximate strong simulation of P

up to total variation distance ϵ refers to the computational task of strongly simulating a probability distribution Q, which is ϵ close to P in total variation distance (see Supplemental Material for a formal definition [37]).

The classical algorithm for strong simulation of Gaussian circuits with non-Gaussian input states from Theorem 2 in [36] can be readily applied to coherent state samplers. Combining this result with our construction, we obtain a general classical algorithm for approximate strong simulation of bosonic quantum computations, whose complexity scales with the stellar rank of both the input state and the measurement setup. We state the result in the case of pure state input and projective measurements and refer to Theorem 2 in the Supplemental Material [37] for the general theorem and its proof:

Theorem 1.—Let $|\boldsymbol{\psi}\rangle$ be an m-mode pure state of stellar rank $r^\star(\boldsymbol{\psi})$ and core state support size s. For all $k \in \{1, \ldots, m\}$, let $\hat{Y}_k$ be an observable with eigenbasis $\{|y_k\rangle\}_{y_k \in \mathcal{Y}_k}$, and let $r_k^\star = \sup_{y_k \in \mathcal{Y}_k} r^\star(y_k)$. Let $r := r_{\boldsymbol{\psi}}^\star + \sum_k r_k^\star$ be the total stellar rank of the setup. Then, the measurement of $\hat{Y}_1, \ldots, \hat{Y}_m$ on $|\boldsymbol{\psi}\rangle$ over an exponentially large outcome space can be approximately strongly simulated up to total variation distance $\exp(-\mathrm{poly}m)$ in time $\mathcal{O}(s^2 r^3 2^r + \mathrm{poly}m)$.

The total variation distance in the theorem results from the approximation used in Eq. (3). This strong simulation algorithm competes with state-of-the art classical algorithms for certain bosonic architectures [36], but applies to a much wider class of quantum computations—essentially any bosonic computation. The time complexity in Theorem 1 is a worst-case complexity, based on the fastest known classical algorithm for computing the hafnian [50], and may be reduced for particular instances. On the other hand, due to its broad applicability, our simulation technique may be outperformed by classical simulation algorithms targeting specific classes of bosonic circuits [51–55]. Nonetheless, Theorem 1 may be used primarily as a tool for identifying necessary resources for bosonic quantum computational advantage: it establishes the stellar rank as a necessary non-Gaussian property.

Non-Gaussian entanglement.—Now that we have shown that any bosonic computation can be connected to a coherent state sampler, we aim to identify physical resources that are required to reach a quantum advantage with coherent state sampling beyond the stellar rank. We resort to a basic model of coherent state sampler, where we consider sampling from a given N-mode state $\hat{\sigma}$. The probability density corresponding to a certain set of complex measurement outcomes $\alpha_1, \ldots, \alpha_N$ in the N output detectors is given by the Husimi Q function of the state $\hat{\sigma}$: $Q(\vec{\alpha}|\hat{\sigma}) = (1/\pi^N)\langle\vec{\alpha}|\hat{\sigma}|\vec{\alpha}\rangle$, where $\vec{\alpha} = (\alpha_1, \ldots, \alpha_N)^\top$. By having put all the quantum resources of the sampling protocol at the level of the state, the hardness of the sampling problem can now be directly related to properties of the resourceful state's Q function.

Under basic assumptions, we can efficiently sample classically from the Q function of any separable mixed state (see Supplemental Material for a discussion [37]). Hence, quantum entanglement of the input state is a necessary requirement in the design of a coherent state sampler that is hard to simulate. However, it turns out that not all forms of entanglement are equally suitable. In previous works [34,56], we have discussed the concept of passive separability: a quantum state is said to be passively separable if at least one mode basis exists in which the state is separable. In other words, for a passively separable state, any entanglement can be undone by an interferometer built with beam splitters and phase shifters.

The concept of passive separability becomes essential when we combine it with the properties of coherent states. Let $\hat{U}$ describe a passive N-mode linear optics interferometer in the sense that $\hat{U}^\dagger \hat{a}_k \hat{U} = \sum_j U_{jk} \hat{a}_j$, where U is an $N \times N$ unitary matrix. The action of $\hat{U}$ on an N-mode coherent state is given by $\hat{U}|\vec{\alpha}\rangle = |U\vec{\alpha}\rangle$. This simple identity implies that, for all passive linear optics transformations, $Q(\vec{\alpha}|\hat{\tau}) = Q(U\vec{\alpha}|\hat{U}\,\hat{\tau}\,\hat{U}^\dagger)$. By definition, for any state $\hat{\tau}$ that is passively separable, there is at least one transformation $\hat{U}$ such that $\hat{U}\,\hat{\tau}\,\hat{U}^\dagger$ is separable. This, in turn, means that we can efficiently sample from the distribution $Q(\vec{\alpha}|\hat{U}\,\hat{\tau}\,\hat{U}^\dagger)$. Hence, we can sample a vector $\vec{\alpha}$ from $Q(\vec{\alpha}|\hat{\tau})$ by first sampling $\vec{\beta}$ distributed according to $Q(\vec{\beta}|\hat{U}\,\hat{\tau}\,\hat{U}^\dagger)$ and subsequently identifying $\vec{\alpha} = U^\dagger\vec{\beta}$. Thus, we find that we can efficiently simulate the coherent state sampling from any passively separable state.

To reach a quantum computational advantage with a coherent state sampler, we thus have to use input states that are not passively separable. This requirement immediately excludes all Gaussian states, since these are always passively separable [57]. The lack of passive separability can therefore be seen as non-Gaussian entanglement in the sense that it is a form of entanglement that persists in any mode basis and cannot be extracted based solely on the state's covariance matrix. It thus highlights the presence of non-Gaussian features in the state's correlations.

We emphasize that there are other intuitive notions of non-Gaussian entanglement. When we call states that are separable through general Gaussian operations (i.e., a combination of interferometers and squeezing operations) Gaussian separable, one could say that only states that are not Gaussian separable have non-Gaussian entanglement. To understand what notion of non-Gaussian entanglement is necessary for reaching a quantum computational advantage with coherent state sampling, we consider the seminal example of boson sampling. Through Eq. (3), we find that ideal boson sampling with n input photons and an m-mode interferometer $\hat{U}_{\mathrm{BS}}$ corresponds to coherent state sampling from a state given by $|\Psi\rangle \propto \hat{\mathcal{U}}(\hat{U}_{\mathrm{BS}} \otimes \mathbb{1}_{\mathrm{aux}})|\Psi_{\mathrm{total}}\rangle$, where $\hat{\mathcal{U}}$ is a tensor product of two-mode squeezers and where the state $|\Psi_{\mathrm{total}}\rangle$ is a $2n$-photon Fock state that combines the

input state of the boson sampler with n auxiliary photons, given by

$$|\Psi_{\text{total}}\rangle = [\underbrace{|1\rangle \otimes \ldots \otimes |1\rangle}_{n} \otimes \underbrace{|0\rangle \otimes \ldots \otimes |0\rangle}_{m-n}] \otimes [\underbrace{|1\rangle \otimes \ldots \otimes |1\rangle}_{n}]_{\text{aux}}. \quad (5)$$

Boson sampling is known to be a hard problem, so exact coherent state sampling from the state $|\Psi\rangle$ is also classically hard [58]. The structure of this state nicely highlights the three fundamental types of nonclassicality that are required: non-Gaussian resources in $|\Psi_{\text{total}}\rangle$, large-scale entanglement through $\hat{U}_{\text{BS}}$, and squeezing through $\hat{\boldsymbol{\mathcal{U}}}$. Furthermore, the order of the elements is essential: the state $|\Psi\rangle$ is not passively separable because the squeezing operations in $\hat{\boldsymbol{\mathcal{U}}}$ and the non-Gaussian features in $|\Psi_{\text{total}}\rangle$ are local in a different mode basis. However, $\hat{\boldsymbol{\mathcal{U}}}(\hat{U}_{\text{BS}} \otimes \mathbb{1}_{\text{aux}})$ is a Gaussian operation and $|\Psi_{\text{total}}\rangle$ is separable. This means that the state $|\Psi\rangle$ is thus Gaussian separable but not passive separable. Hence, there are Gaussian-separable states leading to coherent state sampling that cannot be efficiently simulated. We thus propose to define non-Gaussian entanglement as the type of entanglement that is present in states that are not passively separable. This amounts to defining it operationally as a type of entanglement that is necessary to achieve computationally hard coherent state sampling.

Conclusion.—In this Letter, we argue that any bosonic sampling computation can be mapped to a corresponding coherent state sampling computation. Our construction allows us to derive a general classical algorithm for strong simulation of bosonic computations, whose time complexity scales with the stellar rank of the input state and the measurement setup of the computation.

We see our Letter in the first instance as providing a useful method to analyze the resources in sampling setups, because all resources in coherent state sampling are situated at the level of the state. As such, we also find that coherent state sampling with passively separable states can be simulated efficiently. We therefore find that the lack of passive separability rather than the lack of Gaussian separability is the operationally useful type of non-Gaussian entanglement.

Our key reduction in Eq. (3) shows that any non-Gaussian resource in the measurement is introduced in the coherent state sampler through auxiliary photons. The total number of auxiliary photons in the coherent state sampler ultimately corresponds to the total stellar rank of the measurement setup. These photons must be entangled in a fundamentally non-Gaussian way to achieve the necessary sampling complexity. For pure states, this non-Gaussian entanglement also implies one of the previous requirements for reaching a quantum computational advantage: Wigner negativity [30]. Yet, for mixed states, it remains an open question how the necessity of Wigner negativity translates to the coherent state sampler.

Typical sampling setups such as (Gaussian) boson sampling correspond to reasonably simple coherent state samplers that mix local non-Gaussian resources through a multimode Gaussian transformation. However, in the multimode bosonic state space, much more exotic states can be conceived. Preparing such states would require multimode non-Gaussian unitary transformations, and it would be interesting to understand whether they have any additional computational resourcefulness.

We thank Frédéric Grosshans for inspiring discussions. This work was supported by the ANR JCJC project NoRdiC (ANR-21-CE47-0005) and Plan France 2030 project NISQ2LSQ (ANR-22-PETQ-0006). U. C. acknowledges funding provided by the Institute for Quantum Information and Matter, a NSF Physics Frontiers Center (NSF Grant No. PHY-1733907).

*ulysse.chabaud@inria.fr
†mattia.walschaers@lkb.upmc.fr

[1] D. Deutsch and R. Jozsa, Rapid solution of problems by quantum computation, Proc. R. Soc. A **439**, 553 (1992).
[2] D. R. Simon, On the power of quantum computation, SIAM J. Comput. **26**, 1474 (1997).
[3] P. W. Shor, Polynomial-time algorithms for prime factorization and discrete logarithms on a quantum computer, SIAM Rev. **41**, 303 (1999).
[4] There is some ambiguity in literature surrounding the terms "quantum supremacy," "quantum advantage," and "quantum speedup." In this Letter, we use the term "quantum computational advantage" to refer to any quantum computational protocol that cannot be efficiently executed by a classical machine.
[5] M. J. Bremner, R. Jozsa, and D. J. Shepherd, Classical simulation of commuting quantum computations implies collapse of the polynomial hierarchy, Proc. R. Soc. A **467**, 459 (2011).
[6] S. Aaronson and A. Arkhipov, The computational complexity of linear optics, in *Proceedings of the Forty-Third Annual ACM Symposium on Theory of Computing*, STOC '11 (Association for Computing Machinery, New York, 2011), pp. 333–342, 10.1145/1993636.1993682.
[7] S. Boixo, S. V. Isakov, V. N. Smelyanskiy, R. Babbush, N. Ding, Z. Jiang, M. J. Bremner, J. M. Martinis, and H. Neven, Characterizing quantum supremacy in near-term devices, Nat. Phys. **14**, 595 (2018).
[8] F. Arute *et al.*, Quantum supremacy using a programmable superconducting processor, Nature (London) **574**, 505 (2019).
[9] F. Pan, K. Chen, and P. Zhang, Solving the Sampling Problem of the Sycamore Quantum Circuits, Phys. Rev. Lett. **129**, 090502 (2022).
[10] E. Knill, R. Laflamme, and G. J. Milburn, A scheme for efficient quantum computation with linear optics, Nature (London) **409**, 46 (2001).

[11] U. Leonhardt, *Essential Quantum Optics*, 1st ed. (Cambridge University Press, Cambridge, England, 2010).
[12] M. Gu, C. Weedbrook, N. C. Menicucci, T. C. Ralph, and P. van Loock, Quantum computing with continuous-variable clusters, Phys. Rev. A **79**, 062318 (2009).
[13] X. Su, Y. Zhao, S. Hao, X. Jia, C. Xie, and K. Peng, Experimental preparation of eight-partite cluster state for photonic qumodes, Opt. Lett. **37**, 5178 (2012).
[14] M. Chen, N. C. Menicucci, and O. Pfister, Experimental Realization of Multipartite Entanglement of 60 Modes of a Quantum Optical Frequency Comb, Phys. Rev. Lett. **112**, 120505 (2014).
[15] W. Asavanant, Y. Shiozawa, S. Yokoyama, B. Charoensombutamon, H. Emura, R. N. Alexander, S. Takeda, J.-i. Yoshikawa, N. C. Menicucci, H. Yonezawa, and A. Furusawa, Generation of time-domain-multiplexed two-dimensional cluster state, Science **366**, 373 (2019).
[16] M. V. Larsen, X. Guo, C. R. Breum, J. S. Neergaard-Nielsen, and U. L. Andersen, Deterministic generation of a two-dimensional cluster state, Science **366**, 369 (2019).
[17] Y. Cai, J. Roslund, G. Ferrini, F. Arzani, X. Xu, C. Fabre, and N. Treps, Multimode entanglement in reconfigurable graph states using optical frequency combs, Nat. Commun. **8**, 15645 (2017).
[18] J. E. Bourassa, R. N. Alexander, M. Vasmer, A. Patil, I. Tzitrin, T. Matsuura, D. Su, B. Q. Baragiola, S. Guha, G. Dauphinais, K. K. Sabapathy, N. C. Menicucci, and I. Dhand, Blueprint for a scalable photonic fault-tolerant quantum computer, Quantum **5**, 392 (2021).
[19] A. P. Lund, A. Laing, S. Rahimi-Keshari, T. Rudolph, J. L. O'Brien, and T. C. Ralph, Boson Sampling from a Gaussian State, Phys. Rev. Lett. **113**, 100502 (2014).
[20] T. Douce, D. Markham, E. Kashefi, E. Diamanti, T. Coudreau, P. Milman, P. van Loock, and G. Ferrini, Continuous-Variable Instantaneous Quantum Computing is Hard to Sample, Phys. Rev. Lett. **118**, 070503 (2017).
[21] C. S. Hamilton, R. Kruse, L. Sansoni, S. Barkhofen, C. Silberhorn, and I. Jex, Gaussian Boson Sampling, Phys. Rev. Lett. **119**, 170501 (2017).
[22] U. Chabaud, T. Douce, D. Markham, P. van Loock, E. Kashefi, and G. Ferrini, Continuous-variable sampling from photon-added or photon-subtracted squeezed states, Phys. Rev. A **96**, 062307 (2017).
[23] L. Chakhmakhchyan and N. J. Cerf, Boson sampling with Gaussian measurements, Phys. Rev. A **96**, 032326 (2017).
[24] H.-S. Zhong *et al.*, Quantum computational advantage using photons, Science **370**, 1460 (2020).
[25] H.-S. Zhong *et al.*, Phase-Programmable Gaussian Boson Sampling Using Stimulated Squeezed Light, Phys. Rev. Lett. **127**, 180502 (2021).
[26] L. S. Madsen *et al.*, Quantum computational advantage with a programmable photonic processor, Nature (London) **606**, 75 (2022).
[27] A. Deshpande, A. Mehta, T. Vincent, N. Quesada, M. Hinsche, M. Ioannou, L. Madsen, J. Lavoie, H. Qi, J. Eisert, D. Hangleiter, B. Fefferman, and I. Dhand, Quantum computational advantage via high-dimensional Gaussian boson sampling, Sci. Adv. **8**, 7894 (2022).
[28] E. Wigner, On the quantum correction for thermodynamic equilibrium, Phys. Rev. **40**, 749 (1932).
[29] D. Gross, Hudson's theorem for finite-dimensional quantum systems, J. Math. Phys. (N.Y.) **47**, 122107 (2006).
[30] A. Mari and J. Eisert, Positive Wigner Functions Render Classical Simulation of Quantum Computation Efficient, Phys. Rev. Lett. **109**, 230503 (2012).
[31] V. Veitch, N. Wiebe, C. Ferrie, and J. Emerson, Efficient simulation scheme for a class of quantum optics experiments with non-negative Wigner representation, New J. Phys. **15**, 013037 (2013).
[32] L. García-Álvarez, C. Calcluth, A. Ferraro, and G. Ferrini, Efficient simulatability of continuous-variable circuits with large Wigner negativity, Phys. Rev. Res. **2**, 043322 (2020).
[33] U. Chabaud, G. Ferrini, F. Grosshans, and D. Markham, Classical simulation of Gaussian quantum circuits with non-Gaussian input states, Phys. Rev. Res. **3**, 033018 (2021).
[34] U. Chabaud and S. Mehraban, Holomorphic representation of quantum computations, Quantum **6**, 831 (2022).
[35] U. Chabaud, D. Markham, and F. Grosshans, Stellar Representation of Non-Gaussian Quantum States, Phys. Rev. Lett. **124**, 063605 (2020).
[36] U. Chabaud, G. Ferrini, F. Grosshans, and D. Markham, Classical simulation of Gaussian quantum circuits with non-Gaussian input states, Phys. Rev. Res. **3**, 033018 (2021).
[37] See Supplemental Material at http://link.aps.org/supplemental/10.1103/PhysRevLett.130.090602 for a brief introduction to the stellar formalism and detailed proofs of the results presented in the main text, which includes Refs. [38–46].
[38] I. E. Segal and G. W. Mackey, *Mathematical Problems of Relativistic Physics* (American Mathematical Society, Providence, 1963), Vol. 2.
[39] V. Bargmann, On a Hilbert space of analytic functions and an associated integral transform part I, Commun. Pure Appl. Math. **14**, 187 (1961).
[40] M. Amy, D. Maslov, M. Mosca, and M. Roetteler, A Meet-in-the-Middle Algorithm for Fast Synthesis of Depth-Optimal Quantum Circuits, IEEE Trans. Comput.-Aided Des. Integr. Circuits Syst. **32**, 818 (2013).
[41] M. Beverland, E. Campbell, M. Howard, and V. Kliuchnikov, Lower bounds on the non-Clifford resources for quantum computations, Quantum Sci. Technol. **5**, 035009 (2020).
[42] F. Hong-Yi, H. R. Zaidi, and J. R. Klauder, New approach for calculating the normally ordered form of squeeze operators, Phys. Rev. D **35**, 1831 (1987).
[43] A. Ferraro, S. Olivares, and M. G. Paris, Gaussian states in continuous variable quantum information, arXiv:quant-ph/0503237.
[44] B. M. Terhal and D. P. DiVincenzo, Classical simulation of noninteracting-fermion quantum circuits, Phys. Rev. A **65**, 032325 (2002).
[45] H. Pashayan, J. J. Wallman, and S. D. Bartlett, Estimating Outcome Probabilities of Quantum Circuits Using Quasiprobabilities, Phys. Rev. Lett. **115**, 070501 (2015).
[46] A. W. Harrow and A. Montanaro, Quantum computational supremacy, Nature (London) **549**, 203 (2017).

[47] U. Chabaud, G. Roeland, M. Walschaers, F. Grosshans, V. Parigi, D. Markham, and N. Treps, Certification of non-gaussian states with operational measurements, PRX Quantum **2**, 020333 (2021).
[48] A. Lvovsky, P. Grangier, A. Ourjoumtsev, V. Parigi, M. Sasaki, and R. Tualle-Brouri, Production and applications of non-Gaussian quantum states of light, arXiv:2006.16985.
[49] R. W. Boyd, *Nonlinear Optics* (Academic Press, New York, 2020).
[50] A. Björklund, B. Gupt, and N. Quesada, A faster hafnian formula for complex matrices and its benchmarking on a supercomputer, J. Exp. Algorithmics **24**, 1 (2019).
[51] N. Quesada, J. M. Arrazola, and N. Killoran, Gaussian boson sampling using threshold detectors, Phys. Rev. A **98**, 062322 (2018).
[52] R. García-Patrón, J. J. Renema, and V. Shchesnovich, Simulating boson sampling in lossy architectures, Quantum **3**, 169 (2019).
[53] J. J. Renema, Simulability of partially distinguishable superposition and Gaussian boson sampling, Phys. Rev. A **101**, 063840 (2020).
[54] J. E. Bourassa, N. Quesada, I. Tzitrin, A. Száva, T. Isacsson, J. Izaac, K. K. Sabapathy, G. Dauphinais, and I. Dhand, Fast simulation of Bosonic qubits via Gaussian functions in phase space, PRX Quantum **2**, 040315 (2021).
[55] C. Calcluth, A. Ferraro, and G. Ferrini, Efficient simulation of Gottesman-Kitaev-Preskill states with Gaussian circuits, Quantum **6**, 867 (2022).
[56] M. Walschaers, C. Fabre, V. Parigi, and N. Treps, Entanglement and Wigner Function Negativity of Multimode Non-Gaussian States, Phys. Rev. Lett. **119**, 183601 (2017).
[57] M. Walschaers, C. Fabre, V. Parigi, and N. Treps, Statistical signatures of multimode single-photon-added and -subtracted states of light, Phys. Rev. A **96**, 053835 (2017).
[58] When multiplicative estimation or additive estimation up to exponentially small error of a single outcome probability is an instance of a #P-hard problem, which is the case for boson sampling, the use of Stockmeyer's algorithm implies that any efficient classical simulation of exact sampling would collapse the polynomial hierarchy of complexity classes [6,59]. This argument directly applies to the corresponding instance of coherent state sampling.
[59] D. Hangleiter and J. Eisert, Computational advantage of quantum random sampling, arXiv:2206.04079.

3

ENGINEERING NON-GAUSSIAN STATES

LIST OF ARTICLES

1. **M. Walschaers**, C. Fabre, V. Parigi, and N. Treps, *Entanglement and Wigner function negativity of multimode non-Gaussian states*, Phys. Rev. Lett. **119**, 183601 (2017).
2. **M. Walschaers**, C. Fabre, V. Parigi, and N. Treps, *Statistical signatures of multimode single-photon added and subtracted states of light*, Phys. Rev. A **96**, 053835 (2017).
3. **M. Walschaers**, S. Sarkar, V. Parigi, and N. Treps, *Tailoring Non-Gaussian Continuous-Variable Graph States*, Phys. Rev. Lett. **121**, 220501 (2018).
4. **M. Walschaers**, Y.-S. Ra, and N. Treps, *Mode-dependent-loss model for multimode photon-subtracted states*, Phys. Rev. A **100**, 023828 (2019).
5. Y.-S. Ra, A. Dufour, **M. Walschaers**, C. Jacquard, T. Michel, C. Fabre, N. Treps, *Non-Gaussian quantum states of a multimode light field*, Nat. Phys. **16**, 144–147(2020).
6. **M. Walschaers** and N. Treps, *Remote generation of Wigner-negativity through Einstein-Podolsky-Rosen steering*, Phys. Rev. Lett. **124**, 150501 (2020).
7. V. Cimini, M. Barbieri, N. Treps, **M. Walschaers**, V. Parigi, *Neural networks for detecting multimode Wigner-negativity*, Phys. Rev. Lett. **125**, 160504 (2020).
8. **M. Walschaers**, V. Parigi, N. Treps, *Practical Framework for Conditional Non-Gaussian Quantum State Preparation*, PRX Quantum **1**, 020305 (2020).
9. U. Chabaud, G. Roeland, **M. Walschaers**, F. Grosshans, V. Parigi, D. Markham, and N. Treps, *Certification of Non-Gaussian States with Operational Measurements*, PRX Quantum **2**, 020333 (2021).
10. A. O. C. Davis, **M. Walschaers**, V. Parigi and N. Treps, *Conditional preparation of non-Gaussian quantum optical states by mesoscopic measurement*, New J. Phys. **23** 063039 (2021).
11. **M. Walschaers**, *Non-Gaussian Quantum States and Where to Find Them*, PRX Quantum **2**, 030204 (2021).
12. Y. Xiang, S. Liu, J. Guo, Q. Gong, N. Treps, Q. He, **M. Walschaers** *Quantification of Wigner Negativity Remotely Generated via Einstein-Podolsky-Rosen Steering*, npj Quantum Information **8**, 21 (2022).
13. **M. Walschaers**, B. Sundar, N. Treps, L. D. Carr, V. Parigi, *Emergent complex quantum networks in continuous-variables non-Gaussian states*, Quantum Sci. Technol. **8** 035009 (2023).
14. **M. Walschaers**, *On Quantum Steering and Wigner Negativity*, Quantum **7**, 1038 (2023).

3.1 PHOTON SUBTRACTION

In Section 2.2 we identified several resources required for reaching a quantum computational advantage: Wigner negativity, a high stellar rank, and non-Gaussian entanglement[1]. My work on quantum state engineering has mainly centered on studying techniques to generate these resources in quantum optics experiments. Tools that are particularly popular in quantum optics are photon subtraction and –to a lesser extent– photon addition (Lvovsky, Grangier, et al., 2020; Ourjoumtsev, Tualle-Brouri, et al., 2006; Parigi et al., 2007; Ra et al., 2020; Wenger et al., 2004; Zavatta et al., 2007).

The core idea behind photon subtraction is rather old (Dakna et al., 1997) and in a single-mode setting it has long been well understood. In a multimode context, photon subtraction was also known to modify entanglement properties of the state (Navarrete-Benlloch et al., 2012; Ourjoumtsev, Dantan, et al., 2007; Zhang et al., 2022), which we will discuss in more detail in Section 5. However, in a multimode setting, it can be significantly more challenging to add or subtract photons in a mode-selective way (Averchenko, Jacquard, et al., 2016; Averchenko, Thiel, et al., 2014; Roeland et al., 2022). When I first got interested in continuous-variable quantum optics, I tried to understand the properties of such multimode photon-subtracted states. Our first big achievement was the (admittedly rather complicated) derivation of a "plug and play" expression for the Wigner function of such states (Walschaers, Fabre, et al., 2017a,b; Walschaers, Ra, et al., 2019). Providing a closed expression for a Wigner function of and arbitrary single-photon-subtracted state in function of the covariance matrix and mean field of the initial Gaussian state, and the mode in which the photon is subtracted turned out to be very useful for applications that range from efficiently modelling experiments (Ra et al., 2020) to generating huge amounts of training data for machine learning algorithms (Cimini et al., 2020). On top, our framework also provides a simple recipe for calculating marginals, without the need for slow integration procedures.

The simple access to reduced states allows us to study the spread of non-Gaussian features through multimode systems after photon subtraction (Walschaers, Sarkar, et al., 2018). It came as a surprise that non-Gaussian features spread through continuous-variable cluster states over a finite graph distance of exactly two nodes removed from the node in which the photon is subtracted. This feature was later also confirmed experimentally (Ra et al., 2020) in a work where we demonstrated the first fully mode-selective photon subtraction. These results on the spread of non-Gaussian features motivated a follow-up question: *when does Wigner-negativity, a highly non-Gaussian feature, spread to different modes in a multimode system?* This question was the main motivation for all the work in Section 3.2.

The techniques used in (Walschaers, Fabre, et al., 2017a,b) are based on calculating high-order correlations between quadratures and are hard to generalise to a scenario where multiple photons are subtracted. This difficulty is nicely shown in (Cardin

1 In the sense of a lack of passive separability

and Quesada, 2022; Gagatsos and Guha, 2019), where one effectively shows that the computation of such correlation functions is of a similar complexity as Gaussian Boson Sampling. Alternatively, the connection between n-photon subtraction and collecting n-clicks in a Gaussian Boson Sampler can also be obtained via our general framework of (Chabaud and Walschaers, 2023). For this reason, it is fruitful to resort to the techniques of (Phillips et al., 2019; Walschaers, Kuipers, Urbina, et al., 2016) to try and understand features of multi-photon subtracted states. In (Walschaers, Treps, et al., 2020) we combined correlations of the type (2.1) with techniques from *network science* to understand how non-Gaussian features appear in the correlations between modes as a consequence of photon subtraction. Our numerical framework can accommodate an unlimited number of photon subtractions, provided they are all in the same mode. This work shows, as expected, that photon subtraction generally increases the correlations between the modes in a graph state. We also find that the finer details of structure of correlations (and their reaction to photon subtraction) depends strongly on the features of the network of C_Z gates, that builds the initial Gaussian graph state. This work highlights that the network perspective is highly useful to build heuristics for understanding photon subtraction on a large scale. It is also a useful guide for proving more rigorous results [see Appendix B of (Walschaers, Treps, et al., 2020)]. At the same time, this approach has its limitations in studying quantum phenomena, since it is not directly clear how the features of these correlation networks translate to an understanding of *quantum* correlations. We will come back to this topic in Chapter 5.

3.2 GENERATING WIGNER NEGATIVITY

As mentioned in the previous section, our work on photon subtraction led us to a simple question that started out as a simple curiosity: *what does it take to propagate Wigner negativity through a multimode system?* Initially, we mainly attacked this question from the point of view of photon subtraction and framed it more specifically on a bipartite setting, where one party goes by the name Alice and the other is known as Bob. When Alice and Bob each hold some modes of a multimode Gaussian state, we wondered when a photon subtraction in one of Alice's modes would create a Wigner negative states on Bob's side. The answer was surprisingly profound: the initial Gaussian state must be such that Bob is able to perform Gaussian steering (Kogias, Lee, et al., 2015) on the mode in which Alice subtracts the photon. If on top, we allow Alice to first perform a Gaussian operation on her subsystem, we can even show that this Gaussian steering is necessary and sufficient (Walschaers and Treps, 2020). This means that Gaussian steering from Alice to Bob is the one and only resource that allows Alice to remotely create Wigner negativity in Bob's subsystems through photon subtraction. This result was experimentally confirmed in the work of Liu et al., 2022

Even though this initial work suggests the existence of a fundamental connection between quantum steering and Wigner negativity, the connection between these two

important quantum phenomena was only shown for the very specific context of photon subtraction. This connection was significantly deepened through a follow-up work (Walschaers, Parigi, et al., 2020), which is also included here in Section 3.4. In this work, we derive the core equation (23) that can be understood as Bayes' theorem for Wigner functions. This version of Bayes theorem differs from the classical version in that the conditional probabilities are replaced by quasi-probabilities and can thus be negative. Even if Alice and Bob initially share a Gaussian state, a measurement (or other conditional operation) on Alice's subsystem can induce negative conditional quasi-probabilities. Crucially, we show that $\langle \hat{A} \rangle_{\mathbf{g}|\vec{x}_\mathbf{f}}$ can only be negative if Bob can steer Alice's subsystem with Gaussian measurements. This thus means that Gaussian steering from Bob to Alice is *necessary* for Alice to remotely create Wigner negativity in Bob's subsystem, *regardless of the measurement Alice performs*. However, we also showed that with some operations it is just impossible for Alice to create Wigner negativity in Bob's subsystem. In particular, when Alice performs an operation that is described by a positive Wigner function, there is no hope for Alice to create Wigner negativity in Bob's subsystem. In (Walschaers, Parigi, et al., 2020) we show that photon addition is such an operation. In Section IV.B of (Walschaers, 2021), it was also shown that the framework of (Walschaers, Parigi, et al., 2020) can also be used as an alternative technique to derive our results on Wigner functions for photon subtracted states.

Gaussian quantum steering is a rather restrictive phenomenon once we go to a multipartite scenario (Reid, 2013; Xiang, Kogias, et al., 2017). In particular, Gaussian steering comes with a series of strict monogamy relations. For example, in a Gaussian setting, whenever Alice can steer Bob, it is impossible for Charlie to also steer Bob. Such monogamy relations naturally carry over to remotely generated Wigner negativity, and we show that is constrains how negativity can be distributed (Xiang, Liu, et al., 2022). In the previously mentioned example, an operation on Bob's subsystem can create Wigner negativity in Alice's subsystem, but not in Charlie's. More generally phrased, because of monogamy relations, an operation on a single mode can also only create Wigner negativity in at most one mode.

Yet, all of these results rely on the core assumption that Alice, Bob, and any other parties initially share a Gaussian state. It is thus natural to wonder whether the connection between the remote generation of Wigner negativity and quantum steering survives scrutiny when the assumption of Gaussianity is dropped. This is the subject of my most recent work on the topic (Walschaers, 2023). In this general scenario Alice and Bob can share any Wigner function, but we assume that Bob's reduced state has no Wigner negativity. Apart from that, we impose no constraints on the global state. We show that the framework for describing conditional quantum state preparation of (Walschaers, Parigi, et al., 2020) still applies under these conditions. The manuscript explores under which conditions Alice can remotely induce Wigner-negativity in Bob's subsystem by performing some quantum operation (typically a measurement). First of all, we show that if Bob can steer Alice's system with Wigner-positive measurements,

there is always a conditional operation that Alice can perform to induce Wigner-negativity on Bob's subsystem. However, through a series of reasonably simple counter examples, we show that quantum steering is *not necessary* for this task, nor is any other type of quantum correlation.

Through these works, the connection between quantum steering and the conditional generation o Wigner negativity have been extensively investigated. We reached the conclusion that in general quantum steering with Wigner-positive measurements is *sufficient* for the remote preparation of Wigner negativity. However, quantum steering is not a necessary recourse. The exception is the case where Alice and Bob share a Gaussian state, where Gaussian steering is also a necessary requirement.

3.3 OUTLOOK

Our key motivation in this chapter was to understand conditional techniques to experimentally generate Wigner negativity, one o the key resources for reaching a quantum computational advantage, as previously discussed in Section 2.2. While the fundamental questions surrounding the generation of Wigner negativity and its relation to quantum steering have largely been answered by the works mentioned in 'Section 3.2, there remain many challenges in quantum state engineering. These are related, on the one hand, to practical implementations, and, on the other hand, to the generation of resources other than Wigner negativity.

From the practical point of view, there are direct generalisations of mode-selective photon subtraction (Ra et al., 2020) that can be thought of. Notably, the techniques of (Walschaers, Parigi, et al., 2020) were used in (Walschaers, 2021) to describe mode-selective photon subtracted states, and they can in principle be extended to the subtraction of multiple photons. In particular, for two- and three-photon subtraction we may hope to obtain closed analytical expressions. This is currently a work in progress. Such work fits in a more general context, where generalised photon subtraction has been proposed as a way of creating important non-Gaussiann states such as GKP (Gottesman et al., 2001) and Schrödinger cat states (Bourassa et al., 2021; Eaton, González-Arciniegas, et al., 2022; Fukui et al., 2022; D. Su et al., 2019; Takase et al., 2021).

In contrast to most works on quantum state engineering, our approach is primarily focused on generating resources rather than specific quantum states. In the context of our discussion in Section 2.2 it is natural to wonder whether a study, similar to Section 3.2, can be executed for other resources. The first resource that comes to mind is non-Gaussian entanglement. In Chapter 5 we will explore this question in further detail and show that photon subtraction can create non-Gaussian quantum correlations. However, one can also consider other resources such as non-linear squeezing (Kala et al., 2022), which we are currently doing together with the group of R. Filip.

3.4 **article:** PRACTICAL FRAMEWORK FOR CONDITIONAL NON-GAUSSIAN QUANTUM STATE PREPARATION

Practical Framework for Conditional Non-Gaussian Quantum State Preparation

Mattia Walschaers,* Valentina Parigi, and Nicolas Treps
Laboratoire Kastler Brossel, Sorbonne Université, CNRS, ENS-PSL Research University, Collège de France, 4 place Jussieu, Paris F-75252, France

(Received 24 August 2020; accepted 5 October 2020; published 22 October 2020)

We develop a general formalism, based on the Wigner function representation of continuous-variable quantum states, to describe the action of an arbitrary conditional operation on a multimode Gaussian state. We apply this formalism to several examples, thus showing its potential as an elegant analytical tool for simulating quantum optics experiments. Furthermore, we also use it to prove that Einstein-Podolsky-Rosen steering is a necessary requirement to remotely prepare a Wigner-negative state.

DOI: 10.1103/PRXQuantum.1.020305

I. INTRODUCTION

In continuous-variable (CV) quantum physics, Gaussian states have long been a fruitful topic of research [1–10]. They appear naturally as the ground states of systems of many noninteracting particles in the form of thermal states [11], or as the coherent states that describe the light emitted by a laser [3]. Through nonlinear processes, it is possible to reduce the noise beyond the shot noise limit (at the price of increased noise in a complementary observable), and create squeezed states [12–17]. For the purpose of metrology, such squeezed states are often enough to obtain a significant boost in performance [18–21].

On theoretical grounds, Gaussian states are relatively easy to handle [8,9]. The quantum statistics of the continuous-variable observables (e.g., the quadratures in quantum optics) are described by Gaussian Wigner functions. All interesting quantum features can be deduced from the covariance matrix that characterises this Gaussian distribution on phase space. Hence, whenever the number of modes remains finite, the techniques of symplectic matrix analysis are sufficient to study Gaussian quantum states. This has generated an extensive understanding of the entanglement properties of Gaussian states [22–27], and recently it has also led to the development of a measure for quantum steering (see [28]) of Gaussian states with Gaussian measurements [29–32], which we refer to as Einstein-Podolsky-Rosen (EPR) steering.

Even though they have many advantages, Gaussian states are of limited use to quantum technologies beyond sensing. They have been shown to be easily simulated on classical devices [33], and in particular Wigner negativity is known to be a necessary resource for reaching a quantum computation advantage [34]. However, it should be stressed that recent work has found large classes of Wigner negative states that can also be simulated easily [35]. In other words, Wigner negativity is necessary but not sufficient to reach a quantum computation advantage [36].

In the particular case of CV quantum computation, Gaussian states play an essential role in the measurement-based approach [37]. In this paradigm, one establishes large Gaussian entangled states, known as cluster states, which form the backbone of the desired quantum routine [38]. Several recent breakthroughs have led to the experimental realisation of such states [39–43]. Nevertheless, to execute quantum algorithms that cannot be simulated efficiently, one must induce Wigner negativity. In the spirit of measurement-based quantum computation, this feature is induced by measuring non-Gaussian observables, e.g., the number of photons, on a subset of modes [44–47]. Such a measurement then projects the remainder of the system into a non-Gaussian state. The exact properties of the resulting state depend strongly on the result of the measurement.

The conditional preparation of non-Gaussian quantum states is common procedure in quantum optics experiments [48]. Basic examples include the heralding of single-photon Fock states after parametric down-conversion [49–51], photon addition and subtraction [52–57], and known schemes to prepare more exotic states such as Schrödinger-cat [58,59] or Gottesman-Kitaev-Preskill states [60]. It should be noted that conditioning on the measurement of Gaussian observables can also be relevant in certain protocols [61]. Remarkably, though, a practical framework to describe the effect of arbitrary conditional operations on arbitrary Gaussian states is still lacking. Notable

*mattia.walschaers@lkb.upmc.fr

exceptions where one does study arbitrary initial states usually rely on specific choices for the conditional measurement.

Here, in Sec. III, we introduce a practical framework to describe the resulting Wigner function for a quantum state that is conditionally prepared by measuring a subset of modes of a Gaussian multimode state. The techniques used in this work are largely based on classical multivariate probability theory and provide a conceptually new understanding of these conditioned states. In Sec. IV, we unveil the most striking consequence of this new framework: we can formally prove that EPR steering in the initial Gaussian state is a necessary requirement for the conditional preparation of Wigner-negative states, regardless of the measurement upon which we condition. This solidifies a previously conjectured general connection between EPR steering and Wigner negativity. As shown in Sec. V, our framework reproduces a range of known state-preparation schemes and can be used to treat more advanced scenarios, which could thus far not be addressed by other analytical methods. First, however, we review the phase-space description of multimode CV systems in Sec. II.

II. PHASE-SPACE DESCRIPTION OF MULTIMODE CONTINUOUS-VARIABLE SYSTEMS

The CV approach studies quantum systems with an infinite-dimensional Hilbert space $\mathcal{H}$ based on observables, $\hat{x}$ and $\hat{p}$, that have a continuous spectrum and obey the canonical commutation relation $[\hat{x},\hat{p}] = 2i$ (the factor 2 is chosen to normalise the vacuum noise to 1). Common examples include the position and momentum operators in mechanical systems, or the amplitude and phase quadratures in quantum optics. In this work, we use quantum optics terminology, but the results equally apply to any other system that is described by the algebra of canonical commutation relations (i.e., any bosonic system).

In a single-mode system, the quadrature observables $\hat{x}$ and $\hat{p}$ determine the optical phase space. The latter is a two-dimensional real space, where the axes denote the possible measurement outcomes for $\hat{x}$ and $\hat{p}$. It is common practice to represent a given state $\hat{\rho}$ by means of its measurement statistics for $\hat{x}$ and $\hat{p}$ on this optical phase space, as in statistical physics. However, because $\hat{x}$ and $\hat{p}$ are complementary observables, they cannot be measured simultaneously, and thus, *a priori*, we cannot construct a joint probability distribution of phase space that reproduces the correct marginals to describe the measurement statistics of the quadratures. Therefore, the phase-space representation of quantum states are quasiprobability distributions. The quasiprobability distribution that reproduces the measurement statistics of the quadrature observables as its marginals is known as the Wigner function [62–64]

$$W(x,p) = \frac{1}{(2\pi)^2}\int_{\mathbb{R}^2} \mathrm{tr}[\hat{\rho}e^{i(\alpha_1\hat{x}+\alpha_2\hat{p})}]e^{-i(\alpha_1 x+\alpha_2 p)}\,d\alpha_1\,d\alpha_2. \tag{1}$$

For some quantum states, this function has the peculiar property of reaching negative values. This Wigner negativity is a genuine hallmark of quantum physics, and it is understood to be crucial in reaching a quantum computational advantage.

Here, we consider a multimode system comprising m modes. Every mode comes with its own infinite-dimensional Hilbert space, associated to a two-dimensional phase space, and observables $\hat{x}_j$ and $\hat{p}_j$. The total optical phase space is, thus, a real space $\mathbb{R}^{2m}$ with a symplectic structure $\Omega = \bigoplus_m \omega$, where the two-dimensional matrix ω is given by

$$\omega = \begin{pmatrix} 0 & -1 \\ 1 & 0 \end{pmatrix}. \tag{2}$$

Therefore, Ω has the properties $\Omega^2 = -\mathbb{1}$ and $\Omega^T = -\Omega$. Any normalised vector $\vec{f} \in \mathbb{R}^{2m}$ defines a single optical mode with an associated phase space $\mathrm{span}\{\vec{f}, \Omega\vec{f}\}$ (i.e., when $\vec{f}$ generates the phase-space axis associated with the amplitude quadrature of this mode, $\Omega\vec{f}$ generates the axis for the associated phase quadrature). Henceforth, we refer to the subsystem associated with the phase-space $\mathrm{span}\{\vec{f}, \Omega\vec{f}\}$ as "the mode f". Every point $\vec{\alpha} \in \mathbb{R}^{2m}$ can also be associated with a generalised quadrature observable

$$\hat{q}(\vec{\alpha}) = \sum_{k=1}^{m}(\alpha_{2k-1}\hat{x}_k + \alpha_{2k}\hat{p}_k). \tag{3}$$

These observables satisfy the general canonical commutation relation $[\hat{q}(\vec{\alpha}), \hat{q}(\vec{\beta})] = -i\vec{\alpha}^T\Omega\vec{\beta}$. Physically, such observable $\hat{q}(\vec{\alpha})$ can be measured with a homodyne detector by selecting the mode that is determined by the direction of $\vec{\alpha}$, and multiplying the detector outcome by $\|\vec{\alpha}\|$. In our theoretical treatment, such generalised quadratures are useful to define the quantum characteristic function of any multimode state $\hat{\rho}$,

$$\chi_{\hat{\rho}}(\vec{\alpha}) = \mathrm{tr}[\hat{\rho}\,\exp\{i\hat{q}(\vec{\alpha})\}] \tag{4}$$

for an arbitrary point $\vec{\alpha}$ in phase space. The multimode Wigner function of the state is then obtained as the Fourier transform of the characteristic function

$$W(\vec{x}) = \frac{1}{(2\pi)^{2m}}\int_{\mathbb{R}^{2m}} \chi_{\hat{\rho}}(\vec{\alpha})e^{-i\vec{\alpha}^T\vec{x}}\,d\vec{\alpha}, \tag{5}$$

where $\vec{x} \in \mathbb{R}^{2m}$ can, again, be any point in the multimode phase space, and the coordinates of $\vec{x}$ represent possible measurement outcomes for $\hat{x}_j$ and $\hat{p}_j$.

The Wigner function can be used to represent and characterise an arbitrary quantum state of the multimode system. In the same spirit, we can also define the phase-space representation of an arbitrary observable $\hat{A}$ as

$$W_{\hat{A}}(\vec{x}) = \frac{1}{(2\pi)^{2m}} \int_{\mathbb{R}^{2m}} \mathrm{tr}[\hat{A} \exp\{i\hat{q}(\vec{\alpha})\}] e^{-i\vec{\alpha}^T \vec{x}}\, d\vec{\alpha}, \quad (6)$$

such that we can fully describe the measurement statistics of an arbitrary quantum observable on phase space, by invoking the identity

$$\mathrm{tr}[\hat{\rho}\hat{A}] = (4\pi)^m \int_{\mathbb{R}^{2m}} W_{\hat{A}}(\vec{x}) W(\vec{x})\, d\vec{x} \quad (7)$$

to evaluate expectation values. In practice, it is often challenging to obtain Wigner functions for arbitrary states or observables, but in some cases they can take convenient forms.

A particular class of convenient states are Gaussian states, where the Wigner function $W(\vec{x})$ is a Gaussian. As a consequence, the Wigner function is positive, and can thus be interpreted as a probability distribution. This Gaussian distribution is completely determined by a covariance matrix V, and mean field $\vec{\xi}$, such that the Wigner function takes the form

$$W(\vec{x}) = \frac{e^{-(1/2)(\vec{x}-\vec{\xi})^T V^{-1} (\vec{x}-\vec{\xi})}}{(2\pi)^m \sqrt{\det V}}. \quad (8)$$

This forms the basis of our preparation procedure for non-Gaussian states as we assume that our initial multimode system is prepared in such a Gaussian state.

To perform the conditional state preparation, we divide the m-mode system into two subsets of orthogonal modes, $\mathbf{f} = \{f_1, \ldots, f_l\}$ and $\mathbf{g} = \{g_1, \ldots, g_{l'}\}$ with $l + l' = m$, and perform a measurement on the modes in $\mathbf{g}$. We can then describe the subsystems of modes $\mathbf{f}$ and $\mathbf{g}$ by phase spaces $\mathbb{R}^{2l}$ and $\mathbb{R}^{2l'}$, respectively. As such, the joint phase space can be mathematically decomposed as $\mathbb{R}^{2m} = \mathbb{R}^{2l} \oplus \mathbb{R}^{2l'}$. A general point $\vec{x}$ in the multimode phase space $\mathbb{R}^{2m}$ can thus be decomposed as $\vec{x} = \vec{x}_{\mathbf{f}} \oplus \vec{x}_{\mathbf{g}}$, where $\vec{x}_{\mathbf{f}}$ and $\vec{x}_{\mathbf{g}}$ describe the phase-space coordinates associated with the sets of modes $\mathbf{f}$ and $\mathbf{g}$, respectively. In particular, $\vec{x}_{\mathbf{f}}$ can be expanded in a particular modes basis $f_1, \ldots, f_l$ as $\vec{x}_{\mathbf{f}} = (x_{f_1}, p_{f_1}, \ldots, x_{f_l}, p_{f_l})$, where the coordinates x_{f_j} and p_{f_j} are obtained as

$$x_{f_j} = \vec{x}^T \vec{f}_j, \quad (9)$$

$$p_{f_j} = \vec{x}^T \Omega \vec{f}_j. \quad (10)$$

A completely analogous treatment is possible for the coordinates associated with the set of modes $\mathbf{g}$.

III. CONDITIONAL OPERATIONS IN PHASE SPACE

In quantum optics, we associate a Hilbert space (more precisely, a Fock space) to each of these modes. The Hilbert space $\mathcal{H}$ of the entire system can then be structured as $\mathcal{H} = \mathcal{H}_{\mathbf{f}} \otimes \mathcal{H}_{\mathbf{g}}$, where $\mathcal{H}_{\mathbf{f}}$ ($\mathcal{H}_{\mathbf{g}}$) describes the quantum states of the set of orthogonal modes $\mathbf{f}$ ($\mathbf{g}$). Formally, the state of our full m-mode system is then described by a density matrix $\hat{\rho}$ that acts on $\mathcal{H}$.

Within this manuscript, we perform a conditional operation in the set of modes $\mathbf{g}$, which we describe through a (not necessarily normalised) set of Kraus operators [65] $\hat{X}_j$ that act on $\mathcal{H}_{\mathbf{g}}$ [66]:

$$\hat{\rho} \mapsto \frac{\sum_j \hat{X}_j \hat{\rho} \hat{X}_j^\dagger}{\mathrm{tr}[\sum_j \hat{X}_j^\dagger \hat{X}_j \hat{\rho}]}. \quad (11)$$

Such a conditional operation naturally arises as a post-measurement state, when $\hat{X}_j$ is a projector, or when $\hat{A} = \sum_j \hat{X}_j^\dagger \hat{X}_j$ is a more general positive operator-valued measure (POVM) element, as represented in the sketch in Fig. 1. The positive semidefinite operator $\hat{A}$ is useful to express the reduced state of the set of modes $\mathbf{f}$:

$$\hat{\rho}_{\mathbf{f}|\hat{A}} = \frac{\mathrm{tr}_{\mathbf{g}}[\hat{A}\hat{\rho}]}{\mathrm{tr}[\hat{A}\hat{\rho}]}. \quad (12)$$

Here $\mathrm{tr}_{\mathbf{g}}$ denotes the partial trace of the Hilbert space $\mathcal{H}_{\mathbf{g}}$ associated with the set of mode $\mathbf{g}$. Our general goal is to understand the properties of the state $\hat{\rho}_{\mathbf{f}|\hat{A}}$.

As we are interested in the Wigner function for the state of the subset of modes $\mathbf{f}$, we translate Eq. (12) to its phase-space representation. We initialize the total system in a Gaussian state with Wigner function $W(\vec{x})$. Subsequently, we also define the Wigner function $W_{\hat{A}}(\vec{x}_{\mathbf{g}})$ of the positive operator $\hat{A}$, which is a function that is defined according to Eq. (6) on the phase space that describes the subset of modes $\mathbf{g}$. As such, we find that

$$W_{\mathbf{f}|\hat{A}}(\vec{x}_{\mathbf{f}}) = \frac{\int_{\mathbb{R}^{2l'}} W_{\hat{A}}(\vec{x}_{\mathbf{g}}) W(\vec{x})\, d\vec{x}_{\mathbf{g}}}{\int_{\mathbb{R}^{2m}} W_{\hat{A}}(\vec{x}_{\mathbf{g}}) W(\vec{x})\, d\vec{x}}. \quad (13)$$

Because $\hat{A}$ is a positive semidefinite operator, the denominator is a positive constant.

As presented in Eq. (13), the Wigner function $W_{\mathbf{f}|\hat{A}}(\vec{x}_{\mathbf{f}})$ is impractical to use and its properties are not apparent. Hence, we now introduce some mathematical tools to obtain a more insightful expression for $W_{\mathbf{f}|\hat{A}}(\vec{x}_{\mathbf{f}})$. First, we use the fact that, for Gaussian states, $W(\vec{x})$ is a probability distribution on phase space, such that we can define the

conditional probability distribution through

$$W(\vec{x}_{\mathbf{g}} \mid \vec{x}_{\mathbf{f}}) = \frac{W(\vec{x})}{W_{\mathbf{f}}(\vec{x}_{\mathbf{f}})}, \tag{14}$$

where $W_{\mathbf{f}}(\vec{x}_{\mathbf{f}})$ is the reduced Gaussian state for the set of modes $\mathbf{f}$,

$$W_{\mathbf{f}}(\vec{x}_{\mathbf{f}}) = \int_{\mathbb{R}^{2l'}} W(\vec{x})\, d\vec{x}_{\mathbf{g}}. \tag{15}$$

Because $W(\vec{x})$ is a Gaussian probability distribution, the conditional probability distribution $W(\vec{x}_{\mathbf{g}} \mid \vec{x}_{\mathbf{f}})$ is also a Gaussian distribution [67] given by

$$W(\vec{x}_{\mathbf{g}} \mid \vec{x}_{\mathbf{f}}) = \frac{\exp[-(1/2)(\vec{x}_{\mathbf{g}} - \vec{\xi}_{\mathbf{g}|\vec{x}_{\mathbf{f}}})^T V_{\mathbf{g}|\vec{x}_{\mathbf{f}}}^{-1}(\vec{x}_{\mathbf{g}} - \vec{\xi}_{\mathbf{g}|\vec{x}_{\mathbf{f}}})]}{(2\pi)^{l'}\sqrt{\det V_{\mathbf{g}|\vec{x}_{\mathbf{f}}}}} \tag{16}$$

with covariance matrix

$$V_{\mathbf{g}|\vec{x}_{\mathbf{f}}} = V_{\mathbf{g}} - V_{\mathbf{gf}} V_{\mathbf{f}}^{-1} V_{\mathbf{gf}}^T, \tag{17}$$

where $V_{\mathbf{g}}$ and $V_{\mathbf{f}}$ are the covariance matrices describing the subsets of modes $\mathbf{g}$ and $\mathbf{f}$ in the initial state, whereas $V_{\mathbf{gf}}$ describes all the initial Gaussian correlations between those subsets. Note that this covariance matrix is the same for all points $\vec{x}_{\mathbf{f}} \in \mathbb{R}^{2l}$, which is a particular property of Gaussian conditional probability distributions. Furthermore, the distribution $W(\vec{x}_{\mathbf{g}} \mid \vec{x}_{\mathbf{f}})$ also contains a displacement

$$\vec{\xi}_{\mathbf{g}|\vec{x}_{\mathbf{f}}} = \vec{\xi}_{\mathbf{g}} + V_{\mathbf{gf}} V_{\mathbf{f}}^{-1}(\vec{x}_{\mathbf{f}} - \vec{\xi}_{\mathbf{f}}), \tag{18}$$

where $\vec{\xi}_{\mathbf{g}}$ and $\vec{\xi}_{\mathbf{f}}$ describe the displacements of the initial state in the sets of modes $\mathbf{g}$ and $\mathbf{f}$, respectively.

Generally, the phase-space probability distribution $W(\vec{x}_{\mathbf{g}} \mid \vec{x}_{\mathbf{f}})$ is not a valid Wigner function of a well-defined quantum state, in the sense that it would violate the Heisenberg inequality. However, it does remain a well-defined probability distribution, i.e., it is normalised and positive. Thus, it still has interesting properties that we can exploit to formulate a general expression for $W_{\mathbf{f}|\hat{A}}(\vec{x}_{\mathbf{f}})$. Let us first use Eq. (14) to recast Eq. (13) in the following form:

$$W_{\mathbf{f}|\hat{A}}(\vec{x}_{\mathbf{f}}) = \frac{\int_{\mathbb{R}^{2l'}} W_{\hat{A}}(\vec{x}_{\mathbf{g}}) W(\vec{x}_{\mathbf{g}} \mid \vec{x}_{\mathbf{f}}) W_{\mathbf{f}}(\vec{x}_{\mathbf{f}})\, d\vec{x}_{\mathbf{g}}}{\int_{\mathbb{R}^{2m}} W_{\hat{A}}(\vec{x}_{\mathbf{g}}) W(\vec{x})\, d\vec{x}} \tag{19}$$

$$= \frac{[\int_{\mathbb{R}^{2l'}} W_{\hat{A}}(\vec{x}_{\mathbf{g}}) W(\vec{x}_{\mathbf{g}} \mid \vec{x}_{\mathbf{f}})\, d\vec{x}_{\mathbf{g}}] W_{\mathbf{f}}(\vec{x}_{\mathbf{f}})}{\int_{\mathbb{R}^{2m}} W_{\hat{A}}(\vec{x}_{\mathbf{g}}) W(\vec{x})\, d\vec{x}}. \tag{20}$$

Subsequently, we can define

$$\langle \hat{A} \rangle_{\mathbf{g}|\vec{x}_{\mathbf{f}}} = (4\pi)^{l'} \int_{\mathbb{R}^{2l'}} W_{\hat{A}}(\vec{x}_{\mathbf{g}}) W(\vec{x}_{\mathbf{g}} \mid \vec{x}_{\mathbf{f}})\, d\vec{x}_{\mathbf{g}}, \tag{21}$$

which is the expectation value of the phase-space representation of $\hat{A}$ with respect to the probability distribution $W(\vec{x}_{\mathbf{g}} \mid \vec{x}_{\mathbf{f}})$. Similarly, we can use Eq. (7) to introduce the notation

$$\langle \hat{A} \rangle = \mathrm{tr}[\hat{A}\hat{\rho}] = (4\pi)^{l'} \int_{\mathbb{R}^{2m}} W_{\hat{A}}(\vec{x}_{\mathbf{g}}) W(\vec{x})\, d\vec{x} \tag{22}$$

for the expectation value of $\hat{A}$ in the state ρ. Finally, we can use Eqs. (21) and (22) to recast Eq. (20) in the form

$$W_{\mathbf{f}|\hat{A}}(\vec{x}_{\mathbf{f}}) = \frac{\langle \hat{A} \rangle_{\mathbf{g}|\vec{x}_{\mathbf{f}}}}{\langle \hat{A} \rangle} W_{\mathbf{f}}(\vec{x}_{\mathbf{f}}). \tag{23}$$

The major advantage of this formulation is that $\langle \hat{A} \rangle_{\mathbf{g}|\vec{x}_{\mathbf{f}}}$ represents the average with respect to a Gaussian probability distribution, such that one can use several computational techniques that are well known for Gaussian integrals. A notable property is the factorisation of higher moments in multivariate Gaussian distributions, such that $\langle \hat{A} \rangle_{\mathbf{g}|\vec{x}_{\mathbf{f}}}$ can generally be expressed algebraically in terms of the components of $V_{\mathbf{g}|\vec{x}_{\mathbf{f}}}$ and $\vec{\xi}_{\mathbf{g}|\vec{x}_{\mathbf{f}}}$ (for more details, see the Appendix).

Finally, we remark that $\langle \hat{A} \rangle_{\mathbf{g}|\vec{x}_{\mathbf{f}}} = \langle \hat{A} \rangle$ in the absence of correlations between the set of modes $\mathbf{g}$ that are conditioned upon and the set of modes $\mathbf{f}$ for which we construct the reduced state. This result is directly responsible for the previously obtained results related to the spread of non-Gaussian features in cluster states [68].

IV. EINSTEIN-PODOLSKY-ROSEN STEERING AND WIGNER NEGATIVITY

When two systems are connected through a quantum correlation, one can, in some cases, perform quantum steering [28]. Colloquially, we say that a subsystem $\mathcal{X}$ can steer a subsystem $\mathcal{Y}$ when measurements of certain observables in $\mathcal{X}$ can influence the conditional measurement statistics of observables in $\mathcal{Y}$ beyond what is possible with classical correlations. Ultimately, in quantum steering one studies properties of conditional quantum states as compared to a local hidden variable model for any observables X and Y, acting on $\mathcal{X}$ and $\mathcal{Y}$, respectively. Contrary to the case of Bell nonlocality, quantum steering considers an asymmetric local hidden variable model:

$$P(X = x, Y = y) = \sum_{\lambda} P(\lambda) P(X = x \mid \lambda) P_Q(Y = y \mid \lambda). \tag{24}$$

Here one assumes that the probability distributions $P_Q(Y = y \mid \lambda)$ of steered party $\mathcal{Y}$ follow the laws of quantum mechanics. For the party $\mathcal{X}$, which performs the steering, no such assumption is made and any probability distribution is allowed. Such a local hidden variable model can typically be falsified, either by brute force computational methods [69] or via witnesses [70]. These methods have

been applied in a variety of contexts to experimentally observe quantum steering [31,32,71–77].

A paradigmatic example is found when performing homodyne measurements on the EPR state [78]: when the entanglement in the system is sufficiently strong, one can condition the $\hat{x}$ and $\hat{p}$ quadrature measurements in $\mathcal{Y}$ on the outcome of the same quadrature measurement in $\mathcal{X}$. The obtained conditional probability distributions for the quadrature measurements in $\mathcal{Y}$ can violate the Heisenberg inequality, even when averaged over all measurement outcomes in $\mathcal{X}$. The violations of such a conditional inequality are impossible with classical correlations, but are a hallmark of quantum steering.

Quantum steering can occur in all types of quantum states, with all kinds of measurements. In CV quantum physics, one often refers to the particular case of Gaussian states that can be steered through Gaussian measurements as EPR steering. Recently, other forms of steering for Gaussian states have been developed under the name of nonclassical steering [79]. In this approach, one checks whether Gaussian measurements in $\mathcal{X}$ can induce a nonclassical conditional state in $\mathcal{Y}$. Throughout this work, the focus lies on EPR steering, where the systems $\mathcal{X}$ and $\mathcal{Y}$ are the sets of modes **f** and **g**, respectively.

In previous work, we showed that EPR steering is a necessary prerequisite to remotely generate Wigner negativity through photon subtraction [80]. More precisely, when a photon is subtracted in a mode g, the reduced state Wigner function of a correlated mode f can only be nonpositive if mode f is able to steer mode g. When one allows for an additional Gaussian transformation on mode g prior to photon subtraction, we found that EPR steering from f to g is also a sufficient condition to reach Wigner negativity in mode f.

The formalism that is developed in the previous section allows us to generalize this previous result to arbitrary conditional operations on an arbitrary number of modes.

Theorem 1. *For any initial Gaussian state $\hat{\rho}$ and any conditional operation $\hat{A}$ in Eq. (12), EPR steering between the set of modes* **f** *and the set of modes* **g** *is necessary to induce Wigner negativity in $W_{\mathbf{f}|\hat{A}}(\vec{x}_\mathbf{f})$.*

Proof. Gaussian EPR steering is generally quantified through the properties of $V_{\mathbf{g}|\vec{x}_\mathbf{f}}$. In particular, one can show that the set of modes in **f** can jointly steer the set of modes **g** if and only if $V_{\mathbf{g}|\vec{x}_\mathbf{f}}$ violates the Heisenberg inequality [29,30]. The crucial consequence is that $W(\vec{x}_\mathbf{g} \mid \vec{x}_\mathbf{f})$, as given by Eq. (16), is itself a well-defined Gaussian quantum state when the modes in **f** *cannot* steer the modes **g**. For all possible $\vec{x}_\mathbf{f}$, we can thus associate this Gaussian quantum state with a density matrix $\hat{\rho}_{\mathbf{g}|\vec{x}_\mathbf{f}}$.

The crucial observation is that $\langle\hat{A}\rangle_{\mathbf{g}|\vec{x}_\mathbf{f}}$, as defined in Eq. (21), is the expectation value of $\hat{A}$ in a well-defined quantum state $\rho_{\mathbf{g}|\vec{x}_\mathbf{f}}$ for any $\vec{x}_\mathbf{f}$. Because $\hat{A}$ is a positive semidefinite operator, we directly find that

$$\langle\hat{A}\rangle_{\mathbf{g}|\vec{x}_\mathbf{f}} = \mathrm{tr}[\rho_{\mathbf{g}|\vec{x}_\mathbf{f}}\hat{A}] \geqslant 0 \quad \text{for all } \vec{x}_\mathbf{f} \in \mathbb{R}^{2l}. \tag{25}$$

Therefore, the overall conditional Wigner function $W_{\mathbf{f}|\hat{A}}(\vec{x}_\mathbf{f})$ in Eq. (23) is non-negative. We can only achieve $\langle\hat{A}\rangle_{\mathbf{g}|\vec{x}_\mathbf{f}} < 0$ for certain points $\vec{x}_\mathbf{f} \in \mathbb{R}^{2l}$ when $V_{\mathbf{g}|\vec{x}_\mathbf{f}}$ violates the Heisenberg inequality. This concludes that in absence of EPR steering $W_{\mathbf{f}|\hat{A}}(\vec{x}_\mathbf{f}) \geqslant 0$. ■

Note that the steps in this proof rely heavily on the fact that the initial state is Gaussian. For other types of quantum states, we cannot directly relate quantum steering to the properties of $W(\vec{x}_\mathbf{g} \mid \vec{x}_\mathbf{f})$.

V. EXAMPLES

A. Heralding

In the first example, we consider a scenario where a photon-number-resolving measurement is performed on one of the output modes, which can be considered a special case of the situation considered in Ref. [47]. Heralding is ubiquitous in quantum optics, as it is one of the most common tools to generate single-photon Fock states [49–51].

To study heralding, we use Eq. (23) where a measurement of the number of photons n in a single mode g is performed. We assume that this measurement is optimal, and, thus, that we project on a Fock state $|n\rangle$. In this case, we set $\hat{A} = |n\rangle\langle n|$, and therefore we obtain

$$W_{\hat{A}}(\vec{x}_g) = \sum_{k=0}^{n} \binom{n}{k} \frac{(-1)^{n+k}\|\vec{x}_g\|^{2k}}{k!} \frac{e^{-(1/2)\|\vec{x}_g\|^2}}{2\pi}, \tag{26}$$

where we used the closed form of the Laguerre polynomial. Hence, we can now use this expression to calculate $\langle|n\rangle\langle n|\rangle_{g|\vec{x}_\mathbf{f}}$. In this calculation, we must evaluate

$$W_{\hat{A}}(\vec{x}_g)W(\vec{x}_g \mid \vec{x}_\mathbf{f}) = \sum_{k=0}^{n} \binom{n}{k} \frac{(-1)^{n+k}\|\vec{x}_g\|^{2k}}{k!} \frac{\exp[-(1/2)(\vec{x}_g - \vec{\xi}_{g|\vec{x}_\mathbf{f}})^T V_{g|\vec{x}_\mathbf{f}}^{-1}(\vec{x}_g - \vec{\xi}_{g|\vec{x}_\mathbf{f}}) - \|\vec{x}_g\|^2]/2}{4\pi^2\sqrt{\det V_{g|\vec{x}_\mathbf{f}}}}, \tag{27}$$

and we can recast

$$\exp\left[-\tfrac{1}{2}(\vec{x}_g-\vec{\xi}_{g|\vec{x}_\mathbf{f}})^T V_{g|\vec{x}_\mathbf{f}}^{-1}(\vec{x}_g-\vec{\xi}_{g|\vec{x}_\mathbf{f}})-\tfrac{1}{2}\|\vec{x}_g\|^2\right] = e^{-(1/2)[(\mathbb{1}+V_{g|\vec{x}_\mathbf{f}})\vec{x}_g-\vec{\xi}_{g|\vec{x}_\mathbf{f}}]^T[V_{g|\vec{x}_\mathbf{f}}(\mathbb{1}+V_{g|\vec{x}_\mathbf{f}})]^{-1}[(\mathbb{1}+V_{g|\vec{x}_\mathbf{f}})\vec{x}_g-\vec{\xi}_{g|\vec{x}_\mathbf{f}}]} \times e^{-(1/2)\vec{\xi}_{g|\vec{x}_\mathbf{f}}^T[\mathbb{1}+V_{g|\vec{x}_\mathbf{f}}]^{-1}\vec{\xi}_{g|\vec{x}_\mathbf{f}}}. \tag{28}$$

After a substitution in the integral, we then find that

$$\langle|n\rangle\langle n|\rangle_{g|\vec{x}_\mathbf{f}} = 2\det(\mathbb{1}+V_{g|\vec{x}_\mathbf{f}})^{-1/2} e^{-(1/2)\vec{\xi}_{g|\vec{x}_\mathbf{f}}^T[\mathbb{1}+V_{g|\vec{x}_\mathbf{f}}]^{-1}\vec{\xi}_{g|\vec{x}_\mathbf{f}}} \sum_{k=0}^{n}\binom{n}{k}\frac{(-1)^{n+k}}{k!} \times \int_{\mathbb{R}^2}\frac{\|(\mathbb{1}+V_{g|\vec{x}_\mathbf{f}})^{-1}\vec{x}_g\|^{2k} e^{-(1/2)(\vec{x}_g-\vec{\xi}_{g|\vec{x}_\mathbf{f}})^T\sigma^{-1}(\vec{x}_g-\vec{\xi}_{g|\vec{x}_\mathbf{f}})}}{2\pi\sqrt{\det\sigma}}\,d\vec{x}_g, \tag{29}$$

where we defined $\sigma = V_{g|\vec{x}_\mathbf{f}}(\mathbb{1}+V_{g|\vec{x}_\mathbf{f}})$, which is now the covariance matrix of a new Gaussian probability distribution. The final expression is then determined by the moments of the Gaussian distribution with covariance matrix σ and displacement $\vec{\xi}_{g|\vec{x}_\mathbf{f}}$. Even though this expression is relatively elegant, it can be remarkably tedious to compute for larger values of n.

First, let us focus on the experimentally relevant case where $n=1$ as an illustration. The evaluation of Eq. (29) is than conducted by calculating the second moments of a Gaussian distribution, such that we ultimately find that

$$W_{\mathbf{f}|\,|1\rangle\langle 1|}(\vec{x}_\mathbf{f}) = \left\{\|(\mathbb{1}+V_{g|\vec{x}_\mathbf{f}})^{-1}\vec{\xi}_{g|\vec{x}_\mathbf{f}}\|^2+\mathrm{tr}[(\mathbb{1}+V_{g|\vec{x}_\mathbf{f}})^{-1}V_{g|\vec{x}_\mathbf{f}}]-1\right\} \times \frac{\det(\mathbb{1}+V_g)^{1/2}}{\det(\mathbb{1}+V_{g|\vec{x}_\mathbf{f}})^{1/2}}\frac{e^{-(1/2)\vec{\xi}_{g|\vec{x}_\mathbf{f}}^T[\mathbb{1}+V_{g|\vec{x}_\mathbf{f}}]^{-1}\vec{\xi}_{g|\vec{x}_\mathbf{f}}}}{\mathrm{tr}[(\mathbb{1}+V_g)^{-1}V_g]-1}W_\mathbf{f}(\vec{x}_\mathbf{f}), \tag{30}$$

where we set $\vec{\xi}_g=0$, thus assuming that there is no mean field in mode g. We note that this function reaches negative values if and only if $\mathrm{tr}[(\mathbb{1}+V_{g|\vec{x}_\mathbf{f}})^{-1}V_{g|\vec{x}_\mathbf{f}}]<1$. Using Williamson's decomposition, as we did in Ref. [80], it can be shown that this condition can only be fulfilled when the set of modes $\mathbf{f}$ can perform EPR steering in mode g, or, in other words, when $V_{g|\vec{x}_\mathbf{f}}$ violates the Heisenberg inequality. This is exactly what we can expect from our general result in Sec. IV.

In general, we know that the Wigner function (23) can only be negative when $V_{g|\vec{x}_\mathbf{f}}$ is not a covariance matrix of a well-defined quantum state. However, determining the existence of zeroes of this Wigner function is a cumbersome task. For heralding with $n>1$, we therefore restrict to numerical simulations using a specific initial state.

This specific initial state is generated by mixing two squeezed thermal states on a balance beam splitter, where one of the output modes will serve as f, and the other as g. In the limiting case where the initial thermal noise vanishes, we recover the well-known EPR state that manifests perfect photon-number correlations between modes f and g. In this case, it is clear that a detection of n photons in mode g will herald the state $|n\rangle$ in mode f. However, by introducing thermal noise, the photon-number correlations fade and the properties of the heralded state in mode f are less clear. Thermal noise will also gradually reduce the EPR steering in the system, such that the Wigner negativity in mode f will vanish when the thermal noise becomes too strong. Hence, with this example we can study the interplay between Wigner negativity and EPR steering in a controlled setting.

The squeezed thermal state is characterised by a covariance matrix $V=\mathrm{diag}[\delta/s,\delta s]$, where δ denotes the amount of initial thermal noise, and s is the squeezing parameter. We initially start with two copies of such a state, and

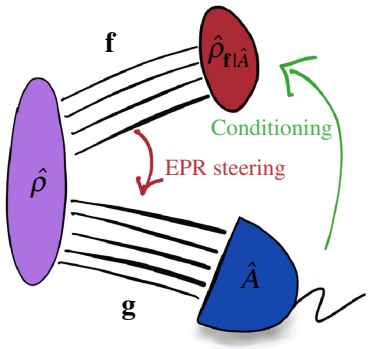

FIG. 1. Sketch of the conditional state-preparation scenario: a multimode quantum state with density matrix $\hat{\rho}$ is separated over two subsets of modes, $\mathbf{f}$ and $\mathbf{g}$. A measurement is performed on the modes in $\mathbf{g}$, yielding a result associated with a POVM element $\hat{A}$. Conditioning on this measurement outcome "projects" the subset of mode $\mathbf{f}$ into a state $\hat{\rho}_{\mathbf{f}|\hat{A}}$. The directional EPR steering, discussed in Sec. IV, is highlighted.

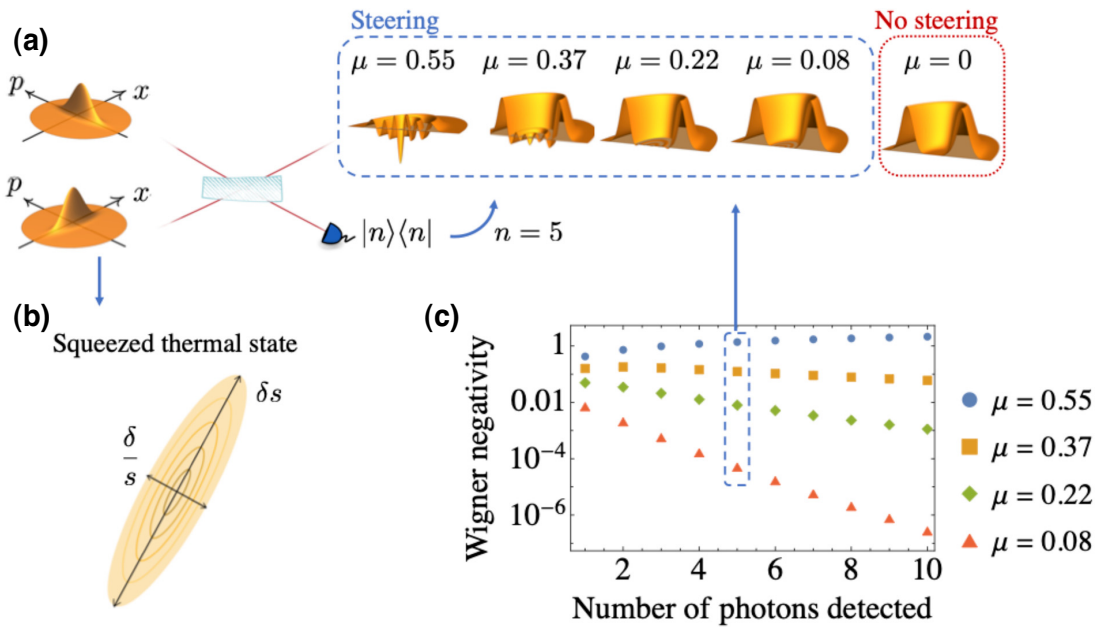

FIG. 2. Photon heralding with a particular Gaussian input state, generated by mixing two equal squeezed thermal states (b) on a balanced beam splitter (a). On one of the outputs of the beam splitter, a projective measurement is performed on the Fock state $|n\rangle$, which heralds a non-Gaussian state in the other mode. The Wigner functions of this non-Gaussian state are shown for the case where $n = 5$, with varying degrees of EPR steering μ, controlled by varying the thermal noise δ for a fixed squeezing $s = 5$ dB. The Wigner negativity, measured by $\mathcal{N}$ given in Eq. (32), is shown in (c) for varying degrees of EPR steering and a varying number of measured photons n.

rotate the phase of one of them by $\pi/2$ (see Fig. 2). When both modes are mixed on a beam splitter, the resulting state manifests EPR steering depending on parameters δ and s, which can be quantified through [30]

$$\mu = \max\left\{0, -\tfrac{1}{2}\log\det V_{g|\vec{x}_f}\right\}, \tag{31}$$

where we explicitly use the fact that $V_{g|\vec{x}_f}$ is a two-dimensional matrix. When we then postselect on the number of photons, n, measured in one output mode, we herald a conditional non-Gaussian state in the other mode. In Fig. 2, we show the resulting Wigner functions for the case where the detected number of photons is $n = 5$. When the amount of EPR steering is varied (note that $\mu = 0.55$ corresponds to the pure state), we see that the resulting Wigner function rapidly loses Wigner negativity. In full agreement with our general result of the previous section, we also find that the Wigner negativity vanishes when there is no EPR steering.

A more quantitative study of the Wigner negativity can be found in panel (c) of Fig. 2, where we vary both the amount of steering μ and the number of detected photons n. The Wigner negativity is measured by the quantity [81–83]

$$\mathcal{N} = \int_{\mathbb{R}^2} |W_{f|\hat{A}}(\vec{x}_f)|\, d\vec{x}_f - 1. \tag{32}$$

When the state is pure (here for $\mu = 0.55$), a detection of n photons in one mode herald a Fock state $|n\rangle$ in the other mode and the Wigner negativity thus increases with n. However, once the state is no longer pure and the steering decreases, we observe the existence of an optimal value n for which the maximal amount of Wigner negativity is obtained. For very weak EPR steering (e.g., $\mu = 0.08$ in this calculation), this optimal value is obtained for $n = 1$.

This numerical study shows the fruitfulness of our presented framework to study a very concrete heralding scheme. Furthermore, the example confirms the relationship between Gaussian EPR steering and Wigner negativity.

B. Photon-added and -subtracted states

Ideal photon addition and subtraction are defined by acting with a creation operator $\hat{a}^\dagger$ or annihilation operator $\hat{a}$, respectively, on the quantum state. In practice, these operations are often realised by using some form of heralding [52], which we treated in the previous example. However,

it tends to be more convenient to use the idealised model, based on creation and annihilation operators, and it has been shown experimentally that this model is highly accurate. This model also fits the conditional state framework of Eq. (11), where we set $\hat{X}_j$ to be a creation or annihilation operator.

In multimode systems, photon addition and subtraction have been considered for their entanglement properties, which sprouted a range of theoretical [84–91] and experimental [92–94] results. Many of the obtained theoretical results rely on the purity of the initial Gaussian state, and are hard to generalise to arbitrary Gaussian states. In recent years, there has been some progress in developing analytical tools to describe general photon subtracted states [91, 95], but it remains challenging to use these techniques to evaluate entanglement measures. Therefore, related questions have been investigated, such as, for example, the spread of non-Gaussian features in multimode systems [68,80,96,97].

The framework presented in this manuscript is particularly fruitful to investigate the spread of non-Gaussian features through photon addition or subtraction. We first show how the results of Ref. [80] can be recovered via Eq. (23). Then, we use the present framework to provide analytical results for the states that can be obtained by subtracting multiple photons in a multimode system.

1. Adding or subtracting a single photon

We start by studying the addition and subtraction of a single photon. The scenario for photon-subtracted states was studied in detail in Ref. [80] and our goal in this example is to show how these previous results can be obtained in the context of our present framework. Furthermore, we also study photon addition, which has not yet been considered in the context of the remote generation of Wigner negativity.

Creation and annihilation operators are by construction operators that act on a single mode g. In the single-photon scenario, we find the photon-subtracted state

$$\hat{\rho}_- = \frac{\hat{a}_g \hat{\rho} \hat{a}_g^\dagger}{\mathrm{tr}[\hat{n}_g \hat{\rho}]} \tag{33}$$

and the photon-added state

$$\hat{\rho}_+ = \frac{\hat{a}_g^\dagger \hat{\rho} \hat{a}_g}{\mathrm{tr}[(\hat{n}_g + \mathbb{1})\hat{\rho}]}. \tag{34}$$

These states clearly fit the framework of Eq. (11). In the context of Eq. (12), the reduced state of the set of modes $\mathbf{f}$ is obtained by choosing $\hat{A} = \hat{n}_g$ and $\hat{A} = \hat{n}_g + \mathbb{1}$ for photon subtraction and addition, respectively. We can then use Eq. (23) to obtain the Wigner function in the subset of modes $\mathbf{f}$, for which we must evaluate $\langle \hat{n}_g \rangle_{g|\vec{x}_\mathbf{f}}$. To this end, we evaluate the Wigner function of the number operator, which is given by

$$W_{\hat{n}_g}(\vec{x}_g) = \frac{1}{16\pi}(\|\vec{x}_g\|^2 - 2), \tag{35}$$

such that we directly find that

$$\langle \hat{n}_g \rangle_{g|\vec{x}_\mathbf{f}} = \tfrac{1}{4}(\mathrm{tr} V_{g|\vec{x}_\mathbf{f}} + \|\vec{\xi}_{g|\vec{x}_\mathbf{f}}\|^2 - 2), \tag{36}$$

where the dependence on $\vec{x}_\mathbf{f}$ comes from $\vec{\xi}_{g|\vec{x}_\mathbf{f}}$. Thus, we find that, for the photon-subtracted state,

$$W^-_{\mathbf{f}|\hat{n}_g}(\vec{x}_\mathbf{f}) = \frac{\mathrm{tr} V_{g|\vec{x}_\mathbf{f}} + \|\vec{\xi}_{g|\vec{x}_\mathbf{f}}\|^2 - 2}{\mathrm{tr} V_g + \|\vec{\xi}_g\|^2 - 2} W_\mathbf{f}(\vec{x}_\mathbf{f}). \tag{37}$$

From this result, we immediately observe that the potential Wigner negativity of these states depends on whether or not $\mathrm{tr} V_{g|\vec{x}_\mathbf{f}} < 2$. In Ref. [80] it was shown through the Williamson decomposition that $\mathrm{tr} V_{g|\vec{x}_\mathbf{f}} \leqslant 2\sqrt{\det V_{g|\vec{x}_f}}$. This directly implies that EPR steering (31) is a necessary condition to reach Wigner negativity. It is instructive to emphasise that

$$\|\vec{\xi}_{g|\vec{x}_\mathbf{f}}\|^2 = \|\vec{\xi}_g + V_{g\mathbf{f}} V_\mathbf{f}^{-1}(\vec{x}_\mathbf{f} - \vec{\xi}_\mathbf{f})\|^2, \tag{38}$$

from which one ultimately retrieves the expression

$$W^-_{\mathbf{f}|\hat{n}_g}(\vec{x}_\mathbf{f}) = \frac{\{\|\vec{\xi}_g + V_{g\mathbf{f}} V_\mathbf{f}^{-1}(\vec{x}_\mathbf{f} - \vec{\xi}_\mathbf{f})\|^2 + \mathrm{tr} V_{g|\vec{x}_\mathbf{f}} - 2\}}{\mathrm{tr} V_g + \|\vec{\xi}_g\|^2 - 2} W_\mathbf{f}(\vec{x}_\mathbf{f}),$$

which is the result that was derived in Ref. [80].

For the photon-added state, we can perform a completely analogous computation with

$$W_{\hat{n}_g + \mathbb{1}}(\vec{x}_g) = \frac{1}{16\pi}(\|\vec{x}_g\|^2 + 2), \tag{39}$$

from which we find that

$$W^+_{\mathbf{f}|\hat{n}_g}(\vec{x}_\mathbf{f}) = \frac{\mathrm{tr} V_{g|\vec{x}_\mathbf{f}} + \|\vec{\xi}_{g|\vec{x}_\mathbf{f}}\|^2 + 2}{\mathrm{tr} V_g + \|\vec{\xi}_g\|^2 + 2} W_\mathbf{f}(\vec{x}_\mathbf{f}). \tag{40}$$

This result immediately shows that this Wigner function is always positive, which implies that it is impossible to remotely create Wigner negativity through photon addition.

In previous work, we highlighted that photon addition always creates Wigner negativity in the mode where the photon is added [91]. What we observe in Eq. (40) can be understood as the complementary picture for the other modes. This result also highlights an operational difference between photon subtraction and addition: photon addition is a more powerful tool to locally create Wigner negativity, whereas photon subtraction has the potential to create Wigner negativity nonlocally (i.e., in modes that can steer the mode in which the photon is subtracted).

2. Subtracting multiple photons

When multiple photons are added or subtracted, or when we chain combinations of addition and subtraction operations, the evaluation of $\langle \hat{A} \rangle_{\mathbf{g}|\vec{x}_\mathbf{f}}(\vec{x}_\mathbf{f})$ will rapidly become more complicated. A general strategy to approach this problem avoids the explicit evaluation of $W_{\hat{A}}(\vec{x}_\mathbf{g})$, but rather uses standard techniques for the evaluation of moments of multivariate Gaussian distributions. This ultimately boils down to applying Wick's theorem [98] and summing over all matchings (see the Appendix for details). Even though this task can be implemented numerically, the corresponding analytical expressions quickly become intractable.

To illustrate this method, we consider the multimode scenario where two photons are subtracted in different orthogonal modes, g_1 and g_2, which implies that the conditioning implements the map

$$\rho \mapsto \frac{\hat{a}_{g_1}\hat{a}_{g_2}\hat{\rho}\hat{a}^\dagger_{g_2}\hat{a}^\dagger_{g_1}}{\mathrm{tr}[\hat{n}_{g_1}\hat{n}_{g_2}\hat{\rho}]}. \tag{41}$$

This implies that we must apply our formalism with $\hat{A} = \hat{n}_{g_1}\hat{n}_{g_2}$. To treat this problem with the technique of matchings, we use the Gaussian identity (note that we do not explicitly write the dependence on $\vec{x}_\mathbf{f}$ to simplify notation)

$$\begin{aligned}
&\langle \hat{n}_{g_1}\hat{n}_{g_2}\rangle_{\mathbf{g}|\vec{x}_\mathbf{f}} \\
&\quad = \left|\langle \hat{a}_{g_1}\rangle_{\mathbf{g}|\vec{x}_\mathbf{f}}\right|^2 \left|\langle \hat{a}_{g_2}\rangle_{\mathbf{g}|\vec{x}_\mathbf{f}}\right|^2 + \langle \hat{n}_{g_1}\rangle'_{\mathbf{g}|\vec{x}_\mathbf{f}} \left|\langle \hat{a}_{g_2}\rangle_{\mathbf{g}|\vec{x}_\mathbf{f}}\right|^2 \\
&\qquad + \langle \hat{n}_{g_2}\rangle'_{\mathbf{g}|\vec{x}_\mathbf{f}} \left|\langle \hat{a}_{g_1}\rangle_{\mathbf{g}|\vec{x}_\mathbf{f}}\right|^2 + \langle \hat{a}^\dagger_{g_1}\hat{a}_{g_2}\rangle'_{\mathbf{g}|\vec{x}_\mathbf{f}}\langle \hat{a}^\dagger_{g_2}\rangle_{\mathbf{g}|\vec{x}_\mathbf{f}}\langle \hat{a}_{g_1}\rangle_{\mathbf{g}|\vec{x}_\mathbf{f}} \\
&\qquad + \langle \hat{a}^\dagger_{g_1}\hat{a}_{g_2}\rangle'_{\mathbf{g}|\vec{x}_\mathbf{f}}\langle \hat{a}^\dagger_{g_2}\hat{a}_{g_1}\rangle'_{\mathbf{g}|\vec{x}_\mathbf{f}} + \langle \hat{a}^\dagger_{g_1}\hat{a}^\dagger_{g_2}\rangle'_{\mathbf{g}|\vec{x}_\mathbf{f}}\langle \hat{a}_{g_1}\hat{a}_{g_2}\rangle'_{\mathbf{g}|\vec{x}_\mathbf{f}} \\
&\qquad + \langle \hat{n}_{g_1}\rangle'_{\mathbf{g}|\vec{x}_\mathbf{f}}\langle \hat{n}_{g_2}\rangle'_{\mathbf{g}|\vec{x}_\mathbf{f}} + \langle \hat{a}^\dagger_{g_2}\hat{a}_{g_1}\rangle'_{\mathbf{g}|\vec{x}_\mathbf{f}}\langle a^\dagger_{g_1}\rangle_{\mathbf{g}|\vec{x}_\mathbf{f}}\langle \hat{a}_{g_2}\rangle_{\mathbf{g}|\vec{x}_\mathbf{f}} \\
&\qquad + \langle \hat{a}^\dagger_{g_1}\hat{a}^\dagger_{g_2}\rangle'_{\mathbf{g}|\vec{x}_\mathbf{f}}\langle \hat{a}_{g_1}\rangle_{\mathbf{g}|\vec{x}_\mathbf{f}}\langle \hat{a}_{g_2}\rangle_{\mathbf{g}|\vec{x}_\mathbf{f}} \\
&\qquad + \langle \hat{a}_{g_1}\hat{a}_{g_2}\rangle'_{\mathbf{g}|\vec{x}_\mathbf{f}}\langle \hat{a}^\dagger_{g_1}\rangle_{\mathbf{g}|\vec{x}_\mathbf{f}}\langle \hat{a}^\dagger_{g_2}\rangle_{\mathbf{g}|\vec{x}_\mathbf{f}},
\end{aligned} \tag{42}$$

where $\langle\cdot\rangle'_{\mathbf{g}|\vec{x}_\mathbf{f}}$ denotes the nondisplaced version of the distribution. We can immediately identify

$$\langle \hat{a}_{g_1}\rangle_{\mathbf{g}|\vec{x}_\mathbf{f}} = \tfrac{1}{2}(\vec{\xi}^T_{\mathbf{g}|\vec{x}_\mathbf{f}}\vec{g}_1 + i\vec{\xi}^T_{\mathbf{g}|\vec{x}_\mathbf{f}}\Omega\vec{g}_1); \tag{43}$$

subsequently, from Eq. (36), we obtain

$$\langle \hat{n}_{g_1}\rangle'_{\mathbf{g}|\vec{x}_\mathbf{f}} = \tfrac{1}{4}(\mathrm{tr}V_{g_1|\vec{x}_\mathbf{f}} - 2), \tag{44}$$

and finally we find new types of terms that are given by

$$\begin{aligned}
\langle \hat{a}^\dagger_{g_1}\hat{a}^\dagger_{g_2}\rangle'_{\mathbf{g}|\vec{x}_\mathbf{f}} = \tfrac{1}{4}[&\vec{g}_1^T V_{\mathbf{g}|\vec{x}_\mathbf{f}}\vec{g}_2 - \vec{g}_1^T\Omega^T V_{\mathbf{g}|\vec{x}_\mathbf{f}}\Omega\vec{g}_2 \\
&- i(\vec{g}_1^T V_{\mathbf{g}|\vec{x}_\mathbf{f}}\Omega\vec{g}_2 + \vec{g}_1^T\Omega^T V_{\mathbf{g}|\vec{x}_\mathbf{f}}\vec{g}_2)]
\end{aligned} \tag{45}$$

and

$$\begin{aligned}
\langle \hat{a}^\dagger_{g_1}\hat{a}_{g_2}\rangle'_{\mathbf{g}|\vec{x}_\mathbf{f}} = \tfrac{1}{4}[&\vec{g}_1^T V_{\mathbf{g}|\vec{x}_\mathbf{f}}\vec{g}_2 + \vec{g}_1^T\Omega^T V_{\mathbf{g}|\vec{x}_\mathbf{f}}\Omega\vec{g}_2 \\
&+ i(\vec{g}_1^T V_{\mathbf{g}|\vec{x}_\mathbf{f}}\Omega\vec{g}_2 - \vec{g}_1^T\Omega^T V_{\mathbf{g}|\vec{x}_\mathbf{f}}\vec{g}_2)].
\end{aligned} \tag{46}$$

The computation required to obtain the final result is tedious but straightforward. We find that

$$\begin{aligned}
&\langle \hat{n}_{g_1}\hat{n}_{g_2}\rangle_{\mathbf{g}|\vec{x}_\mathbf{f}} \\
&\quad = \tfrac{1}{16}[(\mathrm{tr}V_{g_1|\vec{x}_\mathbf{f}} + \|\vec{\xi}_{g_1|\vec{x}_\mathbf{f}}\|^2 - 2)(\mathrm{tr}V_{g_2|\vec{x}_\mathbf{f}} \\
&\qquad + \|\vec{\xi}_{g_2|\vec{x}_\mathbf{f}}\|^2 - 2) + 2\mathrm{tr}(C^TC) + 4\vec{\xi}^T_{g_1|\vec{x}_\mathbf{f}}C\vec{\xi}_{g_2|\vec{x}_\mathbf{f}}],
\end{aligned} \tag{47}$$

where we have defined the submartix C as the off-diagonal block of $V_{\mathbf{g}|\vec{x}_\mathbf{f}}$ via

$$V_{\mathbf{g}|\vec{x}_\mathbf{f}} = \begin{pmatrix} V_{g_1|\vec{x}_\mathbf{f}} & C \\ C^T & V_{g_2|\vec{x}_\mathbf{f}} \end{pmatrix}. \tag{48}$$

Nonzero entries in the block C can occur due to various causes. First, they can be due to a correlation between the modes g_1 and g_2 in the initial Gaussian state [as seen from the term $V_\mathbf{g}$ in Eq. (17)]. However, nontrivial entries in C also arise when modes g_1 and g_2 are both correlated to the same modes in $\mathbf{f}$, which is induced by the term $V_\mathbf{gf}V_\mathbf{f}^{-1}V_\mathbf{gf}^T$ in Eq. (17).

Result (47) directly shows the appearance of a trivial term, $(\mathrm{tr}V_{g_1|\vec{x}_\mathbf{f}} + \|\vec{\xi}_{g_1|\vec{x}_\mathbf{f}}\|^2 - 2)(\mathrm{tr}V_{g_1|\vec{x}_\mathbf{f}} + \|\vec{\xi}_{g_1|\vec{x}_\mathbf{f}}\|^2 - 2)$, which multiplies the effect of photon subtraction in g_1 with that of photon subtraction in g_2. However, when both modes are sufficiently "close" to each other, we find the additional terms $2\mathrm{tr}(C^TC) + 4\vec{\xi}^T_{g_1|\vec{x}_\mathbf{f}}C\vec{\xi}_{g_2|\vec{x}_\mathbf{f}}$, which can be interpreted as some form of interference between the two photon subtractions.

In Fig. 3 we provide an illustration, where we inject three pure squeezed vacuum states into a series of beam splitters to generate an entangled three-mode state from which we subtract two photons. The first two squeezed vacuum states have 5 dB squeezing in opposite quadratures and are mixed on the beam splitter with 75% transmittance. One of the output ports will serve as mode g_1, whereas the other is injected into a section beam splitter of 25% transmittance. In the other input port of this beam splitter, we inject the third squeezed vacuum state, which is also squeezed by 5 dB. One of the output ports of the 25% transmittance beam splitter serves as mode g_2, and in the other output port we find mode f, which is the mode for which we reconstruct the output Wigner function using Eq. (47). Photon subtraction is represented by a highly transmitting beam splitter that sends a small amount of light to a photon detector. Two-photon subtraction then happens when both detectors click at the same time, and we can condition the state in mode f upon this detection outcome. This postselection scheme effectively implements the operators $\hat{a}_{g_1}$ and $\hat{a}_{g_2}$ on modes g_1 and g_2, respectively.

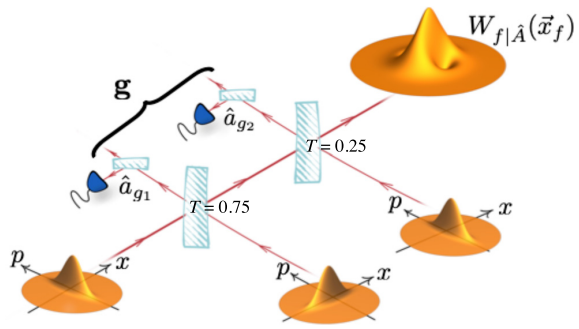

FIG. 3. Conditional state Wigner function $W_{f|\hat{A}}(\vec{x}_f)$, obtained by subtracting a photon in two of the three modes in a three-mode entangled state. This entangled state is generated by mixing three squeezed vacuum states in a sequence of beam splitters with transmittances of 75% (left) and 25% (right). Two of the squeezed vacuum states are squeezed by 5 dB in the x quadrature (left, right) and one is squeezed by 5 dB along the p quadrature (middle). The photon subtraction is represented by highly transmitting beam splitters that send a small fraction of light to a photon detector, which effectively implements the operators $\hat{a}_{g_1}$ and $\hat{a}_{g_2}$ on the modes g_1 and g_2, respectively.

We observe that the conditional state $W_{f|\hat{A}}(\vec{x}_f)$ with $\hat{A} = \hat{n}_{g_1}\hat{n}_{g_2}$ reaches negative values in two distinct regions of phase space. Indeed, with the Williamson decomposition of $V_{\mathbf{g}|\vec{x}_f}$ we can quantify [30] the strength of EPR steering from mode f to the set of modes $\mathbf{g}$ to be $\mu = 0.548$. Furthermore, the fact that there are two negativity regions is a hallmark of the subtraction of two photons. This example shows that our framework is a highly versatile tool for CV quantum state engineering.

Finally, we consider the complementary scenario where two photons are subtracted from one mode. In this case, we can still use the perfect matching technique (42), when creation and annihilation operators are in normal ordering. In this case, we obtain $\hat{A} = \hat{a}_g^\dagger\hat{a}_g^\dagger\hat{a}_g\hat{a}_g$, and analogously to Eq. (42), we find that

$$\langle \hat{a}_g^\dagger\hat{a}_g^\dagger\hat{a}_g\hat{a}_g\rangle_{g|\vec{x}_\mathbf{f}} = \tfrac{1}{16}[(\mathrm{tr}V_{g|\vec{x}_\mathbf{f}} + \|\vec{\xi}_{g|\vec{x}_\mathbf{f}}\|^2)^2 + 2\mathrm{tr}(V_{g|\vec{x}_\mathbf{f}}^2) + 4\vec{\xi}_{g|\vec{x}_\mathbf{f}}^T(V_{g|\vec{x}_\mathbf{f}} - 2\mathbb{1})\vec{\xi}_{g|\vec{x}_\mathbf{f}} - 8\mathrm{tr}V_{g|\vec{x}_\mathbf{f}} + 8]. \tag{49}$$

This result can then be directly inserted into Eq. (23) to obtain the final conditional state for the set of modes $\mathbf{f}$ when two photons are subtracted in mode g. As expected, the subtraction of two photons can induce Wigner negativity only when there is EPR steering from the modes $\mathbf{f}$ to mode g.

As such, we have shown that our framework allows us to analytically describe conditional non-Gaussian states in a regime that is highly challenging for many other methods. For example, it is highly challenging to approach the problem with the correlation function methods of Ref. [91], even though this method is highly successful for single-photon subtraction in multimode states.

These methods can in principle be extended to deal with higher numbers of added and/or subtracted photons in various modes. However, it must be emphasised that one will quickly encounter practical boundaries as finding all possible matchings is a computationally hard problem [99]. Finding an exact description of the Wigner function that is obtained by subtracting a large number of photons from a subset of an entangled Gaussian state seems to be a computationally hard problem that has its roots in graph theory. The problem of finding all matchings also lies at the basis of Gaussian boson sampling [100,101], and it is not expected to be easy to overcome. The problem of Gaussian boson sampling can in turn also be related to CV sampling from photon-added or -subtracted states [102].

VI. CONCLUSIONS

We present a general framework that describes the Wigner function that is obtained by applying an arbitrary operation on a subset of modes of a multimode Gaussian state, and conditioning the remaining modes on this operation. The most natural way of interpreting this scenario is by considering this operation to be a measurement, such that the state of the remaining modes is obtained by post-selecting on a specific measurement outcome, as is the case for heralding. However, this framework can also be used to study the nonlocal effects of photon addition and subtraction.

Our framework relies heavily on classical probability theory, and in particular on properties of conditional probability distributions (14). We use the fact that Gaussian states have positive Wigner functions, such that associated conditional probability distributions on phase space are well defined as probability distributions (but not necessarily as quantum states, because they can violate the Heisenberg inequality). In this regard, our general results (21)–(22) are valid for all initial states with a positive Wigner function.

Gaussian states are not only the most relevant initial states from an experimental point of view, they also have the theoretical advantage of leading to a Gaussian conditional probability distribution. The latter is an enormous advantage for evaluating the crucial quantity $\langle\hat{A}\rangle_{\mathbf{g}|\vec{x}_\mathbf{f}}$, as defined in Eq. (21). On a more fundamental level, we note that the covariance matrix (17) of this Gaussian conditional probability distribution is essential in the theory of EPR steering. This observation allows us to directly prove that EPR steering is a necessary prerequisite for the conditional preparation of Wigner negativity, regardless of the conditional operation that is performed.

In previous work, we already showed that Gaussian EPR steering is also a sufficient ingredient for the remote preparation of Wigner negativity, in the sense that there always exists a combination of a Gaussian operation and photon subtraction in the modes **g** that induces Wigner negativity in the modes **f**. We thus establish a fundamental relation between Gaussian EPR steering and the ability to prepare a Wigner-negative state in correlated modes. This result is particularly important in the light of measurement-based quantum computation, where large Gaussian cluster states form the backbone for implementing a quantum algorithm. The actual computation is then executed by performing measurements (or more general operations) on some modes of the cluster, in order to project the remainder of the system in a desired quantum state. To claim that such a computation is universal, one must be able to induce Wigner negativity. Our results therefore show that EPR steering is an essential figure of merit in these cluster states in order to claim that a cluster state is suitable for universal quantum computation.

From a practical point of view, the examples in Sec. V show that our framework is highly versatile. However, the boundaries of analytical treatments are also highlighted. Even though the obtained Eq. (21) for $\langle\hat{A}\rangle_{\mathbf{g}|\vec{x}_\mathbf{f}}$ is easy to interpret conceptually, the actual evaluation can still be challenging. Regardless, we must emphasise that the elegance and simplicity of our framework does allow us to obtain results with far greater ease than previously possible. Many of the methods known in the literature are either hard to generalise to arbitrary Gaussian initial states [44,59], focused on one particular measurement or operation [47,91,95], or are just generally hard to interpret or use analytically. Our framework can be applied to any initial Gaussian state, and any conditional operation, provided the Wigner function of $\hat{A}$ is known.

As such, our results provide a starting point for investigating a wide range of new questions related to multimode conditional preparation of non-Gaussian states. By establishing a fundamental relation between EPR steering and Wigner negativity, we specifically highlight that this framework is also suited to obtain general analytical results, which is often challenging in the study of states that are both highly non-Gaussian and highly multimode.

APPENDIX: MATCHINGS

In Sec. 2, we refer to the method of perfect matchings to evaluate $\langle\hat{A}\rangle_{\mathbf{g}|\vec{x}_\mathbf{f}}$, which we present here with more rigour and detail.

The technique of perfect matchings is a common practice to evaluate correlation functions in Gaussian states, which can be traced back to works such as Refs. [5,98]. In formal terms, we consider a Gaussian (also known as "quasifree" in the mathematical physics literature) functional $\langle\cdot\rangle_{\mathbf{g}|\vec{x}_\mathbf{f}}$ on the algebra of observables for the canonical commutation relations [11]. A defining property of such functionals is that truncated correlation functions [5] for any product of more than two creation and annihilation operators vanish. This property is the direct analog of the cumulants of a multivariate Gaussian distribution and it implies that the functional $\langle\cdot\rangle_{\mathbf{g}|\vec{x}_\mathbf{f}}$ is fully determined by the quantities $\langle\hat{a}_{g_1}^\dagger\hat{a}_{g_2}^\dagger\rangle'_{\mathbf{g}|\vec{x}_\mathbf{f}} = \langle\hat{a}_{g_1}\hat{a}_{g_2}\rangle'^{*}_{\mathbf{g}|\vec{x}_\mathbf{f}}$, $\langle\hat{a}_{g_1}^\dagger\hat{a}_{g_2}\rangle'_{\mathbf{g}|\vec{x}_\mathbf{f}}$, and $\langle\hat{a}_{g_1}^\dagger\rangle_{\mathbf{g}|\vec{x}_\mathbf{f}} = \langle\hat{a}_{g_1}\rangle^*_{\mathbf{g}|\vec{x}_\mathbf{f}}$. Here the $\langle\cdot\rangle'_{\mathbf{g}|\vec{x}_\mathbf{f}}$ is the nondisplaced version of the functional, which is formally defined as

$$\langle\hat{a}_{g_1}^\#\hat{a}_{g_2}^\#\rangle'_{\mathbf{g}|\vec{x}_\mathbf{f}} = \langle\hat{a}_{g_1}^\#\hat{a}_{g_2}^\#\rangle_{\mathbf{g}|\vec{x}_\mathbf{f}} - \langle\hat{a}_{g_1}^\#\rangle_{\mathbf{g}|\vec{x}_\mathbf{f}}\langle\hat{a}_{g_2}^\#\rangle_{\mathbf{g}|\vec{x}_\mathbf{f}}, \tag{A1}$$

where $\hat{a}_{g_1}^\#$ can be either a creation or an annihilation operator. We can then write the following general property of the Gaussian functional:

$$\langle\hat{a}_{g_1}^\dagger\cdots\hat{a}_{g_n}^\dagger\hat{a}_{g_{n+1}}\cdots\hat{a}_{g_{n+m}}\rangle_{\mathbf{g}|\vec{x}_\mathbf{f}} = \sum_{M\in\mathcal{M}}\prod_{\{j_1,j_2\}\in M}\langle\hat{a}_{j_1}^\#\hat{a}_{j_2}^\#\rangle'_{\mathbf{g}|\vec{x}_\mathbf{f}}\prod_{\{k\}\in M}\langle\hat{a}_k^\#\rangle_{\mathbf{g}|\vec{x}_\mathbf{f}}. \tag{A2}$$

Here $\mathcal{M}$ is the set of all "matchings" for the set $\{g_1,\ldots,g_{n+m}\}$. We use the term matching to refer to a partition of the set $\{g_1,\ldots,g_{n+m}\}$ in subsets with either one or two elements. An example of such a possible matching is given by $M = \{\{g_1,g_2\},\ldots,\{g_{n-1},g_n\},\{g_n\},\ldots,\{g_{n+m}\}\}$. For each partition $M\in\mathcal{M}$, we then evaluate the product of associated two-point and one-point functions, where any pair $\{j_1,j_2\}\in M$ is associated with $\langle\hat{a}_{j_1}^\#\hat{a}_{j_2}^\#\rangle'_{\mathbf{g}|\vec{x}_\mathbf{f}}$ and $\{k\}\in M$ is associated with $\langle\hat{a}_k^\#\rangle_{\mathbf{g}|\vec{x}_\mathbf{f}}$. Note that, for $i = g_1,\ldots,g_n$, the operator $\hat{a}_i^\#$ is a creation operator, whereas, for $i = g_{n+1},\ldots,g_{n+m}$, it is an annihilation operator.

The problem of finding all matchings is a well-known problem in graph theory. To make the connection, we can represent each element of the set $\{g_1,\ldots,g_{n+m}\}$ as a vertex in a full connected graph, and then consider the resulting partitions as the matchings of this graph [99]. The number of terms in Eq. (A2) quickly explodes as the number of creation and annihilation operators increases, which ultimately makes the problem of evaluating $\langle\hat{a}_{g_1}^\dagger\cdots\hat{a}_{g_n}^\dagger\hat{a}_{g_{n+1}}\cdots\hat{a}_{g_{n+m}}\rangle_{\mathbf{g}|\vec{x}_\mathbf{f}}$ computationally hard.

A subtle point in our treatment of $\langle\hat{A}\rangle_{\mathbf{g}|\vec{x}_\mathbf{f}}$ is that $\langle\cdot\rangle_{\mathbf{g}|\vec{x}_\mathbf{f}}$ is not an expectation value of a Gaussian quantum state. Hence, it is legitimate to wonder up to what extent the techniques of Gaussian quantum states can be used to evaluate $\langle\hat{A}\rangle_{\mathbf{g}|\vec{x}_\mathbf{f}}$. From its definition in Eq. (21), it can be deduced that $\langle\cdot\rangle_{\mathbf{g}|\vec{x}_\mathbf{f}}$ is a functional on the algebra of observables. It directly inherits the Gaussian properties from $W(\vec{x}_\mathbf{g}\mid\vec{x}_\mathbf{f})$, such that it is a Gaussian functional. In particular, property (A2) can be directly traced back to the structure of the moments of the multivariate Gaussian probability distribution $W(\vec{x}_\mathbf{g}\mid\vec{x}_\mathbf{f})$. The Gaussian functional $\langle\cdot\rangle_{\mathbf{g}|\vec{x}_\mathbf{f}}$ is not associated to a state because it is not a positive functional, i.e., we can find positive operators $\hat{A}$ for which $\langle\hat{A}\rangle_{\mathbf{g}|\vec{x}_\mathbf{f}} < 0$.

For a Gaussian functional on the algebra of canonical commutation relations to be equivalent to a quantum state, one must impose additional constraints on the functional to guarantee positivity [5,11]. These constraints ultimately boil down to imposing the Heisenberg inequality.

ACKNOWLEDGMENTS

V.P. acknowledges financial support from the European Research Council under the Consolidator Grant COQCOoN (Grant No. 820079)

[1] E. Schrödinger, Der stetige übergang von der mikro- zur makromechanik, Naturwissenschaften **14**, 664 (1926).
[2] E. H. Kennard, Zur quantenmechanik einfacher bewegungstypen, Z. Phys. **44**, 326 (1927).
[3] R. J. Glauber, Coherent and incoherent states of the radiation field, Phys. Rev. **131**, 2766 (1963).
[4] E. C. G. Sudarshan, Equivalence of Semiclassical and Quantum Mechanical Descriptions of Statistical Light Beams, Phys. Rev. Lett. **10**, 277 (1963).
[5] D. W. Robinson, The ground state of the Bose gas, Commun. Math. Phys. **1**, 159 (1965).
[6] R. Hudson, When is the wigner quasi-probability density non-negative?, Rep. Math. Phys. **6**, 249 (1974).
[7] R. Simon, N. Mukunda, and B. Dutta, Quantum-noise matrix for multimode systems: U(n) invariance, squeezing, and normal forms, Phys. Rev. A **49**, 1567 (1994).
[8] S. L. Braunstein and P. van Loock, Quantum information with continuous variables, Rev. Mod. Phys. **77**, 513 (2005).
[9] C. Weedbrook, S. Pirandola, R. García-Patrón, N. J. Cerf, T. C. Ralph, J. H. Shapiro, and S. Lloyd, Gaussian quantum information, Rev. Mod. Phys. **84**, 621 (2012).
[10] G. Adesso, S. Ragy, and A. R. Lee, Continuous variable quantum information: Gaussian states and beyond, Open Syst. Inf. Dynam. **21**, 1440001 (2014).
[11] A. Verbeure, *Many-Body Boson Systems: Half a Century Later*, Theoretical and Mathematical Physics(Springer, London, New York, 2011).
[12] H. P. Yuen, Two-photon coherent states of the radiation field, Phys. Rev. A **13**, 2226 (1976).
[13] R. E. Slusher, L. W. Hollberg, B. Yurke, J. C. Mertz, and J. F. Valley, Observation of Squeezed States Generated by Four-Wave Mixing in an Optical Cavity, Phys. Rev. Lett. **55**, 2409 (1985).
[14] L.-A. Wu, H. J. Kimble, J. L. Hall, and H. Wu, Generation of Squeezed States by Parametric Down Conversion, Phys. Rev. Lett. **57**, 2520 (1986).
[15] R. M. Shelby, M. D. Levenson, S. H. Perlmutter, R. G. DeVoe, and D. F. Walls, Broad-Band Parametric Deamplification of Quantum Noise in an Optical Fiber, Phys. Rev. Lett. **57**, 691 (1986).
[16] A. Heidmann, R. J. Horowicz, S. Reynaud, E. Giacobino, C. Fabre, and G. Camy, Observation of Quantum Noise Reduction on Twin Laser Beams, Phys. Rev. Lett. **59**, 2555 (1987).
[17] H. Vahlbruch, M. Mehmet, K. Danzmann, and R. Schnabel, Detection of 15 db Squeezed States of Light and Their Application for the Absolute Calibration of Photoelectric Quantum Efficiency, Phys. Rev. Lett. **117**, 110801 (2016).
[18] C. M. Caves, Quantum-mechanical noise in an interferometer, Phys. Rev. D **23**, 1693 (1981).
[19] N. Treps, N. Grosse, W. P. Bowen, C. Fabre, H.-A. Bachor, and P. K. Lam, A quantum laser pointer, Science **301**, 940 (2003).
[20] J. Aasi *et al.*, Enhanced sensitivity of the ligo gravitational wave detector by using squeezed states of light, Nat. Photonics **7**, 613 (2013).
[21] R. Schnabel, Squeezed states of light and their applications in laser interferometers, Phys. Rep. **684**, 1 (2017).
[22] L.-M. Duan, G. Giedke, J. I. Cirac, and P. Zoller, Inseparability Criterion for Continuous Variable Systems, Phys. Rev. Lett. **84**, 2722 (2000).
[23] R. Simon, Peres-Horodecki Separability Criterion for Continuous Variable Systems, Phys. Rev. Lett. **84**, 2726 (2000).
[24] R. F. Werner and M. M. Wolf, Bound Entangled Gaussian States, Phys. Rev. Lett. **86**, 3658 (2001).
[25] S. L. Braunstein, Squeezing as an irreducible resource, Phys. Rev. A **71**, 055801 (2005).
[26] G. Adesso and F. Illuminati, Entanglement in continuous-variable systems: Recent advances and current perspectives, J. Phys. A: Math. Theor. **40**, 7821 (2007).
[27] S. Gerke, J. Sperling, W. Vogel, Y. Cai, J. Roslund, N. Treps, and C. Fabre, Full Multipartite Entanglement of Frequency-Comb Gaussian States, Phys. Rev. Lett. **114**, 050501 (2015).
[28] R. Uola, A. C. S. Costa, H. C. Nguyen, and O. Gühne, Quantum steering, Rev. Mod. Phys. **92**, 015001 (2020).
[29] H. M. Wiseman, S. J. Jones, and A. C. Doherty, Steering, Entanglement, Nonlocality, and the Einstein-Podolsky-Rosen Paradox, Phys. Rev. Lett. **98**, 140402 (2007).
[30] I. Kogias, A. R. Lee, S. Ragy, and G. Adesso, Quantification of Gaussian Quantum Steering, Phys. Rev. Lett. **114**, 060403 (2015).
[31] X. Deng, Y. Xiang, C. Tian, G. Adesso, Q. He, Q. Gong, X. Su, C. Xie, and K. Peng, Demonstration of Monogamy Relations for Einstein-Podolsky-Rosen Steering in Gaussian Cluster States, Phys. Rev. Lett. **118**, 230501 (2017).
[32] Y. Cai, Y. Xiang, Y. Liu, Q. He, and N. Treps, Versatile multipartite einstein-podolsky-rosen steering via a quantum frequency comb, Phys. Rev. Res. **2**, 032046 (2020).
[33] S. D. Bartlett, B. C. Sanders, S. L. Braunstein, and K. Nemoto, Efficient Classical Simulation of Continuous Variable Quantum Information Processes, Phys. Rev. Lett. **88**, 097904 (2002).
[34] A. Mari and J. Eisert, Positive Wigner Functions Render Classical Simulation of Quantum Computation Efficient, Phys. Rev. Lett. **109**, 230503 (2012).
[35] L. García-Álvarez, C. Calcluth, A. Ferraro, and G. Ferrini, Efficient simulatability of continuous-variable circuits with large wigner negativity, arXiv:2005.12026 [quant-ph] (2020).

[36] S. Rahimi-Keshari, T. C. Ralph, and C. M. Caves, Sufficient Conditions for Efficient Classical Simulation of Quantum Optics, Phys. Rev. X **6**, 021039 (2016).

[37] M. Gu, C. Weedbrook, N. C. Menicucci, T. C. Ralph, and P. van Loock, Quantum computing with continuous-variable clusters, Phys. Rev. A **79**, 062318 (2009).

[38] P. van Loock, C. Weedbrook, and M. Gu, Building gaussian cluster states by linear optics, Phys. Rev. A **76**, 032321 (2007).

[39] X. Su, Y. Zhao, S. Hao, X. Jia, C. Xie, and K. Peng, Experimental preparation of eight-partite cluster state for photonic qumodes, Opt. Lett. **37**, 5178 (2012).

[40] M. Chen, N. C. Menicucci, and O. Pfister, Experimental Realization of Multipartite Entanglement of 60 Modes of a Quantum Optical Frequency Comb, Phys. Rev. Lett. **112**, 120505 (2014).

[41] Y. Cai, J. Roslund, G. Ferrini, F. Arzani, X. Xu, C. Fabre, and N. Treps, Multimode entanglement in reconfigurable graph states using optical frequency combs, Nat. Commun. **8**, 15645 (2017).

[42] W. Asavanant, Y. Shiozawa, S. Yokoyama, B. Charoensombutamon, H. Emura, R. N. Alexander, S. Takeda, J.-I. Yoshikawa, N. C. Menicucci, H. Yonezawa, and A. Furusawa, Generation of time-domain-multiplexed two-dimensional cluster state, Science **366**, 373 (2019).

[43] M. V. Larsen, X. Guo, C. R. Breum, J. S. Neergaard-Nielsen, and U. L. Andersen, Deterministic generation of a two-dimensional cluster state, Science **366**, 369 (2019).

[44] J. Fiurášek, R. García-Patrón, and N. J. Cerf, Conditional generation of arbitrary single-mode quantum states of light by repeated photon subtractions, Phys. Rev. A **72**, 033822 (2005).

[45] R. Tualle-Brouri, A. Ourjoumtsev, A. Dantan, P. Grangier, M. Wubs, and A. S. Sørensen, Multimode model for projective photon-counting measurements, Phys. Rev. A **80**, 013806 (2009).

[46] A. P. Lund, A. Laing, S. Rahimi-Keshari, T. Rudolph, J. L. O'Brien, and T. C. Ralph, Boson Sampling from a Gaussian State, Phys. Rev. Lett. **113**, 100502 (2014).

[47] D. Su, C. R. Myers, and K. K. Sabapathy, Conversion of gaussian states to non-gaussian states using photon-number-resolving detectors, Phys. Rev. A **100**, 052301 (2019).

[48] A. I. Lvovsky, P. Grangier, A. Ourjoumtsev, V. Parigi, M. Sasaki, and R. Tualle-Brouri, Production and applications of non-gaussian quantum states of light, arXiv:2006.16985 [quant-ph] (2020).

[49] C. K. Hong and L. Mandel, Experimental Realization of a Localized One-Photon State, Phys. Rev. Lett. **56**, 58 (1986).

[50] A. I. Lvovsky, H. Hansen, T. Aichele, O. Benson, J. Mlynek, and S. Schiller, Quantum State Reconstruction of the Single-Photon Fock State, Phys. Rev. Lett. **87**, 050402 (2001).

[51] A. M. Brańczyk, T. C. Ralph, W. Helwig, and C. Silberhorn, Optimized generation of heralded fock states using parametric down-conversion, New J. Phys. **12**, 063001 (2010).

[52] J. Wenger, R. Tualle-Brouri, and P. Grangier, Non-Gaussian Statistics from Individual Pulses of Squeezed Light, Phys. Rev. Lett. **92**, 153601 (2004).

[53] A. Ourjoumtsev, R. Tualle-Brouri, J. Laurat, and P. Grangier, Generating optical schrödinger kittens for quantum information processing, Science **312**, 83 (2006).

[54] A. Zavatta, S. Viciani, and M. Bellini, Quantum-to-classical transition with single-photon-added coherent states of light, Science **306**, 660 (2004).

[55] V. Parigi, A. Zavatta, M. Kim, and M. Bellini, Probing quantum commutation rules by addition and subtraction of single photons to/from a light field, Science **317**, 1890 (2007).

[56] V. A. Averchenko, C. Jacquard, V. Thiel, C. Fabre, and N. Treps, Multimode theory of single-photon subtraction, New J. Phys. **18**, 083042 (2016).

[57] Y.-S. Ra, A. Dufour, M. Walschaers, C. Jacquard, T. Michel, C. Fabre, and N. Treps, Non-gaussian quantum states of a multimode light field, Nat. Phys. **16**, 144 (2020).

[58] M. Dakna, T. Anhut, T. Opatrný, L. Knöll, and D.-G. Welsch, Generating Schrödinger-cat-like states by means of conditional measurements on a beam splitter, Phys. Rev. A **55**, 3184 (1997).

[59] G. S. Thekkadath, B. A. Bell, I. A. Walmsley, and A. I. Lvovsky, Engineering Schrödinger cat states with a photonic even-parity detector, Quantum **4**, 239 (2020).

[60] M. Eaton, R. Nehra, and O. Pfister, Non-gaussian and gottesman–kitaev–preskill state preparation by photon catalysis, New J. Phys. **21**, 113034 (2019).

[61] M. Lassen, L. S. Madsen, M. Sabuncu, R. Filip, and U. L. Andersen, Experimental demonstration of squeezed-state quantum averaging, Phys. Rev. A **82**, 021801(R) (2010).

[62] E. Wigner, On the quantum correction for thermodynamic equilibrium, Phys. Rev. **40**, 749 (1932).

[63] K. E. Cahill and R. J. Glauber, Density operators and quasiprobability distributions, Phys. Rev. **177**, 1882 (1969).

[64] M. Hillery, R. O'Connell, M. Scully, and E. Wigner, Distribution functions in physics: Fundamentals, Phys. Rep. **106**, 121 (1984).

[65] K. Kraus, General state changes in quantum theory, Ann. Phys. **64**, 311 (1971).

[66] On the full multimode Hilbert space, the operator will take the form $\mathbb{1} \otimes \hat{X}_j$, but for simplicity we will just denote it as $\hat{X}_j$.

[67] R. J. Muirhead, in *Aspects of Multivariate Statistical Theory*, Wiley Series in Probability and Statistics (Wiley, Hoboken, 2008), p. 1.

[68] M. Walschaers, S. Sarkar, V. Parigi, and N. Treps, Tailoring Non-Gaussian Continuous-Variable Graph States, Phys. Rev. Lett. **121**, 220501 (2018).

[69] D. Cavalcanti and P. Skrzypczyk, Quantum steering: A review with focus on semidefinite programming, Rep. Prog. Phys. **80**, 024001 (2017).

[70] E. G. Cavalcanti, S. J. Jones, H. M. Wiseman, and M. D. Reid, Experimental criteria for steering and the einstein-podolsky-rosen paradox, Phys. Rev. A **80**, 032112 (2009).

[71] D. J. Saunders, S. J. Jones, H. M. Wiseman, and G. J. Pryde, Experimental epr-steering using bell-local states, Nat. Phys. **6**, 845 (2010).

[72] A. J. Bennet, D. A. Evans, D. J. Saunders, C. Branciard, E. G. Cavalcanti, H. M. Wiseman, and G. J. Pryde, Arbitrarily Loss-Tolerant Einstein-Podolsky-Rosen Steering

Allowing a Demonstration Over 1 km of Optical Fiber with no Detection Loophole, Phys. Rev. X **2**, 031003 (2012).

[73] V. Händchen, T. Eberle, S. Steinlechner, A. Samblowski, T. Franz, R. F. Werner, and R. Schnabel, Observation of one-way einstein–podolsky–rosen steering, Nat. Photonics **6**, 596 (2012).

[74] D. H. Smith, G. Gillett, M. P. de Almeida, C. Branciard, A. Fedrizzi, T. J. Weinhold, A. Lita, B. Calkins, T. Gerrits, H. M. Wiseman, S. W. Nam, and A. G. White, Conclusive quantum steering with superconducting transition-edge sensors, Nat. Commun. **3**, 625 (2012).

[75] J. Schneeloch, P. B. Dixon, G. A. Howland, C. J. Broadbent, and J. C. Howell, Violation of Continuous-Variable Einstein-Podolsky-Rosen Steering with Discrete Measurements, Phys. Rev. Lett. **110**, 130407 (2013).

[76] S. Kocsis, M. J. W. Hall, A. J. Bennet, D. J. Saunders, and G. J. Pryde, Experimental measurement-device-independent verification of quantum steering, Nat. Commun. **6**, 5886 (2015).

[77] A. Cavaillès, H. Le Jeannic, J. Raskop, G. Guccione, D. Markham, E. Diamanti, M. D. Shaw, V. B. Verma, S. W. Nam, and J. Laurat, Demonstration of Einstein-Podolsky-Rosen Steering Using Hybrid Continuous- and Discrete-Variable Entanglement of Light, Phys. Rev. Lett. **121**, 170403 (2018).

[78] M. D. Reid and P. D. Drummond, Quantum Correlations of Phase in Nondegenerate Parametric Oscillation, Phys. Rev. Lett. **60**, 2731 (1988).

[79] M. Frigerio, S. Olivares, and M. G. A. Paris, Non-classical steering and the gaussian steering triangoloids, arXiv:2006.11912 [quant-ph] (2020).

[80] M. Walschaers and N. Treps, Remote Generation of Wigner Negativity through Einstein-Podolsky-Rosen Steering, Phys. Rev. Lett. **124**, 150501 (2020).

[81] R. Takagi and Q. Zhuang, Convex resource theory of non-gaussianity, Phys. Rev. A **97**, 062337 (2018).

[82] F. Albarelli, M. G. Genoni, M. G. A. Paris, and A. Ferraro, Resource theory of quantum non-gaussianity and wigner negativity, Phys. Rev. A **98**, 052350 (2018).

[83] A. Kenfack and K. Życzkowski, Negativity of the wigner function as an indicator of non-classicality, J. Opt. B: Quantum Semiclassical Opt. **6**, 396 (2004).

[84] T. Opatrný, G. Kurizki, and D.-G. Welsch, Improvement on teleportation of continuous variables by photon subtraction via conditional measurement, Phys. Rev. A **61**, 032302 (2000).

[85] S. Olivares, M. G. A. Paris, and R. Bonifacio, Teleportation improvement by inconclusive photon subtraction, Phys. Rev. A **67**, 032314 (2003).

[86] R. García-Patrón, J. Fiurášek, N. J. Cerf, J. Wenger, R. Tualle-Brouri, and P. Grangier, Proposal for a Loophole-Free Bell Test Using Homodyne Detection, Phys. Rev. Lett. **93**, 130409 (2004).

[87] A. Kitagawa, M. Takeoka, M. Sasaki, and A. Chefles, Entanglement evaluation of non-gaussian states generated by photon subtraction from squeezed states, Phys. Rev. A **73**, 042310 (2006).

[88] Y. Yang and F.-L. Li, Entanglement properties of non-gaussian resources generated via photon subtraction and addition and continuous-variable quantum-teleportation improvement, Phys. Rev. A **80**, 022315 (2009).

[89] C. Navarrete-Benlloch, R. García-Patrón, J. H. Shapiro, and N. J. Cerf, Enhancing quantum entanglement by photon addition and subtraction, Phys. Rev. A **86**, 012328 (2012).

[90] T. Das, R. Prabhu, A. Sen(De), and U. Sen, Superiority of photon subtraction to addition for entanglement in a multimode squeezed vacuum, Phys. Rev. A **93**, 052313 (2016).

[91] M. Walschaers, C. Fabre, V. Parigi, and N. Treps, Entanglement and Wigner Function Negativity of Multimode Non-Gaussian States, Phys. Rev. Lett. **119**, 183601 (2017).

[92] A. Ourjoumtsev, A. Dantan, R. Tualle-Brouri, and P. Grangier, Increasing Entanglement between Gaussian States by Coherent Photon Subtraction, Phys. Rev. Lett. **98**, 030502 (2007).

[93] H. Takahashi, J. S. Neergaard-Nielsen, M. Takeuchi, M. Takeoka, K. Hayasaka, A. Furusawa, and M. Sasaki, Entanglement distillation from Gaussian input states, Nat. Photonics **4**, 178 (2010).

[94] O. Morin, K. Huang, J. Liu, H. Le Jeannic, C. Fabre, and J. Laurat, Remote creation of hybrid entanglement between particle-like and wave-like optical qubits, Nat. Photonics **8**, 570 (2014).

[95] C. N. Gagatsos and S. Guha, Efficient representation of gaussian states for multimode non-gaussian quantum state engineering via subtraction of arbitrary number of photons, Phys. Rev. A **99**, 053816 (2019).

[96] I. A. Fedorov, A. E. Ulanov, Y. V. Kurochkin, and A. I. Lvovsky, Quantum vampire: Collapse-free action at a distance by the photon annihilation operator, Optica **2**, 112 (2015).

[97] K. G. Katamadze, G. V. Avosopiants, Y. I. Bogdanov, and S. P. Kulik, How quantum is the "quantum vampire" effect?: Testing with thermal light, Optica **5**, 723 (2018).

[98] G. C. Wick, The evaluation of the collision matrix, Phys. Rev. **80**, 268 (1950).

[99] L. Lovász and M. D. Plummer, *Matching Theory* (AMS Chelsea Publishing, Providence, RI, 2009).

[100] C. S. Hamilton, R. Kruse, L. Sansoni, S. Barkhofen, C. Silberhorn, and I. Jex, Gaussian Boson Sampling, Phys. Rev. Lett. **119**, 170501 (2017).

[101] K. Brádler, P.-L. Dallaire-Demers, P. Rebentrost, D. Su, and C. Weedbrook, Gaussian boson sampling for perfect matchings of arbitrary graphs, Phys. Rev. A **98**, 032310 (2018).

[102] U. Chabaud, T. Douce, D. Markham, P. van Loock, E. Kashefi, and G. Ferrini, Continuous-variable sampling from photon-added or photon-subtracted squeezed states, Phys. Rev. A **96**, 062307 (2017).

4

QUANTUM-INSPIRED METROLOGY

LIST OF ARTICLES

1. G. Sorelli, M. Gessner, **M. Walschaers**, and N. Treps, *Optimal observables and estimators for practical superresolution imaging*, Phys. Rev. Lett. **127**, 123604 (2021).
2. G. Sorelli, M. Gessner, **M. Walschaers**, and N. Treps, *Moment-based superresolution: Formalism and applications*, Phys. Rev. A **104**, 033515 (2021).
3. G. Sorelli, M. Gessner, **M. Walschaers**, and N. Treps, *Quantum limits for resolving Gaussian sources*, Phys. Rev. Research **4**, L032022 (2022).
4. I. Karuseichyk, G. Sorelli, **M. Walschaers**, N. Treps, and M. Gessner, *Resolving mutually-coherent point sources of light with arbitrary statistics*, Phys. Rev. Research **4**, 043010 (2022).
5. G. Sorelli, M. Gessner, N. Treps, **M. Walschaers**, *Gaussian quantum metrology for mode-encoded parameters*, arXiv:2202.10355
6. T. Linowski, K. Schlichtholz, G. Sorelli, M. Gessner, **M. Walschaers**, N. Treps, Ł. Rudnicki, *Application range of crosstalk-affected spatial demultiplexing for resolving separations between unbalanced sources*, arXiv:2211.09157
7. K. Schlichtholz, T. Linowski, **M. Walschaers**, N. Treps, Ł. Rudnicki, G. Sorelli, *Practical tests for sub-Rayleigh source discriminations with imperfect demultiplexers*, arXiv:2303.02654
8. C. Rouvière, D. Barral, A. Grateau, I.a Karuseichyk, G. Sorelli, **M. Walschaers**, N. Treps, *Ultra-sensitive separation estimation of optical sources*, arXiv:2306.11916

4.1 ASPECTS OF QUANTUM METROLOGY

Even though the topic of quantum metrology has a long history in our group (Pinel et al., 2013; Treps et al., 2003), it is a reasonably new subject for me personally. I became involved in this work due to a growing theoretical activity that followed our group's demonstration of distance estimation through spatial-mode demultiplexing (Boucher et al., 2020). This work is based on a mix of old idea (Treps et al., 2003) on using spatial-mode demultiplexing to estimate the position of a beam and more recent results that show that similar techniques can be applied to estimate the distance between two incoherent sources with high precision (Tsang et al., 2016). Our theoretical endeavours on this subject mainly revolve around rigorous methods to take into account experimental imperfections and their impact on the precision with which we can estimate

parameters (Gessner, Fabre, et al., 2020; Karuseichyk et al., 2022; Sorelli et al., 2021a,b). We will come back to these specific problems in Section 4.2, but first we introduce some basic concepts and techniques of quantum metrology which are complementary to what we have introduced in Chapter 1.

In our work, we specifically focus on the context of parameter estimation where the quantum state $\hat{\rho}_\theta$ depends on a parameter θ. Our aim is to use quantum measurements (see Section 1.1.4) to estimate the value of θ as accurately as possible. If we choose to measure a POVM $\{\hat{P}_a\}$, this means we are going to use the probability density

$$P(a|\theta) = \mathrm{Tr}(\hat{P}_a \hat{\rho}_\theta) \tag{4.1}$$

to estimate the exact value of θ. There are a range of methods to do so, ranging from error propagation and the method of moments to maximum likelihood estimation (Kay, 1993; Van Trees, 2001). Generally speaking, we simply define the likelihood $\mathcal{L}(\theta|A)$ as the probability to observe outcomes $A = \{a_1, \ldots, a_N\}$ given a parameter θ. When we perform maximum likelihood estimation, we are just choosing the estimator θ_{est} such that the function $\mathcal{L}(\theta|A)$ is maximized in $\theta = \theta_{\text{est}}$. In our specific setting, we usually consider that we perform many independent runs of an experiment, such that the likelihood function is given by

$$\mathcal{L}(\theta|A) = P(a_1|\theta) \ldots P(a_N|\theta). \tag{4.2}$$

However, when the samplers are not independent, the definition generalises to $\mathcal{L}(\theta|A) = P(A|\theta)$, which is now the joint probability distribution for the measurement outcomes.

A very fundamental result in estimation theory is the Cramér-Rao bound. This result puts a lower bound on the precision $\Delta\theta_{\text{est}}$ that can be achieved for the estimator θ_{est} of the parameter θ. In experimental terms, it tells us what is the smallest error bar that can be reached when experimentally determining θ. The fundamental result states that

$$\Delta\theta_{\text{est}} \geq \frac{1}{\sqrt{F_\theta[\mathcal{L}]}}, \tag{4.3}$$

where $F_\theta[\mathcal{L}]$ is the *Fisher information* given that the actual value of the parameter is θ and given the likelihood function $\mathcal{L}(\theta|A)$. Mathematically, the Fisher information is defined as

$$F_\theta[\mathcal{L}] = \int_{\mathcal{A}} \left(\frac{\partial}{\partial\theta} \log \mathcal{L}(\theta|A) \right)^2 P(A|\theta) dA. \tag{4.4}$$

In our specific experimental case, we can use (4.2) to write that

$$F_\theta[\mathcal{L}] = N \int_{\mathcal{A}} \left(\frac{\partial}{\partial\theta} \log P(a|\theta) \right)^2 P(a|\theta) da = N F_\theta[P], \tag{4.5}$$

where we slightly abuse notation to highlight that $F_\theta[P]$ is the Fisher information obtained from the distribution (4.1). Thus, if we have N independent repetitions of the

same experimental measurement, we find that the precision of the parameter estimation is limited by

$$\Delta\theta_{\text{est}} \geq \frac{1}{\sqrt{NF_\theta[P]}}. \tag{4.6}$$

Of course, this limit depends on the distributions $P(a|\theta)$ and thus also on the POVM $\{\hat{P}_a\}$ we choose to measure.

In quantum metrology, one often studies the *quantum Fisher information* rather than the Fisher information for any specific POVM. The quantum Fisher information is quite simply defined as the maximum achievable Fisher information over all possible measurements

$$\mathcal{F}_Q[\hat{\rho}_\theta] = \max_{\hat{P}_a} F_\theta[P], \tag{4.7}$$

in other words, the quantum Fisher information is related to the highest achievable sensitivity of a state for sensing the parameter θ. Using different states, we can still change the precision with which we can estimate a parameter, but the quantum Fisher information gives us the best precision we can possibly get for a given state.

A priori, equation (4.7) may not seem very useful. After all, maximising over all possible measurement is hard to do. However, this is where one of the most important results of quantum metrology kicks in: one can explicitly calculate the quantum Fisher information. To understand this, we first of all introduce the Hellinger distance between two probability distributions $P(a)$ and $Q(a)$

$$d_H^2[P,Q] = \frac{1}{2}\int_{\mathcal{A}} \left(\sqrt{P(a)} - \sqrt{Q(a)}\right)^2 da. \tag{4.8}$$

We are now going to evaluate this distance for the probabilities in (4.1) and specifically compare $P(a|\theta)$ and $P(a|\theta+\delta\theta)$, it can be shown through Taylor expansion that

$$d_H^2[P(.|\theta), P(.|\theta+\delta\theta)] = \frac{F_\theta[P]}{8}\delta\theta^2 + \mathcal{O}(\delta\theta^3) \tag{4.9}$$

Which clearly highlights why the Fisher information is also referred to as the statistical speed with which the probability distribution changes when we change the parameter θ. It literally measures how sensitive the distribution is to small changes in the parameter.

In quantum information theory, the Hellinger distance can be related to the Bures distance between two quantum states $\hat{\rho}$ and $\hat{\sigma}$

$$d_B^2[\hat{\rho},\hat{\sigma}] = 1 - \text{Tr}\left(\sqrt{\sqrt{\hat{\rho}}\hat{\sigma}\sqrt{\hat{\rho}}}\right) \tag{4.10}$$

it can be shown, for example in Chapter 9 of Nielsen and Chuang, 2012, that

$$d_B^2[\hat{\rho},\hat{\sigma}] = \max_{\hat{P}_a} d_H^2[P,Q], \tag{4.11}$$

where we assume that $P(a) = \mathrm{Tr}(\hat{\rho}\hat{P}_a)$ and $Q(a) = \mathrm{Tr}(\hat{\sigma}\hat{P}_a)$. The Bures distance between two states is thus the maximal statistical distance between the measurements that can be performed on these states. We can now combine the definition (4.7), the identity (4.9), and the result (4.11), to obtain that

$$d_B^2[\hat{\rho}_\theta, \hat{\rho}_{\theta+\delta\theta}] = \frac{\mathcal{F}_Q[\hat{\rho}_\theta]}{8}\delta\theta^2 + \mathcal{O}(\delta\theta^3), \tag{4.12}$$

In other words, the quantum Fisher information $\mathcal{F}_Q[\hat{\rho}_\theta]$ can be obtained from the Bures distance between the state for a given parameter, and a state for a small variation of that parameter. The real question is now: in practice, does this result help us to calculated $\mathcal{F}_Q[\hat{\rho}_\theta]$?

It is, in general, rather hard to calculate $d_B^2[\hat{\rho}_\theta, \hat{\rho}_{\theta+\delta\theta}]$. Yet, we can use the result to derive much more useful results. What follows is a derivation that is inspired by (Braunstein and Caves, 1994; Hübner, 1992). Let us start by defining

$$\hat{A}(\delta\theta) = \sqrt{\sqrt{\hat{\rho}_\theta}\hat{\rho}_{\theta+\delta\theta}\sqrt{\hat{\rho}_\theta}}. \tag{4.13}$$

Because

$$\frac{\partial^2}{\partial\delta\theta^2} d_B^2[\hat{\rho}_{\theta+\delta\theta}, \hat{\rho}_\theta]\Big|_{\delta\theta=0} = \frac{\mathcal{F}_Q[\hat{\rho}_\theta]}{4}, \tag{4.14}$$

we find that

$$\mathcal{F}_Q[\hat{\rho}_\theta] = -4\mathrm{Tr}\ddot{\hat{A}}(0). \tag{4.15}$$

Here we introduce the short-hand notation $\dot{\hat{A}}(\theta) = \partial\hat{A}(\theta)/\partial\theta$. First of all, let us simplify notation by setting

$$\frac{\partial}{\partial\delta\theta}\hat{\rho}_{\theta+\delta\theta}\Big|_{\delta\theta=0} = \partial_\theta\hat{\rho}_\theta, \tag{4.16}$$

$$\frac{\partial^2}{\partial\delta\theta^2}\hat{\rho}_{\theta+\delta\theta}\Big|_{\delta\theta=0} = \partial_\theta^2\hat{\rho}_\theta. \tag{4.17}$$

We can now start from $\hat{A}^2(\delta\theta)$ and use these expressions to obtain the identities

$$\hat{A}(0)\dot{\hat{A}}(0) + \dot{\hat{A}}(0)\hat{A}(0) = \sqrt{\hat{\rho}_\theta}\partial_\theta\hat{\rho}_\theta\sqrt{\hat{\rho}_\theta}. \tag{4.18}$$

$$2\dot{\hat{A}}(0)^2 + \ddot{\hat{A}}(0)\hat{A}(0) + \hat{A}(0)\ddot{\hat{A}}(0) = \sqrt{\hat{\rho}_\theta}\partial_\theta^2\hat{\rho}_\theta\sqrt{\hat{\rho}_\theta}. \tag{4.19}$$

Since $\hat{A}(0)$ is not necessarily invertible, we immediately take the ansatz that some observable $\hat{L}_\theta$ exists such that

$$\partial_\theta\hat{\rho}_\theta = \frac{1}{2}(\hat{L}_\theta\hat{\rho}_\theta + \hat{\rho}_\theta\hat{L}_\theta), \tag{4.20}$$

and insert it in (4.18), such that we find

$$\hat{\rho}_\theta\dot{\hat{A}}(0) + \dot{\hat{A}}(0)\hat{\rho}_\theta = \frac{1}{2}\left(\sqrt{\hat{\rho}_\theta}\hat{L}_\theta\sqrt{\hat{\rho}_\theta}\hat{\rho}_\theta + \hat{\rho}\sqrt{\hat{\rho}_\theta}\hat{L}_\theta\sqrt{\hat{\rho}_\theta}\right). \tag{4.21}$$

Notice that we used $\hat{A}(0) = \hat{\rho}_\theta$. Thus, we recover that

$$\dot{\hat{A}}(0) = \frac{1}{2}\sqrt{\hat{\rho}_\theta}\hat{L}_\theta\sqrt{\hat{\rho}_\theta}. \tag{4.22}$$

Now let us insert this into (4.19), such that we can write

$$\ddot{\hat{A}}(0)\hat{\rho}_\theta + \hat{\rho}_\theta\ddot{\hat{A}}(0) = -\frac{1}{2}\sqrt{\hat{\rho}_\theta}\hat{L}_\theta\hat{\rho}_\theta\hat{L}_\theta\sqrt{\hat{\rho}_\theta} + \sqrt{\hat{\rho}_\theta}\partial_\theta^2\hat{\rho}_\theta\sqrt{\hat{\rho}_\theta}. \tag{4.23}$$

Even though we may not be able to invert $\hat{\rho}_\theta$, it is always diagonalisable. This means that we can identify a basis of eigenvectors $|k\rangle$, with $\hat{\rho}_\theta|k\rangle = p_k|k\rangle$. It is convenient to multiply both sides of the equality with $\langle k|$ from the right, and with $|k\rangle$ from the left. We then find that

$$2p_k\langle k|\ddot{\hat{A}}(0)|k\rangle = -\frac{1}{2}\sqrt{p_k}\sqrt{p_k}\langle k|\hat{L}_\theta\hat{\rho}_\theta\hat{L}_\theta|k\rangle + \sqrt{p_k}\sqrt{p_k}\langle k|\partial_\theta^2\hat{\rho}_\theta|k\rangle. \tag{4.24}$$

As a next step, we can write

$$\begin{aligned}
\mathrm{Tr}\ddot{\hat{A}}(0) &= \sum_k \langle k|\ddot{\hat{A}}(0)|k\rangle && \text{(4.25a)}\\
&= -\frac{1}{4}\sum_k \langle k|\hat{L}_\theta\hat{\rho}_\theta\hat{L}_\theta|k\rangle + \frac{1}{2}\sum_k\langle k|\partial_\theta^2\hat{\rho}_\theta|k\rangle && \text{(4.25b)}\\
&= -\frac{1}{4}\mathrm{Tr}[\hat{L}_\theta^2\hat{\rho}_\theta]. && \text{(4.25c)}
\end{aligned}$$

Note that here we used that $\sum_k\langle k|\partial_\theta^2\hat{\rho}_\theta|k\rangle = \mathrm{Tr}[\partial_\theta^2\hat{\rho}_\theta] = \partial_\theta^2\mathrm{Tr}[\hat{\rho}_\theta] = 0$. Inserting this into (4.15) then ultimately leads again to the result

$$\mathcal{F}_Q[\hat{\rho}_\theta] = \mathrm{Var}[\hat{L}_\theta]. \tag{4.26}$$

Note that we used that $\mathrm{Tr}[\hat{L}_\theta\hat{\rho}_\theta] = 0$, which can be directly obtained by taking the trace on both sides of the equality in (4.20).

The above reasoning shows that the quantum Fisher information can be obtained from the symmetric logarithmic derivative $\hat{L}_\theta$ as shown in (4.26). The caveat is that the symmetric logarithmic derivative is implicitly defined through (4.20), and solving this equation is generally extremely challenging. Yet, there are a series of cases where more explicit results are known. For example, when the the parameter is implemented by a unitary transformation. In that case we can find $\hat{\rho}_\theta$ by solving the von Neumann equation

$$\partial_\theta\hat{\rho}_\theta = -i[\hat{G}_\theta, \hat{\rho}_\theta], \tag{4.27}$$

and in particular, we find that

$$-i[\hat{G}_\theta, \hat{\rho}_\theta] = \frac{1}{2}(\hat{L}_\theta\hat{\rho}_\theta + \hat{\rho}_\theta\hat{L}_\theta). \tag{4.28}$$

Multiplying from the left with $\langle j|$ and from the right with $|k\rangle$ leads to

$$\frac{1}{2}(p_k + p_j)\langle j|\hat{L}_\theta|k\rangle = -i(p_k - p_j)\langle j|\hat{G}_\theta|k\rangle, \tag{4.29}$$

where we use that $\hat{\rho}_\theta|n\rangle = p_n|n\rangle$. We then immediately find that

$$\langle j|\hat{L}_\theta|k\rangle = -2i\frac{(p_k - p_j)}{(p_k + p_j)}\langle j|\hat{G}_\theta|k\rangle \tag{4.30}$$

We can then write

$$\mathcal{F}_Q[\hat{\rho}_\theta] = \mathrm{Var}[\hat{L}_\theta] = \sum_j p_j\langle j|\hat{L}_\theta^2|j\rangle = \sum_{j,k} p_j \left|\langle j|\hat{L}_\theta|k\rangle\right|^2 \tag{4.31a}$$

$$= 4\sum_{j,k} p_j \frac{(p_k - p_j)^2}{(p_k + p_j)^2}\left|\langle j|\hat{G}_\theta|k\rangle\right|^2. \tag{4.31b}$$

After a considerable amount of algebra, we find the convenient expression

$$\mathcal{F}_Q[\hat{\rho}_\theta] = \mathrm{Var}[\hat{L}_\theta] = 4\mathrm{Tr}[\hat{\rho}_\theta\hat{G}_\theta^2] - 8\sum_{j,k}\frac{p_k p_j}{(p_k + p_j)}\left|\langle j|\hat{G}_\theta|k\rangle\right|^2. \tag{4.32}$$

This immediately has as a consequence that $\mathcal{F}_Q[\hat{\rho}_\theta] = \mathrm{Var}[\hat{L}_\theta]. \leq 4\mathrm{Tr}[\hat{\rho}\hat{G}_\theta^2]$. It also shows that, whenever the parameter is implemented in a unitary way, we can find the quantum Fisher information when we know the generator, the eigenvalues and eigenvectors of the density matrix $\hat{\rho}_\theta$. This is in particular useful when the generator itself does not depend on the parameter. In an actual experiment, the expression (4.32) for the quantum Fisher information is only useful if we can perform a full quantum state tomography and a full process tomography to get the generator. Usually such tasks are extremely costly, but there might be some connection to recent result in quantum machine learning (Huang, Kueng, and Preskill, 2020; Huang, Kueng, Torlai, et al., 2022; Wilde et al., 2022).

The quantum Fisher information for Gaussian states can be calculated explicitly, as demonstrated in references (Monras, 2013; Šafránek et al., 2015; Serafini, 2017). Our group primarily focuses on parameter estimation using these states, making these results highly relevant. However, it is important to note that the theoretical framework discussed above only considers the quantum state, not the optical modes. In the context of imaging and other types of optical sensing, changes in the parameter not only alter the state, but also the optical modes themselves (Treps et al., 2003). This point is crucial to understanding the difficulty of the distance estimation problem (Tsang et al., 2016) and will be discussed further in Section 4.2.

Before we move on to the next section, it is important to address one final question: *what is it all good for?* Of course, one can now evaluate the quantum Fisher information, and from this conclude that

$$\Delta\theta_{\mathrm{est}} \geq \frac{1}{\sqrt{N\mathcal{F}_Q[\hat{\rho}_\theta]}}, \tag{4.33}$$

no matter what type of measurement we are performing. However, in practice, we always have an experimental setup with specific experimental measurements. This means that we can always get a tighter lower bound by calculating the actual Fisher information for our setup. So what is the actual application of the quantum Fisher information?

The beauty of the quantum Fisher information is that it provides the ultimate precision limit, determined only by the quantum fluctuations coming form the state. Braunstein and Caves, 1994 showed that a projective measurement on the eigenvectors of $\hat{L}_\theta$ saturates the quantum Fisher information, and thus the symmetric logarithmic derivative immediately gives us an optimal measurement. However, this optimal measurement is far from unique. As a matter of fact, any measurement that leads to a saturation of equation (4.33) is optimal. For example, in Karuseichyk et al., 2022 we use the method of moments (Gessner, Smerzi, et al., 2019, 2020) to get an easy to calculate crude estimation of the parameter. For many states, this crude estimation turns out to saturate the quantum Fisher information, and thus it is impossible to do better by using any more refined data analysis or measurements. This is a example that illustrates how, in parameter estimation problems, it is often crucial to get a grasp on the quantum Fisher information to understand fundamental limits, and on the experimental data analysis to understand practical limits. In the following chapter we discuss this issue for the paradigmatic problem of distance estimation.

4.2 ENCODING PARAMETERS IN MODES AND STATES

Section 1.1 has shown us that quantum optics is an interplay of modes and states. The quantum metrology framework of Section 4.1 described in great detail how quantum states change as a function of a parameter, and how we can use these changes to estimate the value of that parameter. However, what happens when the parameter actually changes the modes? To gain some understanding in this question, let us consider a simple example and consider a classical optics context.

We start by studying a simple single-mode light beam, with an electric field given by

$$\boldsymbol{E}^{(+)}(\boldsymbol{r},t) = \mathcal{E}\alpha\boldsymbol{u}(x,y)e^{i(kz-t\omega)}, \tag{4.34}$$

such that we have light propagating in the z-direction, with some transverse field profile given by mode $\boldsymbol{u}(x,y)$. We are now going to displace the beam by a distance d in the x-direction, such that we get a parameter dependent field

$$\boldsymbol{E}_d^{(+)}(\boldsymbol{r},t) = \mathcal{E}\alpha\boldsymbol{u}(x-d,y)e^{i(kz-t\omega)}. \tag{4.35}$$

Even though the light will always remain single-mode, changing the value of d actually changes the mode $\boldsymbol{u}(x-d,y)$, and thus the parameter estimation problem is actually not a single-mode problem. To understand this, it is useful to resort to a Taylor expansion:

$$\boldsymbol{u}(x-d,y) = \boldsymbol{u}(x,y) - d\frac{\partial}{\partial x}\boldsymbol{u}(x,y) + \frac{d^2}{2}\frac{\partial^2}{\partial x^2}\boldsymbol{u}(x,y) + \dots \tag{4.36}$$

Assuming that $\boldsymbol{u}(x,y)$ has some nice mathematical properties (as would for example be the case for a Gaussian beam), the functions $\partial^n \boldsymbol{u}(x,y)/\partial x^n$ can be re-normalized to form a mode basis. These derivative modes thus give us a way of representing our action of the parameter in a fixed mode-basis that is independent of the value of the parameter. In return for using these parameter-independent modes the problem has now become manifestly multimode. However, at the same time, the expansion (4.36) suggest that all relevant information of the parameter is already contained in the value of the field in mode $\partial \boldsymbol{u}(x,y)/\partial x$. This information can in principle be readily extracted with homodyne detection, as was done in Ansquer et al., 2021 for time-frequency modes.

More generally speaking, we can always consider a parameter-dependent light field and expand it in a parameter-independent mode basis

$$\boldsymbol{E}_d^{(+)}(\boldsymbol{r},t) = \sum_k \mathcal{E}_k \alpha_k(d)\boldsymbol{u}_k(\boldsymbol{r},t), \tag{4.37}$$

which can readily be quantised as

$$\hat{\boldsymbol{E}}_d^{(+)}(\boldsymbol{r},t) = \sum_k \mathcal{E}_k \hat{a}_k(d)\boldsymbol{u}_k(\boldsymbol{r},t). \tag{4.38}$$

because here the creation and annihilation operators change with the parameter d, we can see this as a description of the action of the parameter in the Heisenberg picture. Generally speaking, we can write this action in terms of a quantum channel

$$\hat{a}_k(d) = \Lambda_d(\hat{a}_k). \tag{4.39}$$

Because the parameter d acts on all creation operators individually, we write that

$$\Lambda_d[f(\hat{a}_1^\dagger,\dots,\hat{a}_m^\dagger,\hat{a}_1,\dots,\hat{a}_m)] = f(\hat{a}_1^\dagger(d),\dots,\hat{a}_m^\dagger(d),\hat{a}_1(d),\dots,\hat{a}_m(d)), \tag{4.40}$$

for any analytical function f, regardless of the operator ordering. This mathematically means that any parameter that "changes the shape of the modes" can equivalently be implemented by a quantum channel that is a $*$-automorphism in the Heisenberg picture that, according to (4.39) does not mix creation and annihilation operators. This gives us a very limited set of quantum channels. We can directly calculate that

$$\frac{\partial}{\partial d}\Lambda_d[\hat{a}_1^\# \dots \hat{a}_m^\#] = \sum_k \hat{a}_1^\#(d)\dots\hat{a}_{k-1}^\#(d)\left(\frac{\partial}{\partial d}\hat{a}_k^\#(d)\right)\hat{a}_{k+1}^\#(d)\dots\hat{a}_m^\#(d), \tag{4.41}$$

where $\hat{a}_l^{\#}$ can be a creation or an annihilation operator (this just reflects that regardless of operator ordering we always get the same result). This shows that the dynamics is entirely determined by $\partial \hat{a}_k^{\#}(d)/\partial d$. Combining all these constraints we find that the channel Λ_d must be unitary and have a generator of the form

$$\hat{G} = \sum_{k,l} G_{k,l} \hat{a}_k^\dagger \hat{a}_l. \tag{4.42}$$

This actually give us the description of a generator of an interferometer or, in other words, a change in mode basis. Since we typically describe the quantum Fisher information as a property of the state, we can equally define the action of the parameter in the Schrödinger picture as

$$\hat{\rho}_d = \Lambda_d^*(\hat{\rho}) = e^{-id\hat{G}} \hat{\rho} e^{id\hat{G}}, \tag{4.43}$$

where we formally note Λ_d^* as the dual map of Λ_d. We can then use equation (4.32) to explicitly calculate the quantum Fisher information. Note that this result on parameter estimation with parameters that change the form of optical modes was obtained by Gessner, Treps, et al., 2022 using different techniques. They also provide an explicit expression for $G_{k,l}$ in (4.42).

Elegant as the above derivation may be, it only covers a very idealised aspect of parameter estimation with parameter-dependent modes. In a more general scenario, we expect to have not only changes in mode shape, but also other processes. As such, the parameter can affect both the state and the modes. This appears naturally in imaging problems, where a finite aperture can both impact the mode shape and cause optical losses. This is the typical scenario in the problem of distance estimation between two point sources (Lupo and Pirandola, 2016; Sorelli et al., 2021a,b).

The problem of distance estimation in imaging is old and was already studied by lord Rayleigh and Abbe in the late nineteenth century. For a long time, this problem was assumed to be constrained by the diffraction limit, but a range of superresolution protocols have since profoundly changed our understanding. However, it is only recently that the framework of spatial-mode demultiplexing has shown that superresolution can be achieved using only passive linear optics (Tsang et al., 2016). The key difficulty of this setup is sketched in Figure 1: while the sources initially emit light in two distinct orthogonal modes with annihilation operators $\hat{s}_1$ and $\hat{s}_2$, the imaging system smears out the modes and makes them overlap if the sources are too close. This highlights that the action of the imaging system is not merely a change of mode basis, but a non-unitary operation that does not preserve the orthogonality of the modes and typically a considerable amount of energy emitted by the sources is lost.

There are a range of methods to deal with this imaging problem. A priori, one could model everything on the level of modes and describe the process as a transformation from an orthogonal to a non-orthogonal mode basis. In some sense, this approach is

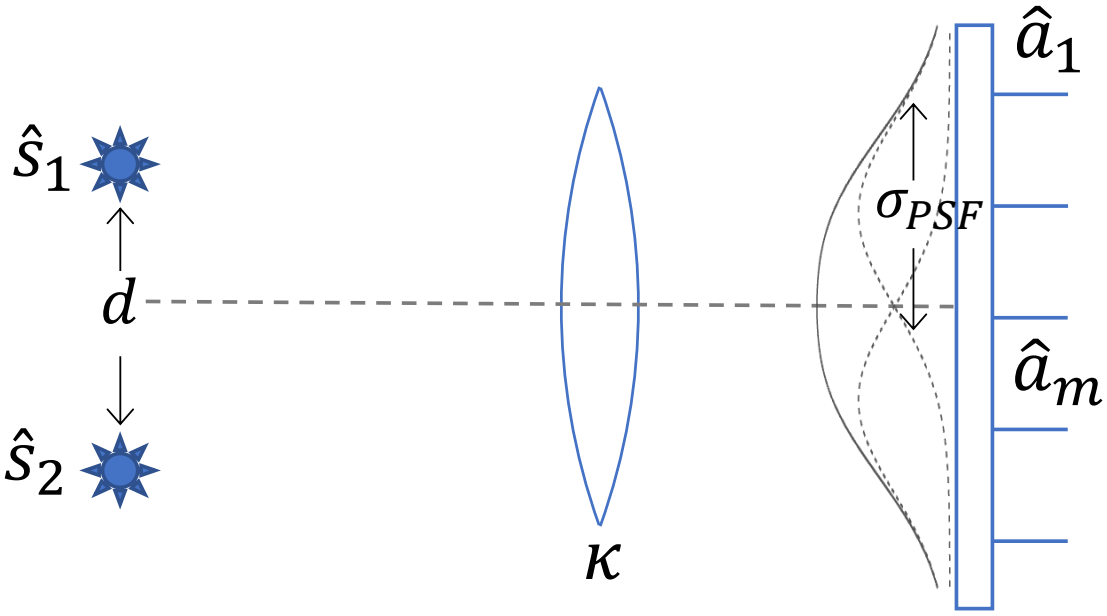

Figure 1: Schematic representation of the separation estimation setup.

followed by Fiderer et al., 2021, even though the theoretical framework is not that of modes and states. Alternatively, one can also rely on orthogonalisation procedures and rely on an additional loss model (Karuseichyk et al., 2022; Lupo and Pirandola, 2016; Sorelli et al., 2021a,b).

Regardless of the approach that is used to describe a setting with parameter-dependent modes and states, it is in general not possible to rely on a elegant formula such as equation (4.32) to obtain the quantum Fisher information for this problem. As we mentioned before, as long as the states are Gaussian we can rely on the general results (Monras, 2013; Šafránek et al., 2015; Serafini, 2017). In principle, we can apply the technique (4.38) to transform the full problem into a problem where the parameter acts on the state and use the Gaussian results. However, in practice equation (4.38) leaves us with an infinite number of modes, which makes the problem intractable. The big innovation in our recent work (Sorelli et al., 2022a) is to develop a practical way of defining a finite parameter-independent mode basis that contains all the information about the parameter and allows us to calculate the quantum Fisher information for arbitrary Gaussian states even when the parameter changes the mode basis. This framework notably allowed us to derive the quantum Fisher information for the separation estimation problem for any case where the initial sources are prepared in a Gaussian state (Sorelli et al., 2022b). Combining our results with a bound derived by Lupo and Pirandola, 2016, we can show that coherent states are practically optimal for separation

estimation. Furthermore, we have shown that the method of moments can practically saturate the quantum Fisher information in this optimal case (Karuseichyk et al., 2022), which means that separation estimation that approaches the ultimate quantum limit could be practically possible. Even though one should expect experimental imperfection to impose some limitations (Sorelli et al., 2021a,b), we have recently shown that it is experimentally possible to reach sensitivities that are orders of magnitude below the Rayleigh limit (Rouvière et al., 2023). Furthermore, we show that distance estimation close to the quantum limit is within reach.

4.3 OUTLOOK

Mode-demultiplexing offers a whole new way of looking at the information encoded in light, and therefore opens many new doors for sensing and imaging. From the practical point of view, our results in (Sorelli et al., 2022a) highlight the potential applications of these techniques in the spectral domain by multiplexing in interesting bases of time-frequency modes. This could allow us to look at problems such as synchronisation of pulses, which may in turn have application for the calibration of Boson Sampling setups (Walschaers, Kuipers, and Buchleitner, 2016). Also in imaging applications there are a range of interesting problems that remain to be addressed. On the one hand, one could wonder whether these techniques have applications in recognising shapes of objects (Grace and Guha, 2022; Pushkina et al., 2021). On the other hand, one could also consider a context with dynamical sources and attempt to estimate their trajectories. Both of these extensions are challenging from a theoretical point of view because we either cannot describe the problem as an estimation of a finite number of parameters, or we have to deal with a very limited number of data-points. We foresee that this will require entirely different theoretical techniques, for example based on Bayesian statistics.

For a more fundamental theoretical point of view, we can again consider a notion of quantum advantage and wonder how about the requirements to achieve sensitivities beyond what is possible with classical light. In this case, it is already known that squeezing is a useful resource (Treps et al., 2003), but one can wonder about the operational role of non-Gaussian features such as stellar rank and Wigner negativity. There has been some work that suggests (Arvidsson-Shukur et al., 2020) that negativity in the Kirkwood–Dirac quasiprobability distribution plays an important role in improving metrological sensitivity. However, it is not clear how the negativity in this quasiprobability distirbution can be related to Wigner negativity.

Most practical results about the quantum Fisher information rely on the diagonalisation of the state's density matrix. However, continuous-variable systems are often more conveniently dealt with in a phase space representation and knowing the Wigner function does not guarantee a practical way of finding the density matrix, let alone diagonalise it. To this end, it may be useful to use phase space calculus such as in

(1.50c) may be useful to translate the equation (4.20) directly to phase space. However, this still requires us to solve an integral equation to obtain the Wigner function of the symmetric logarithmic derivative $\hat{L}$. A potential avenue for the future is to find classes of states and parameters for which the phase space representation of equation (4.20) can be solved explicitly.

4.4 **article:** GAUSSIAN QUANTUM METROLOGY FOR MODE-ENCODED PARAMETERS: GENERAL THEORY AND IMAGING APPLICATIONS

Gaussian quantum metrology for mode-encoded parameters

Giacomo Sorelli[1,2], Manuel Gessner[3], Nicolas Treps[1], and Mattia Walschaers[1]

[1]Laboratoire Kastler Brossel, Sorbonne Université, ENS-Université PSL, CNRS, Collège de France, 4 Place Jussieu, F-75252 Paris, France

[2]Fraunhofer IOSB, Ettlingen, Fraunhofer Institute of Optronics, System Technologies and Image Exploitation, Gutleuthausstr. 1, 76275 Ettlingen, Germany

[3]Departament de Física Teòrica, IFIC, Universitat de València, CSIC, C/ Dr. Moliner 50, 46100 Burjassot (València), Spain

Quantum optical metrology aims to identify ultimate sensitivity bounds for the estimation of parameters encoded into quantum states of the electromagnetic field. In many practical applications, including imaging, microscopy, and remote sensing, the parameter of interest is not only encoded in the quantum state of the field, but also in its spatio-temporal distribution, i.e. in its mode structure. In this mode-encoded parameter estimation setting, we derive an analytical expression for the quantum Fisher information valid for arbitrary multimode Gaussian fields. To illustrate the power of our approach, we apply our results to the estimation of the transverse displacement of a beam and to the temporal separation between two pulses. For these examples, we show how the estimation sensitivity can be enhanced by adding squeezing into specific modes.

1 Introduction

A fundamental task in quantum metrology is to identify the ultimate sensitivity limit in the estimation of a parameter encoded into a quantum state. Even under ideal conditions, when all technical noise sources are removed, quantum noise poses unavoidable limitations to such estimation. In spite of that, quantum parameter estimation theory provides the tools to reduce noise by optimizing the output measurements. This optimization leads to the quantum Cramér Rao lower bound, which states that the minimal uncertainty $\Delta\vartheta$ of the estimator of a parameter ϑ is inversely proportional to the quantum Fisher information of the quantum state $\hat{\rho}_\vartheta$ where the parameter is encoded (Helstrom, 1976; Holevo, 2011; Paris, 2009; Pezzè and Smerzi, 2014; Giovannetti *et al.*, 2011; Tóth and Apellaniz, 2014). This bound can be further optimized by finding quantum states that, for a given parameter, maximize the value of the quantum Fisher information.

Electromagnetic fields play a privileged role as metrological probes in a variety of branches of science and technology, ranging from imaging and microscopy (Taylor and Bowen, 2016; Tsang, 2019), to remote sensing with lidars and radars (Giovannetti *et al.*, 2001; Zhuang *et al.*, 2017; Huang *et al.*, 2021), to gravitational wave detection (Acernese *et al.*, 2019; Tse *et al.*, 2019). In several of these applications, the parameter of interest does not only modify the quantum state of the probe light, but also its spatio-temporal distribution. Such a spatio-temporal distribution is conveniently described in terms of *modes*. i.e. normalized solutions of Maxwell's equations in vacuum (Fabre and Treps, 2020). For example, spatial modes of light describe the different components of an image, while the properties of an optical pulse are encoded into frequency-time modes.

Previous works in this context of *mode-encoded parameter estimation* focused on specific problems. For example, the case where the total light's intensity is not affected by the parameter, but its distribution among different modes is, was considered for the estimation of a small lateral beam displacement (Treps *et al.*, 2002, 2003), or in the estimation of spectral parameters of a frequency comb (Cai *et al.*, 2021). A general theory for this fixed-intensity scenario was recently presented by Gessner *et al.* (2022). Two different (mathematically equivalent) problems, that lately attracted a lot of attention, are the estimation of the separation between two point sources analysed through a diffraction-limited imaging system (Tsang *et al.*, 2016; Paúr *et al.*, 2016; Boucher *et al.*, 2020) or the temporal separation between two pulses (Ansari *et al.*, 2021; De *et al.*, 2021; Mazelanik *et al.*, 2022). For these problems, the parameter of interest is encoded in the shape of two (spatial or temporal) modes in the detection plane with separation-dependent pop-

ulations (Lupo and Pirandola, 2016). Pushed by the need to go beyond these case studies, in this work, we study mode-encoded parameter estimation with arbitrary multimode Gaussian states, i.e. photonics quantum states fully defined by the first two moments of their quadratures (Holevo, 1975; Weedbrook *et al.*, 2012; Adesso *et al.*, 2014).

Gaussian states play a central role in quantum optics: they describe important classical states such as coherent states, representing lasers operating above threshold, and thermal states, describing fully incoherent light. Furthermore, non-classical Gaussian states can be produced deterministically in non-linear optical processes. Among the latter states, there are squeezed states, whose reduced quantum noise has been proposed as a useful resource since the early days of quantum parameter estimation (Caves, 1981), and is now a key ingredient of several quantum-enhanced metrological schemes (Treps *et al.*, 2003; Pezzé and Smerzi, 2008; Acernese *et al.*, 2019; Tse *et al.*, 2019). While previous studies of the quantum Fisher information for Gaussian states exist (Pinel *et al.*, 2012; Monras, 2013; Šafránek *et al.*, 2015; Jiang, 2014), they focused on the estimation of parameters defining the first two moments of the quadratures, e.g. mean field, phase, and squeezing.

The aim of this work is to overcome these limitations, to study the estimation of parameters encoded in the spatio-temporal profile of the electromagnetic field, and therefore to broaden the applicability of Gaussian quantum metrology to new fields of technology such as imaging, microscopy, and temporal (or spectral) beam profiling. As examples of such applications, we reconsider the estimation of the transverse displacement of a beam and the temporal separations between two pulses: For the former case, we extend the results for coherent beams of (Pinel *et al.*, 2012) to thermal beams, we show that squeezing in the right mode provides a quantum enhancement also in this case, and we discuss how to include the effect of thermal noise and losses. For the latter, we confirm known results for thermal (Nair and Tsang, 2016; Lupo and Pirandola, 2016) and coherent pulses (Sorelli *et al.*, 2022), and we investigate the possibility of a quantum enhancement populating additional modes with squeezed light.

Our paper is organized as follows: First, in Sec. 2, we recall some basic facts about Gaussian states and quantum parameter estimation. We then derive the analytical expression of the quantum Fisher information for mode-encoded parameter estimation with Gaussian states, in Sec. 3. Section 4 contains the application of our results to the estimation of the transverse displacement of a beam and the temporal separation of two pulses. Section 5 concludes our work.

2 Preliminaries

2.1 Gaussian states

An $N-$mode continuous variable (CV) (Braunstein and van Loock, 2005; Serafini, 2017) quantum system can be described by choosing a *mode basis*, i.e. a set $\{u_k(\mathbf{r},t)\}_{k=1}^{N}$ of solutions of Maxwell's equations, orthonormal with respect to the inner product

$$(u_k|u_l) = \int d^3\mathbf{r} u_k^*(\mathbf{r},t)u_l(\mathbf{r},t) = \delta_{kl}, \qquad (1)$$

and associating with each mode $u_k(\mathbf{r},t)$ a pair of quadrature operators $\hat{q}_k = (\hat{a}_k + \hat{a}_k^\dagger)$ and $\hat{p}_k = i(\hat{a}_k^\dagger - \hat{a}_k)$, where $\hat{a}_k^\dagger$ and $\hat{a}_k$ are standard creation and annihilation operators. If we group all quadratures in the $2N-$dimensional vector $\hat{\mathbf{x}} = (\hat{q}_1, \hat{p}_1, \ldots, \hat{q}_n, \hat{p}_n)^\top$, from the canonical commutation relations $[\hat{a}_k, \hat{a}_l^\dagger] = \delta_{kl}$ for annihilation operators, we obtain

$$[\hat{x}_j, \hat{x}_k] = 2i\Omega_{jk}, \qquad (2)$$

with the symplectic form $\Omega = \bigoplus_{k=1}^{N} \omega_k$, and $\omega_k = i\sigma_y$, where we have introduced the notation $\sigma_{i=x,y,z}$ for the standard 2×2 Pauli matrices. Our preferred *phase space* representation of an $N-$mode CV quantum state with density matrix $\hat{\rho}$, and characteristic function $\chi(\mathbf{y}) = \mathrm{tr}\left[\exp\left(-i\mathbf{y}^\top \Omega \hat{\mathbf{x}}\right)\hat{\rho}\right]$, is the Wigner function

$$W(\mathbf{x}) = \int \frac{d\mathbf{y}^{2N}}{(2\pi)^{2N}} e^{-i\mathbf{y}^\top \Omega \mathbf{x}} \chi(\mathbf{y}). \qquad (3)$$

In this work, we restrict ourselves to the study of Gaussian states. $N-$mode Gaussian states are CV states with Gaussian Wigner function (Holevo, 1975; Weedbrook *et al.*, 2012; Adesso *et al.*, 2014)

$$W(\mathbf{x}) = \frac{\exp\left[-(\mathbf{x}-\bar{\mathbf{x}})^\top \sigma^{-1}(\mathbf{x}-\bar{\mathbf{x}})/2\right]}{(2\pi)^N \sqrt{\det \sigma}}, \qquad (4)$$

which are completely determined by the displacement vector $\bar{\mathbf{x}} = \langle \hat{\mathbf{x}} \rangle$, and the covariance matrix

$$\sigma_{jk} = \frac{1}{2}\left\langle \{(\hat{x}_j - \bar{x}_j), (\hat{x}_k - \bar{x}_k)\} \right\rangle, \qquad (5)$$

where $\{\cdot,\cdot\}$ denotes the anticommutator, and $\langle\cdot\rangle$ the expectation value $\langle\cdot\rangle = \mathrm{tr}\left[\cdot\hat{\rho}\right]$. For every physical

state, the covariance matrix satisfies the uncertainty inequality (Simon *et al.*, 1994)

$$\sigma + i\Omega \geq 0. \tag{6}$$

A useful property of the covariance matrix is that, according to Williamson theorem (Williamson, 1936), it can be decomposed as

$$\sigma = S\nu S^\top, \quad \text{with} \quad \nu = \bigoplus_{k=1}^{N} \nu_k \mathbb{1}_2, \tag{7}$$

where S is a symplectic matrix, i.e. $S\Omega S^\top = \Omega$, we introduced the notation $\mathbb{1}_n$ for the $n-$dimensional identity matrix, and ν is a diagonal matrix whose element are known as *symplectic eigenvalues*. The uncertainty inequality (6) implies that the symplectic eigenvalues must be larger than unity, i.e. $\nu_k \geq 1$.

2.2 Mode and state transformations

Let us recall that the space of solutions of Maxwell's equation is a Hilbert space (Fabre and Treps, 2020; Walschaers, 2021). Accordingly, different mode bases are connected via unitary transformations

$$u_k(\mathbf{r}, t) = \sum_{l=1}^{N} U_{kl} v_l(\mathbf{r}, t), \tag{8a}$$

$$v_k(\mathbf{r}, t) = \sum_{l=1}^{N} U^*_{lk} u_l(\mathbf{r}, t), \tag{8b}$$

with $U_{kl} = (v_l|u_k)$. Under mode basis changes, creation operators follow the same transformation rules as the modes (Fabre and Treps, 2020), which implies that the quadrature vector transforms according to

$$\hat{\mathbf{x}}' = O\hat{\mathbf{x}}, \tag{9}$$

with O an orthogonal symplectic matrix, i.e $OO^\top = O^\top O = \mathbb{1}_{2N}$ and $O^\top \Omega O = \Omega$, with elements $O_{2k-1,2l-1} = \mathrm{Re}\,[U_{kl}]$, $O_{2k,2l-1} = -\mathrm{Im}\,[U_{kl}]$, $O_{2k-1,2l} = \mathrm{Im}\,[U_{kl}]$ and $O_{2k,2l} = \mathrm{Re}\,[U_{kl}]$.

A mode basis change is a particular case of a Gaussian channel: a completely positive, trace preserving map transforming Gaussian states into Gaussian states. Such channels are completely determined by their transformation rules for the displacement vector and the covariance matrix (Holevo and Werner, 2001)

$$\bar{\mathbf{x}}' = \mathcal{T}\bar{\mathbf{x}} + \bar{\mathbf{z}}, \tag{10a}$$

$$\sigma' = \mathcal{T}\sigma\mathcal{T}^\top + \mathcal{N}, \tag{10b}$$

where $\bar{\mathbf{z}}$ is a real $2N-$dimensional vector, while $\mathcal{T}$ and $\mathcal{N}$ are $2N \times 2N$ real matrices with $\mathcal{N} = \mathcal{N}^\top$ and satisfying the positivity condition $\mathcal{N} + i\mathcal{T}\Omega\mathcal{T}^\top \geq i\Omega$. From Eq. (9) is easy to see that a mode basis change is a Gaussian channel (see Eqs. (10)) with $\mathcal{N} = 0$ and $\mathcal{T} = O$.

2.3 Quantum estimation theory

Let us now assume that we want to estimate a parameter ϑ encoded in a quantum state $\hat{\rho}_\vartheta$ from M independent measurements of a given positive operator-valued measure (POVM) defined by the operators $\hat{K}_\mu$. Using classical post-processing techniques, from the measurements' results, we can extract an unbiased estimator $\tilde{\vartheta}$ of the parameter as well as its standard deviation $\Delta\tilde{\vartheta}$. The latter is bounded according to the Cramér-Rao inequality (Helstrom, 1976; Holevo, 2011; Paris, 2009; Pezzè and Smerzi, 2014; Giovannetti *et al.*, 2011)

$$\Delta\tilde{\vartheta} \geq \frac{1}{\sqrt{M\mathcal{F}_{\vartheta,\hat{K}_\mu}}} \tag{11}$$

with the Fisher information $\mathcal{F}_{\vartheta,\hat{K}_\mu}$ defined by

$$\mathcal{F}_{\vartheta,\hat{K}_\mu} = \sum_\mu p(\mu|\vartheta) \left[\partial_\vartheta \log\left(p(\mu|\vartheta)\right)\right]^2 \tag{12}$$

where $p(\mu|\vartheta) = \mathrm{Tr}\left[\hat{K}_\mu \hat{\rho}_\vartheta\right]$ is the conditional probability of obtaining the result μ for a given value of ϑ, and we introduced the compact notation $\partial_\vartheta \cdot = \partial \cdot / \partial\vartheta$ for the derivative. The Fisher information optimized over all possible POVMs

$$F_\vartheta = \max_{\hat{K}_\mu} \mathcal{F}_{\vartheta,\hat{K}_\mu}, \tag{13}$$

is the quantum Fisher information (QFI), and establishes the ultimate metrological sensitivity (Braunstein and Caves, 1994). In general, the QFI can be computed as

$$F_\vartheta = \mathrm{Tr}\left[\hat{\mathcal{L}}^2_\vartheta \hat{\rho}_\vartheta\right], \tag{14}$$

where $\hat{\mathcal{L}}_\vartheta$ is the symmetric logarithmic derivative (SLD), implicitly defined by the equation (Helstrom, 1976; Holevo, 2011; Paris, 2009; Pezzè and Smerzi, 2014; Giovannetti *et al.*, 2011)

$$2\partial_\vartheta \hat{\rho}_\vartheta = \hat{\mathcal{L}}_\vartheta \hat{\rho}_\vartheta + \hat{\rho}_\vartheta \hat{\mathcal{L}}_\vartheta. \tag{15}$$

When ρ_ϑ is an $N-$mode Gaussian state defined by the displacement vector $\bar{\mathbf{x}}$ and the covariance matrix

σ, the SLD is quadratic in the quadratures (Monras, 2013; Šafránek *et al.*, 2015)

$$\hat{\mathcal{L}}_\vartheta = L_\vartheta^{(0)} + \mathbf{L}_\vartheta^{(1)\top}\hat{\mathbf{x}} + \frac{1}{2}\hat{\mathbf{x}}^\top L_\vartheta^{(2)}\hat{\mathbf{x}} \tag{16}$$

with

$$L_\vartheta^{(0)} = -\frac{1}{2}\,\mathrm{Tr}\left[\sigma L_\vartheta^{(2)}\right] - \mathbf{L}_\vartheta^{(1)\top}\bar{\mathbf{x}} - \frac{1}{2}\bar{\mathbf{x}}^\top L_\vartheta^{(2)}\bar{\mathbf{x}} \tag{17a}$$

$$\mathbf{L}_\vartheta^{(1)} = \sigma^{-1}\left(\partial_\vartheta\bar{\mathbf{x}}\right) - L_\vartheta^{(2)}\bar{\mathbf{x}} \tag{17b}$$

$$L_\vartheta^{(2)} = \frac{1}{2}\sum_{l=0}^{3}\sum_{jk=1}^{N}\frac{a_{jk}^{(l)}}{\nu_j\nu_k - (-1)^l}\left(S^\top\right)^{-1}A_{jk}^{(l)}S^{-1} \tag{17c}$$

where S and ν are the symplectic matrix and the symplectic eigenvalues obtained from the Williamson decomposition of σ as introduced in Eq. (7), while $a_{jk}^{(l)} = \mathrm{Tr}\left[A_{jk}^{(l)}S^{-1}(\partial_\vartheta\sigma)(S^\top)^{-1}\right]$, with $A_{jk}^{(l)}$ a set $2n\times 2n$ matrices that are zero everywhere except in the jk block where they are given by $\omega/\sqrt{2}$, $\sigma_z/\sqrt{2}$, $\mathbb{1}_2/\sqrt{2}$ and $\sigma_x/\sqrt{2}$ for $l = 0, 1, 2$ and 3, respectively. Substituting Eqs. (16) and (17) into Eq. (14) and using the properties of the characteristic function (Serafini, 2017), we can write the QFI for a Gaussian state as

$$F_\vartheta = F_\sigma + F_{\bar{\mathbf{x}}}, \tag{18}$$

with

$$F_\sigma = \mathrm{Tr}\left[L_\vartheta^{(2)}(\partial_\vartheta\sigma)\right] \tag{19a}$$

$$= \frac{1}{2}\sum_{l=0}^{3}\sum_{jk=1}^{N}\frac{\left(a_{jk}^{(l)}\right)^2}{\nu_j\nu_k - (-1)^l},$$

$$F_{\bar{\mathbf{x}}} = \left(\partial_\vartheta\bar{\mathbf{x}}\right)^\top\sigma^{-1}(\partial_\vartheta\bar{\mathbf{x}}). \tag{19b}$$

where F_σ and $F_{\bar{\mathbf{x}}}$ are the contribution to the QFI coming from variations of the covariance matrix σ and the displacement vector $\bar{\mathbf{x}}$, respectively.

3 Mode-encoded parameter estimation

Let us consider the estimation of a parameter ϑ encoded into a Gaussian state $\hat{\rho}_\vartheta$ expressed into an $n-$dimensional mode basis $u_k[\vartheta](\mathbf{r},t)$, with n the smallest number of modes necessary to describe the system. We will refer to the Hilbert space spanned by these modes as $\mathcal{H}_n = \mathrm{span}\left(\{u_k[\vartheta](\mathbf{r},t)\}\right)$. Since every basis of the mode Hilbert space $\mathcal{H}_n$ would provide a description of the quantum state $\hat{\rho}_\vartheta$ in terms of the smallest number n of modes, the choice of the mode basis $u_k[\vartheta](\mathbf{r},t)$ is not unique. Despite this freedom of choice, in the most general parameter estimation scenarios, every mode basis $u_k[\vartheta](\mathbf{r},t)$ will be parameter-dependent. The latter fact implies that the Gaussian state $\hat{\rho}_\vartheta$ depends on ϑ not only explicitly through the displacement vector $\bar{\mathbf{x}}_\vartheta$ and the covariance σ_ϑ, but also implicitly through the mode functions $u_k[\vartheta](\mathbf{r},t)$. Our goal is this section is to calculate the QFI (18) taking into account both these dependences.

3.1 Separation of mode and state parameter dependence

Our first step is to make the parameter dependence coming from the modes $u_k[\vartheta](\mathbf{r},t)$ explicit in the covariance matrix and displacement vector of the quantum state $\hat{\rho}_\vartheta$. To this goal, we express them into a parameter-independent basis $v_k(\mathbf{r},t)$: Using Eq. (9), we get

$$\sigma_I = O\sigma_\vartheta O^T, \tag{20a}$$

$$\bar{\mathbf{x}}_I = O\bar{\mathbf{x}}_\vartheta, \tag{20b}$$

where we introduced the subscripts I and ϑ to identify quantities in the parameter-independent and parameter-dependent bases, respectively. Naturally, the choice of the parameter-independent basis $v_k(\mathbf{r},t)$ is not unique. However, since this basis does not contain any information on the parameter, its choice does not affect the final expression for the QFI, as will become clear at the end of our calculation.

Given that n is the smallest number of modes necessary to represent the state $\hat{\rho}_\vartheta$, the parameter independent basis $v_k(\mathbf{r},t)$ must have dimension $N \geq n$. To take into account this change in dimension, we complement the state in the parameter-dependent mode basis with $N-n$ vacuum modes, so that we can write the covariance matrix σ_ϑ in block diagonal form as

$$\sigma_\vartheta = \begin{pmatrix} V_n & 0 \\ 0 & \mathbb{1}_{2(N-n)} \end{pmatrix}, \tag{21}$$

and the displacement vector as $\bar{\mathbf{x}}_\vartheta = (\bar{\mathbf{x}}_n^\top, 0, \cdots, 0)^\top$. To isolate the action of O on the n initially populated modes, it is convenient to rewrite it as a 1×2 block matrix

$$O = \begin{pmatrix} O_n & O_{N-n} \end{pmatrix}, \tag{22}$$

with O_n and O_{N-n} a $2N \times 2n$ and a $2N \times 2(N-n)$ matrices, respectively. Some useful properties of these matrices and their derivatives are reported in App. A. Substituting Eqs. (22) and (21) into Eq. (20a), and using the properties of the matrices O_n and O_{N-n} (See Eq. (83b) in App. A), we can rewrite the covariance matrix in the mode-independent basis as

$$\sigma_I = O_n(V_n - \mathbb{1}_{2n})O_n^\top + \mathbb{1}_{2N}. \tag{23}$$

Analogously, using Eq. (22) into Eq. (20b), we can rewrite the displacement vector as

$$\bar{\mathbf{x}}_I = O_n \bar{\mathbf{x}}_n. \tag{24}$$

Equations (23) and (24) provide a description of the Gaussian state $\hat{\rho}_\vartheta$ where the parameter dependence is fully expressed in the covariance matrix σ_I and the displacement vector $\mathbf{x}_I$. In particular, the transformation properties of the n initially populated modes appear now explicitly through the matrix O_n. In the following, we are going to use these expressions to compute the two terms in Eq. (18).

3.2 Covariance matrix contribution to the quantum Fisher information

We start with the calculation of F_σ (see Eq. (19a)), which describes the contribution to the sensitivity due to variations of the covariance matrix. Let us start by taking the derivative of the covariance matrix σ_I in the parameter independent basis with respect to the parameter

$$\begin{aligned}\partial_\vartheta \sigma_I = &\left(\partial_\vartheta O_n\right)(V_n - \mathbb{1}_{2n})O_n^\top \\ &+ O_n(V_n - \mathbb{1}_{2n})\left(\partial_\vartheta O_n^\top\right) + O_n\left(\partial_\vartheta V_n\right)O_n^\top.\end{aligned} \tag{25}$$

To compute the quadratic term of the SLD $L_\vartheta^{(2)}$ (see Eq. (17c)), we need the Williamson decomposition $\sigma_I = S_I \nu_I S_I^T$ of the covariance matrix σ_I. Using Eqs. (21) and (22), we can connect it to the Williamson decomposition $V_n = S_n \nu S_n^T$ of the covariance of the n initially populated modes in the parameter dependent basis $u_n[\vartheta](\mathbf{r}, t)$, and obtain

$$S_I = \begin{pmatrix} O_n S_n & O_{N-n}\end{pmatrix}, \tag{26a}$$

$$\nu_I = \nu \oplus \mathbb{1}_{2(N-n)}. \tag{26b}$$

Accordingly, using the properties of the matrix O (see App. A for details), we can write

$$S_I^{-1}\left(\partial_\vartheta \sigma_I\right)\left(S_I^\top\right)^{-1} = \begin{pmatrix} B_n & B_\partial^\top & 0 \\ B_\partial & 0 & 0 \\ 0 & 0 & 0\end{pmatrix}, \tag{27}$$

with

$$\begin{aligned}B_n = &S_n^{-1} D_n^\top \left(V_n - \mathbb{1}_{2n}\right)\left(S_n^\top\right)^{-1} \\ &+ S_n^{-1}\left(V_n - \mathbb{1}_{2n}\right) D_n \left(S_n^\top\right)^{-1} \\ &+ S_n^{-1}\left(\partial_\vartheta V_n\right)\left(S_n^\top\right)^{-1},\end{aligned} \tag{28a}$$

$$B_\partial = D_\partial^\top \left(V_n - \mathbb{1}_{2n}\right)\left(S_n^\top\right)^{-1}. \tag{28b}$$

Here, D_n is a $2n \times 2n$ matrix and D_∂ is a $2n \times 2m$ matrix, constructed using, respectively, the coefficients $c_{kl}[\vartheta]$ and $c'_{kl}[\vartheta]$ of the expansion

$$\begin{aligned}\partial_\vartheta u_k[\vartheta](\mathbf{r}, t) = &\sum_{l=1}^{n} c_{kl}[\vartheta] u_l[\vartheta](\mathbf{r}, t) \\ &+ \sum_{l=1}^{m} c'_{kl}[\vartheta] u'_l[\vartheta](\mathbf{r}, t),\end{aligned} \tag{29}$$

where the modes $u'_l[\vartheta](\mathbf{r}, t)$ form an $m(\leq n)-$dimensional basis of the mode Hilbert space $\mathcal{H}_\partial = \text{span}\left(\{\partial_\vartheta u_k[\vartheta](\mathbf{r}, t)\}\right) \setminus \mathcal{H}_n$ (See App. A). Accordingly, the diagonal block B_n contains a *mode contribution* (first two terms in Eq. (28a)) due to the portion of the derivatives $\partial_\vartheta u_k[\vartheta](\mathbf{r}, t)$ within the space of the initially populated modes $\mathcal{H}_n$, and a contribution given by the explicit dependence of the covariance matrix V_n on the parameter. On the other hand, the off-diagonal blocks B_∂ and $B_\partial^\top$ only contain the mode contribution due to the leakage of the derivatives $\partial_\vartheta u_k[\vartheta](\mathbf{r}, t)$ from $\mathcal{H}_n$ to $\mathcal{H}_\partial$.

Using Eq. (27), we can calculate the coefficients $a_{jk}^{(l)}$ in Eq. (17c), which result in

$$a_{jk}^{(l)} = \begin{cases} \text{Tr}\left[A_{jk}^{(l)} B_n\right] & 1 \leq j,k \leq n \\ \text{Tr}\left[\tilde{A}_{jk}^{(l)\top} B_\partial\right] & 1 \leq j \leq n, n < k \leq (n+m) \\ \text{Tr}\left[\tilde{A}_{jk}^{(l)} B_\partial^\top\right] & n < k \leq (n+m), 1 \leq j \leq n \\ 0 & j,k > (n+m)\end{cases} \tag{30}$$

where $\tilde{A}_{jk}^{(l)}$ are $m \times n$ blocks of the matrices $A_{ij}^{(l)}$. Finally, using Eq. (19a) and Eq. (26b), we can write the covariance matrix contribution to the QFI as

$$\begin{aligned}F_\sigma = &\frac{1}{2}\sum_{l=0}^{3}\sum_{jk=1}^{n} \frac{\left(a_{jk}^{(l)}\right)^2}{\nu_j \nu_k - (-1)^l} \\ &+ \frac{1}{2}\sum_{l=0}^{3}\sum_{j=1}^{n}\sum_{k=1}^{m} \frac{\left(a_{j,k+n}^{(l)}\right)^2 + \left(a_{k+n,j}^{(l)}\right)^2}{\nu_j - (-1)^l}.\end{aligned} \tag{31}$$

The sum in the first term in Eq. (31) only runs over the n initially populated modes. Accordingly, it describes the contribution to the QFI given by variations

of the state within the n initially populated modes $u_n[\vartheta](\mathbf{r},t)$. On the other hand, the second term in Eq. (31) contains a sum over the n initially populated modes $u_n[\vartheta](\mathbf{r},t)$ and another over their m orthonormalized derivatives $u'_n[\vartheta](\mathbf{r},t)$. Therefore, it takes into account the contribution to the QFI due to the coupling between the initially populated modes and their derivatives induced by parameter variations. Finally, let us note that Eq. (31) is completely determined by the covariance matrix V_n of the state $\hat{\rho}_\vartheta$ in the n initially populated modes $u_k[\vartheta](\mathbf{r},t)$, and by the shape of the modes themselves, but, as anticipated, it does not depend on the choice of the auxiliary parameter-independent basis $v_k(\mathbf{r},t)$.

3.3 Displacement vector contribution to the quantum Fisher information

We now move on to compute $F_{\bar{\mathbf{x}}}$, as given by Eq. (19b), which takes into account the contribution to the QFI coming from variations of the displacement vector $\bar{x}_I$. To compute this term, we need the derivative of Eq. (24)

$$\partial_\vartheta \bar{\mathbf{x}}_I = (\partial_\vartheta O_n)\bar{x}_n + O_n(\partial_\vartheta \bar{\mathbf{x}}_n), \tag{32}$$

and the inverse of the covariance matrix σ_I that, thanks to Eq. (22), we can write as

$$\sigma_I^{-1} = O_n V_n^{-1} O_n^\top + O_{N-n} O_{N-n}^\top. \tag{33}$$

Finally, combining Eqs. (32) and (33), and using the properties of the matrices O_n and O_{N-n} (see App. A), we obtain

$$\begin{aligned} F_{\bar{\mathbf{x}}} = {} & (\partial_\vartheta \bar{\mathbf{x}}_n)^\top V_n^{-1} (\partial_\vartheta \bar{\mathbf{x}}_n) \\ & + (\partial_\vartheta \bar{\mathbf{x}}_n)^\top V_n^{-1} D_n^\top \bar{\mathbf{x}}_n + \bar{\mathbf{x}}_n^\top D_n V_n^{-1} (\partial_\vartheta \bar{\mathbf{x}}_n) \\ & + \bar{\mathbf{x}}_n^\top \left(D_n V_n^{-1} D_n^\top + D_\partial D_\partial^\top \right) \bar{\mathbf{x}}_n. \end{aligned} \tag{34}$$

Similarly to what we observed for F_σ, $F_{\bar{\mathbf{x}}}$ only depends on the displacement vector $\bar{\mathbf{x}}_n$ in the n initially populated modes $u_k[\vartheta](\mathbf{r},t)$ and their shapes. Moreover, we note that the first term in in Eq. (34) only depends on variations of the displacement vector $\bar{\mathbf{x}}_n$, while the last term only depends on changes of the shapes of the n initially populated modes $u_k[\vartheta](\mathbf{r},t)$. On the other hand, in the two middle terms appear both $(\partial_\vartheta \bar{\mathbf{x}}_n[\vartheta])$ and D_n. Accordingly, they combine mode variations with changes in the displacement vector.

4 Application to spatial and temporal resolution

4.1 Spatial beam positioning

4.1.1 A single populated mode

As a first example, we consider the estimation of the transverse displacement d of a light beam whose spatial profile is defined by the mode $u_0[d](\mathbf{r}) = u(\mathbf{r}-\mathbf{r}_0)$ with $\mathbf{r}_0 = (d,0)$, where, without loss of generality, we assumed the beam to be displaced along the x axis. Furthermore, we consider the mode $u[d](\mathbf{r})$ to have a well-defined parity, s.t. it is orthogonal to its derivative: $(\partial_d u_0|u_0) = 0$. Under these assumptions, we have $D_n = 0$ and $D_\partial = \eta \mathbb{1}_2$, with $\eta = ||\partial_d u(\mathbf{r}-\mathbf{r}_0)||$. In this context, η quantifies the spatial extent of the beam we want to localize, e.g. for a Gaussian mode $u(\mathbf{r}) = \exp(-|\mathbf{r}|^2/2w^2)/\sqrt{\pi w^2}$, we have $\eta^2 = 1/2w^2$.

This estimation problem is fully defined by the mode $u_0[d](\mathbf{r})$. As a consequence, the mean field contribution to the QFI (34) simplifies to

$$F_{\bar{\mathbf{x}}} = (\partial_d \mathbf{x}_0)^\top V_0^{-1} (\partial_d \mathbf{x}_0) + \eta^2 ||\mathbf{x}_0||^2, \tag{35}$$

and we can write the covariance contribution to the QFI (31) as

$$F_v = \frac{1}{2}\sum_{l=0}^{3} \left(\frac{a_l^2}{\nu_0^2 - (-1)^l} + \frac{b_l^2}{\nu_0 - (-1)^l} \right), \tag{36}$$

where we defined the coefficients

$$a_l^2 = \mathrm{tr}\left[A_l S_0^{-1} (\partial_d V_0) (S_0^\top)^{-1} \right]^2, \tag{37a}$$

$$\begin{aligned} b_l^2 = {} & \eta^2 \,\mathrm{tr}\left[A_l \left(V_0 - \mathbb{1}_2\right) \left(S_0^\top\right)^{-1} \right]^2 \\ & + \eta^2 \,\mathrm{tr}\left[A_l S_0^{-1} \left(V_0 - \mathbb{1}_2\right) \right]^2, \end{aligned} \tag{37b}$$

with

$$\begin{aligned} A_0 = i\sigma_y/\sqrt{2};\ A_1 = \sigma_z/\sqrt{2}; \\ A_2 = \mathbb{1}_2/\sqrt{2};\ A_3 = \sigma_x/\sqrt{2}, \end{aligned} \tag{38}$$

where we recall $\sigma_{x,y,z}$ are Pauli matrices.

We can now evaluate Eqs. (35) and (36) for different states of the mode $u_0[d](\mathbf{r})$. Let us start by considering a coherent state $|\alpha\rangle$, defined by the complex amplitude α that can be parameter dependent. Accordingly, we have $\bar{\mathbf{x}}_0 = 2(\mathrm{Re}[\alpha], \mathrm{Im}[\alpha])$ and $V_0 = \mathbb{1}_2$. In this case, is not hard to verify that the covariance matrix contribution (36) vanishes, $F_v = 0$,

and the QFI is fully determined by the displacement term (35), which reduces to

$$F_{d,\mathrm{coh}} = |\partial_d \alpha|^2 + 4\eta^2 N_0, \tag{39}$$

where we introduced the mean photon number $N_0 = |\alpha|^2$. The second term in Eq. (39) presents a shot-noise scaling and is inversely proportional to the beam size: small displacements of a larger beam are harder to estimate. On the other hand, the first term in Eq. (39) takes into account how α depends on the transverse displacement of the beam. Such a dependence could be induced by position-dependent losses.

Let us now consider the localization of a thermal beam, for which we have $\bar{\mathbf{x}}_0 = 0$ and $V_0 = (2N_0 + 1)\mathbb{1}_2$. As opposed to the coherent case discussed above, in this case the displacement contribution (35) vanishes, and the QFI is fully determined by the covariance matrix term (36). Since V_0 is proportional to the identity, the only nonzero coefficients in Eqs. (37) are $a_2^2 = 8(\partial_d N_0)^2$ and $b_2^2 = 16 N_0^2 \eta^2$, resulting in

$$F_{d,\mathrm{th}} = \frac{(\partial_d N_0)^2}{N_0(N_0+1)} + 4\eta^2 N_0. \tag{40}$$

The $4\eta^2 N_0$ term is identical to the one in Eq. (39). Accordingly, when the mean photon number N_0 does not depend explicitly on the transverse displacement, we have the same QFI for thermal and coherent beams. On the other hand, the explicit dependence of the mean photon number N_0 on the parameter induces a quite different dependence. To make this difference more explicit, we use $N_0 = |\alpha|^2$ to rewrite this term in function of the mean photon number N_0 also in the coherent case. Accordingly, we get $|\partial_d \alpha|^2 = (\partial_d N_0)^2 / N_0$, which is a factor N_0+1 larger than the corresponding term in the thermal case. As a consequence, if the $d-$dependence of mean photon number dominates the QFI, such as in the case of strong displacement-dependent losses, coherent states provide a significant advantage over thermal states. This is due to the fact that for coherent states, a variation of the mean photon number consists in a change of mean field, while for thermal states it is a change of the covariance matrix, and the former is more efficient than the latter in making two Gaussian distributions distinguishable.

4.1.2 Populating the derivative mode

It was demonstrated by Pinel *et al.* (2012); Gessner *et al.* (2022), that the QFI (39) can be enhanced by adding squeezing to the derivative mode $\partial_d u_0[d](\mathbf{r})$. In the following, we will see how our formalism recovers this result, to extend it to different states of the mode $u_0[d](\mathbf{r})$ and to take into account losses in the squeezed derivative mode.

When populating the derivative mode, the mode Hilbert space $\mathcal{H}_n$, as introduced in Sec. 3, is spanned by $u_0[d](\mathbf{r}) = u(\mathbf{r} - \mathbf{r}_0)$ and its normalized derivative $u_1[d](\mathbf{r}) = \partial_d u_0(\mathbf{r} - \mathbf{r}_0)/\eta$. On the other hand, the mode Hilbert space $\mathcal{H}_\partial$ (see Sec. 3) only contains the second derivative mode $u_2[d](\mathbf{r}) = (\partial_d u_1[d](\mathbf{r}) - \xi u_0[d](\mathbf{r}))/\zeta$, with $\xi = (\partial_d u_1 | u_0)$ and $\zeta = ||\partial_d u_1[d](\mathbf{r}) - \xi u_0[d](\mathbf{r})||$. Accordingly, we have

$$D_n = \begin{pmatrix} 0 & \eta\mathbb{1}_2 \\ \xi\mathbb{1}_2 & 0 \end{pmatrix}, \quad D_\partial = \begin{pmatrix} 0 \\ \zeta\mathbb{1}_2 \end{pmatrix}. \tag{41}$$

Furthermore, we assume that the derivative mode $u_1[d](\mathbf{r})$ has no mean field so that the mean field vector can be written as $\bar{\mathbf{x}}^\top = (q_0, p_0, 0, 0)$. Therefore, the mean field term of the QFI (34) results in

$$F_{\bar{\mathbf{x}}} = \mathbf{y}^T V^{-1} \mathbf{y} = (\partial_d \bar{\mathbf{x}}_0^\top, \eta \bar{\mathbf{x}}_0^\top) V^{-1} \begin{pmatrix} \partial_d \bar{\mathbf{x}}_0 \\ \eta \bar{\mathbf{x}}_0 \end{pmatrix}. \tag{42}$$

As noted by Pinel *et al.* (2012), the QFI (42) can be rewritten as a function of a unique element of the inverse covariance matrix V_v^{-1}

$$F_{\bar{\mathbf{x}}} = ||\mathbf{y}||^2 (V_v^{-1})_{0,0}, \tag{43}$$

where $(V_v)_{0,0}$ is the variance of the $q-$quadrature of mode

$$\begin{aligned} v_0[d](\mathbf{r}, t) = &\frac{(\partial_d q_0 + i\partial_d p_0)}{||\mathbf{y}||} u_0[d](\mathbf{r}, t) \\ &+ \frac{\eta(q_0 + i p_0)}{||\mathbf{y}||} u_1[d](\mathbf{r}, t) \end{aligned} \tag{44}$$

Accordingly, for states with a nonzero mean field and a parameter-independent covariance matrix (e.g. coherent states), it is necessary and sufficient to squeeze the q quadrature of mode $v_0[d](\mathbf{r})$ to quantum enhance our beam positioning capability. It is interesting to observe that, if the mean field vector does not depend explicitly on the beam displacement d, i.e. $\partial_d q_0 = \partial_d p_0 = 0$, the mode $v_0[d](\mathbf{r})$ equals (up to a global phase) the derivative mode $u_1[d](\mathbf{r})$, which is orthogonal to the mode $u_0[d](\mathbf{r})$ that defines the beam shape. In this case, this effect has been exploited experimentally to enhance position estimation with a so called *quantum laser pointer* (Treps *et al.*, 2003). In a more general scenario, e.g. in presence

of position-dependent losses, Eq. (44) prescribes to squeeze a mode $v_0[d](\mathbf{r})$ which is partially overlapping with $u_0[d](\mathbf{r})$.

Let us now discuss how the covariance matrix term of the QFI is modified by population in the derivative mode $u_1[d](\mathbf{r})$. For simplicity, we will focus on the case where the population of mode $u_1[d](\mathbf{r})$ is fully uncorrelated with that of mode $u_0[d](\mathbf{r})$, therefore, the covariance matrix takes the block diagonal form

$$V = \begin{pmatrix} V_0 & 0 \\ 0 & V_1 \end{pmatrix}. \tag{45}$$

Under these assumptions, the covariance matrix contribution to the QFI (31) takes the form

$$F_v = \frac{1}{2}\sum_{l=0}^{3}\left(\frac{a_l^2}{\nu_0^2-(-1)^l} + \frac{\tilde{b}_l^2}{\nu_0\nu_1-(-1)^l} + \frac{d_l^2}{\nu_1-(-1)^l}\right), \tag{46}$$

where we have defined the coefficients

$$a_l^2 = \mathrm{tr}\left[A_l S_0^{-1}(\partial_\vartheta V_0)(S_0^\top)^{-1}\right]^2, \tag{47a}$$

$$\begin{aligned}\tilde{b}_l^2 = &\left(\eta\,\mathrm{tr}\left[A_l S_1^{-1}\left(V_0-\mathbb{1}_2\right)\left(S_0^\top\right)^{-1}\right]\right. \\ &\left.+\,\xi\,\mathrm{tr}\left[A_l S_1^{-1}\left(V_1-\mathbb{1}_2\right)\left(S_0^\top\right)^{-1}\right]\right)^2 \\ &+\left(\eta\,\mathrm{tr}\left[A_l S_0^{-1}\left(V_0-\mathbb{1}_2\right)\left(S_1^{-1}\right)^\top\right]^2\right. \\ &\left.+\,\xi\,\mathrm{tr}\left[A_l S_0^{-1}\left(V_1-\mathbb{1}_2\right)\left(S_1^{-1}\right)^\top\right]\right)^2,\end{aligned} \tag{47b}$$

$$\begin{aligned}d_l^2 = &\,\zeta^2\,\mathrm{tr}\left[A_l S_1^{-1}\left(V_1-\mathbb{1}_2\right)\right]^2 \\ &+\zeta^2\,\mathrm{tr}\left[A_l\left(V_1-\mathbb{1}_2\right)\left(S_1^{-1}\right)^\top\right]^2.\end{aligned} \tag{47c}$$

To further illustrate how to use Eq. (46) in practice, let us now consider the localisation of a thermal beam $u_0[d](\mathbf{r})$ aided by a squeezed vacuum state in the derivative mode $u_1[d](\mathbf{r})$. Accordingly, we have

$$V_0 = (2N_0+1)\mathbb{1}_2, \quad V_1 = \begin{pmatrix} e^{-2r} & 0 \\ 0 & e^{2r} \end{pmatrix}, \tag{48}$$

which corresponds to

$$S_0 = \mathbb{1}_2, \quad \text{with} \quad S_1 = \begin{pmatrix} e^{-r} & 0 \\ 0 & e^{r} \end{pmatrix}, \tag{49}$$

with $\nu_0 = 2N_0+1$ and $\nu_1 = 1$. Under these assumptions, the only nonzero coefficients are $a_2^2 = 2(2N_0'+1)^2$, $\tilde{b}_1^2 = 16(N_0\eta-\xi)^2\sinh^2 r$, $\tilde{b}_2^2 = 16N_0^2\eta^2\cosh^2 r$, and $d_1^2 = 2\zeta^2\sinh^2 r$. Substituting into Eq. (46), we obtain the following expression the QFI (for a zero mean state, the contribution in Eq. (43) vanishes)

$$\begin{aligned}F_{d,\mathrm{th-sq}} = &\frac{(\partial_d N_0)^2}{N_0(N_0+1)} + \frac{4(N_0\eta-\xi)^2 N_1}{N_0+1} \\ &+ 4N_0\eta^2(N_1+1) + 4\zeta^2 N_1,\end{aligned} \tag{50}$$

where we have introduced the number of photons $N_1 = \sinh^2 r$ in the squeezed derivative mode. Given that a thermal state has no preferred direction in phase space, we find that the result in Eq. (50) remains valid if we modify the squeezing direction. Furthermore, we can see that the QFI (50) is always larger than the one in Eq. (40) for a thermal state alone. This becomes particularly evident if we assume that N_0 does not explicitly depend on the parameter, and we consider the $N_0 \gg N_1 \gg 1$ limit, where we have $F_{d,\mathrm{th-sq}} \sim 4N_0(2N_1+1)\eta^2 \sim 2N_0\eta^2 e^{2r} \sim e^{2r}F_{d,\mathrm{th}}/2$.

It is interesting to compare this result, with the quantum enhancement achievable with a coherent state in mode $u_0[d](\mathbf{r})$. For simplicity, let us consider the case where the mean field $\bar{\mathbf{x}}_0$ does not depend explicitly on the transverse beam displacement d. In such a case, combining Eq. (43) with Eq. (50) (setting the number of thermal photons to zero), we obtain

$$F_{d,\mathrm{coh-sq}} = 4N_0\eta^2 e^{2r} + 4(\xi^2+\zeta^2)N_1. \tag{51}$$

The second term is negligible for $N_0 \gg N_1$, and we obtain $F_{d,\mathrm{coh-sq}} \sim e^{2r}F_{d,\mathrm{coh}}$. Accordingly, for the positioning a bright thermal beam aided with a squeezed state in the derivative mode, we have a quantum enhancement which is just a factor two smaller than that we obtain adding squeezing in the derivative mode $u_1[d](\mathbf{r})$ when the mode $u_0[d](\mathbf{r})$ is in a coherent state. We can understand this result by considering a thermal state as an ensemble average over coherent states with Gaussian distributed amplitudes and uniformly distributed phases. Accordingly, when adding squeezing in the derivative mode, the relative orientation between the coherent states in the ensemble and the squeezing will result sometimes in an enhancement and sometimes in a reduction of the sensitivity (see Eq. (43)). To make this statement more quantitative, we compute from Eqs. (43) and (50) the average QFI of a coherent state in mode $u_0[d](\mathbf{r})$ combined with a squeezed vacuum state in the normalized derivative mode $u_1[d](\mathbf{r})$ with ran-

dom, uniformly distributed squeezing directions

$$F_{d,\mathrm{avg}} = \frac{4N_0\eta^2}{2\pi}\int (e^{2r}\cos^2\phi + e^{-2r}\sin^2\phi)d\phi + 4(\xi^2+\zeta^2)N_1 \\ = 4N_0\eta^2\cosh 2r + 4(\xi^2+\zeta^2)N_1. \tag{52}$$

While in general, the convexity of the QFI ensures $F_{d,\mathrm{avg}} \geq F_{d,\mathrm{th-sq}}$, for $N_0 \gg N_1 \gg 1$ we have $F_{d,\mathrm{avg}} \sim 2N_0\eta^2 e^{2r} \sim F_{d,\mathrm{th-sq}}$, which supports our interpretation that the the quantum advantage enabled by squeezing for thermal states can be seen as an average over the sensitivity enhancements/diminutions obtained for coherent states.

We demonstrated above how squeezing in the normalized derivative mode $u_1[d](\mathbf{r})$ can lead to a sensitivity enhancement in the estimation of the displacement of a Gaussian beam. However, in practical situations it is hard to get a squeezed state which is not corrupted by noise. To illustrate what happens in these more practical scenarios, let us consider a thermal state in mode $u_0[d](\mathbf{r})$ and the derivative mode $u_1[d](\mathbf{r})$ populated with an arbitrary zero-mean Gaussian state, i.e. a squeezed thermal state. Accordingly, we have

$$V_1 = (2N_T+1)\begin{pmatrix} e^{-2r} & 0 \\ 0 & e^{2r}\end{pmatrix}, \tag{53}$$

where r quantifies the squeezing strength, while N_T quantifies the amout of thermal noise. Accordingly, the matrix S_1 in Eq. (49) remains the same, while the symplectic eigenvalue become $\nu_1 = 2N_T+1$. The total photon number in the derivative mode for such a state is given by $N_1 = N_T + N_S + 2N_TN_S$, with the squeezing contribution given by $N_S = \sinh^2 r$. Following the same steps as above, we now obtain the following expression for the covariance matrix contribution to the QFI (46)

$$F_{d,\mathrm{th-g}} = \frac{(N_0')^2}{N_0(N_0+1)} + \frac{4N_S\left(\xi(N_T+1)-\eta N_0\right)^2}{2N_0N_T+N_0+N_T+1} \\ + \frac{4(N_S+1)\left(\eta^2N_0^2 + N_0N_T\left(2\eta\xi+\zeta^2(2N_T+1)\right)\right)}{2N_0N_T+N_0+N_T} \\ + \frac{4N_T^2(N_S+1)\left(\zeta^2+\xi^2\right)}{2N_0N_T+N_0+N_T} + 4N_S\zeta^2(N_T+1), \tag{54}$$

which reduces to Eq. (50) when $N_T = 0$. On the other hand, when $N_S = 0$ and the population of the derivative mode becomes purely thermal, we obtain

$$F_{d,\mathrm{th-th}} = \frac{(N_0')^2}{N_0(N_0+1)} + 4\frac{(\eta N_0+\xi N_1)^2}{2N_0N_1+N_0+N_1} \\ + 4\zeta^2N_1, \tag{55}$$

and it is not hard to show that $F_{d,\mathrm{th-th}}$ (55) is always smaller than the $F_{d,\mathrm{th-sq}}$ (50): unsurprisingly, populating the derivative mode with squeezing is always better than populating that with thermal noise. In fact, for small values of N_1, the QFI $F_{d,\mathrm{th-th}}$ (55) is even smaller than that for an unpopulated derivative mode $F_{d,\mathrm{th}}$ (40). To better illustrate this interplay between squeezing and thermal noise, we introduce the following parametrisation

$$N_S = \chi N_1 \quad \text{and} \quad N_T = \frac{(1-\chi)N_1}{1+2\chi N_1}, \tag{56}$$

which allows to vary the amount of squeezing and thermal noise while keeping constant the total number of photons N_1 in the derivative mode. In particular, for $\chi = 1$ the derivative mode is purely squeezed, while for $\chi = 0$ it is purely thermal, so that we can refer to χ as the *squeezing fraction*. If we further assume that the beam we are trying to localize is Gaussian, i.e. $u(\mathbf{r}) = \exp(-|\mathbf{r}|^2/2w^2)/\sqrt{\pi w^2}$, we show that for $\chi \geq 1/2$ and $N_1 > 0$, the QFI (54) is always larger than that for unpopulated derivative mode, i.e. for $N_1 = 0$. On the other hand, as presented in Fig. 1, for $\chi < 1/2$ and small N_1 we obtain a worse sensitivity compared to that when the derivative mode is in vacuum.

Optical metrology protocols are generally very sensitive to photon losses, it is therefore important to illustrate how such losses can be taken account. Accordingly, it is useful to note that for a thermal state of mode $u_0[d](\mathbf{r})$, and an arbitrary zero-mean Gaussian state of the derivative mode $u_1[d](\mathbf{r})$, the QFI maintains the form (54) even after losses. In fact, it is sufficient to perform the following substitutions

$$N_0 = N_0^{\mathrm{in}}\kappa_0 \tag{57}$$

$$N_T = \frac{1}{2}\left(\left[\left(2\kappa_1(2N_S^{\mathrm{in}}N_T^{\mathrm{in}} + N_T^{\mathrm{in}} + N_S^{\mathrm{in}}) + 1\right)^2 - 4N_S^{\mathrm{in}}(2N_T^{\mathrm{in}}+1)^2(N_S^{\mathrm{in}}+1)\right]^{1/2} - 1\right) \tag{58}$$

$$\sinh(2r) = \kappa_1\frac{2N_T^{\mathrm{in}}+1}{2N_T+1}\sinh\left(2r^{\mathrm{in}}\right), \tag{59}$$

where κ_0 and κ_1 are the attenuation coefficients of the two modes $u_0[d](\mathbf{r})$, and $u_1[d](\mathbf{r})$, respectively;

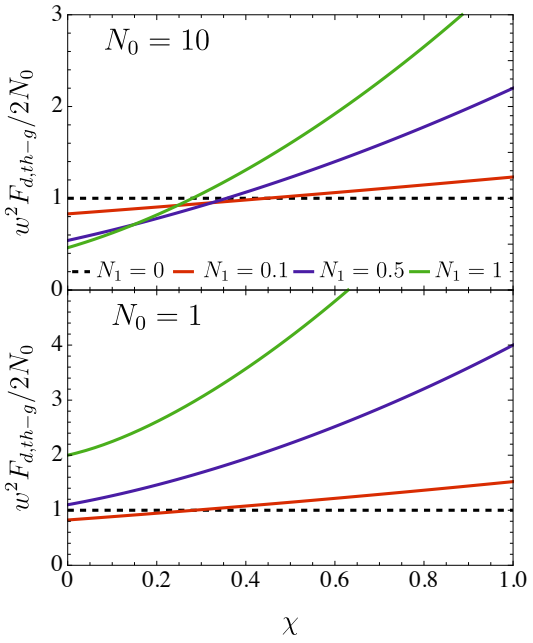

Figure 1: QFI (normalized by its maximum value when $u_1[d](\mathbf{r})$ is in vacuum) for the estimation of the transverse shift d of a thermal Gaussian beam with mean photon number $N_0 = 10$ (top) and $N_0 = 1$ (bottom), assisted by a thermal squeezed state with mean photon number N_1, as function of the squeezing fraction χ.

while N_0^{in}, N_T^{in} and $N_S^{\text{in}} = \sinh^2 r^{\text{in}}$ are the populations of the mode $u_0[d](\mathbf{r})$, and the thermal and squeezing components of the population of the mode $u_1[d](\mathbf{r})$, respectively. Finally, in some applications, the attenuation coefficients κ_0 and κ_1 can be parameter dependent. In those cases, not only N_0 depends on the transverse displacement d (as taken into account by the first term in Eq. (54)), but also N_T and r. This leads to an additional term in the QFI which takes the form

$$\frac{1}{2}\sum_{l=0}^{3}\frac{\text{tr}\left[A_l S_1^{-1}\partial_d V_1\left(S_1^{-1}\right)^\top\right]^2}{\nu_1^2-(-1)^l} \tag{60}$$
$$= \frac{((2N_T+1)(\partial_d r)\cosh r - 2(\partial_d N_T)\sinh r)^2}{4N_T(N_T+1)+2}$$
$$+ \frac{((2N_T+1)(\partial_d r)\sinh r - 2(\partial_d N_T)\cosh r)^2}{4N_T(N_T+1)}.$$

4.2 Temporal separation between pulses

As a second example, we consider the estimation of the time delay τ between two light pulses with the same temporal profile defined by the mode $u(t)$, which for simplicity, we will assume to be real and even, i.e. $u(t) = u(-t)$. From a parameter estimation point of view, this problem is most interesting when the separation τ between the pulses is smaller than (or comparable to) the pulse width. In this context, there is a finite overlap between the modes $u(t-\tau/2)$ and $u(t+\tau/2)$ (see Fig. 2)

$$\delta = \int u(t-\tau/2)u(t+\tau/2)dt. \tag{61}$$

Accordingly, as discussed by Lupo and Pirandola (2016); Sorelli *et al.* (2021a,b) for the spatial domain, it is convenient to describe the problem in terms of the two orthonormal modes

$$u_0[\tau](t) = \frac{u(t-\tau/2)+u(t+\tau/2)}{\sqrt{2(1+\delta)}}, \tag{62a}$$
$$v_0[\tau](t) = \frac{u(t-\tau/2)-u(t+\tau/2)}{\sqrt{2(1-\delta)}}. \tag{62b}$$

We are interested in computing the QFI for the estimation of τ, when the two modes (62), and eventually their derivatives, are populated. Accordingly, we complement the modes (62) with their orthonormalized first and second derivatives (see App. B for detailed calculations):

$$u_1[\tau](t) = \partial_\tau u_0[\tau](t)/\eta_u \tag{63a}$$
$$v_1[\tau](t) = \partial_\tau v_0[\tau](t)/\eta_v \tag{63b}$$
$$u_2[\tau](t) = (\partial_\tau u_1[\tau](t) - \xi_u u_0[\tau](t))/\zeta_u \tag{63c}$$
$$v_2[\tau](t) = (\partial_\tau v_1[\tau](t) - \xi_v v_0[\tau](t))/\zeta_v, \tag{63d}$$

where $\eta_u = ||\partial_\tau u_0[\tau](t)||$, $\eta_v = ||\partial_\tau v_0[\tau](t)||$, $\xi_u = (\partial_\tau u_1|u_0)$, $\xi_v = (\partial_\tau v_1|v_0)$, $\zeta_u = ||\partial_\tau u_1[\tau](t) - \xi_u u_0[\tau](t)||$ and $\zeta_u = ||\partial_\tau v_1[\tau](t) - \xi_v v_0[\tau](t)||$. The shapes of the modes $u_i[\tau](t)$ and $v_i[\tau](t)$ for the specific case of Gaussian pulses $u(t) = e^{-t^2/2w^2}/(\pi w^2)^{1/4}$ are presented in Fig. 2. Using the modes (62) and (63), we can express the matrices D_n and D_∂ (see Sec. 3.2) as

$$D_n = \begin{pmatrix} 0 & D_\eta \\ D_\xi & 0 \end{pmatrix}, \quad D_\partial = (0,0,D_\zeta)^\top, \quad \text{with}$$
$$D_\eta = \begin{pmatrix} \eta_u \mathbb{1}_2 & 0 \\ 0 & \eta_v \mathbb{1}_2 \end{pmatrix}, \; D_\xi = \begin{pmatrix} \xi_u \mathbb{1}_2 & 0 \\ 0 & \xi_v \mathbb{1}_2 \end{pmatrix},$$
$$D_\zeta = \begin{pmatrix} \zeta_u \mathbb{1}_2 & \zeta_v \mathbb{1}_2 \end{pmatrix}. \tag{64}$$

We have now specified all the mode-related quantities needed to compute the QFI for the estimation of the temporal separation τ between pulses. To proceed, we now make some further assumptions on the

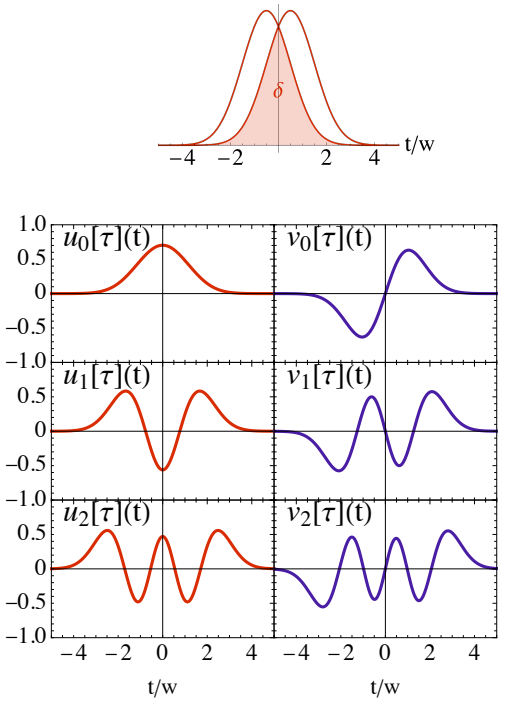

Figure 2: (top) Two Gaussian pulses temporally separated by $\tau = w$, with their overlap δ represented as a shaded area. (bottom) Set of orthonormal modes constructed from the two Gaussian pulses and their first and second derivatives with respect to τ. All modes have definite parity, in particular the modes $u_i[\tau](t)$ (left - red) are even functions, while the modes $v_i[\tau](t)$ (right - blue) are odd functions.

quantum state of the pulses. In particular, we consider the modes $u_0[\tau](t)$ and $v_0[\tau](t)$ to be in a general Gaussian state, and we allow for auxiliary population of the orthogonalized first derivative modes $u_1[\tau](t)$ and $v_1[\tau](t)$ with no mean field[1]. Accordingly, we can write the mean field vector as $\bar{\mathbf{x}}^\top = (\bar{\mathbf{x}}_0^\top, 0)$, with $\bar{\mathbf{x}}_0 = (q_{u_0}, p_{u_0}, q_{v_0}, p_{v_0})$. The mean field term of the QFI (34) can then be expressed as

$$F_{\bar{\mathbf{x}}} = (\partial_\tau \bar{\mathbf{x}}_0, D_n \bar{\mathbf{x}}_0)^\top V^{-1} (\partial_\tau \bar{\mathbf{x}}_0, D_n \bar{\mathbf{x}}_0) \tag{65}$$

Similarly to what we discussed in Sec. 4.1, for every state with a nonzero mean field, i.e. with $||\bar{\mathbf{x}}_0|| \neq 0$, there always exists a mode basis where $(\partial_\tau \bar{\mathbf{x}}_0, D_n \bar{\mathbf{x}}_0)$ has only one nonzero component. In other words, there always exists an orthogonal transformation O s.t. $O(\partial_\tau \bar{\mathbf{x}}_0, D_n \bar{\mathbf{x}}_0) = (\sqrt{||\partial_\tau \bar{\mathbf{x}}_0||^2 + ||D_\eta \bar{\mathbf{x}}_0||^2}, 0, 0, 0)$. Accordingly the QFI only depends on the inverse covariance matrix element $\left(O^T V^{-1} O\right)_{0,0}$. Therefore, the use of quantum resources, such as squeezing, to increase such matrix element can lead to an enhanced sensitivity (Pinel *et al.*, 2012).

Let us now have a look at the covariance matrix contribution to the QFI (31). To this goal, we will make the simplifying assumption that the population of the derivative modes $u_1[\tau](t)$ and $v_1[\tau](t)$ is uncorrelated with that of the symmetric and antisymmetric superpositions $u_0[\tau](t)$ and $v_0[\tau](t)$ of the pulses we want to separate, so that we can write the covariance matrix in block diagonal form

$$V = \begin{pmatrix} V_0 & 0 \\ 0 & V_1 \end{pmatrix}. \tag{66}$$

Under these assumptions, the covariance matrix contribution to the QFI takes the form

$$F_V = \frac{1}{2} \sum_{l=0}^{3} \sum_{jk=0,1} \left(\frac{\left(a_l^{jk}\right)^2}{\nu_0^j \nu_0^k - (-1)^l} + \frac{\left(b_l^{jk}\right)^2}{\nu_0^j \nu_1^k - (-1)^l} + \frac{\left(c_l^{jk}\right)^2}{\nu_1^j \nu_1^k - (-1)^l} + \frac{\left(d_l^{jk}\right)^2}{\nu_1^j - (-1)^l} \right), \tag{67}$$

where we introduced the coefficients

$$\left(a_l^{jk}\right)^2 = \left(\mathrm{tr}\left[A_l^{(jk)} \partial_\tau V_0\right]\right)^2, \tag{68a}$$

$$\left(b_l^{jk}\right)^2 = \Big(\mathrm{tr}\Big\{A_l^{(jk)} S_0^{-1} \Big[D_\xi^T (V_1 - \mathbb{1}_4) + (V_0 - \mathbb{1}_4) D_\eta\Big] \left(S_1^{-1}\right)^\top \Big\}\Big)^2 + \Big(\mathrm{tr}\Big\{A_l^{(jk)} S_1^{-1} \Big[D_\xi^T (V_1 - \mathbb{1}_4) + (V_0 - \mathbb{1}_4) D_\eta\Big] \left(S_0^{-1}\right)^\top \Big\}\Big)^2, \tag{68b}$$

$$\left(c_l^{jk}\right)^2 = \left(\mathrm{tr}\left[A_l^{(jk)} \partial_\tau V_1\right]\right)^2, \tag{68c}$$

$$\left(d_l^{jk}\right)^2 = \left(\mathrm{tr}\left\{A_l^{(jk)} D_\zeta (V_1 - \mathbb{1}_4) \left(S_1^{-1}\right)^\top \right\}\right)^2, \tag{68d}$$

with the matrices $A_l^{(jk)}$ as defined in Sec. 2.3 and ν_0^j (ν_1^j) the symplectic eigenvalues of the covariance matrix V_0 (V_1). Accordingly, we have four groups

[1] Note that we allow for correlations (classical or quantum) between the modes $u_0[\tau](t)$ and $v_0[\tau](t)$. To focus on the role of squeezing in the derivative modes, in the examples contained this paper, we do not consider such correlations. However, we studied their role in diffraction-limited imaging in Sorelli *et al.* (2022).

of addends in the QFI (67): The first one, depending on the coefficients a_l^{jk}, describes the contribution of the population of the symmetric $u_0[\tau](t)$ and antisymmetric $v_0[\tau](t)$ superpositions of the two pulses. These terms are nonzero if and only if the covariance matrix V_0 explicitly depends on the temporal separation, i.e. $\partial_\tau V_0 \neq 0$. Similarly, the third group of addends, depending on the coefficients c_l^{jk}, takes into account the population of the derivative modes $u_1[\tau](t)$ and $v_1[\tau](t)$, and is nonzero if and only if $\partial_\tau V_1 \neq 0$. The second group of addends, containing the coefficients b_l^{jk}, takes into account how variations of the temporal separation τ leads to coupling between the modes $u_0[\tau](t)$, $v_0[\tau](t)$ and their derivative $u_1[\tau](t)$, $v_1[\tau](t)$. Finally, the addends containing the coefficients d_l^{jk} take into account how due to variations of τ the derivative modes $u_1[\tau](t)$, $v_1[\tau](t)$ couple to the second derivative modes $u_2[\tau](t)$ and $v_2[\tau](t)$.

Let us now evaluate the QFI (67) for a specific quantum state of the two pulses. In particular, we are interested in two equally-bright fully-incoherent pulses whose intensity distribution is given by

$$\begin{aligned} I(t) &= \langle \hat{E}^\dagger(t)\hat{E}(t)\rangle \\ &= N_0(|u(t-\tau/2)|^2 + |u(t+\tau/2)|^2), \end{aligned} \tag{69}$$

where we introduced the mean number of photons per pulse N_0, and the electric field operator $\hat{E}(t) = \sum_j \left(\hat{a}_j u_j[\tau](t) + \hat{b}_j v_j[\tau](t)\right)$, with $\hat{a}_j$ and $\hat{b}_j$ the annihilation operators associated with the even and odd modes $u_j[\tau](t)$ and $v_j[\tau](t)$, respectively (see Fig. 2). It is not hard to see that the intensity distribution $I(t)$ (69) is achieved by a thermal state of the modes $u_0[\tau](t)$ and $v_0[\tau](t)$, with mean photon numbers $N_u = N_0(1+\delta)$ and $N_v = N_0(1-\delta)$, respectively. Such a state has no mean field $\bar{\mathbf{x}}_0 = 0$, so that its QFI is fully determined by Eq. (67), and has a covariance matrix

$$V_0 = \begin{pmatrix} (2N_0(1+\delta)+1)\,\mathbb{1}_2 & 0 \\ 0 & (2N_0(1-\delta)+1)\,\mathbb{1}_2 \end{pmatrix}. \tag{70}$$

In Sec. 4.1, we have seen that adding squeezing to the derivative mode improve the sensitivity, even for the spatial localization of an incoherent thermal beam. To verify, whether this is the case also for the temporal separation between two thermal pulses, we assume the derivative modes $u_1[\tau](t)$ and $v_1[\tau](t)$ to be populated by two independent, equally-squeezed vacuum states, described by the covariance matrix

$$V_1 = \begin{pmatrix} e^{-2r} & 0 & 0 & 0 \\ 0 & e^{2r} & 0 & 0 \\ 0 & 0 & e^{-2r} & 0 \\ 0 & 0 & 0 & e^{2r} \end{pmatrix}. \tag{71}$$

For such a quantum state, the QFI (67) takes the form (see App. C for the explicit calculation of the coefficients (68))

$$\begin{aligned} F_{\tau,\mathrm{th-sq}} = {} & \frac{2N_0\left[1+N_0(1+\delta^2)\right](\partial_\tau\delta)^2}{(1-\delta^2)\left[(1+N_0)^2-(N_0\delta)^2\right]} \\ & + 2(\zeta_u^2+\zeta_v^2)\sinh^2 r \\ & + 4N_0\left[\eta_u^2(1+\delta)+\eta_v^2(1-\delta)\right]\cosh^2 r \\ & + 4\frac{\left(N_0(1+\delta)\eta_u-\xi_u\right)^2}{1+N_0(1+\delta)}\sinh^2 r \\ & + 4\frac{\left(N_0(1-\delta)\eta_v-\xi_v\right)^2}{1+N_0(1-\delta)}\sinh^2 r. \end{aligned} \tag{72}$$

The behavior of the QFI (72), for Gaussian pulses, is plotted as red lines in Fig. 3.

For comparison, we will now also evaluate the QFI for the temporal separation of two equally bright fully coherent pulses. As opposed to Eq. (69), in this case the intensity distribution also contains an interference term depending on the relative phase ϕ between the coherent pulses

$$\begin{aligned} I(t) &= \langle \hat{E}^\dagger(t)\hat{E}(t)\rangle \\ &= N_0(|u(t-\tau/2)|^2 + |u(t+\tau/2)|^2) \\ &\quad + 2N_0 u(t-\tau/2)u(t+\tau/2)\cos\phi. \end{aligned} \tag{73}$$

Such an intensity distribution can be obtained by populating the modes $u_0[\tau](t)$ and $v_0[\tau](t)$ with coherent states, whose covariance matrix is the identity $V_0 = \mathbb{1}_4$, and whose mean field is given by $\bar{\mathbf{x}}_0 = (\bar{\mathbf{x}}_u, \bar{\mathbf{x}}_v)^\top$, with

$$\bar{\mathbf{x}}_u = \sqrt{2N_0(1+\delta)}(1+\cos\phi, \sin\phi) \tag{74a}$$

$$\bar{\mathbf{x}}_v = \sqrt{2N_0(1-\delta)}(1-\cos\phi, -\sin\phi). \tag{74b}$$

In particular, from Eqs. (74), we can see that for in-phase ($\phi = 0$) coherent pulses, the mean field is fully determined by the q quadrature of mode $u_0[\tau](t)$. Similarly, when the two coherent pulses are out of phase ($\phi = \pi$) the mean field is fully determined by the q quadrature of mode $v_0[\tau](t)$. As we did for thermal sources, we are going to consider the derivative modes $u_1[\tau](t)$ and $v_1[\tau](t)$ by two independent

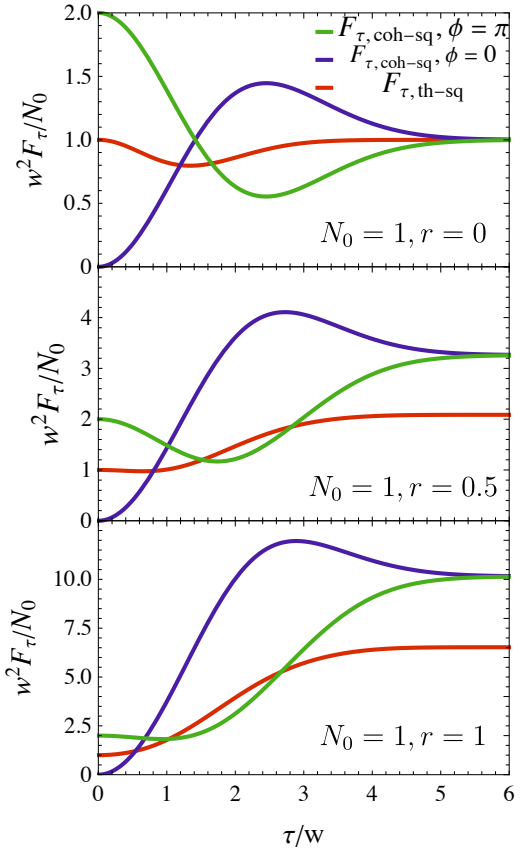

Figure 3: QFI (Normalized to its maximum value for thermal states in modes $u_0[\tau](t)$ and $v_0[\tau](t)$) for the estimation of the temporal separation τ between two thermal (red) or coherent pulses, either in phase (blue) or out of phase (green), as a function of the temporal separation τ in units of the pulse width w. For each panel, we considered a mean photon number of $N_0 = 1$ per pulse, and different levels of squeezing in the derivative modes, as quantified by the parameter $r = 0$ (top), $r = 0.5$ (middle), and $r = 1$ (bottom). The pulse shape is assumed Gaussian $u(t) = e^{-t^2/2w^2}/(\pi w^2)^{1/4}$ for all panels.

squeezed vacuum states (see Eqs. (66) and (71)). Under these assumptions, the covariance matrix contribution to the QFI can be obtained simply by setting $N_0 = 0$ into Eq. (72). Accordingly, we have

$$F_{\tau,\mathrm{coh-sq}} = F_{\bar{\mathbf{x}},\mathrm{coh-sq}} + F_{\tau,\mathrm{th-sq}}|_{N_0=0}\,, \tag{75}$$

where the displacement term $F_{\bar{\mathbf{x}},\mathrm{coh-sq}}$ can be computed from Eq. (65), and reads

$$\begin{aligned} F_{\bar{\mathbf{x}},\mathrm{coh-sq}} &= (\partial_\tau \bar{\mathbf{x}}_0)^\top V_0^{-1}(\partial_\tau \bar{\mathbf{x}}_0) + \bar{\mathbf{x}}_0^\top D_\eta V_1^{-1} D_\eta \bar{\mathbf{x}}_0 \\ &= \frac{2N_0(1-\delta\cos\phi)(\partial_\tau\delta)^2}{1-\delta^2} \\ &\quad + 2N_0 e^{2r}\eta_u^2(1+\delta)(1+\cos\phi)^2 \\ &\quad + 2N_0 e^{2r}\eta_v^2(1-\delta)(1-\cos\phi)^2 \\ &\quad + 2N_0 e^{-2r}\sin^2\phi[\eta_u(1+\delta)+\eta_v(1-\delta)]. \end{aligned} \tag{76}$$

We can see that, when the two coherent pulses are either in phase ($\phi = 0$) or out of phase ($\phi = \pi$), the last line in Eq. (76) vanishes and only the squeezing-enhanced term proportional to e^{2r} survives. This is consistent with the fact that the covariance matrix V_1 (71) presents squeezing along the q quadrature of modes $u_1[\tau](t)$ and $v_1[\tau](t)$, and for $\phi = 0, \pi$ the mean field (74) has a vanishing p quadrature. The QFI for the separation τ between in phase and out of phase coherent pulses are presented as blue and green lines in Fig. 3.

Let us now compare the expressions for the QFI for thermal and coherent pulses aided by squeezing in the derivative modes reported in Eqs. (72) and (75), respectively. We start by comparing the behaviours for vanishingly small separations $\tau \to 0$. In this regime (see App. B), we have $(\partial_\tau\delta)^2/(1-\delta^2) \sim (\Delta k)^2$, with

$$(\Delta k)^2 = \int [\partial_t u(t)]^2 dt, \tag{77}$$

and $\eta_u \sim \eta_v \sim \xi_u \sim \xi_v \sim \zeta_u \sim \zeta_v \sim 0$, which implies

$$F_{\tau,\mathrm{th-sq}} \xrightarrow{\tau\to 0} 2N_0(\Delta k)^2, \tag{78a}$$

$$F_{\tau,\mathrm{coh-sq}} \xrightarrow{\tau\to 0} 2N_0(\Delta k)^2(1+\cos\phi). \tag{78b}$$

Accordingly, independently of the squeezing value r, the QFI for in phase coherent pulses vanishes for $\tau \to 0$, while that for out of phase coherent pulses is twice the one for incoherent pulses (see Fig. 3 where for Gaussian pulses we have $(\Delta k)^2 = 1/2w^2$).

To better understand this behavior, let us recall that the quantum state of the finite overlap δ between the two pulses induces a $\tau-$dependent population of the symmetric and antisymmetric modes $u_0[\tau](t)$ and $v_0[\tau](t)$. It is this dependence on temporal separation, which enters the QFI through $\partial_\tau\bar{\mathbf{x}}_0$ (in the coherent case) and $\partial_\tau V_0$ (in the incoherent case), that dominates the QFI behavior for $\tau \to 0$. This implies that the population of the derivative modes $u_1[\tau](t)$ and $v_1[\tau](t)$, and in the particular the squeezing thereof, has no impact on the $\tau \to 0$ behavior of the QFI.

On the contrary, for separations much larger than the pulses' width, i.e. $\tau\Delta k \gg 1$, the overlap δ tends to zero, and the populations of the modes $u_0[\tau](t)$ and $v_0[\tau](t)$ become parameter independent. The QFI is then dominated by the noise in derivative modes $u_1[\tau](t)$ and $v_1[\tau](t)$. In particular, we have

$$F_{\tau,\mathrm{th-sq}} \xrightarrow{\tau\to\infty} 2(\Delta k)^2 \left(2\sinh^2 r + N_0 \cosh 2r\right), \tag{79a}$$

$$F_{\tau,\mathrm{coh-sq}|\phi=0,\pi} \xrightarrow{\tau\to\infty} 2(\Delta k)^2 \left(2\sinh^2 r + N_0 e^{2r}\right). \tag{79b}$$

Accordingly, for large temporal separations τ we have a squeezing enhancement. Such an enhancement is always larger for coherent pulses than for thermal pulses. However, similarly to what we observed for the spatial localization of a beam, the QFI enhancement for large τ in the coherent case is at most a factor two larger than that in the thermal one.

5 Conclusion

In this paper, we determined the ultimate sensitivity limit for the estimation of a parameter encoded into the quantum state as well as the mode structure of a multimode Gaussian state of the electromagnetic field. In particular, we presented an analytical expression for the QFI, bounding the estimation sensitivity through the Cramér-Rao lower bound, which can be calculated from the first two moments of the states and the dependence on the parameter of the mode functions. Such an expression expands the field of use of Gaussian quantum metrology to the estimation of parameters encoded into the spatio-temporal distribution of an electromagnetic signal. We illustrated how to apply our general formalism by studying two paradigmatic problems: the estimation of the transverse displacement of a beam, and of the temporal separation between two pulses.

In the study of the transverse displacement we showed that if the mean photon number of the beam is independent of its transverse position, the displacement of a coherent and thermal beam can be estimated with the same sensitivity. On the other hand, if the mean number of photons N_0 in the beam depends on its transverse displacement, e.g. because of position dependent losses, this dependence adds an additional term to the QFI which is $\sim N_0$ times larger for coherent beams than for thermal ones. Furthermore, we showed that the sensitivity in the estimation of a transverse displacement can be enhanced by adding squeezing to a mode shaped like the derivative of the beam. Such a squeezing-enabled quantum enhancement is at most a factor two larger for coherent beams than for thermal ones.

We then moved to the time domain and considered the estimation of the temporal separation between two coherent or thermal pulses. Such pulses are described by two temporal modes (the symmetric and anti-symmetric superpositions of the pulses) whose shape and populations depend on the separation parameter τ. We showed that the interplay between these two dependences plays a fundamental role in the choice of which modes one needs to squeeze to achieve a quantum enhancement. For large temporal separations, when the pulses have a negligible overlap, they are are most sensitive to the changes in the mode shapes. Accordingly, in this regime a quantum enhancement is possible by adding squeezing to the derivatives of the symmetric and anti-symmetric superpositions of the pulses. As for the transverse displacement estimation, the quantum enhancement achieved for coherent pulses is at most a factor two larger than the one obtained for thermal ones. On the other hand, for small temporal separations, when the pulses have a significant overlap, the QFI is dominated by how photons redistributes among the symmetric and anti-symmetric superpositions of the pulses. As a consequence, populating the derivative modes has no effect on the sensitivity in this regime.

Our approach could be readily applied to other mode-encoded parameter estimation scenarios in various field of science and technology ranging from astronomy to microscopy (Gessner *et al.*, 2022). Moreover, parameters encoded into time-frequency modes appears in the characterization of frequency combs (Cai *et al.*, 2021), or in radars that estimate the distance of a reflecting target from the temporal profile of chirped pulses (Van Trees, 2002, 2001) (recent studies have addressed this problem in the quantum regime (Zhuang and Shapiro, 2022; Gessner *et al.*, 2022)). Finally, the applicability of our approach could be further broadened by considering the simultaneous estimation of multiple parameters (Nichols *et al.*, 2018).

Acknowledgments

We are very grateful to Claude Fabre for our illuminating discussions on the role of modes in quantum optical metrology, which have been a main

source of inspiration for this work. We also thank Ilya Karuseichyk for useful discussion. This work was partially funded by French ANR under COSMIC project (ANR-19-ASTR0020-01). This work received funding from the European Union's Horizon 2020 research and innovation programme under Grant Agreement No. 899587. This work was carried out during the tenure of an ERCIM 'Alain Bensoussan' Fellowship Programme. This work was funded by MCIN/AEI/10.13039/501100011033 and the European Union "NextGenerationEU" PRTR fund [RYC2021-031094-I]. This work has been founded by the Ministry of Economic Affairs and Digital Transformation of the Spanish Government through the QUANTUM ENIA project call - QUANTUM SPAIN project, by the European Union through the Recovery, Transformation and Resilience Plan - NextGenerationEU within the framework of the Digital Spain 2026 Agenda, and by the CSIC Interdisciplinary Thematic Platform (PTI+) on Quantum Technologies (PTI-QTEP+).

A Properties of the basis-change matrices

Here we derive some useful properties of the matrix O, and its blocks O_n and O_N from the properties of the n initially populated modes $\{u_k[\vartheta](\mathbf{r},t)\}$ and their derivatives $\{\partial_\vartheta u_k[\vartheta](\mathbf{r},t)\}$. Let us start by recalling the following Hilbert space definitions:

$$\mathcal{H}_n = \mathrm{span}\left(\{u_k[\vartheta](\mathbf{r},t)\}\right), \tag{80}$$
$$\mathcal{H}_\partial = \mathrm{span}\left(\{\partial_\vartheta u_k[\vartheta](\mathbf{r},t)\}\right) \setminus \mathcal{H}_n. \tag{81}$$

We now assume that m is the number of derivatives $\partial_\vartheta u_k[\vartheta](\mathbf{r},t)$ that are linearly independent from the n initially populated modes, i.e. $\dim(\mathcal{H}_\partial) = m$. Accordingly, up to a reordering of the basis $\{\partial_\vartheta u_k[\vartheta](\mathbf{r},t)\}$, we can always construct a basis of $\mathcal{H}_\partial$ using the orthonormalized version $u'_k[\vartheta](\mathbf{r},t)$ of the derivatives of the first m initially populated modes $\partial_\vartheta u_k[\vartheta](\mathbf{r},t)$.

We can now choose the modes $u'_k[\vartheta](\mathbf{r},t)$ as the first m among the $N-n$ auxiliary vacuum modes that we use to describe the quantum state of the system in the parameter dependent basis. In light of this, it is convenient to further decompose the matrix O_{N-n} as

$$O_{N-n} = \begin{pmatrix} O_\partial & O_{N-n-m} \end{pmatrix}, \tag{82}$$

where O_∂ and O_{N-n-m} are matrices of dimensions $2N\times 2m$ and $2N\times 2(N-n-m)$, respectively. From the orthogonality of O, we can obtain the following relations:

$$O_k^\top O_l = \delta_{kl}\mathbb{1}_{\dim(O_k)}, \tag{83a}$$
$$\sum_k O_k O_k^\top = \mathbb{1}_{2N}, \tag{83b}$$

where the sum in Eq. (83b) runs over the total number of column blocks we decomposed the matrix O into.

Let us now compute the derivative of the matrix O_n. In Sec. 2.2, we have seen that that O is composed by 2×2 blocks containing the mode overlaps. Accordingly, it is sufficient to specify the derivative of the kl block of O_n, which reads

$$\partial_\vartheta \left(O_n\right)_{kl} = \begin{pmatrix} \mathrm{Re}\left[(v_l|\partial_\vartheta u_k[\vartheta])\right] & -\mathrm{Im}\left[(v_l|\partial_\vartheta u_k[\vartheta])\right] \\ \mathrm{Im}\left[(v_l|\partial_\vartheta u_k[\vartheta])\right] & \mathrm{Re}\left[(v_l|\partial_\vartheta u_k[\vartheta])\right] \end{pmatrix} \tag{84}$$

Combining Eqs. (84) and (29), we obtain

$$\partial_\vartheta O_n = O_n D_n^\top + O_\partial D_\partial^\top, \tag{85}$$

where D_n and D_∂ are a $2n\times 2n$ and a $2n\times 2m$ matrices, respectively. Their kl blocks are given by

$$(D_n)_{kl} = \begin{pmatrix} \mathrm{Re}\left(c_{kl}[\vartheta]\right) & -\mathrm{Im}\left(c_{kl}[\vartheta]\right) \\ \mathrm{Im}\left(c_{kl}[\vartheta]\right) & \mathrm{Re}\left(c_{kl}[\vartheta]\right) \end{pmatrix}, \tag{86}$$

$$(D_\partial)_{kl} = \begin{pmatrix} \mathrm{Re}\left(c'_{kl}[\vartheta]\right) & -\mathrm{Im}\left(c'_{kl}[\vartheta]\right) \\ \mathrm{Im}\left(c'_{kl}[\vartheta]\right) & \mathrm{Re}\left(c'_{kl}[\vartheta]\right) \end{pmatrix}. \tag{87}$$

Using Eqs. (85) and (83), we then obtain

$$O_n^\top(\partial_\vartheta O_n) = D_n^\top, \tag{88a}$$
$$O_{(N-n)}^\top(\partial_\vartheta O_n) = (D_\partial, 0)^\top. \tag{88b}$$

Let us conclude this appendix with few words on the coefficients $c_{kl}[\vartheta]$ and $c'_{kl}[\vartheta]$. The first are simply given by the overlaps of the initially populated modes with their derivatives $c_{kl}[\vartheta] = (u_l[\vartheta]|\partial_\vartheta u_k[\vartheta])$. On the other hand, there exist several orthonormalization methods that can be used to construct the modes $u'_k[\vartheta](\mathbf{r},t)$, leading to different expressions for the coefficients $c'_{kl}[\vartheta]$. For example, using the Gram-Schmidt procedure, the modes $u'_k[\vartheta](\mathbf{r},t)$ can be constructed iteratively as $u'_k[\vartheta](\mathbf{r},t) = \tilde{u}'_k[\vartheta](\mathbf{r},t)/\sqrt{(\tilde{u}'_k[\vartheta]|\tilde{u}'_k[\vartheta])}$ with

$$\begin{aligned}\tilde{u}'_k[\vartheta](\mathbf{r},t) = {} & \partial_\vartheta u_k[\vartheta](\mathbf{r},t) \\ & - \sum_{j=1}^{n}(u_j[\vartheta]|\partial_\vartheta u_k[\vartheta])u_j[\vartheta](\mathbf{r},t) \\ & - \sum_{j=1}^{k-1}(u'_j[\vartheta]|\partial_\vartheta u_k[\vartheta])u'_j[\vartheta](\mathbf{r},t).\end{aligned} \tag{89}$$

Accordingly, the coefficients $c'_{kl}[\vartheta]$ are given by

$$c'_{kl}[\vartheta] = \begin{cases} \sqrt{(\tilde{u}'_k[\vartheta]|\tilde{u}'_k[\vartheta])} & \text{for } k = l \\ (u'_j[\vartheta]|\partial_\vartheta u_k[\vartheta]) & \text{for } k < l \\ 0 & k > l \end{cases}, \tag{90}$$

resulting in a lower-triangular block matrix D_∂.

B Derivative modes for temporal separation estimation

B.1 General expressions

In this appendix, we construct the orthogonalized first and second derivatives of the modes $u_0[d](t)$ and $u_0[d](t)$. Let us start by computing the derivatives of Eqs. (62) with respect to the parameter τ:

$$\partial_d u_0[\tau](t) = \frac{-\partial_t u(t-\tau/2) + \partial_x u(x+\tau/2)}{2\sqrt{2(1+\delta)}} - \delta' \frac{u_0[\tau](t)}{2(1+\delta)}, \tag{91a}$$

$$\partial_d v_0[\tau](t) = \frac{-\partial_t u(t-\tau/2) - \partial_t u(t+\tau/2)}{2\sqrt{2(1-\delta)}} + \delta' \frac{v_0[\tau](t)}{2(1-\delta)}, \tag{91b}$$

where we introduced $\delta' = \partial_\tau \delta$. We assumed that our pulses are symmetric, i.e. $u(t) = u(-t)$. We thus have $(\partial_t u|u) = 0$, which, combined with

$$\delta' = -\int \partial_t u(t-\tau/2) u(t+\tau/2) dt + \int u(t-\tau/2) \partial_t u(t+\tau/2) dt, \tag{92}$$

implies that $(\partial_\tau v_0|u_0) = (\partial_\tau u_0|v_0) = 0$. Consequently, the orthogonalised first derivative modes are simply given by

$$u_1[\tau](t) = \partial_\tau u_0[\tau](t)/\eta_u, \tag{93a}$$

$$v_1[\tau](t) = \partial_\tau v_0[\tau](t)/\eta_v, \tag{93b}$$

with

$$\eta_u^2 = ||\partial_\tau u_0[\tau](t)||^2 = \frac{(\Delta k)^2 - \beta}{4(1+\delta)} - \frac{(\delta')^2}{4(1+\delta)^2}, \tag{94a}$$

$$\eta_v^2 = ||\partial_\tau v_0[\tau](t)||^2 = \frac{(\Delta k)^2 + \beta}{4(1-\delta)} - \frac{(\delta')^2}{4(1-\delta)^2}, \tag{94b}$$

where we introduced

$$(\Delta k)^2 = \int [\partial_t u(t)]^2 dt, \quad \text{and} \tag{95}$$

$$\beta = \int \partial_t u(t-\tau/2) \partial_t u(t+\tau/2) dt. \tag{96}$$

We now move to the construction of the orthonormalized second derivatives. The fact that the modes $u_1[\tau](t)$ and $v_1[\tau](t)$ have, by construction, opposite parity implies that $(\partial_\tau u_1|u_1) = (\partial_\tau v_1|v_1) = 0$, and $(\partial_\tau u_1|v_1) = -(\partial_\tau v_1|u_1)$. Let us then evaluate $(\partial_d u_1|v_1)$ explicitly

$$\begin{aligned}(\partial_\tau u_1|v_1) &= \frac{(\partial_\tau u_1|\partial_\tau v_0)}{\eta_v} \\ &= \frac{(\partial_\tau^2 u_0|\partial_\tau v_0)}{\eta_u \eta_v} - \frac{\eta'_u}{\eta_v \eta_u^2}(\partial_\tau u_0|\partial_\tau v_0) \\ &= \frac{(\partial_\tau^2 u_0|\partial_\tau v_0)}{\eta_u \eta_v},\end{aligned} \tag{97}$$

where in the last step we used that $u_0[\tau](t)$ and $v_0[\tau](t)$ are even and odd functions of t, respectively. The second derivative of $u_0(x)$ and $v_0(x)$ can be rewritten as

$$\partial_t^2 u_0[\tau](t) = \frac{f_u[\tau](t)}{4\sqrt{2(1+\delta)}} - \frac{\delta'}{1+\delta}\partial_d u_0[\tau](t) + C_u u_0[\tau](t), \tag{98a}$$

$$\partial_t^2 v_0[\tau](t) = \frac{f_v[\tau](t)}{4\sqrt{2(1-\delta)}} + \frac{\delta'}{1-\delta}\partial_d v_0[\tau](t) + C_v v_0[\tau](t), \tag{98b}$$

with

$$f_u[\tau](t) = \partial_t^2 u(t-\tau/2) + \partial_t^2 u(t+\tau/2), \tag{99}$$

$$f_v[\tau](t) = \partial_t^2 u(t-\tau/2) - \partial_t^2 u(t+\tau/2), \tag{100}$$

and

$$C_u = \frac{(\delta')^2 - 2(1+\delta)\delta''}{4(1+\delta)^2}, \tag{101}$$

$$C_v = \frac{(\delta')^2 + 2(1-\delta)\delta''}{4(1-\delta)^2}, \tag{102}$$

where we have introduced the second derivative of the overlap parameter $\delta'' = \partial_\tau^2 \delta$. Using $(\partial_\tau u_0|\partial_\tau v_0) = (u_0|\partial_\tau v_0) = 0$, from Eq. (98a) we have

$$\begin{aligned}&(\partial_d u_1|v_1) \propto \\ &\int \partial_t^2 u(t+\tau)\partial_t u(t) dt + \int \partial_t^2 u(-t-\tau)\partial_t u(-t) dt \\ &= \int \partial_t^2 u(t+\tau)\partial_t u(t) dt - \int \partial_t^2 u(t+\tau)\partial_t u(t) dt \\ &= 0,\end{aligned} \tag{103}$$

where we used that the pulse shape $u(t)$ is an even function of t. Therefore, the orthogonalized second derivative modes are given by

$$u_2[\tau](t) = (\partial_d u_1[\tau](t) - \xi_u u_0([\tau](t))/\zeta_u, \quad (104)$$
$$v_2[\tau](t) = (\partial_d v_1[\tau](t) - \xi_v v_0[\tau](t))/\zeta_v, \quad (105)$$

with $\xi_u = (\partial_\tau u_1|u_0)$, $\xi_v = (\partial_\tau v_1|v_0)$, $\zeta_u = ||\partial_\tau u_1[\tau(t) - \xi_u u_0[\tau](t)||$ and $\zeta_v = ||\partial_\vartheta v_1[\vartheta](t) - \xi_v v_0[\vartheta](t)||$.

Let us explicitly calculate ξ_u and ξ_v. This can be achieved by using Eqs. (98a), (98b) and by noting that

$$\begin{aligned}\int &\partial_t^2 \left[u(t-\tau/2) \pm u(t+\tau/2)\right] \quad (106)\\ &\times \left[u(t-\tau/2) \pm u(t-\tau/2)\right] dt\\ &= -\int \left[\partial_t u(t-\tau/2) \pm \partial_t u(t+\tau/2)\right]^2 dt\\ &= -2(\Delta k)^2 \mp 2\beta,\end{aligned}$$

where we used partial integration and made the reasonable assumption that the pulse shape $u(t)$ goes to zero at infinity. We then get

$$\xi_u = \frac{1}{\eta_u}\left(\frac{(\delta')^2 - 2(1+\delta)\delta''}{4(1+\delta)^2} - \frac{(\Delta k)^2+\beta}{4(1+\delta)}\right) \quad (107a)$$
$$= \frac{(\delta')^2 - 2(1+\delta)\delta'' - (1+\delta)\left((\Delta k)^2+\beta\right)}{(1+\delta)\sqrt{(1+\delta)\left((\Delta k)^2-\beta\right) - (\delta')^2}},$$
$$\xi_v = \frac{1}{\eta_v}\left(\frac{(\delta')^2 + 2(1-\delta)\delta''}{4(1-\delta)^2} - \frac{(\Delta k)^2-\beta}{4(1-\delta)}\right) \quad (107b)$$
$$= \frac{(\delta')^2 + 2(1-\delta)\delta'' - (1+\delta)\left((\Delta k)^2-\beta\right)}{(1-\delta)\sqrt{(1-\delta)\left((\Delta k)^2+\beta\right) - (\delta')^2}}.$$

Let us now compute explicitly the normalization constants of the modes $u_2[\tau](t)$ and $v_2[\tau](t)$

$$\begin{aligned}\zeta_u^2 &= ||\partial_\tau u_1[\tau](t) - \xi_u u_0[\tau](t)||^2 \quad (108a)\\ &= ||\partial_\tau u_1[\tau](t)||^2 + \xi_u^2 - 2\xi_u(\partial_\tau u_1|u_0)\\ &= ||\partial_\tau u_1[\tau](t)||^2 - \xi_u^2,\\ \zeta_v^2 &= ||\partial_\tau v_1[\tau](t) - \xi_v v_0[\tau](t)||^2 \quad (108b)\\ &= ||\partial_\tau v_1[\tau](t)||^2 + \xi_v^2 - 2\xi_v(\partial_\tau v_1|v_0)\\ &= ||\partial_\tau v_1[\tau](t)||^2 - \xi_v^2.\end{aligned}$$

We can then expand

$$||\partial_\tau u_1[\tau](t)||^2 = \left|\left|\frac{\partial_\tau^2 u_0[\tau](t)}{\eta_u} - \frac{(\partial_\tau \eta_u)^2}{\eta_u^2}\partial_\tau u_0[\tau](t)\right|\right|^2 \quad (109a)$$
$$= \frac{||\partial_\tau^2 u_0||^2 + (\partial_\tau \eta_u)^2}{\eta_u^2} - 2\frac{\partial_\tau \eta_u}{\eta_u^3}(\partial_\tau^2 u_0|\partial_\tau u_0),$$
$$||\partial_\tau v_1[\tau](t)||^2 = \left|\left|\frac{\partial_\tau^2 v_0[\tau](t)}{\eta_v} - \frac{(\partial_\tau \eta_v)^2}{\eta_v^2}\partial_\tau v_0[\tau](t)\right|\right|^2 \quad (109b)$$
$$= \frac{||\partial_\tau^2 v_0[\tau](t)||^2 + (\partial_\tau \eta_v)^2}{\eta_v^2} - 2\frac{\partial_\tau \eta_v}{\eta_v^3}(\partial_\tau^2 v_0|\partial_\tau v_0).$$

From Eqs. (98a) and (98b), we then have

$$||\partial_\tau^2 u_0[\tau](t)||^2 = \frac{||f_u[\tau](t)||^2}{32(1+\delta)} + \frac{(\delta')^2\eta_u^2}{(1+\delta^2)} + C_u^2 \quad (110a)$$
$$- \frac{\delta'(f_u|\partial_\tau u_0)}{4\sqrt{2}(1+\delta)^{3/2}} - C_u\frac{2(\Delta k)^2+2\beta}{\sqrt{2(1+\delta)}}$$
$$||\partial_\tau^2 v_0[\tau](t)||^2 = \frac{||f_v[\tau](t)||^2}{32(1-\delta)} + \frac{(\delta')^2\eta_v^2}{(1-\delta^2)} + C_v^2 \quad (110b)$$
$$+ \frac{\delta'(f_v|\partial_\tau v_0)}{4\sqrt{2}(1-\delta)^{3/2}} - C_v\frac{2(\Delta k)^2-2\beta}{\sqrt{2(1-\delta)}},$$

with

$$||f_u[\tau](t)||^2 = 2(\sigma+\epsilon) \quad (111a)$$
$$||f_v[\tau](t)||^2 = 2(\sigma-\epsilon), \quad (111b)$$

and

$$(f_u|\partial_d u_0) = \frac{(\Delta k)^2+\beta}{1+\delta}\delta' + \frac{\beta'}{\sqrt{2(1+\delta)}}, \quad (112a)$$
$$(f_v|\partial_d v_0) = \frac{(\Delta k)^2-\beta}{1-\delta}\delta' + \frac{\beta'}{\sqrt{2(1-\delta)}}, \quad (112b)$$

where we defined

$$\sigma = \int \left|\partial_t^2 u(t)\right|^2 dt, \quad (113a)$$
$$\epsilon = \int \partial_t^2 u(t-\tau/2)\partial_t^2 u(t-\tau/2)dx. \quad (113b)$$

Since the expressions of the mode quantities (especially ζ_u and ζ_v) computed above for a generic

pulse shape $u(t)$ are fairly complicated, we present their explicit expressions for a Gaussian pulse $u(t) = e^{-t^2/2w^2}/(\pi w^2)^{1/4}$ in the following:

$$\eta_u = \frac{\sqrt{\tau^2 + 4w^2 \sinh\left(\frac{\tau^2}{4w^2}\right)}\operatorname{sech}\left(\frac{\tau^2}{8w^2}\right)}{8w^2}, \quad (114)$$

$$\eta_v = \frac{\sqrt{4w^2 \sinh\left(\frac{\tau^2}{4w^2}\right) - \tau^2}\operatorname{csch}\left(\frac{\tau^2}{8w^2}\right)}{8w^2}, \quad (115)$$

$$\xi_u = -\frac{\sqrt{\tau^2 + 4w^2 \sinh\left(\frac{\tau^2}{4w^2}\right)}\operatorname{sech}\left(\frac{\tau^2}{8w^2}\right)}{8w^2}, \quad (116)$$

$$\xi_v = -\frac{\sqrt{4w^2 \sinh\left(\frac{\tau^2}{4w^2}\right) - \tau^2}\operatorname{csch}\left(\frac{\tau^2}{8w^2}\right)}{8w^2}, \quad (117)$$

$$\zeta_u^2 = \frac{2w^2 \sinh\left(\frac{\tau^2}{2w^2}\right) - \tau^2\left(1 + \cosh\left(\frac{\tau^2}{4w^2}\right)\right)}{\left(\tau^2 + 4w^2 \sinh\left(\frac{\tau^2}{4w^2}\right)\right)^2} \quad (118)$$

$$+ \frac{(\tau^4 + 16w^4)\sinh\left(\frac{\tau^2}{4w^2}\right)}{4w^2\left(\tau^2 + 4w^2 \sinh\left(\frac{\tau^2}{4w^2}\right)\right)^2}$$

$$\zeta_v^2 = \frac{2w^2 \sinh\left(\frac{\tau^2}{2w^2}\right) - \tau^2\left(1 - \cosh\left(\frac{\tau^2}{4w^2}\right)\right)}{\left(\tau^2 - 4w^2 \sinh\left(\frac{\tau^2}{4w^2}\right)\right)^2} \quad (119)$$

$$- \frac{(\tau^4 + 16w^4)\sinh\left(\frac{\tau^2}{4w^2}\right)}{4w^2\left(\tau^2 - 4w^2 \sinh\left(\frac{\tau^2}{4w^2}\right)\right)^2}.$$

Note that the fact that $\eta_{u,v}^2 = \xi_{u,v}^2$ is a peculiarity of Gaussian pulses and it is not true in general.

B.2 Small τ behaviour

Arguably, the most interesting regime for temporal separation estimation is that of small τ. Therefore, in the following, we discuss the behaviour of the quantities computed above for $\tau \to 0$. Let us start by considering the following series expansions

$$\delta = 1 - (\Delta k)^2 \frac{\tau^2}{2} + \sigma \frac{\tau^4}{24} + \mathcal{O}(\tau^6), \quad (120a)$$

$$\beta = (\Delta k)^2 - \sigma \frac{\tau^2}{2} + \mathcal{O}(\tau^4), \quad (120b)$$

$$\epsilon = \sigma + \mathcal{O}(\tau^2). \quad (120c)$$

Using Eqs. (120), it is possible to show that for $\tau \sim 0$ we have $\eta_u \sim \eta_v \sim \xi_u \sim \xi_v \sim \zeta_u \sim \zeta_v \sim \tau$. For example, for Gaussian pulses we have

$$\eta_u = \frac{\tau}{4\sqrt{2}w^2} + \mathcal{O}\left(\tau^2\right), \quad (121a)$$

$$\eta_v = \frac{\tau}{4\sqrt{6}w^2} + \mathcal{O}\left(\tau^2\right), \quad (121b)$$

$$\xi_u = -\frac{\tau}{4\sqrt{2}w^2} + \mathcal{O}\left(\tau^2\right), \quad (121c)$$

$$\xi_v = -\frac{\tau}{4\sqrt{6}w^2} + \mathcal{O}\left(\tau^2\right), \quad (121d)$$

$$\zeta_u = \frac{\tau}{4\sqrt{3}w^2} + \mathcal{O}\left(\tau^2\right), \quad (121e)$$

$$\zeta_v = \frac{\tau}{4\sqrt{5}w^2} + \mathcal{O}\left(\tau^2\right). \quad (121f)$$

This behaviour implies that the contribution to the QFI coming from the coefficients b_l^{jk} and d_l^{jk} vanishes for $\tau \to 0$ (see Eqs.(68) and App. C).

C Calculation of the QFI (72)

In this Appendix, we explicitly compute the coefficients (68) that lead to the QFI (72) for the estimation of the temporal separation τ between two incoherent thermal pulses aided by two squeezed vacuum states in the derivative modes $u_1[\tau](t)$ and $v_1[\tau](t)$ defined by the covariance matrices V_0 (70) and V_1 (71).

First, we note that V_0 (70) is already in Williamson form. Therefore, the symplectic matrix S_0 entering in Eqs. (68) is the identity $S_0 = \mathbb{1}_4$, while for the symplectic eigenvalues we have $\nu_0^0 = 2N_0(1+\delta)+1$ and $\nu_0^1 = 2N_0(1-\delta)+1$. On the other hand, the Williamson decomposition V_1 (71) is achieved by the squeezing matrix

$$S_1 = \begin{pmatrix} e^{-r} & 0 & 0 & 0 \\ 0 & e^{r} & 0 & 0 \\ 0 & 0 & e^{-r} & 0 \\ 0 & 0 & 0 & e^{r} \end{pmatrix}, \quad (122)$$

with symplectic eigenvalues $\nu_1^{0,1} = 1$.

To compute the coefficients a_l^{jk}, we need the derivative of the matrix V_0 (70). The latter depends on the temporal separation τ only through the overlap parameter δ. Accordingly, we have

$$\partial_\tau V_0 = \begin{pmatrix} 2N_0(\partial_\tau \delta)\mathbb{1}_2 & 0 \\ 0 & -2N_0(\partial_\tau \delta)\mathbb{1}_2 \end{pmatrix}. \quad (123)$$

Since $\partial_\tau V_0$ is diagonal, the only nonzero a_l^{jk} coefficients are

$$\left(a_2^{00}\right)^2 = \left(a_2^{11}\right)^2 = 8N_0(\partial_\tau \delta). \quad (124)$$

Using $S_0 = \mathbb{1}_4$, and the fact that all matrices D_ξ, D_η, and V_0 are diagonal, we have $\left(b_l^{jk}\right)^2 = 2\left(\mathrm{tr}\left\{A_l^{(jk)} M_b\right\}\right)^2$, where we introduced the matrix

$$M_b = \begin{pmatrix} X_u + Y_u & 0 & 0 & 0 \\ 0 & X_u - Y_u & 0 & 0 \\ 0 & 0 & X_v + Y_v & 0 \\ 0 & 0 & 0 & X_v - Y_v \end{pmatrix}, \tag{125}$$

with

$$X_u = N_0(1+\delta)\eta_u \cosh r, \tag{126a}$$
$$X_v = N_0(1-\delta)\eta_v \cosh r, \tag{126b}$$
$$Y_u = [N_0(1+\delta)\eta_u - \xi_u] \sinh r, \tag{126c}$$
$$Y_v = [N_0(1-\delta)\eta_v - \xi_v] \sinh r. \tag{126d}$$

Consequently, the only nonzero b_l^{jk} coefficients are

$$\left(b_1^{00}\right)^2 = 8\left[N_0(1+\delta)\eta_u - \xi_u\right]^2 \sinh^2 r, \tag{127a}$$
$$\left(b_2^{00}\right)^2 = 8N_0^2(1+\delta)^2\eta_u^2 \cosh^2 r, \tag{127b}$$
$$\left(b_1^{11}\right)^2 = 8\left[N_0(1-\delta)\eta_v - \xi_v\right]^2 \sinh^2 r, \tag{127c}$$
$$\left(b_2^{11}\right)^2 = 8N_0^2(1-\delta)^2\eta_v^2 \cosh^2 r. \tag{127d}$$

We assumed the covariance matrix V_1 of the derivative modes $u_1[\tau](t)$ and $v_1[\tau](t)$ to be parameter independent, i.e. $\partial_\tau V_1 = 0$, which leads to $c_l^{(jk)} = 0$ for all l, j and k.

Finally, we can write the d_l^{jk} coefficients as

$$\left(d_l^{jk}\right)^2 = 2\left(\mathrm{tr}\left\{A_l^{(jk)} M_d\right\}\right)^2 \tag{128}$$

with

$$M_d = D_\zeta(V_1 - \mathbb{1}_4)S_1^{-1} = 2\sinh r \begin{pmatrix} \zeta_u\sigma_z & 0 \\ 0 & \zeta_v\sigma_z \end{pmatrix}. \tag{129}$$

As consequence, the only nonzero d_l^{jk} coefficients are

$$\left(d_1^{00}\right)^2 = 8\zeta_u^2 \sinh^2 r, \tag{130a}$$
$$\left(d_1^{11}\right)^2 = 8\zeta_v^2 \sinh^2 r. \tag{130b}$$

Substituting the coefficients in Eqs. (124), (127) and (130) into Eq. (67), we then obtain the QFI (72).

References

C. W. Helstrom, *Quantum detection and estimation theory*, Vol. 3 (Academic press, New York, 1976).

A. S. Holevo, *Probabilistic and statistical aspects of quantum theory*, Vol. 1 (Springer, Berlin, 2011).

M. G. A. Paris, International Journal of Quantum Information **07**, 125 (2009).

L. Pezzè and A. Smerzi, in *Proceedings of the International School of Physics "Enrico Fermi"*, Course 188, Varenna, edited by G. M. Tino and M. A. Kasevich (IOS Press, Amsterdam, 2014) pp. 691 – 741.

V. Giovannetti, S. Lloyd, and L. Maccone, Nature Photonics **5**, 222 (2011).

G. Tóth and I. Apellaniz, Journal of Physics A: Mathematical and Theoretical **47**, 424006 (2014).

M. A. Taylor and W. P. Bowen, Physics Reports **615**, 1 (2016).

M. Tsang, Contemporary Physics **60**, 279 (2019).

V. Giovannetti, S. Lloyd, and L. Maccone, Nature **412**, 417 (2001).

Q. Zhuang, Z. Zhang, and J. H. Shapiro, Phys. Rev. A **96**, 040304 (2017).

Z. Huang, C. Lupo, and P. Kok, PRX Quantum **2**, 030303 (2021).

F. Acernese *et al.* (Virgo Collaboration), Phys. Rev. Lett. **123**, 231108 (2019).

M. Tse *et al.* (LIGO Collaboration), Phys. Rev. Lett. **123**, 231107 (2019).

C. Fabre and N. Treps, Rev. Mod. Phys. **92**, 035005 (2020).

N. Treps, U. Andersen, B. Buchler, P. K. Lam, A. Maître, H.-A. Bachor, and C. Fabre, Phys. Rev. Lett. **88**, 203601 (2002).

N. Treps, N. Grosse, W. P. Bowen, C. Fabre, H.-A. Bachor, and P. K. Lam, Science **301**, 940 (2003).

Y. Cai, J. Roslund, V. Thiel, C. Fabre, and N. Treps, npj Quantum Information **7**, 82 (2021).

M. Gessner, N. Treps, and C. Fabre, arXiv:2201.04050 (2022).

M. Tsang, R. Nair, and X.-M. Lu, Phys. Rev. X **6**, 031033 (2016).

M. Paúr, B. Stoklasa, Z. Hradil, L. L. Sánchez-Soto, and J. Rehacek, Optica **3**, 1144 (2016).

P. Boucher, C. Fabre, G. Labroille, and N. Treps, Optica **7**, 1621 (2020).

V. Ansari, B. Brecht, J. Gil-Lopez, J. M. Donohue, J. Řeháček, Z. c. v. Hradil, L. L. Sánchez-Soto, and C. Silberhorn, PRX Quantum **2**, 010301 (2021).

S. De, J. Gil-Lopez, B. Brecht, C. Silberhorn, L. L. Sánchez-Soto, Z. c. v. Hradil, and J. Řeháček, Phys. Rev. Res. **3**, 033082 (2021).

M. Mazelanik, A. Leszczyński, and M. Parniak, Nature Communications **13**, 691 (2022).

C. Lupo and S. Pirandola, Phys. Rev. Lett. **117**, 190802 (2016).

A. Holevo, IEEE Transactions on Information Theory **21**, 533 (1975).

C. Weedbrook, S. Pirandola, R. García-Patrón, N. J. Cerf, T. C. Ralph, J. H. Shapiro, and S. Lloyd, Reviews of Modern Physics **84**, 621 (2012).

G. Adesso, S. Ragy, and A. R. Lee, Open Systems & Information Dynamics **21**, 1440001 (2014).

C. M. Caves, Phys. Rev. D **23**, 1693 (1981).

L. Pezzé and A. Smerzi, Phys. Rev. Lett. **100**, 073601 (2008).

O. Pinel, J. Fade, D. Braun, P. Jian, N. Treps, and C. Fabre, Phys. Rev. A **85**, 010101 (2012).

A. Monras, arXiv:1303.3682 (2013).

D. Šafránek, A. R. Lee, and I. Fuentes, New Journal of Physics **17**, 073016 (2015).

Z. Jiang, Phys. Rev. A **89**, 032128 (2014).

R. Nair and M. Tsang, Phys. Rev. Lett. **117**, 190801 (2016).

G. Sorelli, M. Gessner, M. Walschaers, and N. Treps, Phys. Rev. Res. **4**, L032022 (2022).

S. L. Braunstein and P. van Loock, Rev. Mod. Phys. **77**, 513 (2005).

A. Serafini, *Quantum continuous variables: a primer of theoretical methods* (Tayor & Francis, Milton Park, 2017).

R. Simon, N. Mukunda, and B. Dutta, Phys. Rev. A **49**, 1567 (1994).

J. Williamson, American Journal of Mathematics **58**, 141 (1936).

M. Walschaers, PRX Quantum **2**, 030204 (2021).

A. S. Holevo and R. F. Werner, Phys. Rev. A **63**, 032312 (2001).

S. L. Braunstein and C. M. Caves, Phys. Rev. Lett. **72**, 3439 (1994).

G. Sorelli, M. Gessner, M. Walschaers, and N. Treps, Phys. Rev. Lett. **127**, 123604 (2021a).

G. Sorelli, M. Gessner, M. Walschaers, and N. Treps, Phys. Rev. A **104**, 033515 (2021b).

H. L. Van Trees, *Detection, estimation, and modulation theory, part I: detection, estimation, and linear modulation theory* (John Wiley & Sons, New York, 2002).

H. L. Van Trees, *Detection, estimation, and modulation theory, part III: Radar-Sonar Signal Processing and Gaussian Signals in Noise* (John Wiley & Sons, New York, 2001).

Q. Zhuang and J. H. Shapiro, Phys. Rev. Lett. **128**, 010501 (2022).

R. Nichols, P. Liuzzo-Scorpo, P. A. Knott, and G. Adesso, Phys. Rev. A **98**, 012114 (2018).

5

NON-GAUSSIAN QUANTUM CORRELATIONS

LIST OF ARTICLES

1. **M. Walschaers**, C. Fabre, V. Parigi, and N. Treps, *Entanglement and Wigner function negativity of multimode non-Gaussian states*, Phys. Rev. Lett. **119**, 183601 (2017).
2. **M. Walschaers**, C. Fabre, V. Parigi, and N. Treps, *Statistical signatures of multimode single-photon added and subtracted states of light*, Phys. Rev. A **96**, 053835 (2017).
3. **M. Walschaers**, *Non-Gaussian Quantum States and Where to Find Them*, PRX Quantum **2**, 030204 (2021).
4. K. Zhang, J. Jing, N. Treps, and **M. Walschaers**, *Maximal entanglement increase with single-photon subtraction*, Quantum **6**, 704 (2022).
5. C. E. Lopetegui, M. Gessner, M. Fadel, N. Treps, and **M. Walschaers**, *Homodyne Detection of Non-Gaussian Quantum Steering*, PRX Quantum **3**, 030347 (2022).
6. U. Chabaud and **M. Walschaers**, *Resources for bosonic quantum computational advantage*, Phys. Rev. Lett. **130**, 090602 (2023)
7. D. Barral, M. Isoard, G. Sorelli, M. Gessner, N. Treps, **M. Walschaers**, *Metrological detection of purely-non-Gaussian entanglement*, arXiv:2301.03909

5.1 FRAMEWORK FOR NON-GAUSSIAN ENTANGLEMENT

Ever since Bell's groundbreaking work (Bell, 1964), quantum correlations are at the forefront of fundamental developments in quantum physics. They are one of the core features that distinguish quantum and classical physics. It is thus no surprise that quantum entanglement lies at the heart of many proposed quantum technologies. Quantum correlations also have a long history in continuous-variable systems, after all, the seminal paper by Einstein et al., 1935 was written in a continuous-variable language. Schrödinger, 1935, 1936 formulated a crucial reply to the EPR paper, defining what would later become known as quantum steering. Therefore, the concept of quantum steering was historically first considered in the context of continuous-variable quantum optics (Reid, 1989; Reid and Drummond, 1988). At a later stage, tools for studying more general quantum entanglement in continuous-variable systems were introduced (Duan et al., 2000; Loock and Furusawa, 2003; R. Simon, 2000). Because these continuous-

variable methods are based on the covariance matrix, they are practical to use in experiments (Bowen et al., 2003).

On the other hand, entanglement witnesses and measures based on the covariance matrix have their limitations. In Chabaud and Walschaers, 2023 (see Section 2.4) we argued that we need a type of entanglement that cannot be undone through changes in mode basis to achieve a quantum computational advantage. However, using the Williamson (Williamson, 1936) and Bloch-Messiah (Braunstein, 2005) decompositions, we can show (Walschaers, Fabre, et al., 2017b) that there is always a mode basis in which the covariance matrix does not show any entanglement. This means that the "non-Gaussian entanglement" that is relevant for reaching a quantum computational advantage cannot be studied via the covariance matrix of the state.

Initially, we studied non-Gaussian entanglement in the context of photon subtraction. This operation is known to typically increase entanglement (Navarrete-Benlloch et al., 2012). By using an entanglement measure known as Rényi-2 entanglement (based on the Rényi-2 entropy), we showed that the subtraction of a single photon can at most increase the entanglement by an amount $\log 2$ (Zhang et al., 2022). This amount corresponds exactly to the maximal amount of entanglement that can be created by sending a photon through a beam splitter. Using the techniques of Walschaers, Fabre, et al., 2017a one can furthermore show that this entanglement increase cannot be seen in the covariance matrix of the state. Furthermore, we can also use Rényi-2 entanglement to show that photon subtraction in a superposition of modes can create entanglement between these modes, even is previously there was none (Walschaers, 2021). However, in the presence of a mean field there are rare cases where photon subtraction can deteriorate entanglement.

Photon-subtracted states are a useful and relevant case study, but they are insufficient to fully understand the phenomenon of non-Gaussian entanglement. The development of a more general framework to study non-Gaussian entanglement is a major topic in my current research, and in the remainder of this section I give a short overview of the main lines of work we are pursuing.

First of all, one should note that there is no general definition of non-Gaussian entanglement that is agreed upon in literature. For example, one might argue that any non-Gaussian state with entanglement is non-Gaussian entangled. However, we introduced a more restrictive notion of non-Gaussian entanglement as the counterpart of passive separability (Walschaers, Fabre, et al., 2017a,b), a concept that was already introduced in Section 2.2. Formally, a state $\hat{\rho}$ is said to be passively separable when there is a passive linear optics transformation $\hat{U}$ such that $\hat{U}\hat{\rho}\hat{U}^\dagger$ is separable. This means that if we study the state in the right mode basis, it will behave as a separable state. We can see this as a type of non-Gaussian entanglement because all Gaussian states are passively separable (Walschaers, Fabre, et al., 2017b).

Passive separability is perhaps more elegant to understand on the level of the Wigner function, where we can write that

$$W_{\hat{U}\hat{\rho}\hat{U}^\dagger}(\vec{x}) = W_{\hat{\rho}}(O^\top \vec{x}), \tag{5.1}$$

where O is the symplectic orthonormal matrix given by (1.19) that corresponds to $\hat{U}$. A state $\hat{\rho}$ is therefore said to be *passively separable* (Walschaers, Fabre, et al., 2017b) whenever there is an orthonormal symplectic matrix $O^\top$ such that

$$W_{\hat{\rho}}(O\vec{x}) = \int_\Gamma p(\gamma) W_{\hat{\rho}_A}(\vec{x}_A) W_{\hat{\rho}_B}(\vec{x}_B) d\gamma. \tag{5.2}$$

Here we introduced a bit of additional notation. First, we assume that we are separating the state in a bipartition of two subsystems A and B, where A contains m_A modes and B contains m_B modes, such that $m_A + m_B = m$. The coordinates $\vec{x}_A$ ($\vec{x}_B$) describe the phase space of subsystem A (B) and $\vec{x} = \vec{x}_A \oplus \vec{x}_B$. Finally, when dealing with mixed states we must include a label γ for the states in the mixture, and a distribution $p(\gamma)$. For multimode light, it is easy to see how one could extend the concept of passive separability to a multipartite setting and ask, for example, when there is a mode basis in which the state is fully separable. Any state which is not passively separable, and thus for which no O exists such that (5.2) holds, can now be considered non-Gaussian entangled. This is the notion of entanglement that is shown to be necessary for reaching a quantum computational advantage in Chabaud and Walschaers, 2023.

We can also think of these notions in a slightly different way. Passively separable states are those states in which the entanglement could have been created with passive linear optics. One could in this spirit define Gaussian separable states as states in which the entanglement could have been created by any Gaussian unitary transformation. In this regard, it suffices to generalise (5.2) by replacing the orthogonal symplectic transformation by any Gaussian transformation. In other words, a state is Gaussian separable if there is a symplectic matrix S such that

$$W_{\hat{\rho}}(S\vec{x}) = \int_\Gamma p(\gamma) W_{\hat{\rho}_A}(\vec{x}_A) W_{\hat{\rho}_B}(\vec{x}_B) d\gamma. \tag{5.3}$$

One can of course argue that the most natural definition of non-Gaussian entanglement is as the counterpart of Gaussian separability. In other words, a state would only be considered non-Gaussian entangled if no Gaussian transformation could create the entanglement. In this regard, it is useful to highlight that every passively separable state is also Gaussian separable. Which means that one notion of non-Gaussian entanglement is stricter than the other. It is useful to highlight that there are Gaussian separable states that can lead to a quantum computational advantage (Chabaud and Walschaers, 2023), making passive separability the more important concept from an operation point of view.

To get a more formal understanding of passive- and Gaussian separability, it is useful to first study pure states. To do so, we will base ourselves on results by Chabaud,

Ferrini, et al., 2021; Chabaud and Mehraban, 2022. Here the authors study a dense class of multimode states $|\psi\rangle$ that is given by

$$|\psi\rangle = \hat{G}|C\rangle. \tag{5.4}$$

Here, $\hat{G}$ is a Gaussian unitary transformation, and $|C\rangle$ is known as a *core state*. Core states of stellar rank N are superpositions of Fock states and can thus be written by

$$|C\rangle = \sum_{\substack{n_1,\dots,n_m=0 \\ n_1+\cdots+n_m\leq N}} c_{n_1,\dots,n_m}|n_1,\dots,n_m\rangle \tag{5.5}$$

States of the type (5.4) have the advantage of "separating" the Gaussian and non-Gaussian part in a clean way. To see this, one might look at the Wigner function of the state and realise that

$$W_{|\psi\rangle}(\vec{x}) = W_{|C\rangle}(S\vec{x}), \tag{5.6}$$

where S is the symplectic transformation that corresponds to $\hat{G}$. This clearly shows that all non-Gaussian features in $|\psi\rangle$ are directly inherited from its core state $|C\rangle$. Yet, the symplectic transformation S can generate entanglement and therefore we cannot simply discard it.

Because of equation (5.6), it seems appealing to characterise passive- and Gaussian separability in terms of properties of the core state's Wigner function that are invariant under Gaussian transformations (for Gaussian separability) or basis changes (for passive separability). However, this is surprisingly difficult, and it is leaving a lot of additional structure of the states unexploited. Notably, we can gain a lot by using that the core states are pure and of form (5.5). These ideas have been briefly explored by Chabaud and Mehraban, 2022, and here we present a slightly modified version of their arguments.

When we ask the question whether $|\psi\rangle$ is *passively separable*, we wonder whether a mode basis change can render $W_{|\psi\rangle}(\vec{x})$ separable in the sense of (5.2). Using the Bloch-Messiah decomposition, we can rewrite $S = O_1 K O_2$, where K is a diagonal symplectic matrix that implement local squeezing operations. When we then use the structure of the core state (5.5), we find that it's Wigner function is a polynomial multiplied by a Gaussian. Because the state is pure, the state can only be separable if the Wigner function factorises. This can only happen when we avoid cross-terms in the exponential part of the Wigner function. The only mode basis where these cross-terms are absent, is the one where the squeezing effects in S are local. Finally, note that local squeezing has no influence on entanglement in the specific mode basis. This leads us to the important relation

$$|\psi\rangle \text{ is passively separable} \iff W_{|C\rangle}(O_2\vec{x}) \text{ is factorized.} \tag{5.7}$$

In other words, $|\psi\rangle$ is passively separable if and only if $|C\rangle$ is separable in the mode-basis where the squeezing in $|\psi\rangle$ is local.

The question of Gaussian separability is more subtle because Gaussian transformations give us much more freedom. In particular, the question is now whether a transformation S' exists for which $W_{|\boldsymbol{\psi}\rangle}(S'\vec{x})$ is factorized. As for passive separability, these Wigner functions can only be factorized when there are not cross terms in the Gaussian part of the Wigner functions. However, this leaves the freedom to choose S' such that $S'S = O$, a symplectic orthonormal matrix. As such, we find that $W_{|\boldsymbol{\psi}\rangle}(S'\vec{x}) = W_{|\boldsymbol{C}\rangle}(O\vec{x})$. Because $|\boldsymbol{C}\rangle$ is a core state, any mode-basis change O leaves the Gaussian part unchanged such that no Gaussian cross terms appear. This leads us to the conclusion that (Chabaud and Mehraban, 2022)

$$|\boldsymbol{\psi}\rangle \text{ is Gaussian separable} \iff |\boldsymbol{C}\rangle \text{ is passively separable.} \tag{5.8}$$

Which clearly establishes that non-Gaussian entanglement of pure states of the type (5.4) can be understood by studying the properties of the core states $|\boldsymbol{C}\rangle$.

Even though the problem is now significantly simplified by restricting to a specific class of states (5.5), any systematic study to understand (passive) separability of core states is still to be carried out. This is currently a major topic of research in our group. A combination of our work (Chabaud and Walschaers, 2023) and (Mari and Eisert, 2012) makes it tempting to study these concepts in terms of Wigner negativity. However, this turns out to be remarkably difficult and we find it to be more appropriate to apply the stellar formalism of Chabaud, Markham, et al., 2020 (a detailed introduction can be found in Section III.D of the article in Section 1.3).

The stellar formalism is based on the stellar function $F^{\star}_{|\boldsymbol{\psi}\rangle}(\vec{\xi})$. This function can be interpreted as a representation of the state $|\boldsymbol{\psi}\rangle$ in the over-complete basis of coherent states $|\vec{\xi}\rangle$, which were defined in (1.61). Mathematically, it is given by

$$F^{\star}_{|\boldsymbol{\psi}\rangle}(\vec{\xi}) = \langle\vec{\xi}|\boldsymbol{\psi}\rangle e^{\frac{1}{8}\|\vec{\xi}\|^2}. \tag{5.9}$$

For a core state $|\boldsymbol{C}\rangle$, the stellar function $F^{\star}_{|\boldsymbol{C}\rangle}(\vec{\xi})$ is a multivariate polynomial and its properties can be understood by studying the manifolds that are determined by $F^{\star}_{|\boldsymbol{C}\rangle}(\vec{\xi}) = 0$. In particular, for the problem of Gaussian separability of $|\boldsymbol{\psi}\rangle$, we wonder whether there is a symplectic orthogonal transformation such that the manifolds generated by the associated core state $F^{\star}_{|\boldsymbol{C}\rangle}(O\vec{\xi}) = 0$ can be included entirely in the subsection of phases space associated with A or B.

Preliminary results using these ideas show that single-photon subtracted states are always Gaussian separable, because the manifold determined by $F^{\star}_{|\boldsymbol{C}\rangle}(O\vec{\xi}) = 0$ is a single-mode hyperplane that can be "turned" by O to coincide with either A or B. For a state of the form $|\boldsymbol{C}\rangle \propto |2,0\rangle + |0,2\rangle$, we can show Gaussian separability because the manifold of zeros is given by two perpendicular single-mode hyperplanes (such that a well-chosen O aligns one hyperplane in A while jointly aligning the second one in B). Various other core states, such as $|\boldsymbol{C}\rangle \propto |N,0\rangle + |0,N\rangle$ with $N > 2$, $|\boldsymbol{C}\rangle \propto |2,0\rangle + |0,1\rangle$, and $|\boldsymbol{C}\rangle = \sqrt{\lambda}|2,0\rangle + \sqrt{1-\lambda}|0,2\rangle$ with $\lambda \in (0,1)$ can all be shown to be not passively

separable. As a consequence, no state $|\psi\rangle = \hat{G}|C\rangle$ that is generated by acting with a Gaussian on one of these core states, is Gaussian separable. Note that for passive separability of $|\psi\rangle = \hat{G}|C\rangle$, we do not have the freedom to alter the orientation of the manifolds and we simply have to consider $F^{\star}_{|C\rangle}(O_2\vec{\xi}) = 0$, where O_2 is fixed by $\hat{G}$. We thus see that, for most $\hat{G}$ the state $|\psi\rangle = \hat{G}|C\rangle$ with $|C\rangle \propto |2,0\rangle + |0,2\rangle$ will not be passively separable. Using the same argument, we can show that multimode single-photon subtracted states are typically not passively separable.

This generally shows that we can relate the problem of passive and Gaussian separability of pure states of finite stellar rank to a problem of algebraic geometry. Even though this might not be practical to actually generate or witness entanglement in experimental setups, it does help us get a fundamental understanding of the structure of non-Gaussian entangled states.

The problem becomes considerably more involved when we consider mixed states. The most natural definitions for passive and Gaussian separability are probably the ones given by equations (5.2) and (5.3), respectively. When we consider these definitions for a mixed state $\hat{\rho}$, they imply the existence of a pure-state decomposition such that all these pure states are passively or Gaussian separable by the same passive linear optics or Gaussian unitary transformation. A priori, we see no reason why a mixture of passively (Gaussian) separable pure states $|\psi_1\rangle, \ldots, |\psi_n\rangle$, that are separated by *different* passive linear optics (Gaussian unitary) transformations, would be passively (Gaussian) separable in the sense of equation (5.2) (equation (5.3)).

It is useful to go back to the operational point of view and consider the protocol of Chabaud and Walschaers, 2023. Clearly a mixture of passively separable pure states would not be resourceful for coherent state sampling. Assuming the pure state decomposition is known, one might simply choose a pure state from the mixture and easily simulate the sampling for the chosen state. This thus calls for a notion of *genuine non-Gaussian entanglement*, where we consider a state to be non-Gaussian entangled only when it cannot be written as a mixture of pure passively (or Gaussian) separable states. This would be particularly natural since it excludes non-Gaussian mixtures of Gaussian states. The disadvantage, however, is that genuine non-Gaussian entanglement may be even harder to witness experimentally.

5.2 METROLOGICAL DETECTION PROTOCOLS

The detection of non-Gaussian quantum correlations forms an important bottleneck in its study. As pointed out at the beginning of the previous section, non-Gaussian entanglement cannot be understood merely from measuring the covariance matrix of the state. As a consequence, typical Gaussian witnesses (Duan et al., 2000; Loock and Furusawa, 2003; R. Simon, 2000) will not work. For this reason, a series of more advanced counterparts have been proposed (Gessner, Pezzè, et al., 2016; Gneiting and

Hornberger, 2011; Levi et al., 2015; Walborn et al., 2009). In the context of quantum steering similar efforts have been made to go beyond the strictly Gaussian scenario (Kogias, Skrzypczyk, et al., 2015; Schneeloch et al., 2013; Yadin et al., 2021). In the light of Chapter 4, we are particularly interested in the work of Gessner, Pezzè, et al., 2016 and Yadin et al., 2021 where a metrological advantage is used to witness entanglement.

Gessner, Pezzè, et al., 2016 studies a scenario in which one tries to witness entanglement between two parties, Alice and Bob, that share a state $\hat{\rho}_{AB}$. Both parties are going to implement the same parameter θ in a unitary way with a local generator $\hat{G}_A$ for Alice and $\hat{G}_B$ for Bob. Using properties of the quantum Fisher information and of the variance, the authors showed that

$$\mathcal{F}_Q[\hat{\rho}_{AB}] \geq \mathrm{Var}[\hat{G}_A] + \mathrm{Var}[\hat{G}_B] \implies \rho_{AB} \text{ is entangled.} \tag{5.10}$$

Here we used that the generators $\hat{G}_A$ and $\hat{G}_B$ are independent of the parameter, such that the quantum Fisher information itself also becomes independent of the value of the parameter. The witness thus shows that a state is entangled whenever we can outperform the best possible sensitivity that can be achieved with separable states (given by $\mathrm{Var}[\hat{G}_A] + \mathrm{Var}[\hat{G}_B]$).

While this witness can be shown to always outperform variance-based techniques, it does also come with the difficulty of actually having to calculate the quantum Fisher information. In particular for continuous-variable systems where the density matrix of the state often is not known, this is a serious difficulty because it means that explicit expressions for the quantum Fisher information such as (4.32) cannot be used. As a solution, we proposed to use the definition (4.7) of the quantum Fisher information, which states that it simply is the maximal Fisher information over all measurements. It is thus only a matter of finding the appropriate measurement such that

$$\mathcal{F}[P] \geq \mathrm{Var}[\hat{G}_A] + \mathrm{Var}[\hat{G}_B]. \tag{5.11}$$

Generally speaking this is a hard task, but in the spirit of continuous-variable quantum information processing it is natural to aim for homodyne measurements. In Barral et al., 2023 we use these metrological techniques to study entanglement for photon subtracted states of Section 3.1. We show specifically how entanglement that is invisible in the covariance matrix could potentially be measured by using multimode homodyne measurements with only two different phase settings. In this case, the parameter θ is implemented by a displacement operator, such that the generators are quadrature operators, and the parameter can be equally estimated using quadrature operators. Furthermore, we show how these techniques are feasible with a finite number of measurement outcomes. Currently, we are trying to improve these detection schemes by using techniques from machine learning in the same spirit as we previously did for Wigner negativity (Cimini et al., 2020).

Similar metrological techniques have been developed to test quantum steering based on the average quantum fisher information of conditional states Yadin et al., 2021.

The practical approach to witnessing steering in the continuous-variable setup is also based on using the Fisher information for homodyne detection instead of the quantum Fisher information. The details of this work (Lopetegui et al., 2022) can be found in (5.3), where we strongly rely on the knowledge of the Wigner function for photon subtracted states to show under which conditions quantum steering can be witnessed in non-Gaussian states.

The above techniques for detecting entanglement have been proven to work in a regime where the typical Gaussian toolbox, based on the covariance matrix, fails. Nevertheless, the method still only allows us to witness entanglement in a fixed basis, whereas we would ultimately desire a mode-basis-independent entanglement witness. When we think of the Hahn-Banach separation theorem, an entanglement witness could take the form of an observable $\hat{W}$ with the property that $\mathrm{Tr}[\hat{W}\hat{\rho}] > 0$ for all separable states $\hat{\rho}$ (Terhal, 2000). In our specific case, we are on top looking for a $\hat{W}$ that is invariant under mode basis changes or more general Gaussian unitary transformations. However, finding such observables is highly challenging. We hope that techniques like the ones we previously used for certifying the stellar rank of a state (Chabaud, Roeland, et al., 2021) may be of use.

5.3 **article:** HOMODYNE DETECTION OF NON-GAUSSIAN QUANTUM STEERING

Homodyne Detection of Non-Gaussian Quantum Steering

Carlos E. Lopetegui,[1,2] Manuel Gessner,[1,3] Matteo Fadel,[4] Nicolas Treps,[1] and Mattia Walschaers[1,*]

[1] *Laboratoire Kastler Brossel, Sorbonne Université, CNRS, ENS-Université PSL, Collège de France, 4 Place Jussieu, Paris F-75252, France*

[2] *Laboratoire de Physique de l'Ecole Normale Supérieure, ENS, Université PSL, CNRS, Sorbonne Université, Université de Paris, Paris F-75005, France*

[3] *ICFO-Institut de Ciències Fotòniques, The Barcelona Institute of Science and Technology, Av. Carl Friedrich Gauss 3, Castelldefels, Barcelona 08860, Spain*

[4] *Department of Physics, ETH Zürich, Zürich 8093, Switzerland*

(Received 7 February 2022; revised 28 July 2022; accepted 1 August 2022; published 29 September 2022)

Quantum correlations are at the core of current developments in quantum technologies. Certification protocols of entanglement and steering, suitable for continuous-variable non-Gaussian states are scarce and generally highly demanding from an experimental point of view. We propose a protocol based on Fisher information for witnessing steering in general continuous-variable bipartite states, through homodyne detection. It proves to be relevant for the detection of non-Gaussian steering in scenarios where witnesses based on Gaussian features like the covariance matrix are shown to fail.

DOI: 10.1103/PRXQuantum.3.030347

I. INTRODUCTION

In 1935 Einstein, Podolsky, and Rosen introduced what came to be known as the EPR paradox [1], challenging, through the argument of local realism, the completeness of quantum mechanics. In his early response [2,3], Schrödinger addressed the issue of spooky action, troubled by the paradox arising from the capability of one part of a bipartite system to instantaneously *steer* the state of the other through appropriate local measurements. These works received notorious attention after the seminal paper by Bell [4], who proposed a strong test for locality itself. In 2007, Wisemann *et al.* [5] provided an operational benchmark for steering, from which they proved that the set of states that manifest steering are a strict subset of the set of entangled states and a strict superset of those that violate Bell inequalities. This definition can be understood in terms of a scenario where two parties, Alice and Bob, share a state. Alice has to convince Bob that the state they share is entangled, while Bob does not actually trust Alice, i.e., he does not assume her measurements to be in accordance with the constraints imposed by quantum physics. Alice will communicate the results of her measurements and then Bob can measure the state on his part of the system. Whenever Bob can verify the presence of a quantum correlation based only on the information provided by Alice and his own measurement results, we say that there is quantum steering from Alice to Bob.

The relevance of the characterization of steering goes beyond the interest in fundamental questions as it is a relevant resource in quantum information protocols [6,7], like one-sided device-independent quantum key distribution [8–10], certification of random number generators [11,12], quantum metrology [13], and quantum channel discrimination [14]. These one-sided device-independent approaches to quantum information protocols are settled in between the fully device-independent protocols that require the violation of Bell inequalities for certification, and the entanglement-based protocols, which are less restrictive, but also slightly less secure [15–17].

The problem of steering characterization for Gaussian states has been widely studied [18,19], and a well-defined measure has been established [20–22], based on the symplectic spectrum of the conditioned covariance matrix. However, for many applications in quantum technologies, one requires non-Gaussian states. For example, non-Gaussian features are necessary to reach a quantum computational advantage [23], and for quantum error correction [24]. Any application that relies on entanglement distillation must be non-Gaussian [25] and common entanglement distillation protocols effectively create non-Gaussian quantum correlations [26,27]. Such non-Gaussian quantum correlations become particularly

*mattia.walschaers@lkb.upmc.fr

relevant in quantum metrology, where they often lead to an improvement in sensitivity [28–31].

A general characterization of steering in non-Gaussian scenarios has been elusive so far. One possible approach relies on conditional quantum state tomography and semidefinite programming [32]. Alternatively, many protocols are based on second-order correlations [18], and for non-Gaussian states, these protocols require non-Gaussian measurements [33]. The latter is twofold undesired. First, it is appealing to rely strictly on Gaussian continuous-variable (CV) measurements, such as homodyne detection. Second, we want to probe the non-Gaussian features of the state, and thus must avoid introducing any additional non-Gaussian features through the measurement. In this spirit, we aim for a general protocol purely based on homodyne detection. Even though methods based on hierarchies have been proposed [34], these can require significant experimental and computational overhead when high-order moments are involved. Thus, rather than only focusing on moments of the measurement outcomes, our protocol will exploit the full measurement statistics.

We tackle the problem of witnessing quantum steering with a toolbox based on quantum metrology [30,31,35]. The steering capacity in a bipartite system was formally linked to an enhancement in the capability to estimate certain parameters [13]. We adapt this approach to the experimental context and limitations of CV quantum optics and show its relevance for non-Gaussian states. For that, we consider single-photon-subtracted states as a probe system. In the context of non-Gaussian states, photon subtraction, offers an experimentally feasible way to attain Wigner negativity in a controlled way [36,37]. This approach offers a very flexible way to generate different kinds of states [38] and in particular purely non-Gaussian features can be studied by appropriately choosing the mode in which the photon is subtracted [36]. These states are a relevant probe since pure photon-subtracted squeezed vacuum states have been shown to manifest quantum steering that cannot be detected by variance-based criteria [39]. We also show that our metrological approach detects more non-Gaussian steerable states than the entropic criterion of Ref. [40], even though the latter also exploits full homodyne statistics.

II. PROTOCOL

A. Protocol for general quantum states

We now formulate the steering detection scheme as a metrological protocol, following Ref. [13]. We consider the scenario in which Bob attempts to estimate a phase ξ generated by a Hamiltonian $\hat{H}$ that acts on his side of the system. Without any further information than that which he can extract from direct measurements in the displaced state $\hat{\rho}^B_\xi = \exp(-i\xi\hat{H})\hat{\rho}^B\exp(i\xi\hat{H})$, the maximal precision that he can achieve using an arbitrary unbiased estimator ξ_{est} is limited by the quantum Fisher information (QFI) $F_Q(\hat{\rho}^B,\hat{H})$, the central quantity in quantum metrology [30,31,35]. In the present scenario, where the parameter to be estimated is implemented by a unitary transformation, generated by a Hamiltonian, there is a practical expression for the QFI for a state $\hat{\rho}^B = \sum_k r_k|r_k\rangle\langle r_k|$:

$$F_Q(\hat{\rho}^B,\hat{H}) = 4\mathrm{Tr}[\hat{\rho}^B\hat{H}^2] - 8\sum_{j,k}\frac{r_k r_j}{r_k+r_j}|\langle r_j|\hat{H}|r_k\rangle|^2. \tag{1}$$

Note that this expression requires us to know the eigenvalues r_k and associated eigenvectors $|r_k\rangle$. However, in many physical systems, and notably CV systems where the density matrix is infinite dimensional, these quantities are often not known.

The QFI represents the sensitivity of state $\hat{\rho}^B$ under small perturbations generated by $\hat{H}$. This idea is formalized in the quantum Cramér-Rao bound on the variance of the estimator

$$\mathrm{Var}(\xi_{\text{est}}) \geq \frac{1}{nF_Q(\hat{\rho}^B,\hat{H})}, \tag{2}$$

where n is the number of repetitions of the measurement protocol. The inequality can be saturated by choosing the optimal measurement observable and estimator.

Nevertheless, Bob's state might be correlated with another system. Let us assume that Alice possesses this second party, and will assist Bob in his estimation protocol by sending him information about her measurement setup and outcome. Alice's assistance may improve Bob's estimation precision even when correlations are purely classical. Local complementarity sets a limit to this improvement that can only be overcome when there is quantum steering [13]. The average sensitivity attainable by Bob following assistance by Alice, is upper bounded by the conditional QFI

$$F_Q^{B|A}(\mathcal{A},\hat{H}) := \max_{\hat{X}}\int p(a|\hat{X})F_Q^B(\hat{\rho}^B_{a|\hat{X}},\hat{H})da, \tag{3}$$

and we introduce the assemblage as a function $\mathcal{A}$ that maps the observable $\hat{X}$ and one of its measurement outcomes a to

$$\mathcal{A}(a,\hat{X}) := p(a|\hat{X})\hat{\rho}^B_{a|\hat{X}}, \tag{4}$$

where $p(a|\hat{X})$ is the probability distribution for Alice's outcomes a after measurement of the observable $\hat{X}$, and $\hat{\rho}^B_{a|\hat{X}}$ is the conditioned state on Bob's side that is obtained after such a measurement.

In this context the confirmation of quantum steering consists in showing that assemblage (4) cannot be

described with a hidden state model given by

$$\mathcal{A}(a,\hat{X}) = \int d\lambda p(\lambda) p(a|\hat{X},\lambda)\hat{\sigma}^B_\lambda. \tag{5}$$

Note, moreover, that the implementation of a local phase ξ preserves the structure of the local hidden state model. If the state Bob and Alice share is consistent with the structure of Eq. (5), the following inequality holds [13]:

$$F_Q^{B|A}(\mathcal{A},\hat{H}) \leq 4\mathrm{Var}_Q^{B|A}(\mathcal{A},\hat{H}). \tag{6}$$

Here $\mathrm{Var}_Q^{B|A}(\mathcal{A},\hat{H})$ represents the quantum conditional variance

$$\mathrm{Var}_Q^{B|A}(\mathcal{A},\hat{H}) := \min_{\hat{X}} \int p(a|\hat{X})\mathrm{Var}(\hat{\rho}^B_{a|\hat{X}},\hat{H})da \tag{7}$$

that is obtained after minimization over all possible measurement setups by Alice. Here we encounter the variance of $\hat{H}$ in the state $\rho^B_{a|\hat{X}}$, given by

$$\mathrm{Var}(\hat{\rho}^B_{a|\hat{X}},\hat{H}) := \mathrm{Tr}[\hat{\rho}^B_{a|\hat{X}}\hat{H}^2] - \mathrm{Tr}[\hat{\rho}^B_{a|\hat{X}}\hat{H}]^2. \tag{8}$$

Together with the Cramér-Rao bound, inequality (6) implies the uncertainty relation [13]

$$\mathrm{Var}(\xi_{\mathrm{est}})\mathrm{Var}_Q^{B|A}(\mathcal{A},\hat{H}) \geq \frac{1}{4n} \tag{9}$$

between the phase displacement estimator ξ_{est} and its generator $\hat{H}$, whose violation constitutes an EPR paradox.

Inequality (6) can be thought of as a way to witness steering through its relevance for metrological tasks. The extent to which a given assemblage violates the inequality is captured by the steering witness

$$S_{\max}(\mathcal{A}) = \max_{\{\hat{H},\mathrm{Tr}(\hat{H}^2)=1\}} \left[F_Q^{B|A}(\mathcal{A},\hat{H}) - 4\mathrm{Var}_Q^{B|A}(\mathcal{A},\hat{H})\right]^+, \tag{10}$$

where $[x]^+ = \max\{0,x\}$. Moreover, Reid's criterion [41] can be derived as a weaker version of this witness. It can be shown [13] that

$$F_Q^{B|A}(\mathcal{A},\hat{H}) \geq \frac{|\langle[\hat{H},\hat{M}]\rangle_{\hat{\rho}^B}|^2}{\mathrm{Var}_Q^{B|A}(\mathcal{A},\hat{M})} \tag{11}$$

holds for arbitrary assemblages $\mathcal{A}$ and observables $\hat{H}$ and $\hat{M}$. Combined with inequality (6), we introduce the following measure for the violation of Reid's variance-based steering witness:

$$S_R(\mathcal{A}) = \max_{\{\hat{H},\mathrm{Tr}(\hat{H}^2)=1\}} \left[\frac{|\langle[\hat{H},\hat{M}]\rangle_{\hat{\rho}^B}|^2}{\mathrm{Var}_Q^{B|A}(\mathcal{A},\hat{M})} - 4\mathrm{Var}_Q^{B|A}(\mathcal{A},\hat{H})\right]^+. \tag{12}$$

This witness is very commonly used to witness steering in Gaussian states with quadrature operators [41]. Furthermore, Eq. (11) directly implies that $S_{\max}(\mathcal{A}) \geqslant S_R(\mathcal{A})$.

B. Homodyne protocol for continuous-variable systems

In this section, we translate the general protocol of the previous section to the specific context of multimode quantum optics [36,42]. We rely on quadrature displacements as the phase estimation probe, which can be easily implemented by shifting the Wigner function [43] in phase space. Experimentally, such a displacement results in a simple shift of the measured quadrature histograms, which implies that the effect of the parameter can be easily "simulated" in postprocessing. This will allow us to develop a framework to witness steering based entirely on homodyne detection.

Our starting point is the M-mode electric field operator

$$\hat{E}^+(\mathbf{r},t) = \sum_{j=1}^{M} \epsilon_j \hat{a}_j u_j(\mathbf{r},t), \tag{13}$$

where the $u_i(\mathbf{r},t)$ are a set of orthonormal solutions of Maxwell equations (classical modes), ϵ_j is a constant that carries the dimensions of the field, and the $\hat{a}_j$ are the annihilation operators corresponding to modes u_j of the bosonic field. In CV quantum optics the fundamental observables are the real and complex components of these operators, defined as

$$\hat{a}_j = \frac{\hat{q}_j + i\hat{p}_j}{2}, \tag{14}$$

where $\hat{q}_j$ and $\hat{p}_j$ are the amplitude and phase quadratures of the electric field, respectively, which satisfy the canonical commutation relation $[\hat{q}_j,\hat{p}_k] = 2i\delta_{j,k}$. The measurement outcomes for these observables are represented in optical phase space, which has a symplectic structure associated with the form

$$\Omega = \bigoplus_{j=1}^{M} \begin{pmatrix} 0 & -1 \\ 1 & 0 \end{pmatrix}. \tag{15}$$

We can now define vectors of quadrature operators

$$\vec{\hat{x}} = (\hat{q}_1,\hat{p}_1,\ldots,\hat{q}_M,\hat{p}_M)^\top, \tag{16}$$

and translate the commutation relation to $[\hat{x}_j,\hat{x}_k] = 2i\Omega_{jk}$.

To represent quantum states in optical phase space, we resort to a quasiprobability distribution, the Wigner function. Even though this representation can reach negative values and is thus not a joint probability distribution for quadratures, its marginals describe the probabilities of measurement outcomes for individual quadrature observables [36]. We focus on states of a bipartite system that are completely described by its Wigner function $W(\vec{x}_A \oplus \vec{x}_B)$ in a phase space of dimension $\mathbb{R}^{2m} \oplus \mathbb{R}^{2m'}$, where $\vec{x}_A$ ($\vec{x}_B$) stands for the phase space coordinates of subsystem A (B) that consists of m (m') modes.

A direct application of the protocol in Sec. II A would require us to obtain the QFI F_Q^B. This is in general a notoriously difficult task as it involves the reconstruction of the density matrix, which is often unfeasible in a CV setting. However, the QFI is lower bounded by its classical counterpart

$$F_Q^B(\hat{\rho}^B, \hat{H}) \geq F_\xi^B[P]. \tag{17}$$

The classical Fisher information (FI) characterizes the best precision that can be obtained for estimating ξ by using the results of a specific measurement. It is defined as

$$F_\xi^B[P] := \int_{\mathbb{R}} P(q|\xi)\left(\frac{\partial \mathcal{L}(q|\xi)}{\partial \xi}\right)^2 dq, \tag{18}$$

where $\mathcal{L}(q|\xi) = \log[P(q|\xi)]$ represents the logarithmic likelihood associated with the probability density of measurement outcomes q, after implementation of the parameter ξ. More formally phrased, $P(q|\xi) = \mathrm{Tr}[\hat{\rho}_\xi^B \hat{\Pi}_q]$, where $\hat{\Pi}_q$ forms a positive operator-valued measure such that $\int \hat{\Pi}_q dq = \mathbb{1}$. For CV systems, it is natural to choose $\hat{H}$ to be a quadrature operator, and $\hat{\Pi}_q = |q\rangle\langle q|$ to correspond to homodyne measurements.

Relation (17) is particularly appealing as it shows that any violation of inequality (6) based on the classical FI is a lower bound for the exact violation based on the QFI. The downside of relying on the classical FI is that one may fail to witness steering that could otherwise be detected by using a better measurement scheme. However, the classical FI already provides a strict improvement over Reid's criterion (12). We show that this improvement is sufficient to witness non-Gaussian steering.

In what follows we summarize the protocol to witness steering for a bipartite CV system; see Fig. 1. We have two sets of modes that are, in principle, mutually entangled: one in possession of Alice and one in possession of Bob. In her modes, Alice performs a homodyne detection that is characterized by a normalized vector $\vec{f}$ in Alice's phase space, which means that she measures the quadrature $\hat{x}_A^{\vec{f}} = \vec{f}^{\top}\vec{\hat{x}}$. When she obtains the measurement result x_0, Bob's state will be transformed into a state described

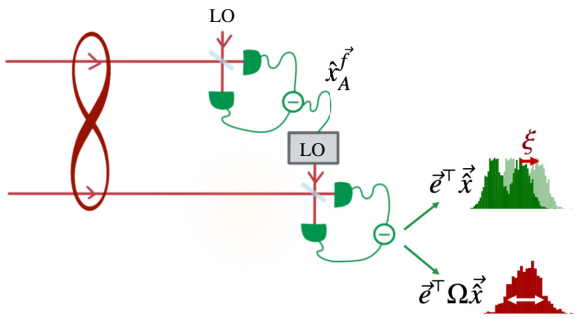

FIG. 1. Metrological protocol on which we base the witnessing of steering for bipartite CV states. Alice performs homodyne detection on the mode she owns and communicates to Bob the quadrature she chose to measure and its outcome. Based on this information, Bob tunes the local oscillator (LO) to choose what quadrature to measure in order to better estimate the displacement ξ generated by $\hat{D}(\xi) = \exp[-i\xi\vec{e}^{\top}\Omega\vec{\hat{x}}/2]$, such that the Hamiltonian is given by $\hat{H} = \vec{e}^{\top}\Omega\vec{\hat{x}}/2$.

by the conditional Wigner function

$$W^{B|A}(\vec{x}_B|x_A^{\vec{f}} = x_0) = \frac{\int_{\mathbb{R}^{2m}} W(\vec{x}_A \oplus \vec{x}_B)\delta(\vec{f}^{\top}\vec{x}_A - x_0)d\vec{x}_A}{\int_{\mathbb{R}^{2m}\oplus\mathbb{R}^{2m'}} W(\vec{x}_A \oplus \vec{x}_B)\delta(\vec{f}^{\top}\vec{x}_A - x_0)d\vec{x}_A d\vec{x}_B}. \tag{19}$$

Bob estimates a local quadrature displacement $W^{B|A}(\vec{x}_B) \mapsto W^{B|A}(\vec{x}_B - \xi\vec{e})$ on his subsystem. The parameter of interest ξ here corresponds to the extent of this displacement, which is generated by the Hamiltonian $\hat{H} = \vec{e}^{\top}\Omega\vec{\hat{x}}/2$ with $\vec{e}$ a normalized vector in Bob's phase space. In the spirit of Eq. (10), to witness steering, we optimize over all possible choices of displacement axis, and thus maximize over $\vec{e}$.

To study Bob's sensitivity for such an estimation, we evaluate the quantities involved in inequality (10), but we replace the QFI with the classical FI (18). To compute the classical FI, we fix the observable $\hat{M}$. A logical choice is to measure the displaced quadrature, given by $\hat{M} = \vec{e}^{\top}\vec{\hat{x}}$. This means that $P(q \mid \xi)$ in Eq. (18) is the marginal of the Wigner function (19) along the phase space axis $\vec{e}$. The probability of obtaining an outcome q when measuring the quadrature along $\vec{e}$ is given by

$$P^B_{x_0|\vec{f}}(q) = \int_{\mathbb{R}^{2m'}} \delta(\vec{e}^{\top}\vec{x}_B - q) W^{B|A}(\vec{x}_B|x_A^{\vec{f}} = x_0)d\vec{x}_B. \tag{20}$$

The displaced profile is obtained by the map $q \mapsto q - \xi$ on the marginal distribution, such that we can write

$$P^B_{x_0|\vec{f}}(q|\xi) = P^B_{x_0|\vec{f}}(q - \xi). \tag{21}$$

The resulting conditional classical FI for a fixed choice of Bob's displacement and measurement (determined by $\vec{e}$),

optimized over all homodyne observables ($\vec{f}$) on Alice's side, is defined as

$$F^{B|A}_{\text{hom}}\left(\mathcal{A}, \frac{\vec{e}^{\top}\Omega\hat{\vec{x}}}{2}\right) = \max_{\vec{f}\in\mathbb{R}^{2m}} \int_{\mathbb{R}} P_A(x^{\vec{f}}_A = x_0) F^B_{\xi}[P^B_{x_0|\vec{f}}]dx_0. \tag{22}$$

Here, $P_A(x^{\vec{f}}_A = x_0)$ is the marginal of the Wigner function along the quadrature measured by Alice. To check whether there is some mode in Alice's subsystem that can steer Bob's, the optimization runs over all possible choices of $\vec{f}$. One could refine the question and restrict $\vec{f}$ to the phase space of one specific mode to test whether this particular mode can steer Bob's subsystem.

To compute the conditional variance of the generator $\vec{e}^{\top}\Omega\hat{\vec{x}}/2$, we also use a marginal of the conditional Wigner function (19). From definition (7), we find that the conditional variance is given by

$$\text{Var}^{B|A}_{\text{hom}}\left(\mathcal{A}, \frac{\vec{e}^{\top}\Omega\hat{\vec{x}}}{2}\right) = \min_{\vec{f}\in\mathbb{R}^{2m}} \frac{1}{4}\int_{\mathbb{R}} P_A(x^{\vec{f}}_A = x_0) \times \text{Var}\left(\hat{\rho}^B_{x_0|\vec{f}}, \vec{e}^{\top}\Omega\hat{\vec{x}}\right)dx_0, \tag{23}$$

where $\text{Var}(\hat{\rho}^B_{x_0|\vec{f}}, \vec{e}^{\top}\Omega\hat{\vec{x}})$ is the variance of the quadrature corresponding to the generator $\vec{e}^{\top}\Omega\hat{\vec{x}}$. To compute this quantity, we introduce the probability of obtaining an outcome p when we measure the quadrature along the axis $\Omega\vec{e}$:

$$\tilde{P}^B_{x_0|\vec{f}}(p) = \int_{\mathbb{R}^{2m'}} \delta(\vec{e}^{\top}\Omega\vec{x}_B - p) W^{B|A}(\vec{x}_B|x^{\vec{f}}_A = x_0)d\vec{x}_B. \tag{24}$$

This distribution allows us to compute

$$\text{Var}\left(\hat{\rho}^B_{x_0|\vec{f}}, \vec{e}^{\top}\Omega\hat{\vec{x}}\right) = \int_{\mathbb{R}} p^2 \tilde{P}^B_{x_0|\vec{f}}(p)dp - \left(\int_{\mathbb{R}} p\tilde{P}^B_{x_0|\vec{f}}(p)dp\right)^2. \tag{25}$$

In other words, Alice first chooses a mode and quadrature to measure. Bob then also chooses a mode and a quadrature to measure depending on Alice's choice. Alice communicates her measurement outcomes to Bob, and Bob will group his measurement outcomes depending on Alice's result.

Finally, in analogy to the general definition (10), which optimizes over all Hamiltonians, we optimize our homodyne steering witness over all possible displacement vectors. This leads to the final witness

$$S^{\text{hom}}_{\max}(\mathcal{A}) = \max_{\vec{e}\in\mathbb{R}^{2m'}} \left[F^{B|A}_{\text{hom}}\left(\mathcal{A}, \frac{\vec{e}^{\top}\Omega\hat{\vec{x}}}{2}\right) - \text{Var}^{B|A}_{\text{hom}}\left(\mathcal{A}, \vec{e}^{\top}\Omega\hat{\vec{x}}\right)\right]^+ \tag{26}$$

for quantum steering with the specialized homodyne-based protocol. Note that we have used the fact that $4\text{Var}^{B|A}_{\text{hom}}(\mathcal{A}, \vec{e}^{\top}\Omega\hat{\vec{x}}/2) = \text{Var}^{B|A}_{\text{hom}}(\mathcal{A}, \vec{e}^{\top}\Omega\hat{\vec{x}})$.

Even though our protocol is formulated in a fully multimode context, it will effectively detect quantum steering between two optical modes, one given by $\vec{f}$ on Alice's side and one given by $\vec{e}$ on Bob's system. Optimizing over the possible choices of $\vec{f}$ and $\vec{e}$ gives us a sufficient criterion for steering from Alice to Bob, but one can make the protocol more general by measuring multiple quadratures simultaneously on both Alice's and Bob's side of the system. Because this extension is technically rather involved, but physically straightforward, we present it separately in the Appendix.

Witness (26) for our homodyne-based protocol is a lower bound for the steering witness proposed in Ref. [13] that relies on the QFI. At the same time, we can define a version of Reid's criterion (12) restricted to homodyne measurements by setting $\hat{H} = \vec{e}^{\top}\Omega\hat{\vec{x}}$ and $\hat{M} = \vec{e}^{\top}\hat{\vec{x}}$, which leads to

$$S^{\text{hom}}_{R}(\mathcal{A}) = \max_{\vec{e}\in\mathbb{R}^{2m'}} \left[\frac{1}{\text{Var}^{B|A}_{\text{hom}}(\mathcal{A}, \vec{e}^{\top}\hat{\vec{x}})} - \text{Var}^{B|A}_{\text{hom}}(\mathcal{A}, \vec{e}^{\top}\Omega\hat{\vec{x}})\right]^+. \tag{27}$$

Here, we find the quantity $\text{Var}^{B|A}_{\text{hom}}(\mathcal{A}, \vec{e}^{\top}\hat{\vec{x}})^{-1}$ that quantifies the sensitivity of estimating ξ based only on the average measurement outcome of $\vec{e}^{\top}\hat{\vec{x}}$. Because of the relation between the method of moments and the Fisher information [31], this is always smaller than the sensitivity set by the FI. We thus find the hierarchy $S^{\text{hom}}_{R}(\mathcal{A}) \leq S^{\text{hom}}_{\max}(\mathcal{A}) \leq S_{\max}(\mathcal{A})$. Interestingly, there are states for which $S^{\text{hom}}_{\max}(\mathcal{A}) < S_R(\mathcal{A})$ as the general version of Reid's criterion allows for highly non-Gaussian operators $\hat{H}$ and $\hat{M}$.

Finally, it is interesting to explicitly compare $S^{\text{hom}}_{R}(\mathcal{A})$ and $S^{\text{hom}}_{\max}(\mathcal{A})$ for Gaussian states. When Alice conditions on a homodyne measurement, she performs a Gaussian operation on the state. When the global state is Gaussian, Alice's measurement will create a Gaussian conditional state $\rho^B_{x_0|\vec{f}}$ on Bob's subsystem [44]. Because the state is Gaussian, it is characterized by a Gaussian Wigner function and its marginals are also Gaussian. Therefore, the probability distribution $P^B_{x_0|\vec{f}}(q|\xi)$ in Eq. (21) is Gaussian and only its mean value depends on the parameter ξ.

In this case, a simple calculation shows that $F_{\xi}^{B}[P^{B}_{x_0|\vec{f}}] = 1/\mathrm{Var}(\hat{\rho}^{B}_{x_0|\vec{f}}, \vec{e}^{\top}\hat{\vec{x}})$. This leads us to the following identity for Gaussian states:

$$F^{B|A}_{\mathrm{hom}}\left(\mathcal{A}, \frac{\vec{e}^{\top}\Omega\hat{\vec{x}}}{2}\right) = \max_{\vec{f}\in\mathbb{R}^{2m}} \int_{\mathbb{R}} P_A(x_A^{\vec{f}} = x_0) \times \frac{1}{\mathrm{Var}(\hat{\rho}^{B}_{x_0|\vec{f}}, \vec{e}^{\top}\hat{\vec{x}})} dx_0. \tag{28}$$

A second important element for Gaussian states is that $\mathrm{Var}(\hat{\rho}^{B}_{x_0|\vec{f}}, \vec{e}^{\top}\Omega\hat{\vec{x}})$ is independent of actual measurement result x_0 on Alice's side [44]. In other words, we find that

$$F^{B|A}_{\mathrm{hom}}\left(\mathcal{A}, \frac{\vec{e}^{\top}\Omega\hat{\vec{x}}}{2}\right) = \max_{\vec{f}\in\mathbb{R}^{2m}} \frac{1}{\mathrm{Var}(\hat{\rho}^{B}_{x_0|\vec{f}}, \vec{e}^{\top}\hat{\vec{x}})}. \tag{29}$$

From the same argument, it follows that

$$\frac{1}{\mathrm{Var}^{B|A}_{\mathrm{hom}}(\mathcal{A}, \vec{e}^{\top}\hat{\vec{x}})} = \max_{\vec{f}\in\mathbb{R}^{2m}} \frac{1}{\mathrm{Var}(\hat{\rho}^{B}_{x_0|\vec{f}}, \vec{e}^{\top}\hat{\vec{x}})}, \tag{30}$$

which ultimately shows that

$$S_R^{\mathrm{hom}}(\mathcal{A}) = S_{\max}^{\mathrm{hom}}(\mathcal{A}) \quad \text{for Gaussian states.} \tag{31}$$

This shows that our metrological formalism based on quadrature measurements can only outperform Reid's criterion based on quadrature variances when we are dealing with non-Gaussian states.

Reid's criterion as captured by $S_R^{\mathrm{hom}}(\mathcal{A})$ is also a lower bound for a different steering witness that can be derived from Ref. [40]. In this work, an entropy-based witness is introduced, constructed based on the Shannon entropies of the distributions $P^{B}_{x_0|\vec{f}}(q)$ and $\tilde{P}^{B}_{x_0|\vec{f}}(p)$:

$$h(P|x_A^{\vec{f}} = x_0) = -\int_{\mathbb{R}} P^{B}_{x_0|\vec{f}}(q) \log P^{B}_{x_0|\vec{f}}(q) dq, \tag{32}$$

$$h(\tilde{P}|x_A^{\vec{f}} = x_0) = -\int_{\mathbb{R}} \tilde{P}^{B}_{x_0|\vec{f}}(p) \log \tilde{P}^{B}_{x_0|\vec{f}}(p) dp. \tag{33}$$

We can then define

$$h^{B|A}(\mathcal{A}, \vec{e}^{\top}\hat{\vec{x}}) = \min_{\vec{f}\in\mathbb{R}^{2m}} \int_{\mathbb{R}} P_A(x_A^{\vec{f}} = x_0) h(P|x_A^{\vec{f}} = x_0) dx_0, \tag{34}$$

$$h^{B|A}(\mathcal{A}, \vec{e}^{\top}\Omega\hat{\vec{x}}) = \min_{\vec{f}\in\mathbb{R}^{2m}} \int_{\mathbb{R}} P_A(x_A^{\vec{f}} = x_0) h(\tilde{P}|x_A^{\vec{f}} = x_0) dx_0. \tag{35}$$

The original steering criterion that was proposed can be translated to our context as

$$h^{B|A}(\mathcal{A}, \vec{e}^{\top}\hat{\vec{x}}) + h^{B|A}(\mathcal{A}, \vec{e}^{\top}\Omega\hat{\vec{x}}) < \log(2\pi e). \tag{36}$$

It is particularly useful to note that

$$\mathrm{Var}^{B|A}_{\mathrm{hom}}\left(\mathcal{A}, \frac{\vec{e}^{\top}\Omega\hat{\vec{x}}}{2}\right)\mathrm{Var}^{B|A}_{\mathrm{hom}}\left(\mathcal{A}, \frac{\vec{e}^{\top}\hat{\vec{x}}}{2}\right) \geqslant \frac{e^{2h^{B|A}(\mathcal{A}, \vec{e}^{\top}\hat{\vec{x}})} e^{2h^{B|A}(\mathcal{A}, \vec{e}^{\top}\Omega\hat{\vec{x}})}}{(2\pi e)^2}. \tag{37}$$

When we combine this with the entropic inequality (36), we can propose the steering witness

$$S_H(\mathcal{A}) = \max_{\vec{e}\in\mathbb{R}^{2m'}} \left[2\pi e^{1-2h^{B|A}(\mathcal{A}, \vec{e}^{\top}\hat{\vec{x}})} - \frac{e^{2h^{B|A}(\mathcal{A}, \vec{e}^{\top}\Omega\hat{\vec{x}})-1}}{2\pi}\right]^{+}. \tag{38}$$

In the limit for Gaussian states, we find that $S_H(\mathcal{A}) = S_R^{\mathrm{hom}}(\mathcal{A})$. For more general states, we find that $S_H(\mathcal{A}) \geqslant S_R^{\mathrm{hom}}(\mathcal{A})$. To compare the metrological witness to the entropic one, we combine a relation between the Fisher information and Shannon entropy [45] with Jensen's inequality to prove that

$$F^{B|A}_{\mathrm{hom}}\left(\mathcal{A}, \frac{\vec{e}^{\top}\Omega\hat{\vec{x}}}{2}\right) \geq 2\pi e^{1-2h^{B|A}(\mathcal{A}, \vec{e}^{\top}\hat{\vec{x}})}. \tag{39}$$

However, the variance and entropy power are also related to each, which was, for example, used to obtain inequality (37). This leads to the inequality

$$\mathrm{Var}^{B|A}_{\mathrm{hom}}\left(\mathcal{A}, \frac{\vec{e}^{\top}\Omega\hat{\vec{x}}}{2}\right) \geq \frac{e^{2h^{B|A}(\mathcal{A}, \vec{e}^{\top}\Omega\hat{\vec{x}})-1}}{2\pi}. \tag{40}$$

When we combine inequalities (39) and (40), we cannot establish a clear relation between the entropic witness $S_H(\mathcal{A})$ and the metrological witness $S_{\max}^{\mathrm{hom}}(\mathcal{A})$. We explore which one of these two witnesses, based on the same homodyne measurement statistics, performs better for non-Gaussian states.

In Sec. IV, we explore the potential of the metrological protocol for an important class of two-mode non-Gaussian states, presented in Sec. III, under ideal detection conditions. Details about the experimental estimation of these quantities for realistic detection schemes are provided in Sec. V.

III. MODE-SELECTIVE PHOTON SUBTRACTION

The protocol described in the previous section is valid for any CV system, regardless of the nature of the state that

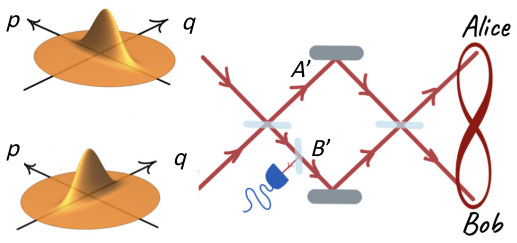

FIG. 2. Parameterized probe states: the non-Gaussian state obtained by subtracting one photon from one mode of a two-mode squeezed state is passed through a beam splitter with a tunable transmissivity $\tau = \sin^2(\theta)$.

we consider, as long as we have access to the marginals of the Wigner function along the desired axes in the phase space of each of the subsystems. In this section we introduce the probe states that we consider throughout this paper, namely, photon-subtracted states. Different approaches can be followed to describe the generation of these states and obtain their Wigner function [36,46–48].

We focus on two-mode photon-subtracted states, where one mode is sent to Alice and the other to Bob. These states are generated through the setup sketched in Fig. 2: two single-mode squeezed-vacuum states, squeezed in opposite quadratures, are mixed on a balanced beam splitter to generate an EPR state. A single photon is subtracted in one of the two output modes, and the resulting state is mixed on a second beam splitter with a variable reflectivity $\cos\theta$.

To accommodate losses and other experimental imperfections, we consider an arbitrary Gaussian two-mode state without mean field. We start by considering the state in the basis of EPR modes, which we denote A' and B', such that we have

$$W_G(\vec{x}) = \frac{e^{-\vec{x}^\top V^{-1}\vec{x}/2}}{(2\pi)^2\sqrt{\det V}}, \tag{41}$$

where V is the 4×4 covariance matrix of the state and $\vec{x} = \vec{x}_{A'} \oplus \vec{x}_{B'} = (x_{A'}, p_{A'}, x_{B'}, p_{B'})^\top$ contains the coordinates in phase space. Subsequently, we subtract a photon in the first mode A', such that the relevant Wigner function is given by [36]

$$W^-(\vec{x}) = \frac{\|P_{A'}(\mathbb{1} - V^{-1})\vec{x}\|^2 - \mathrm{Tr}(P_{A'}V^{-1}) + 2}{\mathrm{Tr}(V_{A'} - \mathbb{1})} W_G(\vec{x}), \tag{42}$$

where $P_{A'}$ is a projector on the first mode, given by

$$P_{A'} = \begin{pmatrix} 1 & 0 & 0 & 0 \\ 0 & 1 & 0 & 0 \\ 0 & 0 & 0 & 0 \\ 0 & 0 & 0 & 0 \end{pmatrix}, \tag{43}$$

and $V_{A'}$ is the covariance matrix for the reduced state of the first mode, given by $V_{A'} = P_{A'}VP_{A'}$.

In the ideal setting of Fig. 2, we can describe the covariance matrix as

$$V = \frac{1}{2}\begin{pmatrix} r_1 + 1/r_2 & 0 & 1/r_2 - r_1 & 0 \\ 0 & r_2 + 1/r_1 & 0 & r_2 - 1/r_1 \\ 1/r_2 - r_1 & 0 & r_1 + 1/r_2 & 0 \\ 0 & r_2 - \frac{1}{r_1} & 0 & r_2 + 1/r_1 \end{pmatrix}, \tag{44}$$

where $r_i = 10^{s_i/10}$ with s_i representing the squeezing parameter of the squeezed mode $i = 1, 2$, given in decibels (dB), and the squeezing is applied in opposite quadratures.

Photon losses can be described in an open quantum system approach, as an interaction of the system with the environment [49]. When the losses are the same in both modes, the effect can be entirely absorbed within the covariance matrix, regardless of whether they act before or after the photon subtraction. The effect of losses can then be modeled by modifying the covariance matrix in the following way:

$$V \mapsto (1 - \eta)V + \eta\mathbb{1} \tag{45}$$

with $\eta \in [0, 1]$ representing the amount of loses.

We apply a tuneable beam splitter after the local photon subtraction. The parameter θ, which parameterizes the non-Gaussian states, determines the transmissivity of the beam splitter [$T = \sin^2(\theta) \in [0, 1]$], whose effect on the quadratures of the phase space is described by the matrix

$$M(\theta) = \begin{pmatrix} \cos(\theta) & 0 & \sin(\theta) & 0 \\ 0 & \cos(\theta) & 0 & \sin(\theta) \\ -\sin(\theta) & 0 & \cos(\theta) & 0 \\ 0 & -\sin(\theta) & 0 & \cos(\theta) \end{pmatrix}. \tag{46}$$

The Wigner function of the resulting state that is sent to Alice and Bob is then written as

$$W^-_\theta(\vec{x}_A \oplus \vec{x}_B) = W^-(M(\theta)^T\vec{x}). \tag{47}$$

The set of non-Gaussian probe states include $\theta = 0$ and $\theta = \pi/2$, i.e., zero transmissivity and zero reflectivity, which leave the state untouched (up to a swap of the modes). In the former case, the photon is subtracted in Alice's mode, whereas in the latter case it is subtracted in Bob's mode. Here, we expect an enhancement of Gaussian quantum correlations of the EPR state through the generation of non-Gaussian features. On the other hand, $\theta = \pi/4$ would undo the correlations in the absence of photon subtraction. However, if a photon is subtracted, the second beam splitter delocalizes the non-Gaussian features

of the state over Alice's and Bob's modes. In this case, we witness a purely non-Gaussian quantum correlation, exclusively generated after photon subtraction, as no correlation is encoded in the covariance matrix of the corresponding state. This implies that Gaussian protocols like those based on Reid's criteria are expected to fail to witness steering.

IV. IDEAL DETECTION OF NON-GAUSSIAN QUANTUM STEERING

In this section we consider the protocol established in Sec. II for detection of steering using as probe states the photon subtracted states introduced in Sec. III. We first consider ideal results, neglecting the effect of any losses in the system. After that, we study the effect of losses in each possible scenario in an analytical way.

A. Gaussian witnesses for quantum steering

Before considering the non-Gaussian scenario, with the double purpose of validating the protocol and setting up comparison for the forthcoming results, we analyze steering in Gaussian two-mode squeezed states (i.e., before photon subtraction in Fig. 2).

Because Alice and Bob only control a single mode, we can simplify our notation compared to Sec. II B, by naming the measured quadratures on Bob's side

$$\hat{q} := \vec{e}^{\top}\vec{\hat{x}}, \tag{48}$$

$$\hat{p} := \vec{e}^{\top}\Omega\vec{\hat{x}}. \tag{49}$$

Alice's choice of a phase space axis is equivalent to choosing an angle φ such that she measures

$$\hat{x}_A(\varphi) := \cos\varphi\hat{q}_A + \sin\varphi\hat{p}_A, \tag{50}$$

which means that $\hat{x}_A(\varphi)$ is any quadrature in Alice's mode.

In Fig. 3, we present the results obtained when we consider an EPR state by setting equal squeezing values, i.e., $s \equiv s_1 = s_2$, in Eq. (44). We analyze the violation of the metrological inequality after homodyne detection by Alice, considering the largest possible violation obtained over all possible choices of the quadrature on Bob's side over which the displacement takes place, as prescribed by the maximization in Eq. (26). As there is no global phase dependence in the EPR state, Alice is completely free to choose one measurement setting φ. Bob will thus have to choose $\vec{e}$ such that $\hat{q}$ is maximally correlated with $\hat{x}_A(\varphi)$. This choice immediately fixes the second quadrature $\hat{p}$ that Bob will measure through Eq. (49). The largest value of the steering witness (26) will then be obtained if Alice chooses a second measurement setting that measures the quadrature that is most strongly correlated with $\hat{p}$. A key property of the state is that the correlation between Alice's and Bob's measurements is the strongest when they measure the same quadrature (i.e., when their homodyne measurements are in phase), which means that Alice's second setting should be set to $\varphi + \pi/2$.

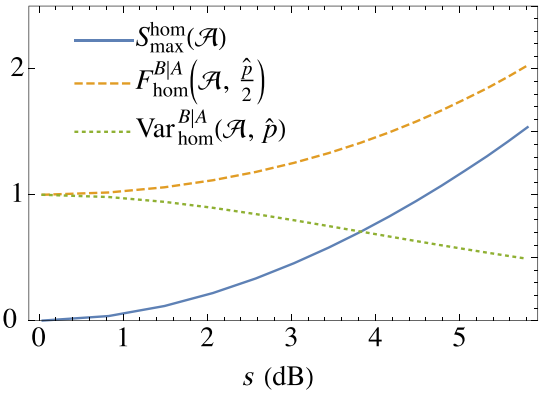

FIG. 3. Witnessing steering in two-mode squeezed states with equal squeezing in both modes as a function of the squeezing level s. We show the results using the steering witness (26), which is in this case identical to Reid's criterion $S^{\mathrm{hom}}_{R}(\mathcal{A})$ (recall that any value larger than zero implies quantum steering). We choose Alice's measurement settings (50) as $\varphi = 0$ and $\varphi = \pi/2$ to achieve a maximal value of the steering witness (see the main text). An optimization is performed over all possible choices of the generator of displacements on Bob's side.

In Fig. 4, we show the effect of photon losses (45) for the same type of states as in Fig. 3, for 3-dB squeezing. The latter is relevant to further understand the relation between Gaussian and non-Gaussian steering and the fundamental differences that can arise between one and the other.

B. Quantum steering after local photon subtraction

Moving now to the non-Gaussian realm, the natural first scenario to consider is the subtraction of one

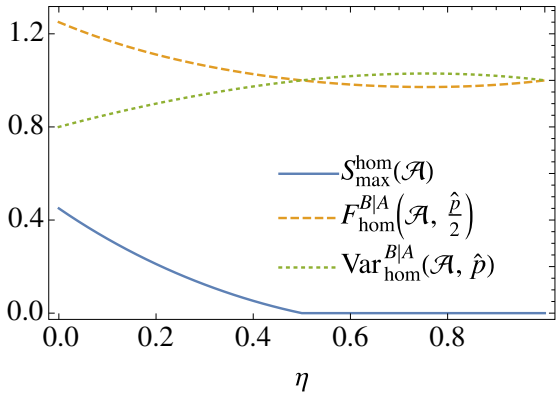

FIG. 4. Effect of losses in the steering witness (26) for a two-mode squeezed state, as considered in Fig. 3 for a level of squeezing of $s = 3$ dB.

photon in one of the two correlated modes A' or B', in the previously considered Gaussian scenario. This corresponds to $\theta = 0$ or $\theta = \pi/2$ in the tuneable beam splitter in Fig. 2. A recent result shows that Gaussian steering before photon subtraction is a sufficient condition for remotely generating Wigner negativity [50]. In the following we explore a complementary property and investigate how local photon subtraction affects the steering of the state.

States obtained by local photon subtraction are nonsymmetric. Wigner negativity, for example, is only present in the reduced state of the mode complementary to that where the photon is subtracted. However, the Wigner negativity of the two-mode Wigner function is larger than the single-mode Wigner negativity [51], which indicates the presence of nonlocal effects. In the same way, one would expect that steering, which is intrinsically a one-sided property, should not behave in the same way in both directions, i.e., steering from the mode where the photon is subtracted to the complementary mode is expected to be different from the steering in the opposite direction. To check this, in Fig. 5 we show the steering witness, as measured in the two directions. For the green curves, we use Reid's criterion (27), which leads to strongly asymmetric results, as no EPR steering from the mode where the photon is subtracted is observed. Yet, remarkably, the metrological witness (26) not only witnesses steering from the photon subtracted mode, but actually leads to a larger value for the steering witness. This observation contrasts with what one would expect from Reid's criterion, thus clearly showing new non-Gaussian behavior. In a more operational sense, this result shows that non-Gaussian steering from the photon-subtracted mode to the complementary mode can considerably enhance the inference of displacements in the complementary mode. The entropic witness (38) is also shown to detect steering from the photon-subtracted mode, but only when there is sufficient squeezing in the initial squeezed modes. This means that there is non-Gaussian steering that can be detected by the metrological witness, but not by the entropic one. Furthermore, we observe that the metrological witness systematically produces larger values than the entropic one (both coincide for Gaussian steering).

In Fig. 6, we consider the effect of losses, as we did previously for Gaussian states. The goal is to understand how resilient the witnesses are and how they are connected to the Gaussian scenario. As discussed in Sec. III, uniform losses in photon-subtracted states can be modeled by modifying the initial Gaussian covariance matrix as if the losses occurred at this initial stage. In other words, we analyze how photon subtraction affects Fig. 4, with the remark that steering is not symmetric, as we already discussed in Fig. 5.

There are some remarkable features observed in Fig. 6. In the first place, as we previously observed in Fig. 5 in the absence of losses, steering from the photon-subtracted mode seems to be stronger than the steering from the complementary mode, in the sense that a larger violation of inequality (6) is attained. Nevertheless, when we consider the effect of losses, we observe a much faster decay in the former that renders it harder to witness in a real experiment. For the entropic witness (38), we see a somewhat slower decay. However, given that the initial value of the witness in the absence of losses is much smaller

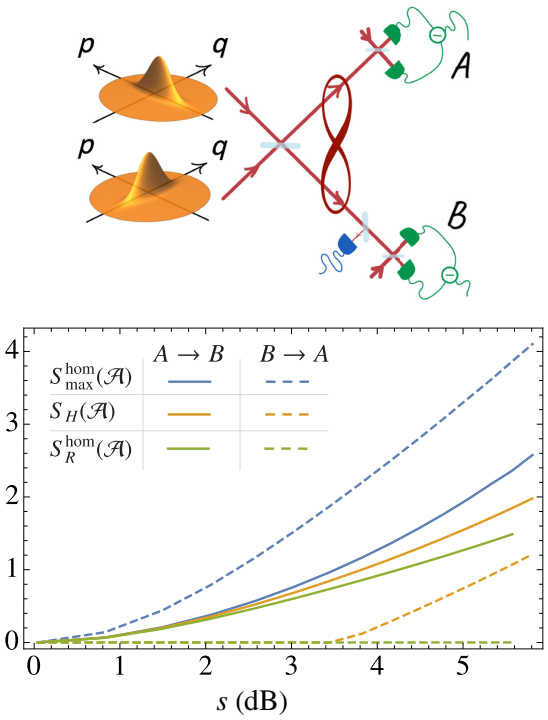

FIG. 5. Steering in photon-subtracted states corresponding to the choices of $\theta = 0$ and $\theta = \pi/2$ in the tuneable beam splitter in Fig. 2. Solid curves correspond to A steering B, whereas dashed lines correspond to the scenario where B is steering A. In green we show the observations arising from the application of Reid's criterion $S^{\text{hom}}_R(\mathcal{A})$ in Eq. (27). In this case, no steering from the mode where the photon is subtracted can be observed. In blue, we plot the steering witness $S^{\text{hom}}_{\text{max}}(\mathcal{A})$ in Eq. (26) for the same set of states and we can see that a violation of the inequality is attained in the direction where no Gaussian EPR steering is observed through Reid's criteria, and remarkably, this violation is larger than in the opposite direction. This represents a remarkable signature of non-Gaussian steering. In orange we finally show that the entropic witness can pick up on steering from B to A only when there is a sufficient amount of steering. On the one hand, this clearly highlights the capabilities of the entropic witness to detect non-Gaussian steering. On the other hand, it also shows that the metrological witness can detect steering in parameter regimes where the entropic witness cannot. We also observe that in both directions $S^{\text{hom}}_R(\mathcal{A}) \leq S_H(\mathcal{A}) \leq S^{\text{hom}}_{\text{max}}(\mathcal{A})$.

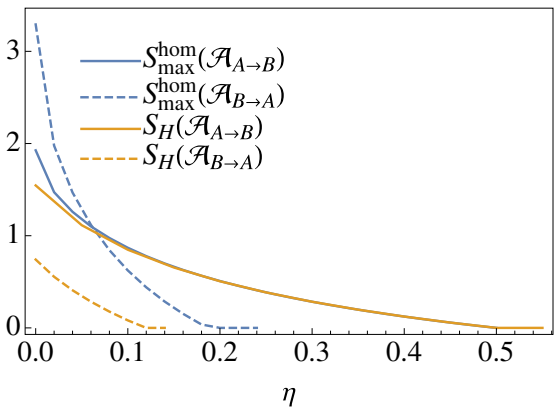

FIG. 6. Steering in photon-subtracted states corresponding to the choices of $\theta = 0$ and $\theta = \pi/2$ in Fig. 2, after uniform loss η [Eq. (45)]. In particular, we consider the photon subtraction in a 5-dB squeezed state. In accordance with Fig. 5, we can observe that in the absence of losses the violation of inequality (6) is larger when we consider the steering from the photon-subtracted mode than in the other direction. Yet, with increasing losses, the former decreases much faster (vanishing at 18% losses) than the steering from the complementary mode (vanishing at 50% losses, as in Fig. 4). When comparing the metrological witness $S^{\text{hom}}_{\max}(\mathcal{A})$ to the entropic witness $S_H(\mathcal{A})$, we observe that, for the steering from A to B (where the steering resembles Gaussian steering) and the larger values of η, both witnesses coincide. However, the metrological witness clearly outperforms the entropic one. We even find parameter ranges where the metrological witness detects steering that goes undetected by the entropic witness.

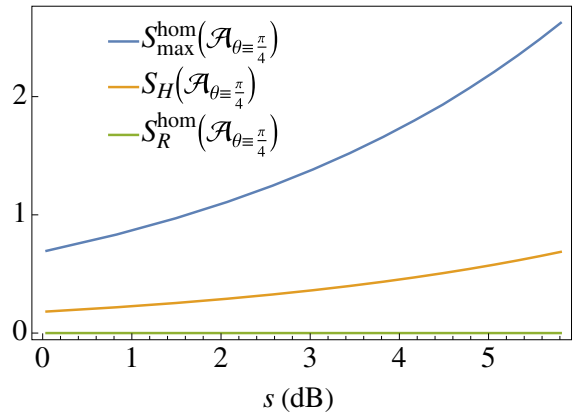

FIG. 7. Witnessing non-Gaussian steering for the state generated by having $\theta = \pi/4$ in the second beam splitter in Fig. 2. In green we show the absence of violation of Reid's criterion, expressed in the form of witness (27). In blue and orange we observe how an increasing violation of the metrological and entropic inequalities, respectively, are obtained as the squeezing level increases, starting from a finite value of witnesses (26) and (38) for arbitrarily low squeezing.

than for the metrological witness, we still find that the entropic witness is less tolerant to losses. On the other hand, regardless of the witness we use, steering from the complementary mode goes away for the same amount of losses as the Gaussian steering does. These observations, together with the impossibility of witnessing the steering from the photon-subtracted mode using Reid's criterion, lead us to interpret the steering from the complementary mode as an enhanced type of Gaussian steering, while the steering from the photon-subtracted mode appears to be purely non-Gaussian, stronger, but less resilient to losses. This behavior is equivalent for other values of squeezing, and the amount of losses required to destroy the steering from the photon-subtracted state increases with it.

C. Purely non-Gaussian quantum steering

The most striking shortcomings of considering Gaussian measurements of steering do naturally arise when we consider purely non-Gaussian correlations. In the present section we analyze the steering in the state obtained after setting $\theta = \pi/4$ in the second beam splitter in Fig. 2. The final state is equivalent to the state that would be obtained by subtracting a single photon from a superposition of the two initially uncorrelated squeezed modes, which is a nonlocal non-Gaussian operation. The non-Gaussian nature of these correlations can be seen in the Wigner function (42), whose Gaussian part factorizes for $\theta = \pi/4$. In Fig. 7, we show the analysis of the steering as a function of the squeezing level for this scenario. We consider, as before, two equally squeezed modes, squeezed in opposite quadratures, i.e., setting $r_1 = r_2$ in Eq. (44). We show how Reid's criterion fails to witness any quantum steering in this case, while we witness steering through witnesses (26) and (38). Even for arbitrarily low amounts of squeezing we find that these witnesses do not tend to zero, which is fundamentally different to the scenario obtained after local photon subtraction. Thus, we observe that, by means of a nonlocal non-Gaussian operation, a finite amount of steering is created for arbitrarily low squeezing. This observation is in agreement with that obtained when measuring entanglement in this kind of non-Gaussian state [36], and can intuitively be understood in the following way: for an arbitrarily low amount of squeezing, both modes are to good approximation a superposition of vacuum and two-photon Fock states. After photon subtraction in a balanced superposition of the two, we obtain an entangled two-mode state, given by $(|01\rangle + |10\rangle)/\sqrt{2}$, which is a Bell state.

In this case of purely non-Gaussian steering, both the metrological and entropic witnesses have been shown to be effective. However, in Fig. 8 we explore how both witnesses behave in the presence of losses. As for Fig. 6, we once again find that the metrological witness is more resilient to losses. Similar plots can be produced for all squeezing levels, showing the same behavior.

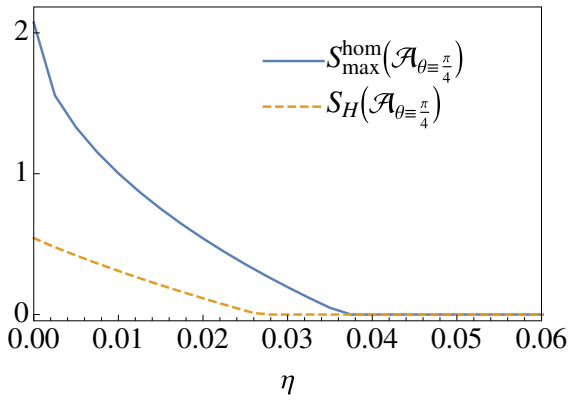

FIG. 8. Effect of photon losses on purely non-Gaussian steering, quantified by both the metrological witness (blue solid curve) and the entropic witness (dashed orange curve) for the state generated with $\theta = \pi/4$ in the second beam splitter in Fig. 2.

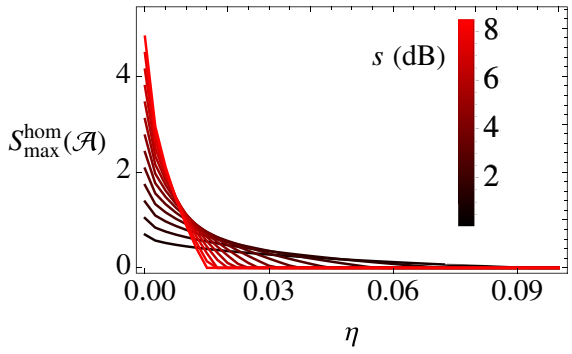

FIG. 9. Effect of photon losses on purely non-Gaussian steering for the state generated with $\theta = \pi/4$ in the second beam splitter in Fig. 2. We observe a reduction in the resilience to noise as the level of squeezing in the initial states increase. The latter might be linked to the fact that the effect of losses is more severe in single-mode squeezed states the larger the squeezing is [52].

Summing up all our comparisons between the entropic and metrological witnesses, we conclude that there are cases where the metrological witness can detect steering that goes undetected by the entropic witness. We find no opposite case, leading us to suggest that, for single-photon-subtracted states, the metrological witness tends to outperform the entropic one. Therefore, we focus our attention on the metrological witness in the remainder of this article.

In Fig. 9, we show how witness (26) behaves for these states under the effect of uniform photon losses. The behavior is very different to what we observe in the Gaussian scenario. First, we observe a very weak resilience to noise compared to the former one. Yet, the most striking feature is that this resilience decreases as the level of squeezing (and thus steering) increases, contrary to what happens in the correlated basis ($\theta = 0$), even for the steering from the mode in which the photon is subtracted.

Finally, in Fig. 10, we show a comparison of how the witness (26) behaves in the different scenarios that we have considered, namely, the Gaussian case and the photon-subtracted states obtained by the procedure described in Fig. 2 for $\theta = 0$, considering both steering from Alice to Bob and from Bob to Alice, and for the purely non-Gaussian case $\theta = \pi/4$.

V. REALISTIC DETECTION OF NON-GAUSSIAN QUANTUM STEERING

The approach followed so far considers the ideal scenario in which we can condition the state in Bob's steered mode on a definite outcome of Alice's measure. Yet, clearly, the latter is equivalent, from an experimental point of view, to having access to an infinite amount of data, namely, to sample the whole continuum of possible outcomes. In this section we approach the problem in a more realistic fashion, by discretizing the set of Alice's measurement outcomes, in a way that we no longer condition Bob's state on a single outcome but rather on a mixture of the conditioned states belonging to a given *bin* on Alice's side.

First, we analyze this scenario in an analytic way, to understand the limitations of this procedure. Later, keeping in mind the results from the former analysis, we consider the more realistic scenario, in which we study the protocol by simulating homodyne detection with rejection sampling.

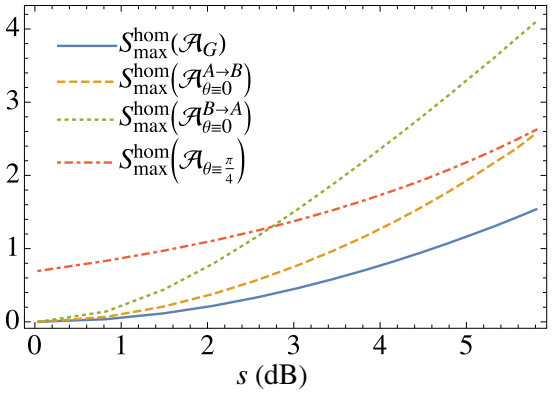

FIG. 10. Comparison of the behavior of the steering witness in the different scenarios considered so far. Here $\mathcal{A}_G$ denotes the assemblage corresponding to the Gaussian state; $\mathcal{A}_{\theta=\{0,\pi/4\}}$ denote the assemblages corresponding to the states generated through the choices $\theta = \{0, \pi/4\}$ in the tuneable beam splitter in Fig. 2; $\mathcal{A}^{A\to B(B\to A)}_{\theta=0}$ denote the two nonequivalent directions in which steering can occur in the case $\theta = 0$—the convention is the same as in Fig. 5.

A. Conditioning on finite data

Following the previous idea, the measurement outcomes that Alice communicates are rather determined by a histogram than by a probability density of continuous quadrature measurement outcomes. Therefore, we partition the real line corresponding to the outcomes of the quadrature measured by Alice in a series of n bins

$$\mathcal{I} = \{\mathcal{I}_1, \ldots, \mathcal{I}_n\}, \tag{51}$$

such that $\mathbb{R} = \bigcup_k \mathcal{I}_k$ and we note that $\mathcal{I}_k = [l_{k-1}, l_k)$ with $l_0 = -\infty$ and $l_n = \infty$. The probability of measurement outcomes now is described by

$$P_A[x_A(\varphi) \in \mathcal{I}_k] = \int_{l_{k-1}}^{l_k} P_A[x_A(\varphi) = x_0] dx_0, \tag{52}$$

where $x_A(\varphi)$ stands for the quadrature measured by Alice, for which we keep the notation introduced in Sec. IV for two-mode states. An assemblage then gives a discrete sum of the form

$$\mathcal{A}(\mathcal{I}_k, \hat{x}_A(\varphi)) = P_A[x_A(\varphi) \in \mathcal{I}_k] \hat{\rho}^B_{\mathcal{I}_k|\varphi}, \tag{53}$$

where

$$\hat{\rho}^B_{\mathcal{I}_k|\varphi} = \int_{l_{k-1}}^{l_k} P_A[x_A(\varphi) = x_0] \hat{\rho}^B_{x_0|\varphi} dx_0 \tag{54}$$

is the conditional state on Bob's side after the measurement by Alice of quadrature $x_A(\varphi)$ falls in bin $\mathcal{I}_k$. This state is a mixture of all the conditional states conditioned on definite quadrature outcomes, with a weight given by the marginal probability density $P[x_A(\varphi)]$.

The conditional FI now has to be calculated considering the discrete assemblage

$$F^{B|A}_{\text{disc}}(\mathcal{A}, \hat{H}) = \max_{\varphi \in [0,2\pi)} \sum_k P_A[x_A(\varphi) \in \mathcal{I}_k] F^B_\xi[P^B_{\mathcal{I}_k|\varphi}], \tag{55}$$

where $F^B_\xi[P^B_{\mathcal{I}_k|\varphi}]$ is computed according to Eq. (18), with $P^B_{\mathcal{I}_k|\varphi}(x|\xi)$ being the marginal along the displaced quadrature, characterized by $\vec{e}$, conditioned on the displacement ξ. This probability density can be obtained as $P^B_{\mathcal{I}_k,\varphi}(x|\xi) = \int_{l_{k-1}}^{l_k} P_A[x_A(\varphi) = x_0] P^B_{x_0|\varphi}(x|\xi) dx_0$. Because of the convexity of the FI, we find that

$$F^{B|A}_{\text{disc}}(\mathcal{A}, \hat{H}) \leq F^{B|A}_{\text{hom}}(\mathcal{A}, \hat{H}), \tag{56}$$

where $F^{B|A}_{\text{hom}}(\mathcal{A}, \hat{H})$ is the conditional FI when no coarse graining is considered.

If we consider the estimation of displacements ξ along the position quadrature $\hat{q}$ in Eq. (48), generated by the Hamiltonian $\hat{H} = \hat{p}/2$, using Eq. (49),

$$F^{B|A}_{\text{disc}}\left(\mathcal{A}, \frac{\hat{p}}{2}\right) = \max_{\varphi \in [0,2\pi)} \sum_k P_A[x_A(\varphi) \in \mathcal{I}_k] \int_{\mathbb{R}} P^B_{\mathcal{I}_k|\varphi}(q - \xi) \times \left\{ \frac{\partial \log[P^B_{\mathcal{I}_k|\varphi}(q - \xi)]}{\partial \xi} \right\}^2 dq, \tag{57}$$

where we have made use of the identity $P^B_{\mathcal{I}_k|\varphi}(q|\xi) = P^B_{\mathcal{I}_k|\varphi}(q - \xi)$.

The conditional variance of the generator $\hat{p}/2$ is calculated in a similar way,

$$\text{Var}^{B|A}_{\text{disc}}\left(\mathcal{A}, \frac{\hat{p}}{2}\right) = \min_{\varphi \in [0,2\pi)} \sum_k P_A[x_A(\varphi) \in \mathcal{I}_k] \times \text{Var}\left(\hat{\rho}^B_{\mathcal{I}_k|\varphi}, \frac{\hat{p}}{2}\right), \tag{58}$$

where the variance $\text{Var}(\hat{\rho}^B_{\mathcal{I}_k|\varphi}, \hat{p}/2)$ in the conditional state $\hat{\rho}^B_{\mathcal{I}_k|\varphi}$ in Eq. (54) is calculated in full analogy to Eq. (25).

For the examples in Fig. 11, the (typically unequal) sizes of the different bins are optimized to maximize the witness. Because the photon-subtracted states have no mean field, we choose bins that are symmetric around the origin to reflect the structure of the exact quadrature statistics. We show the behavior of the steering witness (10) against the level of squeezing of the initial two-mode state for the case of purely non-Gaussian steering corresponding to the choice $\theta = \pi/4$ in the second beam splitter in Fig. 2. Being able to witness steering in this challenging regime while considering realistic discretization of the measurement results is particularly encouraging for the prospect of experimental implementations of this method.

In Fig. 12 we analyze how binning the spectrum of outcomes of Alice's measurements affects the capability to witness the steering under the influence of photon losses. As expected, measurements with fewer bins, which lead to weaker violations of witness (6), also show a smaller tolerance to losses.

B. Detecting quantum steering on homodyne data

In this section we present a *realistic* analysis of the protocol that we have presented. So far, we have considered in an exact way the marginals of the Wigner functions. In an experimental implementation we would have to infer these probability densities from the outcomes of the homodyne measurements, or compute directly some of the quantities involved. To study such a scenario, we simulate experimental data through rejection sampling from the theoretical probability densities.

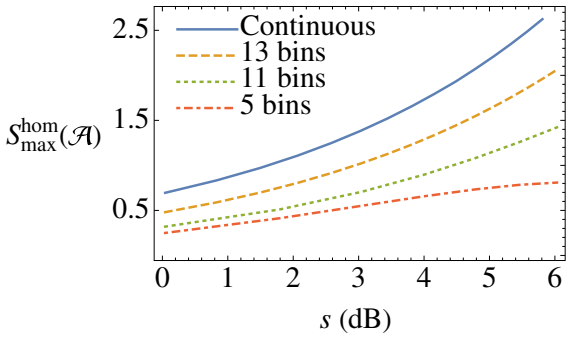

FIG. 11. Effect of discretization of the quadrature outcomes on Alice's side on the witness of steering for the two-mode photon-subtracted state with $\theta = \pi/4$ in the tuneable beam splitter in Fig. 2. Below five bins it is not possible to witness steering as we fail to capture important features of the probability density. Nevertheless, a good violation of inequality (6) is possible starting from five bins.

As we have observed so far, in the states that we have considered the largest violations are obtained when considering displacements along the q or p quadratures, conditioned on measurements in the same quadrature on Alice's side. This is particularly suited for an experimental implementation as simultaneous locking of the local oscillators in the phase and amplitude quadrature is already possible in homodyne detection schemes. Therefore, the data that we simulate for each measurement are sampled from the joint probability distribution of the same quadratures of both Bob's and Alice's modes, which can be theoretically obtained by integrating the Wigner function (47) over the remaining quadratures. To better represent realistic experimental settings, the states that we consider will be slightly different from those that we analyzed before. In particular, the squeezing of the two modes will not be exactly

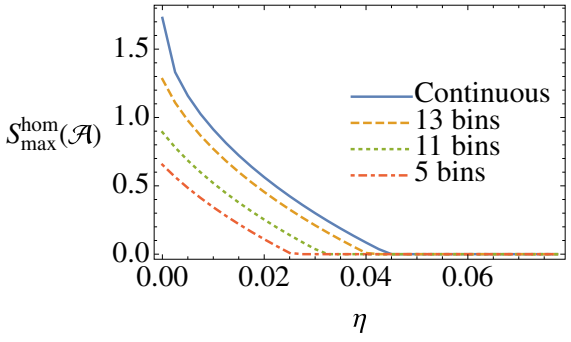

FIG. 12. Effect of losses in the witness of steering in the same kind of states as in Fig. 11 for a level of squeezing of 4 dB. As expected, the steering witness is reduced with increasing losses, but again, for a reasonably low number of bins, such as 13, the resilience is almost the same as in the pure loss-free scenario.

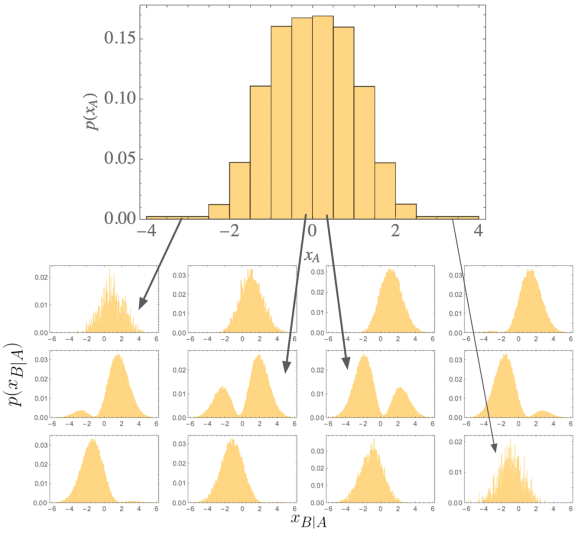

FIG. 13. Schematic representation of the analysis of the simulated data. The histogram in the top represents the outcome statistics of measurements of Alice's position quadrature. The panels below each represent the conditional statistics of the position quadrature of Bob's mode, corresponding to each of the bins of Alice's histogram. Wide tails, compared to the rest of the bins, are considered in order to guarantee sufficient statistics for the reconstruction of the states conditioned on less likely outcomes.

the same. Thus, the choice of quadratures previously mentioned is not the optimal one, but it will always provide a lower bound for the actual value of the witness.

In what follows, we discuss the protocol for the analysis of the data. Let us consider the simultaneous measurement of the momentum quadrature. The ideal reconstruction of the assemblage implies the inference of the probability density on Alice's side, and for each possible outcome, the reconstruction of the conditioned state. As mentioned in the previous subsection, this is an unfeasible experimental task, even more so if we consider the fact that one actually undersamples the tails of the distributions on Alice's side, in a way that reconstructing the statistics of its corresponding conditioned state is impossible. To overcome this issue, we have to build a histogram on Alice's side, and analyze Bob's statistics conditioned on each bin of the histogram (Fig. 13). It is important to remark that the histogram has to be inhomogeneous: the bins in the tails must encompass a larger region in order to avoid spurious contributions from undersampled data.

Computing the conditional variance is a rather straightforward task. On the other side, the computation of the FI from the discrete outcomes is more subtle. The most common procedure to experimentally estimate the FI relies on the computation of the Hellinger distance (statistical distance) between the reference probability density and the displaced ones [53–55].

With a parameter-dependent probability density $P(q|\xi)$ and a reference $P(q|0)$, the Hellinger distance is defined as

$$d_H^2(\xi) = \frac{1}{2}\int_q \left(\sqrt{P(q|\xi)} - \sqrt{P(q|0)}\right)^2 dq. \tag{59}$$

Expanding $P(q|\xi)$ to first order in ξ, it is possible to show that

$$d_H^2(\xi) = \frac{F}{8}\xi^2 + \mathcal{O}(\xi^3), \tag{60}$$

where F is shorthand for the Fisher information $F_{\xi=0}[P]$. Hence, it is enough to perform a quadratic fitting of the Hellinger distance to estimate the FI F. The latter is particularly well suited for our analysis as the displaced probability distributions can be obtained by just shifting the reference one. Such a postprocessing displacement of the measurement outcomes does not require experimentally implementing the displacements, which is much more demanding. In an experimental implementation we have access to relative frequencies $\{\mathcal{F}(q|\xi)\}$ rather than the exact probabilities $P(q|\xi)$ required above. In this context Eq. (60) is valid only as an approximation, given the fact that $\mathcal{F}(q|\xi) = P(q|\xi) + \delta\mathcal{F}(q|\xi)$, with $\delta\mathcal{F}(q|\xi)$ a statistical fluctuation that arises due to finite sample size. Because of normalization, $\sum_q \delta\mathcal{F}(q|\xi) = 0$, where the sum runs over all possible values of q, which for CV systems will be given by all possible bins in which the outcome of the measurement might fall. If we define the histograms $f\,(0) = \{\mathcal{F}(q|0)\}_q$ and $f\,(\xi) = \{\mathcal{F}(q|\xi)\}_q$ for a sample of n experimental measurements, we have [53]

$$\langle d_H^2(f\,(0), f\,(\xi))\rangle = c_0 + \left(\frac{F}{8} + c_2\right)\xi^2 + \mathcal{O}(\xi^3, \delta\mathcal{F}(q|\xi)^3) \tag{61}$$

with

$$c_0 = \frac{N-1}{4n}, \qquad c_2 \approx \frac{F(1+N)}{32n}, \tag{62}$$

where $\langle d_H^2(f\,(0), f\,(\xi))\rangle$ is the sample average of the Hellinger distance between the two relative frequencies, n is the number of measurements, and m is the number of values of q for which $\mathcal{F}(q|\xi) \neq 0$. Observe that the previous formula converges asymptotically to (60). This implies that the estimation of F is asymptotically unbiased, with the bias decreasing as $1/n$.

In Figs. 14 and 15 we study the influence of losses on the estimation of the steering witness (10) based on a finite set of $n = 10^5$ data points. In most experiments, it is unrealistic to have exactly the same squeezing in each mode. Therefore, the specific values of the squeezing in Alice's and Bob's initial states (at the left of Fig. 2) are chosen arbitrarily. We choose $s_1 = 3.2$ dB and $s_2 = 2.6$ dB since these lie in an experimentally relevant range. The obtained violation is below the exact result $S_{\max}^{\text{hom}}$ (dashed line) obtained when considering the exact Wigner function of the system for the same set of parameters.

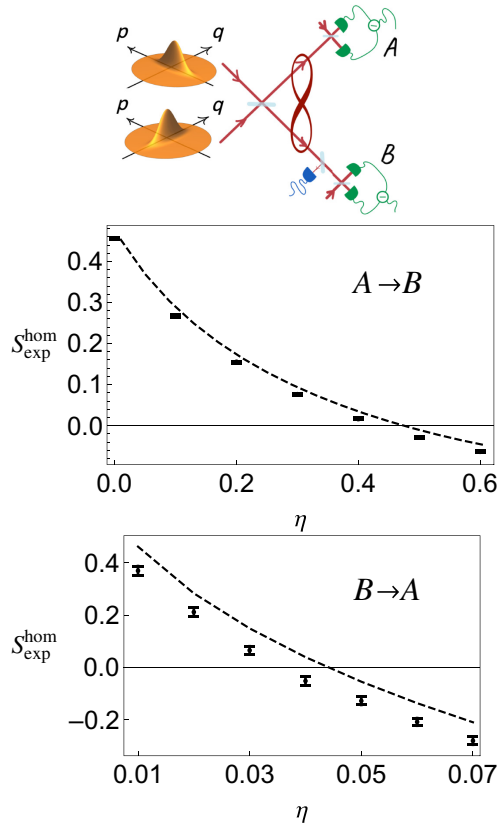

FIG. 14. Numerical simulations of the effect of losses in the witness of steering estimation (10). The state that we consider is defined by the choice of $\theta = 0$ in the preparation scheme, i.e., the state resulting after local photon subtraction in one of two correlated squeezed modes, with inhomogeneous squeezing $s_1 = 3.2$ dB and $s_2 = 2.6$ dB. The plot in the top corresponds to the steering from the mode complementary to that where the photon is subtracted. The bottom plot corresponds to the steering from the mode where the photon is subtracted. Dashed lines correspond to the exact analytical results obtained considering binning on the steering side. Error bars correspond to statistical errors and uncertainties on the fit. We can observe that the steering from the photon-subtracted state, which is not observed using Gaussian criteria, vanishes somewhere between 3% and 4% losses, while the steering in the complementary direction persists for larger losses.

In Fig. 14, we investigate this system in the correlated basis, i.e., the cases $\theta = 0$, where Bob subtracts a photon. Subsequently, we analyze the steering from Alice to Bob and from Bob to Alice. As before, the case where Alice steers Bob can be studied using Reid's criterion, as

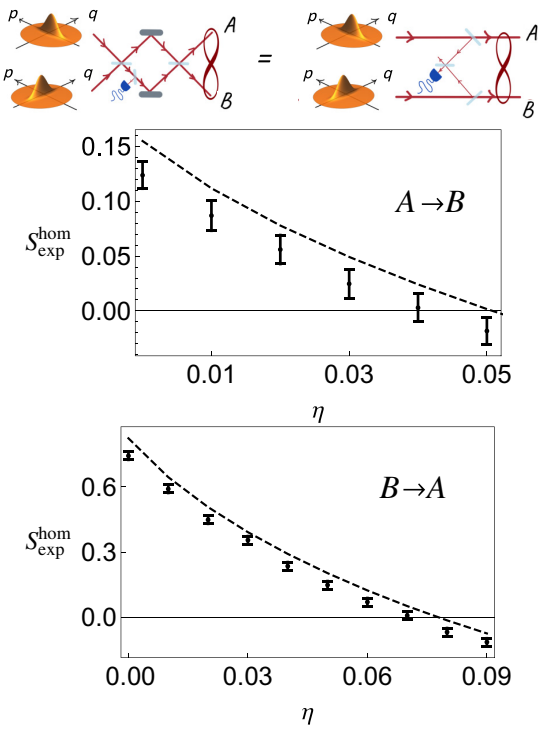

FIG. 15. Numerical simulations of the effect of losses in the witness of steering estimation (10). The top panel represents the state preparation with $\theta = \pi/4$, i.e., delocalized photon subtraction from a two-mode squeezed state with inhomogeneous squeezing $s_1 = 3.2$ dB and $s_2 = 2.6$ dB. Dashed lines correspond to the exact analytical results obtained considering binning on the steering side with a perfect measurement of the Fisher information (as in Sec. V A), while points are obtained by inferring the Fisher information from the finite data using the Hellinger distance method (see the text). Error bars correspond to statistical errors and uncertainties on the fit. Contrary to the results showed for homogeneous squeezing, here we can observe a remarkable difference in the steering in the two complementary directions.

shown in Fig. 5(a), indicating that it is essentially a case of Gaussian steering. Also in these simulations, based on a finite number of data points, this Gaussian character translates to a much greater resilience against losses. However, for steering from Bob to Alice—which cannot be witnessed through Reid's criterion—we observe a much more detrimental effect of losses. Because non-Gaussian features are typically very sensitive to losses, a possible origin of this sensitivity is that the steering is dominated by non-Gaussian features of the state. This conjecture is supported by Fig. 6, which shows that the protocol is much more loss resistant when the correlations have some Gaussian features.

To fully explore the feasibility of our method for witnessing non-Gaussian steering, we show the case for $\theta = \pi/4$ in Fig. 15. In this scenario, all the correlations in the state (be it quantum or classical) originate from the non-Gaussian part of the Wigner function (47) and no quantum correlation can be witnessed based on its covariance matrix. In other words, this is a state where all quantum steering is purely non-Gaussian in nature. Again, we observe a much more detrimental effect of losses compared to the top panel of Fig. 14. However, due to the asymmetry in the steering of the two modes, we observe a much larger value for the steering witness when considering steering from the lesser squeezed mode to the more squeezed modes. This higher value also comes with a higher robustness to losses. From an experimental point of view, the tolerable loss values remain very small in both cases. Nevertheless, these simulations show that in sufficiently pure systems it is possible to witness non-Gaussian quantum steering using exclusively homodyne detection with an experimentally feasible protocol.

VI. CONCLUSIONS AND OUTLOOK

We proposed a protocol for witnessing steering in CV systems. The protocol is based on the metrological steering criterion first proposed in Ref. [13], and relies solely on homodyne detection. The latter makes it suitable for current experimental capabilities. The protocol is shown to succeed in detecting quantum steering in non-Gaussian states, even in scenarios where protocols based on Gaussian features, like Reid's criterion, are shown to fail, when restricted to quadrature measurements. A comparison between our metrological protocol and the entropic witness presented in Ref. [40] shows that our protocol consistently outperforms the entropic one. This adds to a similar conclusion that was reached in Ref. [56] for a comparison between metrological and entropic entanglement witnesses. It remains an interesting open question whether there is a formal way of proving that the metrological witness is always larger than the entropic one. Such a proof could potentially lead to new insights into the relation between the Fisher information and entropy.

A realistic simulation of data from a continuous-variable experiment includes the effects of loss, data discretization, and the scalable extraction of the Fisher information. Our results show that non-Gaussian quantum steering can be detected with a feasible number of measurements. Even for reasonably small numbers of samples ($n = 10^5$), the violation of inequality (6) can be observed with several standard deviations, considering around 3 dB of squeezing, albeit requiring rather low losses. Rather than a feature of our specific protocol, the high sensitivity to losses for these states might be an indication of the fragile nature of non-Gaussian quantum steering. We should emphasize that our metrological witness is based on the same experimental implementation as Reid's criterion for quadrature operators. However, the postprocessing of the measurement data is significantly more involved in our approach.

The relevance of our protocol is not merely experimental. Non-Gaussian quantum correlations are notoriously difficult to study in CV systems. For the most complete descriptions of CV states, one generally resorts to quasiprobability distributions. However, it is highly challenging to use such objects to study quantum correlations (Bell inequalities are a notable exception [57,58]). The techniques in Sec. II B provide a useful way to analytically study the presence of metrologically useful non-Gaussian quantum steering based purely on the marginal of the Wigner function.

ACKNOWLEDGMENTS

This work is supported by the ANR JCJC project NoRdiC (ANR-21-CE47-0005). It is also partially funded by the European Union's Horizon 2020 research and innovation programme under Grant Agreement No. 899587, the Marie Skłodowska-Curie Grant Agreement No. 847648 with fellowship code LCF/BQ/PI21/11830025, and the QuantERA programme through the project ApresSF. M.G. acknowledges the LabEx ENS-ICFP: ANR-10-LABX-0010/ANR-10-IDEX-0001-02 PSL* and the Ministerio de Ciencia e Innovación (MCIN)/Agencia Estatal de Investigación (AEI) through Grant No. PID2020-115761RJ-I00, and support received from a "la Caixa" Foundation fellowship (ID 100010434). This work was supported within the QuantERA II Programme that has received funding from the European Union's Horizon 2020 research and innovation programme under Grant Agreement No 101017733.

APPENDIX: GENUINELY MULTIMODE PROTOCOL

The protocol that was proposed in Sec. II B effectively describes a witness for steering between two modes in a larger multimode system. In this section, we provide an extension of the protocol in a more general multimode setting. The resulting steering witness is strictly better for testing the steering between Alice and Bob, but it comes with considerably more experimental overhead and parameters to optimize.

First of all, let us consider Alice's subsystem that contains m modes. Rather than just choosing one axis $\vec{f}$ in Alice's phase space along which to measure, we can choose any set of axes that are not connected to the same mode. Formulated differently, for any mode basis in Alice's subsystem, we can measure one quadrature in each mode and condition on the joint outcome for all these measurements.

To formalize this idea, let us first consider an orthonormal symplectic basis $\mathcal{F}$ of Alice's phase space, given by

$$\mathcal{F} = \{\vec{f}_1, \Omega f_1, \ldots, \vec{f}_m, \Omega \vec{f}_m\}, \tag{A1}$$

where $\vec{f}_k$ are all vectors in $\mathbb{R}^{2M}$ with M the number of modes in the global system that contains both Alice and Bob. One can think of $\mathcal{F}$ as one of the infinitely many ways of identifying axes in Alice's phase in a way such that $\vec{f}_k$ and Ωf_k always belong to the same mode (we could say that the axis generated by $\vec{f}_k$ represents the measurements of the q quadrature in this mode and Ωf_k generates the axis that represents its p quadrature).

The vectors $\vec{f}_1, \ldots, \vec{f}_m$ by construction now correspond to m axes in phase space that can be jointly measured. When we perform such a measurement and postselect on a series of measurement outcomes $x_1, \ldots, x_m$ for each one of these axes, we find that Bob's Wigner function is transformed into

$$W^{B|A}(\vec{x}_B | x_A^{\vec{f}_1} = x_1, \ldots, x_A^{\vec{f}_m} = x_m) = \frac{\int_{\mathbb{R}^{2m}} W(\vec{x}_A \oplus \vec{x}_B) \prod_{k=1}^{m} \delta(\vec{f}_k^{\top} \vec{x}_A - x_k) d\vec{x}_A}{P_A(x_A^{\vec{f}_1} = x_1, \ldots, x_A^{\vec{f}_m} = x_m)}, \tag{A2}$$

where we define

$$P_A(x_A^{\vec{f}_1} = x_1, \ldots, x_A^{\vec{f}_m} = x_m) = \int_{\mathbb{R}^{2m} \oplus \mathbb{R}^{2m'}} W(\vec{x}_A \oplus \vec{x}_B) \prod_{k=1}^{m} \delta(\vec{f}_k^{\top} \vec{x}_A - x_k) d\vec{x}_A d\vec{x}_B. \tag{A3}$$

Equation (A2) thus directly generalizes Eq. (19).

On Bob's side of the system, we are now going to use this Wigner function to study the effect of a change in the mean field. One particular feature of such displacement operations is that they are generated by a quadrature operator, which means that they are always acting along a well-defined axis $\vec{e}$ in Bob's phase space. The parameter of interest thus affects Bob's conditional state as

$$W^{B|A}(\vec{x}_B|x_A^{\vec{f}_1}=x_1,\ldots,x_A^{\vec{f}_m}=x_m)\mapsto W^{B|A}(\vec{x}_B-\xi\vec{e}|x_A^{\vec{f}_1}=x_1,\ldots,x_A^{\vec{f}_m}=x_m). \tag{A4}$$

Because on Bob's side we implement a parameter with a single-mode generator, the calculation of the conditional variance generalizes in a straightforward fashion as

$$\begin{aligned}\mathrm{Var}_{\mathrm{hom}}^{B|A}\left(\mathcal{A},\frac{\vec{e}^{\top}\Omega\vec{\hat{x}}}{2}\right)=\min_{\mathcal{F}}\frac{1}{4}\int_{\mathbb{R}^m}&P_A(x_A^{\vec{f}_1}=x_1,\ldots,x_A^{\vec{f}_m}=x_m)\\&\times\mathrm{Var}\big(\hat{\rho}^B_{x_1,\ldots,x_m|\vec{f}_1,\ldots,\vec{f}_m},\vec{e}^{\top}\Omega\vec{\hat{x}}\big)dx_1\cdots dx_m,\end{aligned} \tag{A5}$$

where $\mathrm{Var}(\hat{\rho}^B_{x_1,\ldots,x_m|\vec{f}_1,\ldots,\vec{f}_m},\vec{e}^{\top}\Omega\vec{\hat{x}})$ is the variance of the quadrature corresponding to the generator $\vec{e}^{\top}\Omega\vec{\hat{x}}$. To compute this quantity, we use exactly the same subspace of phase space as before, generated by all vectors orthogonal to $\Omega\vec{e}$:

$$\mathcal{P}^{\perp}=\{\vec{x}_B\in\mathbb{R}^{2m'}\mid\vec{e}^{\top}\Omega\vec{x}_B=0\}. \tag{A6}$$

We then calculate the measurement statistics for the quadrature $\vec{e}^{\top}\Omega\vec{\hat{x}}$ as

$$\tilde{P}^B_{x_1,\ldots,x_m|\vec{f}_1,\ldots,\vec{f}_m}(p)=\int_{\mathcal{P}^{\perp}}W^{B|A}(\vec{x}_B|x_A^{\vec{f}_1}=x_1,\ldots,x_A^{\vec{f}_m}=x_m)d\vec{x}^B, \tag{A7}$$

where p denotes the values along the single remaining phase space axis generated by $\vec{e}^{\top}\Omega\vec{\hat{x}}$. This distribution allows us to compute

$$\begin{aligned}&\mathrm{Var}\big(\hat{\rho}^B_{x_1,\ldots,x_m|\vec{f}_1,\ldots,\vec{f}_m},\vec{e}^{\top}\Omega\vec{\hat{x}}\big)\\&\quad=\int_{\mathbb{R}}p^2\tilde{P}^B_{x_1,\ldots,x_m|\vec{f}_1,\ldots,\vec{f}_m}(p)\,dp-\left(\int_{\mathbb{R}}p\tilde{P}^B_{x_1,\ldots,x_m|\vec{f}_1,\ldots,\vec{f}_m}(p)\,dp\right)^2.\end{aligned} \tag{A8}$$

In practice, this is still the variance of only one quadrature operator in Bob's conditional state. From an experimental point of view, this can be considered a significant advantage due to limited overhead.

The biggest difference appears on the level of the Fisher information. In Eq. (22), we only use the specific displaced quadrature along the phase space axis $\vec{e}$. However, more generally speaking, we can use any set of quadratures in Bob's subsystem to estimate the displacement strength ξ. To formalize this idea, we are going to consider the case where we use m' (the number of modes in Bob's subsystem) jointly measurable quadratures to estimate ξ. To do so, we use the Wigner function (A2) and integrate out all the complementary quadratures. To maximize the efficiency of the parameter estimation, we always consider cases where the full displacement is contained within the set of quadratures that is used to estimate it.

For this purpose, let us introduce a symplectic orthonormal basis $\mathcal{G}$ of Bob's phase space $\mathbb{R}^{2m'}$:

$$\mathcal{G}=\{\vec{g}_1,\Omega\vec{g}_1,\ldots,\vec{g}_{m'},\Omega\vec{g}_{m'}\}. \tag{A9}$$

A crucial additional constraint that is imposed on this basis is that some $\alpha_k\in\mathbb{R}$ with $\sum_k\alpha_k^2=1$ exist such that

$$\vec{e}=\alpha_1\vec{g}_1+\cdots+\alpha_{m'}\vec{g}_{m'}. \tag{A10}$$

This demand is important, because we are going to measure quadratures along the phase space axes generated by $\vec{g}_1,\ldots,\vec{g}_{m'}$. When doing so, we generalize Eq. (20) to

$$P^B_{x_1,\ldots,x_m|\vec{f}_1,\ldots,\vec{f}_m}(q_1,\ldots,q_{m'})=\int_{\mathbb{R}^{2m'}}\prod_{k=1}^{m'}\delta(\vec{g}_k^{\top}\vec{x}_B-q_k)W^{B|A}(\vec{x}_B|x_A^{\vec{f}_1}=x_1,\ldots,x_A^{\vec{f}_m}=x_m)d\vec{x}_B. \tag{A11}$$

The action of the displacement now becomes a bit more subtle, in the sense that

$$P^B_{x_1,\ldots,x_m|\vec{f}_1,\ldots,\vec{f}_m}(q_1,\ldots,q_{m'} \mid \xi) = P^B_{x_1,\ldots,x_m|\vec{f}_1,\ldots,\vec{f}_m}(q_1-\alpha_1\xi,\ldots,q_{m'}-\alpha_{m'}\xi \mid \xi). \tag{A12}$$

The Fisher information for estimating ξ using this multivariate distribution can be calculated by a straightforward extension of Eq. (18), such that we find that

$$F^B_\xi[P^B_{x_1,\ldots,x_m|\vec{f}_1,\ldots,\vec{f}_m}] = \int_{\mathbb{R}^{m'}} P^B_{x_1,\ldots,x_m|\vec{f}_1,\ldots,\vec{f}_m}(q_1,\ldots,q_{m'} \mid \xi)\left(\frac{\partial \mathcal{L}(q_1,\ldots,q_{m'} \mid \xi)}{\partial \xi}\right)^2 dq_1\cdots dq_{m'}. \tag{A13}$$

The conditional Fisher information then becomes

$$F^{B|A}_{\text{hom}}\left(\mathcal{A}, \frac{\vec{e}^\top \Omega \vec{\hat{x}}}{2}\right) = \max_{\mathcal{F}} \int_{\mathbb{R}^m} P_A(x_A^{\vec{f}_1} = x_1,\ldots,x_A^{\vec{f}_m} = x_m) F^B_\xi[P^B_{x_1,\ldots,x_m|\vec{f}_1,\ldots,\vec{f}_m}]dx_1\cdots dx_m. \tag{A14}$$

Note that we maximize over all possible bases for Alice's phase space $\mathcal{F}$, as given by Eq. (A1).

Combining all the above elements now leads us to formulate a fully multimode version of the metrological witness (26):

$$S^{\text{hom}}_{\max}(\mathcal{A}) = \max_{\vec{e}\in\mathbb{R}^{2m'};\mathcal{G}} \left[F^{B|A}_{\text{hom}}\left(\mathcal{A}, \frac{\vec{e}^\top \Omega \vec{\hat{x}}}{2}\right) - \text{Var}^{B|A}_{\text{hom}}(\mathcal{A}, \vec{e}^\top \Omega \vec{\hat{x}})\right]^+ \tag{A15}$$

with the terms now defined through Eqs. (A5) and (A14). Furthermore, we note that we must maximize this value over all possible choices of displacement directions and subsequently all the possible ways of constructing a basis $\mathcal{G}$ of Bob's phase space according to Eq. (A9). Of course, in practice, any displacement direction and measurement basis that allows us to obtain a value of $S^{\text{hom}}_{\max}(\mathcal{A})$ that is significantly larger than zero (significant as compared to an experimental error bar) is sufficient to certify quantum steering from Alice to Bob.

The steering witness in Eq. (A15) is guaranteed to outperform the version in Eq. (26) in which Bob only measures the displaced quadrature. However, it is clear that having to optimize several homodyne detectors to function simultaneously clearly requires much more experimental overhead than using a single detector. This thus imposes the question of whether there is a strict advantage in using the multimode witness (A15), where Alice and Bob measure all their quadratures simultaneously.

For Alice's measurements, we explore the case where no individual mode (regardless of the mode basis) can steer Bob, but where we require the use of several modes at the same time. On Bob's side, the matter is more related to metrology. Because the displacement is anyway generated by a generator that acts on one specific mode, it is logical to wonder whether only measuring the displaced quadrature operator is sufficient to extract all information on ξ. There is an argument to suggest that this is typically not the case. When in the state given by Eq. (A2), the mode in which the displacement acts is entangled to other modes; a measurement of only the displaced quadrature will trace out the other modes, which effectively leads to decoherence. This suggests that in these cases Eq. (A15) could detect steering that remains hidden when the simpler form (26) is used. This can be verified by comparing the obtained FI to the QFI if the latter can be calculated.

A detailed study of all these extra effects would require us to perform additional case studies for different kinds of multimode states. However, such a study requires a more dedicated effort and is considered to be beyond the scope of this work.

[1] A. Einstein, B. Podolsky, and N. Rosen, Can quantum-mechanical description of physical reality be considered complete? Phys. Rev. **47**, 777 (1935).
[2] E. Schrödinger, Discussion of probability relations between separated systems, Math. Proc. Camb. Philos. Soc. **31**, 555 (1935).
[3] E. Schrödinger, Probability relations between separated systems, Math. Proc. Camb. Philos. Soc. **32**, 446 (1936).
[4] J. S. Bell, On the Einstein Podolsky Rosen paradox, Phys. Phys. Fiz. **1**, 195 (1964).
[5] H. M. Wiseman, S. J. Jones, and A. C. Doherty, Steering, Entanglement, Nonlocality, and the Einstein-Podolsky-Rosen Paradox, Phys. Rev. Lett. **98**, 140402 (2007).
[6] R. Uola, A. C. S. Costa, H. C. Nguyen, and O. Gühne, Quantum steering, Rev. Mod. Phys. **92**, 015001 (2020).

[7] R. Gallego and L. Aolita, Resource theory of steering, Phys. Rev. X **5**, 041008 (2015).

[8] C. Branciard, E. G. Cavalcanti, S. P. Walborn, V. Scarani, and H. M. Wiseman, One-sided device-independent quantum key distribution: Security, feasibility, and the connection with steering, Phys. Rev. A **85**, 010301 (2012).

[9] T. Gehring, V. Händchen, J. Duhme, F. Furrer, T. Franz, C. Pacher, R. F. Werner, and R. Schnabel, Implementation of continuous-variable quantum key distribution with composable and one-sided-device-independent security against coherent attacks, Nat. Commun. **6**, 8795 (2015).

[10] N. Walk, S. Hosseini, J. Geng, O. Thearle, J. Y. Haw, S. Armstrong, S. M. Assad, J. Janousek, T. C. Ralph, T. Symul, H. M. Wiseman, and P. K. Lam, Experimental demonstration of Gaussian protocols for one-sided device-independent quantum key distribution, Optica **3**, 634 (2016).

[11] Y. Z. Law, L. P. Thinh, J.-D. Bancal, and V. Scarani, Quantum randomness extraction for various levels of characterization of the devices, J. Phys. A: Math. Theor. **47**, 424028 (2014).

[12] E. Passaro, D. Cavalcanti, P. Skrzypczyk, and A. Acín, Optimal randomness certification in the quantum steering and prepare-and-measure scenarios, New J. Phys. **17**, 113010 (2015).

[13] B. Yadin, M. Fadel, and M. Gessner, Metrological complementarity reveals the Einstein-Podolsky-Rosen paradox, Nat. Commun. **12**, 2410 (2021).

[14] M. Piani and J. Watrous, Necessary and Sufficient Quantum Information Characterization of Einstein-Podolsky-Rosen Steering, Phys. Rev. Lett. **114**, 060404 (2015).

[15] A. Acín, N. Brunner, N. Gisin, S. Massar, S. Pironio, and V. Scarani, Device-Independent Security of Quantum Cryptography Against Collective Attacks, Phys. Rev. Lett. **98**, 230501 (2007).

[16] N. Brunner, D. Cavalcanti, S. Pironio, V. Scarani, and S. Wehner, Bell nonlocality, Rev. Mod. Phys. **86**, 419 (2014).

[17] R. Horodecki, P. Horodecki, M. Horodecki, and K. Horodecki, Quantum entanglement, Rev. Mod. Phys. **81**, 865 (2009).

[18] E. G. Cavalcanti, S. J. Jones, H. M. Wiseman, and M. D. Reid, Experimental criteria for steering and the Einstein-Podolsky-Rosen paradox, Phys. Rev. A **80**, 032112 (2009).

[19] M. D. Reid, P. D. Drummond, W. P. Bowen, E. G. Cavalcanti, P. K. Lam, H. A. Bachor, U. L. Andersen, and G. Leuchs, Colloquium: The Einstein-Podolsky-Rosen paradox: From concepts to applications, Rev. Mod. Phys. **81**, 1727 (2009).

[20] I. Kogias, A. R. Lee, S. Ragy, and G. Adesso, Quantification of Gaussian Quantum Steering, Phys. Rev. Lett. **114**, 060403 (2015).

[21] L. Lami, C. Hirche, G. Adesso, and A. Winter, Schur Complement Inequalities for Covariance Matrices and Monogamy of Quantum Correlations, Phys. Rev. Lett. **117**, 220502 (2016).

[22] L. Lami, C. Hirche, G. Adesso, and A. Winter, From log-determinant inequalities to Gaussian entanglement via recoverability theory, IEEE Trans. Inf. Theory **63**, 7553 (2017).

[23] A. Mari and J. Eisert, Positive Wigner Functions Render Classical Simulation of Quantum Computation Efficient, Phys. Rev. Lett. **109**, 230503 (2012).

[24] J. Niset, J. Fiurášek, and N. J. Cerf, No-Go Theorem for Gaussian Quantum Error Correction, Phys. Rev. Lett. **102**, 120501 (2009).

[25] J. Eisert, S. Scheel, and M. B. Plenio, Distilling Gaussian States with Gaussian Operations is Impossible, Phys. Rev. Lett. **89**, 137903 (2002).

[26] H. Takahashi, J. S. Neergaard-Nielsen, M. Takeuchi, M. Takeoka, K. Hayasaka, A. Furusawa, and M. Sasaki, Entanglement distillation from Gaussian input states, Nat. Photonics **4**, 178 (2010).

[27] A. Ourjoumtsev, A. Dantan, R. Tualle-Brouri, and P. Grangier, Increasing Entanglement between Gaussian States by Coherent Photon Subtraction, Phys. Rev. Lett. **98**, 030502 (2007).

[28] L. Pezzé and A. Smerzi, Entanglement, Nonlinear Dynamics, and the Heisenberg Limit, Phys. Rev. Lett. **102**, 100401 (2009).

[29] M. Gessner, A. Smerzi, and L. Pezzè, Metrological Nonlinear Squeezing Parameter, Phys. Rev. Lett. **122**, 090503 (2019).

[30] V. Giovannetti, S. Lloyd, and L. Maccone, Advances in quantum metrology, Nat. Photonics **5**, 222 (2011).

[31] L. Pezzè, A. Smerzi, M. K. Oberthaler, R. Schmied, and P. Treutlein, Quantum metrology with nonclassical states of atomic ensembles, Rev. Mod. Phys. **90**, 035005 (2018).

[32] A. Cavaillès, H. Le Jeannic, J. Raskop, G. Guccione, D. Markham, E. Diamanti, M. D. Shaw, V. B. Verma, S. W. Nam, and J. Laurat, Demonstration of Einstein-Podolsky-Rosen Steering Using Hybrid Continuous- and Discrete-Variable Entanglement of Light, Phys. Rev. Lett. **121**, 170403 (2018).

[33] Y. Xiang, B. Xu, L. Mišta, T. Tufarelli, Q. He, and G. Adesso, Investigating Einstein-Podolsky-Rosen steering of continuous-variable bipartite states by non-Gaussian pseudospin measurements, Phys. Rev. A **96**, 042326 (2017).

[34] I. Kogias, P. Skrzypczyk, D. Cavalcanti, A. Acín, and G. Adesso, Hierarchy of Steering Criteria Based on Moments for All Bipartite Quantum Systems, Phys. Rev. Lett. **115**, 210401 (2015).

[35] G. Tóth and I. Apellaniz, Quantum metrology from a quantum information science perspective, J. Phys. A: Math. Theor. **47**, 424006 (2014).

[36] M. Walschaers, Non-Gaussian Quantum States and Where to Find Them, PRX Quantum **2**, 030204 (2021).

[37] U. Chabaud, G. Roeland, M. Walschaers, F. Grosshans, V. Parigi, D. Markham, and N. Treps, Certification of Non-Gaussian States with Operational Measurements, PRX Quantum **2**, 020333 (2021).

[38] Y.-S. Ra, A. Dufour, M. Walschaers, C. Jacquard, T. Michel, C. Fabre, and N. Treps, Non-Gaussian quantum states of a multimode light field, Nat. Phys. **16**, 144 (2020).

[39] P. Chowdhury, T. Pramanik, A. S. Majumdar, and G. S. Agarwal, Einstein-Podolsky-Rosen steering using quantum correlations in non-Gaussian entangled states, Phys. Rev. A **89**, 012104 (2014).

[40] S. P. Walborn, A. Salles, R. M. Gomes, F. Toscano, and P. H. Souto Ribeiro, Revealing Hidden Einstein-Podolsky-Rosen Nonlocality, Phys. Rev. Lett. **106**, 130402 (2011).
[41] M. D. Reid, Demonstration of the Einstein-Podolsky-Rosen paradox using nondegenerate parametric amplification, Phys. Rev. A **40**, 913 (1989).
[42] C. Fabre and N. Treps, Modes and states in quantum optics, Rev. Mod. Phys. **92**, 035005 (2020).
[43] E. Wigner, On the quantum correction for thermodynamic equilibrium, Phys. Rev. **40**, 749 (1932).
[44] C. Weedbrook, S. Pirandola, R. García-Patrón, N. J. Cerf, T. C. Ralph, J. H. Shapiro, and S. Lloyd, Gaussian quantum information, Rev. Mod. Phys. **84**, 621 (2012).
[45] A. Stam, Some inequalities satisfied by the quantities of information of Fisher and Shannon, Inf. Control **2**, 101 (1959).
[46] M. Walschaers, C. Fabre, V. Parigi, and N. Treps, Entanglement and Wigner Function Negativity of Multimode Non-Gaussian States, Phys. Rev. Lett. **119**, 183601 (2017).
[47] M. Walschaers, C. Fabre, V. Parigi, and N. Treps, Statistical signatures of multimode single-photon-added and -subtracted states of light, Phys. Rev. A **96**, 053835 (2017).
[48] D. Braun, P. Jian, O. Pinel, and N. Treps, Precision measurements with photon-subtracted or photon-added Gaussian states, Phys. Rev. A **90**, 013821 (2014).
[49] M. Walschaers, Y.-S. Ra, and N. Treps, Mode-dependent-loss model for multimode photon-subtracted states, Phys. Rev. A **100**, 023828 (2019).
[50] M. Walschaers, V. Parigi, and N. Treps, Practical Framework for Conditional Non-Gaussian Quantum State Preparation, PRX Quantum **1**, 020305 (2020).
[51] Y. Xiang, S. Liu, J. Guo, Q. Gong, N. Treps, Q. He, and M. Walschaers, Distribution and quantification of remotely generated Wigner negativity, npj Quantum Inf. **8**, 21 (2022).
[52] in *A Guide to Experiments in Quantum Optics*, Chapter 9 (John Wiley & Sons Ltd, Weinheim, 2019), p. 303.
[53] H. Strobel, W. Muessel, D. Linnemann, T. Zibold, D. B. Hume, L. Pezzè, A. Smerzi, and M. K. Oberthaler, Fisher information and entanglement of non-Gaussian spin states, Science **345**, 424 (2014).
[54] W. K. Wootters, Statistical distance and Hilbert space, Phys. Rev. D **23**, 357 (1981).
[55] S. L. Braunstein and C. M. Caves, Statistical Distance and the Geometry of Quantum States, Phys. Rev. Lett. **72**, 3439 (1994).
[56] M. Gessner, L. Pezzè, and A. Smerzi, Efficient entanglement criteria for discrete, continuous, and hybrid variables, Phys. Rev. A **94**, 020101 (2016).
[57] K. Banaszek and K. Wódkiewicz, Testing Quantum Nonlocality in Phase Space, Phys. Rev. Lett. **82**, 2009 (1999).
[58] M. D'Angelo, A. Zavatta, V. Parigi, and M. Bellini, Tomographic test of Bell's inequality for a time-delocalized single photon, Phys. Rev. A **74**, 052114 (2006).

6

CONCLUSIONS

Throughout the past decade, continuous-variable quantum systems have seen a surge in popularity, motivated by the developments in bosonic error correction codes, realisations of Gaussian boson sampling, and real-world applications such as the use of squeezing in gravitational wave detection. These developments have lured researcher from a variety of fields, e.g., superconducting circuits, into exploring the continuous-variable degrees of freedom of their systems. This has recently led to a series of impressive continuous-variable experiments (Campagne-Ibarcq et al., 2020; Lescanne et al., 2020; Neeve et al., 2022).

Where the continuous-variable approach was long seen as a niche, it is gradually becoming more mainstream. While this creates a very dynamic and increasingly well-funded research environment, it also boosts competition. Among these competitors, we now also count large industry players such as Xanadu (optics) and Amazon (superconducting circuits). This regularly forces us to take a few steps back and reflect about our place in this dynamical landscape.

In this Habilitation thesis, I tried to show that we consciously choose to stay away from well-defined road maps with clearly outlined technical challenges to overcome, but rather pursue a free exploration of the interesting physics that surrounds continuous-variable quantum technologies. In my research, this is reflected by a growing focus on quantum resources, *i.e.*, useful features of quantum states. Works such as Mari and Eisert, 2012 and Albarelli et al., 2018; Takagi and Zhuang, 2018 have strongly motivated my interest in understanding the prerequisites for generating Wigner negativity. However, our recent results in Chabaud and Walschaers, 2023 provide a strong motivation to explore other resources, such as non-Gaussian entanglement and stellar rank.

This thesis highlights how the theory research in our group is evolving towards a structure in which we explore three core elements of these quantum resources: creation (see Chapter 3), characterisation (see Chapter 5), and their applications (see Chapters 2 and 4). The research lines in these three directions are strongly intertwined, and ultimately we hope that the exploration of applications in quantum computing and quantum metrology will ultimately help us identify new relevant quantum resources. This has now put us on the track of non-Gaussian entanglement, which will be the

central resource that we will study in the near future.

In the long-run, we hope that many of the different pieces of the puzzle on quantum advantages will ultimately click together. On the one hand, the negativity of phase-space representations of the state seems like a key ingredient. Negativity of some quasiprobability distributions have been identified as a crucial resource for reaching a quantum computational advantage (Mari and Eisert, 2012; Rahimi-Keshari et al., 2016) and negativity of other quasiprobability distributions are known to lead to some form of quantum metrological advantage (Arvidsson-Shukur et al., 2020). Negativity of the Wigner function has also been connected to a continuous-variable type of contextuality (Booth et al., 2022; Spekkens, 2008), and in turn contextuality is a known to provide the "magic" in measurement-based quantum computing (Howard et al., 2014). On the other hand, it is still unclear how resources such as a high stellar rank and non-Gaussian entanglement (Chabaud and Walschaers, 2023) fit into this picture.

Considering quantum metrological advantages, it remains a serious open question whether non-Gaussian resources can provide a sufficiently large improvement to make it worth the effort of generating those resources in the first place. Our metrological detection techniques for non-Gaussian entanglement (Barral et al., 2023; Lopetegui et al., 2022) suggest that non-Gaussian entanglement could have useful metrological properties. However, these metrological witnesses compare metrological sensitivity to other properties of the state. Were we only to focus on the metrological sensitivity, it is not guaranteed that there are not separable Gaussian states than can lead to the same performance. The cases we have consider so far suggest that this typically is the case. This suggests that in the future it will be crucial to delineate operational settings to reach a meaningful comparison between the metrological properties of different types of quantum states.

BIBLIOGRAPHY

[1]S. Aaronson and A. Arkhipov, "The Computational Complexity of Linear Optics", in Proceedings of the Forty-third Annual ACM Symposium on Theory of Computing, STOC '11 (2011), pp. 333–342.

[2]S. Aaronson and A. Arkhipov, "Bosonsampling is Far from Uniform", Quantum Info. Comput. **14**, 1383–1423 (2014).

[3]F. Albarelli, M. G. Genoni, M. G. A. Paris, and A. Ferraro, "Resource theory of quantum non-Gaussianity and Wigner negativity", Phys. Rev. A **98**, 052350 (2018).

[4]M. Ansquer, V. Thiel, S. De, B. Argence, G. Gredat, F. Bretenaker, and N. Treps, "Unveiling the dynamics of optical frequency combs from phase-amplitude correlations", Physical Review Research **3**, 033092 (2021).

[5]D. R. M. Arvidsson-Shukur, N. Yunger Halpern, H. V. Lepage, A. A. Lasek, C. H. W. Barnes, and S. Lloyd, "Quantum advantage in postselected metrology", Nature Communications **11**, 3775 (2020).

[6]V. A. Averchenko, C. Jacquard, V. Thiel, C. Fabre, and N. Treps, "Multimode theory of single-photon subtraction", New J. Phys. **18**, 083042 (2016).

[7]V. A. Averchenko, V. Thiel, and N. Treps, "Nonlinear photon subtraction from a multimode quantum field", Phys. Rev. A **89**, 063808 (2014).

[8]G. A. Baker, "Formulation of Quantum Mechanics Based on the Quasi-Probability Distribution Induced on Phase Space", Physical Review **109**, 2198–2206 (1958).

[9]D. Barral, M. Isoard, G. Sorelli, M. Gessner, N. Treps, and M. Walschaers, *Metrological detection of purely-non-Gaussian entanglement*, Jan. 2023.

[10]S. D. Bartlett, B. C. Sanders, S. L. Braunstein, and K. Nemoto, "Efficient Classical Simulation of Continuous Variable Quantum Information Processes", Physical Review Letters **88**, 097904 (2002).

[11]J. S. Bell, "On the einstein-podolsky-rosen paradox", Physics **1**, 195–200 (1964).

[12]P. Bertet, A. Auffeves, P. Maioli, S. Osnaghi, T. Meunier, M. Brune, J. M. Raimond, and S. Haroche, "Direct Measurement of the Wigner Function of a One-Photon Fock State in a Cavity", Physical Review Letters **89**, 200402 (2002).

[13]M. E. O. Bezerra and V. Shchesnovich, *Families of bosonic suppression laws beyond the permutation symmetry principle*, Jan. 2023.

[14]R. I. Booth, U. Chabaud, and P.-E. Emeriau, "Contextuality and Wigner Negativity Are Equivalent for Continuous-Variable Quantum Measurements", Physical Review Letters **129**, 230401 (2022).

[15]P. Boucher, C. Fabre, G. Labroille, and N. Treps, "Spatial optical mode demultiplexing as a practical tool for optimal transverse distance estimation", Optica **7**, 1621 (2020).

[16]J. E. Bourassa, R. N. Alexander, M. Vasmer, A. Patil, I. Tzitrin, T. Matsuura, D. Su, B. Q. Baragiola, S. Guha, G. Dauphinais, K. K. Sabapathy, N. C. Menicucci, and I. Dhand, "Blueprint for a Scalable Photonic Fault-Tolerant Quantum Computer", Quantum **5**, 392 (2021).

[17]W. P. Bowen, N. Treps, B. C. Buchler, R. Schnabel, T. C. Ralph, H.-A. Bachor, T. Symul, and P. K. Lam, "Experimental investigation of continuous-variable quantum teleportation", Phys. Rev. A **67**, 032302 (2003).

[18]V. Boyer, A. M. Marino, R. C. Pooser, and P. D. Lett, "Entangled Images from Four-Wave Mixing", Science **321**, 544–547 (2008).

[19]S. L. Braunstein, "Squeezing as an irreducible resource", Phys. Rev. A **71**, 055801 (2005).

[20]S. L. Braunstein and C. M. Caves, "Statistical distance and the geometry of quantum states", Physical Review Letters **72**, 3439–3443 (1994).

[21]M. J. Bremner, R. Jozsa, and D. J. Shepherd, "Classical simulation of commuting quantum computations implies collapse of the polynomial hierarchy", Proceedings of the Royal Society A: Mathematical, Physical and Engineering Sciences **467**, 459–472 (2010).

[22]M. A. Broome, A. Fedrizzi, S. Rahimi-Keshari, J. Dove, S. Aaronson, T. C. Ralph, and A. G. White, "Photonic Boson Sampling in a Tunable Circuit", Science **339**, 794–798 (2013).

[23]E. Brunner, A. Buchleitner, and G. Dufour, "Many-body coherence and entanglement probed by randomized correlation measurements", Physical Review Research **4**, 043101 (2022).

[24]Y. Cai, J. Roslund, G. Ferrini, F. Arzani, X. Xu, C. Fabre, and N. Treps, "Multimode entanglement in reconfigurable graph states using optical frequency combs", Nat. Commun. **8**, 15645 (2017).

[25]P. Campagne-Ibarcq, A. Eickbusch, S. Touzard, E. Zalys-Geller, N. E. Frattini, V. V. Sivak, P. Reinhold, S. Puri, S. Shankar, R. J. Schoelkopf, L. Frunzio, M. Mirrahimi, and M. H. Devoret, "Quantum error correction of a qubit encoded in grid states of an oscillator", Nature **584**, 368–372 (2020).

[26]Y. Cardin and N. Quesada, *Photon-number moments and cumulants of Gaussian states*, Dec. 2022.

[27]J. Carolan, J. D. A. Meinecke, P. J. Shadbolt, N. J. Russell, N. Ismail, K. Wörhoff, T. Rudolph, M. G. Thompson, J. L. O'Brien, J. C. F. Matthews, and A. Laing, "On the experimental verification of quantum complexity in linear optics", Nature Photonics **8**, 621–626 (2014).

[28]U. Chabaud, T. Douce, D. Markham, P. van Loock, E. Kashefi, and G. Ferrini, "Continuous-variable sampling from photon-added or photon-subtracted squeezed states", Phys. Rev. A **96**, 062307 (2017).

[29]U. Chabaud, G. Ferrini, F. Grosshans, and D. Markham, "Classical simulation of Gaussian quantum circuits with non-Gaussian input states", Physical Review Research **3**, 033018 (2021).

[30]U. Chabaud, F. Grosshans, E. Kashefi, and D. Markham, "Efficient verification of Boson Sampling", Quantum **5**, 578 (2021).

[31]U. Chabaud, D. Markham, and F. Grosshans, "Stellar Representation of Non-Gaussian Quantum States", Phys. Rev. Lett. **124**, 063605 (2020).

[32]U. Chabaud and S. Mehraban, "Holomorphic representation of quantum computations", Quantum **6**, 831 (2022).

[33]U. Chabaud, G. Roeland, M. Walschaers, F. Grosshans, V. Parigi, D. Markham, and N. Treps, "Certification of Non-Gaussian States with Operational Measurements", PRX Quantum **2**, 020333 (2021).

[34]U. Chabaud and M. Walschaers, "Resources for Bosonic Quantum Computational Advantage", Physical Review Letters **130**, 090602 (2023).

[35]V. Cimini, M. Barbieri, N. Treps, M. Walschaers, and V. Parigi, "Neural Networks for Detecting Multimode Wigner Negativity", Physical Review Letters **125**, 160504 (2020).

[36]P. Clifford and R. Clifford, "The Classical Complexity of Boson Sampling", in *Proceedings of the 2018 Annual ACM-SIAM Symposium on Discrete Algorithms (SODA)*, Proceedings (Jan. 2018), pp. 146–155.

[37]A. Crespi, R. Osellame, R. Ramponi, M. Bentivegna, F. Flamini, N. Spagnolo, N. Viggianiello, L. Innocenti, P. Mataloni, and F. Sciarrino, "Suppression law of quantum states in a 3D photonic fast Fourier transform chip", Nature Communications **7**, 10469 (2016).

[38]A. Crespi, R. Osellame, R. Ramponi, D. J. Brod, E. F. Galvão, N. Spagnolo, C. Vitelli, E. Maiorino, P. Mataloni, and F. Sciarrino, "Integrated multimode interferometers with arbitrary designs for photonic boson sampling", Nature Photonics **7**, 545–549 (2013).

[39]T. Curtright, D. Fairlie, and C. Zachos, "Features of time-independent Wigner functions", Physical Review D **58**, 025002 (1998).

[40]M. Dakna, T. Anhut, T. Opatrný, L. Knöll, and D.-G. Welsch, "Generating Schrödinger-cat-like states by means of conditional measurements on a beam splitter", Phys. Rev. A **55**, 3184–3194 (1997).

[41]N. Dangniam and C. Ferrie, "Quantum Bochner's theorem for phase spaces built on projective representations", Journal of Physics A: Mathematical and Theoretical **48**, 115305 (2015).

[42]A. O. C. Davis, M. Walschaers, V. Parigi, and N. Treps, "Conditional preparation of non-Gaussian quantum optical states by mesoscopic measurement", New Journal of Physics **23**, 063039 (2021).

[43]V. Delaubert, N. Treps, M. Lassen, C. C. Harb, C. Fabre, P. K. Lam, and H.-A. Bachor, "${\mathrm{TEM}}_{10}$ homodyne detection as an optimal small-displacement and tilt-measurement scheme", Physical Review A **74**, 053823 (2006).

[44]P. a. M. Dirac, "The Fundamental Equations of Quantum Mechanics", Proceedings of the Royal Society of London A: Mathematical, Physical and Engineering Sciences **109**, 642–653 (1925).

[45]C. Dittel, G. Dufour, M. Walschaers, G. Weihs, A. Buchleitner, and R. Keil, "Totally destructive interference for permutation-symmetric many-particle states", Physical Review A **97**, 062116 (2018).

[46]C. Dittel, G. Dufour, M. Walschaers, G. Weihs, A. Buchleitner, and R. Keil, "Totally Destructive Many-Particle Interference", Physical Review Letters **120**, 240404 (2018).

[47]L.-M. Duan, G. Giedke, J. I. Cirac, and P. Zoller, "Inseparability Criterion for Continuous Variable Systems", Phys. Rev. Lett. **84**, 2722–2725 (2000).

[48]M. Eaton, C. González-Arciniegas, R. N. Alexander, N. C. Menicucci, and O. Pfister, "Measurement-based generation and preservation of cat and grid states within a continuous-variable cluster state", Quantum **6**, 769 (2022).

[49]M. Eaton, A. Hossameldin, R. J. Birrittella, P. M. Alsing, C. C. Gerry, H. Dong, C. Cuevas, and O. Pfister, "Resolution of 100 photons and quantum generation of unbiased random numbers", Nature Photonics, 1–6 (2022).

[50]A. Einstein, B. Podolsky, and N. Rosen, "Can Quantum-Mechanical Description of Physical Reality Be Considered Complete?", Physical Review **47**, 777–780 (1935).

[51]J. Eisert, D. Hangleiter, N. Walk, I. Roth, D. Markham, R. Parekh, U. Chabaud, and E. Kashefi, "Quantum certification and benchmarking", Nature Reviews Physics **2**, 382–390 (2020).

[52]C. Fabre and N. Treps, "Modes and states in quantum optics", Rev. Mod. Phys. **92**, 035005 (2020).

[53]M. Fannes and A. Verbeure, "Gauge transformations and normal states of the CCR", J. Math. Phys. **16**, 2086–2088 (1975).

[54]L. J. Fiderer, T. Tufarelli, S. Piano, and G. Adesso, "General Expressions for the Quantum Fisher Information Matrix with Applications to Discrete Quantum Imaging", PRX Quantum **2**, 020308 (2021).

[55]R. Filip and L. Mišta, "Detecting Quantum States with a Positive Wigner Function beyond Mixtures of Gaussian States", Phys. Rev. Lett. **106**, 200401 (2011).

[56]F. Flamini, N. Spagnolo, and F. Sciarrino, "Photonic quantum information processing: a review", Reports on Progress in Physics **82**, 016001 (2018).

[57]F. Flamini, M. Walschaers, N. Spagnolo, N. Wiebe, A. Buchleitner, and F. Sciarrino, "Validating multi-photon quantum interference with finite data", Quantum Science and Technology **5**, 045005 (2020).

[58]D. Fukuda, G. Fujii, T. Numata, K. Amemiya, A. Yoshizawa, H. Tsuchida, H. Fujino, H. Ishii, T. Itatani, S. Inoue, and T. Zama, "Titanium-based transition-edge photon number resolving detector with 98% detection efficiency with index-matched small-gap fiber coupling", Optics Express **19**, 870–875 (2011).

[59]K. Fukui, S. Takeda, M. Endo, W. Asavanant, J.-i. Yoshikawa, P. van Loock, and A. Furusawa, "Efficient Backcasting Search for Optical Quantum State Synthesis", Physical Review Letters **128**, 240503 (2022).

[60]C. N. Gagatsos and S. Guha, "Efficient representation of Gaussian states for multi-mode non-Gaussian quantum state engineering via subtraction of arbitrary number of photons", Physical Review A **99**, 053816 (2019).

[61]L. García-Álvarez, C. Calcluth, A. Ferraro, and G. Ferrini, "Efficient simulatability of continuous-variable circuits with large Wigner negativity", Physical Review Research **2**, 043322 (2020).

[62]R. García-Patrón, J. J. Renema, and V. Shchesnovich, "Simulating boson sampling in lossy architectures", Quantum **3**, 169 (2019).

[63]M. G. Genoni, M. L. Palma, T. Tufarelli, S. Olivares, M. S. Kim, and M. G. A. Paris, "Detecting quantum non-Gaussianity via the Wigner function", Phys. Rev. A **87**, 062104 (2013).

[64]T. Gerrits, B. Calkins, N. Tomlin, A. E. Lita, A. Migdall, R. Mirin, and S. W. Nam, "Extending single-photon optimized superconducting transition edge sensors beyond the single-photon counting regime", Optics Express **20**, 23798–23810 (2012).

[65]M. Gessner, C. Fabre, and N. Treps, "Superresolution Limits from Measurement Crosstalk", Physical Review Letters **125**, 100501 (2020).

[66]M. Gessner, L. Pezzè, and A. Smerzi, "Efficient entanglement criteria for discrete, continuous, and hybrid variables", Physical Review A **94**, 020101 (2016).

[67]M. Gessner, A. Smerzi, and L. Pezzè, "Metrological Nonlinear Squeezing Parameter", Physical Review Letters **122**, 090503 (2019).

[68]M. Gessner, A. Smerzi, and L. Pezzè, "Multiparameter squeezing for optimal quantum enhancements in sensor networks", Nature Communications **11**, 3817 (2020).

[69]M. Gessner, N. Treps, and C. Fabre, *Quantum Limits on Mode Parameter Estimation*, Jan. 2022.

[70]T. Giordani, F. Flamini, M. Pompili, N. Viggianiello, N. Spagnolo, A. Crespi, R. Osellame, N. Wiebe, M. Walschaers, A. Buchleitner, and F. Sciarrino, "Experimental statistical signature of many-body quantum interference", Nature Photonics **12**, 173–178 (2018).

[71]R. J. Glauber, "Coherent and Incoherent States of the Radiation Field", Phys. Rev. **131**, 2766–2788 (1963).

[72]C. Gneiting and K. Hornberger, "Detecting Entanglement in Spatial Interference", Physical Review Letters **106**, 210501 (2011).

[73]C. Gogolin, M. Kliesch, L. Aolita, and J. Eisert, "Boson-Sampling in the light of sample complexity", arXiv:1306.3995 [quant-ph] (2013).

[74]D. Gottesman, A. Kitaev, and J. Preskill, "Encoding a qubit in an oscillator", Physical Review A **64**, 012310 (2001).

[75]M. R. Grace and S. Guha, "Identifying Objects at the Quantum Limit for Superresolution Imaging", Physical Review Letters **129**, 180502 (2022).

[76]G. Grynberg, A. Aspect, and C. Fabre, *Introduction to quantum optics: from the semi-classical approach to quantized light* (Cambridge, UK ; New York, 2010).

[77]B. C. Hall, "Quantization Schemes for Euclidean Space", in *Quantum Theory for Mathematicians*, edited by B. C. Hall, Graduate Texts in Mathematics (New York, NY, 2013), pp. 255–277.

[78]C. S. Hamilton, R. Kruse, L. Sansoni, S. Barkhofen, C. Silberhorn, and I. Jex, "Gaussian Boson Sampling", arXiv:1612.01199 [quant-ph] (2016).

[79]D. Hangleiter, M. Kliesch, J. Eisert, and C. Gogolin, "Sample Complexity of Device-Independently Certified "Quantum Supremacy"", Physical Review Letters **122**, 210502 (2019).

[80]N. Heurtel, A. Fyrillas, G. de Gliniasty, R. L. Bihan, S. Malherbe, M. Pailhas, B. Bourdoncle, P.-E. Emeriau, R. Mezher, L. Music, N. Belabas, B. Valiron, P. Senellart, S. Mansfield, and J. Senellart, *Perceval: A Software Platform for Discrete Variable Photonic Quantum Computing*, Apr. 2022.

[81]A. C. Hirshfeld and P. Henselder, "Deformation quantization in the teaching of quantum mechanics", American Journal of Physics **70**, 537–547 (2002).

[82]A. S. Holevo, *Statistical Structure of Quantum Theory*, Vol. 67, Lecture Notes in Physics Monographs (Berlin, Heidelberg, 2001).

[83]C. K. Hong, Z. Y. Ou, and L. Mandel, "Measurement of subpicosecond time intervals between two photons by interference", Physical Review Letters **59**, 2044–2046 (1987).

[84]M. Howard, J. Wallman, V. Veitch, and J. Emerson, "Contextuality supplies the 'magic' for quantum computation", Nature **510**, 351–355 (2014).

[85]H.-Y. Huang, R. Kueng, and J. Preskill, "Predicting many properties of a quantum system from very few measurements", Nature Physics **16**, 1050–1057 (2020).

[86]H.-Y. Huang, R. Kueng, G. Torlai, V. V. Albert, and J. Preskill, "Provably efficient machine learning for quantum many-body problems", Science **377**, eabk3333 (2022).

[87]M. Hübner, "Explicit computation of the Bures distance for density matrices", Physics Letters A **163**, 239–242 (1992).

[88]R. L. Hudson, "When is the wigner quasi-probability density non-negative?", Reports on Mathematical Physics **6**, 249–252 (1974).

[89]K. Husimi, "Some Formal Properties of the Density Matrix", Proceedings of the Physico-Mathematical Society of Japan. 3rd Series **22**, 264–314 (1940).

[90]V. Kala, R. Filip, and P. Marek, "Cubic nonlinear squeezing and its decoherence", Optics Express **30**, 31456–31471 (2022).

[91]I. Karuseichyk, G. Sorelli, M. Walschaers, N. Treps, and M. Gessner, "Resolving mutually-coherent point sources of light with arbitrary statistics", Physical Review Research **4**, 043010 (2022).

[92]S. M. Kay, *Fundamentals of statistical signal processing*, Prentice Hall signal processing series (Englewood Cliffs, N.J, 1993).

[93]A. Kenfack and K. Życzkowski, "Negativity of the Wigner function as an indicator of non-classicality", Journal of Optics B: Quantum and Semiclassical Optics **6**, 396–404 (2004).

[94]N. Killoran, J. Izaac, N. Quesada, V. Bergholm, M. Amy, and C. Weedbrook, "Strawberry Fields: A Software Platform for Photonic Quantum Computing", Quantum **3**, 129 (2019).

[95]I. Kogias, A. R. Lee, S. Ragy, and G. Adesso, "Quantification of Gaussian Quantum Steering", Physical Review Letters **114**, 060403– (2015).

[96]I. Kogias, P. Skrzypczyk, D. Cavalcanti, A. Acín, and G. Adesso, "Hierarchy of Steering Criteria Based on Moments for All Bipartite Quantum Systems", Physical Review Letters **115**, 210401 (2015).

[97]G. Labroille, B. Denolle, P. Jian, P. Genevaux, N. Treps, and J.-F. Morizur, "Efficient and mode selective spatial mode multiplexer based on multi-plane light conversion", Optics Express **22**, 15599–15607 (2014).

[98] L. Lachman, I. Straka, J. Hloušek, M. Ježek, and R. Filip, "Faithful Hierarchy of Genuine n-Photon Quantum Non-Gaussian Light", Phys. Rev. Lett. **123**, 043601 (2019).

[99] D. Leibfried, D. M. Meekhof, B. E. King, C. Monroe, W. M. Itano, and D. J. Wineland, "Experimental Determination of the Motional Quantum State of a Trapped Atom", Physical Review Letters **77**, 4281–4285 (1996).

[100] R. Lescanne, M. Villiers, T. Peronnin, A. Sarlette, M. Delbecq, B. Huard, T. Kontos, M. Mirrahimi, and Z. Leghtas, "Exponential suppression of bit-flips in a qubit encoded in an oscillator", Nature Physics **16**, 509–513 (2020).

[101] F. Levi, S. Mostarda, F. Rao, and F. Mintert, "Quantum mechanics of excitation transport in photosynthetic complexes: a key issues review", Reports on Progress in Physics **78**, 082001 (2015).

[102] S. Liu, D. Han, N. Wang, Y. Xiang, F. Sun, M. Wang, Z. Qin, Q. Gong, X. Su, and Q. He, "Experimental Demonstration of Remotely Creating Wigner Negativity via Quantum Steering", Physical Review Letters **128**, 200401 (2022).

[103] P. van Loock and A. Furusawa, "Detecting genuine multipartite continuous-variable entanglement", Physical Review A **67**, 052315 (2003).

[104] C. E. Lopetegui, M. Gessner, M. Fadel, N. Treps, and M. Walschaers, "Homodyne Detection of Non-Gaussian Quantum Steering", PRX Quantum **3**, 030347 (2022).

[105] C. Lupo and S. Pirandola, "Ultimate Precision Bound of Quantum and Subwavelength Imaging", Physical Review Letters **117**, 190802 (2016).

[106] L. G. Lutterbach and L. Davidovich, "Method for Direct Measurement of the Wigner Function in Cavity QED and Ion Traps", Physical Review Letters **78**, 2547–2550 (1997).

[107] A. I. Lvovsky, P. Grangier, A. Ourjoumtsev, V. Parigi, M. Sasaki, and R. Tualle-Brouri, *Production and applications of non-Gaussian quantum states of light* (2020).

[108] A. I. Lvovsky, H. Hansen, T. Aichele, O. Benson, J. Mlynek, and S. Schiller, "Quantum State Reconstruction of the Single-Photon Fock State", Phys. Rev. Lett. **87**, 050402 (2001).

[109] A. I. Lvovsky and M. G. Raymer, "Continuous-variable optical quantum-state tomography", Reviews of Modern Physics **81**, 299–332 (2009).

[110] L. S. Madsen, F. Laudenbach, M. F. Askarani, F. Rortais, T. Vincent, J. F. F. Bulmer, F. M. Miatto, L. Neuhaus, L. G. Helt, M. J. Collins, A. E. Lita, T. Gerrits, S. W. Nam, V. D. Vaidya, M. Menotti, I. Dhand, Z. Vernon, N. Quesada, and J. Lavoie, "Quantum computational advantage with a programmable photonic processor", Nature **606**, 75–81 (2022).

[111] A. Mari and J. Eisert, "Positive Wigner Functions Render Classical Simulation of Quantum Computation Efficient", Phys. Rev. Lett. **109**, 230503 (2012).

[112]R. van der Meer, P. Hooijschuur, F. H. B. Somhorst, P. Venderbosch, M. de Goede, B. Kassenberg, H. Snijders, C. Taballione, J. Epping, H. v. d. Vlekkert, N. Walk, P. W. H. Pinkse, and J. J. Renema, *Experimental demonstration of an efficient, semi-device-independent photonic indistinguishability witness*, Nov. 2021.

[113]R. Mezher and S. Mansfield, *Assessing the quality of near-term photonic quantum devices*, Feb. 2022.

[114]A. Monras, *Phase space formalism for quantum estimation of Gaussian states*, Mar. 2013.

[115]J. E. Moyal, "Quantum mechanics as a statistical theory", Mathematical Proceedings of the Cambridge Philosophical Society **45**, 99–124 (1949).

[116]A. E. Moylett, R. García-Patrón, J. J. Renema, and P. S. Turner, "Classically simulating near-term partially-distinguishable and lossy boson sampling", Quantum Science and Technology **5**, 015001 (2019).

[117]C. Navarrete-Benlloch, R. García-Patrón, J. H. Shapiro, and N. J. Cerf, "Enhancing quantum entanglement by photon addition and subtraction", Phys. Rev. A **86**, 012328 (2012).

[118]B. de Neeve, T.-L. Nguyen, T. Behrle, and J. P. Home, "Error correction of a logical grid state qubit by dissipative pumping", Nature Physics **18**, 296–300 (2022).

[119]R. Nehra, A. Win, M. Eaton, R. Shahrokhshahi, N. Sridhar, T. Gerrits, A. Lita, S. W. Nam, and O. Pfister, "State-independent quantum state tomography by photon-number-resolving measurements", Optica **6**, 1356–1360 (2019).

[120]J. von Neumann, "Die Eindeutigkeit der Schrödingerschen Operatoren", Math. Ann. **104**, 570–578 (1931).

[121]M. A. Nielsen and I. L. Chuang, *Quantum Computation and Quantum Information: 10th Anniversary Edition*, 1st ed. (June 2012).

[122]A. Ourjoumtsev, A. Dantan, R. Tualle-Brouri, and P. Grangier, "Increasing Entanglement between Gaussian States by Coherent Photon Subtraction", Phys. Rev. Lett. **98**, 030502 (2007).

[123]A. Ourjoumtsev, R. Tualle-Brouri, J. Laurat, and P. Grangier, "Generating Optical Schrödinger Kittens for Quantum Information Processing", Science **312**, 83–86 (2006).

[124]V. Parigi, A. Zavatta, M. Kim, and M. Bellini, "Probing Quantum Commutation Rules by Addition and Subtraction of Single Photons to/from a Light Field", Science **317**, 1890–1893 (2007).

[125]D. Petz, *An invitation to the algebra of canonical comutation relations*, Leuven notes in mathematical and theoretical physics Series A 2 (Leuven, 1990).

[126]D. S. Phillips, M. Walschaers, J. J. Renema, I. A. Walmsley, N. Treps, and J. Sperling, "Benchmarking of Gaussian boson sampling using two-point correlators", Physical Review A **99**, 023836 (2019).

[127]O. Pinel, P. Jian, N. Treps, C. Fabre, and D. Braun, "Quantum parameter estimation using general single-mode Gaussian states", Physical Review A **88**, 040102 (2013).

[128]A. A. Pushkina, G. Maltese, J. I. Costa-Filho, P. Patel, and A. I. Lvovsky, "Superresolution Linear Optical Imaging in the Far Field", Physical Review Letters **127**, 253602 (2021).

[129]Y.-S. Ra, A. Dufour, M. Walschaers, C. Jacquard, T. Michel, C. Fabre, and N. Treps, "Non-Gaussian quantum states of a multimode light field", Nature Physics **16**, 144–147 (2020).

[130]S. Rahimi-Keshari, T. C. Ralph, and C. M. Caves, "Sufficient Conditions for Efficient Classical Simulation of Quantum Optics", Phys. Rev. X **6**, 021039 (2016).

[131]M. Reed and B. Simon, *Methods of Modern Mathematical Physics I: Functional Analysis.* 1 edition (New York, Jan. 1980).

[132]M. D. Reid, "Demonstration of the Einstein-Podolsky-Rosen paradox using nondegenerate parametric amplification", Phys. Rev. A **40**, 913–923 (1989).

[133]M. D. Reid, "Monogamy inequalities for the Einstein-Podolsky-Rosen paradox and quantum steering", Physical Review A **88**, 062108 (2013).

[134]M. D. Reid and P. D. Drummond, "Quantum Correlations of Phase in Nondegenerate Parametric Oscillation", Phys. Rev. Lett. **60**, 2731–2733 (1988).

[135]J. J. Renema, A. Menssen, W. R. Clements, G. Triginer, W. S. Kolthammer, and I. A. Walmsley, "Efficient Classical Algorithm for Boson Sampling with Partially Distinguishable Photons", Physical Review Letters **120**, 220502 (2018).

[136]L. Rigovacca, W. S. Kolthammer, C. Di Franco, and M. S. Kim, "Optical nonclassicality test based on third-order intensity correlations", Physical Review A **97**, 033809 (2018).

[137]G. Roeland, S. Kaali, V. R. Rodriguez, N. Treps, and V. Parigi, "Mode-selective single-photon addition to a multimode quantum field", New Journal of Physics **24**, 043031 (2022).

[138]J. Roslund, R. M. de Araújo, S. Jiang, C. Fabre, and N. Treps, "Wavelength-multiplexed quantum networks with ultrafast frequency combs", Nat Photon **8**, 109–112 (2014).

[139]C. Rouvière, D. Barral, A. Grateau, I. Karuseichyk, G. Sorelli, M. Walschaers, and N. Treps, *Ultra-sensitive separation estimation of optical sources*, June 2023.

[140]A. Royer, "Wigner function as the expectation value of a parity operator", Phys. Rev. A **15**, 449–450 (1977).

[141]D. Šafránek, A. R. Lee, and I. Fuentes, "Quantum parameter estimation using multi-mode Gaussian states", New Journal of Physics **17**, 073016 (2015).

[142]J. Schneeloch, C. J. Broadbent, S. P. Walborn, E. G. Cavalcanti, and J. C. Howell, "Einstein-Podolsky-Rosen steering inequalities from entropic uncertainty relations", Physical Review A **87**, 062103 (2013).

[143]E. Schrödinger, "Discussion of Probability Relations between Separated Systems", Mathematical Proceedings of the Cambridge Philosophical Society **31**, 555–563 (1935).

[144]E. Schrödinger, "Probability relations between separated systems", Mathematical Proceedings of the Cambridge Philosophical Society **32**, 446–452 (1936).

[145]A. Serafini, *Quantum Continuous Variables: A Primer of Theoretical Methods*, 1st ed. (Boca Raton, FL : CRC Press, Taylor & Francis Group, [2017] |, July 2017).

[146]B. Seron, L. Novo, A. Arkhipov, and N. J. Cerf, *Efficient validation of Boson Sampling from binned photon-number distributions*, Dec. 2022.

[147]V. S. Shchesnovich, "Partial indistinguishability theory for multiphoton experiments in multiport devices", Physical Review A **91**, 013844 (2015).

[148]P. Shor, "Algorithms for quantum computation: discrete logarithms and factoring", in Proceedings 35th Annual Symposium on Foundations of Computer Science (Nov. 1994), pp. 124–134.

[149]R. Simon, "Peres-Horodecki Separability Criterion for Continuous Variable Systems", Phys. Rev. Lett. **84**, 2726–2729 (2000).

[150]M. A. Soloviev, "Twisted convolution and Moyal star product of generalized functions", Theoretical and Mathematical Physics **172**, 885–900 (2012).

[151]G. Sorelli, M. Gessner, M. Walschaers, and N. Treps, "Moment-based superresolution: Formalism and applications", Physical Review A **104**, 033515 (2021).

[152]G. Sorelli, M. Gessner, M. Walschaers, and N. Treps, "Optimal Observables and Estimators for Practical Superresolution Imaging", Physical Review Letters **127**, 123604 (2021).

[153]G. Sorelli, M. Gessner, M. Walschaers, and N. Treps, *Gaussian quantum metrology for mode-encoded parameters: general theory and imaging applications*, tech. rep. arXiv:2202.10355 (arXiv, Feb. 2022).

[154]G. Sorelli, M. Gessner, M. Walschaers, and N. Treps, *Quantum limits for resolving Gaussian sources*, tech. rep. arXiv:2205.04258 (arXiv, May 2022).

[155]F. Soto and P. Claverie, "When is the Wigner function of multidimensional systems nonnegative?", Journal of Mathematical Physics **24**, 97–100 (1983).

[156]N. Spagnolo, C. Vitelli, M. Bentivegna, D. J. Brod, A. Crespi, F. Flamini, S. Giacomini, G. Milani, R. Ramponi, P. Mataloni, R. Osellame, E. F. Galvão, and F. Sciarrino, "Experimental validation of photonic boson sampling", Nature Photonics **8**, 615–620 (2014).

[157]R. W. Spekkens, "Negativity and Contextuality are Equivalent Notions of Nonclassicality", Phys. Rev. Lett. **101**, 020401 (2008).

[158]J. B. Spring, B. J. Metcalf, P. C. Humphreys, W. S. Kolthammer, X.-M. Jin, M. Barbieri, A. Datta, N. Thomas-Peter, N. K. Langford, D. Kundys, J. C. Gates, B. J. Smith, P. G. R. Smith, and I. A. Walmsley, "Boson Sampling on a Photonic Chip", Science **339**, 798–801 (2013).

[159]I. Straka, L. Lachman, J. Hloušek, M. Miková, M. Mičuda, M. Ježek, and R. Filip, "Quantum non-Gaussian multiphoton light", npj Quantum Information **4**, 1–5 (2018).

[160]I. Straka, A. Predojević, T. Huber, L. Lachman, L. Butschek, M. Miková, M. Mičuda, G. S. Solomon, G. Weihs, M. Ježek, and R. Filip, "Quantum non-Gaussian Depth of Single-Photon States", Physical Review Letters **113**, 223603 (2014).

[161]I. Strandberg, "Simple, Reliable, and Noise-Resilient Continuous-Variable Quantum State Tomography with Convex Optimization", Physical Review Applied **18**, 044041 (2022).

[162]D. Su, C. R. Myers, and K. K. Sabapathy, "Conversion of Gaussian states to non-Gaussian states using photon-number-resolving detectors", Physical Review A **100**, 052301 (2019).

[163]X. Su, Y. Zhao, S. Hao, X. Jia, C. Xie, and K. Peng, "Experimental preparation of eight-partite cluster state for photonic qumodes", Opt. Lett. **37**, 5178–5180 (2012).

[164]E. C. G. Sudarshan, "Equivalence of Semiclassical and Quantum Mechanical Descriptions of Statistical Light Beams", Phys. Rev. Lett. **10**, 277–279 (1963).

[165]R. Takagi and Q. Zhuang, "Convex resource theory of non-Gaussianity", Physical Review A **97**, 062337– (2018).

[166]K. Takase, J.-i. Yoshikawa, W. Asavanant, M. Endo, and A. Furusawa, "Generation of optical Schr\"odinger cat states by generalized photon subtraction", Physical Review A **103**, 013710 (2021).

[167]B. M. Terhal, "Bell inequalities and the separability criterion", Physics Letters A **271**, 319–326 (2000).

[168]M. C. Tichy, "Interference of identical particles from entanglement to boson-sampling", J. Phys. B: At. Mol. Opt. Phys. **47**, 103001 (2014).

[169]M. C. Tichy, "Sampling of partially distinguishable bosons and the relation to the multidimensional permanent", Physical Review A **91**, 022316 (2015).

[170]M. C. Tichy, K. Mayer, A. Buchleitner, and K. Mølmer, "Stringent and Efficient Assessment of Boson-Sampling Devices", Physical Review Letters **113**, 020502 (2014).

[171]M. C. Tichy, M. Tiersch, F. de Melo, F. Mintert, and A. Buchleitner, "Zero-Transmission Law for Multiport Beam Splitters", Physical Review Letters **104**, 220405 (2010).

[172]M. Tillmann, B. Dakić, R. Heilmann, S. Nolte, A. Szameit, and P. Walther, "Experimental boson sampling", Nature Photonics **7**, 540–544 (2013).

[173]E. S. Tiunov, V. V. Tiunova (Vyborova), A. E. Ulanov, A. I. Lvovsky, and A. K. Fedorov, "Experimental quantum homodyne tomography via machine learning", Optica **7**, 448–454 (2020).

[174]N. Treps, N. Grosse, W. P. Bowen, C. Fabre, H.-A. Bachor, and P. K. Lam, "A Quantum Laser Pointer", Science **301**, 940–943 (2003).

[175]M. Tsang, R. Nair, and X.-M. Lu, "Quantum Theory of Superresolution for Two Incoherent Optical Point Sources", Physical Review X **6**, 031033 (2016).

[176]H. L. Van Trees, *Detection, estimation, and modulation theory* (New York, 2001).

[177]V. Veitch, N. Wiebe, C. Ferrie, and J. Emerson, "Efficient simulation scheme for a class of quantum optics experiments with non-negative Wigner representation", New Journal of Physics **15**, 013037 (2013).

[178]B. Vlastakis, G. Kirchmair, Z. Leghtas, S. E. Nigg, L. Frunzio, S. M. Girvin, M. Mirrahimi, M. H. Devoret, and R. J. Schoelkopf, "Deterministically Encoding Quantum Information Using 100-Photon Schrödinger Cat States", Science **342**, 607–610 (2013).

[179]G. Vojetta, F. Guellec, L. Mathieu, K. Foubert, P. Feautrier, and J. Rothman, "Linear photon-counting with HgCdTe APDs", in Advanced Photon Counting Techniques VI, Vol. 8375 (May 2012), pp. 206–223.

[180]K. Wagner, J. Janousek, V. Delaubert, H. Zou, C. Harb, N. Treps, J. F. Morizur, P. K. Lam, and H. A. Bachor, "Entangling the Spatial Properties of Laser Beams", Science **321**, 541–543 (2008).

[181]S. P. Walborn, B. G. Taketani, A. Salles, F. Toscano, and R. L. de Matos Filho, "Entropic Entanglement Criteria for Continuous Variables", Physical Review Letters **103**, 160505 (2009).

[182]M. Walschaers, "Signatures of many-particle interference", Journal of Physics B: Atomic, Molecular and Optical Physics **53**, 043001 (2020).

[183]M. Walschaers, "Non-gaussian quantum states and where to find them", PRX Quantum **2**, 030204 (2021).

[184]M. Walschaers, "On Quantum Steering and Wigner Negativity", Quantum **7**, 1038 (2023).

[185]M. Walschaers, C. Fabre, V. Parigi, and N. Treps, "Entanglement and Wigner Function Negativity of Multimode Non-Gaussian States", Phys. Rev. Lett. **119**, 183601 (2017).

[186]M. Walschaers, C. Fabre, V. Parigi, and N. Treps, "Statistical signatures of multimode single-photon-added and -subtracted states of light", Phys. Rev. A **96**, 053835 (2017).

[187]M. Walschaers, J. Kuipers, and A. Buchleitner, "From many-particle interference to correlation spectroscopy", Physical Review A **94**, 020104 (2016).

[188]M. Walschaers, J. Kuipers, J.-D. Urbina, K. Mayer, M. C. Tichy, K. Richter, and A. Buchleitner, "Statistical benchmark for BosonSampling", New Journal of Physics **18**, 032001 (2016).

[189]M. Walschaers, V. Parigi, and N. Treps, "Practical Framework for Conditional Non-Gaussian Quantum State Preparation", PRX Quantum **1**, 020305 (2020).

[190]M. Walschaers, Y.-S. Ra, and N. Treps, "Mode-dependent-loss model for multimode photon-subtracted states", Physical Review A **100**, 023828 (2019).

[191]M. Walschaers, S. Sarkar, V. Parigi, and N. Treps, "Tailoring Non-Gaussian Continuous-Variable Graph States", Physical Review Letters **121**, 220501– (2018).

[192]M. Walschaers and N. Treps, "Remote Generation of Wigner Negativity through Einstein-Podolsky-Rosen Steering", Phys. Rev. Lett. **124**, 150501 (2020).

[193]M. Walschaers, N. Treps, B. Sundar, L. D. Carr, and V. Parigi, "Emergent complex quantum networks in continuous-variables non-Gaussian states", arXiv:2012.15608 [cond-mat, physics:quant-ph] (2020).

[194]J. Wenger, R. Tualle-Brouri, and P. Grangier, "Non-Gaussian Statistics from Individual Pulses of Squeezed Light", Physical Review Letters **92**, 153601– (2004).

[195]H. Weyl, "Quantenmechanik und Gruppentheorie", Zeitschrift für Physik **46**, 1–46 (1927).

[196]E. Wigner, "On the Quantum Correction For Thermodynamic Equilibrium", Phys. Rev. **40**, 749–759 (1932).

[197]F. Wilde, A. Kshetrimayum, I. Roth, D. Hangleiter, R. Sweke, and J. Eisert, *Scalably learning quantum many-body Hamiltonians from dynamical data*, Sept. 2022.

[198]J. Williamson, "On the Algebraic Problem Concerning the Normal Forms of Linear Dynamical Systems", American Journal of Mathematics **58**, 141–163 (1936).

[199]Y. Xiang, I. Kogias, G. Adesso, and Q. He, "Multipartite Gaussian steering: Monogamy constraints and quantum cryptography applications", Physical Review A **95**, 010101 (2017).

[200]Y. Xiang, S. Liu, J. Guo, Q. Gong, N. Treps, Q. He, and M. Walschaers, "Distribution and quantification of remotely generated Wigner negativity", npj Quantum Information **8**, 21 (2022).

[201]B. Yadin, M. Fadel, and M. Gessner, "Metrological complementarity reveals the Einstein-Podolsky-Rosen paradox", Nature Communications **12**, 2410 (2021).

[202]A. Zavatta, V. Parigi, and M. Bellini, "Experimental nonclassicality of single-photon-added thermal light states", Phys. Rev. A **75**, 052106 (2007).

[203]K. Zhang, J. Jing, N. Treps, and M. Walschaers, "Maximal entanglement increase with single-photon subtraction", Quantum **6**, 704 (2022).

[204]H.-S. Zhong, Y.-H. Deng, J. Qin, H. Wang, M.-C. Chen, L.-C. Peng, Y.-H. Luo, D. Wu, S.-Q. Gong, H. Su, Y. Hu, P. Hu, X.-Y. Yang, W.-J. Zhang, H. Li, Y. Li, X. Jiang, L. Gan, G. Yang, L. You, Z. Wang, L. Li, N.-L. Liu, J. J. Renema, C.-Y. Lu, and J.-W. Pan, "Phase-Programmable Gaussian Boson Sampling Using Stimulated Squeezed Light", Physical Review Letters **127**, 180502 (2021).

[205]H.-S. Zhong, H. Wang, Y.-H. Deng, M.-C. Chen, L.-C. Peng, Y.-H. Luo, J. Qin, D. Wu, X. Ding, Y. Hu, P. Hu, X.-Y. Yang, W.-J. Zhang, H. Li, Y. Li, X. Jiang, L. Gan, G. Yang, L. You, Z. Wang, L. Li, N.-L. Liu, C.-Y. Lu, and J.-W. Pan, "Quantum computational advantage using photons", Science **370**, 1460 (2020).